frontiers | Research Topics

Neuroinflammation and neurodegenerative diseases

Edited by
Pradeep Kumar and Kiran Bhaskar

Published in
Frontiers in Neuroscience

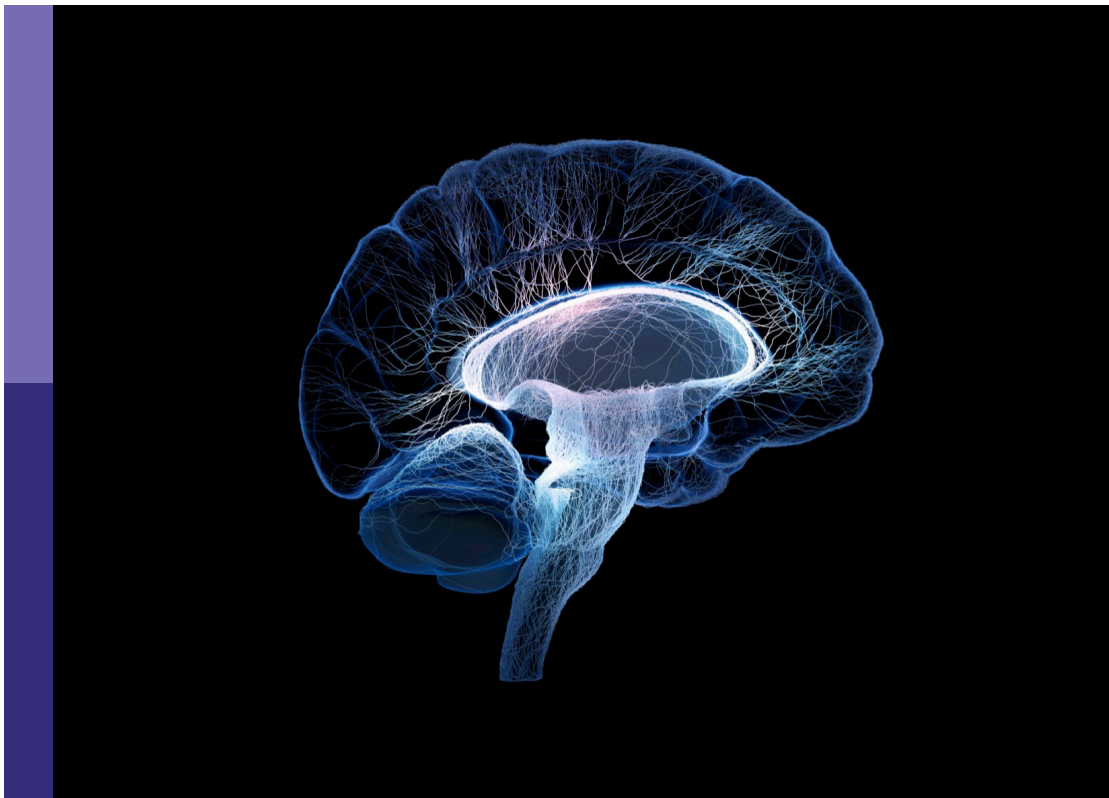

ISSN 1664-8714
ISBN 978-2-8325-6051-8
DOI 10.3389/978-2-8325-6051-8

About Frontiers

Frontiers is more than just an open access publisher of scholarly articles: it is a pioneering approach to the world of academia, radically improving the way scholarly research is managed. The grand vision of Frontiers is a world where all people have an equal opportunity to seek, share and generate knowledge. Frontiers provides immediate and permanent online open access to all its publications, but this alone is not enough to realize our grand goals.

Frontiers journal series

The Frontiers journal series is a multi-tier and interdisciplinary set of open-access, online journals, promising a paradigm shift from the current review, selection and dissemination processes in academic publishing. All Frontiers journals are driven by researchers for researchers; therefore, they constitute a service to the scholarly community. At the same time, the *Frontiers journal series* operates on a revolutionary invention, the tiered publishing system, initially addressing specific communities of scholars, and gradually climbing up to broader public understanding, thus serving the interests of the lay society, too.

Dedication to quality

Each Frontiers article is a landmark of the highest quality, thanks to genuinely collaborative interactions between authors and review editors, who include some of the world's best academicians. Research must be certified by peers before entering a stream of knowledge that may eventually reach the public - and shape society; therefore, Frontiers only applies the most rigorous and unbiased reviews. Frontiers revolutionizes research publishing by freely delivering the most outstanding research, evaluated with no bias from both the academic and social point of view. By applying the most advanced information technologies, Frontiers is catapulting scholarly publishing into a new generation.

What are Frontiers Research Topics?

Frontiers Research Topics are very popular trademarks of the *Frontiers journals series*: they are collections of at least ten articles, all centered on a particular subject. With their unique mix of varied contributions from Original Research to Review Articles, Frontiers Research Topics unify the most influential researchers, the latest key findings and historical advances in a hot research area.

Find out more on how to host your own Frontiers Research Topic or contribute to one as an author by contacting the Frontiers editorial office: frontiersin.org/about/contact

Neuroinflammation and neurodegenerative diseases

Topic editors

Pradeep Kumar — All India Institute of Medical Sciences, India

Kiran Bhaskar — University of New Mexico, United States

Citation

Kumar, P., Bhaskar, K., eds. (2025). *Neuroinflammation and neurodegenerative diseases*. Lausanne: Frontiers Media SA. doi: 10.3389/978-2-8325-6051-8

Table of contents

frontiers | Frontiers in Neuroscience

TYPE Editorial
PUBLISHED 14 February 2025
DOI 10.3389/fnins.2025.1561636

OPEN ACCESS

EDITED AND REVIEWED BY
Mark P. Burns,
Georgetown University, United States

*CORRESPONDENCE
Pradeep Kumar
✉ pradeepguptaneuro@gmail.com

RECEIVED 16 January 2025
ACCEPTED 04 February 2025
PUBLISHED 14 February 2025

CITATION
Kumar P and Bhaskar K (2025) Editorial: Neuroinflammation and neurodegenerative diseases. *Front. Neurosci.* 19:1561636. doi: 10.3389/fnins.2025.1561636

Editorial: Neuroinflammation and neurodegenerative diseases

Pradeep Kumar[1]* and Kiran Bhaskar[2]

[1]Clinical Research Unit, All India Institute of Medical Sciences, New Delhi, India, [2]Department of Molecular Genetics & Microbiology and Neurology, University of New Mexico, Albuquerque, NM, United States

KEYWORDS

neuroinflammation, neurodegenerative disease, biomarkers, neuroprotection, therapeutic interventions

Editorial on the Research Topic
Neuroinflammation and neurodegenerative diseases

Neurodegenerative diseases, characterized by the progressive loss of neuronal structure and function, are among the most devastating health challenges of the modern era (Gadhave et al., 2024). Disorders such as Alzheimer's disease (AD), Parkinson's disease (PD), multiple sclerosis (MS), and amyotrophic lateral sclerosis (ALS) share few common pathological hallmarks: neurodegeneration, neuroinflammation, and impaired brain integrity/connectivity (Cova et al., 2017). This complex interplay of immune-mediated responses in the central nervous system (CNS) integrity has emerged as a pivotal contributor to neuronal damage and disease progression (Jellinger, 2010). The growing body of research on this topic underscores the importance of unraveling the mechanisms of neuroinflammation and restoring brain homeostasis, which will pave the way for innovative therapeutic strategies.

This Research Topic, titled *Neuroinflammation and neurodegenerative diseases,* comprises 14 insightful contributions from leading researchers. Collectively, these studies explore the molecular and cellular underpinnings of neuroinflammation, the diagnostic potential of biomarkers, and promising therapeutic avenues. Additional insights are provided on how peripherally-derived risk factors [such as type 2 diabetes mellitus (T2DM), osteoarthritis, and Coronavirus Disease 2019 (COVID-19)] can have an impact on brain integrity/neuroinflammation. This editorial highlights the key themes and findings presented in this Research Topic.

Unraveling molecular mechanisms

Among variety of neurodegenerative phenotypes, understanding the molecular basis of neuroinflammation is crucial for identifying therapeutic targets. Several studies in this Research Topic shed light on these mechanisms. For instance, the potential role of Calcitonin Gene Related Peptide (CGRP) in synucleinopathies offers insights into the molecular mediators of neuroinflammation (Alexoudi et al.). Likewise, the study on *α-Synuclein-mediated mitochondrial translocation of cofilin-1* elucidates how mitochondrial dysfunction and oxidative stress are intertwined in PD pathology (Yan et al.). The reciprocal roles of retro-elements in regulating memory and immunity, as discussed in one article, further deepen our understanding of the genetic and epigenetic interplay in neurodegeneration (Herbert). Such findings underscore the intricate molecular networks driving oxidative stress and neuroinflammatory processes.

Inflammatory biomarkers and diagnostics

The pursuit of reliable biomarkers for early diagnosis and disease monitoring remains a cornerstone of neurodegenerative research. The diagnostic values of plasma cell-free nuclear DNA (cf-nDNA) and cell-free mitochondrial DNA (cf-mtDNA) for PD and multiple system atrophy, as explored in one study, highlight the promise of liquid biopsy approaches (Ying et al.). Another study associates higher serum lipoprotein-associated phospholipase A_2 (Lp-PLA2) levels with cognitive impairment in PD patients, emphasizing the role of systemic inflammation markers in CNS diseases (Wu et al.).

Many peripheral causes can impact neuronal integrity and trigger neuroinflammation. For example, comprehensive magnetic resonance imaging (MRI) assessments revealing subtle brain findings in non-hospitalized post-COVID patients with cognitive impairment extend the discussion to post-viral neuroinflammatory syndromes (Fineschi et al.). Similarly, Ni et al. observed significant abnormalities in the connectivity and topology of large brain functional networks in T2DM patients. Liu et al. has observed a positive correlation between patients with osteoarthritis and Parkinson's disease. This underscores the relevance of neuroinflammation in broader contexts, including long-term sequelae of infectious, metabolic, and other peripheral degenerative diseases.

Therapeutic approaches and interventions

Targeted therapies to mitigate neuroinflammation hold transformative potential for patients with neurodegenerative diseases. The neuroprotective effects of the aqueous extract of *Swietenia macrophylla* leaf in a PD murine model (Cardoso et al., 2024), along with the cognitive and mood-enhancing properties of diethyl butylmalonate in 5×familial Alzheimer's disease (FAD) mice, exemplify novel pharmacological interventions (Yuan et al.).

Non-pharmacological approaches also show promise. The regulation of microglia through physical exercise, as highlighted in one study, underscores the potential of lifestyle modifications as adjunctive therapies (Strohm and Majewska). These findings align with broader efforts to identify holistic and accessible therapeutic options.

Neuroprotective strategies

Preserving neuronal integrity amidst the challenges of neuroinflammation is a primary objective in neurodegenerative research. The impact of sleep, anxiety, and depression on traumatic brain injury outcomes, analyzed in another contribution, offers insights into the broader psychosocial dimensions of neuroprotection (Fu et al.).

Additionally, the spatiotemporal consistency analysis of cerebral small vessel disease via resting-state functional MRI (rs-fMRI) provides a window into the vascular contributions to neurodegeneration, emphasizing the need for integrated neurovascular protective strategies (Yang et al.).

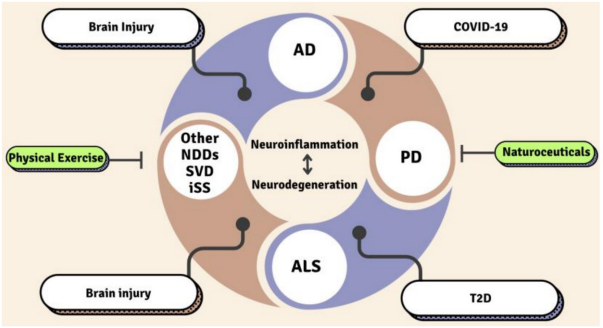

FIGURE 1
Regulators of neurodegeneration and neuroinflammation. SVD, Small Vessel Disease; AD, Alzheimer's Disease; PD, Parkinson's Disease; ALS, Amyotrophic Lateral Sclerosis; T2D, Type 2 Diabetes; iSS, Infratentorial superficial siderosis; NDDs, Neurodegenerative diseases.

Looking ahead

This Research Topic represents a significant step forward in our understanding of neurodegenerative diseases with specific emphasis on neuroinflammation, metabolic condition, and peripheral diseases (Figure 1). The findings bridge gaps between basic science and translational research, providing a roadmap for future investigations. By identifying actionable targets and validating therapeutic interventions, these studies lay the groundwork for innovative solutions to one of modern medicine's most pressing challenges.

We extend our gratitude to all contributors for their invaluable insights and encourage continued interdisciplinary collaboration in this field. Together, we aspire to translate these scientific advances into tangible benefits for patients and their families, ultimately transforming the landscape of neurodegenerative disease management.

Author contributions

PK: Conceptualization, Project administration, Supervision, Writing – original draft, Writing – review & editing. KB: Conceptualization, Supervision, Writing – original draft, Writing – review & editing.

Acknowledgments

The authors are thankful to the contributors to this Research Topic as well as the Editorial support of the Journal.

Conflict of interest

The authors declare that the research was conducted in the absence of any commercial or financial relationships that could be construed as a potential conflict of interest.

Publisher's note

References

Cardoso, V. S. L., Valente-Amaral, A., Monteiro, R. F. M., Meira, C. L. S., de Meira, N. S., da Silva, M. N., et al. (2024). Aqueous extract of Swietenia macrophylla leaf exerts an anti-inflammatory effect in a murine model of Parkinson's disease induced by 6-OHDA. *Front Neurosci.* 18:1351718. doi: 10.3389/fnins.2024.1351718

Cova, I., Markova, A., Campini, I., Grande, G., Mariani, C., and Pomati, S. (2017). Worldwide trends in the prevalence of dementia. *J. Neurol. Sci.* 379, 259–260. doi: 10.1016/j.jns.2017.06.030

Gadhave, D. G., Sugandhi, V. V., Jha, S. K., Nangare, S. N., Gupta, G., Singh, S. K., et al. (2024). Neurodegenerative disorders: mechanisms of degeneration and therapeutic approaches with their clinical relevance. *Ageing Res. Rev.* 99:102357. doi: 10.1016/j.arr.2024.102357

Jellinger, K. A. (2010). Basic mechanisms of neurodegeneration: a critical update. *J. Cell Mol. Med.* 14, 457–487. doi: 10.1111/j.1582-4934.2010.01010.x

frontiers | Frontiers in Neuroscience

TYPE Original Research
PUBLISHED 16 February 2024
DOI 10.3389/fnins.2024.1373358

OPEN ACCESS

EDITED BY
Pradeep Kumar,
All India Institute of Medical Sciences, India

REVIEWED BY
Sotirios Apostolakis,
Metropolitan Hospital, Greece
Malik Ghannam,
University of Iowa Hospitals and Clinics, United States

*CORRESPONDENCE
Weibin Huang
975017548@qq.com

RECEIVED 19 January 2024
ACCEPTED 05 February 2024
PUBLISHED 16 February 2024

CITATION
Deng L, Lin Y, Lin Y and Huang W (2024) Infratentorial superficial siderosis: report of six cases and review of the literature.
Front. Neurosci. 18:1373358.
doi: 10.3389/fnins.2024.1373358

Infratentorial superficial siderosis: report of six cases and review of the literature

Lixia Deng[1,2,3], Yi Lin[1,3,4], Yu Lin[1,3,4] and Weibin Huang[1,3,4]*

[1]Department of Neurology, The First Affiliated Hospital of Fujian Medical University, Fuzhou, Fujian, China, [2]Department of Neurology, The Third Hospital of Xiamen, Xiamen, Fujian, China, [3]Fujian Institute of Neurology, The First Affiliated Hospital, Fujian Medical University, Fuzhou, Fujian, China, [4]Department of Neurology, National Regional Medical Center, Binhai Campus of the First Affiliated Hospital, Fujian Medical University, Fuzhou, Fujian, China

Objectives: To investigate the etiology, clinical manifestations, imaging features, and treatment of patients with infratentorial superficial siderosis (iSS), enhance clinicians' comprehension of this rare disease, and conduct oral deferiprone intervention and subsequent monitoring.

Methods: Six patients diagnosed with iSS based on magnetic resonance imaging (MRI) and susceptibility weighted imaging (SWI) were enrolled from 2021 to 2023 at the First Affiliated Hospital of Fujian Medical University. Their clinical datas were summarized, and the etiology and imaging characteristics were analyzed. Follow-up was conducted through telephone or outpatient visits.

Results: Among the 6 patients, there were 3 males and 3 females. The onset age ranged from 35 to 71 years, with an average onset age of 53 years. The clinical symptoms mainly included acoustic disturbances (6/6), gait imbalance (6/6), dysolfactory (6/6), cognitive impairment (2/6), epilepsy (2/6), and pyramidal tract sign (2/6). Evidence of superficial siderosis was observed on MRI across the cortex, brainstem, cerebellum, and spinal cord in all patients. T2-space sequence MRI revealed two instances of dural tear. During the follow-up period ranging from 1 month to 3 years, three patients who received oral deferiprone treatment showed improvement, whereas the remaining three patients who declined deferiprone treatment demonstrated progression.

Conclusion: The primary clinical manifestations of iSS include bilateral sensorineural hearing disturbances, progressive cerebellar ataxia, and spinal cord lesions. The key diagnostic criteria involve the presence of linear hypointensity on T2-WI in the surface region of the nervous system. Dural tear caused by various factors is considered to be the most common cause of iSS, and its treatment mainly involves surgical intervention for hemorrhagic primary diseases as well as pharmacotherapy with deferiprone.

KEYWORDS

infratentorial superficial siderosis, magnetic resonance imaging, dural tear, deferiprone, T2-weighted imaging

1 Introduction

The superficial siderosis of the central nervous system (SSCNS) is an uncommon neurodegenerative disorder resulting from chronic, recurrent or persistent leakage of minute quantities of erythrocytes into the subarachnoid space. SSCNS can be classified into cortical superficial siderosis (cSS) and infratentorial superficial siderosis (iSS), based on which brain

regions are affected (Wilson et al., 2017). cSS primarily involves the cerebral cortex surface. Clinical manifestations include headache, focal nerve dysfunction, and cognitive impairment. iSS is defined as involvement of at least two sites within the brainstem, cerebellum or spinal cord with or without supratentorial distribution of hemosiderin deposition. The primary clinical manifestations of iSS encompass progressive cerebellar ataxia, sensorineural hearing loss in both ears, and spinal cord lesions. Additional prevalent neurological symptoms include cognitive impairment, epilepsy, hyposmia, dizziness, headache, etc. (Kumar, 2021).

In the past, the diagnosis of iSS primarily relied on postmortem examinations. Pathological analysis revealed deposits of hemosiderin, iron, and ferritin on the surface of the brainstem, cerebellum, and spinal cord, accompanied by secondary nerve cell degeneration, and demyelination changes. However, with the widespread utilization of magnetic resonance imaging (MRI) technology in recent years, an increasing number of cases of iSS have been identified. The presence of hypointense signal loops on the cortical surface, brainstem, cerebellum, and spinal cord can be observed in T2 sequences MRI as well as other iron-sensitive sequences in individuals with superficial siderosis.

Due to the limited number of cases, clinical heterogeneity, inadequate attention to etiological diagnosis, and lack of long-term follow-up data, iSS exhibits a high rate of missed diagnoses, low diagnostic rates, and insufficient treatment rates. It is crucial to accumulate relevant data from clinical and basic research promptly in order to facilitate the diagnosis and treatment of this disease. Therefore, the objective of this study was to prospectively enroll and analyze a cohort of six representative cases with iSS admitted to the First Affiliated Hospital of Fujian Medical University between 2021 and 2023. The study aimed to comprehensively characterize their clinical manifestations, including imaging findings, lumbar puncture results, audiological examinations, and other relevant outcomes. By combining these findings with existing literature evidence, we discussed its pathogenesis, potential etiology factors and treatment options. This comprehensive analysis aims to enhance our understanding and diagnostic capabilities regarding iSS while emphasizing the importance of exploring its underlying causes for developing accurate treatment strategies.

2 Materials and methods

2.1 Population

A total of six patients diagnosed with iSS were recruited from the First Affiliated Hospital of Fujian Medical University between 2021 and 2023. The inclusion criteria for patient selection included: (1) clinical admission with chief complaints of hearing loss, unsteady gait, or cognitive impairment; (2) Hypointense rings were observed on at least two locations within the brainstem, cerebellum, or spinal cord using T2 and other iron-sensitive sequences in MRI imaging.

Abbreviations: SSCNS, superficial siderosis of the central nervous system; iSS, infratentorial superficial siderosis; cSS, cortical superficial siderosis; MRI, magnetic resonance imaging; T2-WI, T2-weighted imaging; SWI, susceptibility weighted imaging; MOCA, montreal cognitive assessment; CSF, cerebrospinal fluid; EEG, electroencephalogram; DSM, digital subtraction myelography.

2.2 Data collection

2.2.1 Demographics

Two highly trained neurologists collected and sorted out the clinical data of 6 patients, including age, gender, age of onset, course of disease, clinical symptoms, and recorded the patient's signs, cognitive scores, imaging, electroencephalogram (EEG), cerebrospinal fluid (CSF) examination results, etc.

2.2.2 Hearing evaluation

Hearing function was assessed using pure-tone audiometry. The hearing levels were represented by 3-frequency averages (3FA, 0.5/1/2 kilohertz, kHz) for both ears; 120 decibel hearing level (dBHL) values were substituted to calculate 3FA at frequencies where the hearing thresholds were not reached. Higher 3FA values represented worse hearing levels.

2.2.3 Cognitive evaluation

Montreal Cognitive Assessment (MOCA): Cognitive function was assessed by MOCA (Beijing version), which includes visuospatial/executive function, naming, abstract/memory, attention/calculation, language, and orientation, is a rapid screening tool for mild cognitive impairment. It assesses a number of different cognitive domains. The total score of this scale is 30, and the normal value is ≥26.

2.2.4 MRI

MR750 3.0 T superconducting magnetic resonance machine produced by Siemens Company of the Germany was used for MRI scanning. Routine T1-WI, T2-WI and SWI were performed in all six patients. T2-space sequence MRI were performed in two cases.

3 Results

3.1 General information

Among the 6 patients, there were an equal number of males and females (3 each), with ages ranging from 45 to 73 years and an average age of 59 years. The onset age ranged from 35 to 71 years, with an average onset age of 53 years. The duration of the disease varied between 1 and 10 years (Table 1).

3.2 Past medical history

None of the six iSS patients had a history of craniocerebral or lumbar trauma, nor did they undergo any related surgeries. Among them, two patients presented with diabetes and one patient exhibited hypertension as comorbidities.

3.3 Clinical symptoms

Among the 6 patients, all exhibited acoustic disturbances (6/6), gait imbalance (6/6), dysolfactory symptoms (6/6), while cognitive impairment, epilepsy, and pyramidal tract sign were present in 2 out of 6 patients each (Table 1).

TABLE 1 Clinical manifestation, cerebrospinal fluid, imaging, etiology, and treatment of the 6 patients with iSS.

case	sex	age (years)	symptoms	symptoms duration (years)	CSF RBC count (*10^9/L)	CSF protein (g/L)	siderosis on imaging	etiology	treatment
1	F	58	a, g, d, p	5	m/v	m/v	severe	dural tear	deferiprone
2	F	56	a, g, d, c	6	m/v	m/v	severe	inconcl.	deferiprone
3	F	67	a, g, d, c, e	1	2.4	0.47	moderate	inconcl.	heteropathy
4	M	73	a, g, d	2	m/v	m/v	moderate	inconcl.	heteropathy
5	M	55	a, g, d, e	5	0.1	0.71	severe	inconcl.	heteropathy
6	M	45	a, g, d, p	10	0.1	0.41	severe	dural tear	deferiprone

F, female; M, male; a, acoustic disturbances (tinnitus, hearing disturbances); g, gait imbalance; d, dysolfactory; c, cognitive impairment; e, epilepsy; p, pyramidal tract sign; CSF, cerebrospinal fluid; RBC, red blood cell; m/v, missing value; inconcl., inconclusive.
Siderosis on imaging was graded as mild (only infratentorial on SWI or T2-weighted images (WI), no or only thin rim on T2), moderate (supratentorial and infratentorial on SWI or T2-WI, thin rim on T2), severe (supratentorial and infratentorial on SWI or T2-WI, thick rim on T2).

3.4 Hearing and vestibular function examination

All six patients successfully completed the hearing function examination, revealing bilateral auditory impairment predominantly affecting high-frequency perception. Additionally, vestibular function assessment was conducted on all six cases, demonstrating a consistent weakness in semicircular canal response.

3.5 MRI

3.5.1 Craniocerebral MRI

All six patients underwent brain MRI examination, and T2 low signal shadow around the cortex, cerebellum, brainstem, and craniocervical junction could be seen in all patients. All the 6 patients had cerebellar atrophy, especially cerebellar vermis.

3.5.2 Spinal cord MRI

A complete spine MRI scan was performed on 6 patients, among whom superficial siderosis was observed in the cervical, thoracic, and lumbar medulla in 4 cases (severe), while it was observed in the cervical and thoracic medulla in 2 cases (moderate). Atrophy of the cervical pulp and thoracic pulp was evident in all 6 cases. T2-space sequence MRI revealed two instances of dural tear (Figure 1).

3.6 EEG

EEG was completed by three out of the six patients, all of whom exhibited a background activity characterized by diffuse slow-wave dominance.

3.7 CSF examination

Three out of the six patients underwent lumbar puncture and CSF examination. The CSF pressure was measured as 190, 105, and 90 mmH2O, respectively, (normal range: 80 ~ 180 mmH2O; conversion factor: 1 mmH2O = 0.0098 kPa). The total red blood cell counts were recorded as 2.4, 0.1, and 0.1 × 10^9/L, respectively, (normal range: 0). White blood cell counts were observed to be at levels of 6, 8, and 4 × 10^6/L, respectively, (normal range: up to a maximum of <8 × 10^6/L). CSF protein concentrations were measured as being at levels of 0.47, 0.71, and 0.41 g/L, respectively, (normal range: 0.15 ~ 0.45 g/L). Glucose and chloride levels remained within normal limits.

3.8 Follow-up observation

After the diagnosis of iSS, patients were subjected to a follow-up period ranging from 1 month to 3 years, either through telephone or outpatient visits. The follow-up outcomes revealed that three patients who received oral deferiprone treatment showed improvement in cognitive function and gait balance, whereas the remaining three patients who declined deferiprone treatment demonstrated progression. The MRI examination conducted after a treatment duration of 2 years revealed no progression in SS (Figure 2).

4 Discussion

SSCNS is a rare central nervous system disorder characterized by the deposition of hemosiderin on the brain and spinal cord surfaces, leading to the development of neurological deficits. The prevalence of SSCNS is higher in the middle-aged and elderly population, with rates of 0.21% among individuals aged 50–69 years and 1.43% among those over 69 years (Pichler et al., 2017). Consistent with previous findings, four out of six patients in this study fell within the age range of 50–69 years.

The classification of iSS is further divided into classic and secondary types based on etiology (Wilson et al., 2017). Classic type iSS (ISS-1) is characterized by the absence of spontaneous or traumatic intracranial hemorrhage that could explain hemosiderin deposition. Conversely, secondary type iSS (ISS-2) refers to cases with a history of spontaneous or traumatic intracranial hemorrhage, such as aneurysm-induced spontaneous intracerebral hemorrhage, ventricular hemorrhage, or surgical trauma. In this study, all 6 patients were diagnosed with iSS-1 type, exhibiting involvement of at least two sites in the brainstem, cerebellum, or spinal cord; moreover, no instances of spontaneous or traumatic intracranial hemorrhage were observed that could account for the deposition of hemosiderin.

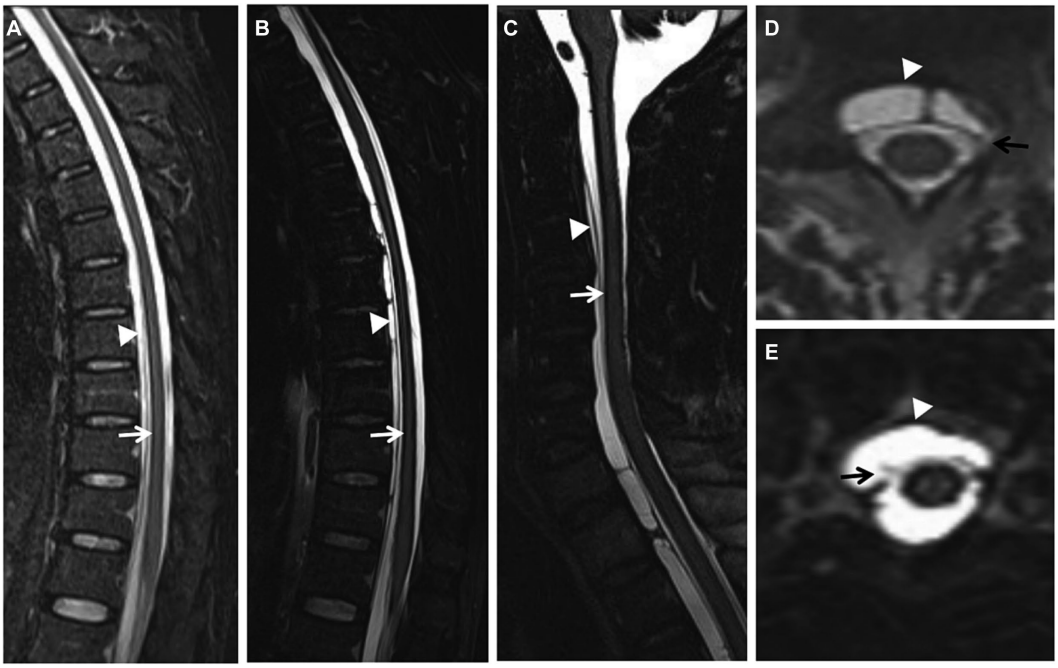

FIGURE 1
(Case 5) Extensive spinal superficial siderosis (SS) (**A–C**; arrows) and ventral epidural fluid collection at the cervical and thoracic levels (**A**–**E**; arrowheads). SS and ventral epidural fluid were more evident on T2-space sequences (**B**) than on T2-weighted images (WI) (**A**). Dural tear at the upper cervical level on axial T2-space sequence (**D**, **E**; arrows).

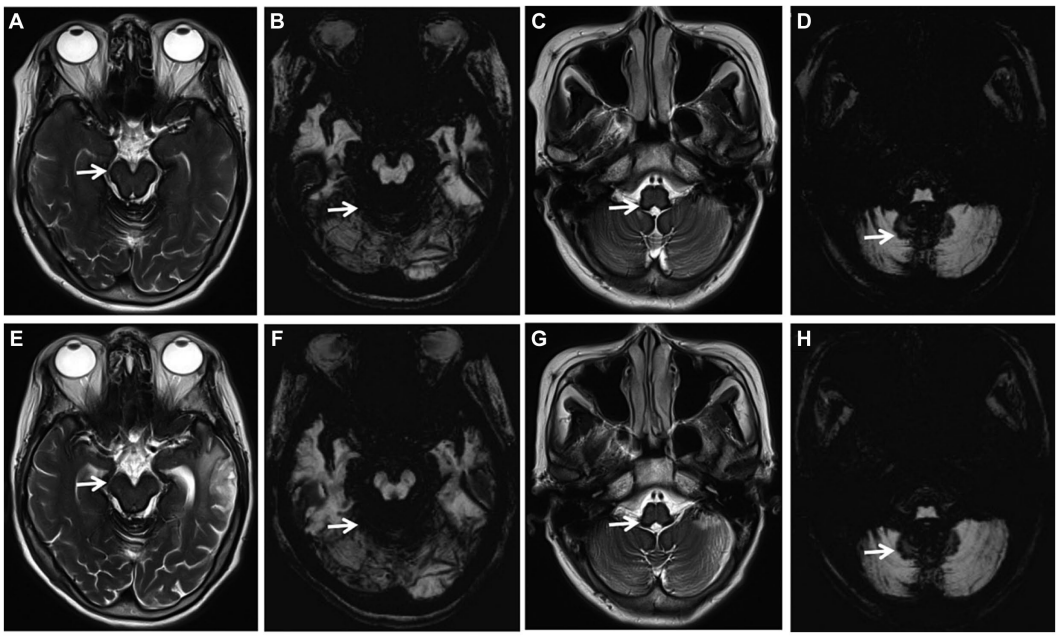

FIGURE 2
(Case 1) Axial T2-weighted images (WI) (**A**, **C**, **E**, **G**; arrows) and axial susceptibility-weighted imaging (SWI) (**B**, **D**, **F**, **H**; arrows) showing extensive SS, no progression of SS before treatment (**A**–**D**) and 2 years after deferiprone treatment (**E–H**).

The clinical manifestations of iSS are dependent on the location and extent of hemosiderin deposition. In this study, all 6 cases involved the cortex, cerebellum, brainstem, I and VIII cranial nerves, and spinal cord. The corresponding clinical manifestations were cognitive impairment (2/6), epilepsy (2/6), gait imbalance (6/6), dysolfactory (6/6), acoustic disturbances (6/6), and pyramidal tract sign (2/6). Specifically: (1) Cognitive impairment and epilepsy: All six patients completed the MOCA assessment, with two demonstrating

varying degrees of cognitive impairment primarily characterized by decreased recent memory, without a significant decline in visuospatial or executive function. This finding significantly diverges from previous studies that indicated cognitive impairment in iSS was predominantly associated with impaired executive function and visual memory (Jang et al., 2019; Chan et al., 2021; Fujii et al., 2023). However, these discrepancies may be attributed to the limited sample size and short follow-up duration. In future investigations, we aim to expand our sample size and extend the follow-up period. In this study, two patients presented with epilepsy; hemosiderin deposition in brain lobes such as the frontal subbasal surface, temporal lobe, and lateral fissure may serve as the pathological basis for seizures. Previous case reports have demonstrated that complete repair of cervical dura mater damage resulted in one patient with iSS not experiencing recurrent symptomatic epilepsy (Xu et al., 2021); (2) Gait imbalance: The main manifestations encompassed trunk ataxia and difficulty in walking straight; only one patient exhibited bilateral finger-nose test instability, suggesting that SSCNS ataxia may primarily involve a balance disorder. This finding is consistent with the study conducted by Weidauer et al. (2023). The cerebellar vermis may exhibit a higher susceptibility due to its abundant population of microglia and Bergmann glia, as well as its close proximity to the dorsal aspect of the fourth ventricle, which exposes it to an increased flow rate of cerebrospinal fluid; (3) Dysolfactory: the 6 patients in this study all complained of dysolfactory, and odor recognition tests all suggested different degrees of dysolfactory. Because the myelin sheath of the olfactory nerve is composed of glial cells, it is more vulnerable to damage (Kharytaniuk et al., 2022); (4) Acoustic disturbances: Pure tone hearing threshold tests were performed in all 6 patients in this study, suggesting binaural symmetric sensorineural hearing loss, and high-frequency hearing loss was more severe, which was consistent with the literature (Kumar, 2021). The VIII cranial nerve exits the brainstem through the pons and has a long period of immersion in the cerebrospinal fluid, and the myelin sheath is formed by glial cells, so it is most vulnerable to damage; (5) Pyramidal tract sign: In this study, 2 of 6 patients had pyramidal tract sign. iSS may be due to epidural hydrops caused by dural defects and the spinal cord is compressed, leading to myelopathy, mainly manifested as pyramidal tract sign, sensory disturbance and dysuria.

There are several potential sources of hemorrhage in SSCNS, including trauma, vascular malformation, central nervous system tumor, and cerebral amyloid angiopathy (CAA). CAA is the most common etiology of cSS in middle-aged and elderly patients (Charidimou et al., 2019a,b, 2020; Koemans et al., 2022) (Table 2). The source of hemorrhage in iSS-1 is generally unclear; however, dural tear has been identified as a common etiology (Takai and Taniguchi, 2021; Friedauer et al., 2023; Schievink et al., 2023) (Table 2). In this study cohort of six patients with iSS-1, two had confirmed dural tears. The pathophysiological of hemosiderin deposition in patients with dural defects is still unclear. However, previous studies have suggested the possible mechanism: CSF leaks into the epidural space through the ventral dural tear, and repetitive bleeding occurs from the epidural vessels that circulate back to the subarachnoid space through the dural tear, leading to hemosiderin deposition on the surface of the brain, and the spinal cord (Takai and Taniguchi, 2021; Yoshii et al., 2022).

With the continuous advancement of neuroimaging techniques, MRI of the brain and spinal cord has emerged as a crucial diagnostic tool for iSS. iSS is characterized by a distinct low T2 linear signal on the surface of the central nervous system in contact with CSF, while SWI exhibits higher sensitivity toward hemosiderin deposition (Stabile et al., 2018; Wagner et al., 2019). In this study, all six patients underwent comprehensive cranial MRI examinations which revealed T2 hypointense shadows surrounding the cortex, cerebellum, brainstem, and craniocervical junction. Complete MRI evaluations of the spinal cord in six cases demonstrated iron deposition signals on its surface along with fluid accumulation within the spinal canal; additionally, two cases showed dural tears using T2-space sequences (Figure 1). Our findings indicate that T2-space sequences are superior to conventional T2 sequences in identifying SS and dural tear due to their enhanced contrast between the dura and CSF. Dural tear represents the most common etiology for iSS; however, fluid accumulation within the spinal canal merely suggests potential cerebrospinal fluid leakage without providing information regarding its exact location. Complementary techniques such as CT myelography, digital subtraction myelography (DSM), or magnetic resonance myelography can be employed to identify fistulas based on institutional experience. Therefore, an initial routine MRI scan encompassing the entire central nervous system should be performed prior to selecting an appropriate imaging modality for fistula detection.

EEG was completed by three out of the six patients, all of whom exhibited a background activity characterized by diffuse slow-wave dominance. The three patients with iSS exhibited extensive cortical superficial siderosis, leading to cortical atrophy, which was characterized by the presence of diffuse slow-wave dominance on the EEG. In future investigations, we will strive to augment the sample size and continuously monitor the EEG performance.

In this study, the average time from onset to diagnosis of iSS was 1–10 years, and the average diagnosis time was about 5 years. We hypothesize that the prolonged interval between symptom onset and iSS diagnosis may be attributed to the following factors: (1) insufficient clinical understanding of the disease, lack of unified

TABLE 2 Differentiation between cSS and iSS.

Items	cSS	iSS
Classification of type	Focal type (≤3 sulci involvement); Disseminated type (>3 sulci involvement)	Type 1 (classical); Type 2 (secondary)
Most common cause	CAA	Dural tear
Clinical presentation	TFNEs, cognitive impairment	Progressive hearing loss, ataxia and myelopathy
Imaging on MRI	Linear hypointensity on T2-WI was restricted to the supratentorial	Linear hypointensity on T2-WI involved at least two sites (brain stem, cerebellum, spinal cord), with or without supratentorial
CSF studies	Red cells	Red cells
Treatment	Surgical removal of the source of bleeding; deferiprone	Surgical removal of the source of bleeding; deferiprone
Differential diagnosis	TIA, migraine with aura, epilepsy, et al.	Spinocerebellar ataxia, et al.

cSS, cortical superficial siderosis; iSS, infratentorial superficial siderosis; CAA, cerebral amyloid angiopathy; TFNEs, transient focal neurologic symptoms; TIA, transient ischemic attack.

diagnostic criteria; (2) some asymptomatic patients with recurrent micro cerebral hemorrhage did not enter the medical procedure; (3) the early symptoms of the disease are mild, and the first MRI examination rate and follow-up rate are not high; (4) there are large inter-individual differences in the absorption of heme iron in brain tissue.

Up to now, there is no recognized and definite treatment for SSCNS, mainly including surgery, drug therapy and other symptomatic treatments: (1) Surgical treatment is suitable for patients with definite hemorrhagic lesions, dural abnormalities, aneurysms, vascular malformations or central nervous system tumors. Among the reported cases, a minority of patients have undergone surgical intervention, and its long-term clinical efficacy remains uncertain (Takai and Taniguchi, 2021; Yoshii et al., 2022); (2) Deferiprone is one of the main treatment methods at present. In literature reports, low-dose deferiprone has a certain curative effect (Kessler et al., 2018; Cossu et al., 2019; Flores Martin et al., 2021), but Sammaraiee et al. (2020) have raised doubts about the safety and tolerance of long-term use of deferiprone treatment in patients with iSS, 40% of the cases withdrew from treatment due to granulocytopenic sepsis and fatigue side effects, of which the largest proportion was granulocytopenic sepsis (30%). Therefore, it is necessary to further study the risk of long-term treatment in the future; (3) Other symptomatic treatments: for patients with hearing loss, the suitableness of cochlear implantation can be evaluated. Although hearing loss is caused by post-cochlear lesions, some patients have different degrees of benefits after cochlear implantation (Artukarslan et al., 2022). In this study, 2 of the 6 patients with iSS were confirmed to have a dural tear, but both refused surgery and received deferiprone treatment, while the other patient without a dural tear was also treated with deferiprone. Three patients who received deferiprone treatment were followed up for 1 month to 3 years, and all showed improvement in gait balance, but no improvement in hearing and olfactory dysfunction. The MRI examination conducted after a treatment duration of 2 years revealed no progression in SS (Figure 2). No side effects were observed in these three patients. Three of the six patients received cochlear implantation, and their hearing was partially improved after surgery, and their quality of life was improved. There are few cases of iSS treated with deferiprone and cochlear implantation in China, and there is a lack of long-term follow-up studies. We will continue to follow up patients to observe the long-term efficacy.

This study has a small sample size and is a single-center study. A prospective international centralized register of patients should be developed to inform the design and conduct of a multicentre, placebo-controlled, randomized clinical trial to unify the diagnostic criteria for iSS, and evaluate the efficacy of deferiprone. Future research should prioritize the following aspects: (1) conducting prospective longitudinal studies to evaluate the therapeutic effects of deferiprone and dural tear repair; (2) investigating the role of biomarkers, such as CSF ferritin; (3) elucidating the precise mechanism underlying chronic erythrocyte leakage in patients with dural tears; and (4) further clarifying the mechanisms responsible for hemosiderin retention and neuronal damage resulting from chronic subarachnoid hemorrhage.

5 Conclusion

iSS is a disease characterized by the deposition of hemosiderin on the surface of the brain, spinal cord and cranial nerves, resulting in sensorineural hearing loss, cerebellar ataxia and pyramidal signs. The linear hypointensity on T2-WI is the main basis for the diagnosis of iSS. The most prevalent etiology of iSS is dural tear resulting from various causes, and the management of this condition primarily encompasses surgical intervention for hemorrhagic primary diseases and pharmacotherapy with deferiprone.

Data availability statement

The original contributions presented in the study are included in the article/supplementary material, further inquiries can be directed to the corresponding author.

Ethics statement

The studies involving humans were approved by the ethics committee of the First Affiliated Hospital of Fujian Medical University ([2021]462). The studies were conducted in accordance with the local legislation and institutional requirements. The participants provided their written informed consent to participate in this study. Written informed consent was obtained from the individual(s) for the publication of any potentially identifiable images or data included in this article.

Author contributions

LD: Data curation, Formal analysis, Investigation, Methodology, Validation, Visualization, Writing – original draft, Writing – review & editing. YiL: Data curation, Investigation, Resources, Supervision, Writing – review & editing. YuL: Data curation, Investigation, Visualization, Writing – review & editing. WH: Data curation, Funding acquisition, Investigation, Supervision, Visualization, Writing – original draft, Writing – review & editing.

Funding

The author(s) declare financial support was received for the research, authorship, and/or publication of this article. This study was supported by the Natural Science Foundation of Fujian Province (2022J05146).

Acknowledgments

We would like to thank all the subjects who participated in the study.

Conflict of interest

The authors declare that the research was conducted in the absence of any commercial or financial relationships that could be construed as a potential conflict of interest.

Publisher's note

References

Artukarslan, E., Matin, F., Donnerstag, F., Gartner, L., Lenarz, T., and Lesinski-Schiedat, A. (2022). Cochlea implantation in patients with superficial hemosiderosis. *Eur. Arch. Otorrinolaringol.* 279, 4363–4370. doi: 10.1007/s00405-021-07198-2

Chan, E., Sammaraiee, Y., Banerjee, G., Martin, A. F., Farmer, S., Cowley, P., et al. (2021). Neuropsychological and neuroimaging characteristics of classical superficial siderosis. *J. Neurol.* 268, 4238–4247. doi: 10.1007/s00415-021-10548-z

Charidimou, A., Boulouis, G., Greenberg, S. M., and Viswanathan, A. (2019a). Cortical superficial siderosis and bleeding risk in cerebral amyloid angiopathy: a meta-analysis. *Neurology* 50, 954–962. doi: 10.1212/WNL.0000000000008590

Charidimou, A., Boulouis, G., Xiong, L., Pasi, M., Roongpiboonsopit, D., Ayres, A., et al. (2019b). Cortical Superficial Siderosis Evolution. *Stroke* 50, 954–962. doi: 10.1161/STROKEAHA.118.023368

Charidimou, A., Perosa, V., Frosch, M. P., Scherlek, A. A., Greenberg, S. M., and van Veluw, S. J. (2020). Neuropathological correlates of cortical superficial siderosis in cerebral amyloid angiopathy. *Brain* 143, 3343–3351. doi: 10.1093/brain/awaa266

Cossu, G., Abbruzzese, G., Forni, G. L., Matta, G., Pinto, V., Ruffinengo, U., et al. (2019). Efficacy and safety of deferiprone for the treatment of superficial siderosis: results from a long-term observational study. *Neurol. Sci.* 40, 1357–1361. doi: 10.1007/s10072-019-03847-x

Flores Martin, A., Shanmugarajah, P., Hoggard, N., and Hadjivassiliou, M. (2021). Treatment response of Deferiprone in infratentorial superficial Siderosis: a systematic review. *Cerebellum* 20, 454–461. doi: 10.1007/s12311-020-01222-7

Friedauer, L., Foerch, C., Steinbach, J., Hattingen, E., Harter, P. N., Armbrust, M., et al. (2023). The acute superficial siderosis syndrome - clinical entity, imaging findings, and histopathology. *Cerebellum* 22, 296–304. doi: 10.1007/s12311-022-01387-3

Fujii, H., Iryo, T., Mine, N., Matsushima, H., and Kitamura, T. (2023). Classical cortical superficial siderosis presenting as extensive higher brain dysfunction with hypoperfusion in the frontoparietal lobe on the (123)I-IMP-SPECT: a case report. *Rinsho Shinkeigaku* 63, 505–512. doi: 10.5692/clinicalneurol.cn-001828

Jang, H., Jang, Y. K., Kim, H. J., Werring, D. J., Lee, J. S., Choe, Y. S., et al. (2019). Clinical significance of amyloid beta positivity in patients with probable cerebral amyloid angiopathy markers. *Eur. J. Nucl. Med. Mol. Imaging* 46, 1287–1298. doi: 10.1007/s00259-019-04314-7

Kessler, R. A., Li, X., Schwartz, K., Huang, H., Mealy, M. A., and Levy, M. (2018). Two-year observational study of deferiprone in superficial siderosis. *CNS Neurosci. Ther.* 24, 187–192. doi: 10.1111/cns.12792

Kharytaniuk, N., Lim, E. A., Chan, E., Pavlou, M., Werring, D. J., and Bamiou, D. E. (2022). Olfactory dysfunction is common in classical infratentorial superficial siderosis of the central nervous system. *J. Neurol.* 269, 6582–6588. doi: 10.1007/s00415-022-11329-y

Koemans, E. A., Voigt, S., Rasing, I., van Harten, T. W., Jolink, W. M. T., Schreuder, F., et al. (2022). Cerebellar superficial Siderosis in cerebral amyloid Angiopathy. *Stroke* 53, 552–557. doi: 10.1161/STROKEAHA.121.035019

Kumar, N. (2021). Superficial Siderosis: a clinical review. *Ann. Neurol.* 89, 1068–1079. doi: 10.1002/ana.26083

Pichler, M., Vemuri, P., Rabinstein, A. A., Aakre, J., Flemming, K. D., Brown, R. D. Jr., et al. (2017). Prevalence and natural history of superficial Siderosis: a population-based study. *Stroke* 48, 3210–3214. doi: 10.1161/STROKEAHA.117.018974

Sammaraiee, Y., Banerjee, G., Farmer, S., Hylton, B., Cowley, P., Eleftheriou, P., et al. (2020). Risks associated with oral deferiprone in the treatment of infratentorial superficial siderosis. *J. Neurol.* 267, 239–243. doi: 10.1007/s00415-019-09577-6

Schievink, W. I., Maya, M. M., Harris, J., Galvan, J., Tache, R. B., and Nuno, M. (2023). Infratentorial superficial Siderosis and spontaneous intracranial hypotension. *Ann. Neurol.* 93, 64–75. doi: 10.1002/ana.26521

Stabile, A., Di Lazzaro, V., Colosimo, C., Piazza, F., Ferrarese, C., and DiFrancesco, J. C. (2018). Idiopathic infratentorial superficial siderosis of the central nervous system: case report and review of literature. *Neurol. Neurochir. Pol.* 52, 102–106. doi: 10.1016/j.pjnns.2017.10.006

Takai, K., and Taniguchi, M. (2021). Superficial siderosis of the central nervous system associated with ventral dural defects: bleeding from the epidural venous plexus. *J. Neurol.* 268, 1491–1494. doi: 10.1007/s00415-020-10319-2

Wagner, F., Buchwalder, M., Wiest, R., Caversaccio, M. D., and Vibert, D. (2019). Superficial Siderosis of the central nervous system: Neurotological findings related to magnetic resonance imaging. *Otol. Neurotol.* 40, 31–37. doi: 10.1097/MAO.0000000000002071

Weidauer, S., Neuhaus, E., and Hattingen, E. (2023). Cerebral superficial Siderosis: Etiology, Neuroradiological features and clinical findings. *Clin. Neuroradiol.* 33, 293–306. doi: 10.1007/s00062-022-01231-5

Wilson, D., Chatterjee, F., Farmer, S. F., Rudge, P., McCarron, M. O., Cowley, P., et al. (2017). Infratentorial superficial siderosis: classification, diagnostic criteria, and rational investigation pathway. *Ann. Neurol.* 81, 333–343. doi: 10.1002/ana.24850

Xu, L., Yuan, C., Wang, Y., Shen, S., and Duan, H. (2021). Superficial siderosis of the central nervous system with epilepsy originating from traumatic cervical injury: illustrative case. *J. Neurosurg. Case Lessons* 1:CASE2114. doi: 10.3171/CASE2114

Yoshii, T., Hirai, T., Egawa, S., Hashimoto, M., Matsukura, Y., Inose, H., et al. (2022). Case report: dural dissection with ventral spinal fluid-filled collection in superficial Siderosis: insights into the pathology from anterior-approached surgical cases. *Front. Neurol.* 13:919280. doi: 10.3389/fneur.2022.919280

frontiers | Frontiers in Neuroscience

TYPE Original Research
PUBLISHED 21 February 2024
DOI 10.3389/fnins.2024.1351718

OPEN ACCESS

EDITED BY
Kiran Bhaskar,
University of New Mexico, United States

REVIEWED BY
Ari Dienel,
University of Texas Health Science Center at Houston, United States
José Ronaldo dos Santos,
Federal University of Sergipe, Brazil

*CORRESPONDENCE
Elizabeth Sumi Yamada
✉ esyamada@ufpa.br

†These authors have contributed equally to this work

RECEIVED 06 December 2023
ACCEPTED 05 February 2024
PUBLISHED 21 February 2024

CITATION
Cardoso VSL, Valente-Amaral A, Monteiro RFM, Meira CLS, de Meira NS, da Silva MN, Pinheiro JJV, Bastos GNT, Felício JS and Yamada ES (2024) Aqueous extract of *Swietenia macrophylla* leaf exerts an anti-inflammatory effect in a murine model of Parkinson's disease induced by 6-OHDA.
Front. Neurosci. 18:1351718.
doi: 10.3389/fnins.2024.1351718

Aqueous extract of *Swietenia macrophylla* leaf exerts an anti-inflammatory effect in a murine model of Parkinson's disease induced by 6-OHDA

Váldina Solimar Lopes Cardoso[1,2†], Anderson Valente-Amaral[1,3†], Rayan Fidel Martins Monteiro[3,4], Clarina Loius Silva Meira[1], Natália Silva de Meira[1], Milton Nascimento da Silva[5], João de Jesus Viana Pinheiro[2,6], Gilmara de Nazareth Tavares Bastos[3,4], João Soares Felício[2,7] and Elizabeth Sumi Yamada[1,2,3*]

[1]Experimental Neuropathology Laboratory, João de Barros Barreto University Hospital, Federal University of Pará, Belém, Brazil, [2]Oncology Research Center and Graduate Program in Oncology and Medical Sciences, João de Barros Barreto University Hospital, Federal University of Pará, Belém, Brazil, [3]Graduate Program in Neuroscience and Cellular Biology, Institute of Biological Sciences, Federal University of Pará, Belém, Brazil, [4]Neuroinflammation Laboratory, Institute of Biological Sciences, Federal University of Pará, Belém, Brazil, [5]Liquid Chromatography Laboratory, Institute of Exact and Natural Science, Federal University of Pará, Belém, Brazil, [6]Laboratory of Pathological Anatomy and Immunohistochemistry, School of Dentistry, Federal University of Pará, Belém, Brazil, [7]Endocrinology Division, University Hospital João de Barros Barreto, Federal University of Pará, Belém, Brazil

Introduction: Parkinson's disease affects 2% of the population aged over 65 years and is the second most common neurodegenerative disorder in the general population. The appearance of motor symptoms is associated with the degeneration of dopaminergic neurons in the nigrostriatal pathway. Clinically significant nonmotor symptoms are also important for severe disability with disease progression. Pharmacological treatment with levodopa, which involves dopamine restitution, results in a temporary improvement in motor symptoms. Among the mechanisms underlying the pathogenesis of the disease are exacerbated oxidative stress, mitochondrial dysfunction, and neuroinflammation. A phytochemical prospecting study showed that the aqueous extract of the leaves from *Swietenia macrophylla* (Melineaceae), known as mahogany, has polyphenols with antioxidant and anti-inflammatory capacity in a significantly higher percentage than leaf extracts from other Amazonian plants. Furthermore, the antioxidant and anti-inflammatory capacity of aqueous extract of mahogany leaf has already been demonstrated in an *in vitro* model. In this study, we hypothesized that the aqueous extract of mahogany leaf (AEML) has a neuroprotective effect in a murine model of Parkinson's disease induced by 6-hydroxidopamine (6-OHDA), due to antioxidant and anti-inflammatory properties of its phenolic compounds.

Methods: Mice were treated daily with the mahogany extract at a dose of 50 mg/kg, starting 7 days before 6-OHDA infusion until post-surgery day 7.

Results and discussion: The animals from the 6-OHDA/mahogany group, which corresponds to animals injected with the toxin and treated with aqueous extract of the mahogany leaf, presented distinct behavioral phenotypes after apomorphine challenge and were therefore subdivided into 2 groups, 6-OHDA/mahogany F1 and 6-OHDA/mahogany F2. The F1 group showed a significant increase in contralateral rotations, whereas the F2 group did not show rotations after the apomorphine stimulus. In the F1 group, there was an increase, although

not significant, in motor performance in the open field and elevated plus maze tests, whereas in the F2 group, there was significant improvement, which may be related to the lesser degree of injury to the nigrostriatal dopaminergic pathway. The TH+ histopathological analysis, a dopaminergic neuron marker, confirmed that the lesion to the nigrostriatal dopaminergic pathway was more pronounced in 6-OHDA/mahogany F1 than in 6-OHDA/mahogany F2. Our main result consisted of signs of improvement in the inflammatory profile in both the F1 and F2 6-OHDA/mahogany groups, such as a lower number of IBA-1+ microglial cells in the ventral striatum and substantia nigra pars compacta and a reduction in GFAP+ expression, an astrocyte marker, in the dorsal striatum. In this study, several bioactive compounds in the aqueous extract of mahogany leaf may have contributed to the observed beneficial effects. Further studies are necessary to better characterize their applicability for treating chronic degenerative diseases with inflammatory and oxidative bases, such as Parkinson's disease.

KEYWORDS

***Swietenia macrophylla*, natural products, polyphenols, Parkinson's disease, neuroinflammation, 6-OHDA model, nigrostriatal pathway**

Introduction

Parkinson's disease (PD) is the second most common neurological disorder with a complex evolution, affecting 2% of the population over the age of 65 and 4% of the population over the age of 80 (Pringsheim et al., 2014; Llibre-Guerra et al., 2022; Okunoye et al., 2022). Currently, the clinical diagnosis of PD is made based on cardinal symptoms: bradykinesia associated with resting tremor, muscle rigidity, and/or postural instability (Kobylecki, 2020; Tolosa et al., 2021). In addition, significant non-motor symptoms, such as anxiety, olfactory disorders, depression, sleep disorders, and autonomic nervous system impairments, are frequently observed. In some patients, these non-motor alterations precede classic motor disorders; in others, they arise with disease progression and contribute to severe disability and reduced quality of life (Braak et al., 2004; Chaudhuri et al., 2006; Tibar et al., 2018).

Although the pathology of PD involves several areas of the basal ganglia, the degeneration of dopaminergic neurons of the nigrostriatal pathway is associated with the onset and evolution of motor symptoms (Kalia and Lang, 2015; Balestrino and Schapira, 2020; MacMahon Copas et al., 2021) However, the cause of PD remains unknown.

Currently, no therapeutic intervention can successfully delay or stop the progression of PD. Therefore, there are not disease-modifying treatments available. The identification of pathophysiological mechanisms underlying PD creates opportunities for the appropriate development of new therapies with disease-modifying potential based on natural agents or compounds that consistently block the primary mechanisms involved in neuronal death (Del Rey et al., 2018; Hung and Schwarzschild, 2020; Jankovic and Tan, 2020).

Swietenia macrophylla is a large tree, known as mahogany, that naturally occurs in tropical and subtropical countries and has ethnomedicinal importance in India, Malaysia, China, and Central and South America (Moghadamtousi et al., 2013). In these countries, traditional people use different parts of this plant for antimicrobial, antioxidant, and antidiabetic purposes. Phytochemical prospecting and biological activity studies found 9 phenolic acids and 18 flavonoids in the aqueous extract from the leaves of *Swietenia macrophylla*, and have demonstrated its antioxidant and anti-inflammatory activity in an *in vitro* model (Pamplona et al., 2015).

Furthermore, the percentage of polyphenols in the aqueous extract of *Swietenia macrophylla* leaf is significantly higher than that in leaf extracts from other Amazonian plants obtained by the same method (Silva et al., 2007). Polyphenols are naturally occurring, non-enzymatic antioxidant compounds that, in low concentrations, are capable of counteracting exacerbated oxidative stress (Kujawska and Jodynis-Liebert, 2018; Ciulla et al., 2019; Singh et al., 2020) In this study, we hypothesized that the aqueous extract of the *Swietenia macrophylla* leaf has neuroprotective effects in a murine model of PD.

Materials and methods

Preparation of the plant extract

The aqueous extract of the mahogany leaf (*Swietenia macrophylla* King) was provided by Dr. Milton da Silva from the Chemistry Institute of the Federal University of Pará. The aerial parts of the plant were identified by a botanist from the Botany Department of the Federal Rural University of Pará, Amazonia, Belém, Pará, Brazil, and a specimen of N° 1,320 was deposited in the Institution's herbarium. The final dilution of the extract was made in physiological saline solution. For more details, see Pamplona et al., 2015.

Animals, treatment, and stereotaxic intervention

We used 28 Swiss male adult mice, weighing between 40–45 g, eight weeks old, from the Evandro Chagas Institute, Ananindeua, Pará; the mice were randomly separated and kept five animals per cage at a controlled temperature of 23 ± 1° C, light/dark cycle of 12/12 h, with water and balanced feed for rodents *ad libitum*. The time for acclimatization of the animals in the experimental laboratory was five days. All procedures were approved by the Ethics Committee on the

Use of Animals of the Federal University of Pará under Technical Report No. 4046270619.

The safety of the aqueous extract of the mahogany leaf (AEML) was previously defined in a subacute oral toxicity trial (data not shown). Based on this result and aiming at allometric conversion, which estimates the use of the equivalent dose as a treatment strategy in humans, we used a dose of 50 mg/kg/day of extract, orally (gavage), for treating animals injected with 6-OHDA or vehicle.

Initially, mice were randomly divided into two groups, one group being pre-treated with aqueous extract of the Mahogany leaf (AEML; $n = 16$) and the other group receiving vehicle ($n = 12$), both orally (gavage), daily, in the morning, for 14 consecutive days. After eight days of treatment, the animals underwent stereotaxis surgery for intrastriatal infusion of 10 µg of 6-OHDA-HCl (Sigma-Aldrich©/A4544) diluted in 2 µL of ascorbic acid (Sigma-Aldrich, USA) or infusion of 2 µL of 0.2% ascorbic acid.

The experimental groups were then renamed as follows: sham/vehicle, received ascorbic acid + saline solution ($n = 6$); sham/mahogany, received ascorbic acid + AEML ($n = 6$); 6-OHDA/vehicle, received 6-OHDA + saline solution ($n = 6$); and 6-OHDA/mahogany, received 6-OHDA + AEML ($n = 10$) (Figure 1).

The experimental design of pre-treatment and post-surgery treatment with AEML aimed to achieve a positive pharmacological effect, preventing damage to the nigrostriatal dopaminergic pathway, caused by the infusion of the toxin. A pilot study of 6-OHDA injection into the dorsal striatum was conducted, and based on statistical analysis, the number of animals used in this study was determined.

Before stereotaxic surgery, the animals were anesthetized with a combination of 75 mg/kg ketamine chloride and 10 mg/kg xylazine hydrochloride ip. They were then positioned in the stereotaxic apparatus (Insight Ltda/EFF333) following the coordinates AP +0.8 mm from the bregma, ML +1.5 mm from the sagittal suture, and DV 3.2 mm from the dura mater (Paxinos and Franklin, 2004). A Hamilton syringe was used to inject 2 µL of 6-OHDA or vehicle into the left dorsal striatum. The injection cannula was kept at the infusion site for 5 min before being slowly withdrawn.

Behavioral tests

All animals were evaluated in the apomorphine-induced rotation test, open field (OF), and elevated plus maze (EPM) on the 14th and 28th day after surgery. In the behavioral assessment room, luminosity was 25–26 Lux (Instrutemp©) and room temperature was 23° ± 1° C; the animals had 1 h of acclimatization and 3 h interval between behavioral assessments. After each evaluation, the apparatus was cleaned with 10% ethanol.

Apomorphine (APO)-induced rotation test

Rotational behavior was induced by apomorphine (Sigma-Aldrich/A4393) at a dose of 0.1 mg/kg (sc), and the animals were

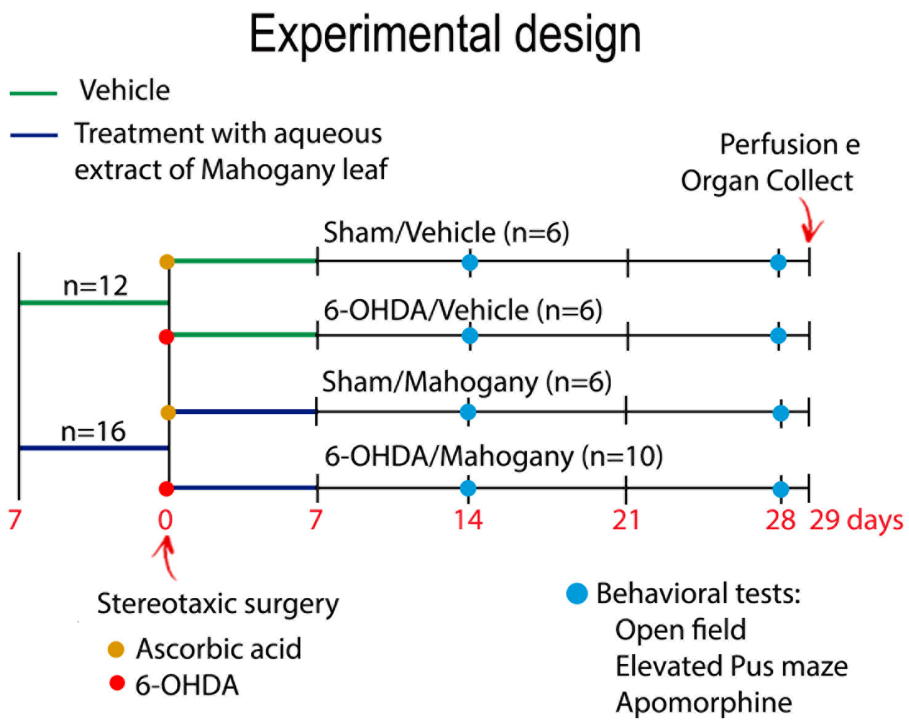

FIGURE 1
Experimental design. Animals were treated with aqueous extract of the mahogany leaf (AEML) at a dose of 50 mg/kg ($n = 16$) or 0.9% NaCl ($n = 12$) for 14 consecutive days (p.o). On the 8th day of the experiment, the animals underwent stereotaxic surgery for intrastriatal infusion of 10 µg of 6-OHDA (yellow circle) or ascorbic acid (red circle). After stereotaxic surgery, the experimental groups were renamed as follows: sham/vehicle, received ascorbic acid + saline solution ($n = 6$); sham/mahogany, received ascorbic acid + AEML ($n = 6$); 6-OHDA/vehicle, received 6-OHDA + saline solution ($n = 6$); and 6-OHDA/mahogany, received 6-OHDA + AEML ($n = 10$). On the 21st and 35th days of the experiment, open field, elevated plus maze, and apomorphine tests were performed (blue circle). Euthanasia was performed on the 36th day.

evaluated for 20 min in a 30 cm diameter arena. The number of rotations is expressed as absolute values.

Open field test (OF)

The open field test was used to evaluate spontaneous locomotion and exploratory activity. The animals were placed in the center of a circular acrylic box with gray walls, measuring 30 cm in height and 30 cm in diameter, for free exploration for 5 min. The videos were analyzed using *ANY-maze USA Software, a video tracking system, version 6.12* (Stoelting Co©, USA), in which the perimeter of the central and peripheral zones was defined. The following behavioral parameters were evaluated: total distance traveled (cm), average speed (cm/s), time and distance traveled in the periphery, and time and distance traveled in the center.

Elevated plus maze (EPM)

The elevated plus maze was used to measure general activity and anxiety-like behavior. The apparatus was 30 cm long and 5 cm wide, with two open and opposing arms, with side edges 0.5 cm high, to ensure that no animal fell from the apparatus, and two closed arms with walls 15 cm high and opposite. The four arms were connected by a 5 cm^2 central platform, and the entire structure was elevated 45 cm from the ground. Each trial lasted 5 min and involved placing the mouse on the central platform with its head facing one of the open arms.

Entry into the arms was considered when all paws crossed the line between the central platform and the arm. Using *the ANY-maze video tracking system, version 6.12* (Stoelting Co©, USA), we outlined the perimeter of the open and closed arms and the central zone. The following parameters were analyzed: total distance traveled (cm), total number of entries into open and closed arms (EOCA), percentage of time spent in open arms (tOA), percentage of time spent in closed arms (tCA), number of entries into open arms (EOA), and number of entries into closed arms (ECA).

Euthanasia and immunohistochemistry

The animals were euthanized with 150 mg/kg of ketamine chloride and 30 mg/kg of xylazine hydrochloride ip; then, transcardial perfusion with 0.1 M PBS and fixation with 4% paraformaldehyde (PFA) were initiated. The brains were collected and post-fixed in 4% PFA for 48 h and then kept in a 30% sucrose solution for 72 h, at 6°C. Subsequently, using a CM1850 cryostat (*Leica Biosystems, Nussloch, Germany*), 40 µm-thick coronal sections of the brain were collected and alternately distributed in six series. After this step, the sections were incubated in the following solutions containing 0.1 M PBS: 0.3% H_2O_2 for 30 min to inactivate endogenous peroxidase activity; 0.3% Triton X-100 for 10 min to permeabilize the sections; and normal donkey serum (NDS; Milipore©) at 5% for 1 h to block nonspecific binding.

After this step, each set of sections was incubated in specific primary antibodies, namely: (i) anti-TH (anti-tyrosine hydroxylase; 1:5.000; *Millipore©, polyclonal, anti-rabbit, AB152*); (ii) anti-IBA-1 (anti-ionized calcium binding adapter molecule 1; 1:10.000, *Wako Pure Chemical Industries Ltd, polyclonal, anti-rabbit #019-19741*); and (iii) anti-GFAP (anti-glial fibrilar acidic protein; 1:10.000; *Millipore©, monoclonal, anti-mouse, G3893*), all for 72 h, at 6°C.

The sections were washed three times for 10 min and incubated in their respective secondary antibodies conjugated to biotin, as follows: donkey anti-rabbit (1:500; *Jackson ImmunoResearch©, 711-065-152*); and donkey anti-mouse (1:500; *Jackson ImmunoResearch©, 711-065-150*), for two 12 h at 6°C. The sections were incubated in the avidin–biotin complex (1:200; *Vectastain Elite®, ABC kit; Vector Laboratories©*) for 1 h.

In the final step, we used DAB-Ni as a substrate to visualize the complex formed from the anti-TH and anti-IBA-1 primary antibodies; and 1% 3,3′-diaminobenzidine solution (DAB; Sigma-Aldrich©, D12384) to visualize the complex formed from the anti-GFAP primary antibody. The sections were washed again, mounted, and dehydrated, and only the series immunostained for GFAP were counterstained with cresyl violet.

Optical density (OD)

TH+ and GFAP+ immunostaining in the dorsal and ventral striatum was analyzed by optical density (OD). We measured three representative sections from the following AP positions: +0.74, +0.38, and + 0.02 mm from the bregma, according to The Mouse Stereotaxy Atlas (Paxinos and Franklin, 2004). The images were captured using a digital camera (*Leica Microsystem Ltd., DFC450, Germany*) attached to a stereomicroscope (*Leica Microsystem Ltd., M205A, Germany*) with image acquisition software (*Leica Application Suit, version 4.2.0, Switzerland*).

The images were transformed into grayscale (8-bit), and optical density quantification was performed using *Fiji ImageJ software* (*version 1.52, National Institutes of Health, USA*). The boundary between the dorsal and ventral STR was defined by a manually drawn horizontal line. In the first two sections, the anatomical reference was the most dorsal point of the lateral ventricle, and in the third section, the anterior commissure, which was adapted from Heuer et al. (2012). Data are expressed as percentages of the contralateral side.

Stereology

The number of microglia in the ventral and dorsal striatum was determined using stereology. From each animal, we used three representative sections from the following anterior–posterior positions: +0.74, +0.38, and, +0.02 mm from the bregma. We defined the counting limit between the dorsal and ventral striatum as the same as that used for the optical density analysis. In the SNpc, the estimation of the number of neurons and glia was also obtained by stereology; we used six representative coronal sections of the midbrain, located between anterior–posterior coordinates-2.80 mm to-3.80 mm from the bregma, according to The Mouse Stereotaxy Atlas (Paxinos and Franklin, 2004).

For the delimitation of the striatum and SNpc, we used 2x magnification, and cells were counted at 40x magnification. We used the STEREOLOGER software (*Stereology Resource Center, Version Inc., 11.0*) coupled to a Nikon Labophot-2 microscope with a control platform for movement of the X, Y, and Z coordinates (*Prior ES111US, Prior Scientific, Fulbourn, Cambridge*). The results were expressed as a percentage in relation to the contralateral side, and the error coefficient was defined as ≤0.1 (Gundersen et al., 1999).

Statistical analysis

The results for apomorphine are expressed as absolute values and were analyzed using a two-tailed paired t-test. Open field and elevated plus maze results are expressed as mean ± SEM. In the Open Field, analysis we applied *two-way ANOVA* and for the other comparisons *one-way* ANOVA and Tukey post-test. In the elevated plus maze, we applied *one-way* ANOVA and Tukey *post hoc* test.

Optical density and stereology data are expressed as mean ± SEM and in statistical analysis, we used *one-way ANOVA*, followed by Tukey *post hoc* test. In all analyses, statistical significance was defined as 95% reliability ($p < 0.05$). We used *GraphPad Prism Inc. software (Version 6.01, 2012)* for statistical analyses and graph creation.

Results

Behavioral tests

Assessment of rotations induced by apomorphine

Contralateral rotations induced by apomorphine were evaluated on the 14th and 28th day after surgery. As expected, animals in the sham/vehicle ($n = 6$) and sham/mahogany ($n = 6$) groups did not rotate after the apomorphine challenge. In the 6-OHDA/vehicle ($n = 6$) group, the average number of rotations on the 14th day post-surgery was 123.0 ± 10.3, with a rate of 6.2 ± 0.5 rotations/min; on the 28th day, the average rotations increased significantly, reaching 177.2 ± 10.9 and a rate of 8.9 ± 0.5 rotations/min ($p = 0.0102$) (Figure 2).

In the 6-OHDA/mahogany group ($n = 10$), 40% of the animals did not present contralateral rotations in the apomorphine challenge. Therefore, we subdivided this group according to the presence or absence of contralateral turns. Animals with contraversive behavior were included in the 6-OHDA/mahogany F1 group ($n = 6$), and animals that did not present contralateral rotations were included in the 6-OHDA/mahogany F2 group ($n = 4$).

In the first apomorphine test, the 6-OHDA/mahogany F1 group presented contralateral turns of 120.2 ± 18.6 (mean ± SEM) at a rate of 6.0 ± 0.9 rotations/min. In the second test, the average number of rotations increased to 172.3 ± 16.4 with a rate of 8.6 ± 0.8 rotations/min ($p = 0.0126$). These results indicate that the nigrostriatal dopaminergic lesion in the 6-OHDA/mahogany F1 group was progressive, and treatment with the aqueous extract of the mahogany leaf did not modify the standard motor behavior in the apomorphine test (Figure 2).

Assessment of locomotor activity and anxiety-like behavior in the open field test

The total distance traveled (cm) and average speed (cm/s) obtained in the open field test were used as parameters of innate exploratory activity. As shown in Figure 3A, on the 14th day, the 6-OHDA/mahogany F2 group had a displacement of 740.1 ± 176.8 cm and an average speed of 2.48 ± 0.58 cm/s. The 6-OHDA/mahogany F1 group had a displacement of 600.3 ± 142.4 cm and an average speed of 2.0 ± 0.47 cm/s, whereas the 6-OHDA/vehicle group had a displacement of only 403.8 ± 94.7 cm, with an average speed of 1.35 ± 0.32 cm/s. Although there was no significant difference between the groups injected with 6-OHDA, the 6-OHDA/mahogany F1 and 6-OHDA/mahogany F2 groups showed a tendency toward motor recovery. Furthermore, the horizontal displacement was aligned with the motor performance of the sham/vehicle group (distance traveled, 798.2 ± 146.4 cm, and average speed, 2.70 ± 0.48 cm/s). The sham/mahogany group showed a mild stimulating effect on ambulation, whereas the 6-OHDA/vehicle group showed horizontal hypoactivity; these two factors significantly accentuated the differences between the groups (distance traveled $p = 0.0078$; average speed, $p = 0.0109$).

In the test carried out on the 28th day post-surgery, the 6-OHDA/mahogany F2 group maintained the trend of motor recovery, with a distance covered of 694.5 ± 189.7 cm and an average speed of 2.33 ± 0.63 cm/s and 6-OHDA/mahogany F1, with a distance covered of 611.2 ± 95.2 cm and an average speed of 2.05 ± 0.32 cm/s; while the 6-OHDA/vehicle group continued to be hypoactive, presenting a displacement of 382.7 ± 82.5 cm and an average speed of 1.27 ± 0.28 cm/s. There was no significant difference between the groups injected with 6-OHDA. The sham/mahogany group showed a mild stimulating effect on ambulation, whereas the 6-OHDA/vehicle group showed horizontal hypoactivity; these two factors significantly

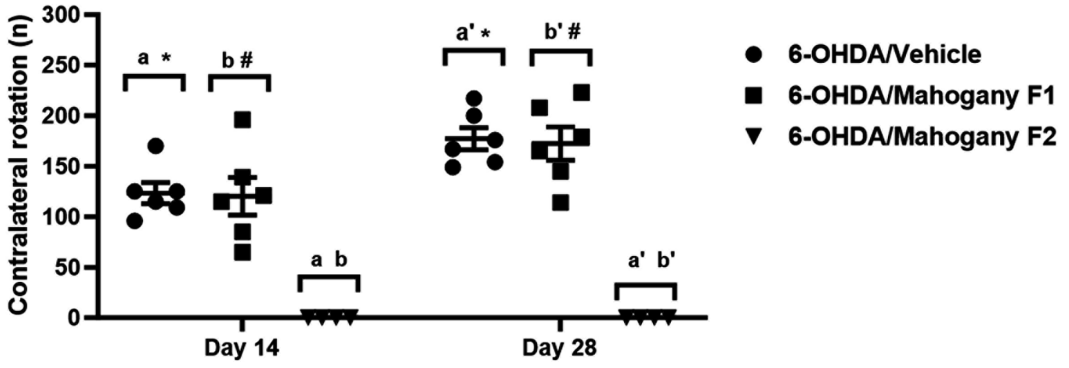

FIGURE 2
Evaluation of contralateral rotations stimulated by apomorphine in animals injected with 6-OHDA and treated with aqueous extract of the mahogany leaf. The symbols indicate: [a]6-OHDA/vehicle vs. 6-OHDA/mahogany F2, day 14, $p < 0.0001$. [b]6-OHDA/mahogany F1vs 6-OHDA/mahogany F2, day 14, $p < 0.0001$. [a']6-OHDA/vehicle vs. 6-OHDA/mahogany F2, day 28, $p < 0.0001$. [b']6-OHDA/ mahogany F1 vs. 6-OHDA/mahogany F2, day 28, $p < 0.0001$. *6-OHDA/vehicle, day 14 vs. day 28; $p = 0.0102$. #6-OHDA/mahogany F1, day 14 vs. day 28; $p = 0.0126$. The results are expressed in mean ± SEM. Two-way ANOVA followed by Tukey's *post hoc* test was used, and statistical significance was defined with 95% confidence ($p < 0.05$).

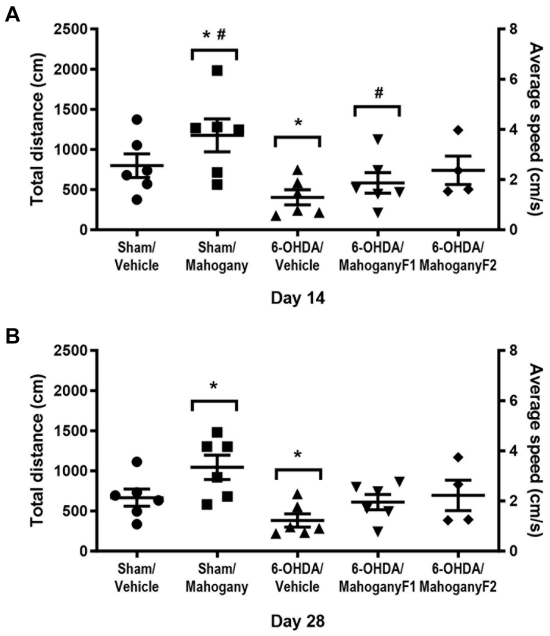

FIGURE 3
Evaluation of exploratory activity in the open field test of animals injected with 6-OHDA or vehicle and treated with aqueous extract of the mahogany leaf. Total distance traveled (cm) and mean speed (cm/s). **(A)** Tests performed on the 14th post-surgery day. The symbols indicate: *sham/mahogany vs. 6-OHDA/vehicle, total distance traveled, $p = 0.0078$, and mean speed, $p = 0.0109$; sham/mahogany vs. 6-OHDA/mahogany F1, total distance traveled, $p = 0.0491$. **(B)** Tests performed on the 28th post-surgery day. The symbol indicates the following: *sham/mahogany vs. 6-OHDA/vehicle, total distance traveled, $p = 0.0052$, and mean speed, $p = 0.0103$. The data are expressed in mean ± SEM. One-way ANOVA followed by Tukey's *post hoc* test, and statistical significance was defined with 95% confidence ($p < 0.05$).

accentuated the differences between the groups (distance traveled, $p = 0.0052$; average speed, $p = 0.0103$).

However, it was observed that the motor performance of the 6-OHDA/mahogany F2 and 6-OHDA/mahogany F1 groups remained equivalent to that of the sham/vehicle group (distance traveled, 666.1 ± 107.0 cm and average speed, 2.20 ± 0.36 cm/s) (Figure 3B).

The percentages of displacement and time on the periphery of the arena on the 14th day post-surgery were as follows: sham/vehicle, 51.6 ± 10.2 and 62.9 ± 9.6%; sham/mahogany F1, 48.2 ± 2.4% and 54.9 ± 5.9%; 6-OHDA/vehicle, 53.6 ± 8.1% and 63.0 ± 5.8%; sham/mahogany F1, 50.5 ± 6.0 and 62.3 ± 8.5; and 6-OHDA/mahogany F2, 63.2 ± 6.2 and 66.4 ± 5.8%, respectively. There was no significant difference between the groups; therefore, the unilateral injection of 6-OHDA into the dorsal striatum did not reproduce aspects related to anxiety-like behavior in the open field test (Figures 4A,B).

On the 28th day, the 6-OHDA/mahogany F2 group showed a more pronounced horizontal displacement in the periphery (85.6 ± 4.3%) and was significantly different from the sham/vehicle group, which had a displacement in the periphery of 65.9 ± 5.4% ($p = 0.0191$). Regarding the percentage of time spent in the periphery, there was no significant difference between the groups (Figures 4C,D).

Assessment of exploratory activity and anxiety-like behavior in the elevated plus maze (EPM)

Exploratory activity was assessed through the total distance traveled and the number of entries into the open and closed arms (EOCA). As shown in Figure 5A, on the 14th day, in the 6-OHDA/mahogany F2 group, the total distance traveled was 866.4 ± 123.9 cm, which represented a significant improvement compared with the 6-OHDA/vehicle group, which had a displacement of 386.6 ± 54.0 cm ($p < 0.05$). The motor performance in the 6-OHDA/mahogany F2 group was compatible with the results presented by the sham/vehicle (881.2 ± 117.5 cm) and sham/mahogany (792.3 ± 94.4 cm) groups.

Regarding the number of entries in open and closed arms, the groups presented the following averages: sham/vehicle, 29.7 ± 6.2; sham/mahogany, 31.1 ± 4.5; 6-OHDA/vehicle, 20.2 ± 5.0; 6-OHDA/mahogany F1, 18.7 ± 4.5; and 6-OHDA/mahogany F2, 31.3 ± 3.1. There was no significant difference when comparing the groups. However, we observed that the 6-OHDA/mahogany F2 group had better motor performance than the model group, although the difference was not significant (Figure 5B).

With the repetition of the test on the 28th day, a reduction in general activity was identified in all groups. Thus, the displacement in the 6-OHDA/mahogany F2 group was 573.0 ± 62.1 cm, 6-OHDA/mahogany F1 was 442.0 ± 132.4 and 6-OHDA/vehicle was 340.7 ± 39.8 cm. Although there was no significant difference between the groups, our data showed that even with the repetition of the test, 6-OHDA/mahogany F2 maintained a strong trend of motor improvement in relation to the model group (Figure 5C).

Regarding the entries in the open and closed frequency parameter, the averages were as follows: sham/vehicle, 24.8 ± 4.5; sham/mahogany, 24.5 ± 4.9; 6-OHDA/vehicle, 18.8 ± 3.5; 6-OHDA/mahogany F1, 20.3 ± 5.2; and 6-OHDA/mahogany F2, 23.2 ± 2.2. There was no statistically significant difference when comparing the groups (Figure 5D). We emphasize that the decrease in the apparatus exploration rate may have been influenced by habituation with repeated tests.

In the two elevated plus maze assessments, the parameters of time in closed arms (CA) and time in open arms (OA) were not affected in the groups injected with 6-OHDA in relation to the sham groups. Likewise, the frequency of visits in the open and closed arms was not affected.

Taken together, these results show that emotionality indices were not influenced by 6-OHDA infusion. These elevated plus maze results corroborate the data obtained in the open field, in which we observed an absence of anxiety-related behavior.

Histopathological analysis

Optical density of TH+ terminals in the dorsal and ventral striatum

For each group, we recorded photomicrographs of representative coronal sections of the striatum. As expected, animals injected with ascorbic acid did not show loss of TH+ immunoreactivity, and a higher density of TH+ fibers was observed in the 6-OHDA/mahogany

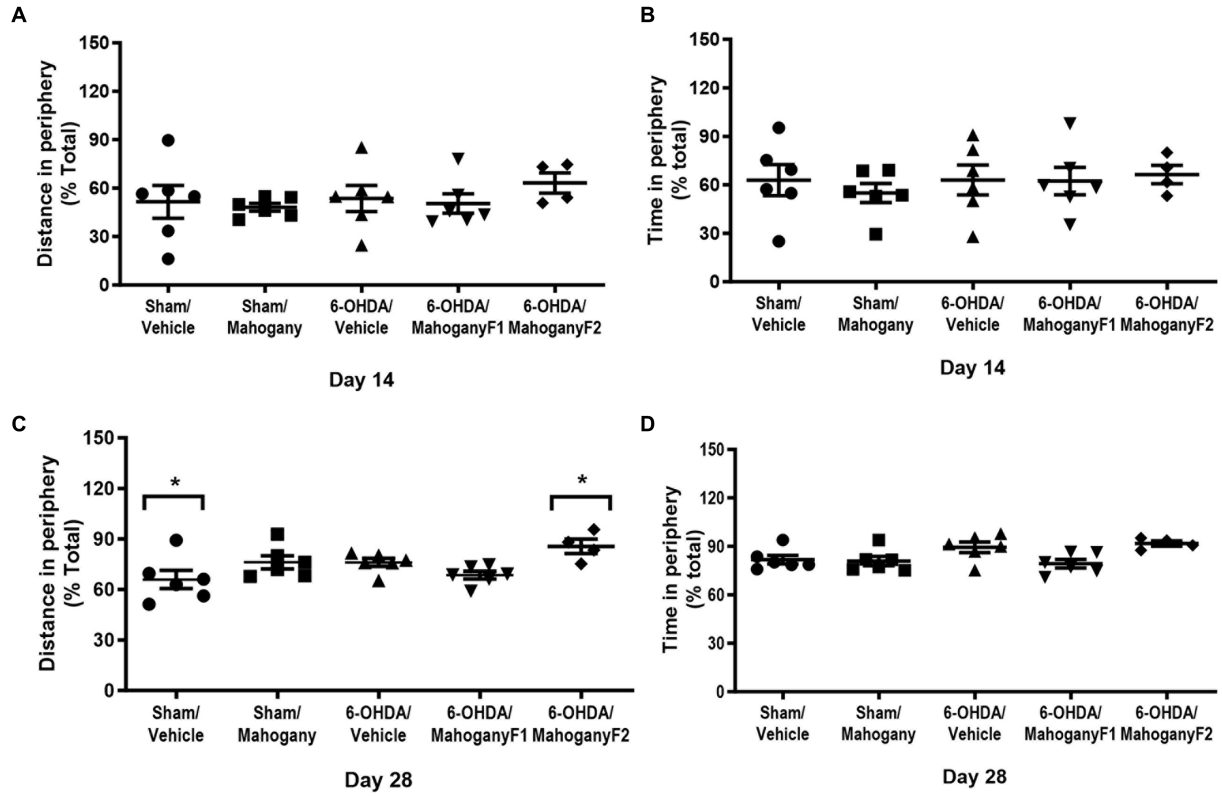

FIGURE 4
Evaluation of anxious-like behavior in the open field test of animals injected with 6-OHDA or vehicle and treated with aqueous extract of the mahogany leaf or vehicle. **(A)** Distance traveled in the periphery on day 14; **(B)** time spent in the periphery on day 14; **(C)** distance traveled in the periphery on day 28; **(D)** time spent in the periphery on day 28. The asterisks above the bars indicate significant differences between the groups. *sham/vehicle vs. 6-OHDA/mahogany, $p = 0.0191$. The data are expressed in mean ± SEM. One-way ANOVA followed by Tukey's *post hoc* test was used, and statistical significance was defined with 95% confidence ($p < 0.05$).

F2 group than in the 6-OHDA/vehicle and 6-OHDA/mahogany F1 groups (Figure 6A).

The 6-OHDA/vehicle group showed a severe and significant reduction in TH⁺ expression in the injected side and only 16.3 ± 5.0% immunostaining in the dorsal striatum. A similar histopathological aspect was identified in the 6-OHDA/mahogany F1 group, with 17.7 ± 4.5% TH+ fibers. In the 6-OHDA/mahogany F2 group, the expression of TH+ in the terminals represented 45.6 ± 12.2% of the remaining TH-immunolabeled fibers (6-OHDA/vehicle vs. 6-OHDA/mahogany F2, $p < 0.008$) (Figure 6C).

Analysis of the optical density of TH+ fibers in the ventral striatum showed that in the 6-OHDA/vehicle group, the percentage of TH⁺ immunostaining remained significantly lower than that in the other groups, with only 21.0 ± 5.5%. A similar histopathological aspect was identified in the 6-OHDA/mahogany F1 group, with 19.7 ± 3.4% of TH+ fibers. In the 6-OHDA/mahogany F2 group, immunostaining was 42.6 ± 8.9%, with an additional contribution of 21.6 ± 6.8% of TH+ fibers in relation to the model (6-OHDA/vehicle vs. 6-OHDA/mahogany F2, $p = 0.0291$) (Figure 6D).

Taken together, the optical density results of the dorsal and ventral striatum confirm that the lesion was more severe in the 6-OHDA/mahogany F1 group than in the 6-OHDA/mahogany F2 group. In addition, the aqueous extract of the mahogany leaf treatment did not interfere with the course of the lesion.

Estimation of the number of TH+ neurons in the substantia nigra pars compacta (SNpc)

In each group, we recorded photomicrographs of the left ventral mesencephalon. As expected, the sham groups did not show loss of TH⁺ immunoreactivity, and the largest volume of TH+ neuron perikarya and branches in the SNpc was observed in the 6-OHDA/mahogany F2 group compared with the 6-OHDA/vehicle group (Figure 6B).

The percentage of TH+ neurons in the SNpc in the 6-OHDA/vehicle group was 35.5 ± 3.9%; a similar histopathological aspect was identified in the 6-OHDA/mahogany F1 group, with 37.4 ± 6.4%, whereas the percentage of remaining dopaminergic neurons in the 6-OHDA/mahogany F2 group was 64.1 ± 8.9% (6-OHDA/vehicle vs. 6-OHDA/mahogany F2, $p = 0.0051$). These data confirm that in the 6-OHDA/mahogany F1 group, lesions were more severe, whereas those in the 6-OHDA/mahogany F2 group were milder.

In the 6-OHDA/mahogany F2 group, neurodegeneration was partial, and compared with the sham/vehicle group, the percentage deficit of TH⁺ neurons in the SNpc was 32.5 ± 6.8% ($p = 0.0008$), and compared with the sham/mahogany group, it was 32.9 ± 6.8% ($p = 0.0007$) (Figure 6E).

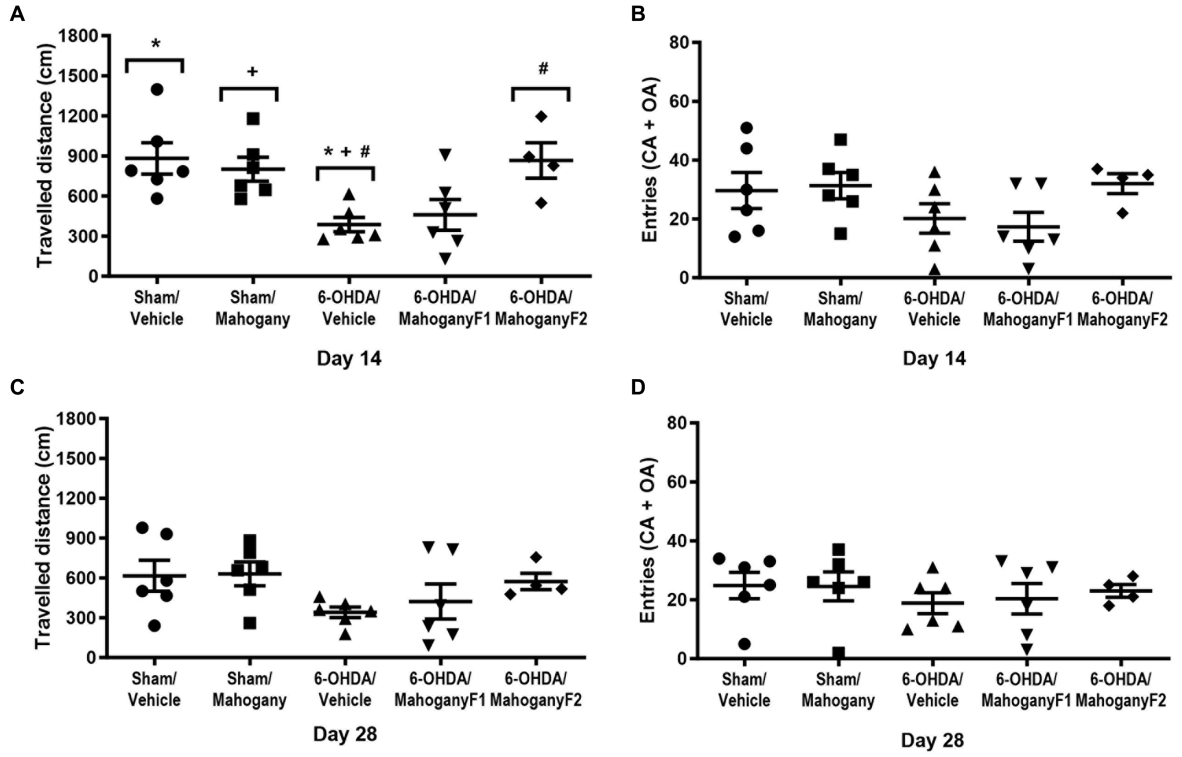

FIGURE 5
Evaluation of exploratory behavior in the Elevated plus maze test, on days 14 and 28 after surgery, of animals injected with 6-OHDA or vehicle and treated with aqueous extract of the mahogany leaf or vehicle. **(A)** Total distance traveled (CM), 14th day. **(B)** Frequency of entries in the open and closed arms, 14th day. **(C)** Total distance traveled (cm), 14th day. **(D)** Frequency of entries in the open and closed arms on day 14. The symbols above the bars indicate significant differences between the groups. * sham/vehicle vs. 6-OHDA/vehicle, $p = 0.0125$; $^{+}$ sham/mahogany vs. 6-OHDA/vehicle, $p = 0.0286$; $^{\#}$6-OHDA/vehicle vs. 6-OHDA mahogany F2, $p = 0.0221$. The data are expressed in mean ± SEM. One-way ANOVA followed by Tukey's *post hoc* test was used, and statistical significance was defined with 95% confidence ($p < 0.05$).

Estimation of the number of microglia IBA-1+ in the dorsal and ventral striatum

From each group, we recorded photomicrographs of the left dorsal striatum (Figure 7A), left ventral striatum (Figure 7B), and left SNpc (Figure 7C). The percentages of IBA-1+ cells in the dorsal striatum were as follows: sham/vehicle, 117.2 ± 9.6%; sham/mahogany, 142.5 ± 5.5%; 6-OHDA/vehicle, 148.9 ± 9.9%; 6-OHDA/mahogany F1, 134.6 ± 15.1%; and 6-OHDA/mahogany F2, 127.6 ± 5.9%. There was no significant difference when comparing the groups (Figure 7D). Despite the lack of statistical significance, the results show that there was an increase in the population of microglia in relation to the contralateral side in the five groups of this study.

These data indicate that in the dorsal striatum, the mechanical injury caused by the needle path contributed to the exacerbated microglial response, whereas the antioxidant potency of the aqueous extract of the mahogany leaf could not overcome the severe local neuroinflammation triggered acutely by the infusion of 6-OHDA.

The percentage of IBA-1^{+} cells in the ventral striatum of the 6-OHDA/mahogany F2 group was 106.8 ± 12.7%, which was significantly lower than that of the 6-OHDA/vehicle group, with 152.7 ± 4.3% ($p = 0.0214$). This result shows that there was a 45.9 ± 14.2% reduction in neuroinflammation in the ventral striatum in the 6-OHDA/mahogany F2 group compared with the model group, suggesting that aqueous extract of the mahogany leaf treatment reduced the progression of neuroinflammation to the ventral striatum (Figure 7E). While the percentage of IBA-1^{+} cells in the ventral striatum of the 6-OHDA/mahogany F1 group was 132 ± 18.9%, there was no significant difference compared with the model group.

Estimation of the number of microglia in the substantia nigra pars compacta (SNpc)

The percentage of IBA-1+ cells in the SNpc in the 6-OHDA/mahogany F2 group was 87.6 ± 9.6%, which was significantly lower than that in the 6-OHDA/vehicle group, which 148.0 ± 7.9% ($p = 0.003$). Thus, these data indicate that treatment with aqueous extract of the mahogany leaf attenuated microglial proliferation by 60.4 ± 12.0% in the 6-OHDA/mahogany F2 group compared with the model group. While the percentage of IBA-1+ cells in the SNpc in the 6-OHDA/mahogany F1 group was 90.1 ± 7.0%, it was also significantly lower than that in the 6-OHDA/vehicle group ($p = 0.001$). These data indicate attenuated microglial proliferation by 57.8 ± 10.5% in the 6-OHDA/mahogany F1 group.

Treatment with the aqueous extract of the mahogany leaf consistently reduced the progression of neuroinflammation in the dopaminergic nigrostriatal pathway of animals injected with 6-OHDA. On the other hand, ascorbic acid injection did not influence microglial proliferation in the SNpc in the sham/vehicle group, whose estimation of IBA-1+ cells was 117.5 ± 7.6%, and in the sham/mahogany group, it was 114.7 ± 7.1% (Figure 7F).

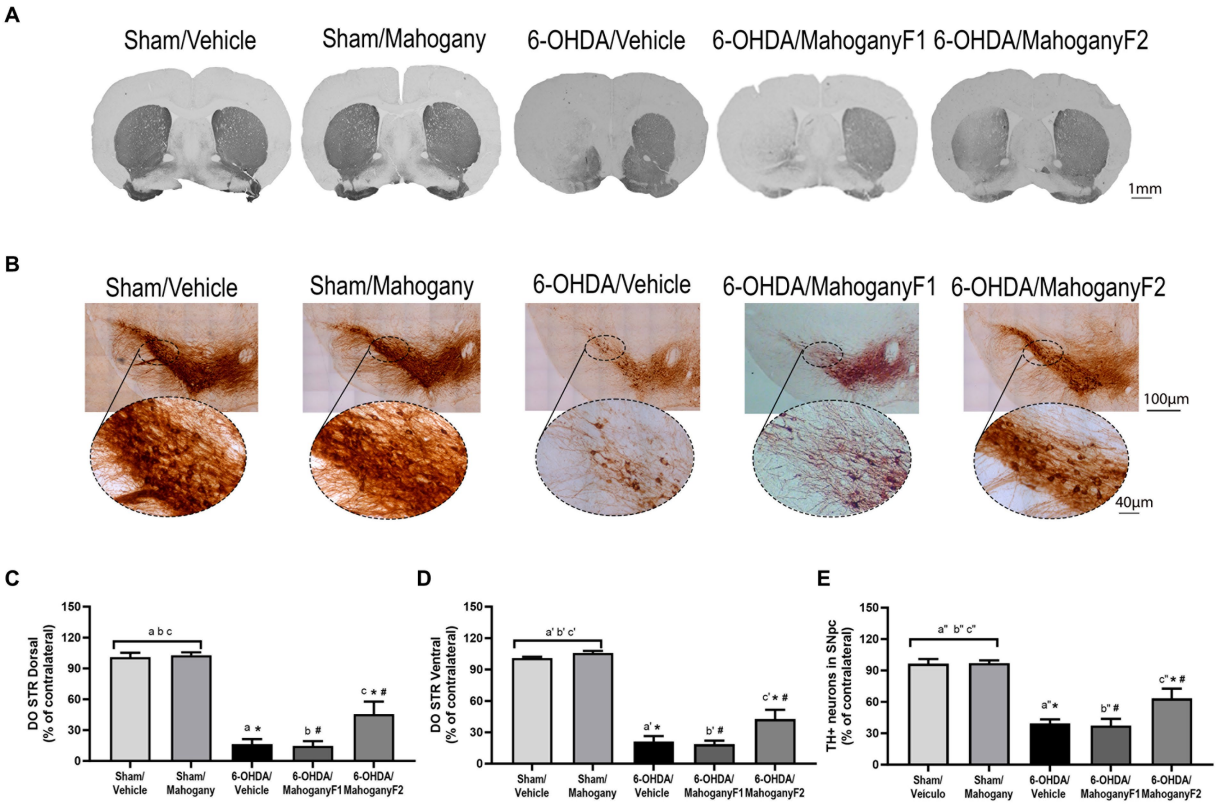

FIGURE 6
Histopathological analysis of animals injected with 6-OHDA or vehicle and treated with aqueous extract of the mahogany leaf or vehicle. **(A)** Photomicrographs of coronal sections of the brain representative of each group. **(B)** Photomicrographs of coronal sections of the ipsilateral ventral midbrain and SNpc. **(C)** Optical density analysis of TH+ fibers in the dorsal striatum. The symbols indicate: [a]sham/vehicle *vs* 6-OHDA/Vehicle, $p < 0{,}0001$; [b]sham/Vehicle *vs* 6-OHDA/mahogany F1, $p < 0{,}0001$; [c]sham/Vehicle *vs* 6-OHDA/mahogany F2, $p < 0{,}0001$; [a]sham/mahogany *vs* 6-OHDA/Vehicle, $p < 0{,}0001$; [b]sham/mahogany *vs* 6-OHDA/mahogany F1, $p < 0{,}0001$; [c]sham/mahogany *vs* 6-OHDA/mahogany F2, $p < 0{,}0001$; *6-OHDA/mahogany F2 *vs* 6-OHDA/vehicle, $p = 0{,}0074$; [#]6-OHDA/mahogany F2 *vs* 6-OHDA/mahogany F1, $p = 0{,}0074$. **(D)** Analysis by optical density of TH+ fibers in ventral striatum. The letters above the bars indicate: [a]sham/Vehicle *vs* 6-OHDA/Vehicle, $p < 0{,}0001$; [b]sham/Vehicle *vs* 6-OHDA/mahogany F1, $p < 0{,}0001$; [c]sham/Vehicle *vs* 6-OHDA/mahogany F2, $p < 0{,}0001$; [a]sham/mahogany *vs* 6-OHDA/Vehicle, $p < 0{,}0001$; [b]sham/mahogany *vs* 6-OHDA/mahogany F1, $p < 0{,}0001$; [c]sham/mahogany *vs* 6-OHDA/mahogany F2, $p < 0{,}0001$; *6-OHDA/mahogany F2 *vs* 6-OHDA/Vehicle, $p = 0{,}0291$; [#] 6-OHDA/mahogany F2 *vs* 6-OHDA/mahogany F1, $p = 0{,}0098$. **(E)** Estimate of the percentage of TH$^+$ neurons in the SNpc. The symbols indicate: [a]sham/Vehicle *vs* 6-OHDA/Vehicle, $p < 0{,}0001$; [b]sham/Vehicle *vs* 6-OHDA/mahogany F1, $p < 0{,}0001$; [c]sham/Vehicle *vs* 6-OHDA/mahogany F2, $p = 0{,}0033$; [a]sham/mahogany *vs* 6-OHDA/Vehicle, $p < 0{,}0001$; [b]sham/mahogany *vs* 6-OHDA/mahogany F1, $p < 0{,}0001$; [c]sham/Vehicle *vs* 6-OHDA/mahogany F2, $p = 0{,}0029$; *6-OHDA/mahogany F2 *vs* 6-OHDA/Vehicle, $p = 0{,}0482$; [#]6-OHDA/mahogany F2 *vs* 6-OHDA/mahogany F2, $p = 0{,}0273$. The data are expressed in mean ± SEM. One-way ANOVA followed by Tukey's *post hoc* test was used, and statistical significance was defined with 95% confidence ($p < 0.05$).

Densitometry of GFAP+ expression in the dorsal and ventral striatum

From each group, we recorded photomicrographs of the left dorsal striatum (Figure 8A), left ventral striatum (Figure 8B), and left SNpc (Figure 8C). Optical density analysis in the dorsal striatum showed that GFAP$^+$ cells in the 6-OHDA/mahogany F1group was 107.2 ± 14.9%, whereas in the 6-OHDA/mahogany F2 group, GFAP+ expression was 104.0 ± 1.8%, which was significantly lower than that in the 6-OHDA/vehicle group, which exhibited 120.9 ± 3.5% ($p = 0.0110$) (Figure 8D). Furthermore, the percentage of optical density in the dorsal striatum in the 6-OHDA/mahogany F2 group was statistically equivalent to that in the sham/vehicle group, with 105.9 ± 2.8%, and sham/mahogany, with 106.2 ± 3.6%. In addition, the 6-OHDA/vehicle group exhibited changes in astrocyte morphology, such as increased soma and thickness of primary processes (Figure 8A).

Regarding immunoreactivity for GFAP+ in the ventral striatum, the data show: sham/vehicle, 106.1 ± 2.3%; sham/mahogany, 107.6 ± 1.4%; 6-OHDA/vehicle, 114.3 ± 1.5%; 6-OHDA/mahogany F1, 111.1 ± 13.3%; and 6-OHDA/mahogany F2, 106.8 ± 5.1%. There was no significant difference between the groups. We observed that the astroglial response was restricted to the 6-OHDA infusion site and did not significantly extend to the ventral striatum (Figure 8E).

Estimation of the number of astrocytes in the substantia nigra pars compacta (SNpc)

GFAP+ cells in the SNpc in the groups injected with the toxin were as follows: 6-OHDA/vehicle, 173.3 ± 17.3%; 6-OHDA/mahogany F1, 197.3 ± 26.4%; and 6-OHDA/mahogany F2, 168.4 ± 16.5%. There was no significant difference between the groups injected with 6-OHDA.

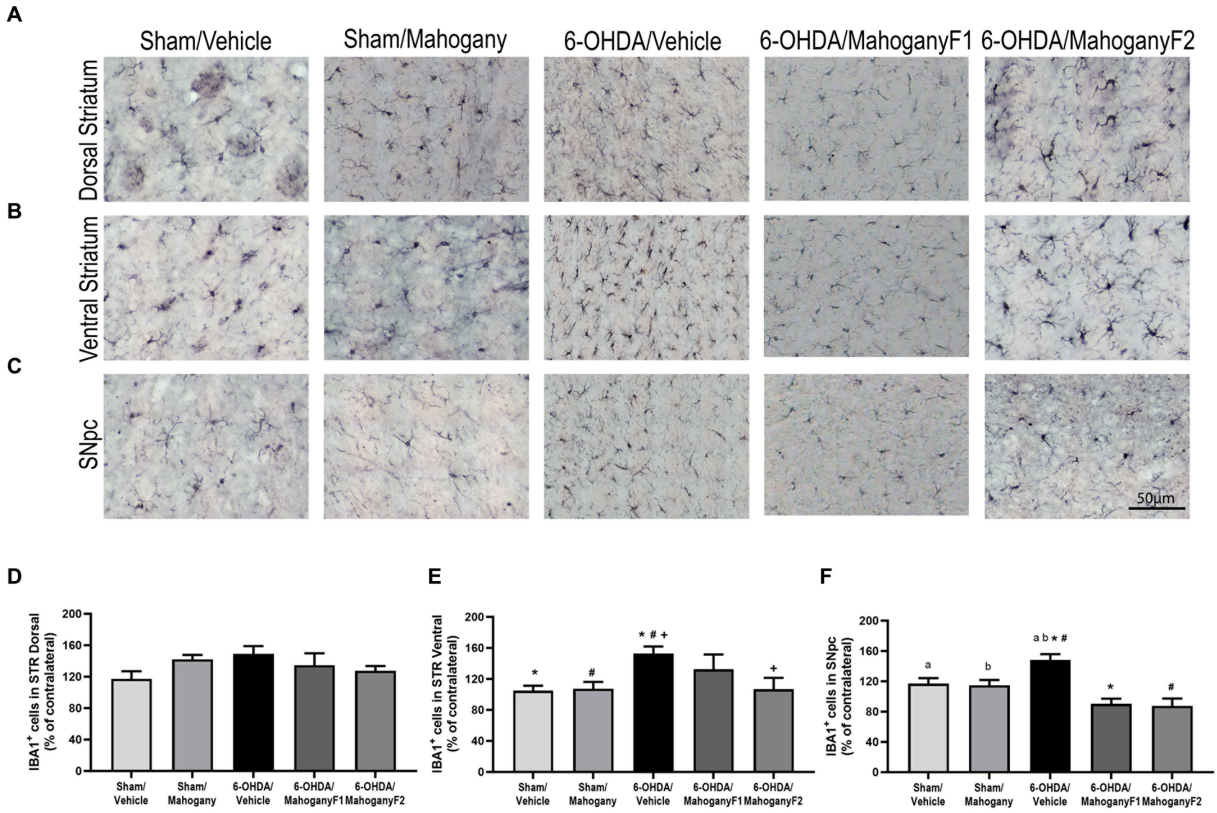

FIGURE 7
Estimation of the percentage of IBA-1+ microglia in the striatum of animals injected with 6-OHDA or vehicle and treated with aqueous extract of the mahogany leaf or vehicle. **(A)** Photomicrographs of coronal sections of the ipsilateral dorsal striatum representative of each group. **(B)** Photomicrographs of coronal sections of the ipsilateral ventral striatum representative of each group. **(C)** Photomicrographs of coronal sections of the ipsilateral SNpc, representative of each group. **(D)** Percentage of IBA-1+ cells in the dorsal striatum. There was no statistically significant difference between the groups. **(E)** Percentage of IBA-1+ cells in the ventral striatum. Symbols indicate: $^{+}$6-OHDA/vehicle vs. 6-OHDA/mahogany F2, $p = 0.0214$; *6-OHDA/vehicle vs. sham/vehicle, $p = 0.0069$; $^{\#}$6-OHDA/vehicle vs. sham/mahogany, $p = 0.0107$. **(F)** Percentage of IBA-1+ cells in SNpc. Symbols indicate: $^{\#}$6-OHDA/vehicle vs. 6-OHDA/mahogany F2, $p = 0.0003$; ^{a}6-OHDA/vehicle vs. sham/vehicle, $p = 0.0487$; ^{b}6-OHDA/vehicle vs. sham/mahogany, $p = 0.0303$. Data are presented as mean ± SEM. One-way ANOVA followed by Tukey's *post hoc* test and statistical significance was defined at a 95% confidence level ($p < 0.05$).

However, the astroglial response in the SNpc of the 6-OHDA-injected groups remained significantly more pronounced compared to the sham/vehicle group, 97.3 ± 4.6% and sham/mahogany group, 100.7 ± 7.8%. The differences between the groups were as follows: 6-OHDA/vehicle vs. sham/vehicle, $p = 0.0184$; 6-OHDA/vehicle vs. sham/mahogany, $p = 0.0356$; 6-OHDA/mahogany F1 vs. sham/vehicle, $p = 0.0184$; 6-OHDA/mahogany F1 vs. sham/mahogany, $p = 0.0042$; 6-OHDA/mahogany F2 vs. sham/vehicle, $p = 0.0263$; and 6-OHDA/mahogany F2 vs. sham/mahogany, $p = 0.0496$ (Figure 8F). These data indicate that in this study, treatment with aqueous extract of the mahogany leaf did not modulate the expression of GFAP in the SNpc of animals injected with 6-OHDA.

Furthermore, we observed that in the groups injected with 6-OHDA, the astrocytes presented with morphological changes characteristic of reactive astrogliosis. These observations are in agreement with data provided in the literature, which show that 6-OHDA injection causes strong and robust astroglial activation, accompanied by permanent cellular changes.

Discussion

Pamplona et al. (2015) conducted phytochemical and biological prospecting studies in the aqueous extract of mahogany leaf (AEML) and found 9 types of phenolic acids and 18 types of flavonoids with antioxidant and anti-inflammatory properties. In the present study, we evaluated the neuroprotective potential of this mahogany extract in a murine model of PD induced by 6-OHDA.

Unilateral injection of 6-OHDA into the striatum causes dopaminergic imbalance between the cerebral hemispheres, and the advancement of nigrostriatal neurodegeneration impacts the hypersensitivity of its receptors in the ipsilateral striatum (Meredith and Kang, 2006; Brooks and Dunnett, 2009). Therefore, motor pathways can be asymmetrically activated through the action of a dopaminergic agonist, generating rotational behavior toward the side contralateral to the lesion (Björklund and Dunnett, 2019; Buhidma et al., 2020). This rotational behavior in lesioned animals is highly reproducible and has been used to establish an index of motor recovery and neuroprotection after exposure to therapeutic drugs (Simola et al., 2007; Buhidma et al., 2020).

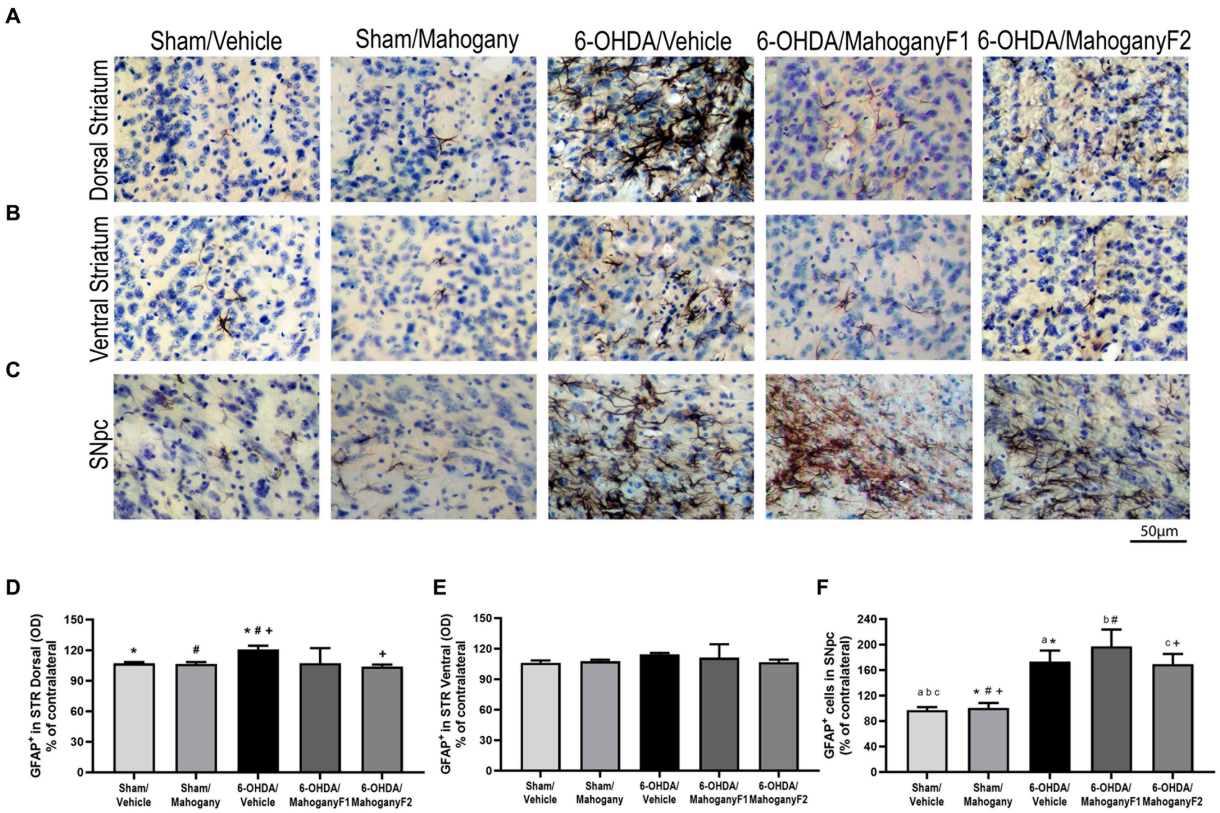

FIGURE 8
Analysis by optical density of GFAP+ immunostaining in the dorsal and ventral striatum and estimate of the percentage of GFAP+ cells in the SNpc of animals injected with 6-OHDA or vehicle and treated with aqueous extract of the mahogany leaf or vehicle. **(A)** Photomicrographs of coronal sections of the ipsilateral dorsal striatum, representative of each group. **(B)** Photomicrographs of coronal sections of the ipsilateral ventral striatum, representative of each group. **(C)** Photomicrographs of coronal sections of the ipsilateral SNpc, representative of each group. **(D)** Analysis by optical density of GFAP+ reactivity in the dorsal striatum. Symbols indicate: *sham/vehicle vs. 6-OHDA/vehicle, $p = 0.0422$; $^{\#}$sham/mahogany vs. 6-OHDA/vehicle, $p = 0.0422$; $^{+}$6-OHDA/vehicle vs. 6-OHDA/mahogany F2, $p = 0.0110$. **(E)** Analysis by optical density of GFAP+ reactivity in the ventral STR. There was no statistically significant difference between the groups. **(F)** Estimation of the percentage of GFAP+ astrocytes in SNpc. Symbols indicate: ^{a}sham/vehicle vs. 6-OHDA/vehicle, $p = 0.0184$; ^{b}sham/vehicle vs. 6-OHDA/mahogany F1, $p = 0.0184$; ^{c}sham/vehicle vs. 6-OHDA/mahogany F2, $p = 0.0263$; *sham/mahogany vs. 6-OHDA/vehicle, $p = 0.0356$; $^{\#}$sham/mahogany vs. 6-OHDA/mahogany F1, $p = 0.0042$; $^{+}$sham/mahogany vs. 6-OHDA/mahogany F1, $p = 0.0496$. Data are presented as mean ± SEM. One-way ANOVA followed by Tukey's *post hoc* test and statistical significance was defined at a 95% confidence level ($p < 0.05$).

In our study, in the 6-OHDA/vehicle group, contralateral rotations became more frequent and vigorous with the progression of the lesion, confirming the successful injection and toxic effect of 6-OHDA in the dorsal striatum. The 6-OHDA/mahogany F1 group showed a significant increase in the average rotations in the second test with apomorphine, indicating a lesion comparable with the 6-OHDA/vehicle group, which was confirmed subsequently in our histopathological evaluation. Thus, EAML treatment did not protect against the progression of the nigrostriatal lesion. In contrast, the 6-OHDA/mahogany F2 group did not show any contralateral rotations after apomorphine challenge, which was compatible with a low degree of lesion in the dopaminergic nigrostriatal pathway, which was also confirmed by histopathology. These results in the F2 group could be due to a technical problem that interfered with the final lesion size after 6-OHDA injection, a neuroprotective effect of the EAML treatment, or a combination of both. At this point, we cannot rule out any of these alternatives.

Motor performance in PD unilateral animal models can also be evaluated using open field (Seibenhener and Wooten, 2015; Willard et al., 2015) and elevated plus maze tests (Carobrez and Bertoglio, 2005; La-Vu et al., 2020). In our study, the sham/mahogany group showed increased motor behavior compared with the 6-OHDA/vehicle group. Results from the elevated plus maze tests showed that the 6-OHDA/mahogany F2 group had significantly better motor performance than the model group in the first test on the 14th post-surgery day. The percentage of entries in the open arms was not affected in either group. In the second test, despite habituation, the 6-OHDA/mahogany F2 group maintained better motor performance than the 6-OHDA/vehicle group. These results are consistent with the data obtained in the open field test, which indicated better motor capacity, in agreement with a lower degree of degeneration in the nigrostriatal dopaminergic pathway in the F2 group compared with the 6-OHDA/vehicle and 6-OHDA/mahogany F1 groups.

In addition to motor disorders, anxiety is a non-motor symptom that affects approximately 35–40% of patients with PD and has a significant impact on patient quality of life (Kano et al., 2011; Dissanayaka et al., 2014; Khatri et al., 2020). Although non-motor symptoms have been little studied, especially in models of unilateral injury, the retrograde neurodegeneration induced by the infusion of 6-OHDA in the striatum resembles the initial stages of PD and has

been used as a tool for investigating neuropsychiatric changes, such as anxiety (Breit et al., 2007). However, studies using different protocols regarding dosis, time, and site of injection have achieved divergent results in relation to anxiety-related behavior (Branchi et al., 2008; Tadaiesky et al., 2008; Prasad and Hung, 2020). In our study, there was no difference between the groups in anxiety-related parameters, both in the open field (not shown) and in the elevated plus maze tests. These results suggest that the observed differences in motor performance between the groups were not due to anxiety-like behavior.

In the histopathological analysis, we found significantly more TH^+ fibers in the striatum and a higher percentage of dopaminergic neurons in the SNpc in the 6-OHDA/mahogany F2 group than in the 6-OHDA/vehicle and 6-OHDA/mahogany F1 groups. Therefore, the histopathological findings confirm the lower degree of lesion in the 6-OHDA/mahogany F2 group, which is compatible with the number of rotations in the apomorphine test, and improved motor performance in the open field and elevated plus maze tests compared with the 6-OHDA/vehicle and 6-OHDA/mahogany F1 groups.

In the present study, we found a significantly higher percentage of microglia in the dorsal striatum, ventral striatum, and SNpc in the 6-OHDA/vehicle group, indicating exacerbated neuroinflammation induced by the toxin. However, in the dorsal striatum, increased microglia staining was also observed in the control groups that were not injected with the toxin, and we attribute this effect to the mechanical injury caused by the needle used for the infusion of the toxin or vehicle. The 6-OHDA groups treated with AEML showed consistently decreased microglial proliferation in the ventral striatum and SNpc, indicating a significant impact on controlling neuroinflammation independent of lesion severity. The absence of apomorphine-induced rotations in the F2 group, even with a loss of 36.7% of nigral dopaminergic neurons, may be due to a decrease in neuroinflammation after treatment with the mahogany extract.

Another important signature of the 6-OHDA-induced injury model is astrocyte hyperreactivity during nigrostriatal dopaminergic projection (Mathiisen et al., 2010; Gradisnik and Velnar, 2023). Astrocytes respond to different types and intensities of perturbations in the CNS and can adopt various context-dependent phenotypes; however, changes in their molecular profile can be reversible (Escartin et al., 2021). *In vivo* studies that used the model of unilateral injection of 6-OHDA into the medial forebrain bundle to induce dopaminergic desensitization in the nigrostriatal pathway showed that in the ipsilateral SNpc, there was a significant increase in GFAP immunoreactivity, including an increase in cell volume and the number of astrocytes of the inflammatory phenotype (Kuter et al., 2018; Jiang et al., 2021).

In our study, the histopathological data from the 6-OHDA/Vehicle group are in agreement with the literature, as the areas in the dorsal striatum and SNpc occupied by hyper-reactive GFAP+ cells were significantly larger than those in the sham groups. Furthermore, these areas were marked by hypertrophic astrocytes soma, thicker primary processes, and densely overlapping branches. These notable morphological changes in astrocytes from the 6-OHDA/vehicle group were correlated with severe degeneration of the nigrostriatal dopaminergic pathway. In contrast, the 6-OHDA/Mahogany F2 group showed less hypertrophy of the soma and densely overlapping branches in the dorsal region, suggesting a modulating effect of AEML treatment. The exacerbation of GFAP+ immunoreactivity in the SNpc of the 6-OHDA/Mahogany F1 and 6-OHDA/Mahogany F2 groups seems to proceed from a distinct source of neuroinflammation because IBA-1+ immunoreactivity was significantly reduced in this nucleus. GFAP hyperreactivity, which diffusely occurred in the SNpc, could be a direct response of astrocytes to 6-OHDA, which reached the cell body via degenerating dopaminergic neurons, or a response to the neurodegenerative process itself.

The percentage of polyphenols in the aqueous extract of the mahogany leaf is significantly higher than that in leaf extracts from other Amazonian plants obtained by the same method (Silva et al., 2007). Some polyphenols found in the phytochemical constitution of mahogany (*Swietenia macrophylla*) are also part of the phytochemical constitution of other plants, and their antioxidant capacity has already been tested in other studies using models of nigrostriatal dopaminergic degeneration induced by toxins, such as: naringerin (Zbarsky et al., 2005; Lou et al., 2014; Kim et al., 2016); resveratrol (Jin et al., 2008; Khan et al., 2010; Wang et al., 2011); quercetin (Haleagrahara et al., 2011); rutin (Moshahid Khan et al., 2012); and myricetin (Ma et al., 2007). In this study, it is conceivable that several bioactive compounds in the aqueous extract of mahogany leaf may jointly contribute to the observed beneficial effects. Further studies are necessary to better characterize their applicability for treating chronic degenerative diseases with inflammatory and oxidative bases, such as Parkinson's disease.

Data availability statement

The raw data supporting the conclusions of this article will be made available by the authors upon request without reservation.

Ethics statement

The animal study was approved by Comissão de Ética no Uso de Animais, Federal University of Pará. The study was conducted in accordance with the local legislation and institutional requirements.

Author contributions

VC: Formal analysis, Investigation, Methodology, Writing – original draft, Writing – review & editing, Conceptualization, Data curation, Supervision. AV-A: Investigation, Methodology, Writing – original draft, Supervision, Writing – review & editing. RM: Investigation, Writing – review & editing, Methodology, Supervision. CM: Investigation, Writing – original draft, Methodology. NM: Investigation, Writing – original draft, Methodology. MS: Validation, Writing – review & editing, Conceptualization, Supervision. JP: Validation, Writing – review & editing, Conceptualization, Supervision. GB: Supervision, Validation, Writing – review & editing, Conceptualization, Methodology. JF: Writing – review & editing, Methodology, Validation. EY: Conceptualization, Formal analysis, Methodology, Supervision, Writing – review & editing, Validation.

Funding

The author(s) declare financial support was received for the research, authorship, and/or publication of this article. Fundação Amazônia de Amparo a Estudos e Pesquisa (FAPESPA ICCAF 115/2014) and PROPESP/UFPA (PAPQ). VC was a scholarship recipient from the Coordenação de Aperfeiçoamento de Pessoal de Nível Superior (CAPES).

Acknowledgments

We thank the Postgraduate Program in Oncology and Medical Sciences linked to the Oncology Research Center of the Federal University of Pará for providing the infrastructure for this study.

Conflict of interest

The authors declare that the research was conducted in the absence of any commercial or financial relationships that could be construed as a potential conflict of interest.

Publisher's note

All claims expressed in this article are solely those of the authors and do not necessarily represent those of their affiliated organizations, or those of the publisher, the editors and the reviewers. Any product that may be evaluated in this article, or claim that may be made by its manufacturer, is not guaranteed or endorsed by the publisher.

References

Balestrino, R., and Schapira, A. H. V. (2020). Parkinson disease. *Eur. J. Neurol.* 27, 27–42. doi: 10.1111/ene.14108

Björklund, A., and Dunnett, S. B. (2019). The amphetamine induced rotation test: a re-assessment of its use as a tool to monitor motor impairment and functional recovery in rodent models of Parkinson's disease. *J. Parkinsons Dis.* 9, 17–29. doi: 10.3233/JPD-181525

Braak, H., Ghebremedhin, E., Rüb, U., Bratzke, H., and Del Tredici, K. (2004). Stages in the development of Parkinson's disease-related pathology. *Cell Tissue Res.* 318, 121–134. doi: 10.1007/s00441-004-0956-9

Branchi, I., D'Andrea, I., Armida, M., Cassano, T., Pèzzola, A., Potenza, R. L., et al. (2008). Nonmotor symptoms in Parkinson's disease: investigating early-phase onset of behavioral dysfunction in the 6-hydroxydopamine-lesioned rat model. *J. Neurosci. Res.* 86, 2050–2061. doi: 10.1002/jnr.21642

Breit, S., Boualibenazzouz, R., Popa, R., Gasser, T., Benabid, A., and Benazzouz, A. (2007). Effects of 6-hydroxydopamine-induced severe or partial lesion of the nigrostriatal pathway on the neuronal activity of pallido-subthalamic network in the rat. *Exp. Neurol.* 205, 36–47. doi: 10.1016/j.expneurol.2006.12.016

Brooks, S. P., and Dunnett, S. B. (2009). Tests to assess motor phenotype in mice: a user's guide. *Nat. Rev. Neurosci.* 10, 519–529. doi: 10.1038/nrn2652

Buhidma, Y., Rukavina, K., Chaudhuri, K. R., and Duty, S. (2020). Potential of animal models for advancing the understanding and treatment of pain in Parkinson's disease. *NPJ Parkinsons Dis.* 6:1. doi: 10.1038/s41531-019-0104-6

Carobrez, A. P., and Bertoglio, L. J. (2005). Ethological and temporal analyses of anxiety-like behavior: the elevated plus-maze model 20 years on. *Neurosci. Biobehav. Rev.* 29, 1193–1205. doi: 10.1016/j.neubiorev.2005.04.017

Chaudhuri, K. R., Healy, D. G., and Schapira, A. H. (2006). Non-motor symptoms of Parkinson's disease: diagnosis and management. *Lancet Neurol.* 5, 235–245. doi: 10.1016/S1474-4422(06)70373-8

Ciulla, M., Marinelli, L., Cacciatore, I., and Di Stefano, A. (2019). Role of dietary supplements in the Management of Parkinson's disease. *Biomol. Ther.* 9:271. doi: 10.3390/biom9070271

Del Rey, N. L.-G., Quiroga-Varela, A., Garbayo, E., Carballo-Carbajal, I., Fernández-Santiago, R., Monje, M. H. G., et al. (2018). Advances in Parkinson's disease: 200 years later. *Front. Neuroanat.* 12:113. doi: 10.3389/fnana.2018.00113

Dissanayaka, N. N. N. W., White, E., O'Sullivan, J. D., Marsh, R., Pachana, N. A., and Byrne, G. J. (2014). The clinical spectrum of anxiety in Parkinson's disease. *Mov. Disord.* 29, 967–975. doi: 10.1002/mds.25937

Escartin, C., Galea, E., Lakatos, A., O'Callaghan, J. P., Petzold, G. C., Serrano-Pozo, A., et al. (2021). Reactive astrocyte nomenclature, definitions, and future directions. *Nat. Neurosci.* 24, 312–325. doi: 10.1038/s41593-020-00783-4

Gradisnik, L., and Velnar, T. (2023). Astrocytes in the central nervous system and their functions in health and disease: a review. *World J. Clin. Cases* 11, 3385–3394. doi: 10.12998/wjcc.v11.i15.3385

Gundersen, H. J. G., Jensen, E. B. V., Kieu, K., and Nielsen, J. (1999). The efficiency of systematic sampling in stereology — reconsidered. *J. Microsc.* 193, 199–211. doi: 10.1046/j.1365-2818.1999.00457.x

Haleagrahara, N., Siew, C. J., Mitra, N. K., and Kumari, M. (2011). Neuroprotective effect of bioflavonoid quercetin in 6-hydroxydopamine-induced oxidative stress biomarkers in the rat striatum. *Neurosci. Lett.* 500, 139–143. doi: 10.1016/j.neulet.2011.06.021

Heuer, A., Smith, G. A., Lelos, M. J., Lane, E. L., and Dunnett, S. B. (2012). Unilateral nigrostriatal 6-hydroxydopamine lesions in mice I: motor impairments identify extent of dopamine depletion at three different lesion sites. *Behav. Brain Res.* 228, 30–43. doi: 10.1016/j.bbr.2011.11.027

Hung, A. Y., and Schwarzschild, M. A. (2020). Approaches to disease modification for Parkinson's disease: clinical trials and lessons learned. *Neurotherapeutics* 17, 1393–1405. doi: 10.1007/s13311-020-00964-w

Jankovic, J., and Tan, E. K. (2020). Parkinson's disease: etiopathogenesis and treatment. *J. Neurol. Neurosurg. Psychiatry* 91, 795–808. doi: 10.1136/jnnp-2019-322338

Jiang, Y., Ma, H., Wang, X., Wang, Z., Yang, Y., Li, L., et al. (2021). Protective effect of the α7 nicotinic receptor agonist PNU-282987 on dopaminergic neurons against 6-hydroxydopamine, regulating anti-neuroinflammatory and the immune balance pathways in rat. *Front. Aging Neurosci.* 12:606927. doi: 10.3389/fnagi.2020.606927

Jin, F., Wu, Q., Lu, Y.-F., Gong, Q.-H., and Shi, J.-S. (2008). Neuroprotective effect of resveratrol on 6-OHDA-induced Parkinson's disease in rats. *Eur. J. Pharmacol.* 600, 78–82. doi: 10.1016/j.ejphar.2008.10.005

Kalia, L. V., and Lang, A. E. (2015). Parkinson's disease. *Lancet* 386, 896–912. doi: 10.1016/S0140-6736(14)61393-3

Kano, O., Ikeda, K., Cridebring, D., Takazawa, T., Yoshii, Y., and Iwasaki, Y. (2011). Neurobiology of depression and anxiety in Parkinson's disease. *Parkinsons Dis.* 2011, 1–5. doi: 10.4061/2011/143547

Khan, M. M., Ahmad, A., Ishrat, T., Khan, M. B., Hoda, M. N., Khuwaja, G., et al. (2010). Resveratrol attenuates 6-hydroxydopamine-induced oxidative damage and dopamine depletion in rat model of Parkinson's disease. *Brain Res.* 1328, 139–151. doi: 10.1016/j.brainres.2010.02.031

Khatri, D. K., Choudhary, M., Sood, A., and Singh, S. B. (2020). Anxiety: an ignored aspect of Parkinson's disease lacking attention. *Biomed. Pharmacother.* 131:110776. doi: 10.1016/j.biopha.2020.110776

Kim, H. D., Jeong, K. H., Jung, U. J., and Kim, S. R. (2016). Naringin treatment induces neuroprotective effects in a mouse model of Parkinson's disease *in vivo*, but not enough to restore the lesioned dopaminergic system. *J. Nutr. Biochem.* 28, 140–146. doi: 10.1016/j.jnutbio.2015.10.013

Kobylecki, C. (2020). Update on the diagnosis and management of Parkinson's disease. *Clin. Med.* 20, 393–398. doi: 10.7861/clinmed.2020-0220

Kujawska, M., and Jodynis-Liebert, J. (2018). Polyphenols in Parkinson's disease: a systematic review of *in vivo* studies. *Nutrients* 10:642. doi: 10.3390/nu10050642

Kuter, K., Olech, Ł., and Głowacka, U. (2018). Prolonged dysfunction of astrocytes and activation of microglia accelerate degeneration of dopaminergic neurons in the rat substantia nigra and block compensation of early motor dysfunction induced by 6-OHDA. *Mol. Neurobiol.* 55, 3049–3066. doi: 10.1007/s12035-017-0529-z

La-Vu, M., Tobias, B. C., Schuette, P. J., and Adhikari, A. (2020). To approach or avoid: an introductory overview of the study of anxiety using rodent assays. *Front. Behav. Neurosci.* 14:145. doi: 10.3389/fnbeh.2020.00145

Llibre-Guerra, J. J., Prina, M., Sosa, A. L., Acosta, D., Jimenez-Velazquez, I. Z., Guerra, M., et al. (2022). Prevalence of parkinsonism and Parkinson disease in urban and rural populations from Latin America: a community based study. *The Lancet Regional Health* 7:100136. doi: 10.1016/j.lana.2021.100136

Lou, H., Jing, X., Wei, X., Shi, H., Ren, D., and Zhang, X. (2014). Naringenin protects against 6-OHDA-induced neurotoxicity via activation of the Nrf2/ARE signaling pathway. *Neuropharmacology* 79, 380–388. doi: 10.1016/j.neuropharm.2013.11.026

Ma, Z.-G., Wang, J., Jiang, H., Liu, T.-W., and Xie, J.-X. (2007). Myricetin reduces 6-hydroxydopamine-induced dopamine neuron degeneration in rats. *Neuroreport* 18, 1181–1185. doi: 10.1097/WNR.0b013e32821c51fe

MacMahon Copas, A. N., McComish, S. F., Fletcher, J. M., and Caldwell, M. A. (2021). The pathogenesis of Parkinson's disease: a complex interplay between astrocytes, microglia, and T lymphocytes? *Front. Neurol.* 12:666737. doi: 10.3389/fneur.2021.666737

Mathiisen, T. M., Lehre, K. P., Danbolt, N. C., and Ottersen, O. P. (2010). The perivascular astroglial sheath provides a complete covering of the brain microvessels: an electron microscopic 3D reconstruction. *Glia* 58, 1094–1103. doi: 10.1002/glia.20990

Meredith, G. E., and Kang, U. J. (2006). Behavioral models of Parkinson's disease in rodents: a new look at an old problem. *Mov. Disord.* 21, 1595–1606. doi: 10.1002/mds.21010

Moghadamtousi, S., Goh, B., Chan, C., Shabab, T., and Kadir, H. (2013). Biological activities and phytochemicals of *Swietenia macrophylla*. *Molecules* 18, 10465–10483. doi: 10.3390/molecules180910465

Moshahid Khan, M., Raza, S. S., Javed, H., Ahmad, A., Khan, A., Islam, F., et al. (2012). Rutin protects dopaminergic neurons from oxidative stress in an animal model of Parkinson's disease. *Neurotox. Res.* 22, 1–15. doi: 10.1007/s12640-011-9295-2

Okunoye, O., Marston, L., Walters, K., and Schrag, A. (2022). Change in the incidence of Parkinson's disease in a large UK primary care database. *NPJ Parkinsons Dis.* 8:23. doi: 10.1038/s41531-022-00284-0

Pamplona, S., Sá, P., Lopes, D., Costa, E., Yamada, E., Silva, C., et al. (2015). *In vitro* cytoprotective effects and antioxidant capacity of phenolic compounds from the leaves of *Swietenia macrophylla*. *Molecules* 20, 18777–18788. doi: 10.3390/molecules201018777

Paxinos, G., and Franklin, K. B. (2004). *The mouse brain in stereotaxic coordinates*. San Diego: Elsevier Academic Press.

Prasad, E. M., and Hung, S.-Y. (2020). Behavioral tests in neurotoxin-induced animal models of Parkinson's disease. *Antioxidants* 9:1007. doi: 10.3390/antiox9101007

Pringsheim, T., Jette, N., Frolkis, A., and Steeves, T. D. L. (2014). The prevalence of Parkinson's disease: a systematic review and meta-analysis. *Mov. Disord.* 29, 1583–1590. doi: 10.1002/mds.25945

Seibenhener, M. L., and Wooten, M. C. (2015). Use of the open field maze to measure locomotor and anxiety-like behavior in mice. *J. Vis. Exp.*:e52434. doi: 10.3791/52434

Silva, E. M., Souza, J. N. S., Rogez, H., Rees, J. F., and Larondelle, Y. (2007). Antioxidant activities and polyphenolic contents of fifteen selected plant species from the amazonian region. *Food Chem.* 101, 1012–1018. doi: 10.1016/j.foodchem.2006.02.055

Simola, N., Morelli, M., and Carta, A. R. (2007). The 6-hydroxydopamine model of parkinson's disease. *Neurotox. Res.* 11, 151–167. doi: 10.1007/BF03033565

Singh, A., Yau, Y. F., Leung, K. S., El-Nezami, H., and Lee, J. C.-Y. (2020). Interaction of polyphenols as antioxidant and anti-inflammatory compounds in brain–liver–gut Axis. *Antioxidants* 9:669. doi: 10.3390/antiox9080669

Tadaiesky, M. T., Dombrowski, P. A., Figueiredo, C. P., Cargnin-Ferreira, E., Da Cunha, C., and Takahashi, R. N. (2008). Emotional, cognitive and neurochemical alterations in a premotor stage model of Parkinson's disease. *Neuroscience* 156, 830–840. doi: 10.1016/j.neuroscience.2008.08.035

Tibar, H., El Bayad, K., Bouhouche, A., Haddou EH, A. B., Benomar, A., Yahyaoui, M., et al. (2018). Non-motor symptoms of Parkinson's disease and their impact on quality of life in a cohort of Moroccan patients. *Front. Neurol.* 9:170. doi: 10.3389/fneur.2018.00170

Tolosa, E., Garrido, A., Scholz, S. W., and Poewe, W. (2021). Challenges in the diagnosis of Parkinson's disease. *Lancet Neurol.* 20, 385–397. doi: 10.1016/S1474-4422(21)00030-2

Wang, Y., Xu, H., Fu, Q., Ma, R., and Xiang, J. (2011). Protective effect of resveratrol derived from Polygonum cuspidatum and its liposomal form on nigral cells in parkinsonian rats. *J. Neurol. Sci.* 304, 29–34. doi: 10.1016/j.jns.2011.02.025

Willard, A. M., Bouchard, R. S., and Gittis, A. H. (2015). Differential degradation of motor deficits during gradual dopamine depletion with 6-hydroxydopamine in mice. *Neuroscience* 301, 254–267. doi: 10.1016/j.neuroscience.2015.05.068

Zbarsky, V., Datla, K. P., Parkar, S., Rai, D. K., Aruoma, O. I., and Dexter, D. T. (2005). Neuroprotective properties of the natural phenolic antioxidants curcumin and naringenin but not quercetin and fisetin in a 6-OHDA model of Parkinson's disease. *Free Radic. Res.* 39, 1119–1125. doi: 10.1080/10715760500233113

frontiers | Frontiers in Neuroscience

TYPE Original Research
PUBLISHED 12 March 2024
DOI 10.3389/fnins.2024.1374567

OPEN ACCESS

EDITED BY
Pradeep Kumar,
All India Institute of Medical Sciences, India

REVIEWED BY
Li Zou,
McGill University, Canada
Xiaoqun Zhu,
First Affiliated Hospital of Anhui Medical University, China

*CORRESPONDENCE
Pengcheng Cai
caipengcheng@hust.edu.cn
Tao Liang
lt-liangtao-lt@163.com

†These authors have contributed equally to this work

RECEIVED 22 January 2024
ACCEPTED 29 February 2024
PUBLISHED 12 March 2024

CITATION
Wu Z, Shu D, Wu S, Cai P and Liang T (2024) Higher serum Lp-PLA2 is associated with cognitive impairment in Parkinson's disease patients.
Front. Neurosci. 18:1374567.
doi: 10.3389/fnins.2024.1374567

Higher serum Lp-PLA2 is associated with cognitive impairment in Parkinson's disease patients

Zubo Wu[1†], Defeng Shu[2†], Suyuan Wu[3], Pengcheng Cai[3*] and Tao Liang[3*]

[1]Department of Pediatrics, Union Hospital, Tongji Medical College, Huazhong University of Science and Technology, Wuhan, China, [2]Department of Obstetrics and Gynecology, Union Hospital, Tongji Medical College, Huazhong University of Science and Technology, Wuhan, China, [3]Department of Clinical Laboratory, Union Hospital, Tongji Medical College, Huazhong University of Science and Technology, Wuhan, China

Objective: To explore the association between lipoprotein-associated phospholipase A2 (Lp-PLA2) and the risk of cognitive impairment in Parkinson's disease (PD-CI).

Methods: A case–control study involving 100 hospitalized PD patients and 60 healthy controls was carried out. Serum Lp-PLA2 level was detected by automatic biochemical analyzer. Based on whether Parkinson's patients have cognitive impairment, PD patients were subdivided to analyze the clinical value of Lp-PLA2. Relationship between Lp-PLA2 and PD-CI risk was analyzed by logistic regression. Diagnostic value of Lp-PLA2 in PD-CI patients was investigated using receiver's operator characteristic curves.

Results: The levels of serum Lp-PLA2 activity in Parkinson's disease with normal cognition (PD-NC) and PD-CI patients were significantly higher than those in healthy controls (HCs), respectively. Furthermore, compared to the PD-NC group, the serum Lp-PLA2 activity level was significantly higher in PD-CI patients. Multivariable logistic regression analysis indicated that higher Lp-PLA2 level was an independent risk factor for PD patients with cognitive impairment. Moreover, the area under the efficacy curve of Lp-PLA2 for predicting PD-CI is 0.659.

Conclusion: Our study shows that higher levels of Lp-PLA2 activity in PD patients are associated with the risk of developing cognitive impairment. Therefore, given the wide availability, safety, and convenience of monitoring serum Lp-PLA2 activity, it may serve as an early biomarker for cognitive impairment in PD patients.

KEYWORDS

Lp-PLA2, Parkinson's disease, cognitive impairment, risk factor, neurodegenerative diseases

1 Introduction

Parkinson's disease (PD) is one of the most common neurodegenerative disorders affecting individuals worldwide (Aarsland et al., 2021). It is characterized by a progressive loss of dopaminergic neurons in the substantia nigra region of the brain leading to motor symptoms that include tremors, rigidity, and bradykinesia. PD has been identified as a multifactorial disorder with both genetic and environmental factors contributing to its pathogenesis (Bloem et al., 2021). In addition to motor symptoms, PD also has a variety of non-motor symptoms. Among them, the most common is cognitive impairment, which can occur in any disease stage of PD and seriously affect the patient's quality of life. In recent years, there has been growing interest in the relationship between PD and cognitive impairment (Aarsland et al., 2021). Cognitive impairment refers to a decline in intellectual and cognitive functions, including memory loss and attention deficits (Weintraub et al., 2022). Depending on the severity, cognitive impairment can be divided into mild cognitive impairment (MCI) and Parkinson's disease dementia (PDD). In most cases, cognitive decline is usually slow and insidious. In recent years, many studies on PD and cognitive impairment have focused on early cognitive changes, especially actively screening for better biomarkers to predict cognitive decline and quickly identify patients at risk of early cognitive impairment (Aarsland et al., 2021). Recent research indicates that a substantial proportion, approximately 30–40%, of individuals with Parkinson's disease (PD) encounter mild cognitive impairment, with a subset of 10–20% advancing to Parkinson's disease-related cognitive impairment (PD-CI) (Aarsland et al., 2021; Wallace et al., 2022). Investigations have proposed a potential correlation between PD-CI and the inherent pathological transformations in PD, as well as modifications in neurotransmitter activity (Zaman et al., 2021; Ye et al., 2023).

Lipoprotein-associated phospholipase A2 (Lp-PLA2) is an enzyme synthesized by macrophages, monocytes, and other inflammatory cells, including endothelial cells in atherosclerotic plaques. It is also found in circulating low-density lipoprotein (LDL) particles. Lp-PLA2 catalyzes the hydrolysis of oxidized phospholipids (OxPLs) which can result in the generation of pro-inflammatory and pro-apoptotic products (Huang et al., 2020). Lp-PLA2 levels have been associated with the severity of atherosclerosis, and high levels of Lp-PLA2 are considered a risk factor for cardiovascular disease (Ridker et al., 2022).

Recent research has suggested that Lp-PLA2 may also be involved in the pathogenesis of cognitive impairment. In one study, Lp-PLA2 levels were found to be higher in individuals with mild cognitive impairment (MCI) and Alzheimer's disease (AD) compared to controls (Davidson et al., 2012; Pokharel et al., 2019; Liu et al., 2023). Another study found that Lp-PLA2 levels were elevated in individuals with type 2 diabetes and that Lp-PLA2 levels were higher in diabetic individuals with cognitive impairment compared to those without cognitive impairment (Cai et al., 2017). Studies have reported the role of Lp-PLA2 in cognitive impairment-related diseases such as Alzheimer's disease and diabetes (Davidson et al., 2012; Feng et al., 2022). These results have shown elevated plasma levels of Lp-PLA2 in patients with these diseases, which are strongly associated with cognitive decline. We have also found in previous studies that serum Lp-PLA2 levels are significantly higher in PD patients compared to healthy individuals, and that Lp-PLA2 levels are positively correlated with disease severity (Wu et al., 2021). However, the relationship between Lp-PLA2 and cognitive impairment associated with PD is unclear. Given the important role of Lp-PLA2 in neurodegenerative diseases such as Alzheimer's disease, it is suspected that they may also play significant roles in PD-CI.

In conclusion, recent research suggests that Lp-PLA2 may play an important role in the development and progression of PD and cognitive impairments. Further investigation is required to determine the exact mechanisms by which Lp-PLA2 contributes to the development of cognitive impairment in PD, and whether Lp-PLA2 could be a potential therapeutic target for the treatment of cognitive impairment in PD.

2 Subjects and methods

2.1 Subjects

A total of 100 hospitalized PD patients from the Department of Neurology, Tongji Medical College Affiliated Union Hospital, Huazhong University of Science and Technology between June 2022 and March 2023 were recruited. There were 58 males and 42 females, and they were aged from 31 to 85 years, with an average of 62.28 ± 11.51 years. All cases were diagnosed by specialists according to typical clinical symptoms and imaging examinations, and in accordance with the diagnostic criteria of PD in the UK Brain Bank (Hughes et al., 2001). The exclusion criteria are as follows: (1) Parkinson's symptoms caused by brain trauma, encephalitis and drugs; (2) essential tremor; (3) PD with tumors, severe infection of the whole body or CNS; (4) PD with severe diseases of the heart, liver and kidney. In addition, a Montreal Cognitive Assessment (MoCA) scale was performed on PD patients to assess their cognitive status. MoCA is mainly based on clinical experience and reference to the cognitive items in the Simple Mental State Assessment Scale (MMSE). The test time is short, and the total score is 0–30 points. The cut-off value is 26, that is, ≥26 is classified as normal cognitive function, <26 is classified as cognitive impairment. According to the MoCA points, PD patients were divided into a PD-NC group ($n = 46$) and a PD-CI group ($n = 54$). The age- and gender-matched control group consisted of 60 healthy subjects (28 males/32 females, median age 55.97 ± 11.23 years), who were recruited from the medical examination center in our hospital and had no evidence of cerebrovascular or inflammatory disease. All subjects were Chinese Han from the same area in Middle China and all gave informed consent. Our study was approved by the ethics committee at Tongji Medical College, Huazhong University of Science and Technology.

2.2 Data collection

After PD patients were admitted to the hospital, their demographic data were obtained in time, including age, gender, disease course, past history, family history, and smoking and drinking habits. Clinical characteristic parameters of PD patients were also collected, such as diastolic blood pressure (DBP), systolic blood pressure (SBP), dyslipidemia, hypertension, diabetes, heart rate, respiratory rate, and body temperature. Patients with a history of hypertension or

TABLE 1 Demographic and clinical characteristics of PD patients and HCs.

Variables	HCs (n = 60)	PD-NC (n = 46)	PD-CI (n = 54)	P-value
Gender (Male/Female)	28/32	28/18	30/24	0.592
Age (years)	57 (49 ~ 63)	57 (51 ~ 63)	71 (63 ~ 75)	<0.001
Disease duration (years)	N.A.	2 (1.0 ~ 5.0)	2 (1.0 ~ 6.0)	0.812
Family history [n (%)]	N.A.	3 (6.52)	3 (5.56)	0.839
Dyslipidemia [n (%)]	N.A.	8 (17.39)	11 (20.37)	0.705
Diabetes mellitus [n (%)]	N.A.	2 (4.35)	4 (7.41)	0.521
Hypertension [n (%)]	N.A.	17 (36.96)	20 (37.04)	0.993
Smoking [n (%)]	N.A.	9 (19.57)	4 (7.41)	0.072
Drinking [n (%)]	N.A.	5 (10.87)	1 (1.85)	0.058
SBP/ (mmHg)	N.A.	134 (122 ~ 146)	134 (123 ~ 151)	0.544
DBP/ (mmHg)	N.A.	84 (77 ~ 93)	83 (78 ~ 90)	0.579
H&Y stage	N.A.	2.00 (1.50 ~ 2.50)	2.75 (1.75 ~ 3.00)	0.019
BMI	N.A.	23.16 (21.22 ~ 24.97)	22.69 (20.60 ~ 25.68)	0.750

N.A., not available.

SBP≧140 mmHg or DBP≧90 mmHg at rest were all diagnosed as hypertension. Diabetes mellitus was diagnosed if the patient was being treated with antidiabetic medications or insulin therapy or had a fasting blood glucose level ≧7.0 mmol/L. We also collected other laboratory parameters upon admission, including alanine aminotransferase (ALT), aspartate aminotransferase (AST), alkaline phosphatase (ALP), glutamyl transpeptidase (GGT), urea nitrogen (BUN), creatinine (Cr), uric acid (UA), cystatin C (Cys C), fasting blood glucose (Glu), cholesterol (TC), triglycerides (TG), high-density lipoprotein (HDL), low-density lipoprotein (LDL), apolipoprotein A (ApoA), apolipoprotein B (ApoB), serum amylase A (SAA), Lipoprotein (a) [Lp(a)], homocysteine (HCY), glucose (GLU), glomerular filtration rate (GFR) and other blood coagulation related indicators.

2.3 Preparation of blood samples

Within 24 h of admission, blood samples were collected with BD™ yellow tubes from peripheral veins of PD patients who had fasted for 12 h. The blood samples were centrifuged at 3,000 rpm and room temperature for 10 min to separate serum. Then the serum was immediately transferred to Eppendorf tubes (EP tubes), labeled and stored in a refrigerator at −80°C until the detection of biochemical factors.

2.4 Measurement of Lp-PLA2

Serum Lp-PLA2 activity was determined by automatic biochemical analyzer AU5800 (Beckerman Coulter). Commercial Lp-PLA2 kits were also provided by Beijing Baiding Bioengineering Co., LTD. The method of Lp-PLA2 activity detection is to use enzymatic method. Lp-PLA2 decomposes the substrate to produce colored products, and the activity results can be obtained by continuous monitoring method. All operations were performed in accordance with the reagent instructions. Strict calibration and quality control procedures were also carried out.

2.5 Statistical analysis

SPSS 22.0 (IBM Co., Armonk, NY, United States) was used for statistical analysis. Normality data was expressed as mean ± standard deviation (SD), and statistically analyzed among groups by t test. Non-normally distributed data were expressed as [median (P50), 25th to 75th percentile (P25 ~ P75)] and compared among groups using *Mann–Whitney U* test. Relationship between any two variables was analyzed using Spearman correlation. The risk factors for PD-CI were determined by logistic regression analysis. After analyzing the difference between the PD-CI group and the PD-NC group, we chose to incorporate those significant indicators into the logistic regression analysis model. The diagnostic value of Lp-PLA2 for PD-CI was evaluated by calculating the area under receiver's operator characteristic (ROC) curve (AUC). In the two-tailed test, $p < 0.05$ was considered statistically significant.

3 Results

3.1 Demographic and clinical characteristics of PD patients with or without cognitive impairment and healthy controls

A total of 100 PD patients and 60 healthy controls (HCs) were recruited in this study. According to the level of cognitive function, the PD patients were divided into 2 groups: 54 PD-CI patients and 46 PD-NC patients. The demographic and clinical characteristics of all participants were summarized in Table 1. The three groups were matched for sex, and there was no age difference between PD-NC and HCs. However, the age of patients in the PD-CI group was significantly higher than in the other two groups. Compared with the PD-NC group, the PD-CI patients had significantly higher H&Y stage than PD-NC group ($p < 0.05$). However, there were no significant differences between the two groups in disease course, family history, dyslipidemia, diabetes history, hypertension, smoking, drinking, BMI, etc. (all $p > 0.05$).

TABLE 2 Comparison of clinical indicators among PD-NC and PD-CI patients and healthy controls.

Variables	HCs (Group A)	PD-NC (Group B)	PD-CI (Group C)	*P* (A vs. B)	*P* (A vs. C)	*P* (B vs. C)
UA/ (μmol/L)	275.4 (224.1 ~ 330.2)	269.5 (216.1 ~ 339.3)	297.4 (239.8 ~ 358.7)	0.975	0.489	0.511
Cys C/ (mg/L)	0.67 (0.63 ~ 0.76)	0.76 (0.66 ~ 0.81)	0.81 (0.72 ~ 0.90)	0.002	<0.001	0.010
TC/ (mmol/L)	4.53 (4.16 ~ 4.90)	4.09 (3.77 ~ 4.82)	4.15 (3.31 ~ 5.11)	0.060	0.125	0.817
TG/ (mmol/L)	0.96 (0.78 ~ 1.21)	1.10 (0.85 ~ 1.34)	0.95 (0.67 ~ 1.42)	0.049	0.966	0.167
HDL/ (mmol/L)	1.47 (1.31 ~ 1.65)	1.21 (1.03 ~ 1.43)	1.10 (0.93 ~ 1.41)	<0.001	<0.001	0.448
LDL/ (mmol/L)	2.44 (2.16 ~ 2.82)	2.38 (2.10 ~ 2.79)	2.36 (1.65 ~ 3.06)	0.975	0.986	0.977
sdLDL/ (mmol/L)	0.56 (0.41 ~ 0.78)	0.72 (0.51 ~ 0.86)	0.63 (0.46 ~ 0.92)	0.027	0.299	0.274
ApoA/ (g/L)	1.53 (1.38 ~ 1.64)	1.26 (1.12 ~ 1.40)	1.17 (1.02 ~ 1.43)	<0.001	<0.001	0.189
ApoB/ (g/L)	0.93 (0.79 ~ 1.05)	0.85 (0.77 ~ 1.00)	0.84 (0.66 ~ 1.10)	0.317	0.768	0.934
Lp(a) / (mg/dL)	11.3 (5.9 ~ 20.8)	16.0 (6.9 ~ 32.4)	17.7 (7.4 ~ 33.4)	0.110	0.026	0.559
Glu/ (mmol/L)	5.0 (4.7 ~ 5.1)	5.0 (4.6 ~ 5.2)	5.2 (4.7 ~ 5.9)	0.868	0.075	0.106
SAA/ (mg/L)	4.1 (3.1 ~ 5.8)	4.8 (3.4 ~ 6.5)	4.9 (3.6 ~ 14.6)	0.120	0.011	0.265
HCY/ (μmol/L)	10.2 (8.1 ~ 12.0)	12.5 (10.8 ~ 15.9)	13.5 (10.3 ~ 17.7)	0.001	<0.001	0.457
GFR	101.48 (94.10 ~ 108.48)	99.50 (94.38 ~ 104.25)	88.94 (81.60 ~ 99.31)	0.344	<0.001	0.001
Lp-PLA2/ (U/L)	394 (333 ~ 426)	415 (363 ~ 477)	481 (386 ~ 547)	0.019	<0.001	0.006

PD, Parkinson's disease; HCs, healthy controls; PD-NC, PD with normal cognition; PD-CI, PD with cognitive impairment.

3.2 Comparison of clinical indicators among PD-NC and PD-CI patients and healthy controls

Compared with the HCs group, the levels of Cys C, HCY and Lp-PLA2 in the PD-NC group and PD-CI group were all significantly higher, while the levels of HDL and ApoA were significantly lower ($p < 0.05$). In addition, only the TG and sdLDL levels in the PD-NC group were found to be higher than that in the HCs group, but no difference was found between the PD-CI group and the HCs group ($p > 0.05$). Besides, only the Lp(a) and SAA levels in the PD-CI group were found to be higher than those in the HCs group, but no difference was found between the PD-NC group and the HCs group ($p > 0.05$). More importantly, the levels of Cys C, GFR, Lp-PLA2 were significantly increased in PD-CI patients compared with PD-NC patients ($p < 0.05$). However, there was no difference in other indicators between the two groups ($p > 0.05$) (Table 2).

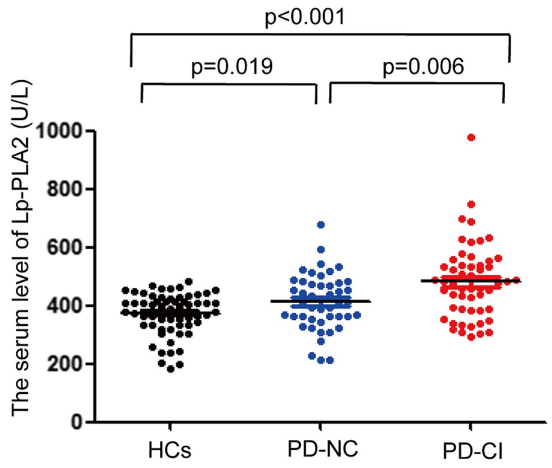

FIGURE 1
Comparison of Lp-PLA2 level among PD-NC, PD-CI and healthy controls.

3.3 The levels of serum Lp-PLA2 activity in PD patients and healthy controls

The levels of serum Lp-PLA2 activity in PD-NC and PD-CI patients were significantly higher than that in HCs, respectively. In addition, compared with the PD-NC group, the serum Lp-PLA2 activity level was significantly higher in PD-CI patients ($p < 0.05$) (Figure 1).

3.4 Correlation analysis between Lp-PLA2 activity and clinical characteristics of PD-CI patients

The correlation between Lp-PLA2 activity and clinical characteristics of PD-CI patients was performed. Our results showed that serum Lp-PLA2 activity level in PD-CI patients was positively correlated with TC ($r = 0.346$, $p = 0.014$), LDL ($r = 0.382$, $p = 0.006$), sdLDL ($r = 0.349$, $p = 0.010$), and ApoB ($r = 0.449$, $p < 0.001$). However, no significant correlations were observed between Lp-PLA2 activity and other laboratory test results (all $p > 0.05$) (Table 3).

3.5 Logistic regression analysis of the risk factors for PD patients with cognitive impairment

A univariate logistic regression analysis was performed to "crudely" explore independent factors that lead to an increased risk of PD-CI, and then multivariate logistic regression was also conducted to further study the risk factors of PD-CI. All variables in Table 4 were

TABLE 3 Correlation analysis between Lp-PLA2 activity and clinical characteristics of PD-CI patients.

Variables	Lp-PLA2		Variables	Lp-PLA2	
	r	*P*-value		*r*	*P*-value
SBP	0.166	0.235	DBP	0.177	0.205
H&Y stage	−0.124	0.371	BMI	−0.031	0.825
TC	0.346	0.014	TG	0.214	0.135
HDL	0.098	0.498	LDL	0.382	0.006
sdLDL	0.349	0.010	ApoA	0.176	0.202
ApoB	0.449	<0.001	Lp(a)	0.017	0.901
SAA	−0.073	0.598	Glu	0.086	0.554
UA	−0.008	0.958	Cys C	−0.201	0.144
GFR	0.179	0.208	HCY	0.049	0.727

entered into the univariate logistic regression model. The results showed that age [odds ratio (OR) 95% confidence interval (CI) = 1.087 (1.042–1.135), $p < 0.001$], Cys C [OR (95%CI) = 23.065 (1.216–437.417), $p = 0.037$], Lp-PLA2 activity [OR (95%CI) = 1.006 (1.002–1.010), $p = 0.006$] were all significantly associated with PD-CI, and higher levels of GFR might be a protective factor for PD-CI [OR (95%CI) = 0.956 (0.926–0.987), $p = 0.006$]. In the multivariate logistic regression analysis in Table 5, we adjusted separately for possible confounders such as age and gender (model 1); age, gender, smoking, drinking (model 2); age, gender, smoking, drinking, hypertension, diabetes, dyslipidemia (model 3). The results revealed that in the above factor-adjusted models, Cys C level was not associated with PD-CI, while the association between Lp-PLA2 activity and the risk of PD-CI was still significantly correlated. In the three models, the OR were 1.008 [(95% CI:1.004–1.013), $p = 0.001$], 1.010 [(95% CI:1.005–1.016), $p < 0.001$] and 1.010 [(95% CI:1.005–1.016), $p < 0.001$], respectively.

TABLE 4 univariate logistic regression analysis of the risk factors for PD patients with cognitive impairment.

	B	S.E.	Walds	*P*-value	OR (95%CI)
Gender	0.219	0.408	0.288	0.592	1.244 (0.560, 2.767)
Age	0.084	0.022	14.830	<0.001	1.087 (1.042, 1.135)
Disease duration	0.013	0.056	0.052	0.820	1.013 (0.908, 1.129)
Family history	0.171	0.842	0.041	0.839	1.186 (0.228, 6.182)
Smoking	1.112	0.639	3.030	0.082	3.041 (0.869, 10.635)
Drinking	1.866	1.115	2.801	0.094	6.463 (0.727, 57.486)
Dyslipidemia	−0.195	0.515	0.143	0.705	0.823 (0.300, 2.259)
Hypertension	−0.003	0.416	0.000	0.993	0.997 (0.441, 2.250)
Diabetes mellitus	−0.565	0.890	0.403	0.525	0.568 (0.099, 3.254)
SBP	0.012	0.011	1.136	0.287	1.012 (0.990, 1.035)
DBP	−0.010	0.019	0.288	0.591	0.990 (0.955, 1.027)
H&Y stage	0.498	0.254	3.857	0.050	1.646 (1.001, 2.706)
BMI	−0.008	0.013	0.374	0.541	0.992 (0.967, 1.018)
TC	−0.022	0.226	0.009	0.924	0.979 (0.629, 1.523)
TG	−0.047	0.279	0.028	0.867	0.954 (0.552, 1.650)
HDL	−0.258	0.605	0.183	0.669	0.772 (0.236, 2.527)
LDL	0.016	0.264	0.004	0.951	1.016 (0.606, 1.706)
sdLDL	−0.153	0.635	0.058	0.809	0.858 (0.247, 2.978)
ApoA	−0.706	0.788	0.804	0.370	0.493 (0.105, 2.312)
ApoB	0.445	0.712	0.392	0.531	1.561 (0.387, 6.296)
Lp(a)	0.007	0.009	0.635	0.426	1.007 (0.989, 1.026)
UA	0.001	0.002	0.305	0.581	1.001 (0.997, 1.006)
Cys C	3.138	1.501	4.370	0.037	23.065 (1.216, 437.417)
GFR	−0.045	0.016	7.516	0.006	0.956 (0.926, 0.987)
Glu	0.392	0.250	2.471	0.116	1.480 (0.908, 2.415)
SAA	0.023	0.015	2.251	0.134	1.023 (0.993, 1.053)
HCY	0.025	0.036	0.483	0.487	1.025 (0.956, 1.099)
Lp-PLA2	0.006	0.002	7.612	0.006	1.006 (1.002, 1.010)

CI, confidence interval; OR, odds ratio.

TABLE 5 multivariate logistic regression analysis of the association between PD patients with cognitive impairment and serum Cys C and Lp-PLA2 activity.

	B	S.E.	Walds	*P*-value	OR (95%CI)
Model 1					
Cys C	1.033	1.645	0.394	0.530	2.809 (0.112, 70.615)
Lp-PLA2	0.008	0.002	11.560	0.001	1.008 (1.004, 1.013)
Model 2					
Cys C	0.707	1.682	0.177	0.674	2.028 (0.075, 54.831)
Lp-PLA2	0.010	0.003	12.932	<0.001	1.010 (1.005, 1.016)
Model 3					
Cys C	0.875	1.769	0.244	0.621	2.398 (0.075, 76.915)
Lp-PLA2	0.010	0.003	12.424	<0.001	1.010 (1.005, 1.016)

CI, confidence interval; OR, odds ratio.
Model 1: adjusting for age, gender; Model 2: adjusting for age, gender, smoking and drinking; Model 3: adjusting for age, gender, smoking, drinking, hypertension, diabetes, dyslipidemia.

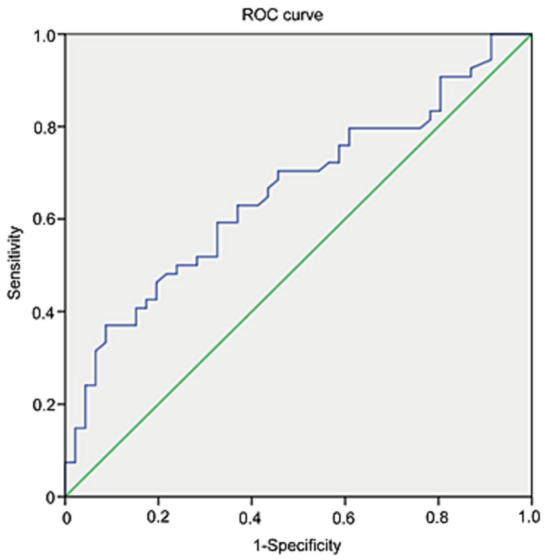

FIGURE 2
The ROC curve of Lp-PLA2 for discrimination between PD-CI patients and PD-NC patients.

3.6 Diagnostic value of Lp-PLA2 for identification of parkinsonian cognitive impairment

ROC analysis was applied to investigate the diagnostic accuracy of Lp-PLA2 activity in distinguishing PD-CI from PD-NC. The area under the curve of Lp-PLA2 activity for PD-CI diagnosis was 0.659 (95% CI: 0.552–0.765). Based on the ROC curve, the Lp-PLA2 concentration cutoff of 523 U/L was relatively high in specificity (91.3%) and low in sensitivity (37%) for distinguishing between PD-CI group and PD-NC group, with a Youden index of 0.283. The ROC curve of Lp-PLA2 activity for discrimination between the PD-CI group and the PD-NC group was shown in Figure 2.

4 Discussion

More and more studies have shown that there are many pathological factors causing cognitive impairment, which may involve oxidative stress, impaired synaptic function, mitochondrial dysfunction, central nervous inflammatory response and other aspects, among which the inflammatory mechanism plays a crucial role (Duggan et al., 2023). Therefore, researchers have been trying to use some relevant biomarkers reflecting vascular and neuroinflammatory damage to diagnose the occurrence of cognitive impairment in the early stage of disease. As an indicator closely related to vascular inflammatory injury, Lp-PLA2 has attracted much attention in cardiovascular and cerebrovascular diseases. Although the roles of Lp-PLA2 in cognitive impairment have been reported, its roles in PD-associated cognitive impairment are still unknown. Continuing our previous research, we collected relevant clinical and laboratory data and conducted a correlation study between Lp-PLA2 and cognitive impairment in patients with Parkinson's disease. In this investigation, we have observed that individuals with Parkinson's disease (PD) who experienced cognitive impairment exhibited elevated levels of serum Lp-PLA2 activity in comparison to PD patients with intact cognitive function. Moreover, we have identified a positive correlation between serum Lp-PLA2 activity and TC, LDL, sdLDL, and ApoB. Furthermore, univariate and multivariate logistic regression analyses were employed to demonstrate that increased Lp-PLA2 activity served as an independent risk factor for cognitive impairment in PD. In addition, we have constructed an ROC diagnostic model centered around Lp-PLA2, which has shown promise in aiding the differentiation between cognitively normal PD patients and those experiencing cognitive impairment. Collectively, these findings provide support for the notion that elevated levels of serum Lp-PLA2 activity may serve as a potential predictive biomarker for cognitive impairment in individuals with PD.

Lipoprotein-associated phospholipase A2 (Lp-PLA2), also referred to as platelet-activating factor acetylhydrolase (PAF-AH), is primarily biosynthesized and excreted by macrophages and lymphocytes. Lp-PLA2 mainly produces Lys phosphatidylcholine (lysoPC) and oxidized non-esterified fatty acids (oxNEFAs) by hydrolyzing oxidized LDL (ox-LDL) to exert pro-inflammatory effects, thereby participating in the occurrence and development of atherosclerosis, as well as plaque stability and plaque rupture (Huang et al., 2020). Therefore, Lp-PLA2 is regarded as a reliable marker reflecting vascular inflammatory injury closely related to atherosclerotic diseases, and has been widely studied in cardiovascular and cerebrovascular diseases. Studies have confirmed that higher level of Lp-PLA2 is an independent predictor of coronary heart disease (Yang et al., 2017), myocardial infarction (Sun et al., 2021), acute cerebral infarction (Tao et al., 2020), and cerebral artery stenosis (Wang et al., 2018), and is also closely related to the patient's admission severity, later treatment, and prognosis. At present, there are still few studies on the roles of Lp-PLA2 in PD. In one of our earlier studies, we have found that higher level of Lp-PLA2 mass is an independent risk factor in PD patients, which is related to the Hoehn-Yahr (H&Y) stage, disease course, and severity of PD, respectively (Wu et al., 2021). In this study, we observed that the Lp-PLA2 activity in PD patients was also significantly higher than that in normal controls.

These results indicate that Lp-PLA2 plays a crucial role in PD. Considering the correlation between Lp-PLA2 and cognitive impairment, we further investigated its relationship with cognitive impairment in PD.

Although some studies have reported the relationship between Lp-PLA2 and cognitive impairment, their conclusions are not consistent. In an earlier study, a small cross-sectional study of 78 AD cases, 59 amnestic mild cognitive impairment cases, and 66 cognitively healthy subjects by Davidson et al. found no significant association between Lp-PLA2 and AD (Davidson et al., 2012). Similar results were also found in the other two researches, which showed no significant correlation between Lp-PLA2 mass or activity and AD (van Himbergen et al., 2012; Savas et al., 2016). However, a recent case–control study revealed that higher Lp-PLA2 was independently associated with AD (Doody et al., 2015). Subjects with higher levels of Lp-PLA2 were almost twice as likely to have AD compared with subjects with Lp-PLA2 levels below the median. In addition, there is also some evidence that Lp-PLA2 is negatively related to cognitive function, and high levels of Lp-PLA2 can contribute to prevent the occurrence of cognitive impairment. Zhu et al. analyzed 87 patients with cerebral small vessel disease (CSVD) and found that Lp-PLA2 was independently associated with cognitive impairment and white matter hyperintensities (WMHs) lesions. The level of Lp-PLA2 mass in CSVD patients with mild or severe cognitive impairment was significantly lower than that in patients with normal cognition. These results may be related to the antioxidant effect of Lp-PLA2 (Zhu et al., 2019). However, a recent study supports the opposite conclusion. Huang et al. also proposed that Lp-PLA2 was an independent risk factor for WMHs, but the level of Lp-PLA2 mass was significantly higher in cognitively impaired CSVD patients than in cognitively normal controls (Huang et al., 2021). Currently, increasing evidence suggest that higher levels of Lp-PLA2 are risk factors for cognitive impairment. In a case–control study, high levels of Lp-PLA2 increased the risk of vascular dementia (VD) and AD, independent of other cardiovascular and inflammatory factors (van Oijen et al., 2006; Doody et al., 2015). In addition, Fitzpatrick et al. conducted a population-based longitudinal study of community residents over the age of 65 years, and the results also confirmed that individuals with elevated Lp-PLA2 mass and activity levels were related to increased risk of dementia at an average of 5.4 years of follow-up. And it was not associated with cardiovascular disease (CVD) and its risk factors. Participants in the highest quartile of Lp-PLA2 mass were 50% more likely to develop dementia than those in the lowest quartile (Fitzpatrick et al., 2014). Jiang et al. performed a large cross-sectional study in a Chinese community population, and the results also showed that elevated level of Lp-PLA2 mass was independently associated with the prevalence of cognitive impairment in Chinese adults (Jiang et al., 2016). Based on the sample size of the study and the duration of follow-up, the conclusion that Lp-PLA2 is regarded as a risk factor for cognitive impairment may be convincing. In addition, Cai et al. also found that the mass and activity of Lp-PLA2 were associated with the risk of mild cognitive impairment in Chinese patients with type 2 diabetes (Cai et al., 2017). Although the above-mentioned multiple studies suggest that Lp-PLA2 may be involved in the pathogenesis of cognitive impairment, the role of Lp-PLA2 in cognitive impairment in PD remains unknown.

Our findings not only indicate an elevation in Lp-PLA2 activity levels in PD patients, but also reveal a significant association between higher Lp-PLA2 activity levels and the risk of cognitive impairment in PD. We first screened for meaningful variables by comparing PD patients with cognitive impairment and cognitively normal patients. Compared with cognitively normal PD patients, we found no statistically significant difference in UA. However, some studies had shown that low levels of UA were associated with cognitive impairment in PD patients, and a decrease in UA levels led to a decrease in antioxidant capacity in PD patients (Pellecchia et al., 2016). But we did not find that in our study. This may be related to the different exclusion criteria. They excluded factors that could possibly modify UA levels in the study, such as treatment with diuretics, non-steroidal anti-inflammatory drugs, or other UA altering agents. In our study, we did not exclude these patients with PD. In addition, we found that Cys C and Lp-PLA2 were significantly elevated in cognitively impaired PD patients compared with cognitively normal PD patients. The elevation of Cys C in PD patients with cognitive impairment was consistent with some researches (Hu et al., 2016). Furthermore, in the univariate logistic regression analysis, both Lp-PLA2 and Cys C were independent risk factors for cognitive impairment in PD. However, after adjustment for different PD risk factors, in the multivariate logistic regression analysis model, only Lp -PLA2 had the value of risk prediction. In order to better distinguish PD patients with cognitive impairment, we further analyzed the diagnostic characteristics of Lp-PLA2 for cognitive impairment in PD using ROC curve, and determined the appropriate diagnostic cut-off value.

Although our findings suggest that higher levels of Lp-PLA2 may be a risk factor for cognitive impairment in PD, its mechanistic roles remain unclear. At present, more evidence supports the formation of cerebrovascular atherosclerosis as important factors in cognitive impairment (Shabir et al., 2018). Given that Lp-PLA2 is involved in the formation and progression of vascular atherosclerosis, we speculate that Lp-PLA2 may lead to cognitive impairment by increasing vascular damage and promoting neurodegeneration. Doody RS et al. did not detect the expression of Lp-PLA2 in the brain tissue of AD patients and controls, but they also suggested that the involvement of Lp-PLA2 in the pathogenesis of AD may be related to its vascular injury (Doody et al., 2015). It has been confirmed that Lp-PLA2 and its main enzyme product lysoPC can participate in diabetic retinopathy by disrupting the blood retinal barrier (BRB) (Canning et al., 2016; Acharya et al., 2017). Based on the structural similarity of the BRB and the blood–brain barrier (BBB), we believe that Lp-PLA2 may also disrupt the BBB, thereby indirectly participating in the development of cognitive impairment in PD. In addition, Lp-PLA2 can also hydrolyze ox-LDL to produce OxNEFA. Therefore, high concentrations of fatty acids make the brain more susceptible to oxidative stress, which may be another important mechanism for triggering cognitive dysfunction (Swomley and Butterfield, 2015). More interesting to us is whether Lp-PLA2 can directly or indirectly participate in the pathogenesis of cognitive impairment in PD by affecting key molecules associated with dementia, such as amyloid β or Tau，which requires further researches to reveal this issue.

Although our study suggests that Lp-PLA2 activity is associated with the risk of cognitive impairment in PD, some limitations remain in this study. First, it is necessary to continue to expand the sample size of PD patients with or without cognitive impairment to further confirm the relationship between Lp-PLA2 and the risk of cognitive impairment in PD. Second, long-term follow-up studies for early PD patients are needed to observe whether subjects with high levels of

Lp-PLA2 develop PD cognitive impairment in later follow-up studies. Third, in our study, we do not consider whether the subjects use lipid-lowering drugs. Some PD patients or the elderly population of normal controls may have taken oral lipid-lowering drugs, which may lead to a decrease in Lp-PLA2 levels to a certain extent, but it generally will not have much impact on our conclusions. Fourth, in our study, some PD patients had a history of hypertension, diabetes, and cerebral infarction, which may have a certain effect on Lp-PLA2 levels. However, considering that the distribution of the above factors was not significantly different between patients with cognitive impairment in PD and cognitively normal patients, we believe that the impact of this potential bias on the conclusions is limited. Fifth, MOCA is used to assess cognitive status in PD patients, and this score does not always accurately reflect cognitive function as it is sometimes affected by the subject's education level. Finally, we only detect the activity of Lp-PLA2, but not its mass. Based on the above problems, whether Lp-PLA2 can be used as a predictive biomarker for the diagnosis of cognitive impairment in PD may require more scientific researches to verify.

5 Conclusion

In conclusion, our study shows that higher levels of Lp-PLA2 activity in PD patients are associated with the risk of developing cognitive impairment. Therefore, given the wide availability, safety, and convenience of monitoring serum Lp-PLA2 activity, it may serve as a predictive biomarker for cognitive impairment in PD patients.

Data availability statement

The original contributions presented in the study are included in the article/supplementary material, further inquiries can be directed to the corresponding authors.

Ethics statement

The studies involving humans were approved by the ethics committee at Tongji Medical College, Huazhong University of Science and Technology. The studies were conducted in accordance with the local legislation and institutional requirements. The participants provided their written informed consent to participate in this study.

Author contributions

ZW: Funding acquisition, Project administration, Writing – original draft, Writing – review & editing. DS: Software, Writing – original draft, Writing – review & editing. SW: Data curation, Writing – original draft. PC: Methodology, Supervision, Validation, Writing – review & editing. TL: Formal analysis, Investigation, Methodology, Project administration, Writing – original draft, Writing – review & editing.

Funding

The author(s) declare that financial support was received for the research, authorship, and/or publication of this article. This study was supported by the Natural Science Foundation Program of Hubei Province (Grant No. 2022CFB181), the Free Innovation Pre-research Fund of Union Hospital of Tongji Medical College, Huazhong University of Science and Technology (Grant No. 2021xhyn059 and No.2023XHYN052).

Conflict of interest

The authors declare that the research was conducted in the absence of any commercial or financial relationships that could be construed as a potential conflict of interest.

Publisher's note

All claims expressed in this article are solely those of the authors and do not necessarily represent those of their affiliated organizations, or those of the publisher, the editors and the reviewers. Any product that may be evaluated in this article, or claim that may be made by its manufacturer, is not guaranteed or endorsed by the publisher.

References

Aarsland, D., Batzu, L., Halliday, G. M., Geurtsen, G. J., Ballard, C., Ray Chaudhuri, K., et al. (2021). Parkinson disease-associated cognitive impairment. *Nat. Rev. Dis. Primers* 7:47. doi: 10.1038/s41572-021-00280-3

Acharya, N. K., Qi, X., Goldwaser, E. L., Godsey, G. A., Wu, H., Kosciuk, M. C., et al. (2017). Retinal pathology is associated with increased blood-retina barrier permeability in a diabetic and hypercholesterolaemic pig model: beneficial effects of the LpPLA(2) inhibitor Darapladib. *Diab. Vasc. Dis. Res.* 14, 200–213. doi: 10.1177/1479164116683149

Bloem, B. R., Okun, M. S., and Klein, C. (2021). Parkinson's disease. *Lancet* 397, 2284–2303. doi: 10.1016/S0140-6736(21)00218-X

Cai, R., Huang, R., Han, J., Sun, H., Sun, J., Xia, W., et al. (2017). Lipoprotein-associated phospholipase A2 is associated with risk of mild cognitive impairment in Chinese patients with type 2 diabetes. *Sci. Rep.* 7:12311. doi: 10.1038/s41598-017-12515-z

Canning, P., Kenny, B. A., Prise, V., Glenn, J., Sarker, M. H., Hudson, N., et al. (2016). Lipoprotein-associated phospholipase A2 (Lp-PLA2) as a therapeutic target to prevent retinal vasopermeability during diabetes. *Proc. Natl. Acad. Sci. USA* 113, 7213–7218. doi: 10.1073/pnas.1514213113

Davidson, J. E., Lockhart, A., Amos, L., Stirnadel-Farrant, H. A., Mooser, V., Sollberger, M., et al. (2012). Plasma lipoprotein-associated phospholipase A2 activity in Alzheimer's disease, amnestic mild cognitive impairment, and cognitively healthy elderly subjects: a cross-sectional study. *Alzheimers Res. Ther.* 4:51. doi: 10.1186/alzrt154

Doody, R. S., Demirovic, J., Ballantyne, C. M., Chan, W., Barber, R., Powell, S., et al. (2015). Lipoprotein-associated phospholipase A2, homocysteine, and Alzheimer's disease. *Alzheimers Dement* 1, 464–471. doi: 10.1016/j.dadm.2015.08.001

Duggan, M. R., Butler, L., Peng, Z., Daya, G. N., Moghekar, A., An, Y., et al. (2023). Plasma proteins related to inflammatory diet predict future cognitive impairment. *Mol. Psychiatry* 28, 1599–1609. doi: 10.1038/s41380-023-01975-7

Feng, F., Chen, Y., Wang, G., Huang, P., Zhu, Q., and Zhou, B. (2022). Correlation of serum CysC, IMA, and Lp-PLA2 levels with type 2 diabetes mellitus patients with lower extremity atherosclerotic occlusive disease. *Front. Surg.* 9:846470. doi: 10.3389/fsurg.2022.846470

Fitzpatrick, A. L., Irizarry, M. C., Cushman, M., Jenny, N. S., Chi, G. C., and Koro, C. (2014). Lipoprotein-associated phospholipase A2 and risk of dementia in the cardiovascular health study. *Atherosclerosis* 235, 384–391. doi: 10.1016/j.atherosclerosis.2014.04.032

Hu, W. D., Chen, J., Mao, C. J., Feng, P., Yang, Y. P., Luo, W. F., et al. (2016). Elevated cystatin C levels are associated with cognitive impairment and progression of Parkinson disease. *Cogn. Behav. Neurol.* 29, 144–149. doi: 10.1097/WNN.0000000000000100

Huang, F., Wang, K., and Shen, J. (2020). Lipoprotein-associated phospholipase A2: the story continues. *Med. Res. Rev.* 40, 79–134. doi: 10.1002/med.21597

Huang, C. J., Zhou, X., Yuan, X., Zhang, W., Li, M. X., You, M. Z., et al. (2021). Contribution of inflammation and Hypoperfusion to white matter Hyperintensities-related cognitive impairment. *Front. Neurol.* 12:786840. doi: 10.3389/fneur.2021.786840

Hughes, A. J., Daniel, S. E., and Lees, A. J. (2001). Improved accuracy of clinicaldiagnosis of Lewy body Parkinson's disease. *Neurology*. 57, 1497–1499. doi: 10.1212/wnl.57.8.1497

Jiang, R., Chen, S., Shen, Y., Wu, J., Chen, S., Wang, A., et al. (2016). Higher levels of lipoprotein associated phospholipase A2 is associated with increased prevalence of cognitive impairment: the APAC study. *Sci. Rep.* 6:33073. doi: 10.1038/srep33073

Liu, L., Zhang, X., Jiang, N., Liu, Y., Wang, Q., Jiang, G., et al. (2023). Plasma lipoprotein-associated phospholipase A2 affects cognitive impairment in patients with cerebral microbleeds. *Neuropsychiatr. Dis. Treat.* 19, 635–646. doi: 10.2147/NDT.S401603

Pellecchia, M. T., Savastano, R., Moccia, M., Picillo, M., Siano, P., Erro, R., et al. (2016). Lower serum uric acid is associated with mild cognitive impairment in early Parkinson's disease: a 4-year follow-up study. *J Neural Transm (Vienna)* 123, 1399–1402. doi: 10.1007/s00702-016-1622-6

Pokharel, Y., Mouhanna, F., Nambi, V., Virani, S. S., Hoogeveen, R., Alonso, A., et al. (2019). ApoB, small-dense LDL-C, Lp(a), LpPLA(2) activity, and cognitive change. *Neurology* 92, e2580–e2593. doi: 10.1212/WNL.0000000000007574

Ridker, P. M., Rifai, N., Macfadyen, J., Glynn, R. J., Jiao, L., Steg, P. G., et al. (2022). Effects of randomized treatment with Icosapent ethyl and a mineral oil comparator on interleukin-1beta, Interleukin-6, C-reactive protein, oxidized low-density lipoprotein cholesterol, homocysteine, lipoprotein(a), and lipoprotein-associated phospholipase A2: a REDUCE-IT biomarker substudy. *Circulation* 146, 372–379. doi: 10.1161/CIRCULATIONAHA.122.059410

Savas, S., Kabaroglu, C., Alpman, A., Sarac, F., Yalcin, M. A., Parildar, Z., et al. (2016). No relationship between lipoprotein-associated phospholipase A2, proinflammatory cytokines, and neopterin in Alzheimer's disease. *Exp. Gerontol.* 77, 1–6. doi: 10.1016/j.exger.2016.01.014

Shabir, O., Berwick, J., and Francis, S. E. (2018). Neurovascular dysfunction in vascular dementia, Alzheimer's and atherosclerosis. *BMC Neurosci.* 19:62. doi: 10.1186/s12868-018-0465-5

Sun, L., Zhu, Z., Shi, M., Jia, Y., Yang, P., Wang, Y., et al. (2021). Causal effect of lipoprotein-associated phospholipase A2 activity on coronary artery disease and myocardial infarction: a two-sample Mendelian randomization study. *Clin. Chim. Acta* 523, 491–496. doi: 10.1016/j.cca.2021.10.039

Swomley, A. M., and Butterfield, D. A. (2015). Oxidative stress in Alzheimer disease and mild cognitive impairment: evidence from human data provided by redox proteomics. *Arch. Toxicol.* 89, 1669–1680. doi: 10.1007/s00204-015-1556-z

Tao, L., Shichuan, W., Detai, Z., and Lihua, H. (2020). Evaluation of lipoprotein-associated phospholipase A2, serum amyloid a, and fibrinogen as diagnostic biomarkers for patients with acute cerebral infarction. *J. Clin. Lab. Anal.* 34:e23084. doi: 10.1002/jcla.23084

Van Himbergen, T. M., Beiser, A. S., Ai, M., Seshadri, S., Otokozawa, S., Au, R., et al. (2012). Biomarkers for insulin resistance and inflammation and the risk for all-cause dementia and alzheimer disease: results from the Framingham heart study. *Arch. Neurol.* 69, 594–600. doi: 10.1001/archneurol.2011.670

Van Oijen, M., Van Der Meer, I. M., Hofman, A., Witteman, J. C., Koudstaal, P. J., and Breteler, M. M. (2006). Lipoprotein-associated phospholipase A2 is associated with risk of dementia. *Ann. Neurol.* 59, 139–144. doi: 10.1002/ana.20721

Wallace, E. R., Segerstrom, S. C., Van Horne, C. G., Schmitt, F. A., and Koehl, L. M. (2022). Meta-analysis of cognition in Parkinson's disease mild cognitive impairment and dementia progression. *Neuropsychol. Rev.* 32, 149–160. doi: 10.1007/s11065-021-09502-7

Wang, Y., Zhou, B., Zhou, P., Yao, Y., Cui, Q., Liu, Y., et al. (2018). Association of lipoprotein-associated phospholipase A2 mass with asymptomatic cerebral artery stenosis. *J. Cell. Mol. Med.* 22, 2329–2336. doi: 10.1111/jcmm.13521

Weintraub, D., Aarsland, D., Biundo, R., Dobkin, R., Goldman, J., and Lewis, S. (2022). Management of psychiatric and cognitive complications in Parkinson's disease. *BMJ* 379:e068718. doi: 10.1136/bmj-2021-068718

Wu, Z., Wu, S., Liang, T., and Wang, L. (2021). Lipoprotein-associated phospholipase A2 is a risk factor for patients with Parkinson's disease. *Front. Neurosci.* 15:633022. doi: 10.3389/fnins.2021.633022

Yang, L., Liu, Y., Wang, S., Liu, T., and Cong, H. (2017). Association between Lp-PLA2 and coronary heart disease in Chinese patients. *J. Int. Med. Res.* 45, 159–169. doi: 10.1177/0300060516678145

Ye, H., Robak, L. A., Yu, M., Cykowski, M., and Shulman, J. M. (2023). Genetics and pathogenesis of Parkinson's syndrome. *Annu. Rev. Pathol.* 18, 95–121. doi: 10.1146/annurev-pathmechdis-031521-034145

Zaman, V., Shields, D. C., Shams, R., Drasites, K. P., Matzelle, D., Haque, A., et al. (2021). Cellular and molecular pathophysiology in the progression of Parkinson's disease. *Metab. Brain Dis.* 36, 815–827. doi: 10.1007/s11011-021-00689-5

Zhu, S., Wei, X., Yang, X., Huang, Z., Chang, Z., Xie, F., et al. (2019). Plasma lipoprotein-associated phospholipase A2 and superoxide dismutase are independent predicators of cognitive impairment in cerebral small vessel disease patients: diagnosis and assessment. *Aging Dis.* 10, 834–846. doi: 10.14336/AD.2019.0304

frontiers | Frontiers in Neuroscience

TYPE Original Research
PUBLISHED 22 May 2024
DOI 10.3389/fnins.2024.1385960

OPEN ACCESS

EDITED BY
Pradeep Kumar,
All India Institute of Medical Sciences, India

REVIEWED BY
Mustapha Muzaimi,
Universiti Sains Malaysia Health Campus, Malaysia
Xiaofei Hu,
Army Medical University, China

*CORRESPONDENCE
Jianquan Zhong
✉ zhongjianquan.2010@qq.com

†These authors have contributed equally to this work and share first authorship

RECEIVED 14 February 2024
ACCEPTED 08 May 2024
PUBLISHED 22 May 2024

CITATION
Yang J, Xiao R, Liu Y, He C, Han L, Xu X, Chen M and Zhong J (2024) Spatiotemporal consistency analysis of cerebral small vessel disease: an rs-fMRI study. *Front. Neurosci.* 18:1385960. doi: 10.3389/fnins.2024.1385960

Spatiotemporal consistency analysis of cerebral small vessel disease: an rs-fMRI study

Jie Yang[1†], Rui Xiao[1†], Yujian Liu[1,2], Chaoliang He[1], Limei Han[1,3], Xiaoya Xu[4], Meining Chen[5] and Jianquan Zhong[1*]

[1]Department of Radiology, Zigong First People's Hospital, Zigong, China, [2]Sichuan Vocational College of Health and Rehabilitation, Zigong, China, [3]North Sichuan Medical College, Nanchong, China, [4]Department of Neurology, Zigong First People's Hospital, Zigong, China, [5]MR Research and Collaboration, Siemens Healthineers, Shanghai, China

Introduction: Cerebral small vessel disease (SVD) affects older adults, but traditional approaches have limited the understanding of the neural mechanisms of SVD. This study aimed to explore the effects of SVD on brain regions and its association with cognitive decline using the four-dimensional (spatiotemporal) consistency of local neural activity (FOCA) method.

Methods: Magnetic resonance imaging data from 42 patients with SVD and 38 healthy controls (HCs) were analyzed using the FOCA values. A two-sample *t* test was performed to compare the differences in FOCA values in the brain between the HCs and SVD groups. Pearson correlation analysis was conducted to analyze the association of various brain regions with SVD scores.

Results: The results revealed that the FOCA values in the right frontal_inf_oper, right temporal_pole_sup, and default mode network decreased, whereas those in the temporal_inf, hippocampus, basal ganglia, and cerebellum increased, in patients with SVD. Most of these varying brain regions were negatively correlated with SVD scores.

Discussion: This study suggested that the FOCA approach might have the potential to provide useful insights into the understanding of the neurophysiologic mechanisms of patients with SVD.

KEYWORDS

cerebral small vessel disease, cognition impairment, four-dimensional (spatiotemporal) consistency of local neural activity, rs-fMRI, SVD score

1 Introduction

Cerebral small vessel disease (SVD) is a prevalent, chronic, and progressive vascular disease among elderly people (Ter Telgte et al., 2018). It encompasses a variety of pathologies and etiologies affecting cerebral small arterioles, arterioles, venules, and capillaries (Cuadrado-Godia et al., 2018). Its main clinical manifestations include various neurologic disorders, such as stroke, cognitive decline, Alzheimer's disease, and abnormal gait. Clinically, it has been found that SVD has common small vessel pathologies and blood-brain barrier (BBB) impairment, and hence, SVD is recognized as a "whole-brain disease" (Shi and Wardlaw, 2016; Li et al., 2018; Ter Telgte et al., 2018; Chojdak-Łukasiewicz et al., 2021). The pathologic mechanisms involved in SVD still remain largely elusive. Imaging markers play a crucial role in diagnosing SVD because of its *in vivo* invisibility.

These markers include white matter hyperintensities (WMH), lacunar infarction (LI), subcortical infarction, cerebral microbleeds (CMBs), and cerebral atrophy (Pantoni, 2010; Litak et al., 2020). Previous studies have proposed a total SVD score based on imaging markers (Staals et al., 2014), which provides a more complete estimate of the full impact of SVD on the brain and correlates with cognitive ability (Staals et al., 2015).

Resting-state functional magnetic resonance imaging (rs-fMRI) is a powerful neuroimaging tool widely used to detect intrinsic brain activity during rest. Several previous studies used amplitude of low-frequency fluctuations (ALFF), regional homogeneity (ReHo), and functional connectivity density (FCD) methods to investigate the impact of SVD on various regions of the brain. They analyzed the changes in ALFF in the whole brain of patients with subcortical ischemic vascular dementia, revealing that the ALFF values in the precuneus, bilateral anterior cingulate cortex, insula, and hippocampus were higher than in the normal group (Liu et al., 2014). Moreover, Ding et al. explored the changes in brain functional connectivity in patients with white matter lesion (WMLs) using the FCD method. They noted the involvement of the regions with altered FCD in cortical regions and caudate (Ding et al., 2016). The ReHo method was used to investigate the changes in neural consistency in patients with WMLs. The results revealed that the decrease in ReHo mainly occurred in the precerebral region, whereas the increase in ReHo mainly occurred in the posterior region (Ding et al., 2017; Orsolini et al., 2021). However, all of the aforementioned measures focused only on the temporal correlation of local adjacent voxels (temporal consistency). They neglected to consider the effect of spatial consistency of spontaneous brain activity signals between neighbors. This might lead to missing useful information in understanding the neuropathologic mechanisms in patients with SVD.

The four-dimensional (spatiotemporal) consistency of local neural activity (FOCA) is a local measurement method first proposed by Dong et al., 2015. It reflects both the temporal homogeneity of local regions and the spatial stability of spontaneous brain activity signals between adjacent time points (Dong et al., 2015). It has been increasingly used in neurologic diseases such as pediatric bipolar disorder (Gao et al., 2021; Guo et al., 2021), frontal lobe epilepsy (Dong et al., 2016), generalized tonic–clonic seizures (Ma et al., 2017), and schizophrenia (Chen et al., 2017). FOCA may provide additional information that can help in understanding brain function (Dong et al., 2015). A high FOCA value indicates low levels of temporal fluctuations and high regional stability. However, the use of this new method of integrating local temporal and spatial information in SVD has not been reported.

Although FOCA can provide a comprehensive view of the time series information of the brain, its application in understanding SVD remains unexplored. This study aimed to fill this research void by investigating the specific effects of SVD on various brain regions using FOCA. Furthermore, we sought to elucidate the relationship between these effects and the cognitive decline often associated with SVD. The findings of this study might contribute substantially to the understanding of the neurophysiologic mechanisms of SVD using the detailed temporal and spatial information provided by FOCA.

2 Materials and methods

2.1 Participants

All research procedures were approved by the hospital Ethics Committee (protocol number: Ethics (Research) No. 98, 2021), and all participants signed written informed consent. Fifty-three SVD patients presenting to our hospital between October 2021 and August 2023 were retrospectively included in this study. The inclusion criteria for patients with SVD were as follows: (1) diagnosis of SVD based on MRI imaging features according to the "Chinese Consensus on Diagnosis and Therapy of Cerebral Small Vessel Diseases 2021" (Hu et al., 2021); (2) no magnetic resonance imaging (MRI) contraindications such as claustrophobia; and (3) absence of notable structural brain abnormalities. The exclusion criteria for patients with SVD were as follows: (1) neurodegenerative diseases or mental disorders such as Alzheimer's disease, Parkinson's disease, or schizophrenia; (2) unrelated neurologic diseases such as epilepsy, stroke, intracranial hemorrhage, or brain tumors; (3) traumatic brain injury or metabolic encephalopathy; and (4) inability to complete the questionnaire due to auditory and visual impairment, speech impairment, or paralysis.

Forty-one healthy controls (HCs) comprised local community residents recruited through advertising. All HCs were required to complete a questionnaire to determine their information on general data and past medical history. In addition, all HCs were required to complete cognitive scale tests, including Mini-Mental State Examination (MMSE). The inclusion criteria for the HCs were no history of neurologic or psychiatric disorders, no cognitive disorders, and no abnormalities in conventional brain MRI images. Also, HCs with no cognitive impairment (MMSE score $\geq$ 25), stroke, or cerebrovascular disease were included. The detailed demographic information on SVD patients and HCs was provided in the results section.

2.2 MRI acquisition

All participants underwent conventional MRI, rs-fMRI, and structural MRI on a 3T MRI scanner (MAGNETOM VIDA, Siemens Healthcare, Erlangen, Germany) with a 64-channel head coil. The rs-fMRI images were acquired using gradient echo planar imaging sequence with the following parameters: repetition time (TR)/echo time (TE) = 1500/30 ms; flip angle = 70°; field of view (FOV) = 240 × 240 mm^2; matrix = 94 × 94; thickness = 3 mm; gap = 0.75 mm; number of slices = 36; and voxel size = 2.5 × 2.5 × 3 mm^3. The total scan time was 6 min 33 s, and a total of 255 images were acquired. Structural MRI scans were acquired using the magnetization prepared 2 rapid acquisition gradient echoes (MP2RAGE) sequence with the following parameters: TR/TE/inversion time (TI1)/TI2 = 5000/2.98/700/2500 ms; flip angle = 4°/5°; matrix = 256 × 256; FOV = 256 × 256 mm^2; thickness = 1.0 mm; number of slices = 176; and voxel size = 1 × 1 × 1 mm^3.

2.3 Data preprocessing

The rs-fMRI data were preprocessed using Statistical Parametric Mapping,[1] as implemented in the Neuroscience Information Toolbox vision 1.3,[2] (Dong et al., 2018). The rs-fMRI data were preprocessed as follows: the first 10 volumes were removed from the rs-fMRI data to ensure that the data is in a stable state; slice time correction; realignment; spatial normalization using individual structural MRI (normalizing to Montreal Neurological Institute space with $3 \times 3 \times 3$ mm^3); and smooth (full width at half maximum, FWHM = 8 mm). The participants with excessive head movement (translation > 2.5 mm or rotation > 2.5 mm) and mean framewise displacement (mFD) greater than 0.5 mm were excluded to avoid the impact of excessive head movement on the subsequent analysis.

2.4 FOCA analysis

The process for calculating the FOCA map for all participants using the NIT v1.3 software involved several steps (Dong et al., 2015). Before generating the FOCA maps, the software first removed various nuisance signals from the unsmoothed rs-fMRI data. These signals included 12 parameters related to head motion, average signals from white matter and cerebrospinal fluid, and any linear trends. Once these signals were removed, the software calculated the FOCA value for each voxel. Then, the FOCA value of each voxel was computed by integrating the temporal correlation among neighboring voxels (26 in total) and the spatial correlation between adjacent time points. After computing the FOCA values for all voxels throughout the brain, these values were normalized. This normalization involved dividing the FOCA value of each voxel by the average FOCA value across the entire brain. Following normalization, the mean FOCA maps were created and then smoothed using an 8-mm FWHM Gaussian kernel. Finally, the whole brain was segmented into 116 distinct regions using the Anatomical Automatic Labeling system, which served as masks for the analysis.

2.5 Total MRI burden of SVD

The SVD score was determined using a previously described 4-point scale with neuroimaging characteristics of SVD, including periventricular WMH or deep WMH, CMBs, LI, and perivascular spaces (PVS) (Staals et al., 2014). The WMH were defined as lesions appearing hyperintense on T2-weighted fluid-attenuated inversion recovery images and graded according to the Fazekas scale (Fazekas et al., 1987; Wardlaw et al., 2013). If the periventricular WMH Fazekas score was 3 or deep WMH Fazekas score was 2 or 3, 1 point was counted. The CMBs were identified and rated using the microbleed anatomical rating scale (Gregoire et al., 2009), and 1 score was counted if CMB was present. The LI was defined as a round or ovoid, subcortical, fluid-filled cavity between 3 and 15 mm in diameter under the cortex (Wardlaw et al., 2013), and 1 point was counted if CMB was present. The PVS were defined as small (<3 mm) structures of high signal on T2-weighted images and low signal on T1-weighted images located in the cerebrospinal fluid or basal ganglia centrum semiovale that followed the orientation of the perforating vessels and ran perpendicular to the brain surface (Doubal et al., 2010). The PVS grade was moderate to severe (2–4) with a score of 1 point. The SVD score ranged from 0 to 4. The images were scored independently by two experienced radiologists. If the results are inconsistent, the two radiologists decide by consensus.

2.6 Statistic analyses

Statistical analyses were performed using the SPM12. The two-sample *t* test was used to analyze FOCA differences between groups, using age, sex, education, head motion (mFD), and total intracranial volume as covariates. Pearson correlation analysis was used to analyze the association between brain regions with intergroup FOCA differences and total SVD scores. The criterion for statistical significance was $P < 0.05$, with a false discovery rate (FDR) used to correct for multiple comparisons (cluster size > 23).

3 Results

3.1 Demographic and clinical characteristics of the participants

A total of 53 patients with SVD and 41 HCs were recruited in this study. Among the patients with SVD, 7 with excessive head movement, 3 with kidney disease, and 1 with cerebral hemorrhage were excluded. In the control group, 3 HCs were excluded due to excessive head movement. Finally, 42 patients with SVD [19 male, 23 female; age (mean ± standard deviation), 68.524 ± 8.805 years], and 38 HCs [15 male, 23 female; age (mean ± standard deviation), 56.237 ± 4.210 years] remained in the final study. No differences were noted in sex, hyperlipidemia, smoking, and drinking. The demographic information and clinical characteristics are presented in **Table 1**.

3.2 Analyzing FOCA values to differentiate SVD from HCs

Significant differences in the FOCA map of SVD were demonstrated using the two-sample *t* test ($P < 0.05$, FDR corrected, and cluster size > 23). Compared with HCs, the decreased FOCA values of SVD were located in the right frontal_inf_oper, right temporal_pole_sup, right precuneus, right parietal_pup, right supramarginal, and left angular regions. The increased FOCA values of SVD were mainly observed in a few bilateral brain regions, including hippocampus, thalamus, cerebelum_9, and fusiform. The increased FOCA values were also observed in right parahippocampal, right cerebelum 4_5, left temporal_inf, left pallidum, left putamen, left cerebelum_10, and vermis_4_5 regions (**Figure 1** and **Table 2**).

1 https://www.fil.ion.ucl.ac.uk/spm/software/spm12/

2 http://www.neuro.uestc.edu.cn/NIT.html

TABLE 1 Demographic information of the healthy controls and patients with SVD.

	SVD (n = 42)	HCs (n = 38)	P-value
Age (year)	47–85 (68.524 ± 8.805)	49–67 (56.237 ± 4.210)	<0.05
Sex (male/female)	19/23	15/23	0.602
Years of education	0–12 (5.476 ± 3.238)	5–16 (10.145 ± 2.490)	<0.05
Vascular risk factors			
Hypertension	27 (64.286%)	6 (15.789%)	<0.05
Diabetes	14 (33.333%)	0	<0.05
Hyperlipidemia	7 (16.667%)	4 (10.526%)	0.964
Smoking	11 (26.190%)	8 (21.053%)	0.590
Drinking	12 (28.571%)	8 (21.053%)	0.438

Data were expressed as the range from min to max (mean ± SD) or number (percentage).
P-value < 0.05 was considered to be statistically significant.
HCs, healthy controls; SD, standard deviation; SVD, cerebral small vessel disease.

3.3 Correlation analysis between total SVD score and FOCA values

The significant correlations between altered brain function value and SVD score are illustrated graphically in Figure 2 (P < 0.05, cluster-level FDR corrected). The SVD score had a negative correlation with the FOCA values of the right hippocampus (r = − 0.392, P = 0.0103), right parahippocampal (r = − 0.433, P = 0.0042), right fusiform (r = − 0.393, P = 0.0096), left pallidum (r = − 0.435, P = 0.0040), right cerebelum_4_5 (r = − 0.402, P = 0.0083), right cerebelum_9 (r = − 0.384, P = 0.0121), left cerebelum_10 (r = − 0.513, P = 0.0005), and Vermis_4_5 (r = − 0.454, P = 0.0025).

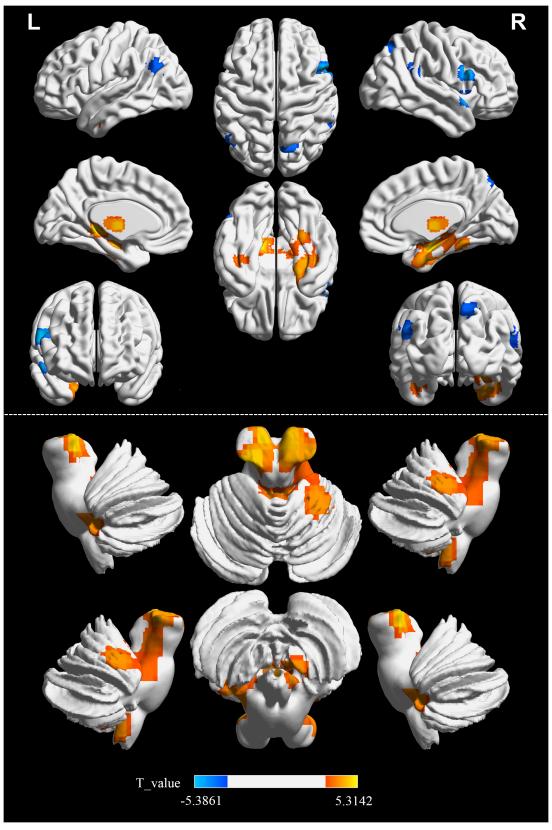

FIGURE 1
Differences in FOCA values between SVD and HCs groups. Cool color represents that the FOCA values was lower in the SVD group than in the HCs group (P < 0.05, FDR corrected, and cluster size > 23). FDR, false discovery rate; FOCA, four-dimensional (spatiotemporal) consistency of local neural activity; HCs, healthy controls; SVD, cerebral small vessel disease.

4 Discussion

This study was novel in investigating the spatiotemporal consistency of local brain spontaneous activity in patients with SVD based on the FOCA value of rs-fMRI. Considerable differences in FOCA values were noted between patients with SVD and HCs. Patients with SVD exhibited decreased FOCA values in certain right and left brain regions but increased FOCA values primarily in the bilateral hippocampus and other specified areas. The negative correlations between SVD scores and FOCA values in specific brain regions provided a preliminary understanding of the impact of SVD on brain function.

Previous studies have demonstrated that FOCA analyzes local spatiotemporal consistency, emphasizing local temporal homogeneity and regional stability of brain activity states (Dong et al., 2015, 2016). This study revealed that patients with SVD had reduced FOCA values in the right precuneus, parietal_sup, supramarginal, and left angular regions, which are parts of the default mode network (DMN). The DMN is a large-scale network consisting of a highly connected cortex combined with self-referential function, emotion, and episodic memory retrieval (Davey et al., 2016; Roberto et al., 2016; Smallwood et al., 2021). We observed reduced FOCA values in these brain regions, suggesting that DMN in patients with SVD may have abnormal spontaneous neural activity. Previous studies have also demonstrated that DMN is a commonly affected network in SVD (Li et al., 2023). This study observed reduced FOCA values in the right frontal_inf_oper and temporal_pole_sup regions. Previous studies have shown that patients with SVD have reduced functional connectivity in the frontal and temporal lobes (Sun et al., 2011; Gu et al., 2022;

TABLE 2 Detailed information on significant differences in each brain region between SVD and HCs groups.

Region	MNI coordinates			Peak *t*_value	Cluster size
	X	*Y*	*Z*		
Hippocampu_L	−18	−33	0	4.87	347
Thalamus_L	−6	−12	3	4.46	
Thalamus_R	6	−12	3	4.34	
Hippocampus_R	36	−9	−18	4.61	407
Fusiform_R	30	−15	−27	4.14	
ParaHippocampal_R	24	−6	−33	4.1	
Cerebelum_4_5_R	18	−30	−27	3.42	
Temporal_Inf_L	−42	−6	−33	3.29	71
Fusiform_L	−39	−18	−27	3.2	
Putamen_L	−30	−6	−6	4.15	39
Pallidum_L	−15	0	0	4.25	
Vermis_4_5	−3	−48	−21	4.3	96
Cerebelum_9_R	9	−45	−54	3.87	29
Cerebelum_10_L	−24	−36	−39	3.85	38
Cerebelum_9_L	−18	−45	−42	3.33	
Temporal_Pole_Sup_R	60	15	−6	−5.18	61
SupraMarginal_R	54	−45	27	−3.82	25
Frontal_Inf_Oper_R	54	12	24	−5.38	79
Angular_L	−51	−66	27	−3.77	40
Parietal_Sup_R	18	−66	48	−3.98	47
Precuneus_R	12	−70	48	−3.27	

HCs, healthy controls; MNI, Montreal Neurological Institute; SVD, cerebral small vessel disease.

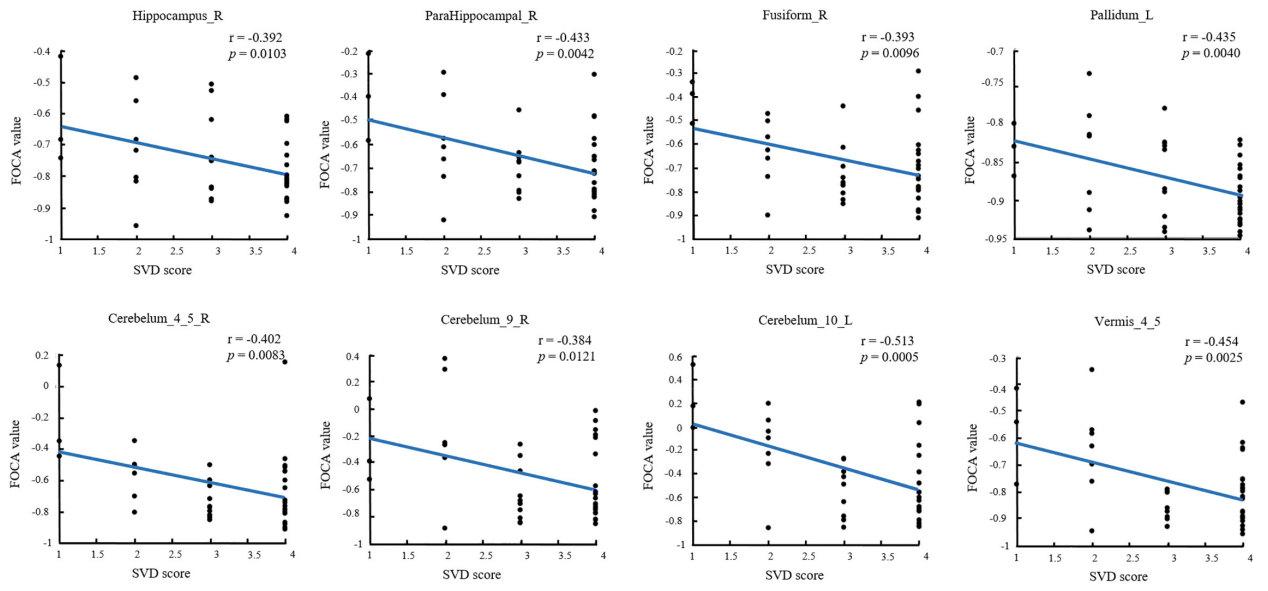

FIGURE 2
Substantial correlations between FOCA values in the brain regions and SVD score ($P < 0.05$, FDR corrected). FDR, false discovery rate; FOCA, four-dimensional (spatiotemporal) consistency of local neural activity.

Yin et al., 2022). Vascular risk factors such as hypertension and diabetes affect the gray matter volume in the frontal and temporal lobes (Gold et al., 2005; Li et al., 2021; Zhang et al., 2022). In this study, SVD patients with hypertension or diabetes were not excluded. This may affect our results due to vascular risk factors. Therefore, we speculate that the decrease in FOCA values in the frontal and temporal lobes of SVD may be caused by multiple factors such as vascular risk factors and decreased connectivity. Our speculation will be confirmed in future work.

Moreover, this study reported increased FOCA values in the hippocampus, thalamus, pallidum, and putamen of patients with SVD, indicating enhanced coordination and stability of neural activity within these regions. Similar results were obtained in studies of other SVD subtypes (Feng et al., 2021; Hu et al., 2022). Several studies have demonstrated that the hippocampus/parahippocampal gyrus is essential for the brain's long-term episodic memory, semantic memory, spatial cognition, learning, emotion, and more (Danjo et al., 2018; Loprinzi, 2019; Maurer and Nadel, 2021; Peng and Burwell, 2021). Meanwhile, the putamen, pallidum, and thalamus are the main components of the basal ganglia located in the deep brain region. The basal ganglia are thought to be crucial in learning and memory. They are associated with executive decision-making and reward, cognition, emotion, and function (Graybiel, 2000; Florio et al., 2018). Further, we demonstrated that the FOCA values of the hippocampus, parahippocampal and pallidum were negatively correlated with the SVD score. A recent study also confirmed that the SVD score was significantly negatively correlated with the overall cognitive function and attention (Hosoya et al., 2023). Linking FOCA values to cognitive functions through SVD scores suggests a hypothesis: alterations in FOCA values might serve a compensatory role. Enhancing the spatiotemporal consistency in brain regions with decreased FOCA values could potentially compensate for neuronal damage and cognitive deficits in these areas, thereby helping to maintain normal daily functions. Further research is needed to validate this hypothesis, ideally through studies that integrate more comprehensive assessments of brain connectivity and cognitive functions to better understand the underlying mechanisms.

Traditionally, the cerebellum has been considered the brain region associated with movement; however, a growing body of research has demonstrated its involvement in more complex functions, including emotional regulation, social processing, and cognitive function. The anterior cerebellar lobe has extensive connections with sensorimotor function, whereas the posterior cerebellar lobe (crus I and VIIb) is involved in cognitive function. The vermis is known to have extensive connections with the limbic structures of the brain, thus demonstrating the involvement of the cerebellum in emotion and emotional behavior (Leggio and Olivito, 2018; Schmahmann, 2019; Pierce and Péron, 2020). This study demonstrated an increase in FOCA values in the vermis. Further, we demonstrated that the FOCA values of cerebellum were negatively correlated with the SVD score. This finding was consistent with previous studies where Ding et al. suggested an increase in ALFF in the cerebellum (Ding et al., 2015), which might be an attempt to recruit more neurons to compensate for cognitive impairment. In addition, the present study demonstrated an increase in FOCA values in the anterior cerebellar region, which was rarely reported in previous studies. This might be because most previous studies focused on the SVD subtype. Another aspect might be the additional information derived using the FOCA method. This might provide new insights into the pathophysiologic mechanisms in patients with SVD. Moreover, several studies have demonstrated that the basal ganglia are closely linked to the cerebral cortex and cerebellum to form a complete network, namely the basal ganglia–cerebellar–cortical network, which is involved in various motor and cognitive functions. However, this is considered to be a complete system that allows us to understand the function of these regions using a completely unique approach (Bostan and Strick, 2018; Milardi et al., 2019; Pierce and Péron, 2020). Future studies should investigate the changes in the loop in patients with SVD.

5 Limitations

This study has a few limitations. Firstly, an age mismatch was seen between patients with SVD and HCs. Therefore, in the statistical analysis, age was removed as a covariate to reduce its impact on the reliability of the results. Secondly, the SVD patients in this study lacks professional scale to evaluate the cognitive function, such as MMSE, which will be further studied in future work.

6 Conclusion

Our results suggest that there is a wide range of spontaneous brain activity abnormalities in patients with SVD, which may be related to cognitive impairment in patients with SVD, and the FOCA method may provide a powerful tool for further understanding the underlying neurophysiological mechanisms of SVD.

Data availability statement

The raw data supporting the conclusions of this article will be made available by the authors, without undue reservation.

Ethics statement

The studies involving humans were approved by the Ethics Committee of Zigong First People's Hospital. The studies were conducted in accordance with the local legislation and institutional requirements. The participants provided their written informed consent to participate in this study.

Author contributions

JY: Methodology, Writing – original draft. RX: Methodology, Writing – original draft. YL: Data curation, Writing – original draft. CH: Investigation, Writing – original draft. LH: Validation, Writing – original draft. XX: Project administration,

Writing – review and editing. MC: Writing – review and editing. JZ: Project administration, Writing – review and editing.

Funding

The author(s) declare that financial support was received for the research, authorship, and/or publication of this article. This project was supported by the Zigong Key Science and Technology Plan in 2021 (No. 2021ZC09) and Zigong Public Hospital Reform and High-Quality Development Demonstration Project in 2023 (No. ZG-KY-2023-008).

Acknowledgments

We thank everyone who helped with this study.

Conflict of interest

MC was employed by company Siemens Healthineers.

The remaining authors declare that the research was conducted in the absence of any commercial or financial relationships that could be construed as a potential conflict of interest.

Publisher's note

References

Bostan, A. C., and Strick, P. L. (2018). The basal ganglia and the cerebellum: Nodes in an integrated network. *Nat. Rev. Neurosci.* 19, 338–350. doi: 10.1038/s41583-018-0002-7

Chen, X., Jiang, Y., Chen, L., He, H., Dong, L., Hou, C., et al. (2017). Altered hippocampo-cerebello-cortical circuit in schizophrenia by a spatiotemporal consistency and causal connectivity analysis. *Front. Neurosci.* 11:25. doi: 10.3389/fnins.2017.00025

Chojdak-Łukasiewicz, J., Dziadkowiak, E., Zimny, A., and Paradowski, B. (2021). Cerebral small vessel disease: A review. *Adv. Clin. Exp. Med.* 30, 349–356. doi: 10.17219/acem/131216

Cuadrado-Godia, E., Dwivedi, P., Sharma, S., Santiago, A. O., Gonzalez, J. R., Balcells, M., et al. (2018). Cerebral small vessel disease: A review focusing on pathophysiology, biomarkers, and machine learning strategies. *J. Stroke* 20:302. doi: 10.5853/jos.2017.02922

Danjo, T., Toyoizumi, T., and Fujisawa, S. (2018). Spatial representations of self and other in the hippocampus. *Science* 359, 213–218. doi: 10.1126/science.aao3898

Davey, C. G., Pujol, J., and Harrison, B. J. (2016). Mapping the self in the brain's default mode network. *Neuroimage* 132, 390–397. doi: 10.1016/j.neuroimage.2016.02.022

Ding, J.-R., Ding, X., Hua, B., Xiong, X., Wang, Q., and Chen, H. (2016). Abnormal functional connectivity density in patients with ischemic white matter lesions: An observational study. *Medicine* 95:e4625. doi: 10.1097/MD.0000000000004625

Ding, X., Ding, J., Hua, B., Xiong, X., Xiao, L., Peng, F., et al. (2017). Abnormal cortical functional activity in patients with ischemic white matter lesions: A resting-state functional magnetic resonance imaging study. *Neurosci. Lett.* 644, 10–17. doi: 10.1016/j.neulet.2017.02.015

Ding, X., Wu, J., Zhou, Z., and Zheng, J. (2015). Specific locations within the white matter and cortex are involved in the cognitive impairments associated with periventricular white matter lesions (PWMLs). *Behav. Brain Res.* 289, 9–18. doi: 10.1016/j.bbr.2015.04.021

Dong, L., Li, H., He, Z., Jiang, S., Klugah-Brown, B., Chen, L., et al. (2016). Altered local spontaneous activity in frontal lobe epilepsy: A resting-state functional magnetic resonance imaging study. *Brain Behav.* 6:e00555. doi: 10.1002/brb3.555

Dong, L., Luo, C., Cao, W., Zhang, R., Gong, J., Gong, D., et al. (2015). Spatiotemporal consistency of local neural activities: A new imaging measure for functional MRI data. *J. Magn. Reson. Imaging* 42, 729–736. doi: 10.1002/jmri.24831

Dong, L., Luo, C., Liu, X., Jiang, S., Li, F., Feng, H., et al. (2018). Neuroscience information toolbox: An open source toolbox for EEG–fMRI multimodal fusion analysis. *Front. Neuroinform.* 12:56. doi: 10.3389/fninf.2018.00056

Doubal, F. N., MacLullich, A. M., Ferguson, K. J., Dennis, M. S., and Wardlaw, J. M. (2010). Enlarged perivascular spaces on MRI are a feature of cerebral small vessel disease. *Stroke* 41, 450–454. doi: 10.1161/STROKEAHA.109.564914

Fazekas, F., Chawluk, J. B., Alavi, A., Hurtig, H. I., and Zimmerman, R. A. (1987). MR signal abnormalities at 1.5 T in Alzheimer's dementia and normal aging. *Am. J. Roentgenol.* 8, 421–426. doi: 10.2214/ajr.149.2.351

Feng, M., Wen, H., Xin, H., Zhang, N., Liang, C., and Guo, L. (2021). Altered spontaneous brain activity related to neurologic dysfunction in patients with cerebral small vessel disease. *Front. Aging Neurosci.* 13:731585. doi: 10.3389/fnagi.2021.731585

Florio, T. M., Scarnati, E., Rosa, I., Di Censo, D., Ranieri, B., Cimini, A., et al. (2018). The basal Ganglia: More than just a switching device. *CNS Neurosci. Ther.* 24, 677–684. doi: 10.1111/cns.12987

Gao, W., Cui, D., Jiao, Q., Su, L., Lu, G., and Yang, R. (2021). Altered spatiotemporal consistency in pediatric bipolar disorder patients with and without psychotic symptoms. *BMC Psychiatry* 21:506. doi: 10.1186/s12888-021-03524-4

Gold, S. M., Dziobek, I., Rogers, K., Bayoumy, A., McHugh, P. F., and Convit, A. (2005). Hypertension and hypothalamo-pituitary-adrenal axis hyperactivity affect frontal lobe integrity. *J. Clin. Endocrinol. Metab.* 90, 3262–3267. doi: 10.1210/jc.2004-2181

Graybiel, A. M. (2000). The basal ganglia. *Curr. Biol.* 10, R509–R511. doi: 10.1016/S0960-9822(00)00593-5

Gregoire, S., Chaudhary, U., Brown, M., Yousry, T., Kallis, C., Jäger, H., et al. (2009). The microbleed anatomical rating scale (MARS): Reliability of a tool to map brain microbleeds. *Neurology* 73, 1759–1766. doi: 10.1212/WNL.0b013e3181c34a7d

Gu, Y., Dong, Q., Xia, X., Tian, X., and Li, X. (2022). Theta oscillation and functional connectivity alterations related to cerebral small vessel disease with working memory impairment. *Clin. Neurophysiol. Off. J. Int. Fed. Clin. Neurophysiol.* 2022:131. doi: 10.21203/rs.3.rs-1045956/v1

Guo, Y., Wang, J., Jiao, Q., Cao, W., Cui, D., Gao, W., et al. (2021). Altered spatiotemporal consistency of corticolimbic circuitry in euthymic pediatric bipolar disorder. *Brain Imaging Behav.* 15, 1290–1299. doi: 10.1007/s11682-020-00327-1

Hosoya, M., Toi, S., Seki, M., Saito, M., Hoshino, T., Yoshizawa, H., et al. (2023). Association between total cerebral small vessel disease score and cognitive function in patients with vascular risk factors. *Hypertens. Res.* 46, 1326–1334. doi: 10.1038/s41440-023-01244-8

Hu, W., Yang, L., Li, X., and Huang, Y. (2021). Chinese consensus on diagnosis and therapy of cerebral small vessel diseases 2021. *Chin. J. Stroke* 16, 716–726.

Hu, Y., Yang, Y., Hou, X., Zhou, Y., and Nie, S. (2022). The influence of white matter hyperintensities severity on functional brain activity in cerebral small vessel disease: An rs-fMRI study. *J. Xray Sci. Technol.* 30, 1213–1227. doi: 10.3233/XST-221218

Leggio, M., and Olivito, G. (2018). Topography of the cerebellum in relation to social brain regions and emotions. *Handb. Clin. Neurol.* 154, 71–84. doi: 10.1016/B978-0-444-63956-1.00005-9

Li, Q., Yang, Y., Reis, C., Tao, T., Li, W., Li, X., et al. (2018). Cerebral small vessel disease. *Cell Transplant.* 27, 1711–1722. doi: 10.1177/0963689718795148

Li, W., Yue, L., and Xiao, S. (2021). Increase in right temporal cortex thickness is related to decline of overall cognitive function in patients with hypertension. *Front. Cardiovasc. Med.* 8:758787. doi: 10.3389/fcvm.2021.758787

Li, Y., Liu, X., Jia, X., Li, H., Jia, X., and Yang, Q. (2023). Structural and functional alterations in cerebral small vessel disease: An ALE-based meta-analysis. *Cereb. Cortex* 33, 5484–5492. doi: 10.1093/cercor/bhac435

Litak, J., Mazurek, M., Kulesza, B., Szmygin, P., Litak, J., Kamieniak, P., et al. (2020). Cerebral small vessel disease. *Int. J. Mol. Sci.* 21:9729. doi: 10.3390/ijms21249729

Liu, C., Li, C., Yin, X., Yang, J., Zhou, D., Gui, L., et al. (2014). Abnormal intrinsic brain activity patterns in patients with subcortical ischemic vascular dementia. *PLoS One* 9:e87880. doi: 10.1371/journal.pone.0087880

Loprinzi, P. (2019). The effects of physical exercise on parahippocampal function. *Physiol. Int.* 106, 114–127. doi: 10.1556/2060.106.2019.10

Ma, S., Jiang, S., Peng, R., Zhu, Q., Sun, H., Li, J., et al. (2017). Altered local spatiotemporal consistency of resting-state BOLD signals in patients with generalized tonic-clonic seizures. *Front. Comput. Neurosci.* 11:90. doi: 10.3389/fncom.2017.00090

Maurer, A. P., and Nadel, L. (2021). The continuity of context: A role for the hippocampus. *Trends Cogn. Sci.* 25, 187–199. doi: 10.1016/j.tics.2020.12.007

Milardi, D., Quartarone, A., Bramanti, A., Anastasi, G., Bertino, S., Basile, G. A., et al. (2019). The cortico-basal ganglia-cerebellar network: Past, present and future perspectives. *Front. Syst. Neurosci.* 13:61. doi: 10.3389/fnsys.2019.00061

Orsolini, S., Marzi, C., Gavazzi, G., Bianchi, A., Salvadori, E., Giannelli, M., et al. (2021). Altered regional brain homogeneity of BOLD signal in CADASIL: A resting state fMRI study. *J. Neuroimaging* 31, 348–355. doi: 10.1111/jon.12821

Pantoni, L. (2010). Cerebral small vessel disease: From pathogenesis and clinical characteristics to therapeutic challenges. *Lancet Neurol.* 9, 689–701. doi: 10.1016/S1474-4422(10)70104-6

Peng, X., and Burwell, R. D. (2021). Beyond the hippocampus: The role of parahippocampal-prefrontal communication in context-modulated behavior. *Neurobiol. Learn. Mem.* 185:107520. doi: 10.1016/j.nlm.2021.107520

Pierce, J. E., and Péron, J. (2020). The basal ganglia and the cerebellum in human emotion. *Soc. Cogn. Affect. Neurosci.* 15, 599–613. doi: 10.1093/scan/nsaa076

Roberto, A., Mohan, A., Jones, K., Carney, M., Liogier-weyback, L., Hwang, S., et al. (2016). The significance of the default mode network (DMN) in neurological and neuropsychiatric disorders: A review. *Yale J. Biol. Med.* 89, 49–57.

Schmahmann, J. D. (2019). The cerebellum and cognition. *Neurosci. Lett.* 688, 62–75. doi: 10.1016/j.neulet.2018.07.005

Shi, Y., and Wardlaw, J. M. (2016). Update on cerebral small vessel disease: A dynamic whole-brain disease. *Stroke Vasc. Neurol.* 1, 83–92. doi: 10.1136/svn-2016-000035

Smallwood, J., Bernhardt, B. C., Leech, R., Bzdok, D., Jefferies, E., and Margulies, D. S. (2021). The default mode network in cognition: A topographical perspective. *Nat. Rev. Neurosci.* 22, 503–513. doi: 10.1038/s41583-021-00474-4

Staals, J., Booth, T., Morris, Z., Bastin, M. E., Gow, A. J., Corley, J., et al. (2015). Total MRI load of cerebral small vessel disease and cognitive ability in older people. *Neurobiol. Aging* 36, 2806–2811. doi: 10.1016/j.neurobiolaging.2015.06.024

Staals, J., Makin, S. D., Doubal, F. N., Dennis, M. S., and Wardlaw, J. M. (2014). Stroke subtype, vascular risk factors, and total MRI brain small-vessel disease burden. *Neurology* 83, 1228–1234. doi: 10.1212/WNL.0000000000000837

Sun, Y.-W., Zhou, Y., Xu, Q., Qian, L.-J., Tao, J., and Xu, J.-R. (2011). Abnormal functional connectivity in patients with vascular cognitive impairment, no dementia: A resting-state functional magnetic resonance imaging study. *Behav. Brain Res.* 223, 388–394. doi: 10.1016/j.bbr.2011.05.006

Ter Telgte, A., Van Leijsen, E. M., Wiegertjes, K., Klijn, C. J., Tuladhar, A. M., and de Leeuw, F.-E. (2018). Cerebral small vessel disease: From a focal to a global perspective. *Nat. Rev. Neurol.* 14, 387–398. doi: 10.1038/s41582-018-0014-y

Wardlaw, J. M., Smith, E. E., Biessels, G. J., Cordonnier, C., Fazekas, F., Frayne, R., et al. (2013). Neuroimaging standards for research into small vessel disease and its contribution to ageing and neurodegeneration. *Lancet Neurol.* 12, 822–838. doi: 10.1016/S1474-4422(13)70124-8

Yin, W., Zhou, X., Li, C., You, M., Wan, K., Zhang, W., et al. (2022). The clustering analysis of time properties in patients with cerebral small vessel disease: A dynamic connectivity study. *Front. Neurol.* 13:913241. doi: 10.3389/fneur.2022.913241

Zhang, J., Liu, Y., Guo, X., Guo, J., Du, Z., He, M., et al. (2022). Causal structural covariance network suggesting structural alterations progression in type 2 diabetes patients. *Front. Hum. Neurosci.* 16:936943. doi: 10.3389/fnhum.2022.936943

frontiers | Frontiers in Neuroscience

TYPE Review
PUBLISHED 07 June 2024
DOI 10.3389/fnins.2024.1420322

OPEN ACCESS

EDITED BY
Pradeep Kumar,
All India Institute of Medical Sciences, India

REVIEWED BY
Shaohua Qi,
Houston Methodist Research Institute, United States
Marcus Augusto-Oliveira,
Federal University of Pará, Brazil
Boyi Zong,
East China Normal University, China

*CORRESPONDENCE
Ania K. Majewska
✉ ania_majewska@urmc.rochester.edu

RECEIVED 19 April 2024
ACCEPTED 20 May 2024
PUBLISHED 07 June 2024

CITATION
Strohm AO and Majewska AK (2024) Physical exercise regulates microglia in health and disease.
Front. Neurosci. 18:1420322.
doi: 10.3389/fnins.2024.1420322

Physical exercise regulates microglia in health and disease

Alexandra O. Strohm[1] and Ania K. Majewska[2,3,4]*

[1]Department of Environmental Medicine, University of Rochester Medical Center, Rochester, NY, United States, [2]Department of Neuroscience, University of Rochester Medical Center, Rochester, NY, United States, [3]Del Monte Institute for Neuroscience, University of Rochester Medical Center, Rochester, NY, United States, [4]Center for Visual Science, University of Rochester Medical Center, Rochester, NY, United States

There is a well-established link between physical activity and brain health. As such, the effectiveness of physical exercise as a therapeutic strategy has been explored in a variety of neurological contexts. To determine the extent to which physical exercise could be most beneficial under different circumstances, studies are needed to uncover the underlying mechanisms behind the benefits of physical activity. Interest has grown in understanding how physical activity can regulate microglia, the resident immune cells of the central nervous system. Microglia are key mediators of neuroinflammatory processes and play a role in maintaining brain homeostasis in healthy and pathological settings. Here, we explore the evidence suggesting that physical activity has the potential to regulate microglia activity in various animal models. We emphasize key areas where future research could contribute to uncovering the therapeutic benefits of engaging in physical exercise.

KEYWORDS

microglia, physical exercise, neurodevelopment, neurodegeneration, aging, environmental exposure

Introduction

It is largely accepted that physical exercise (PE) can promote brain health and cognitive function. Reports in humans show that moderate to vigorous PE can enhance cognition (Colcombe and Kramer, 2003; Angevaren et al., 2008; Hamer et al., 2018; Cheval et al., 2023; James et al., 2023; Li W. et al., 2023). However, the cellular mechanisms that underlie this phenomenon are still an active area of exploration. Traditionally, studies have examined how PE regulates wiring of neuronal connections to enhance cognitive function (Festa et al., 2023). However, recent focus has shifted toward how exercise may regulate inflammation and the immune response in the central nervous system (CNS).

Microglia are the resident immune cells of the CNS responsible for mediating inflammatory responses, tissue maintenance, and synapse remodeling (Li and Barres, 2018; Whitelaw et al., 2023). Many therapeutics are designed to target microglia activity, as it is tightly linked to neuronal health and cognitive function. Under homeostatic conditions, microglia are highly ramified and maintain discrete territories with uniform dispersal throughout the brain (Nimmerjahn et al., 2005). Plasticity, the brain's ability to adapt both functionally and structurally to intrinsic and extrinsic stimuli, is an ongoing process that begins in development and continues throughout a lifespan. Microglia are active participants in plasticity, perpetually undergoing functional and structural changes, extending and retracting their processes to survey their environment and monitor the

functional state of the brain (Nimmerjahn et al., 2005; Wake et al., 2009). In doing this, microglia dynamically interact with synaptic elements to facilitate synapse remodeling (Wake et al., 2009; Tremblay et al., 2010; Paolicelli et al., 2011; Nebeling et al., 2023). These interactions are governed by a variety of signaling pathways and molecules reviewed in Whitelaw et al. (2023), including norepinephrine and BDNF which are known to be produced during PE (see "Exercise Increases Known Modulators of Microglia Activity"). Beyond synapse regulation, microglia serve critical functions in regulating myelination, injury and inflammatory responses, and neurogenesis, reviewed in Bobotis et al. (2024). Perturbations of microglial function have been described in numerous neurological diseases and disorders. Functional changes in microglia are often accompanied by alterations in microglial morphology, number, distribution, and phenotype characterized by altered expression of various molecules (Paolicelli et al., 2022; Bobotis et al., 2024). In certain circumstances, microglial activity can decrease or shift to different functions resulting in a diminished ability to migrate, respond to injury and clear debris (Hefendehl et al., 2014; Thomas et al., 2022). In other cases, microglia can engage in excessive synaptic pruning, or release pro-inflammatory factors that can contribute to cognitive decline (Hong et al., 2016; Pinto et al., 2020). By targeting microglia activity, these processes can be differentially impacted in health and disease. Thus, discovering strategies to modulate microglia activity is of great interest. However, the overall effects of PE on deficits in function and cognition depend on the timing of the exercise intervention. For more discussion on how changes in microglial activity and function can impact the brain during development as well as in health and disease, please see Paolicelli and Ferretti (2017) and Gao et al. (2023).

This review focuses on how PE has been shown to modulate microglia function in different animal models and highlight areas where further research could be beneficial (**Figure 1**). An overview of the comprehensive review process is shown in **Supplementary Figure 1**. Studies were reviewed from the PUBMED search query: ((((exercise[Title/Abstract]) OR (physical exercise[Title/Abstract])) OR (physical activity[Title/Abstract])) AND (microglia[Title/Abstract])) NOT (review[Publication Type]). This resulted in a list of studies which were published over a twenty-year span (between 2003 and November 21, 2023; **Figure 2A**). Select research studies within the scope of this review which were found manually outside the search parameters stated above were also included. Only peer reviewed, primary research studies were included. Data was manually extracted from each study on microglia parameters in various exercise animal models. Studies which only analyzed cytokines were excluded due to their possible contributions from multiple cell types. For a detailed review on how different exercise paradigms impact pro and anti-inflammatory cytokines (please see Mee-Inta et al., 2019). Cytokines were included as a parameter measured if the study measured cytokines from isolated hippocampal microglial or in conjunction with other microglial parameters. Phenotypic parameters encompass measurements of microglia expression of different markers and molecules, including, but not limited to cluster of differentiation 68 (CD68), C-X3-C motif chemokine receptor 1 (CX3CR1), cluster of differentiation 86 (CD86), major histocompatibility complex class 2 (MHCII), insulin-like growth factor 1 (IGF-1), brain-derived neurotrophic factor (BDNF), Complement C1q A Chain (C1QA), mannose receptor (CD206), and galectin-3 (Gal-3). Studies were excluded if they were not available in English, did not use animal models, did not directly measure microglia parameters, or did not include an exercise intervention (**Supplementary Figure 1**). Studies using the types of exercise described in **Figure 2E** were included in this review, which led to the exclusion of one study using "foraging exercise." All studies included in this review and their information is reported in **Supplementary Table 1**.

Physical exercise and microglial activity

There is a clear increase in interest in the effects of physical exercise on microglial function, with more studies being published over time which examine microglial functions in response to physical exercise (**Figure 2A**). Of these studies, the majority used male mice (66.9%), and fewer used females (20.4%). A small percent of studies examined both males and females (7%; **Figure 2B**). Studies in humans have demonstrated sex-differences in sensitivity to exercise, with women showing smaller BDNF changes after exercise on average (Szuhany et al., 2015), highlighting the necessity to use both sexes in animal studies. Furthermore, as microglia phenotypes are sex-dependent (Guneykaya et al., 2018; Ochocka and Kaminska, 2021), there is a clear need for more studies which directly compare male and female responses to physical exercise. Most studies used mouse models (**Figure 2B**), and while many different brain regions were examined, the hippocampus was the most frequently studied brain area (**Figure 2C**). As microglia are regionally heterogenous and exhibit functional differences in different regions (Tan et al., 2020; Ochocka and Kaminska, 2021), it is important for studies to perform regional comparisons in the future. Various microglial parameters were assessed, with most studies examining cell number, phenotype, and morphology (**Figure 2D**). Surprisingly, few have explored how exercise may influence microglia dynamic activities, such as process motility and surveying capacity or soma translocation (**Figure 2D**). When examining the different types of exercise implemented, the majority used treadmill running, a running wheel, and swimming (**Figure 2E**). Additionally, different durations of physical exercise were used, where most animals underwent 1 to 2 months of exercise (**Figure 2F**). Lastly, most studies examined the effects of physical exercise in models of neurodegeneration, followed by stroke, and aging (**Figure 2G**).

Physical exercise and microglia in the healthy brain

In the healthy brain, exercise can improve cognitive function in both humans (Colcombe and Kramer, 2003; Angevaren et al., 2008; Hamer et al., 2018; Cheval et al., 2023; James et al., 2023) and rodents (van Praag et al., 1999a,b). Understanding how exercise modulates microglia activity in the healthy brain could provide insight into the mechanisms behind the positive benefits of exercise, as microglia play important roles in circuit maturation

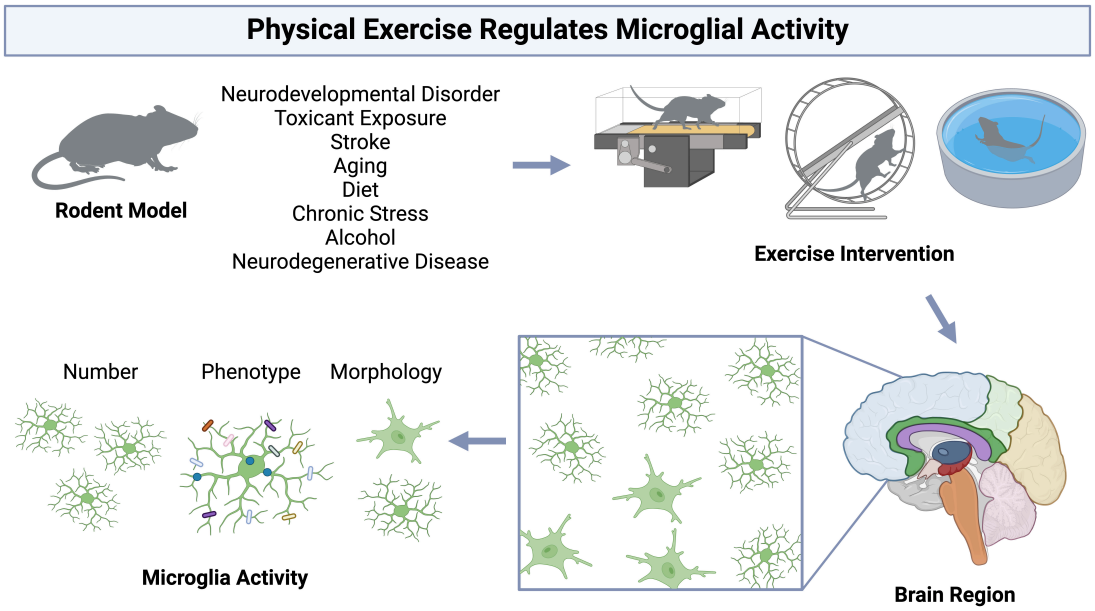

FIGURE 1
Physical exercise regulates microglia activity in rodent models. Figure made with Biorender.com.

and synaptic remodeling in different brain areas (Wake et al., 2009; Tremblay et al., 2010; Paolicelli et al., 2011; Nebeling et al., 2023). There are a limited number of investigations into how exercise may regulate microglia activity exclusively under healthy conditions using rodent models (**Figure 3A**). Males were most frequently used in experiments, with half as many studies employing both males and females (**Figure 3B**). Mouse models were more commonly employed compared to rat models, with C57BL/6 mice being the most utilized strain (**Figure 3B**). Most studies examined the hippocampus (<60%, **Figure 3C**), highlighting a gap in studies examining exercise regulation of microglia in a healthy setting in other brain areas, such as the cerebellum. Studies measured microglial parameters including number, proliferation, phenotype, morphology, cytokines, dynamics, and area (**Figure 3D**). Most used a running wheel for exercise (**Figure 3E**) and animals underwent exercise for either 1-2 or 3-4 weeks (**Figure 3F**). In healthy rats and mice, increased microglial numbers have been reported in the hippocampus (Xu et al., 2016; Sun et al., 2017) and hypothalamus (Soch et al., 2016). In healthy mice, 10 days of voluntary wheel running (VWR) can change microglial proliferation within specific brain areas, with increased proliferation reported in several cortical layers and the hippocampus (Ehninger and Kempermann, 2003; Olah et al., 2009; Ehninger et al., 2011). Despite this increase in proliferation, no changes in morphology were observed (Olah et al., 2009). However, longer durations of VWR can induce changes in the hippocampal microglial phenotype (alterations in CD86/MHCII+, mammalian target of rapamycin (mTOR), CX3CR1 expression) in a healthy setting (Kohman et al., 2013; Lloyd et al., 2017; Williams et al., 2023). Until recently, the effects of exercise on the normal basal surveillance carried out by microglial processes had not been examined. In recent a study, we found one month of VWR did not have effects on primary somatosensory cortical (S1) microglial number, morphology, or dynamics in healthy male or female mice (Strohm et al., 2024). However, it is possible that other forms of exercise, such as treadmill running, or longer durations of exercise could impact microglial dynamics. It is also possible that microglial dynamics are more sensitive to exercise in other brain areas, such as the hippocampus. Of note, hippocampal microglial process dynamics can be regulated by BNDF (Onodera et al., 2021), which is increased with exercise (see below). This was demonstrated by Onodera et al. who observed increases in hippocampal microglial process motility and engulfment of mossy fibers when BDNF was pharmacologically blocked in hippocampal slices (Onodera et al., 2021). Whether exercise is sufficient to alter microglial dynamics in the hippocampus through changes in BDNF remain to be determined. A comprehensive study of different PE paradigms may provide insight into the regional and sex- dependent effects of exercise microglia in healthy settings. Hence, further research is required to draw conclusions regarding the capacity of physical exercise to regulate microglia activity under healthy conditions and the consequences of exercise-induced microglial changes on circuit maintenance.

Physical exercise and microglia in neurodevelopmental models

Microglial play crucial roles in neurodevelopment, engaging in synaptic pruning, regulating neuronal viability and migration, as well as axonal sprouting (Paolicelli and Ferretti, 2017). Dysregulation of their activity is thought to contribute to the pathology of neurodevelopmental disorders. Recent meta-analyses show that physical exercise can improve executive function in children with atypical neurodevelopment (Shi et al., 2024) and reduce social disorders as well as repetitive behaviors in children with autism spectrum disorder (Wang S. et al., 2023). A modest

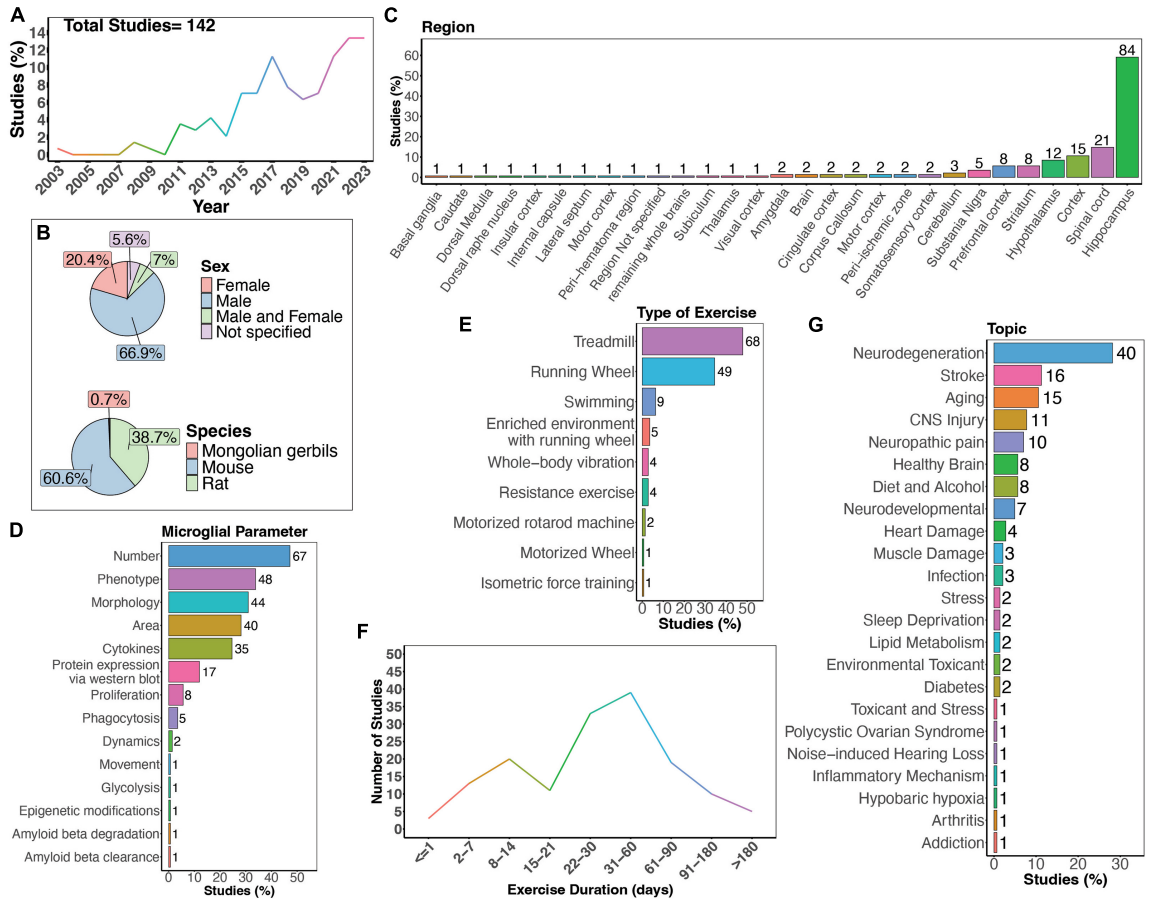

FIGURE 2
Summary of physical exercise and microglia activity. **(A)** Percent of studies published each year within the scope of this review. Total number of studies included in review = 142. **(B)** Percent of studies utilizing male, female, or both sexes (top) and species used (bottom). **(C)** Percent of studies which examine microglia in the brain regions shown. **(D)** Percent of studies which measured microglia parameters shown. **(E)** Percent of studies utilizing different types of exercise paradigms. **(F)** Number of studies implementing exercise paradigms of various durations. **(G)** Percent of studies published on each topic shown. Numbers of studies are included next to the bars for percentage plots. For **(C–E)**, percentages exceed 100% as some studies measured more than one microglial parameter, examined more than one brain region, or implemented more than one form of exercise.

number of studies have sought to understand how PE may regulate microglial function during the progression of neurodevelopmental disorders using rodent models (**Figures 4A,B**). Most of these studies have focused on neurodevelopmental outcomes in males (**Figure 4C**, 57.1%), with Wistar rats being the most utilized strain (**Figure 4C**). Most studies measured microglial parameters in the hippocampus, followed by the cerebellum (**Figures 4D, E**). Exercise inventions were conducted using running wheels, treadmills, or swimming (**Figure 4F**). Interestingly, Shariat et al. (2024) showed that aquatic exercises are effective at improving motor and social skills in children with neurodevelopmental disorders, making the effects of swimming intervention on microglial activity of interest. One study investigated the effectiveness of a swimming intervention in a mouse model of prenatal Zika virus exposure, finding swimming exercise during ZIKA exposure during pregnancy prevented behavioral defects, brain atrophy, and microglial reactivity in the hippocampus (De Sousa et al., 2022). Most studies implemented exercise protocols for 1 month (**Figure 4G**), although one study utilized a 12-day exercise regimen (Gursky et al., 2020) and two implemented exercise protocols for approximately 2 months (Vetreno et al., 2017; Guo et al., 2022).

Physical exercise and microglia in fetal alcohol spectrum disorders

There is evidence suggesting that exercise may offer benefits to children with fetal alcohol spectrum disorders (FASD), as improvements in executive function have been observed following exercise intervention, persisting for up to 3 months post-intervention (Pritchard Orr et al., 2018). Microglia have been suggested to play a role in FASD pathology although this is still under active investigation. In mice, microglia dynamics appear to be minimally affected in both the cortex (Wong et al., 2021) and lobule 4/5 of the cerebellum (Cealie et al., 2023) in a third-trimester equivalent mouse alcohol exposure model of FASD. However, Gursky et al. showed that a similar alcohol exposure increased microglial density and reduced ramification in lobules 1-4 of the cerebellum. Additionally, alcohol-exposed mice exercising for 12 days had decreased microglial density and increased number of ameboid microglia in lobules 1-4 of the cerebellum (Gursky et al., 2020), demonstrating the potential for exercise to reverse some microglial effects in models of alcohol exposure. Furthermore,

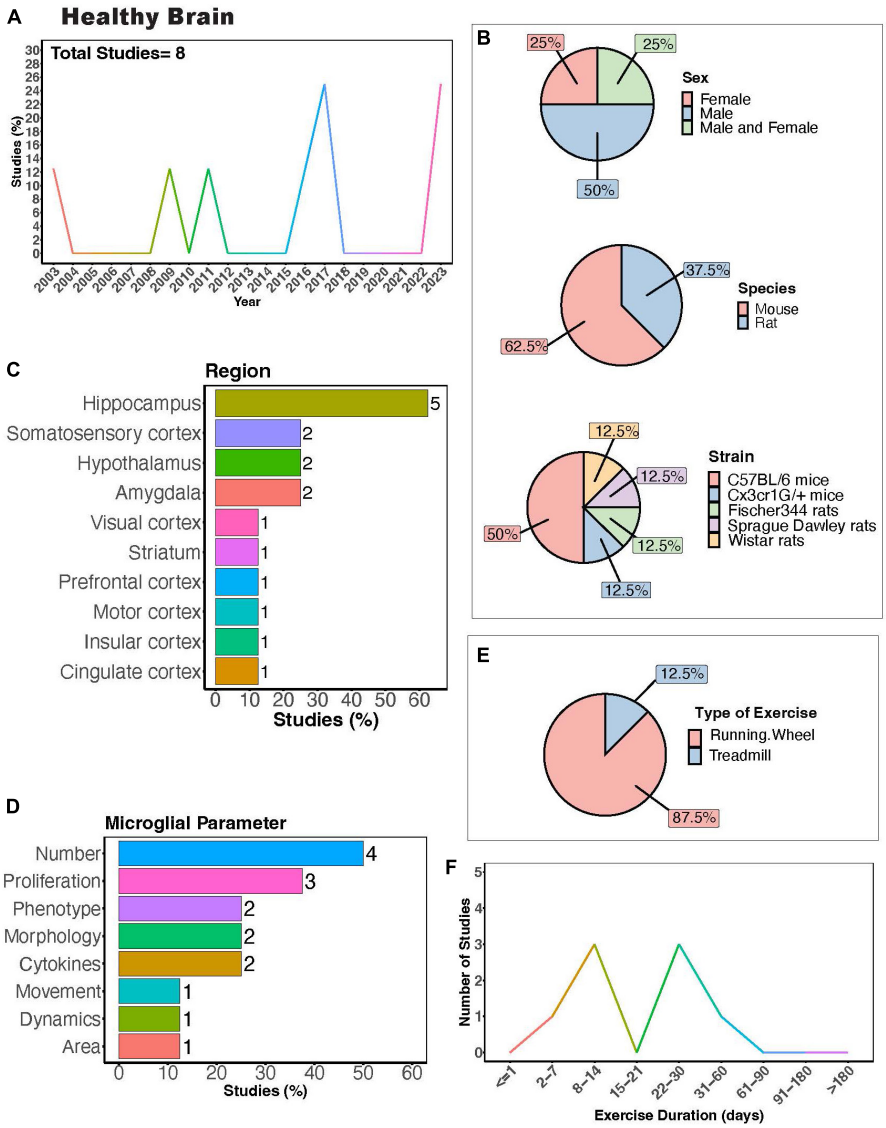

FIGURE 3
Physical exercise and microglia in the healthy brain. **(A)** Percent of studies published each year examining effects of physical exercise on microglia in a healthy setting. Total number of studies = 8. **(B)** Percent of studies utilizing male, female, or both sexes (top), various species (middle), and strain (bottom). **(C)** Percent of studies which examine microglia in the brain regions shown. **(D)** Percent of studies which measured microglia parameters shown. **(E)** Percent of studies utilizing running wheel or treadmill exercise. **(F)** Number of studies implementing exercise paradigms of various durations. Numbers of studies are included next to the bars for percentage plots. For **(C,D)**, percentages exceed 100% as some studies measured more than one microglial parameter or examined more than one brain region.

exercising for 2 months can counteract adolescent intermittent alcohol exposure-induced increases in microglial number (Vetreno et al., 2017), morphological activation (Guo et al., 2022), and pro-inflammatory cytokine production (Guo et al., 2022). Further studies on how PE may regulate microglial function in FASD models could help uncover the therapeutic potential of exercise in FASD.

Physical exercise and microglia in other models of neurodevelopmental disorders

Other rodent models of neurodevelopmental disorders have studied exercise effects on microglia, including developmental valproic acid exposure, cyclin-dependent kinase-like 5-deficiency disorder, and maternal immune activation (**Figure 4B**). In a developmental valproic acid exposure model, Cho et al. (2016) found that treadmill exercise after birth for 1 month ameliorated motor dysfunction and inhibited microglial reactivity in the cerebellum. In a mouse model of cyclin-dependent kinase-like 5-deficiency disorder—a developmental encephalopathy resulting from genetic mutations in the CDKL5 gene—VWR for 1 month in adulthood improved behavioral outcomes and neurogenesis, while also preventing increases in microglial density and cell body size (Mottolese et al., 2023). Furthermore, Andoh et al. (2019) found that VWR in adulthood could reverse behavioral and synaptic deficits in offspring after maternal immune activation, probably by enhancing microglial pruning in the hippocampus.

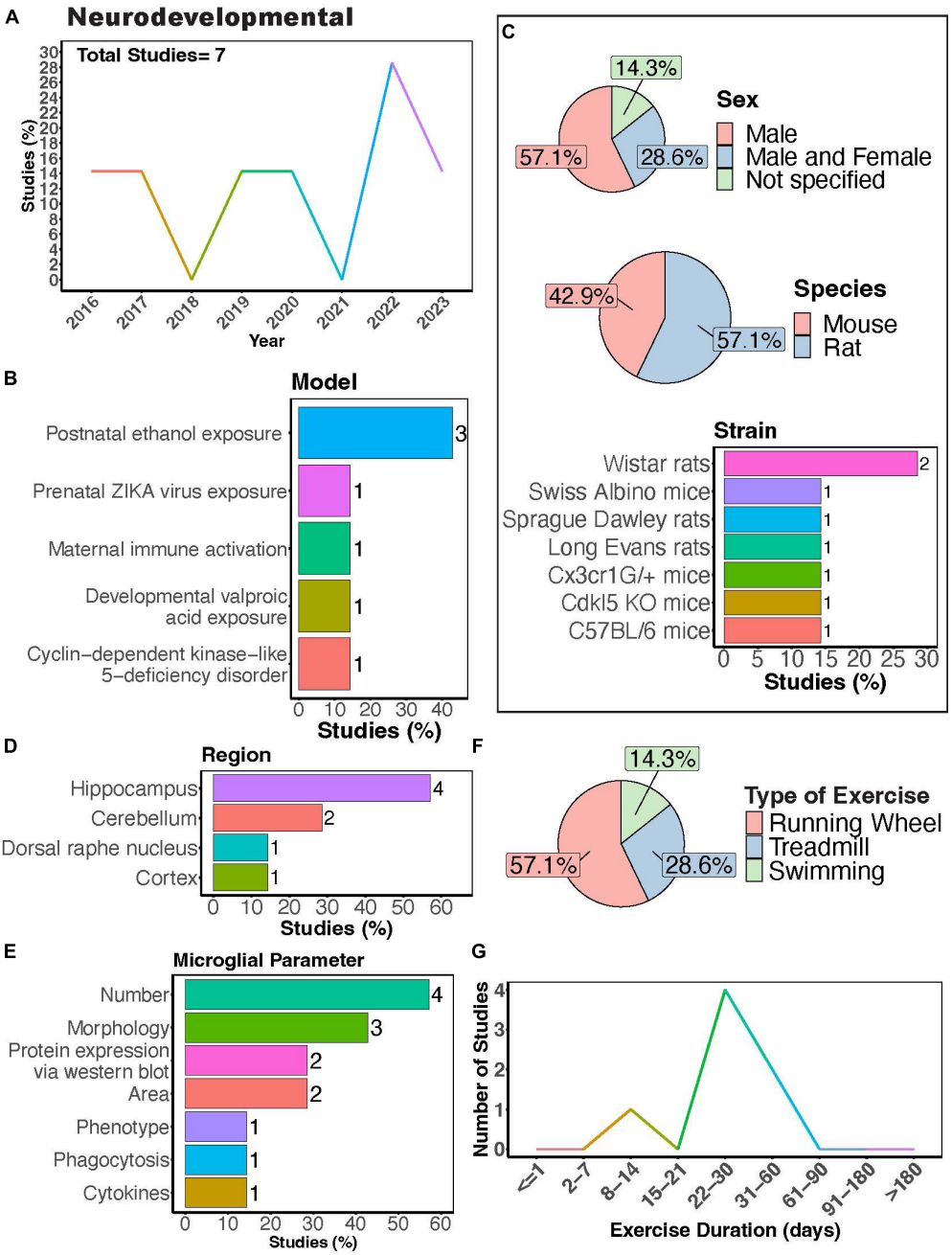

FIGURE 4
Physical exercise and microglia in neurodevelopmental models. **(A)** Percent studies published by year examining effects of physical exercise on microglia in neurodevelopmental models. Total number of studies = 7. **(B)** Percent of studies using various neurodevelopmental models. **(C)** Percent of studies utilizing male, female, or both sexes (top), various species (middle), and strains (bottom). **(D)** Percent of studies which examine microglia in the brain regions shown. **(E)** Percent of studies which measured microglia parameters shown. **(F)** Percent of studies utilizing different types of exercise paradigms. **(G)** Number of studies implementing exercise paradigms of various durations. Numbers of studies are included next to the bars for percentage plots. For **(C–E)**, percentages exceed 100% as some studies used multiple strains, measured more than one microglial parameter, or examined more than one brain region.

These changes were observed in the absence of changes in the density of microglia or CD68 volume. This highlights the ability of exercise to stimulate microglial phagocytic activity, which could be beneficial in neurodevelopmental diseases where microglia fail to prune synapses. Together these studies provide evidence that exercise may be beneficial in counteracting changes in microglia function associated with neurodevelopmental deficiencies.

Novel avenues to explore the role of physical exercise in neurodevelopmental models

There are several other mouse models of autism that could also been used to test the effects of physical activity on microglial function. It would be interesting to test whether exercise

intervention in adulthood would also be useful in the Neuroligin-3 ($NL3^{R451C}$) mouse model of autism, where microglial density, morphology and injury response has been shown to be altered (Matta et al., 2020; Guneykaya et al., 2023). It may also be interesting to test the effectiveness of exercise intervention in multiple ankyrin repeat domains 3 (Shank3) mutant mice, which model autism spectrum disorder, Phelan-McDermid Syndrome, and schizophrenia. Shank3 is an abundant excitatory post-synaptic scaffolding protein and mutant mice show synaptic and behavioral deficits. Microglia exhibit a sex specific expression of Shank 3, with lower expression in male microglia compared to female microglia (Villa et al., 2018). Microglia morphology and density are reported to be unaltered in adult Shank3 mutant mice (Cope et al., 2016). However, a newer report shows changes in transcriptomic expression of microglial genes in several regions between juvenile and adult Shank3 mutant mice (Yoo et al., 2022). It is therefore possible that microglia may have altered functions at different developmental stages in this model. Whether physical activity could counter some of these microglial changes in these models have not yet been tested.

It is also possible that the benefits of exercise could extend to other neurodevelopmental diseases, such as fragile X syndrome. Fragile X syndrome is the most common cause of inherited intellectual disability caused by hypermethylation of the Fmr1 gene, which impairs translation of Fragile X messenger ribonucleoprotein 1 protein (FMRP). Exercise can regulate FMRP expression in wild type mice (Yan et al., 2023) and stimulate hippocampal neurogenesis in FMRP-/- mice (Pinar et al., 2018). However, no studies have reported the effects of exercise on microglia activity in a mouse model of fragile X. Moreover, exercise may serve as a beneficial intervention for Rhett syndrome, a severe disorder that is caused by the loss of function of X-linked methyl-CpG-binding protein 2 (Mecp2). In humans, some reports suggest treadmill walking may benefit females with Rett syndrome (Larsson et al., 2018; Stahlhut et al., 2020). These results are mirrored in mouse models of Rhett syndrome, where forced exercise improved coordination and anxiety in Mecp2-null mice (Yue et al., 2021). Microglia have been implicated in the pathogenesis of Rett syndrome in MECP2-null mice both in the early (Zhao et al., 2017) and end stages of the disease (Schafer et al., 2016). Therefore, testing different durations and timing of exercise intervention in this model could help uncover whether benefits of exercise may be tied to changes in microglial activity. Altogether, knowledge on the effects of physical activity in neurodevelopmental model remain limited and there is great opportunity for further research.

Physical exercise regulates microglia during aging

As the population continues to age, understanding how PE may regulate microglia during aging holds significant value. In elderly humans, increasing evidence indicates that higher levels of PE can regulate microglial morphology, potentially predicting changes in synaptic protein expression or cognitive function (Casaletto et al., 2022). There is a consensus that cognitive function declines without widespread neuronal loss during healthy aging (Gómez-Isla et al., 1996; Freeman et al., 2008), contrasting observations in neurodegenerative diseases where cognitive deficits are associated with synaptic loss and abnormalities. In congruence with this, microglial phenotypes observed in aging are thought to be distinct from those seen in neurodegenerative diseases. In the aging rodent brain, microglia become "primed" with an exaggerated inflammatory response (Perry and Holmes, 2014) and shift to more pro-inflammatory phenotype characterized by increases in MHCII, CD68, CD86, and complement receptor 3 (CR3) expression (Perry et al., 1993; Kohman et al., 2013; Giorgetti et al., 2019), rendering them more sensitive to insults or stimuli. An example of this "primed" response to insult was demonstrated in stroke models, where aged microglia exhibited distinct differences in expression of interferon regulatory factors 4 and 5 *in vivo* (Ngwa et al., 2022) and enhanced phagocytosis capacity and more cytoplasmic inclusions *in vitro* (Ngwa et al., 2021) following stroke. Furthermore, microglia in aged mice exhibit differences in morphology and number compared to adult mice, mirroring changes observed in post-mortem human samples (Davies et al., 2017; Edler et al., 2021). Generally, microglia display less ramified processes with increased cell soma size with age (Perry et al., 1993; Hefendehl et al., 2014; Davies et al., 2017; Tejera et al., 2019). Such decreases in microglial process ramification have been reported in multiple brain regions with age, including the cortex (Hefendehl et al., 2014; Davies et al., 2017; Tejera et al., 2019), hippocampus (Aires et al., 2021), and retina (Damani et al., 2011; Choi et al., 2022). Changes in microglia numbers and distribution with age are conflicting, with some studies reporting increases in microglia density in the hippocampus (Mouton et al., 2002), cortex (Tremblay et al., 2012) and retina (Damani et al., 2011), while others report no differences (Long et al., 1998; Choi et al., 2022), and some show decreases (Hayakawa et al., 2007; Adachi et al., 2010). In the spinal cord, the overall microglial cell area was increased in aged mice with a non-significant trend toward increased cell numbers (Giorgetti et al., 2019). The substantia nigra follows a similar trend, with age-related increases in microglial area and number (Wang T. F. et al., 2022). Microglial dynamics also change with age and by region. In the cortex, microglia process motility decreases with age, while soma movement increases (Hefendehl et al., 2014). Similar age-related decreases in microglial motility have been observed in the retina (Damani et al., 2011). In the hippocampus, microglia process surveillance decreases in aged mice, with no alterations in motility (Aires et al., 2021). Overall, there is strong evidence that aged microglia function differently than younger microglia, and regulating or preventing some of these morphological, dynamic, and phenotypic changes could be used in the treatment of age-related neurocognitive diseases.

The interest in understanding how PE can regulate microglial activity during aging has remained relatively steady (**Figure 5A**). Many studies exclusively used males (**Figure 5B**, > 65%), again underscoring the necessity for more research including females. Among these studies, the majority employed mouse models, with C57BL/6 mice being the most utilized strain (**Figure 5B**). The overwhelming majority of studies investigated microglial parameters in the hippocampus (**Figure 5C**, > 70%), highlighting a significant gap in our understanding of how exercise may modulate aged microglial activity in other brain regions (**Figures 5C,D**). Most studies utilized a running wheel as the form of exercise, where most subjects underwent exercise for a duration of 1–2 months (**Figures 5E,F**). PE can regulate the phenotype of microglia in

aged mice across various brain regions, including the spinal cord, hippocampus, and cortex (Kohman et al., 2012, 2013; Littlefield et al., 2015; Soto et al., 2015; Giorgetti et al., 2019; Mela et al., 2020). These changes encompass decreased expression of activation markers such as CD86 and MHC II (Kohman et al., 2013) as well as components of the complement pathway (Soto et al., 2015), alongside increased expression of neurotrophic factors like IGF-1 and BDNF in aged microglia (Kohman et al., 2012; Littlefield et al., 2015). Furthermore, exercise can modulate age-related changes in inflammation (interleukin 1- beta (IL-1β)) and signs of senescence (as evidenced by expression of β-Galactosidase and $p16^{INK4A}$) (Mela et al., 2020). Additionally, Mela et al. (2020) found that microglia isolated from aged mice that exercised exhibited altered phagocytic capacity and reduced glycolysis. In aged mice, longer durations of physical exercise ranging from 5 weeks to 6 months consistently reduce numbers of microglia in the hippocampus (Kohman et al., 2012, 2013; Littlefield et al., 2015; He et al., 2017), cortex (Soto et al., 2015; He et al., 2017), and substantia nigra (Wang T. F. et al., 2022). However, two studies implementing an exercise duration of 4 weeks reported no changes in microglial numbers in the hippocampus of aged mice (Vukovic et al., 2012; Singhal et al., 2021). Collectively, these findings indicate a strong effect of exercise on microglial function during aging. Whether exercise can mitigate age-induced changes in microglial soma and process dynamics remains to be determined.

Moreover, exercise has been demonstrated to regulate microglial responses to secondary insults in aged rodents. For instance, exercise prevented *E. coli* infection-induced inflammatory cytokine production and age-related priming in rats (Barrientos et al., 2011). Littlefield et al. found exercise increased the proportion of BDNF+/ ionized calcium-binding adapter molecule 1 (Iba1)+ cells in the hippocampus of aged mice, even in mice subjected to LPS administration (Littlefield et al., 2015). This suggests strong beneficial effects of exercise even in the presence of secondary injury. Microglial morphology has also been shown to be influenced by interactions between age, enriched environments containing running wheels, and Piry viral infection (de Sousa et al., 2015). However, some reports show aged microglia have a dampened injury response to laser ablation in the cortex (Hefendehl et al., 2014; Brawek et al., 2021) and retina (Damani et al., 2011), implying that a decreased response to injury might contribute to exacerbated pathology as individuals age. Whether exercise can ameliorate these differential responses of microglia to different insults with age should be examined.

Physical exercise regulates microglia in neurodegenerative models

Microglia are pivotal in both the development and progression of neurodegenerative disease. When in a reactive state, microglia aid in clearing debris, phagocytose and eliminate protein aggregates, and offer neurotrophic support. Dysfunction in these processes can lead to the accumulation of toxic protein aggregates, further exacerbating neurodegeneration. However, prolonged activation of microglia can trigger chronic neuroinflammation, marked by the release of pro-inflammatory cytokines and reactive oxygen species, thereby promoting neurodegeneration. Notably, "reactive," ameboid microglia have been observed in tissue from human patients with many neurodegenerative diseases (McGeer et al., 1988), including Huntington's disease (HD) (Vonsattel et al., 1985; Sapp et al., 2001), amyotrophic lateral sclerosis (ALS) (Brettschneider et al., 2012; Dols-Icardo et al., 2020), Alzheimer's disease (AD) (Itagaki et al., 1989; Davies et al., 2017; Paasila et al., 2019; Franco-Bocanegra et al., 2021), Multiple sclerosis (MS) (Prineas et al., 2001; van Horssen et al., 2012; Singh et al., 2013; Kuhlmann et al., 2017), and Parkinson's disease (PD) (Knott et al., 1999; Imamura et al., 2003). There has been a growing interest in understanding how PE may influence the activity of microglia in neurodegenerative diseases (**Figure 6A**). The effects of PE on microglia activity are well-studied in the context of neurodegeneration, particularly in rodent models of MS, AD and PD (**Figure 6B**). The majority of studies primarily used male mice (**Figure 6C**, 75%), which poses a problem considering that several neurodegenerative diseases, such as AD and MS, exhibit higher prevalence in females compared to males (Cao et al., 2020; Walton et al., 2020). Possible explanations for the higher experimental usage of males compared to females include historical sex-bias toward male animals in research, variability in experimental results due to the estrous cycle in females, and limited availability of transgenic models of both sexes. Most of these studies used mouse models (**Figure 6C**, 85%) employing various strains to model different neurodegenerative diseases and processes (**Figure 6C**). Although various brain regions have been investigated, most studies assessed microglial parameters in the hippocampus (**Figures 6D, E**, 75%). Treadmill exercise was predominantly employed (**Figure 6F**, 50%), closely followed by running wheels (**Figure 6F**, 30%). Additionally, most studies implemented exercise protocols lasting between 3 weeks and 6 months (**Figure 6G**).

Physical exercise and microglia in Alzheimer's disease

AD is the most common form of dementia, estimated to account for 60–70% of cases, and is characterized by tau and amyloid pathology leading to substantial cognitive impairment (World Health Organization, 2023). However, it is important to note that there are individuals with neuropathological features of AD that do not develop cognitive deficits (Bjorklund et al., 2012). In the case of AD, there is substantial evidence showing PE can exert beneficial effects on cognitive function (López-Ortiz et al., 2023). A recent systematic review of 21 studies showed exercise was associated with a lower risk of AD in humans (López-Ortiz et al., 2023). Physical exercise can also increase network connectivity in humans with mild cognitive impairment (Won et al., 2023). While numerous animal models of AD exist, no model recapitulates all aspects of AD pathology seen in humans. AD animal models commonly utilize mutations in genes related to amyloid beta [amyloid protein precursor (APP), presenilin-1 (PSEN1), presenilin-2 (PSEN2)] and tau [microtubule-associated protein tau (MAPT)] processing, which lead to the formation of plaques and neurofibrillary tangles (Sanchez-Varo et al., 2022; Yokoyama et al., 2022). The predominant strain utilized to study the impact of physical exercise on microglia in AD in animals is

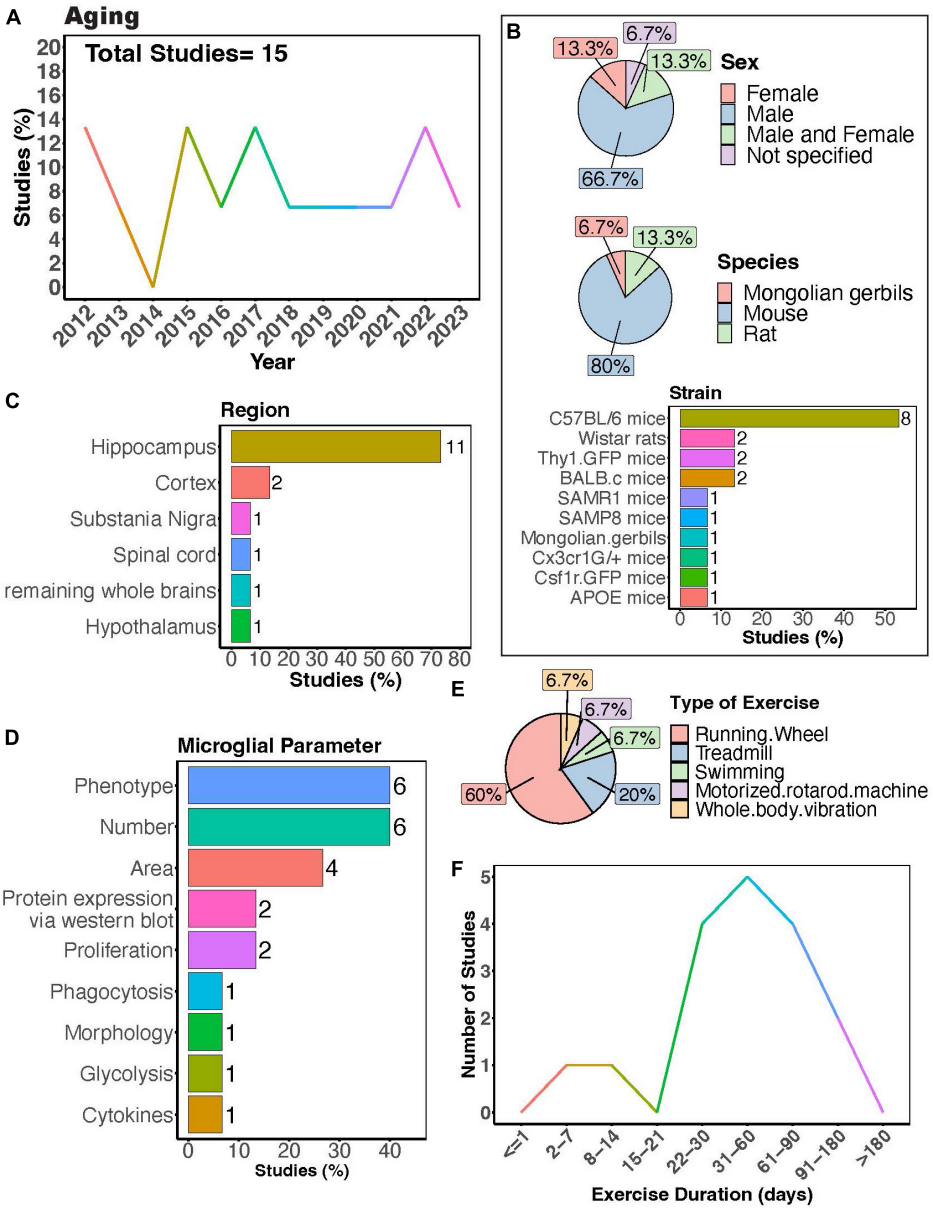

FIGURE 5
Physical exercise regulates microglia during aging. **(A)** Percent studies published by year examining effects of physical exercise on microglia during aging. Total number of studies = 15. **(B)** Percent of studies utilizing male, female, or both sexes (top), various species (middle), and strains (bottom). **(C)** Percent of studies which examine microglia in the brain regions shown. **(D)** Percent of studies which measured microglia parameters shown. **(E)** Percent of studies utilizing different types of exercise paradigms. **(F)** Number of studies implementing exercise paradigms of various durations. Numbers of studies are included next to the bars for percentage plots. For **(B–D)**, percentages exceed 100% as some studies used multiple strains, measured more than one microglial parameter, or examined more than one brain region.

the APP/PS1 mouse model (Figure 6C), in which transgenic mice express human mutant APP and PS1 (Jankowsky et al., 2004). In rodent models, many studies mirror the regulatory effect of exercise on AD pathology seen in humans. Nonetheless, there are some reports that physical exercise is ineffective in regulating AD pathology in 5XFAD, APP/PS1, and Tg2576 mouse models, all characterized by the presence of plaques in the absence of tau pathology (Nichol et al., 2008; Xu et al., 2013; Zhang J. et al., 2018; Belaya et al., 2020; Svensson et al., 2020). One study using female Tg601 mice, which overexpress the wild-type human tau sequence (2N4R), showed exercise promoted neuroinflammation by increasing the number Iba1-positive microglial cells and levels of inflammatory cytokines IL-1β and IL-18 in the hippocampus (Elahi et al., 2016). In terms of specific microglial parameters, conflicting evidence exists regarding the impact of exercise on microglial numbers in AD mice. Some studies suggest that exercise leads to a decrease in microglial numbers (Ke et al., 2011; Leem et al., 2011; Rodríguez et al., 2015; Wang Y. et al., 2023; Yang et al., 2023), while others indicate an increase (Elahi et al., 2016; Xu et al., 2016; Hashiguchi et al., 2020; Zhang S. et al., 2022; Campos et al., 2023), and some findings show no significant change in microglial

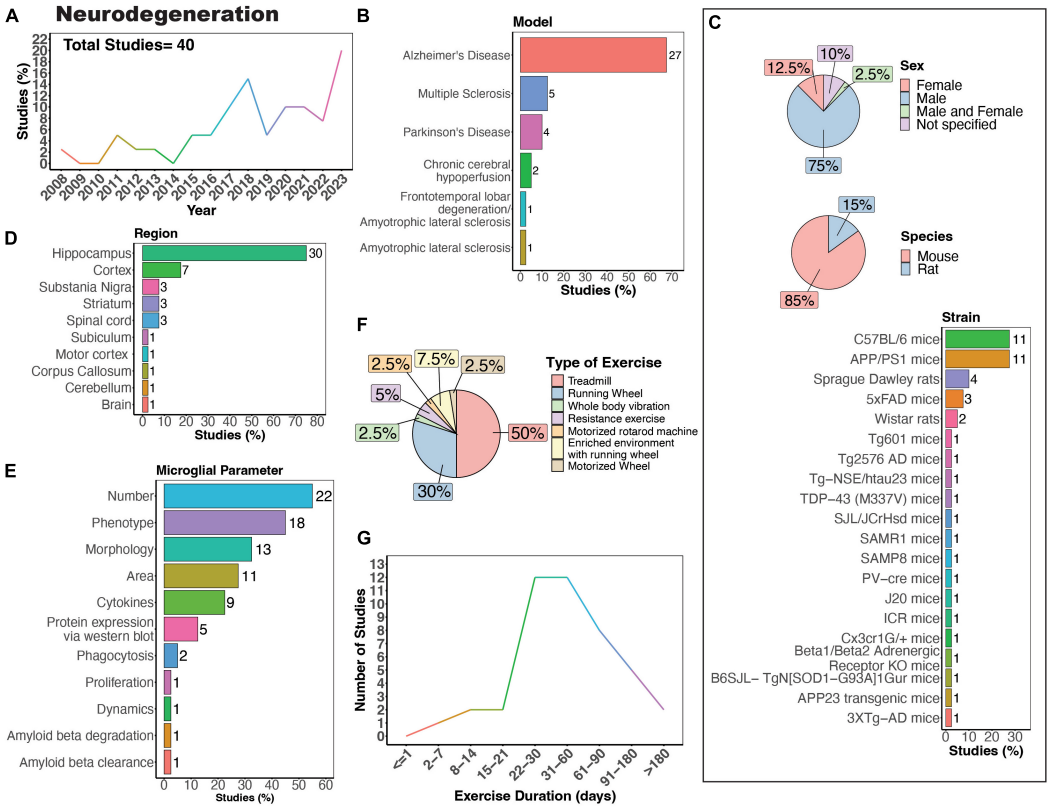

FIGURE 6
Physical exercise and microglia in neurodegenerative diseases. **(A)** Percent studies published by year examining effects of physical exercise on microglia in neurodegenerative models. Total number of studies = 40. **(B)** Percent of studies using models of various neurodegenerative diseases. **(C)** Percent of studies utilizing male, female, or both sexes (top), various species (middle), and strains (bottom). **(D)** Percent of studies which examine microglia in the brain regions shown. **(E)** Percent of studies which measured microglia parameters shown. **(F)** Percent of studies utilizing different types of exercise paradigms. **(G)** Number of studies implementing exercise paradigms of various durations. Numbers of studies are included next to the bars for percentage plots. For **(C–E)** percentages exceed 100% as some studies used multiple strains, measured more than one microglial parameter, or examined more than one brain region.

density in AD mice (Xu et al., 2018; Zhang J. et al., 2018; Ziegler-Waldkirch et al., 2018; Oroszi et al., 2023). In terms of microglial phenotype, exercise can regulate CD68+ (Ziegler-Waldkirch et al., 2018; Zhang S. et al., 2022; Oroszi et al., 2023; Wang Y. et al., 2023), CD86+ (Lu et al., 2017; Zhang et al., 2019; Feng et al., 2023; Yang et al., 2023), triggering receptor expressed on myeloid cells 2 (TREM2) (Zhang L. et al., 2022) and inflammatory molecules (Xu et al., 2016, 2018; Nakanishi et al., 2021; Han et al., 2023) in AD rodent models. Microglia morphology can also be regulated by physical exercise in AD mice, with most studies reporting that exercise reduces the numbers of reactive microglia and increases process ramification (Ke et al., 2011; Leem et al., 2011; Xiong et al., 2015; Xu et al., 2016; Lu et al., 2017; Zhang S. et al., 2022; Feng et al., 2023; Oroszi et al., 2023). However, one study utilizing 3XTg-AD mice, which exhibit plaque pathology and tau pathology at later stages, showed that 9 months of exercise increased hippocampal microglial hypertrophy (microglia surface, volume and somata volume) (Rodríguez et al., 2015), indicating prolonged exercise may have differential regulatory effects compared to exercise of shorter durations. Interestingly, no studies have examined whether physical exercise can regulate the dynamic behavior of microglia in AD models. Such studies could help further uncover mechanisms through which exercise can regulate the function of microglia in the context of neurodegeneration.

Physical exercise and microglia in multiple sclerosis

Exercising 60 min per day, 3 times or more per week, for 8–10 weeks can improve memory and cognitive function in MS patients (Li G. et al., 2023). Several rodent MS models are used to recapitulate different aspects of MS pathology. The cuprizone demyelination model is representative of the relapsing remitting form of MS present in most MS patients, whereas experimental autoimmune encephalomyelitis (EAE) is representative of chronic progressive MS (Ransohoff, 2012; Vega-Riquer et al., 2019). Demyelination, inflammation, microglial activation, astrogliosis, and behavioral disabilities are present in both cuprizone-treated and EAE mice (Ransohoff, 2012; Vega-Riquer et al., 2019). The cuprizone model, however, has a remyelination phase, whereas the EAE model consistently shows immune cell infiltration in the CNS (Ransohoff, 2012; Vega-Riquer et al., 2019). Though limited in number, studies show exercise can regulate microglia function in both cuprizone and EAE models using female mice (Mandolesi

et al., 2019; Rizzo et al., 2021; Zaychik et al., 2021). However, in male mice exercise was unable to prevent cuprizone-induced increases in hippocampal microglia number (Naghibzadeh et al., 2018), indicating potential sex-differences in the effectiveness of exercise intervention. Mifflin et al., also found no effect of exercise on microglia in males or females using an EAE model (Mifflin et al., 2017). Further experimentation using both males and females as well as multiple types and durations of exercise could help uncover the effectiveness of exercise in MS models.

Physical exercise and microglia in Parkinson's disease

PD is the second most common neurodegenerative disease in the elderly population and is characterized by the loss of dopaminergic neurons and formation of Lewy bodies (Poewe et al., 2017). The number of people with PD over age 50 is expected to double between 2006 and 2030, creating an increasing need for effective therapeutic inventions (Dorsey et al., 2007). A recent meta-analysis shows that exercising at least 60 min per day is an effective intervention for enhancing global cognitive function and executive function in PD patients (Kim et al., 2023). However, the mechanisms behind these positive effects remain to be determined. PD is commonly modeled in rodents using exposure to toxicants, such as 1-methyl-4-phenyl-1,2,3,6-tetrahydropyridine (MPTP) or Rotenone. The MPTP and rotenone exposure models both replicate many features of PD, including microglial reactivity, nigrostriatal dopaminergic degeneration, and behavioral deficits (Betarbet et al., 2000, 2006; Du et al., 2001; Sedelis et al., 2001; Zhang J. et al., 2022). However, only the Rotenone exposure model exhibits α-synuclein accumulation and aggregation with formation of Lewy body-like inclusions, mimicking human PD, and this model also shows greater microglia area and numbers in the substantia nigra than the MPTP model (Betarbet et al., 2000, 2006; Zhang J. et al., 2022). Microglia numbers are generally shown to increase in the substantia nigra of PD models, with increases in morphological and phenotypic signs of reactivity (Sung et al., 2012; Gil-Martínez et al., 2018; Lee et al., 2018; Wang W. et al., 2021). While VWR has been reported to be ineffective (Gil-Martínez et al., 2018) in PD models, treadmill exercise is successful in preventing the increase in microglial cell numbers seen in these models (Sung et al., 2012; Lee et al., 2018; Wang W. et al., 2021). One possible explanation is that treadmill running offers a more controlled environment, where researchers can precisely adjust factors such as speed, duration, and incline, which may all impact outcomes. Notably, there is a lack of information on how exercise may impact PD pathology in females, as these studies all used male mice. As women develop PD, and in fact, may experience greater disease severity (Dahodwala et al., 2016), research is needed to discern the effectiveness of exercise in female PD models.

Physical exercise and microglia in Huntington's disease

Nevertheless, PE may not be universally beneficial for all neurodegenerative diseases. HD is a genetically inherited disease caused by a mutation in the gene encoding the Huntington protein which leads to progressive cognitive decline manifesting in involuntary motor movements and its progression does not appear to be sensitive to physical exercise. A systematic review of seventeen studies in humans examining the effects of exercise and cognitive interventions found that exercise intervention may be negligible in HD, even when combined with cognitive interventions (Huynh et al., 2023). Another report showed an absence of cortical plasticity in response to an acute bout of cardiorespiratory exercise in premanifest and early HD patients (Andrews et al., 2022). Though some rodent models of HD have shown that VWR (Pang et al., 2006; van Dellen et al., 2008; Harrison et al., 2013) or treadmill exercise (Stefanko et al., 2017; Caldwell et al., 2020) can improve cognitive outcomes, in one study VWR surprisingly accelerated disease onset in male N171-82Q transgenic HD mice (Potter et al., 2010). Though microglia are believed to facilitate early neuroinflammatory processes in HD patients (Palpagama et al., 2019), clear evidence showing PE can regulate microglial function to alter the manifestation and progression of HD remains to be established, as none of these animal studies examined microglia in the context of physical activity intervention.

Physical exercise and microglia in amyotrophic lateral sclerosis

Strikingly, exercise may be harmful for some neurodegenerative diseases, as is the case for ALS. ALS is the most common motor neuron disease, and it is both rapidly progressive and fatal. A systematic review of ninety-three studies found strenuous anaerobic exercise (such as soccer, long-distance skiing and American football) was a risk factor for ALS (Chapman et al., 2023). The underlying mechanisms behind this remain elusive, though oxidative stress and dysregulated energy metabolism were highlighted as possible mediators of motor neuron stress and degeneration in ALS (Chapman et al., 2023). Microglia are linked to the development of motor neuron pathology in ALS patients (Cooper-Knock et al., 2017). In a mouse model of ALS, exercise increased microglial reactivity, shown by changes in morphology (hypertrophic, intensely stained microglia with thick and stout processes) (Kassa et al., 2017), further supporting the notion that exercise may not be beneficial in treating ALS. Nevertheless, there is some evidence suggesting that exercise can beneficially modulate microglia dynamics. Mutations in the TAR DNA binding protein 43 kDa (TDP-43) are observed in frontotemporal lobar degeneration and ALS and are thought to be partially mediated by microglia dysfunction. A recent study by Wei et al. revealed that microglia in TDP-43 mutant mice exhibited enhanced phagocytic activity and dysregulated soma and process dynamics (Wei et al., 2023). Specifically, TDP-43 induced higher soma migration distances, reduced microglial process territory, increased process velocity, and increased the fraction of retracted processes over an hour-long imaging session (Wei et al., 2023). Two weeks of treadmill exercise at the pre-symptomatic stage restored normal microglial dynamics, reduced CD68 expression, restored morphology changes, and improved motor learning of mutant TDP-43 mice (Wei et al., 2023). This demonstrates the capacity of exercise to regulate microglial dynamics and prevent cognitive dysfunction in a model

of ALS, though further research is needed to explore these effects. Determining how PE differentially regulates microglia in contexts where PE may be ineffective or harmful (HD or potentially ALS), compared to those where PE is reported to be helpful (AD, MS, PD) could provide useful insights into new therapies for neurodegenerative disorders.

Physical exercise regulates microglia function in stroke models

In humans, exercise can improve cognitive function and motor coordination among patients with cognitive impairments after stroke (Li W. et al., 2023). In stroke models, microglia play a complex role- they can promote neuroinflammation, thereby perpetuating damage, yet they can also release anti-inflammatory factors that facilitate repair (Wang Y. et al., 2022). Studies investigating how exercise can regulate microglia functions in stroke often employ animal models of cerebral ischemia, spontaneous hypertension, and intracerebral hemorrhage (ICH) (**Figures 7A,B**). Notably, a significant proportion of these studies focused solely on males (**Figure 7C**, > 80%), indicating a clear research gap concerning females. Rats were predominantly used in these studies (**Figure 7C**, > 80%), with Sprague Dawley rats being the most frequently utilized (**Figure 7C**). Microglial parameters were most frequently examined in the hippocampus, followed by the striatum and hypothalamus (**Figures 7D,E**).

Many of these investigations explored how exercise modulates microglial number and phenotype in stroke models (**Figure 7E**). Treadmill exercise has been shown to influence microglial phenotype after ischemia across various brain regions, including the striatum, corpus callosum, cortex, basal ganglia, and peri-ischemic and peri-hematoma zones (Kinoshita et al., 2021; Lu et al., 2021; Liu et al., 2022; Tamakoshi et al., 2022; Xu et al., 2023). Furthermore, a transgenerational study selecting for low capacity and high-capacity runners found male low-capacity runners had more severe ICH-induced brain injury and greater numbers of major histocompatibility complex class 2 1a (OX-6) positive microglia cells, demonstrating transgenerational regulation of microglia phenotype in a stroke model (He et al., 2013). Both treadmill and swimming exercise have been found to regulate microglial numbers in different brain regions, such as the hypothalamus, hippocampus, basal ganglia, as well as in peri-infarcted and peri-hematoma zones (Kinoshita et al., 2021; Xia et al., 2021; Aguilar-Peralta et al., 2022; Li et al., 2022). However, a single study by Svensson et al. reported no impact of exercise on hippocampal microglial number or phenotype in a cerebral ischemic stroke model (Svensson et al., 2016). Moreover, studies consistently found a decrease in microglia area with exercise intervention in stroke models (Lovatel et al., 2014; Buttler et al., 2017; Zhang et al., 2017; Zhang M. et al., 2018; Gao et al., 2022). Investigations into cytokine levels in stroke models with exercise intervention consistently report reductions in pro-inflammatory cytokines, such as tumor necrosis factor alpha (TNF-α), IL-1β, and interleukin 6 (IL-6) (Masson et al., 2015; Lu et al., 2021; Xia et al., 2021; Gao et al., 2022). Exercise also shifts microglial morphology towards a homeostatic state, characterized by increased process ramification (Li et al., 2022) and length, as well as reduced microglial cell size (Xia et al., 2021). While there are reports indicating altered microglial process motility in ischemic stroke (Morrison and Filosa, 2013), no studies have yet explored how exercise intervention might influence these dynamic properties of microglia.

Treadmill exercise was the predominantly used form of PE, with fewer studies utilizing swimming (**Figure 7F**). This highlights a knowledge gap regarding the potential of voluntary interventions, such as those employing a running wheel, to modulate microglia function. Given that VWR is perceived as less stressful and mirrors a more natural rodent behavior, delving into this paradigm is crucial. Most studies implement injury or ischemia prior to exercise intervention (**Figure 7F**), thus limiting our understanding of potential differences in responses between individuals who were previously active versus sedentary before injury. Exercise durations in these studies vary widely, ranging from 1 to approximately 90 days (**Figure 7G**). Notably, only one study implemented an exercise intervention lasting longer than 2 months. Consequently, future research is necessary to determine whether individuals who engage in regular exercise throughout their lifespan exhibit distinct responses to stroke compared to those leading predominantly sedentary lifestyles.

Exercise interacts with lifestyle factors to modulate microglial activity

It is believed that lifestyles factors, such as exercise, diet, stress, alcohol consumption, and toxicant exposure, influence brain health and cognitive function. Adopting a healthy lifestyle can play a crucial role in reducing neuroinflammation and lowering the risk of developing neurodegenerative and psychiatric disorders (Kip and Parr-Brownlie, 2023). A recent report by Dhana et al. (2024) showed that adopting a healthy lifestyle may facilitate the maintenance of cognitive abilities in older adult). In this context, a healthy lifestyle was characterized by physically activity, eating healthy (increasing green leafy vegetables, nuts, berries, beans, whole grains, seafood, poultry relative to red meats, butter, cheese, sweets, and fried food), and avoiding smoking and limiting alcohol intake (Dhana et al., 2024). How these lifestyle factors interact to influence microglial activity, which can in turn regulate neuronal health, is largely unknown.

In recent years, interest in the influence of physical exercise on microglial activity in the context of diet, alcohol, stress, and toxicant exposure has grown (**Figure 8A**). Numerous studies have investigated how physical exercise regulates microglial activity in rodent models of toxicant exposure (Valdez et al., 2020; Kodali et al., 2021; Wang J. et al., 2021), binge alcohol exposure (Barton et al., 2017a,b; West et al., 2019), diet (Yi et al., 2012; Lima et al., 2014; Yoo et al., 2015; Kang et al., 2016; Yin et al., 2018; Klein et al., 2019; Lang et al., 2020), and chronic stress (Gerecke et al., 2013; Xiao et al., 2021; **Figure 8B**). Most of these studies primarily used male subjects, though females were examined more often than in studies that focused on disease outcomes (**Figure 8C**). Many investigations utilized rat models (**Figure 8C**, 60%), with Long-Evans rats and C57BL/6 mice being the most common strains (**Figure 8C**). Most studies focused on evaluating microglial

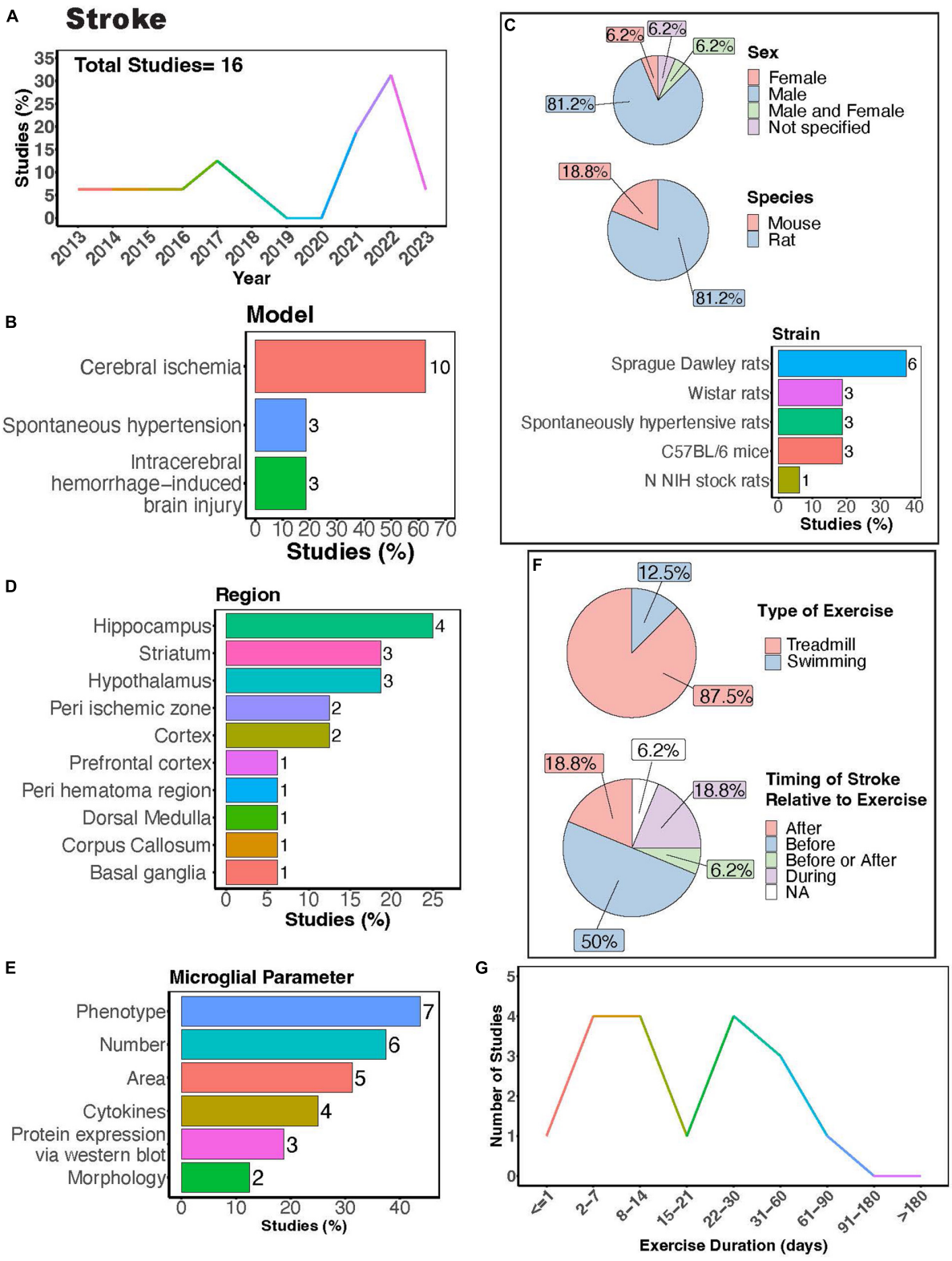

FIGURE 7
Physical exercise regulates microglia in stroke models. **(A)** Percent studies published by year examining effects of physical exercise on microglia in stroke models. Total number of studies = 16. **(B)** Percent of studies using different stroke models. **(C)** Percent of studies utilizing male, female, or both sexes (top), various species (middle), and strain (bottom). **(D)** Percent of studies which examine microglia in the brain regions shown. **(E)** Percent of studies which measured microglia parameters shown. **(F)** Percent of studies utilizing treadmill or swimming exercise (top) and the timing of stroke relative to exercise intervention (before, after, before or after, during, not specified; bottom). Studies where exercise intervention occurs "during" stroke utilized spontaneous hypertensive rats, which exhibit genetically induced increased blood pressure and as such the "stroke" occurred "during" the exercise intervention **(F)**. **(G)** Number of studies implementing exercise paradigms of various durations. Numbers of studies are included next to the bars for percentage plots. For **(D,E)** percentages exceed 100% as some studies used measured more than one microglial parameter or examined more than one brain region.

parameters in the hippocampus (**Figures 8D, E**, 67%) and cortical areas. Exercise interventions were conducted using running wheels (**Figure 8F**, 53.3%) or treadmills (**Figure 8F**, 46.7%), and most studies implemented exercise protocols lasting between 1 and 3 months (**Figure 8G**). Additionally, it is important to consider the timing of exercise intervention relative to the dietary, alcohol, stress, or toxicant exposure. Most studies implemented exercise protocols before or during the diet, alcohol, stress, or toxicant exposure (**Figure 8F**). This reveals a scarcity of literature exploring the potential benefits of exercise intervention after exposure to stress, alcohol, dietary, or toxicants.

Rodent models investigating effects of diet and exercise on microglia activity include high-fat diet or low-fat diet (Yi et al., 2012; Kang et al., 2016; Yin et al., 2018; Klein et al., 2019), diabetes models (Yoo et al., 2015; Lang et al., 2020) as well as treatment with monosodium glutamate (Lima et al., 2014) (MSG; **Figure 8B**). Exercise can attenuate high-fat diet-induced microglial reactivity in the hypothalamus, white matter internal capsule, hippocampus, and cortex (Yi et al., 2012; Kang et al., 2016; Yin et al., 2018; Klein et al., 2019). Although no significant interaction between MSG and exercise was observed in rats, both MSG treatment and exercise increased microglial Iba1+ area in the motor cortex (Lima et al., 2014). In diabetes models, exercise reduced microglial morphological changes, their number, and pro-inflammatory cytokine production (Yoo et al., 2015; Lang et al., 2020). In models of binge alcohol exposure, there is conflicting evidence on the ability of exercise to regulate microglial numbers and morphology, with some reports showing that exercise can regulate these parameters (Barton et al., 2017b; West et al., 2019) while a study by Barton et al. showed no effects on these parameters (Barton et al., 2017a). Nonetheless, Barton et al. did show a significant interaction between binge alcohol exposure and physical exercise, with exercise increasing the number of MHC II+ microglia in female mice exposed to binge alcohol, demonstrating the ability of exercise to regulate microglial phenotype in this model (Barton et al., 2017a). Overall, these studies suggest exercise can interact with dietary exposure to influence microglial activity.

Stress is thought to play a pivotal role in both the development and maintenance of neuropsychiatric disorders like major depression, anxiety disorders, and post-traumatic stress disorder, and is often used to model these conditions in rodents. Although limited, there is evidence that physical exercise can regulate microglia activity in models of chronic stress. Exercise can protect against stress-induced increases in microglial expression of CD68 and Cyclooxygenase 2 (Cox-2), demonstrating the capacity of exercise to induce phenotypic changes in microglial response to stress (Gerecke et al., 2013; Xiao et al., 2021). Xiao et al. also found that exercise attenuated the stressed-induced increases in the number of microglia and pro-inflammatory cytokine IL-1β production in the hippocampus (Xiao et al., 2021). Together these studies suggest that exercise can alleviate stress-induced alterations in microglial function. However, stress can be induced using diverse methods, including models of social stress or non-social stress (such as chronic-restraint stress employed by Gerecke et al., 2013), administered for various durations. It remains to be determined how PE may regulate microglia in these various models of stress and whether these changes are sustained over time.

While environmental toxicants can modulate microglia activity, inducing changes in dynamics (Lowery et al., 2022) and morphology (Yi et al., 2012) indicative of classical microglial reactivity, very few studies have examined exercise regulation of microglia activity in response to toxicant exposure. The models that have include fluoride (Wang J. et al., 2021) and ozone (Valdez et al., 2020) exposure, as well as a model of Gulf war illness, which encompassed daily exposure to mosquito-repellant N, N-diethyl-m-toluamide (DEET), insecticide permethrin (PER), and nerve gas prophylactic drug pyridostigmine bromide (PB), accompanied by 15 min of restraint stress for 4 weeks (Kodali et al., 2021; **Figure 8B**). Wang J. et al. (2021) found that repeated treadmill running attenuated the morphological changes of microglia in the hippocampus of fluoride-exposed mice. Kodali et al. (2021) found that VWR reverses hippocampal microglia morphological changes in a mouse model of Gulf War illness. Both studies highlight the capability of exercise to prevent adverse effects caused by toxicant exposure. In contrast, Valdez et al. found that exercise did not prevent ozone (O3)-induced (1 ppm O3) microglial morphological changes in the hippocampus and the hypothalamus (Valdez et al., 2020). Notably, these studies were restricted to the hippocampus and hypothalamus, suggesting the necessity for exploration of other brain regions in future investigations. Future studies should also examine effects from a broader range of toxicants, considering that individuals are exposed to numerous toxic substances over the course of their lifetimes. For instance, lead (Pb) exposure is known to trigger microglial reactivity and neurological impairment (Liu et al., 2012; Wu et al., 2021; Shvachiy et al., 2023). One proposed mechanism of Pb toxicity involves the activation of nucleotide-binding oligomerization domain, leucine rich repeat and pyrin domain containing (NLRP) and the inflammasome system, an important component of the innate immune response triggered by exposure to other toxicants (Moloudizargari et al., 2019; Su et al., 2021). PE has been shown to regulate the inflammasome system and NLRP expression (Tang et al., 2022). Thus, it is possible that exercise could either prevent or attenuate some of the adverse effects on microglia activity resulting from Pb exposure or other toxicants acting through this pathway. Overall, very little is known regarding PE regulation of microglia activity relative to the vast number of toxicants known to impact brain health.

Exercise increases known modulators of microglia activity

The mechanisms by which exercise elicits microglial changes are unknown, but it is likely that microglia respond to exercise-induced alterations in signaling molecules that broadly affect the function of many brain cell types. The benefits of PE have largely been attributed to increased production of neurotropic factors and enhanced neurogenesis in the hippocampus (van Praag et al., 1999a,b; Olah et al., 2009; Szuhany et al., 2015), which are extensively reviewed elsewhere (Meeusen and De Meirleir, 1995; Vecchio et al., 2018). Interestingly, many of the neurotransmitters and neurotrophic factors that are increased or regulated during PE are known modulators of microglial activity (**Figure 9**; Vecchio et al., 2018; Albertini et al., 2020). Exercise increases neurotrophic factors in both mice and humans, including those that influence cognition such as BDNF, IGF, and nerve growth factor (NGF) (Ding et al., 2006; Arvidsson

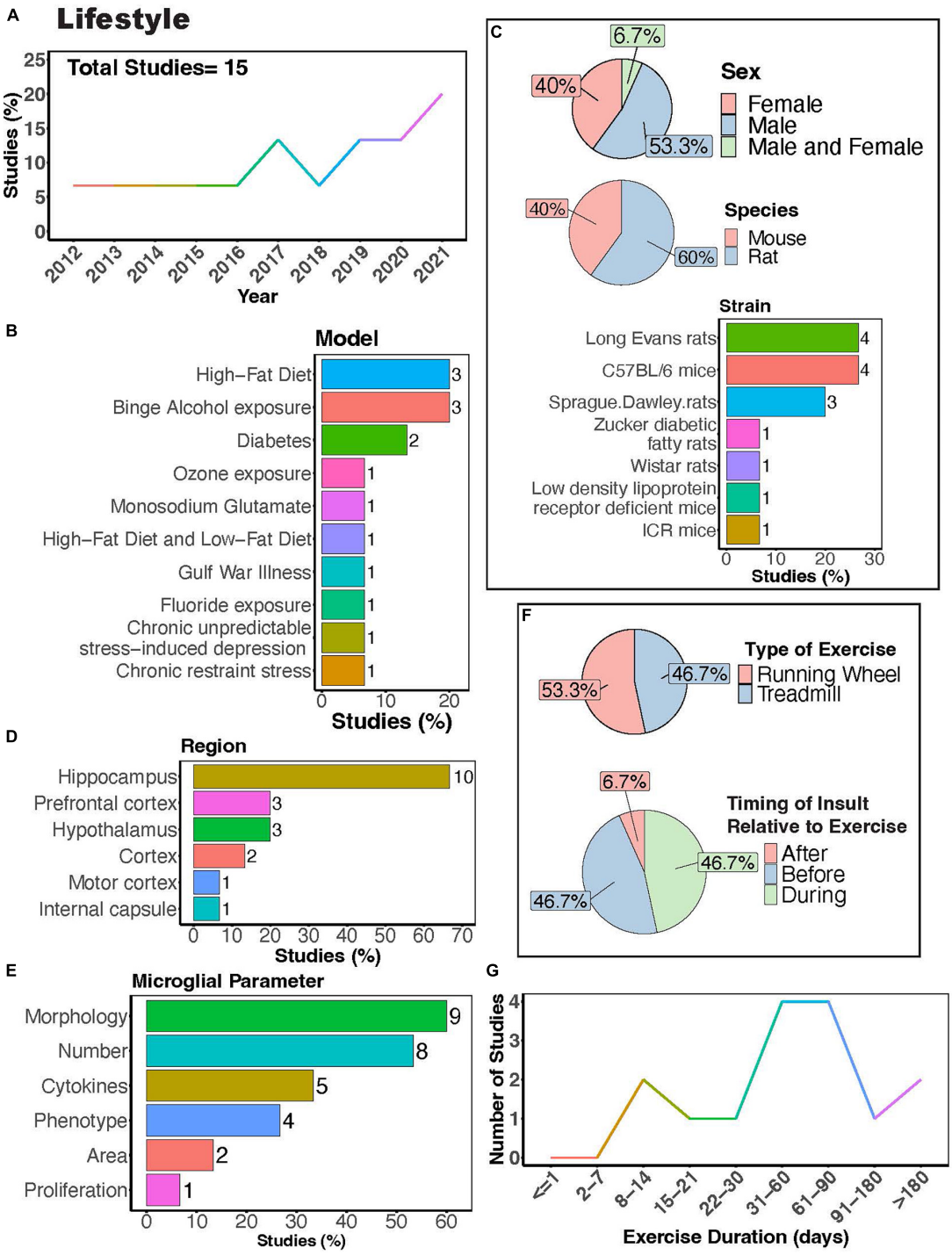

FIGURE 8
Physical exercise interacts with lifestyle factors to modulate microglial activity. **(A)** Percent studies published by year examining effects of physical exercise and lifestyle factors on microglia activity. Total number of studies = 15. **(B)** Percent of studies using different lifestyle models. **(C)** Percent of studies utilizing male, female, or both sexes (top), various species (middle), and strains (bottom). **(D)** Percent of studies which examine microglia in the brain regions shown. **(E)** Percent of studies which measured microglia parameters shown. **(F)** Percent of studies utilizing treadmill or running wheel exercise (top) and the timing of insult (stress, alcohol, environmental, dietary exposure) relative to exercise intervention (before, after, during; bottom). **(G)** Number of studies implementing exercise paradigms of various durations. Numbers of studies are included next to the bars for percentage plots. For **(D,E)** percentages exceed 100% as some studies used measured more than one microglial parameter or examined more than one brain region.

et al., 2018; Żebrowska et al., 2018; Kang et al., 2020). Increases in BDNF with exercise are detected in the hippocampus and cortex (Russo-Neustadt et al., 1999; Adlard et al., 2004; Ploughman et al., 2005; Chen and Russo-Neustadt, 2009), where BDNF can regulate microglia-neuronal interactions, thereby influencing synapse formation and removal (Parkhurst et al.,

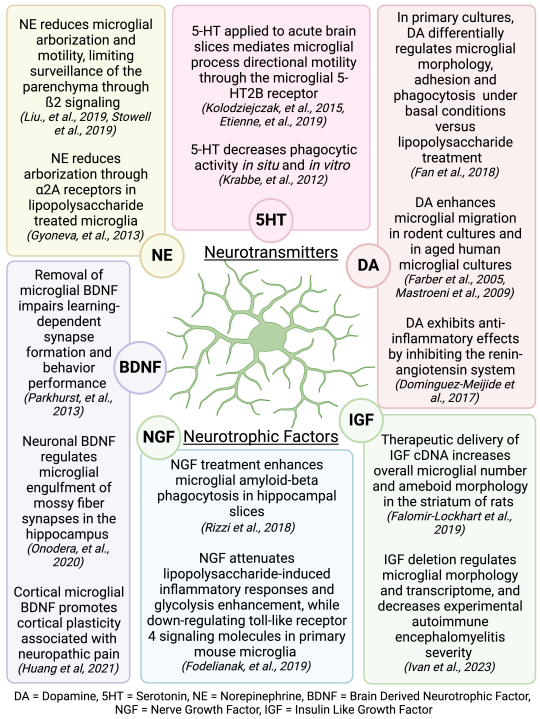

FIGURE 9
Neurotransmitters and neurotrophic factors that are increased during exercise are known regulators of microglial activity. Figure made with Biorender.com.

2013; Huang et al., 2021; Onodera et al., 2021). IGF also increases with exercise in the hippocampus, motor cortex, and striatum (Carro et al., 2000; Ploughman et al., 2005; Chang et al., 2011) and can regulate microglial number, morphology, and mRNA profile (Falomir-Lockhart et al., 2019; Ivan et al., 2023). Exercise-induced increases in NGF have been observed in the hippocampus and cortex (Neeper et al., 1996; Molteni et al., 2002), and can regulate the microglial phenotype, including phagocytic function (Rizzi et al., 2018; Fodelianaki et al., 2019). Exercise-induced increases in neurotransmitters, including norepinephrine, dopamine, and serotonin, are widespread throughout the brain (Vecchio et al., 2018). Norepinephrine regulates microglial arborization and dynamics (Gyoneva and Traynelis, 2013; Liu et al., 2019; Stowell et al., 2019), and has been shown to increase with exercise in many brain areas, including the cerebellum, striatum, hypothalamus, midbrain, cortex, spinal cord, and pons/medulla (Brown et al., 1979; Semenova et al., 1981; Meeusen and De Meirleir, 1995; Pagliari and Peyrin, 1995; Dunn et al., 1996; Dishman et al., 2000). Serotonin levels increase in the hippocampus, midbrain, hypothalamus, striatum, and cortex with exercise (Bailey et al., 1993; Gomez-Merino et al., 2001), and serotonin can regulate microglial phagocytic activity (Krabbe et al., 2012) and directional motility (Kolodziejczak et al., 2015; Etienne et al., 2019). Additionally, exercise increases dopamine in the striatum, nucleus accumbens, midbrain, hypothalamus, and hippocampus (Chaouloff et al., 1987; MacRae et al., 1987; Mathes et al., 2010) and regulates the RAS activity and levels of angiotensin receptors in microglia, resulting in an anti-inflammatory effect (Dominguez-Meijide et al., 2017). Dopamine also regulates microglia migration (Färber et al., 2005; Mastroeni et al., 2009), phagocytosis (Fan et al., 2018), and morphology (Fan et al., 2018). In summary, there is compelling evidence that exercise could regulate microglia activity through one or many of these mechanisms. However, the translatability of these effects to human and how they pertain to changes in cognition remains to be determined. In humans, there is evidence showing exercise-related changes in BDNF are associated with improved executive performance (Hwang et al., 2016). However, a recent study found cognitive improvement following resistance and aerobic exercise was not associated with peripheral biomarkers including adrenaline, noradrenaline, glucose, lactate, cortisol, IGF-1, or BDNF in humans (Ando et al., 2022). Further research is needed to tie exercise-induced changes in central or peripheral biomarkers to altered microglia activity and enhanced cognitive performance.

New frontiers for understanding how exercise regulates microglia

Numerous studies have explored how physical activity can impact microglia in various animal models, yet there are several understudied areas. Advanced *in vivo* imaging techniques allow scientists to track cellular structures over long periods of time, creating a wealth of opportunity to better understand how exercise regulates brain physiology. These methods have already been applied to track blood vessels (Cudmore et al., 2017) and dendritic spines (Chen et al., 2017) chronically over time in living mice undergoing different exercise regimens. However, knowledge regarding how exercise influences microglia dynamic functions is limited. Given the numerous neurotransmitters and neurotrophic factors that are known to regulate microglial activity (**Figure 9**), investigation of the effects of PE on microglia functions in other models is warranted. It is also possible that microglial interactions with specific components of their environment may also be changed by exercise. For example, microglia are known to make physical contacts with dendritic spines to facilitate structural plasticity and regulate neuronal health in different areas of the brain (Tremblay et al., 2010; Nebeling et al., 2023), and these interactions could be differentially regulated by physical activity. Employing reporter mice that label multiple brain structures or cells for chronic *in vivo* imaging could provide deeper insights into how exercise regulates microglial interactions with specific components of their environment over time.

Advancements in sequencing technologies also provide great potential for a comprehensive examination of microglia phenotypes. Several studies reviewed here used bulk tissue RNA sequencing to elucidate the mechanisms behind exercise effects on the brain (Wassouf et al., 2018; Wang J. et al., 2021; Yang et al., 2023). However, this methodology is limited in that it only provides average gene expression patterns across of population of heterogenous cells. However, with the emergence of single cell technologies, which allow researchers to examine changes in gene expression of individual cells, there is ample opportunity to examine microglial states in health and disease within the contexts described in this review (Ochocka and Kaminska, 2021). Indeed, a recent report by Sun et al., used single-cell transcriptomics in young

and old mice exercising for 12 months to identify exercise effects across 14 different tissues (Sun et al., 2023), finding age-related changes in gene expression and increases in IBA1 expression were ameliorated by exercise in the cortex, dentate gyrus, cerebellum, and spinal cord. Intriguingly, the authors found that out all the tissues examined in the study, the aged central nervous system tissues were mostly strongly impacted by exercise, reinforcing the sentiment that there is high potential for exercise to benefit brain health (Sun et al., 2023). Overall, much remains to be discovered regarding the influence of physical exercise on microglial functions within and between brain regions in various diseases states.

Conclusion

There is strong evidence that PE can be beneficial in many rodent models of disease. Despite this, there are several areas where more research on exercise-induced changes in microglial function could yield important insights, particularly in conjunction with other lifestyle factors, where regional- and sex-dependent responses to different exercise paradigms may be more nuanced. Additionally, utilizing PE as an intervention in neurodevelopmental disorders, while challenging, could prove to be effective. Lastly, using newer technologies that allow for *in vivo* tracking of microglia dynamics simultaneously with other cellular structures, and carefully phenotyping microglia on the transcriptomic level during PE could uncover mechanisms underlying the beneficial effects of exercise on cognition.

Author contributions

AS: Conceptualization, Writing – original draft, Writing – review & editing. AM: Funding acquisition, Writing – review & editing.

Funding

The author(s) declare that financial support was received for the research, authorship, and/or publication of this article. This work was supported by T32ES007026 (AS), a Joan Wright Goodman award from the University of Rochester (AS), and NINDS R01 NS114480 (AM).

Conflict of interest

The authors declare that the research was conducted in the absence of any commercial or financial relationships that could be construed as a potential conflict of interest.

Publisher's note

Supplementary material

The Supplementary Material for this article can be found online at: https://www.frontiersin.org/articles/10.3389/fnins.2024.1420322/full#supplementary-material

SUPPLEMENTARY FIGURE 1
Comprehensive literature review process. Studies were reviewed from the PUBMED search query: ((((exercise[Title/Abstract]) OR (physical exercise[Title/Abstract])) OR (physical activity[Title/Abstract])) AND (microglia[Title/Abstract])) NOT (review[Publication Type]). Four research studies within the scope of this review which were found manually outside the search parameters stated above were also included. Data was manually extracted from each study on microglia parameters in various exercise animal models. Reasons for exclusion are as listed.

SUPPLEMENTARY TABLE 1
Information extracted from included studies.

References

Adachi, M., Abe, M., Sasaki, T., Kato, H., Kasahara, J., and Araki, T. (2010). Role of inducible or neuronal nitric oxide synthase in neurogenesis of the dentate gyrus in aged mice. *Metab. Brain Dis.* 25, 419–424. doi: 10.1007/s11011-010-9224-8

Adlard, P., Perreau, V., Engesser-Cesar, C., and Cotman, C. (2004). The timecourse of induction of brain-derived neurotrophic factor mRNA and protein in the rat hippocampus following voluntary exercise. *Neurosci. Lett.* 363, 43–48. doi: 10.1016/j.neulet.2004.03.058

Aguilar-Peralta, A., Gonzalez-Vazquez, A., Tomas-Sanchez, C., Blanco-Alvarez, V., Martinez-Fong, D., Gonzalez-Barrios, J., et al. (2022). Prophylactic zinc administration combined with swimming exercise prevents cognitive-emotional disturbances and tissue injury following a transient hypoxic-ischemic insult in the rat. *Behav. Neurol.* 2022:5388944. doi: 10.1155/2022/5388944

Aires, V., Coulon-Bainier, C., Pavlovic, A., Ebeling, M., Schmucki, R., Schweitzer, C., et al. (2021). CD22 blockage restores age-related impairments of microglia surveillance capacity. *Front. Immunol.* 12:684430. doi: 10.3389/fimmu.2021.684430

Albertini, G., Etienne, F., and Roumier, A. (2020). Regulation of microglia by neuromodulators: modulations in major and minor modes. *Neurosci. Lett.* 733:135000. doi: 10.1016/j.neulet.2020.135000

Ando, S., Komiyama, T., Tanoue, Y., Sudo, M., Costello, J., Uehara, Y., et al. (2022). Cognitive improvement after aerobic and resistance exercise is not associated with peripheral biomarkers. *Front. Behav. Neurosci.* 16:853150. doi: 10.3389/fnbeh.2022.853150

Andoh, M., Shibata, K., Okamoto, K., Onodera, J., Morishita, K., Miura, Y., et al. (2019). Exercise reverses behavioral and synaptic abnormalities after maternal inflammation. *Cell Rep.* 27, 2817–2825.e5. doi: 10.1016/j.celrep.2019.05.015.

Andrews, S., Curtin, D., Coxon, J., and Stout, J. (2022). Motor cortex plasticity response to acute cardiorespiratory exercise and intermittent theta-burst stimulation is attenuated in premanifest and early Huntington's disease. *Sci. Rep.* 12:1104. doi: 10.1038/s41598-021-04378-2

Angevaren, M., Aufdemkampe, G., Verhaar, H., Aleman, A., and Vanhees, L. (2008). Physical activity and enhanced fitness to improve cognitive function in older people without known cognitive impairment. *Cochrane Database Syst. Rev.* 3:CD005381. doi: 10.1002/14651858.CD005381

Arvidsson, D., Johannesson, E., Andersen, L., Karlsson, M., Wollmer, P., Thorsson, O., et al. (2018). A longitudinal analysis of the relationships of physical activity and body fat with nerve growth factor and brain-derived neural factor in children. *J. Phys. Act Health* 15, 620–625. doi: 10.1123/jpah.2017-0483

Bailey, S., Davis, J., and Ahlborn, E. (1993). Neuroendocrine and substrate responses to altered brain 5-HT activity during prolonged exercise to fatigue. *J. Appl. Physiol.* 74, 3006–3012. doi: 10.1152/jappl.1993.74.6.3006

Barrientos, R., Frank, M., Crysdale, N., Chapman, T., Ahrendsen, J., Day, H., et al. (2011). Little exercise, big effects: reversing aging and infection-induced memory deficits, and underlying processes. *J. Neurosci.* 31, 11578–11586. doi: 10.1523/JNEUROSCI.2266-11.2011

Barton, E., Baker, C., and Leasure, J. (2017a). Investigation of sex differences in the microglial response to binge ethanol and exercise. *Brain Sci.* 7:139. doi: 10.3390/brainsci7100139

Barton, E., Lu, Y., Megjhani, M., Maynard, M., Kulkarni, P., Roysam, B., et al. (2017b). Binge alcohol alters exercise-driven neuroplasticity. *Neuroscience* 343, 165–173. doi: 10.1016/j.neuroscience.2016.11.041

Belaya, I., Ivanova, M., Sorvari, A., Ilicic, M., Loppi, S., Koivisto, H., et al. (2020). Astrocyte remodeling in the beneficial effects of long-term voluntary exercise in Alzheimer's disease. *J. Neuroinflammation* 17:271. doi: 10.1186/s12974-020-01935-w

Betarbet, R., Canet-Aviles, R., Sherer, T., Mastroberardino, P., McLendon, C., Kim, J., et al. (2006). Intersecting pathways to neurodegeneration in Parkinson's disease: effects of the pesticide rotenone on DJ-1, alpha-synuclein, and the ubiquitin-proteasome system. *Neurobiol. Dis.* 22, 404–420. doi: 10.1016/j.nbd.2005.12.003

Betarbet, R., Sherer, T., MacKenzie, G., Garcia-Osuna, M., Panov, A., and Greenamyre, J. (2000). Chronic systemic pesticide exposure reproduces features of Parkinson's disease. *Nat. Neurosci.* 3, 1301–1306. doi: 10.1038/81834

Bjorklund, N., Reese, L., Sadagoparamanujam, V., Ghirardi, V., Woltjer, R., and Taglialatela, G. (2012). Absence of amyloid β oligomers at the postsynapse and regulated synaptic Zn2+ in cognitively intact aged individuals with Alzheimer's disease neuropathology. *Mol. Neurodegener.* 7:23. doi: 10.1186/1750-1326-7-23

Bobotis, B., Halvorson, T., Carrier, M., and Tremblay, M. È (2024). Established and emerging techniques for the study of microglia: visualization, depletion, and fate mapping. *Front. Cell Neurosci.* 18:1317125. doi: 10.3389/fncel.2024.1317125

Brawek, B., Skok, M., and Garaschuk, O. (2021). Changing functional signatures of microglia along the axis of brain aging. *Int. J. Mol. Sci.* 22:1091. doi: 10.3390/ijms22031091

Brettschneider, J., Toledo, J., Van Deerlin, V., Elman, L., McCluskey, L., Lee, V., et al. (2012). Microglial activation correlates with disease progression and upper motor neuron clinical symptoms in amyotrophic lateral sclerosis. *PLoS One* 7:e39216. doi: 10.1371/journal.pone.0039216

Brown, B., Payne, T., Kim, C., Moore, G., Krebs, P., and Martin, W. (1979). Chronic response of rat brain norepinephrine and serotonin levels to endurance training. *J. Appl. Physiol. Respir. Environ. Exerc. Physiol.* 46, 19–23. doi: 10.1152/jappl.1979.46.1.19

Buttler, L., Jordão, M., Fragas, M., Ruggeri, A., Ceroni, A., and Michelini, L. (2017). Maintenance of blood-brain barrier integrity in hypertension: a novel benefit of exercise training for autonomic control. *Front. Physiol.* 8:1048. doi: 10.3389/fphys.2017.01048

Caldwell, C., Petzinger, G., Jakowec, M., and Cadenas, E. (2020). Treadmill exercise rescues mitochondrial function and motor behavior in the CAG140 knock-in mouse model of Huntington's disease. *Chem. Biol. Interact.* 315:108907. doi: 10.1016/j.cbi.2019.108907

Campos, H., Ribeiro, D., Hashiguchi, D., Glaser, T., Milanis, M., Gimenes, C., et al. (2023). Neuroprotective effects of resistance physical exercise on the APP/PS1 mouse model of Alzheimer's disease. *Front. Neurosci.* 17:1132825. doi: 10.3389/fnins.2023.1132825

Cao, Q., Tan, C., Xu, W., Hu, H., Cao, X., Dong, Q., et al. (2020). The prevalence of dementia: a systematic review and meta-analysis. *J. Alzheimers Dis.* 73, 1157–1166. doi: 10.3233/JAD-191092

Carro, E., Nuñez, A., Busiguina, S., and Torres-Aleman, I. (2000). Circulating insulin-like growth factor I mediates effects of exercise on the brain. *J. Neurosci.* 20, 2926–2933. doi: 10.1523/JNEUROSCI.20-08-02926.2000

Casaletto, K., Lindbergh, C., VandeBunte, A., Neuhaus, J., Schneider, J., Buchman, A., et al. (2022). Microglial correlates of late life physical activity: relationship with synaptic and cognitive aging in older adults. *J. Neurosci.* 42, 288–298. doi: 10.1523/JNEUROSCI.1483-21.2021

Cealie, M., Douglas, J., Le, L., Vonkaenel, McCall, M., Drew, P., et al. (2023). Developmental ethanol exposure has minimal impact on cerebellar microglial dynamics, morphology, and interactions with Purkinje cells during adolescence. *Front. Neurosci.* 17:1176581. doi: 10.3389/fnins.2023.1176581

Chang, H., Yang, Y., Wang, P., Kuo, C., and Wang, R. (2011). Insulin-like growth factor I signaling for brain recovery and exercise ability in brain ischemic rats. *Med. Sci .Sports Exerc.* 43, 2274–2280. doi: 10.1249/MSS.0b013e318223b5d9

Chaouloff, F., Laude, D., Merino, D., Serrurrier, B., Guezennec, Y., and Elghozi, J. (1987). Amphetamine and alpha-methyl-p-tyrosine affect the exercise-induced imbalance between the availability of tryptophan and synthesis of serotonin in the brain of the rat. *Neuropharmacology* 26, 1099–1106. doi: 10.1016/0028-3908(87)90254-1

Chapman, L., Cooper-Knock, J., and Shaw, P. (2023). Physical activity as an exogenous risk factor for amyotrophic lateral sclerosis: a review of the evidence. *Brain* 146, 1745–1757. doi: 10.1093/brain/awac470

Chen, K., Zhang, L., Tan, M., Lai, C., Li, A., Ren, C., et al. (2017). Treadmill exercise suppressed stress-induced dendritic spine elimination in mouse barrel cortex and improved working memory via BDNF/TrkB pathway. *Transl. Psychiatry* 7:e1069. doi: 10.1038/tp.2017.41

Chen, M., and Russo-Neustadt, A. (2009). Running exercise-induced up-regulation of hippocampal brain-derived neurotrophic factor is CREB-dependent. *Hippocampus* 19, 962–972. doi: 10.1002/hipo.20579

Cheval, B., Darrous, L., Choi, K., Klimentidis, Y., Raichlen, D., Alexander, G., et al. (2023). Genetic insights into the causal relationship between physical activity and cognitive functioning. *Sci. Rep.* 13:5310. doi: 10.1038/s41598-023-32150-1

Cho, H., Kim, T., Ji, E., Park, H., Shin, M., and Baek, S. (2016). Treadmill exercise ameliorates motor dysfunction through inhibition of Purkinje cell loss in cerebellum of valproic acid-induced autistic rats. *J. Exerc. Rehabil.* 12, 293–298. doi: 10.12965/jer.1632696.348

Choi, S., Hill, D., Guo, L., Nicholas, R., Papadopoulos, D., and Cordeiro, M. (2022). Automated characterisation of microglia in ageing mice using image processing and supervised machine learning algorithms. *Sci. Rep.* 12:1806. doi: 10.1038/s41598-022-05815-6

Colcombe, S., and Kramer, A. (2003). Fitness effects on the cognitive function of older adults: a meta-analytic study. *Psychol. Sci.* 14, 125–130. doi: 10.1111/1467-9280.t01-1-01430

Cooper-Knock, J., Green, C., Altschuler, G., Wei, W., Bury, J., Heath, P., et al. (2017). A data-driven approach links microglia to pathology and prognosis in amyotrophic lateral sclerosis. *Acta Neuropathol. Commun.* 5:23. doi: 10.1186/s40478-017-0424-x

Cope, E., Briones, B., Brockett, A., Martinez, S., Vigneron, P., Opendak, M., et al. (2016). Immature neurons and radial glia, but not astrocytes or microglia, are altered in adult Cntnap2 and Shank3 mice, models of autism. *eNeuro* 3:ENEURO.0196-16.2016. doi: 10.1523/ENEURO.0196-16.2016.

Cudmore, R., Dougherty, S., and Linden, D. (2017). Cerebral vascular structure in the motor cortex of adult mice is stable and is not altered by voluntary exercise. *J. Cereb. Blood Flow Metab.* 37, 3725–3743. doi: 10.1177/0271678X16682508

Dahodwala, N., Pei, Q., and Schmidt, P. (2016). Sex differences in the clinical progression of Parkinson's disease. *J. Obstet. Gynecol. Neonatal. Nurs.* 45, 749–756. doi: 10.1016/j.jogn.2016.05.002

Damani, M., Zhao, L., Fontainhas, A., Amaral, J., Fariss, R., and Wong, W. (2011). Age-related alterations in the dynamic behavior of microglia. *Aging Cell.* 10, 263–276. doi: 10.1111/j.1474-9726.2010.00660.x

Davies, D., Ma, J., Jegathees, T., and Goldsbury, C. (2017). Microglia show altered morphology and reduced arborization in human brain during aging and Alzheimer's disease. *Brain Pathol.* 27, 795–808. doi: 10.1111/bpa.12456

de Sousa, A., Dos Reis, R., de Lima, C., de Oliveira, M., Fernandes, T., Gomes, G., et al. (2015). Three-dimensional morphometric analysis of microglial changes in a mouse model of virus encephalitis: age and environmental influences. *Eur. J. Neurosci.* 42, 2036–2050. doi: 10.1111/ejn.12951

De Sousa, R., Peixoto, M., Leite, H., Oliveira, L., Freitas, D., Silva-Júnior, F., et al. (2022). Neurological consequences of exercise during prenatal Zika virus exposure to mice pups. *Int. J. Neurosci.* 132, 1091–1101. doi: 10.1080/00207454.2020.1860970

Dhana, K., Agarwal, P., James, B., Leurgans, S., Rajan, K., Aggarwal, N., et al. (2024). Healthy lifestyle and cognition in older adults with common neuropathologies of dementia. *JAMA Neurol.* 81, 233–239. doi: 10.1001/jamaneurol.2023.5491

Ding, Q., Vaynman, S., Akhavan, M., Ying, Z., and Gomez-Pinilla, F. (2006). Insulin-like growth factor I interfaces with brain-derived neurotrophic factor-mediated synaptic plasticity to modulate aspects of exercise-induced cognitive function. *Neuroscience* 140, 823–833. doi: 10.1016/j.neuroscience.2006.02.084

Dishman, R., Renner, K., White-Welkley, J., Burke, K., and Bunnell, B. (2000). Treadmill exercise training augments brain norepinephrine response to familiar and novel stress. *Brain Res. Bull.* 52, 337–342. doi: 10.1016/s0361-9230(00)00271-9

Dols-Icardo, O., Montal, V., Sirisi, S., López-Pernas, G., Cervera-Carles, L., Querol-Vilaseca, M., et al. (2020). Motor cortex transcriptome reveals microglial key events in amyotrophic lateral sclerosis. *Neurol Neuroimmunol. Neuroinflamm.* 7:e829. doi: 10.1212/NXI.0000000000000829

Dominguez-Meijide, A., Rodriguez-Perez, A., Diaz-Ruiz, C., Guerra, M., and Labandeira-Garcia, J. (2017). Dopamine modulates astroglial and microglial activity via glial renin-angiotensin system in cultures. *Brain Behav. Immun.* 62, 277–290. doi: 10.1016/j.bbi.2017.02.013

Dorsey, E., Constantinescu, R., Thompson, J., Biglan, K., Holloway, R., Kieburtz, K., et al. (2007). Projected number of people with Parkinson disease in the most populous nations, 2005 through 2030. *Neurology* 68, 384–386. doi: 10.1212/01.wnl.0000247740.47667.03

Du, Y., Ma, Z., Lin, S., Dodel, R., Gao, F., Bales, K., et al. (2001). Minocycline prevents nigrostriatal dopaminergic neurodegeneration in the MPTP model of Parkinson's disease. *Proc. Natl. Acad. Sci. U S A.* 98, 14669–14674. doi: 10.1073/pnas.251341998

Dunn, A., Reigle, T., Youngstedt, S., Armstrong, R., and Dishman, R. (1996). Brain norepinephrine and metabolites after treadmill training and wheel running in rats. *Med. Sci. Sports Exerc.* 28, 204–209. doi: 10.1097/00005768-199602000-00008

Edler, M., Mhatre-Winters, I., and Richardson, J. (2021). Microglia in aging and Alzheimer's disease: a comparative species review. *Cells* 10:1138. doi: 10.3390/cells10051138

Ehninger, D., and Kempermann, G. (2003). Regional effects of wheel running and environmental enrichment on cell genesis and microglia proliferation in the adult murine neocortex. *Cereb. Cortex.* 13, 845–851. doi: 10.1093/cercor/13.8.845

Ehninger, D., Wang, L., Klempin, F., Römer, B., Kettenmann, H., and Kempermann, G. (2011). Enriched environment and physical activity reduce microglia and influence the fate of NG2 cells in the amygdala of adult mice. *Cell Tissue Res.* 345, 69–86. doi: 10.1007/s00441-011-1200-z

Elahi, M., Motoi, Y., Matsumoto, S., Hasan, Z., Ishiguro, K., and Hattori, N. (2016). Short-term treadmill exercise increased tau insolubility and neuroinflammation in tauopathy model mice. *Neurosci. Lett.* 610, 207–212. doi: 10.1016/j.neulet.2015.11.010

Etienne, F., Mastrolia, V., Maroteaux, L., Girault, J., Gervasi, N., and Roumier, A. (2019). Two-photon imaging of microglial processes' attraction toward ATP or serotonin in acute brain slices. *J. Vis. Exp.* JoVE. 143:10.3791/58788. doi: 10.3791/58788

Falomir-Lockhart, E., Dolcetti, F., García-Segura, L., Hereñú, C., and Bellini, M. (2019). IGF1 gene therapy modifies microglia in the striatum of senile rats. *Front. Aging Neurosci.* 11:48. doi: 10.3389/fnagi.2019.00048

Fan, Y., Chen, Z., Pathak, J., Carneiro, A., and Chung, C. (2018). Differential regulation of adhesion and phagocytosis of resting and activated microglia by dopamine. *Front. Cell Neurosci.* 12:309. doi: 10.3389/fncel.2018.00309

Färber, K., Pannasch, U., and Kettenmann, H. (2005). Dopamine and noradrenaline control distinct functions in rodent microglial cells. *Mol. Cell Neurosci.* 29, 128–138. doi: 10.1016/j.mcn.2005.01.003

Feng, S., Wu, C., Zou, P., Deng, Q., Chen, Z., Li, M., et al. (2023). High-intensity interval training ameliorates Alzheimer's disease-like pathology by regulating astrocyte phenotype-associated AQP4 polarization. *Theranostics* 13, 3434–3450. doi: 10.7150/thno.81951

Festa, F., Medori, S., and Macrì, M. (2023). Move your body, boost your brain: the positive impact of physical activity on cognition across all age groups. *Biomedicines* 11:1765. doi: 10.3390/biomedicines11061765

Fodelianaki, G., Lansing, F., Bhattarai, P., Troullinaki, M., Zeballos, M., Charalampopoulos, I., et al. (2019). Nerve growth factor modulates LPS - induced microglial glycolysis and inflammatory responses. *Exp. Cell Res.* 377, 10–16. doi: 10.1016/j.yexcr.2019.02.023

Franco-Bocanegra, D., Gourari, Y., McAuley, C., Chatelet, D., Johnston, D., Nicoll, J., et al. (2021). Microglial morphology in Alzheimer's disease and after Aβ immunotherapy. *Sci. Rep.* 11:15955. doi: 10.1038/s41598-021-95535-0

Freeman, S., Kandel, R., Cruz, L., Rozkalne, A., Newell, K., Frosch, M., et al. (2008). Preservation of neuronal number despite age-related cortical brain atrophy in elderly subjects without Alzheimer disease. *J. Neuropathol. Exp. Neurol.* 67, 1205–1212. doi: 10.1097/NEN.0b013e31818fc72f

Gao, C., Jiang, J., Tan, Y., and Chen, S. (2023). Microglia in neurodegenerative diseases: mechanism and potential therapeutic targets. *Signal Transduct. Target Ther.* 8:359. doi: 10.1038/s41392-023-01588-0

Gao, Z., Shen, X., Han, Y., Guo, Y., Li, K., and Bi, X. (2022). Pre-ischemic exercise prevents inflammation and apoptosis by inhibiting MAPK pathway in ischemic stroke. *Transl. Neurosci.* 13, 495–505. doi: 10.1515/tnsci-2022-0268

Gerecke, K., Kolobova, A., Allen, S., and Fawer, J. (2013). Exercise protects against chronic restraint stress-induced oxidative stress in the cortex and hippocampus. *Brain Res.* 1509, 66–78. doi: 10.1016/j.brainres.2013.02.027

Gil-Martínez, A., Cuenca, L., Sánchez, C., Estrada, C., Fernández-Villalba, E., and Herrero, M. (2018). Effect of NAC treatment and physical activity on neuroinflammation in subchronic Parkinsonism; is physical activity essential? *J. Neuroinflammation* 15:328. doi: 10.1186/s12974-018-1357-4

Giorgetti, E., Panesar, M., Zhang, Y., Joller, S., Ronco, M., Obrecht, M., et al. (2019). Modulation of microglia by voluntary exercise or CSF1R inhibition prevents age-related loss of functional motor units. *Cell Rep.* 29, 1539–1554.e7. doi: 10.1016/j.celrep.2019.10.003.

Gómez-Isla, T., Price, J., McKeel, D., Morris, J., Growdon, J., and Hyman, B. (1996). Profound loss of layer II entorhinal cortex neurons occurs in very mild Alzheimer's disease. *J. Neurosci.* 16, 4491–4500. doi: 10.1523/JNEUROSCI.16-14-04491.1996

Gomez-Merino, D., Béquet, F., Berthelot, M., Chennaoui, M., and Guezennec, C. (2001). Site-dependent effects of an acute intensive exercise on extracellular 5-HT and 5-HIAA levels in rat brain. *Neurosci. Lett.* 301, 143–146. doi: 10.1016/s0304-3940(01)01626-3

Guneykaya, D., Ivanov, A., Hernandez, D., Haage, V., Wojtas, B., Meyer, N., et al. (2018). Transcriptional and translational differences of microglia from male and female brains. *Cell Rep.* 24, 2773–2783.e6. doi: 10.1016/j.celrep.2018.08.001.

Guneykaya, D., Ugursu, B., Logiacco, F., Popp, O., Feiks, M., Meyer, N., et al. (2023). Sex-specific microglia state in the Neuroligin-4 knock-out mouse model of autism spectrum disorder. *Brain Behav. Immun.* 111, 61–75. doi: 10.1016/j.bbi.2023.03.023

Guo, Y., Yan, M., Li, L., Zhao, L., and Li, Y. (2022). Treadmill exercise prevents cognitive impairments in adolescent intermittent ethanol rats by reducing the excessive activation of microglia cell in the hippocampus. *Int. J. Mol. Sci.* 23:14701. doi: 10.3390/ijms232314701

Gursky, Z., Johansson, J., and Klintsova, A. (2020). Postnatal alcohol exposure and adolescent exercise have opposite effects on cerebellar microglia in rat. *Int. J. Dev. Neurosci.* 80, 558–571. doi: 10.1002/jdn.10051

Gyoneva, S., and Traynelis, S. (2013). Norepinephrine modulates the motility of resting and activated microglia via different adrenergic receptors. *J. Biol. Chem.* 288, 15291–15302. doi: 10.1074/jbc.M113.458901

Hamer, M., Muniz Terrera, G., and Demakakos, P. (2018). Physical activity and trajectories in cognitive function: english longitudinal study of ageing. *J. Epidemiol. Community Health.* 72, 477–483. doi: 10.1136/jech-2017-210228

Han, H., Zhao, Y., Du, J., Wang, S., Yang, X., Li, W., et al. (2023). Exercise improves cognitive dysfunction and neuroinflammation in mice through Histone H3 lactylation in microglia. *Immun. Ageing* 20:63. doi: 10.1186/s12979-023-00390-4

Harrison, D., Busse, M., Openshaw, R., Rosser, A., Dunnett, S., and Brooks, S. (2013). Exercise attenuates neuropathology and has greater benefit on cognitive than motor deficits in the R6/1 Huntington's disease mouse model. *Exp. Neurol.* 248, 457–469. doi: 10.1016/j.expneurol.2013.07.014

Hashiguchi, D., Campos, H., Wuo-Silva, R., Faber, J., Gomes, da Silva, S., et al. (2020). Resistance exercise decreases amyloid load and modulates inflammatory responses in the APP/PS1 mouse model for Alzheimer's disease. *J. Alzheimers Dis.* 73, 1525–1539. doi: 10.3233/JAD-190729

Hayakawa, N., Kato, H., and Araki, T. (2007). Age-related changes of astorocytes, oligodendrocytes and microglia in the mouse hippocampal CA1 sector. *Mech. Ageing Dev.* 128, 311–316. doi: 10.1016/j.mad.2007.01.005

He, X., Liu, D., Zhang, Q., Liang, F., Dai, G., Zeng, J., et al. (2017). Voluntary exercise promotes glymphatic clearance of amyloid beta and reduces the activation of astrocytes and microglia in aged mice. *Front. Mol. Neurosci.* 10:144. doi: 10.3389/fnmol.2017.00144

He, Y., Liu, W., Koch, L., Britton, S., Keep, R., Xi, G., et al. (2013). Susceptibility to intracerebral hemorrhage-induced brain injury segregates with low aerobic capacity in rats. *Neurobiol. Dis.* 49, 22–28. doi: 10.1016/j.nbd.2012.08.014

Hefendehl, J., Neher, J., Sühs, R., Kohsaka, S., Skodras, A., and Jucker, M. (2014). Homeostatic and injury-induced microglia behavior in the aging brain. *Aging Cell* 13, 60–69. doi: 10.1111/acel.12149

Hong, S., Beja-Glasser, V., Nfonoyim, B., Frouin, A., Li, S., Ramakrishnan, S., et al. (2016). Complement and microglia mediate early synapse loss in Alzheimer mouse models. *Science* 352, 712–716. doi: 10.1126/science.aad8373

Huang, L., Jin, J., Chen, K., You, S., Zhang, H., Sideris, A., et al. (2021). BDNF produced by cerebral microglia promotes cortical plasticity and pain hypersensitivity after peripheral nerve injury. *PLoS Biol.* 19:e3001337. doi: 10.1371/journal.pbio.3001337

Huynh, K., Nategh, L., Jamadar, S., Stout, J., Georgiou-Karistianis, N., and Lampit, A. (2023). Cognition-oriented treatments and physical exercise on cognitive function in Huntington's disease: a systematic review. *J. Neurol.* 270, 1857–1879. doi: 10.1007/s00415-022-11516-x

Hwang, J., Brothers, R., Castelli, D., Glowacki, E., Chen, Y., Salinas, M., et al. (2016). Acute high-intensity exercise-induced cognitive enhancement and brain-derived neurotrophic factor in young, healthy adults. *Neurosci. Lett.* 630, 247–253. doi: 10.1016/j.neulet.2016.07.033

Imamura, K., Hishikawa, N., Sawada, M., Nagatsu, T., Yoshida, M., and Hashizume, Y. (2003). Distribution of major histocompatibility complex class II-positive microglia and cytokine profile of Parkinson's disease brains. *Acta Neuropathol.* 106, 518–526. doi: 10.1007/s00401-003-0766-2

Itagaki, S., McGeer, P., Akiyama, H., Zhu, S., and Selkoe, D. (1989). Relationship of microglia and astrocytes to amyloid deposits of Alzheimer disease. *J. Neuroimmunol.* 24, 173–182. doi: 10.1016/0165-5728(89)90115-x

Ivan, D., Berve, K., Walthert, S., Monaco, G., Borst, K., Bouillet, E., et al. (2023). Insulin-like growth factor-1 receptor controls the function of CNS-resident macrophages and their contribution to neuroinflammation. *Acta Neuropathol. Commun.* 11:35. doi: 10.1186/s40478-023-01535-8

James, S., Chiou, Y., Fatih, N., Needham, L., Schott, J., and Richards, M. (2023). Timing of physical activity across adulthood on later-life cognition: 30 years follow-up in the 1946 British birth cohort. *J. Neurol. Neurosurg. Psychiatry.* 94, 349–356. doi: 10.1136/jnnp-2022-329955

Jankowsky, J., Fadale, D., Anderson, J., Xu, G., Gonzales, V., Jenkins, N., et al. (2004). Mutant presenilins specifically elevate the levels of the 42 residue beta-amyloid peptide in vivo: evidence for augmentation of a 42-specific gamma secretase. *Hum. Mol. Genet.* 13, 159–170. doi: 10.1093/hmg/ddh019

Kang, D., Bressel, E., and Kim, D. (2020). Effects of aquatic exercise on insulin-like growth factor-1, brain-derived neurotrophic factor, vascular endothelial growth factor, and cognitive function in elderly women. *Exp. Gerontol.* 132:110842. doi: 10.1016/j.exger.2020.110842

Kang, E., Koo, J., Jang, Y., Yang, C., Lee, Y., Cosio-Lima, L., et al. (2016). Neuroprotective effects of endurance exercise against high-fat diet-induced hippocampal neuroinflammation. *J. Neuroendocrinol.* 28, 1–10. doi: 10.1111/jne.12385

Kassa, R., Bonafede, R., Boschi, F., Bentivoglio, M., and Mariotti, R. (2017). Effect of physical exercise and anabolic steroid treatment on spinal motoneurons and surrounding glia of wild-type and ALS mice. *Brain Res.* 1657, 269–278. doi: 10.1016/j.brainres.2016.12.029

Ke, H., Huang, H., Liang, K., and Hsieh-Li, H. (2011). Selective improvement of cognitive function in adult and aged APP/PS1 transgenic mice by continuous non-shock treadmill exercise. *Brain Res.* 1403, 1–11. doi: 10.1016/j.brainres.2011.05.056

Kim, R., Lee, T., Lee, H., Ko, D., Lee, J., Shin, H., et al. (2023). Effects of physical exercise interventions on cognitive function in Parkinson's disease: an updated systematic review and meta-analysis of randomized controlled trials. *Parkinsonism Relat. Disord.* 117:105908. doi: 10.1016/j.parkreldis.2023.105908

Kinoshita, K., Hamanaka, G., Ohtomo, R., Takase, H., Chung, K., Lok, J., et al. (2021). Mature adult mice with exercise-preconditioning show better recovery after intracerebral hemorrhage. *Stroke* 52, 1861–1865. doi: 10.1161/STROKEAHA.120.032201

Kip, E., and Parr-Brownlie, L. (2023). Healthy lifestyles and wellbeing reduce neuroinflammation and prevent neurodegenerative and psychiatric disorders. *Front. Neurosci.* 17:1092537. doi: 10.3389/fnins.2023.1092537

Klein, C., Jonas, W., Wiedmer, P., Schreyer, S., Akyüz, L., Spranger, J., et al. (2019). High-fat diet and physical exercise differentially modulate adult neurogenesis in the mouse hypothalamus. *Neuroscience* 400, 146–156. doi: 10.1016/j.neuroscience.2018.12.037

Knott, C., Wilkin, G., and Stern, G. (1999). Astrocytes and microglia in the substantia nigra and caudate-putamen in Parkinson's disease. *Parkinsonism Relat. Disord.* 5, 115–122. doi: 10.1016/s1353-8020(99)00022-x

Kodali, M., Mishra, V., Hattiangady, B., Attaluri, S., Gonzalez, J., Shuai, B., et al. (2021). Moderate, intermittent voluntary exercise in a model of Gulf war illness improves cognitive and mood function with alleviation of activated microglia and astrocytes, and enhanced neurogenesis in the hippocampus. *Brain Behav. Immun.* 97, 135–149. doi: 10.1016/j.bbi.2021.07.005

Kohman, R., Bhattacharya, T., Wojcik, E., and Rhodes, J. (2013). Exercise reduces activation of microglia isolated from hippocampus and brain of aged mice. *J. Neuroinflammation* 10:114. doi: 10.1186/1742-2094-10-114

Kohman, R., DeYoung, E., Bhattacharya, T., Peterson, L., and Rhodes, J. (2012). Wheel running attenuates microglia proliferation and increases expression of a proneurogenic phenotype in the hippocampus of aged mice. *Brain Behav. Immun.* 26, 803–810. doi: 10.1016/j.bbi.2011.10.006

Kolodziejczak, M., Béchade, C., Gervasi, N., Irinopoulou, T., Banas, S., Cordier, C., et al. (2015). Serotonin modulates developmental Microglia via 5-HT2B receptors: potential implication during synaptic refinement of retinogeniculate projections. *ACS Chem. Neurosci.* 6, 1219–1230. doi: 10.1021/cn5003489

Krabbe, G., Matyash, V., Pannasch, U., Mamer, L., Boddeke, H., and Kettenmann, H. (2012). Activation of serotonin receptors promotes microglial injury-induced motility but attenuates phagocytic activity. *Brain Behav. Immun.* 26, 419–428. doi: 10.1016/j.bbi.2011.12.002

Kuhlmann, T., Ludwin, S., Prat, A., Antel, J., Brück, W., and Lassmann, H. (2017). An updated histological classification system for multiple sclerosis lesions. *Acta Neuropathol.* 133, 13–24. doi: 10.1007/s00401-016-1653-y

Lang, X., Zhao, N., He, Q., Li, X., Li, X., Sun, C., et al. (2020). Treadmill exercise mitigates neuroinflammation and increases BDNF via activation of SIRT1 signaling in a mouse model of T2DM. *Brain Res. Bull.* 165, 30–39. doi: 10.1016/j.brainresbull.2020.09.015

Larsson, G., Julu, P., Witt Engerström, I., Sandlund, M., and Lindström, B. (2018). Walking on treadmill with rett syndrome-effects on the autonomic nervous system. *Res. Dev. Disabil.* 83, 99–107. doi: 10.1016/j.ridd.2018.08.010

Lee, J., Kim, T., Park, S., Han, J., Shin, M., Lim, B., et al. (2018). Treadmill exercise improves motor function by suppressing purkinje cell loss in parkinson disease rats. *Int. Neurourol. J.* 22(Suppl. 3), S147–S155. doi: 10.5213/inj.1836226.113

Leem, Y., Lee, Y., Son, H., and Lee, S. (2011). Chronic exercise ameliorates the neuroinflammation in mice carrying NSE/htau23. *Biochem. Biophys. Res. Commun.* 406, 359–365. doi: 10.1016/j.bbrc.2011.02.046

Li, C., Hu, J., Liu, W., Ke, C., Huang, C., Bai, Y., et al. (2022). Exercise intervention modulates synaptic plasticity by inhibiting excessive microglial activation via exosomes. *Front. Cell Neurosci.* 16:953640. doi: 10.3389/fncel.2022.953640

Li, G., You, Q., Hou, X., Zhang, S., Du, L., Lv, Y., et al. (2023). The effect of exercise on cognitive function in people with multiple sclerosis: a systematic review and meta-analysis of randomized controlled trials. *J. Neurol.* 270, 2908–2923. doi: 10.1007/s00415-023-11649-7

Li, Q., and Barres, B. (2018). Microglia and macrophages in brain homeostasis and disease. *Nat. Rev. Immunol.* 18, 225–242. doi: 10.1038/nri.2017.125

Li, W., Luo, Z., Jiang, J., Li, K., and Wu, C. (2023). The effects of exercise intervention on cognition and motor function in stroke survivors: a systematic review and meta-analysis. *Neurol. Sci.* 44, 1891–1903. doi: 10.1007/s10072-023-06636-9

Lima, C., Soares Gde, S., Vitor, S., Andrade-da-Costa, B., Castellano, B., and Guedes, R. (2014). Spreading depression features and Iba1 immunoreactivity in the cerebral cortex of developing rats submitted to treadmill exercise after treatment with monosodium glutamate. *Int. J. Dev. Neurosci.* 33, 98–105. doi: 10.1016/j.ijdevneu.2013.12.008

Littlefield, A., Setti, S., Priester, C., and Kohman, R. (2015). Voluntary exercise attenuates LPS-induced reductions in neurogenesis and increases microglia expression of a proneurogenic phenotype in aged mice. *J. Neuroinflammation* 12:138. doi: 10.1186/s12974-015-0362-0

Liu, M., Liu, X., Wang, W., Shen, X., Che, H., Guo, Y., et al. (2012). Involvement of microglia activation in the lead induced long-term potentiation impairment. *PLoS One 7*:e43924. doi: 10.1371/journal.pone.0043924

Liu, M., Luo, L., Fu, J., He, J., Chen, M., He, Z., et al. (2022). Exercise-induced neuroprotection against cerebral ischemia/reperfusion injury is mediated via alleviating inflammasome-induced pyroptosis. *Exp. Neurol.* 349:113952. doi: 10.1016/j.expneurol.2021.113952

Liu, Y., Ying, Y., Li, Y., Eyo, U., Chen, T., Zheng, J., et al. (2019). Neuronal network activity controls microglial process surveillance in awake mice via norepinephrine signaling. *Nat. Neurosci.* 22, 1771–1781. doi: 10.1038/s41593-019-0511-3

Lloyd, B., Hake, H., Ishiwata, T., Farmer, C., Loetz, E., Fleshner, M., et al. (2017). Exercise increases mTOR signaling in brain regions involved in cognition and emotional behavior. *Behav. Brain Res.* 323, 56–67. doi: 10.1016/j.bbr.2017.01.033

Long, J., Kalehua, A., Muth, N., Calhoun, M., Jucker, M., Hengemihle, J., et al. (1998). Stereological analysis of astrocyte and microglia in aging mouse hippocampus. *Neurobiol. Aging* 19, 497–503. doi: 10.1016/s0197-4580(98)00088-8

López-Ortiz, S., Lista, S., Valenzuela, P., Pinto-Fraga, J., Carmona, R., Caraci, F., et al. (2023). Effects of physical activity and exercise interventions on Alzheimer's disease: an umbrella review of existing meta-analyses. *J. Neurol.* 270, 711–725. doi: 10.1007/s00415-022-11454-8

Lovatel, G., Bertoldi, K., Elsnerb, V., Piazza, F., Basso, C., Moysés Fdos, S., et al. (2014). Long-term effects of pre and post-ischemic exercise following global cerebral ischemia on astrocyte and microglia functions in hippocampus from Wistar rats. *Brain Res.* 1587, 119–126. doi: 10.1016/j.brainres.2014.08.068

Lowery, R., Latchney, S., Peer, R., Lamantia, C., Lordy, K., Opanashuk, L., et al. (2022). Gestational and lactational exposure to 2,3,7,8-tetrachlorodibenzo-p-dioxin primes cortical microglia to tissue injury. *Brain Behav. Immun.* 101, 288–303. doi: 10.1016/j.bbi.2022.01.013

Lu, J., Wang, J., Yu, L., Cui, R., Zhang, Y., Ding, H., et al. (2021). Treadmill exercise attenuates cerebral ischemia-reperfusion injury by promoting activation of M2 microglia via upregulation of Interleukin-4. *Front. Cardiovasc. Med.* 8:735485. doi: 10.3389/fcvm.2021.735485

Lu, Y., Dong, Y., Tucker, D., Wang, R., Ahmed, M., Brann, D., et al. (2017). Treadmill exercise exerts neuroprotection and regulates microglial polarization and oxidative stress in a streptozotocin-induced rat model of sporadic Alzheimer's disease. *J. Alzheimers Dis.* 56, 1469–1484. doi: 10.3233/JAD-160869

MacRae, P., Spirduso, W., Cartee, G., Farrar, R., and Wilcox, R. (1987). Endurance training effects on striatal D2 dopamine receptor binding and striatal dopamine metabolite levels. *Neurosci. Lett.* 79, 138–144. doi: 10.1016/0304-3940(87)90686-0

Mandolesi, G., Bullitta, S., Fresegna, D., De Vito, F., Rizzo, F., Musella, A., et al. (2019). Voluntary running wheel attenuates motor deterioration and brain damage in cuprizone-induced demyelination. *Neurobiol. Dis.* 129, 102–117. doi: 10.1016/j.nbd.2019.05.010

Masson, G., Nair, A., Silva Soares, P., Michelini, L., and Francis, J. (2015). Aerobic training normalizes autonomic dysfunction, HMGB1 content, microglia activation and inflammation in hypothalamic paraventricular nucleus of SHR. *Am. J. Physiol. Heart Circ. Physiol.* 309, H1115–H1122. doi: 10.1152/ajpheart.00349.2015

Mastroeni, D., Grover, A., Leonard, B., Joyce, J., Coleman, P., Kozik, B., et al. (2009). Microglial responses to dopamine in a cell culture model of Parkinson's disease. *Neurobiol. Aging* 30, 1805–1817. doi: 10.1016/j.neurobiolaging.2008.01.001

Mathes, W., Nehrenberg, D., Gordon, R., Hua, K., Garland, T., and Pomp, D. (2010). Dopaminergic dysregulation in mice selectively bred for excessive exercise or obesity. *Behav. Brain Res.* 210, 155–163. doi: 10.1016/j.bbr.2010.02.016

Matta, S., Moore, Z., Walker, F., Hill-Yardin, E., and Crack, P. (2020). An altered glial phenotype in the NL3R451C mouse model of autism. *Sci. Rep.* 10:14492. doi: 10.1038/s41598-020-71171-y

McGeer, P., Itagaki, S., and McGeer, E. (1988). Expression of the histocompatibility glycoprotein HLA-DR in neurological disease. *Acta Neuropathol.* 76, 550–557. doi: 10.1007/BF00689592

Mee-Inta, O., Zhao, Z., and Kuo, Y. (2019). Physical exercise inhibits inflammation and microglial activation. *Cells* 8:691. doi: 10.3390/cells8070691

Meeusen, R., and De Meirleir, K. (1995). Exercise and brain neurotransmission. *Sports Med.* 20, 160–188. doi: 10.2165/00007256-199520030-00004

Mela, V., Mota, B., Milner, M., McGinley, A., Mills, K., Kelly, et al. (2020). Exercise-induced re-programming of age-related metabolic changes in microglia is accompanied by a reduction in senescent cells. *Brain Behav. Immun.* 87, 413–428. doi: 10.1016/j.bbi.2020.01.012

Mifflin, K., Frieser, E., Benson, C., Baker, G., and Kerr, B. (2017). Voluntary wheel running differentially affects disease outcomes in male and female mice with experimental autoimmune encephalomyelitis. *J. Neuroimmunol.* 305, 135–144. doi: 10.1016/j.jneuroim.2017.02.005

Moloudizargari, M., Moradkhani, F., Asghari, N., Fallah, M., Asghari, M., Moghadamnia, A., et al. (2019). NLRP inflammasome as a key role player in the pathogenesis of environmental toxicants. *Life Sci.* 231:116585. doi: 10.1016/j.lfs.2019.116585

Molteni, R., Ying, Z., and Gómez-Pinilla, F. (2002). Differential effects of acute and chronic exercise on plasticity-related genes in the rat hippocampus revealed by microarray. *Eur. J. Neurosci.* 16, 1107–1116. doi: 10.1046/j.1460-9568.2002.02158.x

Morrison, H., and Filosa, J. (2013). A quantitative spatiotemporal analysis of microglia morphology during ischemic stroke and reperfusion. *J. Neuroinflammation* 10:4. doi: 10.1186/1742-2094-10-4

Mottolese, N., Uguagliati, B., Tassinari, M., Cerchier, C., Loi, M., Candini, G., et al. (2023). Voluntary running improves behavioral and structural abnormalities in a mouse model of CDKL5 deficiency disorder. *Biomolecules* 13:1396. doi: 10.3390/biom13091396

Mouton, P., Long, J., Lei, D., Howard, V., Jucker, M., Calhoun, M., et al. (2002). Age and gender effects on microglia and astrocyte numbers in brains of mice. *Brain Res.* 956, 30–35. doi: 10.1016/s0006-8993(02)03475-3

Naghibzadeh, M., Ranjbar, R., Tabandeh, M., and Habibi, A. (2018). Effects of two training programs on transcriptional levels of neurotrophins and glial cells population in hippocampus of experimental multiple sclerosis. *Int. J. Sports Med.* 39, 604–612. doi: 10.1055/a-0608-4635

Nakanishi, K., Sakakima, H., Norimatsu, K., Otsuka, S., Takada, S., Tani, A., et al. (2021). Effect of low-intensity motor balance and coordination exercise on cognitive functions, hippocampal Aβ deposition, neuronal loss, neuroinflammation, and oxidative stress in a mouse model of Alzheimer's disease. *Exp. Neurol.* 337:113590. doi: 10.1016/j.expneurol.2020.113590

Nebeling, F., Poll, S., Justus, L., Steffen, J., Keppler, K., Mittag, M., et al. (2023). Microglial motility is modulated by neuronal activity and correlates with dendritic spine plasticity in the hippocampus of awake mice. *Elife* 12:e83176. doi: 10.7554/eLife.83176

Neeper, S., Gómez-Pinilla, F., Choi, J., and Cotman, C. (1996). Physical activity increases mRNA for brain-derived neurotrophic factor and nerve growth factor in rat brain. *Brain Res.* 726, 49–56.

Ngwa, C., Al Mamun, A., Qi, S., Sharmeen, R., Xu, Y., and Liu, F. (2022). Regulation of microglial activation in stroke in aged mice: a translational study. *Aging* 14, 6047–6065. doi: 10.18632/aging.204216

Ngwa, C., Qi, S., Mamun, A., Xu, Y., Sharmeen, R., and Liu, F. (2021). Age and sex differences in primary microglia culture: a comparative study. *J. Neurosci. Methods* 364:109359. doi: 10.1016/j.jneumeth.2021.109359

Nichol, K., Poon, W., Parachikova, A., Cribbs, D., Glabe, C., and Cotman, C. (2008). Exercise alters the immune profile in Tg2576 Alzheimer mice toward a response coincident with improved cognitive performance and decreased amyloid. *J. Neuroinflammation* 5:13. doi: 10.1186/1742-2094-5-13

Nimmerjahn, A., Kirchhoff, F., and Helmchen, F. (2005). Resting microglial cells are highly dynamic surveillants of brain parenchyma in vivo. *Science* 308, 1314–1318. doi: 10.1126/science.1110647

Ochocka, N., and Kaminska, B. (2021). Microglia diversity in healthy and diseased brain: insights from single-cell omics. *Int. J. Mol. Sci.* 22:3027. doi: 10.3390/ijms22063027

Olah, M., Ping, G., De Haas, A., Brouwer, N., Meerlo, P., Van Der Zee, E., et al. (2009). Enhanced hippocampal neurogenesis in the absence of microglia T cell interaction and microglia activation in the murine running wheel model. *Glia* 57, 1046–1061. doi: 10.1002/glia.20828

Onodera, J., Nagata, H., Nakashima, A., Ikegaya, Y., and Koyama, R. (2021). Neuronal brain-derived neurotrophic factor manipulates microglial dynamics. *Glia* 69, 890–904. doi: 10.1002/glia.23934

Oroszi, T., Geerts, E., Rajadhyaksha, R., Nyakas, C., van Heuvelen, M., and van der Zee, E. (2023). Whole-body vibration ameliorates glial pathological changes in the hippocampus of hAPP transgenic mice, but does not affect plaque load. *Behav Brain Funct.* 19:5. doi: 10.1186/s12993-023-00208-9

Paasila, P., Davies, D., Kril, J., Goldsbury, C., and Sutherland, G. (2019). The relationship between the morphological subtypes of microglia and Alzheimer's disease neuropathology. *Brain Pathol.* 29, 726–740. doi: 10.1111/bpa.12717

Pagliari, R., and Peyrin, L. (1995). Norepinephrine release in the rat frontal cortex under treadmill exercise: a study with microdialysis. *J. Appl. Physiol.* 78, 2121–2130. doi: 10.1152/jappl.1995.78.6.2121

Palpagama, T., Waldvogel, H., Faull, R., and Kwakowsky, A. (2019). The role of microglia and astrocytes in Huntington's disease. *Front. Mol. Neurosci.* 12:258. doi: 10.3389/fnmol.2019.00258

Pang, T., Stam, N., Nithianantharajah, J., Howard, M., and Hannan, A. (2006). Differential effects of voluntary physical exercise on behavioral and brain-derived neurotrophic factor expression deficits in Huntington's disease transgenic mice. *Neuroscience* 141, 569–584. doi: 10.1016/j.neuroscience.2006.04.013

Paolicelli, R., and Ferretti, M. (2017). Function and dysfunction of microglia during brain development: consequences for synapses and neural circuits. *Front. Synaptic. Neurosci.* 9:9. doi: 10.3389/fnsyn.2017.00009

Paolicelli, R., Bolasco, G., Pagani, F., Maggi, L., Scianni, M., Panzanelli, P., et al. (2011). Synaptic pruning by microglia is necessary for normal brain development. *Science* 333, 1456–1458. doi: 10.1126/science.1202529

Paolicelli, R., Sierra, A., Stevens, B., Tremblay, M., Aguzzi, A., Ajami, B., et al. (2022). Microglia states and nomenclature: a field at its crossroads. *Neuron* 110, 3458–3483. doi: 10.1016/j.neuron.2022.10.020

Parkhurst, C., Yang, G., Ninan, I., Savas, J., Yates, J., Lafaille, J., et al. (2013). Microglia promote learning-dependent synapse formation through brain-derived neurotrophic factor. *Cell* 155, 1596–1609. doi: 10.1016/j.cell.2013.11.030

Perry, V., and Holmes, C. (2014). Microglial priming in neurodegenerative disease. *Nat. Rev. Neurol.* 10, 217–224. doi: 10.1038/nrneurol.2014.38

Perry, V., Matyszak, M., and Fearn, S. (1993). Altered antigen expression of microglia in the aged rodent CNS. *Glia* 7, 60–67. doi: 10.1002/glia.440070111

Pinar, C., Yau, S., Sharp, Z., Shamei, A., Fontaine, C., Meconi, A., et al. (2018). Effects of voluntary exercise on cell proliferation and neurogenesis in the dentate gyrus of adult FMR1 knockout mice. *Brain Plast.* 4, 185–195. doi: 10.3233/BPL-170052

Pinto, B., Morelli, G., Rastogi, M., Savardi, A., Fumagalli, A., Petretto, A., et al. (2020). Rescuing over-activated microglia restores cognitive performance in juvenile animals of the Dp(16) mouse model of down syndrome. *Neuron* 108, 887–904.e12. doi: 10.1016/j.neuron.2020.09.010.

Ploughman, M., Granter-Button, S., Chernenko, G., Tucker, B., Mearow, K., and Corbett, D. (2005). Endurance exercise regimens induce differential effects on brain-derived neurotrophic factor, synapsin-I and insulin-like growth factor I after focal ischemia. *Neuroscience* 136, 991–1001. doi: 10.1016/j.neuroscience.2005.08.037

Poewe, W., Seppi, K., Tanner, C., Halliday, G., Brundin, P., Volkmann, J., et al. (2017). Parkinson disease. *Nat. Rev. Dis. Primers* 3:17013. doi: 10.1038/nrdp.2017.13

Potter, M. C., Yuan, C., Ottenritter, C., Mughal, M., and Praag, V. (2010). Exercise is not beneficial and may accelerate symptom onset in a mouse model of Huntington's disease. *PLoS Curr.* 2:RRN1201. doi: 10.1371/currents.RRN1201

Prineas, J., Kwon, E., Cho, E., Sharer, L., Barnett, M., Oleszak, E., et al. (2001). Immunopathology of secondary-progressive multiple sclerosis. *Ann. Neurol.* 50, 646–657. doi: 10.1002/ana.1255

Pritchard Orr, A., Keiver, K., Bertram, C., and Clarren, S. (2018). FAST club: the impact of a physical activity intervention on executive function in children with fetal alcohol spectrum disorder. *Adapt. Phys. Activ. Q.* 35, 403–423. doi: 10.1123/apaq.2017-0137

Ransohoff, R. (2012). Animal models of multiple sclerosis: the good, the bad and the bottom line. *Nat. Neurosci.* 15, 1074–1077. doi: 10.1038/nn.3168

Rizzi, C., Tiberi, A., Giustizieri, M., Marrone, M., Gobbo, F., Carucci, N., et al. (2018). NGF steers microglia toward a neuroprotective phenotype. *Glia* 66, 1395–1416. doi: 10.1002/glia.23312

Rizzo, F., Guadalupi, L., Sanna, K., Vanni, V., Fresegna, D., De Vito, F., et al. (2021). Exercise protects from hippocampal inflammation and neurodegeneration in experimental autoimmune encephalomyelitis. *Brain Behav. Immun.* 98, 13–27. doi: 10.1016/j.bbi.2021.08.212

Rodríguez, J., Noristani, H., and Verkhratsky, A. (2015). Microglial response to Alzheimer's disease is differentially modulated by voluntary wheel running and enriched environments. *Brain Struct. Funct.* 220, 941–953. doi: 10.1007/s00429-013-0693-5

Russo-Neustadt, A., Beard, R., and Cotman, C. (1999). Exercise, antidepressant medications, and enhanced brain derived neurotrophic factor expression. *Neuropsychopharmacology* 21, 679–682. doi: 10.1016/S0893-133X(99)00059-7

Sanchez-Varo, R., Mejias-Ortega, M., Fernandez-Valenzuela, J., Nuñez-Diaz, C., Caceres-Palomo, L., Vegas-Gomez, L., et al. (2022). Transgenic mouse models of alzheimer's disease: an integrative analysis. *Int. J. Mol. Sci.* 23:5404. doi: 10.3390/ijms23105404

Sapp, E., Kegel, K., Aronin, N., Hashikawa, T., Uchiyama, Y., Tohyama, K., et al. (2001). Early and progressive accumulation of reactive microglia in the Huntington disease brain. *J. Neuropathol. Exp. Neurol.* 60, 161–172. doi: 10.1093/jnen/60.2.161

Schafer, D., Heller, C., Gunner, G., Heller, M., Gordon, C., Hammond, T., et al. (2016). Microglia contribute to circuit defects in Mecp2 null mice independent of microglia-specific loss of Mecp2 expression. *Elife* 5:e15224. doi: 10.7554/eLife.15224

Sedelis, M., Schwarting, R., and Huston, J. (2001). Behavioral phenotyping of the MPTP mouse model of Parkinson's disease. *Behav. Brain Res.* 125, 109–125. doi: 10.1016/s0166-4328(01)00309-6

Semenova, T., Ivanov, V., and Tret'yak, T. (1981). Brain levels of noradrenalin, dopamine, and serotonin in rats with different levels of motor activity. *Neurosci. Behav. Physiol.* 11, 153–155. doi: 10.1007/BF01182373

Shariat, A., Najafabadi, M., Dos Santos, I., Anastasio, A., Milajerdi, H., Hassanzadeh, G., et al. (2024). The effectiveness of aquatic therapy on motor and social skill as well as executive function in children with neurodevelopmental disorder: a systematic review and meta-analysis. *Arch. Phys. Med. Rehabil.* 105, 1000–1007. doi: 10.1016/j.apmr.2023.08.025

Shi, P., Zhang, Z., Feng, X., Li, C., and Tang, Y. (2024). Effect of physical exercise in real-world settings on executive function of atypical children: a systematic review and meta-analysis. *Child Care Health Dev.* 50:e13182. doi: 10.1111/cch.13182

Shvachiy, L., Amaro-Leal, Â, Outeiro, T. F., Rocha, I., and Geraldes, V. (2023). Intermittent lead exposure induces behavioral and cardiovascular alterations associated with neuroinflammation. *Cells* 12:818. doi: 10.3390/cells12050818

Singh, S., Metz, I., Amor, S., van der Valk, P., Stadelmann, C., and Brück, W. (2013). Microglial nodules in early multiple sclerosis white matter are associated with degenerating axons. *Acta Neuropathol.* 125, 595–608. doi: 10.1007/s00401-013-1082-0

Singhal, G., Morgan, J., Corrigan, F., Toben, C., Jawahar, M., Jaehne, E., et al. (2021). Short-term environmental enrichment is a stronger modulator of brain glial cells and cervical lymph node T cell subtypes than exercise or combined exercise and enrichment. *Cell Mol. Neurobiol.* 41, 469–486. doi: 10.1007/s10571-020-00862-x

Soch, A., Bradburn, S., Sominsky, L., De Luca, S., Murgatroyd, C., and Spencer, S. (2016). Effects of exercise on adolescent and adult hypothalamic and hippocampal neuroinflammation. *Hippocampus* 26, 1435–1446. doi: 10.1002/hipo.22620

Soto, I., Graham, L., Richter, H., Simeone, S., Radell, J., Grabowska, W., et al. (2015). APOE stabilization by exercise prevents aging neurovascular dysfunction and complement induction. *PLoS Biol.* 13:e1002279. doi: 10.1371/journal.pbio.1002279

Stahlhut, M., Downs, J., Wong, K., Bisgaard, A., and Nordmark, E. (2020). Feasibility and effectiveness of an individualized 12-week; Participation (U-PART) intervention in girls and women with rett syndrome. *Phys. Ther.* 100, 168–179. doi: 10.1093/ptj/pzz138

Stefanko, D., Shah, V., Yamasaki, W., Petzinger, G., and Jakowec, M. (2017). Treadmill exercise delays the onset of non-motor behaviors and striatal pathology in the CAG140 knock-in mouse model of Huntington's disease. *Neurobiol. Dis.* 105, 15–32. doi: 10.1016/j.nbd.2017.05.004

Stowell, R., Sipe, G., Dawes, R., Batchelor, H., Lordy, K., Whitelaw, B., et al. (2019). Noradrenergic signaling in the wakeful state inhibits microglial surveillance and synaptic plasticity in the mouse visual cortex. *Nat. Neurosci.* 22, 1782–1792. doi: 10.1038/s41593-019-0514-0

Strohm, A., O'Connor, T., Oldfield, S., Young, S., Hammond, C., McCall, M., et al. (2024). Cortical microglia dynamics are conserved during voluntary wheel running. *J. Appl. Physiol.* 136, 89–108. doi: 10.1152/japplphysiol.00311.2023

Su, P., Wang, D., Cao, Z., Chen, J., and Zhang, J. (2021). The role of NLRP3 in lead-induced neuroinflammation and possible underlying mechanism. *Environ. Pollut.* 287:117520. doi: 10.1016/j.envpol.2021.117520

Sun, L., Li, X., Wang, F., Zhang, J., Wang, D., Yuan, L., et al. (2017). High-intensity treadmill running impairs cognitive behavior and hippocampal synaptic plasticity of rats via activation of inflammatory response. *J. Neurosci. Res.* 95, 1611–1620. doi: 10.1002/jnr.23996

Sun, S., Ma, S., Cai, Y., Wang, S., Ren, J., Yang, Y., et al. (2023). A single-cell transcriptomic atlas of exercise-induced anti-inflammatory and geroprotective effects across the body. *Innovation* 4:100380. doi: 10.1016/j.xinn.2023.100380

Sung, Y., Kim, S., Hong, H., Park, C., Shin, M., Kim, C., et al. (2012). Treadmill exercise ameliorates dopaminergic neuronal loss through suppressing microglial activation in Parkinson's disease mice. *Life Sci.* 91, 1309–1316. doi: 10.1016/j.lfs.2012.10.003

Svensson, M., Andersson, E., Manouchehrian, O., Yang, Y., Deierborg, T., et al. (2020). Voluntary running does not reduce neuroinflammation or improve non-cognitive behavior in the 5xFAD mouse model of Alzheimer's disease. *Sci. Rep.* 10:1346.

Svensson, M., Rosvall, P., Boza-Serrano, A., Andersson, E., Lexell, J., and Deierborg, T. (2016). Forced treadmill exercise can induce stress and increase neuronal damage in a mouse model of global cerebral ischemia. *Neurobiol. Stress* 5, 8–18. doi: 10.1016/j.ynstr.2016.09.002

Szuhany, K., Bugatti, M., and Otto, M. (2015). A meta-analytic review of the effects of exercise on brain-derived neurotrophic factor. *J. Psychiatr Res.* 60, 56–64. doi: 10.1016/j.jpsychires.2014.10.003

Tamakoshi, K., Maeda, M., Murohashi, N., and Saito, A. (2022). Effect of exercise from a very early stage after intracerebral hemorrhage on microglial and macrophage reactivity states in rats. *Neuroreport* 33, 304–311. doi: 10.1097/WNR.0000000000001782

Tan, Y., Yuan, Y., and Tian, L. (2020). Microglial regional heterogeneity and its role in the brain. *Mol. Psychiatry* 25, 351–367. doi: 10.1038/s41380-019-0609-8

Tang, X., Liao, R., Zheng, L., Yang, L., Ma, Z., Yi, C., et al. (2022). Aerobic exercise reverses the NF-κB/NLRP3 inflammasome/5-HT pathway by upregulating irisin to alleviate post-stroke depression. *Ann. Transl. Med.* 10:1350. doi: 10.21037/atm-22-5443

Tejera, D., Mercan, D., Sanchez-Caro, J., Hanan, M., Greenberg, D., Soreq, H., et al. (2019). Systemic inflammation impairs microglial Aβ clearance through NLRP3 inflammasome. *EMBO J.* 38:e101064. doi: 10.15252/embj.2018101064

Thomas, A., Lehn, M., Janssen, E., Hildeman, D., and Chougnet, C. (2022). Naturally-aged microglia exhibit phagocytic dysfunction accompanied by gene expression changes reflective of underlying neurologic disease. *Sci. Rep.* 12:19471. doi: 10.1038/s41598-022-21920-y

Tremblay, M. È, Lowery, R. L., and Majewska, A. K. (2010). Microglial interactions with synapses are modulated by visual experience. *PLoS Biol.* 8:e1000527. doi: 10.1371/journal.pbio.1000527

Tremblay, M. È, Zettel, M. L., Ison, J. R., Allen, P. D., and Majewska, A. K. (2012). Effects of aging and sensory loss on glial cells in mouse visual and auditory cortices. *Glia* 60, 541–558. doi: 10.1002/glia.22287

Valdez, M., Valdez, J., Freeborn, D., Johnstone, A., and Kodavanti, P. (2020). The effects of ozone exposure and sedentary lifestyle on neuronal microglia and mitochondrial bioenergetics of female long-evans rats. *Toxicol. Appl. Pharmacol.* 408:115254. doi: 10.1016/j.taap.2020.115254

van Dellen, A., Cordery, P., Spires, T., Blakemore, C., and Hannan, A. (2008). Wheel running from a juvenile age delays onset of specific motor deficits but does not alter protein aggregate density in a mouse model of Huntington's disease. *BMC Neurosci.* 9:34. doi: 10.1186/1471-2202-9-34

van Horssen, J., Singh, S., van der Pol, S., Kipp, M., Lim, J., Peferoen, L., et al. (2012). Clusters of activated microglia in normal-appearing white matter show signs of innate immune activation. *J. Neuroinflammation* 9:156. doi: 10.1186/1742-2094-9-156

van Praag, H., Christie, B., Sejnowski, T., and Gage, F. (1999a). Running enhances neurogenesis, learning, and long-term potentiation in mice. *Proc. Natl. Acad. Sci. U S A.* 96, 13427–13431. doi: 10.1073/pnas.96.23.13427

van Praag, H., Kempermann, G., and Gage, F. (1999b). Running increases cell proliferation and neurogenesis in the adult mouse dentate gyrus. *Nat. Neurosci.* 2, 266–270. doi: 10.1038/6368

Vecchio, L., Meng, Y., Xhima, K., Lipsman, N., Hamani, C., and Aubert, I. (2018). The neuroprotective effects of exercise: maintaining a healthy brain throughout aging. *Brain Plast.* 4, 17–52. doi: 10.3233/BPL-180069

Vega-Riquer, J., Mendez-Victoriano, G., Morales-Luckie, R., and Gonzalez-Perez, O. (2019). Five decades of cuprizone, an updated model to replicate demyelinating diseases. *Curr. Neuropharmacol.* 17, 129–141. doi: 10.2174/1570159X15666170717120343

Vetreno, R., Patel, Y., Patel, U., Walter, T., and Crews, F. (2017). Adolescent intermittent ethanol reduces serotonin expression in the adult raphe nucleus and upregulates innate immune expression that is prevented by exercise. *Brain Behav. Immun.* 60, 333–345. doi: 10.1016/j.bbi.2016.09.018

Villa, A., Gelosa, P., Castiglioni, L., Cimino, M., Rizzi, N., Pepe, G., et al. (2018). Sex-specific features of microglia from adult mice. *Cell Rep.* 23, 3501–3511. doi: 10.1016/j.celrep.2018.05.048

Vonsattel, J., Myers, R., Stevens, T., Ferrante, R., Bird, and Richardson, E. (1985). Neuropathological classification of Huntington's disease. *J. Neuropathol. Exp. Neurol.* 44, 559–577. doi: 10.1097/00005072-198511000-00003

Vukovic, J., Colditz, M., Blackmore, D., Ruitenberg, M., and Bartlett, P. (2012). Microglia modulate hippocampal neural precursor activity in response to exercise and aging. *J. Neurosci.* 32, 6435–6443. doi: 10.1523/JNEUROSCI.5925-11.2012

Wake, H., Moorhouse, A., Jinno, S., Kohsaka, S., and Nabekura, J. (2009). Resting microglia directly monitor the functional state of synapses in vivo and determine the fate of ischemic terminals. *J. Neurosci.* 29, 3974–3980. doi: 10.1523/JNEUROSCI.4363-08.2009

Walton, C., King, R., Rechtman, L., Kaye, W., Leray, E., Marrie, R., et al. (2020). Rising prevalence of multiple sclerosis worldwide: insights from the Atlas of MS, third edition. *Mult. Scler.* 26, 1816–1821. doi: 10.1177/1352458520970841

Wang, J., Yue, B., Zhang, X., Guo, X., Sun, Z., and Niu, R. (2021). Effect of exercise on microglial activation and transcriptome of hippocampus in fluorosis mice. *Sci. Total Environ.* 760:143376. doi: 10.1016/j.scitotenv.2020.143376

Wang, S., Chen, D., Yang, Y., Zhu, L., Xiong, X., and Chen, A. (2023). Effectiveness of physical activity interventions for core symptoms of autism spectrum disorder: a systematic review and meta-analysis. *Autism Res.* 16, 1811–1824. doi: 10.1002/aur.3004

Wang, T. F., Wu, S., Pan, B., Tsai, S., and Kuo, Y. (2022). Inhibition of nigral microglial activation reduces age-related loss of dopaminergic neurons and motor deficits. *Cells* 11:481. doi: 10.3390/cells11030481

Wang, W., Lv, Z., Gao, J., Liu, M., Wang, Y., Tang, C., et al. (2021). Treadmill exercise alleviates neuronal damage by suppressing NLRP3 inflammasome and microglial activation in the MPTP mouse model of Parkinson's disease. *Brain Res Bull.* 174, 349–358. doi: 10.1016/j.brainresbull.2021.06.024

Wang, Y., Leak, R., and Cao, G. (2022). Microglia-mediated neuroinflammation and neuroplasticity after stroke. *Front. Cell Neurosci.* 16:980722. doi: 10.3389/fncel.2022.980722

Wang, Y., Zhou, Y., Jiang, L., Wang, S., Zhu, L., Zhang, S., et al. (2023). Long-term voluntary exercise inhibited AGE/RAGE and microglial activation and reduced the loss of dendritic spines in the hippocampi of APP/PS1 transgenic mice. *Exp. Neurol.* 363:114371. doi: 10.1016/j.expneurol.2023.114371

Wassouf, Z., Hentrich, T., Samer, S., Rotermund, C., Kahle, P., Ehrlich, I., et al. (2018). Environmental enrichment prevents transcriptional disturbances induced by alpha-synuclein overexpression. *Front. Cell Neurosci.* 12:112. doi: 10.3389/fncel.2018.00112

Wei, J., Liu, L., Song, X., Lin, B., Cui, J., Luo, L., et al. (2023). Physical exercise modulates the microglial complement pathway in mice to relieve cortical circuitry deficits induced by mutant human TDP-43. *Cell Rep.* 42:112240. doi: 10.1016/j.celrep.2023.112240

West, R., Wooden, J., Barton, E., and Leasure, J. (2019). Recurrent binge ethanol is associated with significant loss of dentate gyrus granule neurons in female rats despite concomitant increase in neurogenesis. *Neuropharmacology* 148, 272–283. doi: 10.1016/j.neuropharm.2019.01.016

Whitelaw, B., Stoessel, M., and Majewska, A. (2023). Movers and shakers: microglial dynamics and modulation of neural networks. *Glia* 71, 1575–1591. doi: 10.1002/glia.24323

Williams, Z., Szyszkowicz, J., Osborne, N., Allehyany, B., Nadon, C., Udechukwu, M., et al. (2023). Sex-specific effects of voluntary wheel running on behavior and the gut microbiota-immune-brain axis in mice. *Brain Behav. Immun. Health* 30:100628. doi: 10.1016/j.bbih.2023.100628

Won, J., Nielson, K., and Smith, J. (2023). Large-scale network connectivity and cognitive function changes after exercise training in older adults with intact cognition and mild cognitive impairment. *J. Alzheimers Dis. Rep.* 7, 399–413. doi: 10.3233/ADR-220062

Wong, E., Strohm, A., Atlas, J., Lamantia, C., and Majewska, A. (2021). Dynamics of microglia and dendritic spines in early adolescent cortex after developmental alcohol exposure. *Dev. Neurobiol.* 81, 786–804. doi: 10.1002/dneu.22843

World Health Organization (2023). *Dementia*. Available online at: https://www.who.int/news-room/fact-sheets/detail/dementia (accessed 19 April, 2024).

Wu, L., Li, S., Pang, S., Zhang, B., Wang, J., He, B., et al. (2021). Effects of lead exposure on the activation of microglia in mice fed with high-fat diets. *Environ. Toxicol.* 36, 1923–1931. doi: 10.1002/tox.23312

Xia, W., Xu, M., Yu, X., Du, M., Li, X., Yang, T., et al. (2021). Antihypertensive effects of exercise involve reshaping of gut microbiota and improvement of gut-brain axis in spontaneously hypertensive rat. *Gut Microbes* 13, 1–24. doi: 10.1080/19490976.2020.1854642

Xiao, K., Luo, Y., Liang, X., Tang, J., Wang, J., Xiao, Q., et al. (2021). Beneficial effects of running exercise on hippocampal microglia and neuroinflammation in chronic unpredictable stress-induced depression model rats. *Transl. Psychiatry* 11:461. doi: 10.1038/s41398-021-01571-9

Xiong, J., Li, S., Sun, Y., Zhang, X., Dong, Z., Zhong, P., et al. (2015). Long-term treadmill exercise improves spatial memory of male APPswe/PS1dE9 mice by regulation of BDNF expression and microglia activation. *Biol. Sport* 32, 295–300. doi: 10.5604/20831862.1163692

Xu, H., Gelyana, E., Rajsombath, M., Yang, T., Li, S., and Selkoe, D. (2016). Environmental enrichment potently prevents microglia-mediated neuroinflammation by human amyloid β-protein oligomers. *J. Neurosci.* 36, 9041–9056. doi: 10.1523/JNEUROSCI.1023-16.2016

Xu, H., Rajsombath, M., Weikop, P., and Selkoe, D. (2018). Enriched environment enhances β-adrenergic signaling to prevent microglia inflammation by amyloid-β. *EMBO Mol. Med.* 10:e8931. doi: 10.15252/emmm.201808931

Xu, J., Zhang, L., Li, M., He, X., Luo, J., Wu, R., et al. (2023). TREM2 mediates physical exercise-promoted neural functional recovery in rats with ischemic stroke via microglia-promoted white matter repair. *J. Neuroinflammation* 20:50. doi: 10.1186/s12974-023-02741-w

Xu, Z., Zhang, L., Wang, Q., Marshall, C., Xiao, N., Gao, J., et al. (2013). Aerobic exercise combined with antioxidative treatment does not counteract moderate- or mid-stage Alzheimer-like pathophysiology of APP/PS1 mice. *CNS Neurosci. Ther.* 19, 795–803. doi: 10.1111/cns.12139

Yan, L., Wang, M., Yang, F., Wang, Y., Wang, S., So, K., et al. (2023). Physical exercise mediates a cortical FMRP-mTOR pathway to improve resilience against chronic stress in adolescent mice. *Transl. Psychiatry* 13:16. doi: 10.1038/s41398-023-02311-x

Yang, J., Yuan, S., Jian, Y., Lei, Y., Hu, Z., Yang, Q., et al. (2023). Aerobic exercise regulates GPR81 signal pathway and mediates complement- microglia axis homeostasis on synaptic protection in the early stage of Alzheimer's disease. *Life Sci.* 331:122042. doi: 10.1016/j.lfs.2023.122042

Yi, C., Al-Massadi, O., Donelan, E., Lehti, M., Weber, J., Ress, C., et al. (2012). Exercise protects against high-fat diet-induced hypothalamic inflammation. *Physiol. Behav.* 106, 485–490. doi: 10.1016/j.physbeh.2012.03.021

Yin, Z., Raj, D., Schaafsma, W., van der Heijden, R., Kooistra, S., Reijne, A., et al. (2018). Low-fat diet with caloric restriction reduces white matter microglia activation during aging. *Front. Mol. Neurosci.* 11:65. doi: 10.3389/fnmol.2018.00065

Yokoyama, M., Kobayashi, H., Tatsumi, L., and Tomita, T. (2022). Mouse models of Alzheimer's disease. *Front. Mol. Neurosci.* 15:912995. doi: 10.3389/fnmol.2022.912995

Yoo, D., Chae, J., Jung, H., Yim, H., Kim, J., Nam, S., et al. (2015). Treadmill exercise is associated with reduction of reactive microgliosis and pro-inflammatory cytokine levels in the hippocampus of type 2 diabetic rats. *Neurol. Res.* 37, 732–738. doi: 10.1179/1743132815Y.0000000015

Yoo, T., Yoo, Y., Kang, H., and Kim, E. (2022). Age, brain region, and gene dosage-differential transcriptomic changes in Shank3-mutant mice. *Front. Mol. Neurosci.* 15:1017512. doi: 10.3389/fnmol.2022.1017512

Yue, Y., Xu, P., Liu, Z., Sun, X., Su, J., Du, H., et al. (2021). Motor training improves coordination and anxiety in symptomatic Mecp2-null mice despite impaired functional connectivity within the motor circuit. *Sci. Adv.* 7:eabf7467. doi: 10.1126/sciadv.abf7467

Zaychik, Y., Fainstein, N., Touloumi, O., Goldberg, Y., Hamdi, L., Segal, S., et al. (2021). High-intensity exercise training protects the brain against autoimmune neuroinflammation: regulation of microglial redox and pro-inflammatory functions. *Front. Cell Neurosci.* 15:640724. doi: 10.3389/fncel.2021.640724

Żebrowska, A., Hall, B., Maszczyk, A., Banaś, R., and Urban, J. (2018). Brain-derived neurotrophic factor, insulin like growth factor-1 and inflammatory cytokine responses to continuous and intermittent exercise in patients with type 1 diabetes. *Diabetes Res. Clin. Pract.* 144, 126–136. doi: 10.1016/j.diabres.2018.08.018

Zhang, J., Guo, Y., Wang, Y., Song, L., Zhang, R., and Du, Y. (2018). Long-term treadmill exercise attenuates Aβ burdens and astrocyte activation in APP/PS1 mouse model of Alzheimer's disease. *Neurosci. Lett.* 666, 70–77. doi: 10.1016/j.neulet.2017.12.025

Zhang, J., Sun, B., Yang, J., Chen, Z., Li, Z., Zhang, N., et al. (2022). Comparison of the effect of rotenone and 1-methyl-4-phenyl-1,2,3,6-tetrahydropyridine on inducing chronic Parkinson's disease in mouse models. *Mol. Med. Rep.* 25:91. doi: 10.3892/mmr.2022.12607

Zhang, L., Liu, Y., Wang, X., Wang, D., Wu, H., Chen, H., et al. (2022). Treadmill exercise improve recognition memory by TREM2 pathway to inhibit hippocampal microglial activation and neuroinflammation in Alzheimer's disease model. *Physiol. Behav.* 251: 113820. doi: 10.1016/j.physbeh.2022.113820

Zhang, M., Zhai, Y., Sun, Y., Zhang, W., Li, Q., Brann, D., et al. (2018). Swimming improves cognitive reserve in ovariectomized rats and enhances neuroprotection after global cerebral ischemia. *Brain Res.* 1692, 110–117. doi: 10.1016/j.brainres.2018.05.020

Zhang, Q., Zhang, J., Yan, Y., Zhang, P., Zhang, W., and Xia, R. (2017). Proinflammatory cytokines correlate with early exercise attenuating anxiety-like behavior after cerebral ischemia. *Brain Behav.* 7:e00854. doi: 10.1002/brb3.854

Zhang, S., Zhu, L., Peng, Y., Zhang, L., Chao, F., Jiang, L., et al. (2022). Long-term running exercise improves cognitive function and promotes microglial glucose metabolism and morphological plasticity in the hippocampus of APP/PS1 mice. *J. Neuroinflammation* 19:34. doi: 10.1186/s12974-022-02401-5

Zhang, X., He, Q., Huang, T., Zhao, N., Liang, F., Xu, B., et al. (2019). Treadmill exercise decreases Aβ deposition and counteracts cognitive decline in APP/PS1 Mice, possibly via hippocampal microglia modifications. *Front. Aging Neurosci.* 11:78. doi: 10.3389/fnagi.2019.00078

Zhao, D., Mokhtari, R., Pedrosa, E., Birnbaum, R., Zheng, D., and Lachman, H. (2017). Transcriptome analysis of microglia in a mouse model of rett syndrome: differential expression of genes associated with microglia/macrophage activation and cellular stress. *Mol. Autism* 8:17. doi: 10.1186/s13229-017-0134-z

Ziegler-Waldkirch, S., d'Errico, P., Sauer, J., Erny, D., Savanthrapadian, S., Loreth, D., et al. (2018). Seed-induced Aβ deposition is modulated by microglia under environmental enrichment in a mouse model of Alzheimer's disease. *EMBO J.* 37, 167–182. doi: 10.15252/embj.201797021

Glossary

PE	physical exercise
CNS	central nervous system
CD68	cluster of differentiation 68
CX3CR1	C-X3-C motif chemokine receptor 1
CD86	cluster of differentiation 86
MHCII	major histocompatibility complex class 2
IGF-1	insulin-like growth factor 1
BDNF	brain-derived neurotrophic factor
C1QA	complement C1q A Chain
CD206	mannose receptor
Gal-3	galectin-3
FASD	fetal alcohol spectrum disorders
mTOR	mammalian target of rapamycin
VWR	voluntary wheel running
CDLK5	cyclin-dependent kinase-like 5
Shank3	multiple ankyrin repeat domains 3
FMRP	fragile X messenger ribonucleoprotein 1 protein
Mecp2	X-linked methyl-CpG-binding protein 2
CR3	complement receptor 3
IL-1β	interleukin-1 beta
IL-18	interleukin 18
IL-6	interleukin 6
Iba1	ionized calcium-binding adapter molecule 1
$NL3^{R451C}$	neuroligin-3
HD	Huntington's disease
ALS	amyotrophic lateral sclerosis
AD	Alzheimer's disease
MS	multiple sclerosis
PD	Parkinson's disease
APP	amyloid protein precursor
PSEN1	presenilin-1
PSEN2	presenilin-2
MAPT	microtubule-associated protein tau
TREM2	triggering receptor expressed on myeloid cells 2
EAE	experimental autoimmune encephalomyeliti
MPTP	1-methyl-4-phenyl-1,2,3,6-tetrahydropyridine
TDP-43	TAR DNA binding protein 43 kDa
ICH	intracerebral hemorrhage
OX-6	major histocompatibility complex class 2 1a
TNF-α	tumor necrosis factor alpha
MSG	monosodium glutamate
Cox-2	cyclooxygenase 2
DEET	N, N-diethyl-m-toluamide
PER	insecticide permethrin
PB	pyridostigmine bromide
O3	ozone
Pb	lead
NLRP	nucleotide-binding oligomerization domain, leucine rich repeat and pyrin domain containing
NGF	nerve growth factor

frontiers | Frontiers in Neuroscience

TYPE Original Research
PUBLISHED 19 August 2024
DOI 10.3389/fnins.2024.1420507

OPEN ACCESS

EDITED BY
Kiran Bhaskar,
University of New Mexico, United States

REVIEWED BY
Mohd Moin Khan,
Brigham and Women's Hospital and Harvard Medical School, United States
Daniel José Barbosa,
University Institute of Health Sciences, Portugal

*CORRESPONDENCE
Yue Wan
✉ wanyue790623@163.com
Xiaorong Deng
✉ dxr9596@163.com

RECEIVED 20 April 2024
ACCEPTED 23 July 2024
PUBLISHED 19 August 2024

CITATION
Yan M, Zhang Q, Chen Y, Zhu C, Wang D, Tan J, He B, Li Q, Deng X and Wan Y (2024) α-Synuclein-mediated mitochondrial translocation of cofilin-1 leads to oxidative stress and cell apoptosis in PD. *Front. Neurosci.* 18:1420507. doi: 10.3389/fnins.2024.1420507

α-Synuclein-mediated mitochondrial translocation of cofilin-1 leads to oxidative stress and cell apoptosis in PD

Mingmin Yan[1,2], Qian Zhang[1], Yu Chen[1], Chenyi Zhu[1], Dan Wang[1], Jie Tan[1], Bihua He[1], Qin Li[1], Xiaorong Deng[1]* and Yue Wan[1]*

[1]Department of Neurology, Hubei No. 3 People's Hospital, School of Medicine, Jianghan University, Wuhan, China, [2]Hubei Key Laboratory of Cognitive and Affective Disorders, Jianghan University, Wuhan, China

Parkinson's disease (PD) is characterized by the accumulation of misfolded α-synuclein protein and the loss of dopaminergic neurons in the substantia nigra. Abnormal α-synuclein aggregates form toxic Lewy bodies, ultimately inducing neuronal injury. Mitochondrial dysfunction was reported to be involved in the neurotoxicity of α-synuclein aggregates in PD. However, the specific mechanism by which abnormal α-synuclein aggregates cause mitochondrial disorders remains poorly defined. Previously, we found that cofilin-1, a member of the actin-binding protein, regulates α-synuclein pathogenicity by promoting its aggregation and spreading *in vitro and in vivo*. In this study, we further investigated the effect of cofilin-1 on α-synuclein induced mitochondrial damage. We discovered that α-synuclein aggregates accelerate the translocation of cofilin-1 to mitochondria, promote its combination with the mitochondrial outer membrane receptor Tom 20, and ultimately activate the oxidative damage and apoptosis pathway in mitochondria. All these results demonstrate the important regulatory role of cofilin-1 in the mitochondrial neurotoxicity of pathological α-synuclein during the progression of PD.

KEYWORDS

α-synuclein, cofilin-1, mitochondria, oxidative stress, apoptosis, Parkinson's disease

Introduction

Parkinson's disease (PD) is a common neurodegenerative disorder characterized by the degeneration of dopamine neurons in the substantia nigra and the accumulation of Lewy bodies in remaining neurons. Misfolded α-synuclein is a key component of intracellular Lewy bodies in PD. It is widely accepted that the formation of pathological α-synuclein aggregates is characteristic of synucleinopathies and directly induces neuronal damage in PD (Bloem et al., 2021). Dysfunction of multiple organelles, including mitochondria, synaptic vesicles, autophagosomes, lysosomes, is considered to be implicated in the toxic consequences of misfolded α-synuclein aggregates (Wong and Krainc, 2017). However, the specific mechanism induced by pathological α-synuclein remains unclear.

Mitochondrial damage is one of the key pathogenic factors that aggravates the α-synuclein pathology in PD. Mutations in the mitochondrial kinase PINK1 and the mitochondrial-binding protein Parkin were identified as the leading causes of autosomal recessive PD (Giasson and Lee, 2001; Valente et al., 2004; Corti et al., 2011). Moreover, multiple studies *in vitro* showed that the translocation of α-synuclein aggregates to mitochondria coincides with increased mitochondrial dysfunction and neuronal damage (Sulzer, 2001; Choi et al., 2022), revealing important roles of mitochondrial homeostasis in the α-synuclein neurotoxicity of PD.

Cofilin is a member of the actin depolymerizing factor (ADF) family, which mainly binds actin and regulates its cytoskeleton dynamics (Beck et al., 2012; Bravo-Cordero et al., 2013). It is abundant in the central nervous system and widely distributed throughout the cell body and neurites, where it regulates actin dynamics, such as cell division, migration, protein trafficking, and synaptic transmission. The N-terminal serine residue at the third site (Ser-3) in cofilin is considered a conserved phosphorylation site related to the activation of cofilin-1 (Arber et al., 1998; Yang et al., 1998). Cofilin-1 is active when Ser-3 is dephosphorylated and becomes inactive when Ser-3 is phosphorylated. It is worth noting that activated dephosphorylated cofilin is involved in the initiation phase of apoptosis in mitochondria (Klamt et al., 2009). Since cofilin is an essential regulator of cytoskeletal and neuronal functions, disruption of its structure and function has profound implications for several neurological disorders (Shaw and Bamburg, 2017). Cofilin dysregulation in rodent models has long been known to induce dendrite reduction and neurodegeneration, exhibiting many neurological symptoms, including behavioral impairment, memory dysfunction, and sleep deprivation (Bamburg and Wiggan, 2002; Jang et al., 2005; Woo et al., 2012).

In our previous study, cofilin-1 was found to promote the aggregation and transmission of pathological α-synuclein *in vivo and vitro* (Yan et al., 2020, 2022), suggesting cofilin-1 may act as one of the key pathogenic factors that aggravate α-synuclein pathology. However, the roles of cofilin-1 in the pathogenesis of α-synuclein and how cofilin regulates the mitochondrial toxicity of α-synuclein are currently unclear.

In this study, we further investigated the regulatory role of cofilin-1 in α-synuclein neurotoxicity. We discovered that α-synuclein aggregates facilitate the activation and redistribution of cofilin-1 in mitochondria. Meanwhile, cofilin-1 aggravates α-synuclein-induced mitochondrial membrane potential (MMP) disturbance by binding to the mitochondrial outer membrane receptor Tom 20, increasing the generation of reactive oxygen species (ROS) and ultimately inducing the mitochondria-mediated intrinsic apoptosis pathway in cells. Together, these results demonstrate the major role of cofilin-1 in regulating α-synuclein-induced mitochondrial damage.

Pathological α-synuclein can exert its neurotoxicity by inducing the translocation of cofilin-1 to the outer mitochondrial membrane, thereby initiating oxidative stress and cell apoptosis. Our study provides new insights into the mitochondrial neurotoxicity of pathological α-synuclein in PD.

Methods

Reagents

Thioflavin T was purchased from Sigma (St. Louis, MO, USA). Lipofectamine-2000, BCA Protein Assay Kit, isopropyl β-D-thiogalactoside (IPTG), and Alexa Fluor 594/488-conjugated secondary antibody were purchased from Thermo Fisher Scientific (Waltham, MA, USA). Mito-track, Caspase 3 Kit, Cell Mitochondria Isolation Kit, rhodamine 123, Hoechst 33342, and propidium iodide (PI) were purchased from Beyotime (Shanghai, China). ROS Kit, MDA Assay Kit, and JC-1 reagents were purchased from Solarbio (Peking, China). Cell Counting Kit-8 (CCK-8) was purchased from Dojindo (Peking, China). In addition, the following reagents and antibodies were used: GAPDH (Proteintech, 60004-1-Ig, Wuhan, China), cofilin (Cell Signaling Technology, 5175, Danvers, MA, USA), p-cofilin (Cell Signaling Technology, 3313, Danvers, MA, USA), S129 (Cell Signaling Technology, 23706, Danvers, MA, USA), α-synuclein (Invitrogen, AHB0261, Carlsbad, CA, USA), ubiqutin (Proteintech, 10201-2-AP, Wuhan, China), Bax (Proteintech, 50599-2-Ig, Wuhan, China), Bcl-2 (Proteintech, 26593-1-AP, Wuhan, China), Cytochrome c (Invitrogen, 45-6100, Carlsbad, CA, USA), Tom 20 (Cell Signaling Technology, 42406, Danvers, MA, USA), HRP-conjugated anti-mouse IgG (BIO-RAD, 170-6516, Hercules, CA, USA), HRP-conjugated anti-rabbit IgG (BIO-RAD, 170-6515, Hercules, CA, USA), Alexa Fluor 594-conjugated goat anti-mouse IgG (Invitrogen, A-11005, Carlsbad, CA, USA), Alexa Fluor 594-conjugated goat anti-rabbit IgG (Invitrogen, A-11012, Carlsbad, CA, USA), DAPI (Biofroxx, EZ3412B205, Germany).

Protein expression and purification of α-synuclein and cofilin-1

The expression and purification of α-synuclein and cofilin-1 were performed as previously described (Yan et al., 2020, 2022). Briefly, α-synuclein and cofilin-1 coding sequences with 6xHis-tag were cloned into the PRK172 plasmid and transduced into the BL21 *E. coli* strain. Cells were cultured in the Luria-Bertani broth medium with 100 mg/mL ampicillin at 37°C. Then, 0.6 mM isopropyl β-D-thiogalactoside (IPTG) was added until the optical density (OD600) reached approximately 0.8, followed by an additional 6-h incubation for protein expression. Then, the α-synuclein protein and cofilin-1 protein were purified through 6xHis Ni-chelating affinity chromatography and eluted at approximately 125 mM imidazole. The purity level was higher than 90%, as demonstrated through the technique known as sodium dodecyl sulfate-polyacrylamide gel electrophoresis (SDS-PAGE). Protein concentrations were determined by the BCA assay (Thermo Fisher, Waltham, MA, USA). α-Synuclein and cofilin-1 proteins were finally lyophilized and stored at −80°C for further analysis.

Preparation of fibrils

To prepare fibrils, lyophilized protein was dissolved in phosphate-buffered saline (PBS) and centrifuged at 100,000 rpm for 1 h at 4°C. The residue was removed, and the soluble α-synuclein or cofilin-1 protein in the supernatant was retained. The protein concentration of the supernatant was determined using the bicinchoninic acid (BCA) assay (Thermo Fisher, Waltham, MA, USA). α-Synuclein aggregation was induced by incubating the above-purified α-synuclein protein at 37°C with shaking at 1,000 rpm for 5 days. Mixed fibrils were made of α-synuclein and cofilin-1 proteins and were incubated in a similar manner. α-Synuclein with or without cofilin-1 fibrillization was confirmed using the thioflavin T fluorescence assay. Briefly, aliquots of 5 μl from the incubation samples were diluted to 100 μl with 25 mM thioflavin T

in PBS and tested at 450 nm excitation and 510 nm emission using the SpectraMax plate reader. The verified α-synuclein aggregates were then sonicated for 30 s with a 0.5-s pulse on/off (Sonics Vibra cell, Newtown, USA), aliquoted, snap-frozen in liquid nitrogen, and finally stored at −80°C.

Induction of α-synuclein aggregation (cell seeding experiment)

After transfecting GST-vector and GST-cofilin-1 into 6-well plates with GFP-α-syn-HEK293 cells, 5 μg of α-synuclein fibrils were transduced into cells the next day. For transduction of α-synuclein fibrils, equal volumes of Lipofectamine 2000 (Thermo Fisher, Waltham, MA, USA) and α-synuclein fibrils solutions were diluted in Opti-MEM medium and mixed to a final concentration of 2.8% (v/v), followed by a 20-min incubation before adding into cell medium. Moreover, 48 h later, the formation and morphology of endogenous α-synuclein inclusions were observed using fluorescence microscopy at different times after adding fibrils.

Primary neuron cultures

Primary mouse cortical neurons dissected from α-synuclein A53T transgenic mice embryos were cultured as previously described. The neurons were infected with adeno-associated viruses (AAVs) or α-synuclein fibrils at 5 days *in vitro*. 1 week later, the neurons were fixed in 4% formaldehyde and stained as below.

Immunofluorescence for neurons and cells

For immunofluorescence, neurons and cells were first fixed and permeabilized with 4% paraformaldehyde supplemented with 1% TX-100 (v/v) for 15 min. The permeabilization solution was then removed and washed three times with PBS. After blocking with a 3% BSA solution at room temperature for 30 min, primary antibodies were added and incubated overnight at 4°C. Coverslips were rinsed three times in PBS for 15 min. Subsequently, the samples were incubated using Alexa Fluor 488/594 anti-mouse/rabbit secondary antibody (1:500) for 1 h and washed three times with PBS. Then, the slides were stained with DAPI (300 nM) for 30 s, washed with PBS again, and finally mounted on glass slides. These slides were observed under an Olympus inverted fluorescence microscope (Olympus TH4-200, Japan). The experiment was repeated at least three times.

Immunostaining for brain samples

The paraffin slices of mouse brain samples were treated with 0.3% H_2O_2 for 10 min. Then, the slices were washed three times in PBS, blocked in 3% BSA for 1 h, and then incubated overnight with primary antibodies at 4°C. The signals were developed with the Histostain-SP kit (Invitrogen, Carlsbad, CA, USA). To detect the colocalization of cofilin-1 and Tom 20 in α-synuclein A53T transgenic mice, the sections were incubated with corresponding primary antibodies overnight at 4°C. Then, the sections were washed three times in PBS and incubated with Alexa Fluor 488/594 anti-mouse/rabbit fluorescent secondary antibody (1:500) for 1 h at room temperature. After being stained with DAPI, the sections were covered with a glass cover using the mounting solution and examined under a fluorescence microscope.

Cell viability assay

Cell viability was detected using the Cell Counting Kit-8 viability assay. Following the manufacturer's instructions, the cells were first transduced with α-synuclein fibrils and mixed fibrils, and then plated at a density of 1×10^4 cells/100 μL in 96-well plates. After 48 h, 10 μL of CCK8 solution was added to each well and incubated at 37°C for 2 h. The medium was then removed and washed twice with PBS. The absorbance was detected at 450 nm by using a Spectra Max Plus 384 Microplate Reader. Cell viability was expressed as the percentage of the control group. The experiment was repeated at least three times.

Western blot analysis

Cells were washed twice with PBS and scraped into an ice-cold NP40 cell lysis buffer containing protease and phosphatase inhibitors for 30 min. The lysate was centrifuged at 15,000 rpm for 15 min at 4°C. The protein concentration was determined in the BCA assay. The supernatant was boiled in an SDS loading buffer. The SDS protein loading buffer (6X) contained 375mM Tris-HCl with pH 6.8, 9% SDS, 50% glycerin, and 0.03% bromophenol blue, and it was diluted to 25 ml with ultrapure water. The samples were separated on SDS/15% polyacrylamide gels, transferred to nitrocellulose membranes (Thermo Fisher Scientific, Waltham, MA, USA) using a semi-dry system (Bio-Rad, Hercules, CA, USA), blocked in 5% non-fat milk (50 mg/ml) in Tris Buffered Saline with Tween-20 (TBST), and incubated with primary antibodies overnight at 4°C. The membranes were washed three times with TBST and then labeled with horseradish peroxidase (HRP)-conjugated secondary antibodies. The signals were detected using enhanced chemiluminescent (ECL) substrates. Image J software was used to measure the density of Western blot bands. The experiment was repeated at least three times.

Triton-X and SDS fractionation of soluble and insoluble α-synuclein

GST-vector and GST-cofilin-1 were transfected into HEK293 cells separately. α-Synuclein fibrils were transduced into cells on the second day. Moreover, 48 h later, the cells were collected. For sequential extraction of soluble and insoluble α-synuclein, the cells were washed twice with PBS and scraped into 1% Triton X-100 (TX-100) containing protease and phosphatase inhibitors. After sonication using a fine probe [0.5-s pulse at an amplitude of 20%, repeated 10 times (using a Ningbo Toshiba Ultrasonic

Cell Crusher JY99-IIDN, China)], cell lysates were incubated on ice for 30 min and centrifuged at 100,000 g for 30 min at 4°C. The supernatant (TX-100 soluble fraction) was collected while the pellet was washed in 1% Triton X-100, sonicated as described earlier, and then centrifuged for another 30 min at 100,000 g. The supernatant was discarded, whereas the pellet (TX-100 insoluble fraction) was resuspended in 2% sodium dodecyl sulfate (SDS) supplemented with protease and phosphatase inhibitors. It was sonicated using a fine probe (0.5-s pulse at an amplitude of 20%, 15 times). Then, the lysate was lysed at room temperature for 30 min and centrifuged. The supernatant was retained as the insoluble fraction. The experiment was repeated at least three times.

Mitochondrial and cytoplasmic extraction

Differential centrifugation was employed to extract mitochondria and cytoplasm from HEK293 cells using the Beyotime Cell Mitochondria Isolation Kit to obtain the cytoplasmic and mitochondrial fractions. According to the manufacturer's instructions, HEK293 cells were lysed in a precooled mitochondrial separation reagent and centrifuged at 600 g for 5 min at 4°C. Subsequently. The supernatant was centrifuged at 11,000 g for 10 min at 4°C to isolate cytoplasmic and mitochondrial fractions. Then, the cytoplasmic supernatant and the pellet containing isolated mitochondria were carefully collected. The mitochondrial preparation was washed several times and resuspended in a mitochondrial stock solution. Finally, the mitochondrial lysate supplemented with the protease inhibitor was prepared for protein analysis.

Determination of intracellular ROS and MDA

To determine the intracellular ROS level, SH-SY5Y cells were incubated with 50 μmol/L DCFH-DA (2′,7′-dichlorodihydrofluorescein diacetate) at 28°C for 30 min in the dark and then washed twice with the PBS buffer. Fluorescent images of intracellular ROS were captured using a fluorescence microscope. According to the manufacturer's instructions, intracellular MDA levels were determined using the Malondialdehyde (MDA) assay kits. First, the treated cells were resuspended in distilled deionized water and the thiobarbituric acid reagent and then heated for 15 min in a boiling water bath. The mixtures were then cooled to room temperature and centrifuged at 3,000 rpm for 5 min to remove the cell debris. The absorbance of the supernatants was measured at 535 nm, and non-specific turbidity was corrected by subtracting the absorbance at 600 and 450 nm.

Detection of mitochondrial membrane potential

Changes in the mitochondrial membrane potential were measured using rhodamine and JC-1 staining methods. Rhodamine 123 staining working solution was added into the SY5Y cells and then incubated at 37°C in a cell culture incubator for 40 min. After being washed twice with cell culture medium, the SY5Y cells were observed under a fluorescence microscope for mitochondrial membrane potential analysis. In addition, a Solarbio mitochondrial membrane sensor kit was used to determine the mitochondrial membrane potential by measuring the potential-dependent accumulation of 5,5′,6,6′-tetrachloro-1,1′,3,3′-tetraethylbenzimidazolylcarbocyanine iodide (JC-1). JC-1 emits red fluorescence while aggregated in the mitochondria of healthy cells. Nevertheless, the dye cannot accumulate in the mitochondria of cells with a collapsed MMP and remains as a monomer, emitting green fluorescence throughout the cell. After being treated with α-synuclein fibrils, cofilin-1, or cofilin mutants for 36 h and washed with PBS, the cells were cultured with JC-1 solution for 20 min at 37°C. Then, the fluorescence intensity was determined using fluorescence microscopy. These experiments were repeated at least three times.

Statistical analyses

All data were expressed as mean ± SEM (standard error of the mean). The statistical analysis was performed using Student's *t*-test for a two-group comparison. When variances were not equal, alternative statistical methods, such as the Mann–Whitney test, were applied. A one-way ANOVA was applied to confirm the significant effects among three or more groups, followed by Tukey's multiple comparisons for *post hoc* tests. A two-way ANOVA was used to analyze the significant effects of grouped data, followed by Bonferroni's multiple comparisons for *post hoc* tests. For the data that were not to be normally distributed, the Kruskal–Wallis test was employed for comparisons, and GraphPad Prism software was used in the above statistical analyses. Differences with $P < 0.05$ were considered significant. All experiments were performed in triplicate for at least three independent trials.

Results

Cofilin-1 promotes the aggregation of α-synuclein *in vitro* and in cells

In our previous study, since purified cofilin-1 *in vitro* was considered to promote the aggregation kinetics of α-synuclein, we further observed the morphology of α-synuclein aggregates with or without cofilin-1 using thioflavin T (ThT) fluorescence staining. The pathological α-synuclein was found to accumulate more abundantly as the concentration of cofilin-1 increased (Figures 1A, B). Furthermore, compared with the pure α-synuclein fibrils, overexpressed cofilin-1 and α-synuclein fibrils in human embryonic kidney 293 (HEK293) cells induced more expression of higher molecular weight species, especially in the insoluble 2% SDS solution (Figures 1C, D). This result represented the overexpression of cofilin-1 together with α-synuclein fibrils, which promoted added aggregation of endogenous α-synuclein in HEK293 cells.

10.3389/fnins.2024.1420507

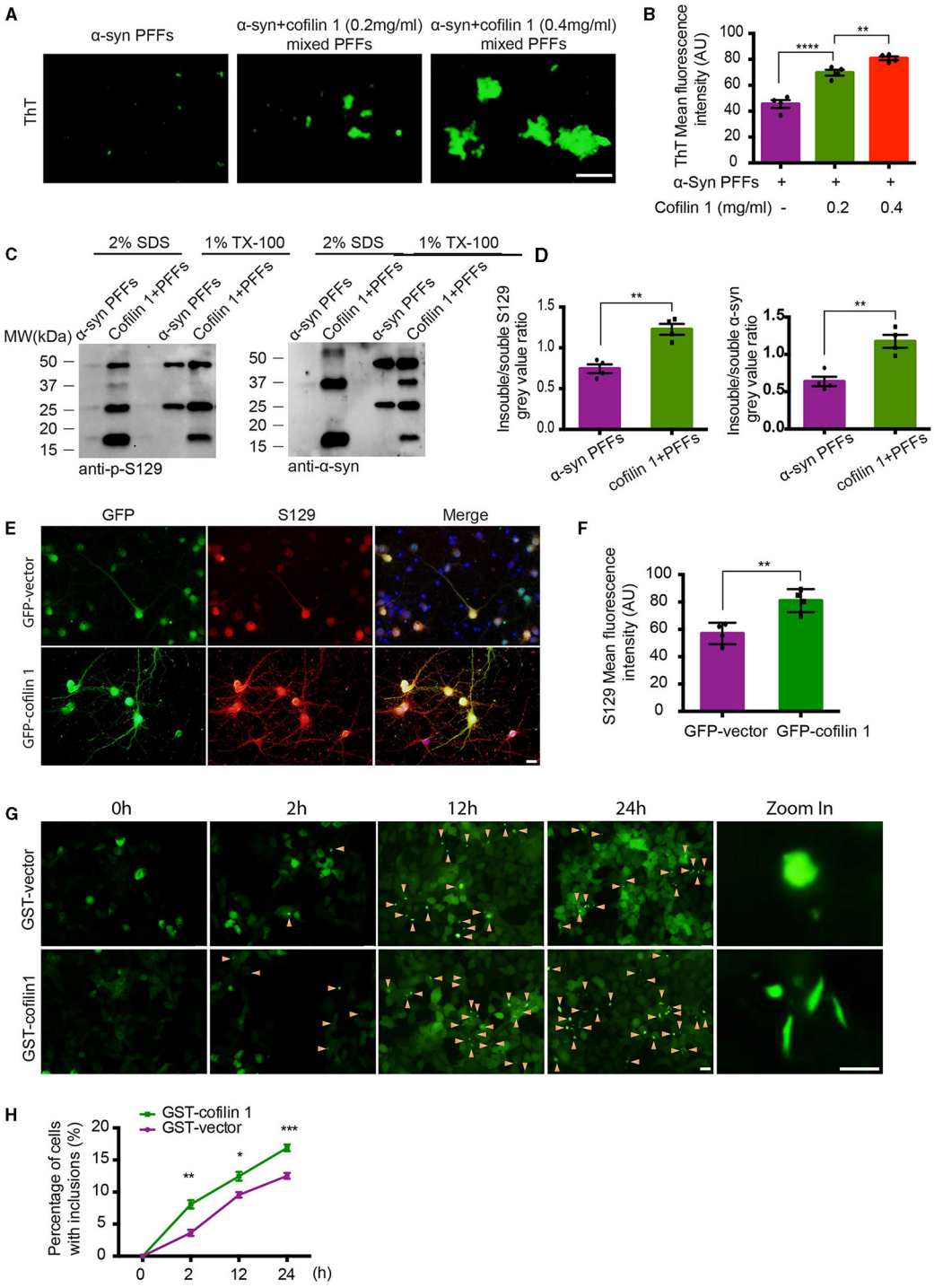

FIGURE 1
Cofilin-1 promotes the aggregation of α-synuclein *in vitro* and in cells. **(A, B)** Thioflavin T fluorescent staining showing α-synuclein aggregation with cofilin-1 in different concentrations. Mixed pre-formed fibrils (PFFs) composed of α-synuclein and cofilin-1 were more aggregated than pure α-synuclein PFFs, especially at high concentrations of cofilin-1. Scale bar, 100 μm. Data are represented as mean ± SEM, $^{**}P < 0.01$, $^{****}P < 0.0001$ by one-way ANOVA. **(C, D)** Western blot analysis of soluble and insoluble p-S129 α-synuclein using triton-X and SDS dissolution test. Compared with pure α-synuclein PFFs, overexpressed cofilin-1 and α-synuclein PFFs in HEK293 cells induced more insoluble α-synuclein aggregates. Quantification of insoluble S129 and α-synuclein. The results are normalized to soluble S129 and α-synuclein. Data are represented as mean ± SEM, $^{**}P < 0.01$ by *t*-test. **(E, F)** Immunostaining for S129 shows that overexpressed cofilin-1 promoted the phosphorylation of α-synuclein in neurons of α-synuclein A53T mice. Scale bar, 20 μm. Data are represented as mean ± SEM, $^{**}P < 0.01$ by *t*-test. **(G)** Cell seeding experiment for intracellular α-synuclein aggregates. Green aggregates (arrows) indicate α-synuclein aggregates. The aggregates in the overexpressed cofilin-1 group were significantly increased at different times compared with the control group, while the aggregate morphology was also inconsistent. Scale bar, 20 μm; Zoom in Scale bar, 5 μm. **(H)** Counting of cells with α-synuclein inclusions. At least 120 cells from at least three fields were counted in the experiments. Data are represented as mean ± SEM, $^{*}P < 0.05$, $^{**}P < 0.01$, and $^{***}P < 0.001$ by two-way ANOVA.

Immunostaining of p-s129 in neurons of α-synuclein A53T mice also supported this result; adeno-associated virus encoding EGFP-cofilin-1 (AAV-GFP-cofilin-1) markedly strengthened the immunoreactivity of p-S129 in neurons compared with the control AAVs (AAV-GFP-vector) (Figures 1E, F). To further investigate the regulation of cofilin-1 on the aggregation of α-synuclein in cells, we used the HEK293 cell line stably transfected with YFP-α-synuclein A53T (YFP-α-syn-HEK293 cells) as reporter cells for the cell seeding experiment. While these cells are transduced with exogenous α-synuclein fibrils, endogenous α-synuclein aggregates into inclusions with visible green fluorescence. We transfected GST-vector and GST-cofilin-1 into the reporter cells, respectively, and transduced with exogenous α-synuclein fibrils the next day. Interestingly, we found that the cells developed globular inclusions only 2 h after treatment with α-synuclein fibrils. The number of intracellular α-synuclein aggregates increased gradually over time, especially when cofilin-1 was overexpressed. However, the overexpression of cofilin-1 promoted the aggregation of endogenous α-synuclein to form different rod-shaped inclusions rather than the globular shapes (Figures 1G, H), suggesting that cofilin-1 promotes the aggregation of α-synuclein into more distinct inclusions, not only *in vitro* but also in cells.

α-Synuclein fibrils facilitate the activation and redistribution of cofilin-1

Since cofilin-1 promotes the aggregation of α-synuclein, we further explored whether α-synuclein aggregates cause their neurotoxicity through cofilin-1. We examined the expression of cofilin-1 in YFP-α-syn-HEK293 cells with α-synuclein fibrils and found that cofilin-1 was mainly expressed in the cytoplasm and protrusions rather than evenly distributed in cells (Figure 2A), suggesting that α-synuclein fibrils promote the redistribution of endogenous cofilin-1. We further verified the effect of α-synuclein fibrils on cofilin-1 in human neuroblastoma cells (SH-SY5Y cells). After transduction of α-synuclein fibrils, we found that cofilin-1 colocalized with the mitochondrial fluorescent probe (Mito-track) (Figure 2B), suggesting that α-synuclein fibrils promote the expression of cofilin-1 in mitochondria. Finally, we transduced HEK293 cells with α-synuclein fibrils and collected cells at different times after adding fibrils. The Western blot analysis showed that the level of p-cofilin-1 gradually declined, while the expression of total cofilin-1 was almost the same (Figures 2C–F). This observation suggests that α-synuclein fibrils induce the decrease in inactive p-cofilin, resulting in an increase in activated cofilin-1. Overall, our results indicate that α-synuclein fibrils facilitate the activation and redistribution of cofilin-1 in cells.

Cofilin-1 aggravates α-synuclein-induced oxidative stress in cells

It has been reported that cofilin-1 initiates the apoptotic pathway and induces oxidative stress in mitochondria. We further verified whether α-synuclein exerts its toxic effects through cofilin-1. We first constructed the point mutation of cofilin-1 as cofilin S3A and cofilin S3D. Cofilin S3A is a continuously activated state, whereas cofilin S3D cannot be activated. Then, we examined the mitochondrial membrane potential in SH-SY5Y cells with Rhodamine. After transducing SH-SY5Y cells with pure α-synuclein fibrils, together with cofilin-1, cofilin S3A, or cofilin S3D separately, the fluorescence intensities were generally increased in α-synuclein fibrils compared with the control group, indicating that the fibrils triggered the mitochondrial membrane damage. Moreover, the overexpression of cofilin-1 exacerbates the loss of mitochondrial membrane potential, especially when dephosphorylated cofilin S3A was overexpressed, while phosphorylated inactive cofilin S3D decreased the loss of membrane potential in mitochondria (Figures 3A, D). Moreover, we stained SH-SY5Y cells using the ROS fluorescence probe DCFH-DA (green) and DHE (red). The fluorescence levels of DCFH-DA and DHE were increased in fibril groups compared with the control group. Similarly, α-synuclein fibrils with the overexpression of cofilin triggered stronger fluorescence intensity than pure α-synuclein fibrils, especially fibrils with cofilin S3A, but the fluorescence intensity was decreased in α-synuclein fibrils with the cofilin S3D group, indicating that ROS levels increased when cofilin-1 was overexpressed with α-synuclein fibrils. Dephosphorylated active cofilin-1 accelerates more severe ROS generation induced by α-synuclein fibrils, whereas inactive cofilin-1 reduces this α-synuclein-induced oxidative stress damage in cells (Figures 3B, C, E, F). Consistent with these results, the MDA level in α-synuclein fibrils group increased more significantly than the control group, while mixed fibrils of α-synuclein and cofilin-1 attenuated the MDA level in SH-SY5Y cells (Figure 3G). These findings suggest that cofilin-1 aggravates oxidative stress induced by α-synuclein fibrils in cells, especially active cofilin-1 instead of phosphorylated inactive cofilin-1.

Overexpression of cofilin-1 accelerates α-synuclein-induced cell apoptosis

We further investigated the effect of cofilin-1 on cell apoptosis induced by α-synuclein fibrils. After the neurons of α-synuclein A53T transgenic mice treated with AAV-GFP-cofilin-1 and AAV-GFP-vector, we found that the reactivities of proteolysis marker ubiquitin were much stronger in neurons with AAV-GFP-cofilin-1 than that in neurons with control AAVs, suggesting that overexpressed cofilin-1 promotes the degradation of proteins (Figures 4A, B). We also assessed the effect of cofilin-1 on apoptosis in SH-SY5Y cells via Hoechst staining. We found that the α-synuclein fibrils group induced more cell apoptosis than the control group, while the apoptotic rate in cells transduced with GFP-cofilin-1 was higher than that with GFP-vector (Figures 4C, D). Similarly, compared with the pure α-synuclein fibrils, the cell viability of mixed fibrils declined significantly, indicating that cofilin-1 reduces cell viability and accelerates α-synuclein-induced cell apoptosis (Figure 4E). To further verify the effect of cofilin-1 on toxic α-synuclein fibrils, we detected

10.3389/fnins.2024.1420507

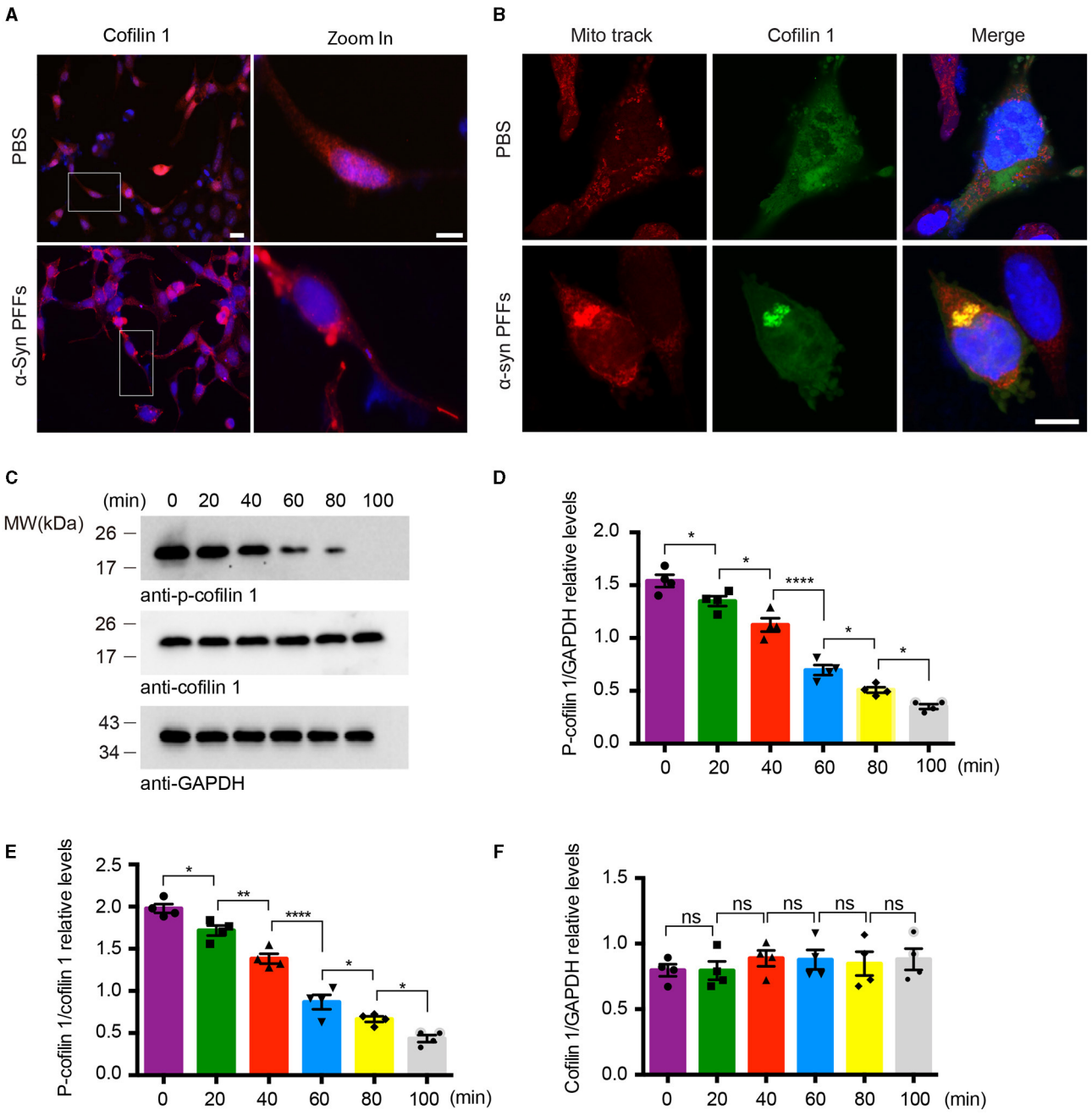

FIGURE 2
α-Synuclein fibrils facilitate the activation and redistribution of cofilin-1. **(A)** Immunostaining showing the redistribution of cofilin-1 in YFP-α-syn-HEK293 cells with α-synuclein fibrils. Scale bar, 20 μm; Zoom in Scale bar, 10 μm. **(B)** Immunofluorescence showing the colocalization of cofilin-1 and Mito-track in SH-SY5Y cells transduced with α-synuclein fibrils. Scale bar, 10 μm. **(C–F)** Western blot detection of p-cofilin-1, total cofilin-1, and GAPDH in HEK293 cells. The expression of non-activated p-cofilin-1 decreased at different times after transducing α-synuclein fibrils. Data are represented as mean ± SEM, $*P < 0.05$, $**P < 0.01$, $****P < 0.0001$. ns, not statistically significant by one-way ANOVA.

the expression of p-S129 and apoptosis-related proteins, Bax, Bcl-2, and cytochrome c. It was well known that proapoptotic protein Bax, anti-apoptotic protein Bcl-2, and cytochrome c played an important role in cell apoptosis. Bcl-2 and Bax proteins were considered to regulate the release of cytochrome c from mitochondria into the cytoplasm, which ultimately triggered the executive apoptotic pathways. As expected, α-synuclein fibrils with transfected cofilin-1 induced more expression of p-S129, Bax, and cytochrome c, while mitochondrial Bcl-2 was significantly reduced in the presence of cofilin-1 (Figures 4F–J). These results suggest that cofilin-1 accelerates α-synuclein-induced cell apoptosis and neurotoxicity.

10.3389/fnins.2024.1420507

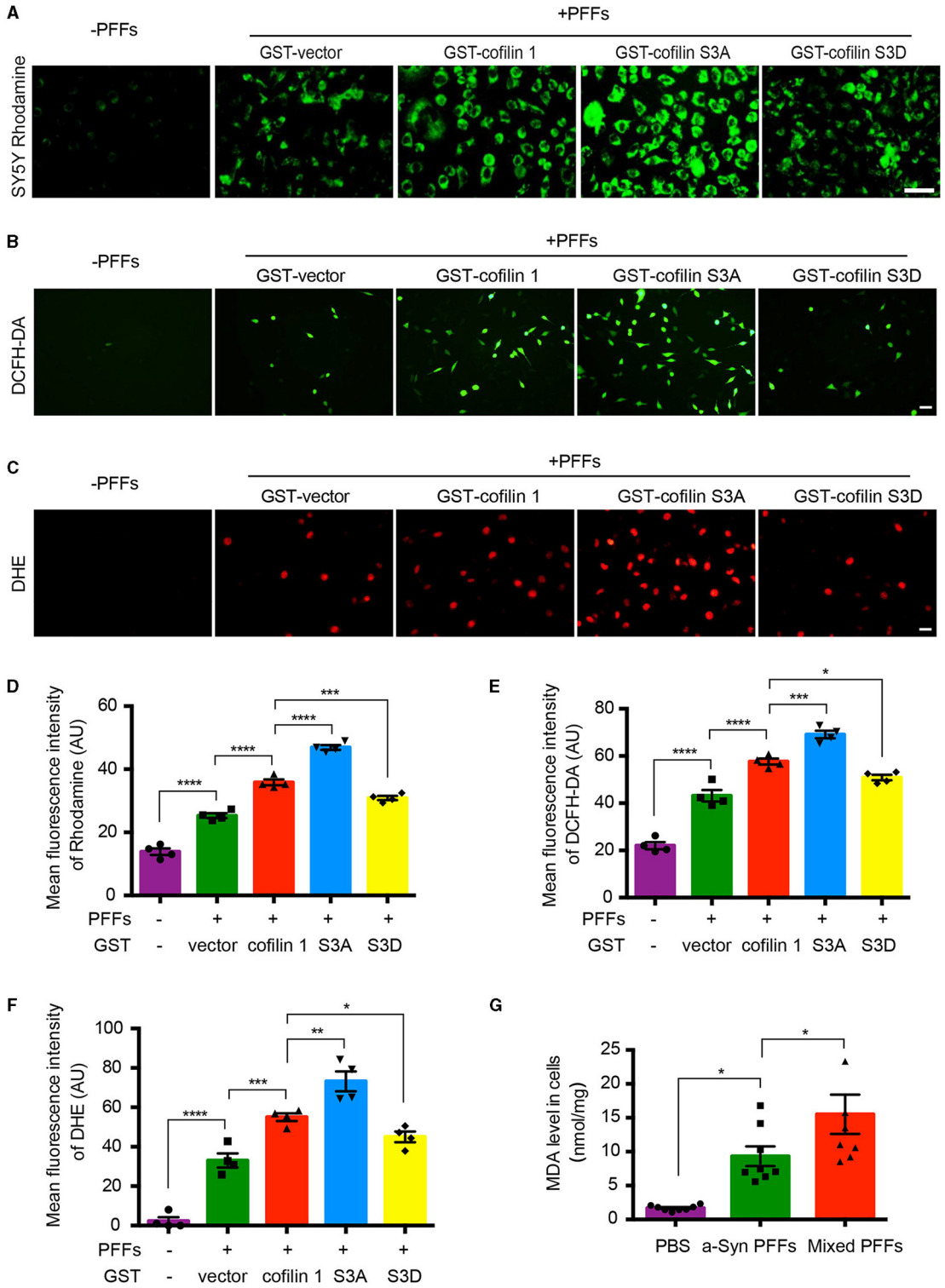

FIGURE 3
Cofilin-1 aggravates α-synuclein-induced oxidative stress in cells. **(A, D)** Detection of the mitochondrial membrane potential in SH-SY5Y cells with Rhodamine. Continuously activated cofilin S3A, but not phosphorylated cofilin S3D, triggered more mitochondrial membrane damage in SH-SY5Y cells. Scale bar, 50 μm. Data are represented as mean ± SEM, ***$P < 0.001$, ****$P < 0.0001$ by one-way ANOVA. **(B, E)** Intracellular ROS was detected by the DCFH-DA probe in SH-SY5Y cells. Cofilin S3A triggered more DCFH (green fluorescence), while cofilin S3D weakened its generation. Scale bar, 50 μm. Data are represented as mean ± SEM, *$P < 0.05$, ***$P < 0.001$, ****$P < 0.0001$ by one-way ANOVA. **(C, F)** Intracellular ROS was detected by the DHE probe in SH-SY5Y cells. DHE (red fluorescence) was reduced in the cofilin S3D group, while cofilin S3A induced more DHE fluorescence intensity. Scale bar, 20 μm. Data are represented as mean ± SEM, *$P < 0.05$, **$P < 0.01$, ***$P < 0.001$, and ****$P < 0.0001$ by one-way ANOVA. **(G)** Quantification of MDA after fibrils transduced into SH-SY5Y cells. The mean MDA values of the PBS, α-synuclein fibrils, and mixed fibrils groups were 1.677, 9.33, and 15.51, respectively. Data are mean ± SEM, *$P < 0.05$ by one-way ANOVA.

10.3389/fnins.2024.1420507

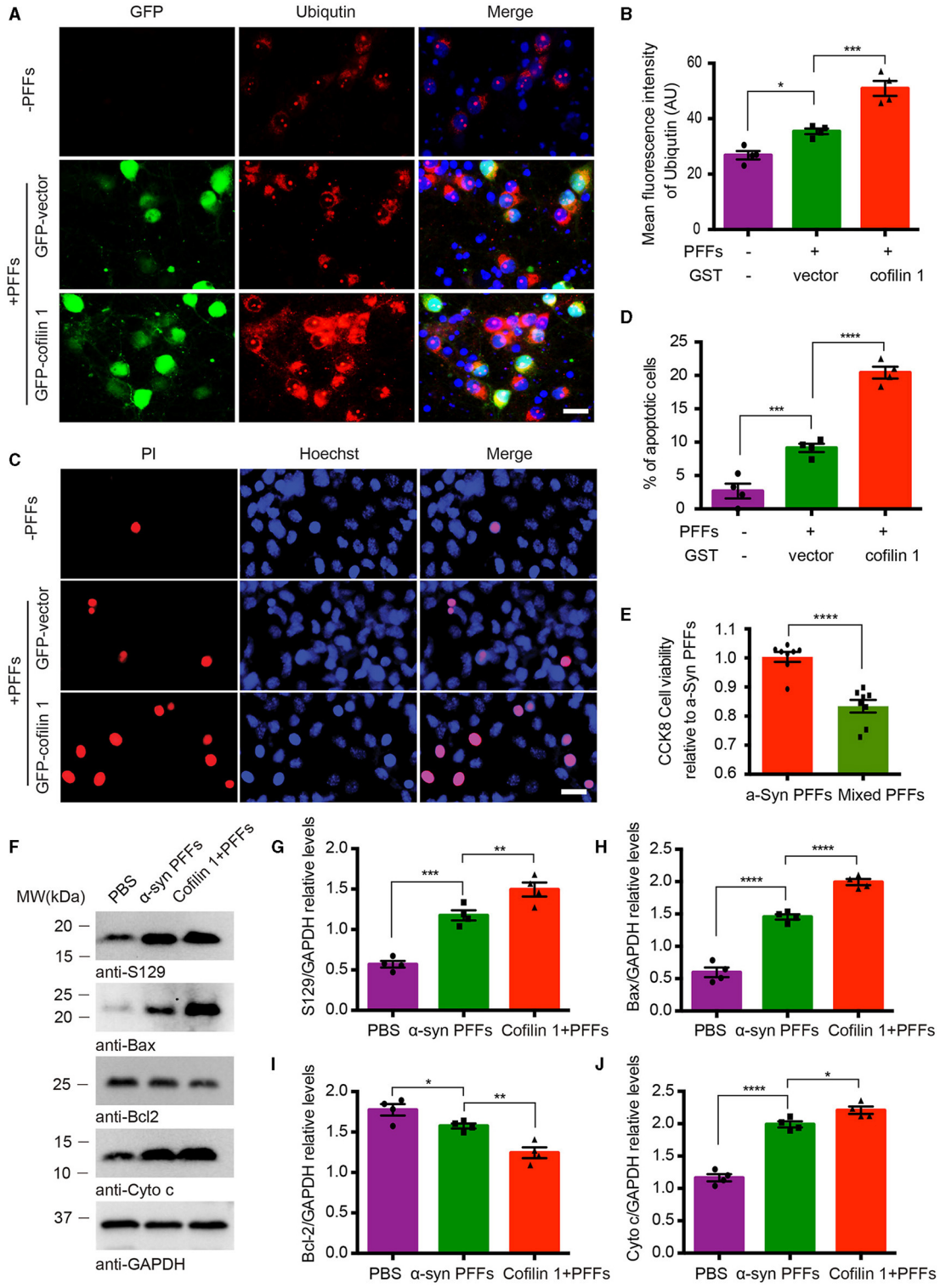

FIGURE 4
Overexpression of cofilin-1 accelerates α-synuclein-induced cell apoptosis. **(A, B)** Immunostaining showing the expression of ubiquitin in neurons of α-synuclein A53T transgenic mice. Overexpressed cofilin-1 promoted the expression of ubiquitin. Scale bar, 20 μm. Data are represented as mean ± SEM, $*P < 0.05$, $***P < 0.001$ by one-way ANOVA. **(C, D)** Detection of cell apoptosis in SH-SY5Y cells via Hoechst staining. Overexpression of cofilin-1 accelerated α-synuclein-induced cell apoptosis. Scale bar, 20 μm. Data are represented as mean ± SEM, $***P < 0.001$, $****P < 0.0001$ by one-way ANOVA. **(E)** CCK8 analysis shows decreased cell viability with mixed fibrils in SH-SY5Y cells. Mixed fibrils reduced the cell viability compared to pure α-synuclein fibrils. Data are represented as mean ± SEM, $****P < 0.0001$ by *t*-test. **(F–J)** Western blot analysis of p-S129 and apoptosis-related proteins Bax, Bcl-2, and cytochrome c. Cytochrome c was tested in the cytosolic fraction, while Bax and Bcl-2 were detected in mitochondria. Quantitative analysis is normalized to GAPDH. Data are represented as mean ± SEM, $*P < 0.05$, $**P < 0.01$, $***P < 0.001$, and $****P < 0.0001$ by one-way ANOVA.

Cofilin-1 binds tom 20 to promote mitochondrial damage and cell apoptosis

Since cofilin-1 accelerates the oxidative stress and cell apoptosis induced by α-synuclein fibrils, we further tested how cofilin-1 regulates its toxicity. We detected the expression of cofilin-1 in α-synuclein A53T transgenic mice. Immunofluorescence staining revealed that cofilin-1 was colocalized with Tom 20 in the brains of α-synuclein A53T mice, whereas cofilin-1 was scattered in the cytoplasm of wild-type mice (Figure 5A), suggesting that α-synuclein promotes the location of cofilin-1 to mitochondria and binds Tom 20. It is consistent with our previous results. Moreover, we further detected the mitochondrial membrane potential damage and apoptosis using the JC-1 assay and caspase-3 kits respectively. The decrease in mitochondrial membrane potential is an early marker event of cell apoptosis. Decreased JC-1 aggregates and increased JC-1 monomers suggest mitochondrial membrane potential damage. We found that α-synuclein fibrils alone induced few immunofluorescences of JC-1 monomers and caspase 3, while cofilin-1, especially active cofilin S3A, aroused much stronger positive immunostaining. Inactive cofilin S3D attenuated the expression of JC-1 monomers and caspase 3 in cells (Figures 5B–F). All these results suggest that cofilin-1 may combine with Tom 20 and induce loss of mitochondrial membrane potential and finally lead to cell apoptosis.

Discussion

PD is an age-related neurodegenerative disorder characterized by the presence of misfolded α-synuclein in neurons and dopaminergic neuron loss in the substantia nigra. Although α-synuclein normally localizes to the presynaptic terminal, its toxic aggregates localize throughout the cell body, which suggests that multiple organelles might be implicated in the α-synuclein toxicity (Wong and Krainc, 2017). Mitochondria are crucial for adenosine triphosphate (ATP) synthesis, calcium storage, lipid metabolism, and neuronal survival (Galluzzi et al., 2012). Mitochondrial dysfunction is the primary step leading to neuronal injury in PD (Exner et al., 2012; Ryan et al., 2015). Numerous reports have described mitochondrial dysfunction in models of pathological α-synuclein (Pech and Verstreken, 2018). α-Synuclein toxicity might directly disrupt mitochondrial homeostasis, given that mice with A53T α-synuclein mutations have increased mitochondrial damage, while dopaminergic neuron degeneration is prevented in mice lacking α-synuclein (Wong and Krainc, 2017). However, there is currently no consensus on how α-synuclein causes its mitochondrial damage.

Cofilin-1 is considered to be activated via dephosphorylation at Ser-3 by slingshot proteins (SSHs) and gets inactivated via phosphorylation by LIM kinases (LIMKs). Although the mechanism of cofilin-mediated actin dynamics has been known for decades, recent studies suggest the profound impacts of cofilin-1 in neurodegenerative diseases. In our previous studies, cofilin-1 was found to be involved in the aggregation and transmission of α-synuclein *in vitro and vivo* (Yan et al., 2020, 2022). However, whether cofilin-1 is involved in the mitochondrial damage of α-synuclein is unknown. Therefore, we investigated the role of cofilin-1 in α-synuclein-mediated mitochondrial impairment in this study. We gained insights into the role of cofilin in α-synuclein-induced mitochondrial dysfunction in PD. We made several novel observations demonstrating that α-synuclein aggregates regulate the distribution of cofilin-1 to mitochondria and cofilin-1 is critical for α-synuclein-induced mitochondrial damage and cell apoptosis. Our findings highlight the critical importance of the cofilin pathway in PD pathogenesis.

Moreover, it has been reported that the translocation of cofilin to mitochondria requires its activated dephosphorylation state, and activated cofilin is necessary for the release of cytochrome c and Bax translocation in mitochondria, which represents the initiation of apoptosis (Chua et al., 2003; Posadas et al., 2012). Multiple studies have confirmed the important role of cofilin-1 in the regulation of apoptosis in mitochondria, where it contributes to mitochondrial membrane depolarization, permeabilization, and the release of proapoptotic factors, thereby leading to neuronal death (Liu et al., 2017). Knockdown of either cofilin or Slingshot phosphatase has a marked neuroprotective effect on neuronal death (Madineni et al., 2016). This is consistent with our results. In our study, the activation and mitochondrial translocation of cofilin-1 induced by α-synuclein fibrils ultimately leads to an increase in caspase 3 and cell apoptosis. Moreover, cofilin-1 was found to bind mitochondrial outer membrane receptor Tom 20, which helps transport proteins into mitochondria. The combination of cofilin-1 and Tom 20 is a key event in α-synuclein-mediated neuronal death. However, the question of whether the entry of cofilin-1 into mitochondria is mediated by Tom 20 remains speculative and requires further verification.

In addition, cofilin functions are also modulated by reactive oxygen species. Studies have shown that ROS-induced cofilin oxidation can induce oxidative stress in ischemic and hemorrhagic strokes (Alhadidi et al., 2016), and the oxidative stress-induced increase in cofilin dephosphorylation is linked to the accumulation of tau tangles and amyloid beta plaques in Alzheimer's disease (Namme et al., 2021). In our study, cofilin-1 also induces reactive oxygen species and their metabolites in PD cell models. Representative images depict the changes in oxidative stress. Mitochondrial damage generally aggravates the process of oxidative stress. The accumulation of ROS can lead to a variety of cellular stress reactions, including DNA damage and the corresponding apoptosis-related signal pathway activation (Hoffmann et al., 2021). It is foreseeable that excessive ROS production induced by cofilin-1 may become involved in aggravating cofilin-1 activation, thereby forming a vicious circle.

Overall, these results strongly suggest that α-synuclein inclusions promote the activation and overstimulation of cofilin-1 in mitochondria, which initiates a series of cytotoxic events, including the production of reactive oxygen species and mitochondrial membrane permeabilization. This leads to the release of apoptogenic factors from the mitochondria, including cytochrome c and apoptosis-inducing factor, which causes caspase 3 activation and triggers neuronal death. Our study describes the molecular mechanism of α-synuclein-mediated neuronal toxicity in mitochondria and provides an overview of cofilin's importance in PD physiology and pathophysiology.

10.3389/fnins.2024.1420507

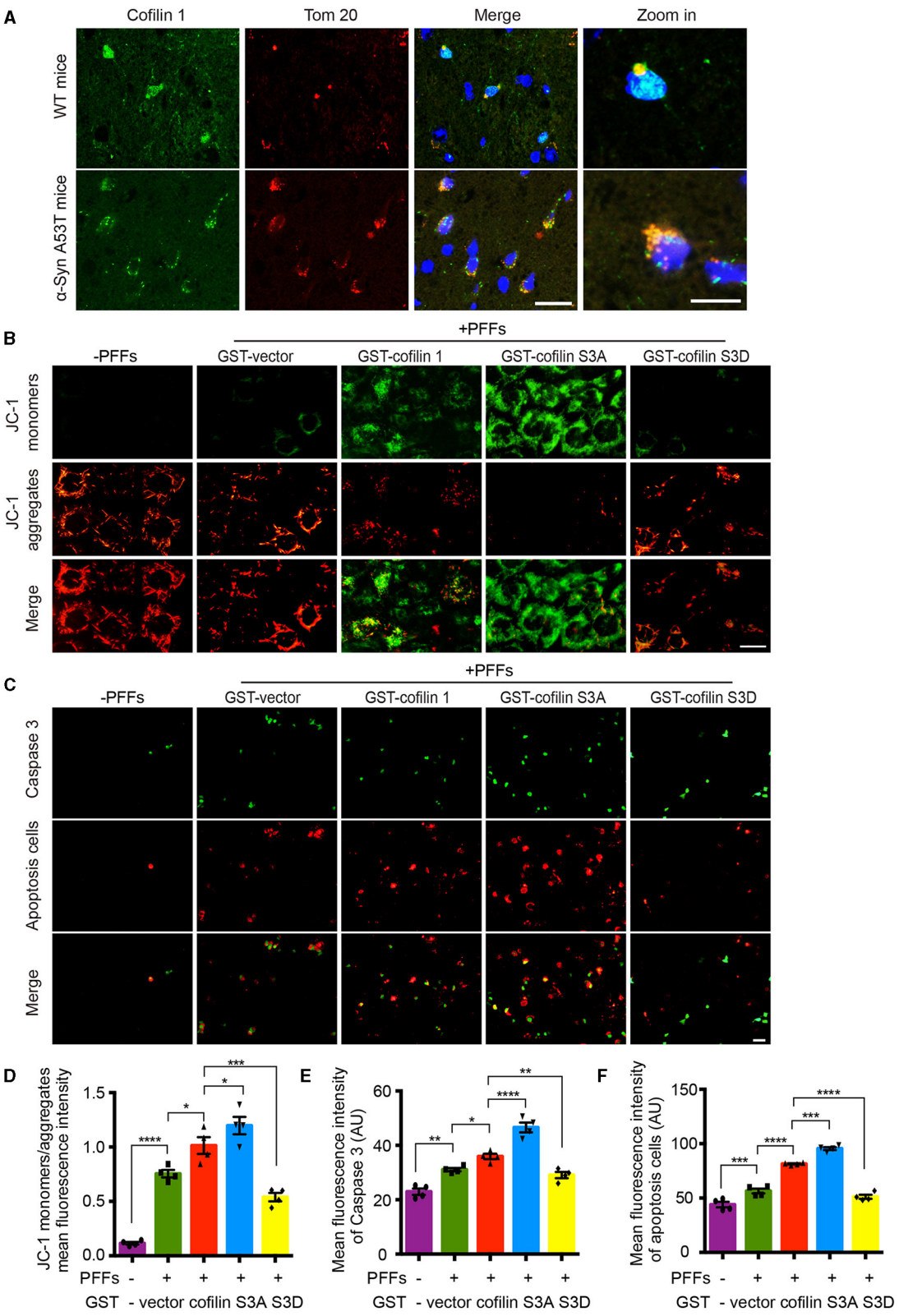

FIGURE 5
Cofilin-1 binds Tom 20 to promote mitochondrial damage and cell apoptosis. **(A)** Immunofluorescence showing the colocalization of cofilin-1 and Tom 20 in α-synuclein A53T transgenic mice. Scale bar, 20 μm; Zoom in Scale bar, 5 μm. **(B, D)** JC-1 kits detect the mitochondrial membrane potential in HEK293 cells. Active cofilin S3A aroused more JC-1 monomers, while inactive cofilin S3D attenuated the expression of JC-1 monomers. Quantification of JC-1 monomers/JC-1 aggregates. Scale bar, 20 μm. Data are represented as mean ± SEM, $^{*}P < 0.05$, $^{***}P < 0.001$, and $^{****}P < 0.0001$ by one-way ANOVA. **(C, E, F)** Caspase 3 staining detecting apoptosis in HEK293 cells. Cofilin-1, especially active cofilin S3A, induced more expression of caspase 3 and cell apoptosis. Scale bar, 50 μm. Data are represented as mean ± SEM, $^{*}P < 0.05$, $^{**}P < 0.01$, $^{***}P < 0.001$, and $^{****}P < 0.0001$ by one-way ANOVA.

Molecular pathways that govern the neurotoxicity of α-synuclein aggregates are attractive therapeutic targets for PD. Phospho-regulation through SSHs and LIMKs is the most critical mechanism, where the Ser-3 residue of cofilin is the specific target. This novel biochemical pathway may thus be a good target for developing future therapeutic molecules for neurodegenerative diseases.

Data availability statement

The original contributions presented in the study are included in the article/supplementary material, further inquiries can be directed to the corresponding authors.

Ethics statement

The animal study was approved by the Animal Care and Use Committee of Renmin Hospital of Wuhan University. The study was conducted in accordance with the local legislation and institutional requirements.

Author contributions

MY: Writing – original draft. QZ: Writing – review & editing, Investigation. YC: Writing – review & editing, Investigation. CZ: Writing – review & editing, Methodology. DW: Writing – review & editing, Methodology. JT: Writing – review & editing, Data curation. BH: Writing – review & editing, Validation. QL: Investigation, Writing – review & editing. XD: Writing – review & editing. YW: Writing – review & editing.

Funding

The author(s) declare financial support was received for the research, authorship, and/or publication of this article. This work was supported by grants from the National Natural Science Foundation of China (No. 82301439), the Natural Science Foundation of Hubei Provincial (Nos. 2022CFB870 and 2022CFB299), and a grant from the Health Commission of Hubei Province Scientific Research Project (No. WJ2023M114).

Conflict of interest

The authors declare that the research was conducted in the absence of any commercial or financial relationships that could be construed as a potential conflict of interest.

Publisher's note

References

Alhadidi, Q., Bin Sayeed, M. S., and Shah, Z. A. (2016). Cofilin as a promising therapeutic target for ischemic and hemorrhagic stroke. *Transl. Stroke Res.* 7, 33–41. doi: 10.1007/s12975-015-0438-2

Arber, S., Barbayannis, F. A., Hanser, H., Schneider, C., Stanyon, C. A., Bernard, O., et al. (1998). Regulation of actin dynamics through phosphorylation of cofilin by LIM-kinase. *Nature* 393, 805–809. doi: 10.1038/31729

Bamburg, J. R., and Wiggan, O. P. (2002). ADF/cofilin and actin dynamics in disease. *Trends Cell Biol.* 12, 598–605. doi: 10.1016/S0962-8924(02)02404-2

Beck, H., Flynn, K., Lindenberg, K. S., Schwarz, H., Bradke, F., Giovanni, D., et al. (2012). Serum Response Factor (SRF)-cofilin-actin signaling axis modulates mitochondrial dynamics. *Proc. Natl. Acad. Sci. USA.* 109, E2523–E2532. doi: 10.1073/pnas.1208141109

Bloem, B. R., Okun, M. S., and Klein, C. (2021). Parkinson's disease. *Lancet* 397, 2284–2303. doi: 10.1016/S0140-6736(21)00218-X

Bravo-Cordero, J. J., Magalhaes, M. A. O., Eddy, R. J., Hodgson, L., and Condeelis, J. (2013). Functions of cofilin in cell locomotion and invasion. *Nat. Rev. Mol. Cell Biol.* 14, 405–415. doi: 10.1038/nrm3609

Choi, M. L., Chappard, A., Singh, B. P., Maclachlan, C., Rodrigues, M., Fedotova, E. I., et al. (2022). Pathological structural conversion of α-synuclein at the mitochondria induces neuronal toxicity. *Nat. Neurosci.* 25, 1134–1148. doi: 10.1038/s41593-022-01140-3

Chua, B. T., Volbracht, C., Tan, K. O., Li, R., Yu, V. C., Mitochondrial, L., et al. (2003). translocation of cofilin is an early step in apoptosis induction. *Nat. Cell Biol.* 5, 1083–1089. doi: 10.1038/ncb1070

Corti, O., Lesage, S., and Brice, A. (2011). What genetics tells us about the causes and mechanisms of Parkinson's disease. *Physiol. Rev.* 91, 1161–1218. doi: 10.1152/physrev.00022.2010

Exner, N., Lutz, A. K., Haass, C., and Winklhofer, K. F. (2012). Mitochondrial dysfunction in Parkinson's disease: molecular mechanisms and pathophysiological consequences. *EMBO J.* 31, 3038–3062. doi: 10.1038/emboj.2012.170

Galluzzi, L., Kepp, O., Trojel-Hansen, C., and Kroemer, G. (2012). Mitochondrial control of cellular life, stress, and death. *Circ. Res.* 111, 1198–1207. doi: 10.1161/CIRCRESAHA.112.268946

Giasson, B. I., and Lee, V. M. Y. (2001). Parkin and the molecular pathways of Parkinson's disease. *Neuron.* 31, 885–888. doi: 10.1016/S0896-6273(01)00439-1

Hoffmann, L., Waclawczyk, M. S., Tang, S., Hanschmann, E. M., Gellert, M., Rust, M. B., et al. (2021). Cofilin1 oxidation links oxidative distress to mitochondrial demise and neuronal cell death. *Cell Death Dis.* 12, 953. doi: 10.1038/s41419-021-04242-1

Jang, D. H., Han, J. H., Lee, S. H., Lee, Y. S., Park, H., Lee, S. H., et al. (2005). Cofilin expression induces cofilin-actin rod formation and disrupts synaptic structure and function in Aplysia synapses. *Proc. Nat. Acad. Sci.* 102, 16072–16077. doi: 10.1073/pnas.0507675102

Klamt, F., Zdanov, S., Levine, R. L., Pariser, A., Zhang, Y., Zhang, B., et al. (2009). Oxidant-induced apoptosis is mediated by oxidation of the actin-regulatory protein cofilin. *Nat. Cell Biol.* 11, 1241–1246. doi: 10.1038/ncb1968

Liu, T., and Wang, F., LePochat, P., Woo, J. A. A., Bukhari, M. Z., Hong, K. W., et al. (2017). Cofilin-mediated neuronal apoptosis via p53 translocation and PLD1 regulation. *Sci. Rep.* 7:11532. doi: 10.1038/s41598-017-09996-3

Madineni, A., Alhadidi, Q., and Shah, Z. A. (2016). Cofilin inhibition restores neuronal cell death in oxygen-glucose deprivation model of ischemia. *Mol. Neurobiol.* 53, 867–878. doi: 10.1007/s12035-014-9056-3

Namme, J. N., Bepari, A. K., and Takebayashi, H. (2021). Cofilin signaling in the CNS physiology and neurodegeneration. *Int. J. Mol. Sci.* 22:10727. doi: 10.3390/ijms221910727

Pech, U., and Verstreken, P. (2018). α-Synuclein and Tau: mitochondrial kill switches. *Neuron*. 97, 3–4. doi: 10.1016/j.neuron.2017.12.024

Posadas, I., Pérez-Martínez, F. C., Guerra, J., Sánchez-Verdú, P., and Ceña, V. (2012). Cofilin activation mediates Bax translocation to mitochondria during excitotoxic neuronal death: Cofilin in excitotoxic death. *J. Neurochem*. 120, 515–527. doi: 10.1111/j.1471-4159.2011.07599.x

Ryan, B. J., Hoek, S., Fon, E. A., and Wade-Martins, R. (2015). Mitochondrial dysfunction and mitophagy in Parkinson's: from familial to sporadic disease. *Trends Biochem. Sci*. 40, 200–210. doi: 10.1016/j.tibs.2015.02.003

Shaw, A. E., and Bamburg, J. R. (2017). Peptide regulation of cofilin activity in the CNS: a novel therapeutic approach for treatment of multiple neurological disorders. *Pharmacol. Therapeut*. 175, 17–27. doi: 10.1016/j.pharmthera.2017.02.031

Sulzer, D. (2001). alpha-synuclein and cytosolic dopamine: stabilizing a bad situation. *Nat. Med*. 7, 1280–1282. doi: 10.1038/nm1201-1280

Valente, E. M., Abou-Sleiman, P. M., Caputo, V., Muqit, M. M. K., Harvey, K., Gispert, S., et al. (2004). Hereditary early-onset Parkinson's disease caused by mutations in PINK1. *Science* 304, 1158–1160. doi: 10.1126/science.1096284

Wong, Y. C., and Krainc, D. (2017). α-synuclein toxicity in neurodegeneration: mechanism and therapeutic strategies. *Nat. Med*. 23, 1–13. doi: 10.1038/nm.4269

Woo, J. A., Jung, A. R., Lakshmana, M. K., Bedrossian, A., Lim, Y., Bu, J. H., et al. (2012). Pivotal role of the RanBP9-cofilin pathway in Aβ-induced apoptosis and neurodegeneration. *Cell Death Differ*. 19, 1413–1423. doi: 10.1038/cdd.2012.14

Yan, M., Meng, L., Dai, L., Zhang, X., Chen, G., Zheng, Y., et al. (2020). Cofilin-1 promotes the aggregation and cell-to-cell transmission of α-synuclein in Parkinson's disease. *Biochem. Biophys. Res. Commun*. 529, 1053–1060. doi: 10.1016/j.bbrc.2020.06.101

Yan, M., Xiong, M., Dai, L., Zhang, X., Zha, Y., Deng, X., et al. (2022). Cofilin-1 promotes the pathogenicity and transmission of pathological α-synuclein in mouse models of Parkinson's disease. *NPJ Parkinsons Dis*. 8:1. doi: 10.1038/s41531-021-00272-w

Yang, N., Higuchi, O., Ohashi, K., Nagata, K., Wada, A., Kangawa, K., et al. (1998). Cofilin phosphorylation by LIM-kinase 1 and its role in Rac-mediated actin reorganization. *Nature* 393, 809–812. doi: 10.1038/31735

frontiers | Frontiers in Neuroscience

TYPE Original Research
PUBLISHED 21 August 2024
DOI 10.3389/fnins.2024.1393740

OPEN ACCESS

EDITED BY
Pradeep Kumar,
All India Institute of Medical Sciences, India

REVIEWED BY
Jinru Zhang,
Second Affiliated Hospital of Soochow University, China
Meng Jia,
University of Pennsylvania, United States

*CORRESPONDENCE
Dalong Wu
✉ wdl198119@163.com
Xinhua Chen
✉ 187098190@qq.com

†These authors have contributed equally to this work

RECEIVED 29 February 2024
ACCEPTED 06 August 2024
PUBLISHED 21 August 2024

CITATION
Liu Y, Zhou X, Chen C, Li X, Pan T, Liu Z, Wu D and Chen X (2024) Association between osteoarthritis with Parkinson's disease in the US (NHANES 2011–2020).
Front. Neurosci. 18:1393740.
doi: 10.3389/fnins.2024.1393740

Association between osteoarthritis with Parkinson's disease in the US (NHANES 2011–2020)

Yang Liu[1†], Xue Zhou[1†], Chunhai Chen[2], Xuefeng Li[1], Ting Pan[2], Ziqi Liu[1], Dalong Wu[2*] and Xinhua Chen[2*]

[1]Changchun University of Chinese Medicine, Changchun, China, [2]The Affiliated Hospital to Changchun University of Chinese Medicine, Changchun, China

Objected: To evaluate the association between osteoarthritis (OA) and Parkinson's disease (PD) in adults in the United States.

Methods: Using 2011–2020 NHANES data, a cross-sectional study of 11,117 adults over the age of 40 was conducted. Univariate logistic regression and multivariate logistic regression were used to analyze the relationship between arthritis and PD. In addition, stratified analysis was used to examine whether the relationship between arthritis and PD was interactive with age, gender, race, education, BMI.

Results: In this study, a total of 11,117 participants were included, and we found that osteoarthritis was positively correlated with the development of PD compared with non-arthritis patients [1.95 (1.44 ~ 2.62)] ($p < 0.001$). After adjusting the covariates, the results are still stable.

Conclusion: PD patients were positively correlated with OA. Among people with OA, there was a 95% increased risk of PD compared to people without arthritis. Therefore, when treating OA, attention should be paid to the increased risk of PD. In the meantime, further studies are needed to explore the link between OA and PD patients.

KEYWORDS

Parkinson's disease, osteoarthritis, cross-sectional study, NHANES, neurodegenerative disease

Introduction

Parkinson's disease (PD) is a prevalent degenerative disorder of the central nervous system, ranking second only to Alzheimer's disease (Hirtz et al., 2007). Epidemiological studies indicate that the incidence of PD rises with age (Savica et al., 2016). The primary clinical manifestations include motor symptoms such as resting tremors, muscle stiffness, bradykinesia, and postural instability (Bledsoe et al., 2023). Characteristic pathological features encompass dopaminergic neuron degeneration and loss, α-synuclein (α-syn) aggregation, and the presence of Lewy bodies (Jankovic and Tan, 2020). Although the pathogenesis of PD remains elusive, emerging evidence suggests a potential role of inflammation in the disease. Various studies have demonstrated that heightened levels of inflammatory mediators can activate microglia, contributing to dopaminergic neuron

degeneration (Lücking et al., 2000; Perry, 2004). Neuroinflammation observed in PD patients may also influence the onset or progression of chronic neurodegenerative conditions (Lücking et al., 2000; Perry, 2004).

Arthritis is an inflammatory disease that affects the joints and surrounding tissues of the body. Studies have shown a rise in its incidence and prevalence over the years (The Lancet, 2017). The types of arthritis include osteoarthritis (OA), rheumatoid arthritis (RA), psoriatic arthritis (PsA), and other forms (Tang, 2019). These types are categorized as inflammatory joint diseases with varying causes (Frangos and Maret, 2020). In the case of OA, inflammation, whether local or systemic, can lead to joint and bone damage, with specific inflammatory factors such as IL-1α, tumor necrosis factor (TNF-α), and C-reactive protein playing a significant role in its development (Hn and Vb, 2015). Similarly, in patients with Parkinson's disease (PD), there are also elevated levels of related inflammatory factors, which differ significantly from those seen in PD alone (Liu T.-W. et al., 2022).

In patients, α-syn can activate inflammatory bodies peripherally, thus triggering peripheral inflammation (Tan et al., 2020). Peripheral inflammation is also considered an essential factor in PD pathogenesis (Fan et al., 2020). The widespread peripheral inflammation may indicate an interaction between osteoarthritis and PD. Studies have shown that C-reactive protein and erythrocyte sedimentation rate are correlated with the prevalence of PD, and they are also biomarkers of arthritis (Fardell et al., 2021; Qu et al., 2023). Additionally, non-steroidal anti-inflammatory drugs (NSAIDs) are commonly used in osteoarthritis treatment, and prolonged use of these medications can lower the risk of PD (Schiess, 2003). Studies have demonstrated that NSAIDs can help maintain neuronal integrity (Casper et al., 2000; Teema et al., 2016). Therefore, it is plausible to assume an association between OA patients taking NSAIDs and PD. However, the results of studies investigating the link between osteoarthritis and Parkinson's disease remain inconclusive.

The existing research on the correlation between osteoarthritis and Parkinson's disease is inconclusive. To further examine this relationship, we conducted a study on a significant sample size sourced from the US National Health and Nutrition Examination Survey (NHANES). This study is believed to be the first to utilize NHANES data in investigating the potential link between osteoarthritis and PD risk.

Materials and methods

Data source

The study utilized data from the NHANES database spanning from 2011 to 2020. The NHANES Database, available at https://www.cdc.gov/nchs/nhanes/index.htm, is a research program aimed at evaluating the health and nutrition status of individuals in the United States, covering various populations and health topics. A decade's worth of data was collected from this database to construct the dataset for the study. Initially, individuals aged 40 and above were considered for exclusion, followed by the exclusion of participants with incomplete personal information. The specific exclusion criteria employed in this study are detailed in Figure 1. Ultimately, the study included a total of 11,117 NHANES participants.

Assessment of Parkinson's disease

In the NHANES database, in conjunction with previous literature (Liu S.-Y. et al., 2022; Liu et al., 2023), individuals taking specific Parkinson's drugs were classified as having Parkinson's disease. This classification was determined based on participants' responses regarding prescription medications. It is important to note that this method is constrained by the medications and codes available in NHANES, requiring individuals to be actively receiving Parkinson's disease medication to be categorized as having the disease. Conversely, those who were not taking the specified medications were classified as not having Parkinson's disease.

Assessment of arthritis

Arthritis diagnosis in the survey was determined based on two key questions. The first question asked participants if a doctor had ever diagnosed them with arthritis. Those who responded "No" were categorized as non-arthritis cases. For those who answered "Yes," a follow-up question inquired about the specific type of arthritis diagnosed. Participants were further classified into osteoarthritis, rheumatoid arthritis, psoriatic arthritis, or other types based on their responses to the second question.

Measurements of other covariates

According to previous research and clinical experience, the key variables examined in this research included demographic factors, personal medical history, and chronic conditions (Zeng et al., 2023, 2024). Demographic factors encompassed age, sex (female, male), race (Mexican American, other Hispanic, non-Hispanic white, non-Hispanic black, other race), marital (married, living with a partner, separated, widowed, divorced, never married), and education ($\leq$9, 9–12, $\geq$12). Prior studies have suggested that nicotine may serve as a protective factor for Parkinson's disease by enhancing the survival of dopaminergic neurons (Liu et al., 2023), hence smoking was considered a significant covariate. Participants were queried about their history of smoking at least 100 cigarettes in their lifetime, with a 'Yes' response indicating a smoker and 'No' indicating a non-smoker. Chronic diseases of interest included diabetes, hypertension, hyperlipidemia, heart disease, stroke, and cancer. Body Mass Index (BMI) was utilized as a standard measure of obesity, with weight and height being measured by trained health professionals. BMI was calculated as weight (kg) divided by height squared (m^2), and both age and BMI were treated as continuous variables.

Statistical analyses

SPSS was utilized for data extraction and cleaning, while the Nhanes R package in R software (v4.2.1) and FreeStatistics (v1.9) were employed for data analysis (Zeng et al., 2024). Categorical variables were presented as frequencies and percentages, whereas continuous variables were depicted as means and standard deviations. To investigate the relationship between arthritis and PD, a multivariate logistic regression model and univariate logistic analysis were

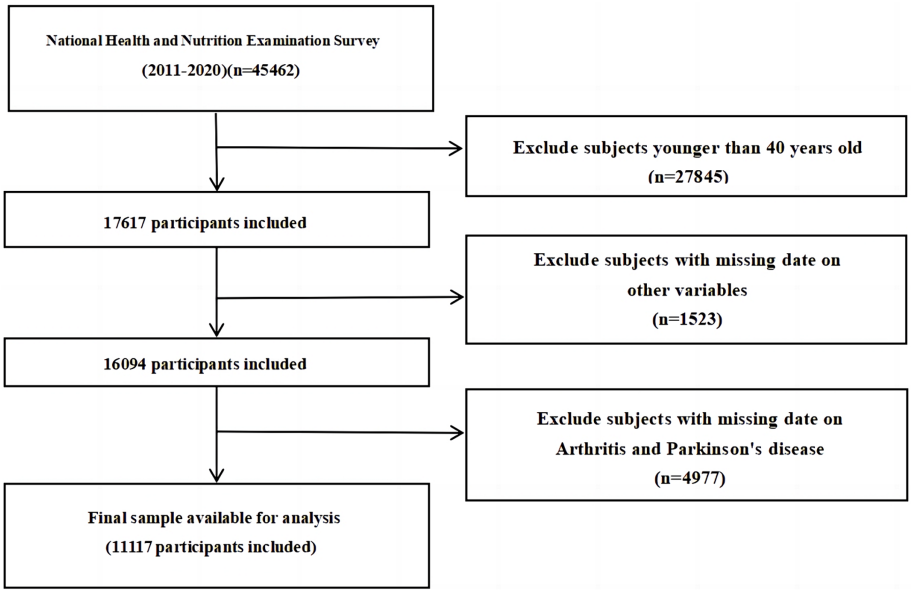

FIGURE 1
Flow diagram of the sample selection from the National Health and Nutrition Examination Survey (NHANES) 2011–2020.

conducted, adjusting for potential confounders. Several models were utilized: Model I with no covariate adjustments, Model II with adjustments for sex, age, race, marital, education, and BMI, Model III with the addition of smoking to the Model II covariates, and Model IV which further adjusted for diabetes, hypertension, hyperlipidemia, heart disease, stroke, and cancer. Univariate regression analysis revealed associations between all these factors and PD. Subgroup analyses were then performed based on age, sex, race, education, and BMI.

Results

Characteristics of participants

The final analysis involved 11,117 participants from NHANES cycles 2011–2020, with 5,150 reporting arthritis, including 2,318 patients with osteoarthritis. Table 1 details the participants' demographic characteristics, smoking history, and chronic complications, revealing differences in the prevalence of conditions like heart disease, stroke, cancer, diabetes, hypertension, and hyperlipemia among the groups. The prevalence of non-arthritis, osteoarthritis, rheumatoid arthritis, and other arthritis among PD patients were 1.8, 4.0, 2.7, and 3.6% respectively, suggesting a correlation between osteoarthritis and PD.

Association between arthritis and PD

In the overall study population of PD patients, univariate regression analysis indicated that PD was positively associated with race, marital, smoking, stroke, osteoarthritis and other arthritis-related factors ($p < 0.05$) (Table 2). Specifically, Non-Hispanic White exhibited a relatively lower risk of PD compared to Mexican American. Furthermore, the prevalence of PD was lower among married individuals compared to their unmarried counterparts (OR: 1.32, 95% CI: 1.05 to 1.67). Patients with a history of stroke demonstrated a significantly higher risk of developing PD. Compared to patients without arthritis, those with OA and other forms of arthritis exhibited a higher likelihood of developing PD, with OR and 95% CI of 2.29 (1.72–3.03) and 2.04 (1.5–2.79), respectively. Our study identified a statistically significant positive correlation between the presence of OA and other types of arthritis and the incidence of PD (Table 2).

Multivariable logistics regression analysis

Table 3 displays the logistic regression findings concerning the relationship between arthritis and PD. The unadjusted model (Model I) indicated an elevated risk of osteoarthritis and other forms of arthritis in relation to PD [2.29 (1.72–3.03), 2.04 (1.5–2.79)]. Upon adjusting for age, sex, race, marital, education, and BMI (Model II), the association between PD and osteoarthritis as well as other arthritis remained significant [1.94 (1.44–2.61), 1.96 (1.42–2.69)]. Further inclusion of smoking in the model (Model III) did not alter the significant relationship between PD and osteoarthritis or other arthritis [1.91 (1.42–2.57), 1.93 (1.4–2.66)]. Finally, after accounting for additional chronic conditions like diabetes, hypertension, hyperlipidemia, heart disease, stroke, and cancer (Model IV), the notable association between PD and osteoarthritis and other arthritis persisted [1.95 (1.44–2.62), 1.96 (1.42–2.71)]. These results suggest a robust and stable correlation between the occurrence of osteoarthritis and Parkinson's disease, with a significant statistical significance ($p < 0.001$).

Subgroup analyses of factors influencing the association between arthritis and PD

The subgroup analysis of the data is depicted in Figure 1. Stratified analyses were conducted to investigate if the association between

10.3389/fnins.2024.1393740

TABLE 1 Data characteristics of the participants.

Variables	Total (*n* = 11,117)	Non-arthritis (*n* = 5,967)	OA (*n* = 2,318)	RA (*n* = 979)	Other (*n* = 1853)
Age, *n* (%)					
<64	6,252 (56.2)	3,820 (64)	1,021 (44)	508 (51.9)	903 (48.7)
>64	4,865 (43.8)	2,147 (36)	1,297 (56)	471 (48.1)	950 (51.3)
Sex, *n* (%)					
Male	5,118 (46.0)	3,087 (51.7)	819 (35.3)	414 (42.3)	798 (43.1)
Female	5,999 (54.0)	2,880 (48.3)	1,499 (64.7)	565 (57.7)	1,055 (56.9)
Race, *n* (%)					
Mexican American	1,087 (9.8)	641 (10.7)	171 (7.4)	113 (11.5)	162 (8.7)
Other Hispanic	1,121 (10.1)	628 (10.5)	170 (7.3)	101 (10.3)	222 (12)
Non-Hispanic White	4,725 (42.5)	2,287 (38.3)	1,352 (58.3)	326 (33.3)	760 (41)
Non-Hispanic Black	2,771 (24.9)	1,453 (24.4)	415 (17.9)	347 (35.4)	556 (30)
Other Race	1,413 (12.7)	958 (16.1)	210 (9.1)	92 (9.4)	153 (8.3)
Marital, *n* (%)					
Married	6,611 (59.5)	3,794 (63.6)	1,342 (57.9)	515 (52.6)	960 (51.8)
Unmarried	4,506 (40.5)	2,173 (36.4)	976 (42.1)	464 (47.4)	893 (48.2)
Education, *n* (%)					
≤9	1,170 (10.5)	614 (10.3)	164 (7.1)	135 (13.8)	257 (13.9)
9–12	3,954 (35.6)	2005 (33.6)	780 (33.6)	414 (42.3)	755 (40.7)
≥12	5,993 (53.9)	3,348 (56.1)	1,374 (59.3)	430 (43.9)	841 (45.4)
BMI, *n* (%)					
Under normal weight	2,485 (22.4)	1,541 (25.8)	447 (19.3)	185 (18.9)	312 (16.8)
Overweight	3,626 (32.6)	2068 (34.7)	684 (29.5)	303 (30.9)	571 (30.8)
Obese	5,006 (45.0)	2,358 (39.5)	1,187 (51.2)	491 (50.2)	970 (52.3)
Smoking, *n* (%)					
No	5,314 (47.8)	2,629 (44.1)	1,201 (51.8)	506 (51.7)	978 (52.8)
Yes	5,803 (52.2)	3,338 (55.9)	1,117 (48.2)	473 (48.3)	875 (47.2)
Heart disease, *n* (%)					
No	891 (8.0)	374 (6.3)	247 (10.7)	93 (9.5)	177 (9.6)
Yes	10,226 (92.0)	5,593 (93.7)	2071 (89.3)	886 (90.5)	1,676 (90.4)
Stroke, *n* (%)					
No	821 (7.4)	348 (5.8)	203 (8.8)	106 (10.8)	164 (8.9)
Yes	10,296 (92.6)	5,619 (94.2)	2,115 (91.2)	873 (89.2)	1,689 (91.1)
Cancer, *n* (%)					
No	1904 (17.1)	822 (13.8)	532 (23)	183 (18.7)	367 (19.8)
Yes	9,213 (82.9)	5,145 (86.2)	1786 (77)	796 (81.3)	1,486 (80.2)
Diabetes, *n* (%)					
No	2,891 (26.0)	1,464 (24.5)	588 (25.4)	304 (31.1)	535 (28.9)
Yes	7,787 (70.0)	4,286 (71.8)	1,629 (70.3)	632 (64.6)	1,240 (66.9)
Border	439 (3.9)	217 (3.6)	101 (4.4)	43 (4.4)	78 (4.2)
Hypertension, *n* (%)					
No	6,999 (63.0)	3,427 (57.4)	1,580 (68.2)	694 (70.9)	1,298 (70)
Yes	4,118 (37.0)	2,540 (42.6)	738 (31.8)	285 (29.1)	555 (30)

(Continued)

TABLE 1 (Continued)

Variables	Total (*n* = 11,117)	Non-arthritis (*n* = 5,967)	OA (*n* = 2,318)	RA (*n* = 979)	Other (*n* = 1853)
Hyperlipemia, *n* (%)					
No	6,169 (55.5)	3,053 (51.2)	1,435 (61.9)	556 (56.8)	1,125 (60.7)
Yes	4,948 (44.5)	2,914 (48.8)	883 (38.1)	423 (43.2)	728 (39.3)
PD, *n* (%)					
No	10,827 (97.4)	5,861 (98.2)	2,226 (96)	953 (97.3)	1787 (96.4)
Yes	290 (2.6)	106 (1.8)	92 (4)	26 (2.7)	66 (3.6)

OA, osteoarthritis; RA, rheumatic arthritis; BMI, body mass index; PD, Parkinson's disease.

TABLE 2 Univariate arthritis analysis.

Variable	OR_95CI	*p*_value
Age:<64 vs. >64	1.21 (0.95 ~ 1.52)	0.117
Sex: Female vs. Male	1.2 (0.95 ~ 1.52)	0.136
Race: ref.=Mexican American		
Other Hispanic	1.25 (0.7 ~ 2.23)	0.443
Non-Hispanic White	2.05 (1.3 ~ 3.23)	**0.002***
Non-Hispanic Black	0.74 (0.44 ~ 1.27)	0.276
Other Race	0.69 (0.37 ~ 1.29)	0.249
Marital: Married vs. Unmarried	1.32 (1.05 ~ 1.67)	**0.019***
Education: ref.≤9		
9–12	1.09 (0.72 ~ 1.66)	0.671
≥12	1.04 (0.69 ~ 1.55)	0.857
BMI	0.99 (0.98 ~ 1.01)	0.403
Smoking: No vs. Yes	0.75 (0.59 ~ 0.95)	**0.016***
Heart Disease: No vs. Yes	0.78 (0.53 ~ 1.15)	0.208
Stroke: No vs. Yes	0.52 (0.36 ~ 0.73)	**<0.001****
Cancer: No vs. Yes	0.94 (0.7 ~ 1.28)	0.713
Diabetes: ref.=No		
Yes	1.03 (0.79 ~ 1.35)	0.826
Border	0.61 (0.28 ~ 1.33)	0.212
Hypertension: No vs. Yes	0.99 (0.78 ~ 1.27)	0.958
Hyperlipemia: No vs. Yes	1.1 (0.87 ~ 1.39)	0.407
Arthritis: ref.=Non-arthritis		
OA	2.29 (1.72 ~ 3.03)	**<0.001****
RA	1.51 (0.98 ~ 2.33)	0.064
Other	2.04 (1.5 ~ 2.79)	**<0.001****

OR, odds ratio; CI, confdence interval.
*$p < 0.05$, **$p < 0.001$. $p < 0.05$ was considered statistically significant.

various types of arthritis and Parkinson's disease differed based on age, sex, race, education, and BMI. Furthermore, the results were validated for all subgroups except for sex, showing consistent findings across all subgroups without any interactions (Figure 2). The findings indicated a significant correlation between osteoarthritis and the risk of developing Parkinson's disease, which was statistically significant ($p < 0.001$).

Discussion

Arthritis, a common disease among the elderly and a trigger for systemic inflammation, has an unclear role in PD. Therefore, it is crucial to investigate the potential correlation between PD and OA from both clinical and social perspectives. Our study examining the relationship between OA and PD revealed a positive association between PD and OA, as well as other forms of arthritis, but not with RA. Through multivariate logistic regression analysis adjusting for confounding factors, we observed a positive correlation between PD and OA risk, while no association was found between RA and PD. Subgroup analysis further supported the stability of these findings.

In this cross-sectional study, we found a clear association between OA and a significant increase in the occurrence of PD. Individuals with OA had a 95 percent higher risk of PD compared to those without arthritis, while no association was observed between RA and PD. This contrasts with findings from previous studies (Liu et al., 2023; Zeng et al., 2024). The discrepancy between our study and others may be attributed to differences in sample populations. Furthermore, our focus on OA during data cleaning may have influenced the results on RA and PD, making the association with RA inconclusive. Our study also revealed a significant correlation between other types of arthritis, such as psoriatic arthritis, and PD. However, due to the limited sample size, further investigation on these types of arthritis was not feasible. Moving forward, larger sample sizes are necessary to explore the relationship between other forms of arthritis and PD.

Arthritis is a degenerative joint disease encompassing OA, RA and other forms. OA is the most prevalent joint disease, characterized by an increase in both systemic and local inflammatory cytokines that contribute to cartilage degradation and impact OA progression (Motta et al., 2023). OA is characterized by cartilage degeneration, synovitis, and changes in subchondral bone, triggering a peripheral inflammatory response. RA, a chronic autoimmune disease, is marked by persistent inflammation in synovial joints. The damage to articular cartilage involves various immune cells like NK cells, B lymphocytes, T lymphocytes, among others (de Lange-Brokaar et al., 2012; Li et al., 2022). Arthritis, a non-specific inflammatory condition, not only inflicts irreversible harm on the synovium but also may contribute to other immune-related disorders like inflammatory bowel disease, systemic lupus erythematosus, diabetes, Graves' disease, and more (Tagoe et al., 2012; Houser and Tansey, 2017; Veronese et al., 2019). The dysregulation of immune homeostasis in patients with arthritis results in an increase in peripheral pro-inflammatory factors and a decrease

TABLE 3 Multivariate logistic regression analysis of the correlation between arthritis and PD.

	Model I	Model II	Model III	Model IV
	OR (95% CI)	OR (95% CI)	OR (95% CI)	OR (95% CI)
Non-arthritis	1 (Ref)	1 (Ref)	1 (Ref)	1 (Ref)
OA	2.29 (1.72 ~ 3.03)**	1.94 (1.44 ~ 2.61)**	1.91 (1.42 ~ 2.57)**	1.95 (1.44 ~ 2.62)**
RA	1.51 (0.98 ~ 2.33)	1.54 (0.99 ~ 2.39)	1.52 (0.98 ~ 2.36)	1.5 (0.96 ~ 2.34)
Other	2.04 (1.5 ~ 2.79)**	1.96 (1.42 ~ 2.69)**	1.93 (1.4 ~ 2.66)**	1.96 (1.42 ~ 2.71)**
P for trend	<0.001	<0.001	<0.001	<0.001

Model I: no adjusted; Model II: adjusted for age + sex + race + marital + education + BMI; Model III: Model II+ smoking; Model IV: Model III + diabetes + hypertension + hyperlipemia + heart disease + stroke + cancer. *$p < 0.05$, **$p < 0.001$. $p < 0.05$ was considered statistically significant.

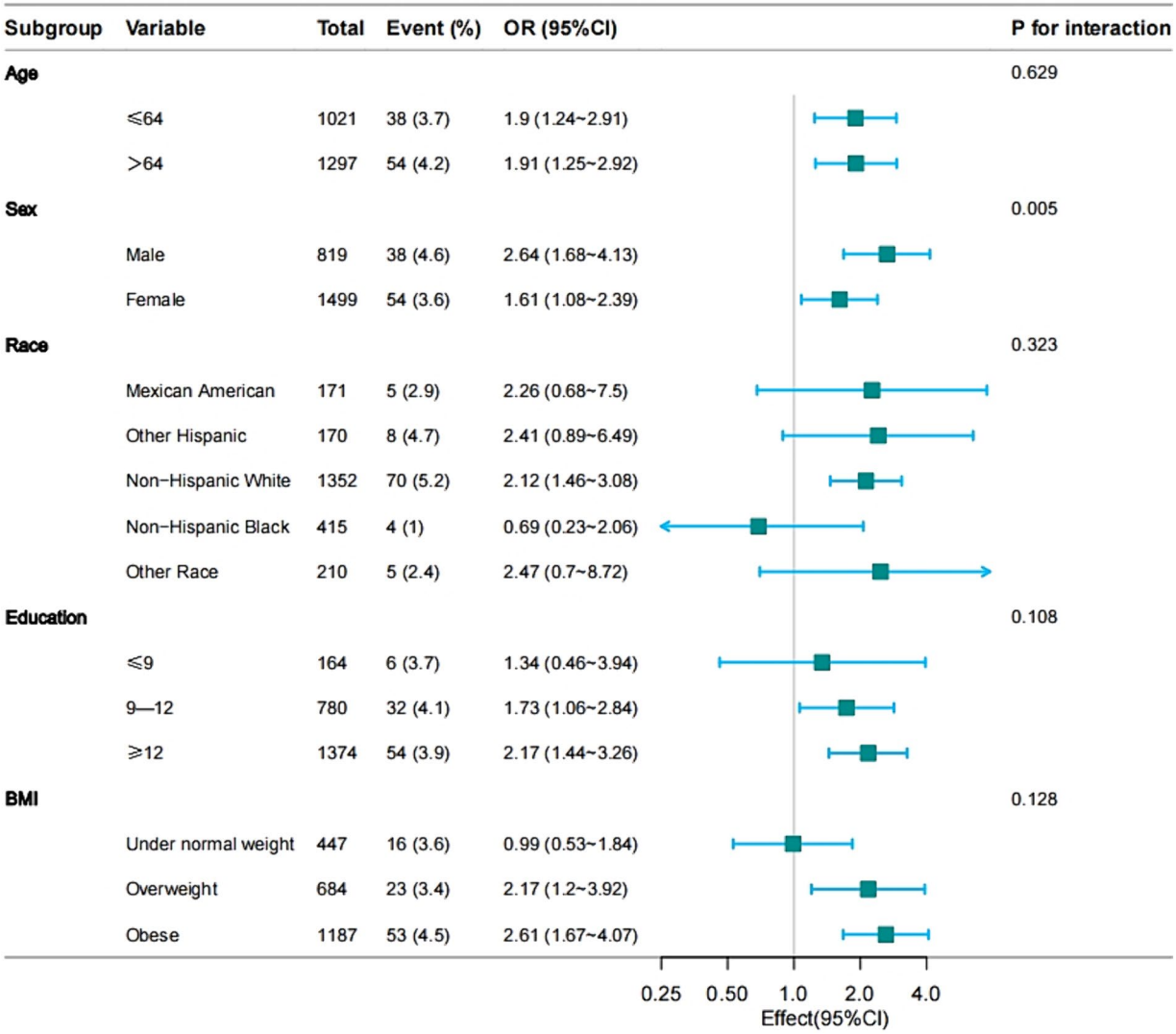

FIGURE 2
Effect size of osteoarthritis on the presence of PD in age, sex, race, education, BMI subgroup.

in anti-inflammatory factors. This imbalance also impacts inflammatory factors and neurotransmitters, which can further enhance the interaction between immune cells and nerves through mutual regulation (Gao et al., 2022). Research indicates that inappropriate peripheral inflammation may trigger a neuroinflammatory response, leading to the disruption of the blood–brain barrier by inflammatory stimuli, potentially contributing to the development of central nervous system disorders (Huang et al., 2021). Moreover, cytokines released by peripheral inflammatory mediators involved in chronic inflammation can activate glial cells, exacerbating

neuroinflammation and directly influencing the function of the blood–brain barrier as well as neurodegenerative processes (Sonar and Lal, 2018). Neuroinflammation is a crucial mechanism in the pathogenesis of PD, serving as both a key factor in disease onset and progression (Zhang et al., 2023). Inflammatory processes can lead to the degeneration of dopamine neurons, which significantly impacts individuals with PD (Lücking et al., 2000; Perry, 2004). Factors such as α-syn misfolding, immune gene polymorphisms, and mitochondrial dysfunction contribute to the development of neuroinflammation in PD patients (Isik et al., 2023). Autopsy studies have confirmed the involvement of microglia-mediated neuroinflammation in the pathogenesis of PD (McGeer et al., 1988). Natural killer cells present in PD patients have been found to effectively degrade α-syn aggregates. Depletion of natural killer cells in α-syn mouse models has been shown to worsen α-syn aggregation and promote dopamine neuron degeneration, suggesting a potential link between peripheral inflammation and PD development (Earls et al., 2020). In addition, elevated levels of systemic inflammatory cytokines have been identified as playing a significant role in the development of PD (Tansey et al., 2022). C-reactive protein (CRP), a key inflammatory marker for arthritis, has been found to have a positive correlation with the prevalence of PD in studies (Qu et al., 2023).

Research indicates that the increase of TNF-α and IL-6 in the bloodstream is also positively associated with PD, suggesting that the elevation of peripheral pro-inflammatory factors may be crucial in the pathogenesis of PD (Chen et al., 2008).

While the root cause of the differing associations between osteoarthritis and Parkinson's disease remains unclear, this study possesses several strengths. Firstly, a significant advantage lies in the utilization of a large and representative sample of Americans gathered through continuous NHANES cycles, enabling the examination of the relationship between osteoarthritis, other forms of arthritis, and PD. Additionally, the potential neuroprotective role of smoking in PD, as indicated by previous studies (Gale and Martyn, 2003; Ascherio and Schwarzschild, 2016), was considered through covariate adjustments, with smoking identified as a crucial variable. Nonetheless, it is important to acknowledge the limitations of our study. Data constraints may have led to missing information, potentially stemming from a lack of awareness or delayed medical attention-seeking. Furthermore, the diagnosis of PD in individuals was primarily based on medication usage, raising concerns about potential biases from patients with other chronic illnesses or mental disorders also taking anti-Parkinson's drugs. As a cross-sectional study, causal relationships cannot be definitively established, and despite adjustments for confounding variables, residual confounding remains a possibility. Thus, a comprehensive controlled trial is warranted. Moreover, the reliance on NHANES data restricted the ability to explore correlations between various types of arthritis and PD individually due to database limitations, necessitating further investigation to validate these findings.

Conclusion

PD patients were positively correlated with OA. Among people with OA, there was a 95% increased risk of PD compared to people without arthritis. Therefore, when treating OA, attention should be paid to the increased risk of PD. In the meantime, further studies are needed to explore the link between OA and PD patients.

Data availability statement

Publicly available datasets were analyzed in this study. This data can be found at: https://www.cdc.gov/nchs/nhanes/index.htm.

Ethics statement

The studies involving humans were approved by National Center for Health Statistics Ethics Review Board. The studies were conducted in accordance with the local legislation and institutional requirements. The participants provided their written informed consent to participate in this study.

Author contributions

YL: Resources, Methodology, Writing – review & editing, Writing – original draft. XZ: Methodology, Writing – review & editing, Writing – original draft. CC: Writing – original draft, Methodology. XL: Writing – original draft, Formal analysis. TP: Writing – original draft, Resources. ZL: Writing – original draft, Resources. DW: Writing – review & editing, Writing – original draft. XC: Writing – review & editing, Writing – original draft.

Funding

The author(s) declare that financial support was received for the research, authorship, and/or publication of this article. This work was supported by the Science and Technology Project of Jilin Provincial Department (20220204006YY) and Development and Reform Commission of Jilin Provincial (2022C041-2).

Acknowledgments

The authors thanks the staff and the participants of the NHANES study for their valuable contributions.

Conflict of interest

The authors declare that the research was conducted in the absence of any commercial or financial relationships that could be construed as a potential conflict of interest.

Publisher's note

References

Ascherio, A., and Schwarzschild, M. A. (2016). The epidemiology of Parkinson's disease: risk factors and prevention. *Lancet Neurol.* 15, 1257–1272. doi: 10.1016/S1474-4422(16)30230-7

Bledsoe, I. O., Yu, J., and Shukla, A. W. (2023). Functional impairment preceding Parkinson disease diagnosis-What's in a Prodrome? *JAMA Neurol.* 80, 130–132. doi: 10.1001/jamaneurol.2022.4157

Casper, D., Yaparpalvi, U., Rempel, N., and Werner, P. (2000). Ibuprofen protects dopaminergic neurons against glutamate toxicity in vitro. *Neurosci. Lett.* 289, 201–204. doi: 10.1016/s0304-3940(00)01294-5

Chen, H., O'Reilly, E. J., Schwarzschild, M. A., and Ascherio, A. (2008). Peripheral inflammatory biomarkers and risk of Parkinson's disease. *Am. J. Epidemiol.* 167, 90–95. doi: 10.1093/aje/kwm260

de Lange-Brokaar, B. J. E., Ioan-Facsinay, A., van Osch, G. J. V. M., Zuurmond, A.-M., Schoones, J., Toes, R. E. M., et al. (2012). Synovial inflammation, immune cells and their cytokines in osteoarthritis: a review. *Osteoarthr. Cartil.* 20, 1484–1499. doi: 10.1016/j.joca.2012.08.027

Earls, R. H., Menees, K. B., Chung, J., Gutekunst, C.-A., Lee, H. J., Hazim, M. G., et al. (2020). NK cells clear α-synuclein and the depletion of NK cells exacerbates synuclein pathology in a mouse model of α-synucleinopathy. *Proc. Natl. Acad. Sci. USA* 117, 1762–1771. doi: 10.1073/pnas.1909110117

Fan, Z., Pan, Y.-T., Zhang, Z.-Y., Yang, H., Yu, S.-Y., Zheng, Y., et al. (2020). Systemic activation of NLRP3 inflammasome and plasma α-synuclein levels are correlated with motor severity and progression in Parkinson's disease. *J. Neuroinflammation* 17:11. doi: 10.1186/s12974-019-1670-6

Fardell, C., Schiöler, L., Nissbrandt, H., Torén, K., and Åberg, M. (2021). The erythrocyte sedimentation rate in male adolescents and subsequent risk of Parkinson's disease: an observational study. *J. Neurol.* 268, 1508–1516. doi: 10.1007/s00415-020-10324-5

Frangos, T., and Maret, W. (2020). Zinc and cadmium in the Aetiology and pathogenesis of osteoarthritis and rheumatoid arthritis. *Nutrients* 13:53. doi: 10.3390/nu13010053

Gale, C., and Martyn, C. (2003). Tobacco, coffee, and Parkinson's disease. *BMJ* 326, 561–562. doi: 10.1136/bmj.326.7389.561

Gao, D., Gao, X., Yang, F., and Wang, Q. (2022). Neuroimmune crosstalk in rheumatoid arthritis. *Int. J. Mol. Sci.* 23:8158. doi: 10.3390/ijms23158158

Hirtz, D., Thurman, D. J., Gwinn-Hardy, K., Mohamed, M., Chaudhuri, A. R., and Zalutsky, R. (2007). How common are the "common" neurologic disorders? *Neurology* 68, 326–337. doi: 10.1212/01.wnl.0000252807.38124.a3

Hn, D., and Vb, K. (2015). Inflammatory biomarkers in osteoarthritis. *Osteoarthr. Cartil.* 23, 1890–1896. doi: 10.1016/j.joca.2015.02.009

Houser, M. C., and Tansey, M. G. (2017). The gut-brain axis: is intestinal inflammation a silent driver of Parkinson's disease pathogenesis? *NPJ Park. Dis.* 3:3. doi: 10.1038/s41531-016-0002-0

Huang, X., Hussain, B., and Chang, J. (2021). Peripheral inflammation and blood-brain barrier disruption: effects and mechanisms. *CNS Neurosci. Ther.* 27, 36–47. doi: 10.1111/cns.13569

Isik, S., Yeman Kiyak, B., Akbayir, R., Seyhali, R., and Arpaci, T. (2023). Microglia mediated Neuroinflammation in Parkinson's disease. *Cells* 12:1012. doi: 10.3390/cells12071012

Jankovic, J., and Tan, E. K. (2020). Parkinson's disease: etiopathogenesis and treatment. *J. Neurol. Neurosurg. Psychiatry* 91, 795–808. doi: 10.1136/jnnp-2019-322338

Li, M., Yin, H., Yan, Z., Li, H., Wu, J., Wang, Y., et al. (2022). The immune microenvironment in cartilage injury and repair. *Acta Biomater.* 140, 23–42. doi: 10.1016/j.actbio.2021.12.006

Liu, T.-W., Chen, C.-M., and Chang, K.-H. (2022). Biomarker of Neuroinflammation in Parkinson's disease. *Int. J. Mol. Sci.* 23:4148. doi: 10.3390/ijms23084148

Liu, S.-Y., Qiao, H.-W., Song, T.-B., Liu, X.-L., Yao, Y.-X., Zhao, C.-S., et al. (2022). Brain microglia activation and peripheral adaptive immunity in Parkinson's disease: a multimodal PET study. *J. Neuroinflammation* 19:209. doi: 10.1186/s12974-022-02574-z

Liu, L., Shen, Q., Bao, Y., Xu, F., Zhang, D., Huang, H., et al. (2023). Association between dietary intake and risk of Parkinson's disease: cross-sectional analysis of survey data from NHANES 2007-2016. *Front. Nutr.* 10:1278128. doi: 10.3389/fnut.2023.1278128

Lücking, C. B., Dürr, A., Bonifati, V., Vaughan, J., De Michele, G., Gasser, T., et al. (2000). Association between early-onset Parkinson's disease and mutations in the parkin gene. *N. Engl. J. Med.* 342, 1560–1567. doi: 10.1056/NEJM200005253422103

McGeer, P. L., Itagaki, S., Boyes, B. E., and McGeer, E. G. (1988). Reactive microglia are positive for HLA-DR in the substantia nigra of Parkinson's and Alzheimer's disease brains. *Neurology* 38, 1285–1291. doi: 10.1212/wnl.38.8.1285

Motta, F., Barone, E., Sica, A., and Selmi, C. (2023). Inflammaging and osteoarthritis. *Clin. Rev. Allergy Immunol.* 64, 222–238. doi: 10.1007/s12016-022-08941-1

Perry, V. H. (2004). The influence of systemic inflammation on inflammation in the brain: implications for chronic neurodegenerative disease. *Brain Behav. Immun.* 18, 407–413. doi: 10.1016/j.bbi.2004.01.004

Qu, Y., Li, J., Qin, Q., Wang, D., Zhao, J., An, K., et al. (2023). A systematic review and meta-analysis of inflammatory biomarkers in Parkinson's disease. *NPJ Park. Dis.* 9:18. doi: 10.1038/s41531-023-00449-5

Savica, R., Grossardt, B. R., Bower, J. H., Ahlskog, J. E., and Rocca, W. A. (2016). Time trends in the incidence of Parkinson disease. *JAMA Neurol.* 73, 981–989. doi: 10.1001/jamaneurol.2016.0947

Schiess, M. (2003). Nonsteroidal anti-inflammatory drugs protect against Parkinson neurodegeneration: can an NSAID a day keep Parkinson disease away? *Arch. Neurol.* 60, 1043–1044. doi: 10.1001/archneur.60.8.1043

Sonar, S. A., and Lal, G. (2018). Blood-brain barrier and its function during inflammation and autoimmunity. *J. Leukoc. Biol.* 103, 839–853. doi: 10.1002/JLB.1RU1117-428R

Tagoe, C. E., Zezon, A., and Khattri, S. (2012). Rheumatic manifestations of autoimmune thyroid disease: the other autoimmune disease. *J. Rheumatol.* 39, 1125–1129. doi: 10.3899/jrheum.120022

Tan, E.-K., Chao, Y.-X., West, A., Chan, L.-L., Poewe, W., and Jankovic, J. (2020). Parkinson disease and the immune system - associations, mechanisms and therapeutics. *Nat. Rev. Neurol.* 16, 303–318. doi: 10.1038/s41582-020-0344-4

Tang, C.-H. (2019). Research of pathogenesis and novel therapeutics in arthritis. *Int. J. Mol. Sci.* 20:1646. doi: 10.3390/ijms20071646

Tansey, M. G., Wallings, R. L., Houser, M. C., Herrick, M. K., Keating, C. E., and Joers, V. (2022). Inflammation and immune dysfunction in Parkinson disease. *Nat. Rev. Immunol.* 22, 657–673. doi: 10.1038/s41577-022-00684-6

Teema, A. M., Zaitone, S. A., and Moustafa, Y. M. (2016). Ibuprofen or piroxicam protects nigral neurons and delays the development of l-dopa induced dyskinesia in rats with experimental parkinsonism: influence on angiogenesis. *Neuropharmacology* 107, 432–450. doi: 10.1016/j.neuropharm.2016.03.034

The Lancet (2017). Managing arthritis in the USA. *Lancet* 389:1076. doi: 10.1016/S0140-6736(17)30765-1

Veronese, N., Cooper, C., Reginster, J.-Y., Hochberg, M., Branco, J., Bruyère, O., et al. (2019). Type 2 diabetes mellitus and osteoarthritis. *Semin. Arthritis Rheum.* 49, 9–19. doi: 10.1016/j.semarthrit.2019.01.005

Zeng, Z., Cen, Y., and Luo, X. (2023). Association between blood selenium with parkinson's disease in the US (NHANES 2011-2020). *Environ. Sci. Pollut. Res. Int.* 30, 117349–117359. doi: 10.1007/s11356-023-30337-7

Zeng, Z., Cen, Y., Xiong, L., Hong, G., Luo, Y., and Luo, X. (2024). Dietary copper intake and risk of Parkinson's disease: a cross-sectional study. *Biol. Trace Elem. Res.* 202, 955–964. doi: 10.1007/s12011-023-03750-9

Zhang, W., Xiao, D., Mao, Q., and Xia, H. (2023). Role of neuroinflammation in neurodegeneration development. *Signal Transduct. Target. Ther.* 8:267. doi: 10.1038/s41392-023-01486-5

frontiers | Frontiers in Neuroscience

TYPE Original Research
PUBLISHED 10 September 2024
DOI 10.3389/fnins.2024.1435218

OPEN ACCESS

EDITED BY
Pradeep Kumar,
All India Institute of Medical Sciences, India

REVIEWED BY
Miren Altuna,
Fundacion CITA Alzheimer, Spain
María González-Nosti,
Universidad de Oviedo, Spain

*CORRESPONDENCE
Serena Fineschi
✉ serena.fineschi@pubcare.uu.se

RECEIVED 19 May 2024
ACCEPTED 07 August 2024
PUBLISHED 10 September 2024

CITATION
Fineschi S, Fahlström M, Fällmar D, Haller S and Wikström J (2024) Comprehensive MRI assessment reveals subtle brain findings in non-hospitalized post-COVID patients with cognitive impairment.
Front. Neurosci. 18:1435218.
doi: 10.3389/fnins.2024.1435218

Comprehensive MRI assessment reveals subtle brain findings in non-hospitalized post-COVID patients with cognitive impairment

Serena Fineschi[1,2]*, Markus Fahlström[3], David Fällmar[3,4], Sven Haller[3,5] and Johan Wikström[3,4]

[1]Department of Public Health and Caring Sciences, Faculty of Medicine, Uppsala University, Uppsala, Sweden, [2]Östhammar Health Care Centre, Östhammar, Sweden, [3]Department of Surgical Sciences, Faculty of Medicine, Uppsala University, Uppsala, Sweden, [4]Department of Radiology, Uppsala University Hospital, Uppsala, Sweden, [5]Division of Radiodiagnostic and Interventional Radiology, Faculty of Medicine, University of Geneva, Geneva, Switzerland

Background: Impaired cognitive ability is one of the most frequently reported neuropsychiatric symptoms in the post-COVID phase among patients. It is unclear whether this condition is related to structural or functional brain changes.

Purpose: In this study, we present a multimodal magnetic resonance imaging study of 36 post-COVID patients and 36 individually matched controls who had a mild form of severe acute respiratory syndrome coronavirus 2 (SARS CoV-2) infection from March 2020 to February 2022. This study aimed to investigate structural and functional brain alterations and their correlation with post-COVID symptoms and neurocognitive functions.

Materials and methods: The study protocol comprised an assessment of physical fatigue [Fatigue Severity Scale (FSS)], mental fatigue (Mental Fatigue Scale (MFS)], depression [Montgomery Asberg Depression Rating Scale (MADRS)], anxiety [Hospital Anxiety and Depression Scale (HAD)], post-COVID Symptoms Severity Score, and neurocognitive status [Repeatable Battery for the Assessment of Neuropsychological Status Update (RBANS)]. The magnetic resonance imaging protocol included morphological sequences, arterial spin labeling (ASL) and dynamic susceptibility contrast-enhanced (DSC) perfusion, diffusion tensor imaging (DTI), and resting-state functional magnetic resonance imaging (fMRI) sequences. Using these protocols, the assessments of macrostructural abnormalities, perfusion, gray matter density, white matter integrity, and brain connectivity were performed.

Results: Post-COVID patients had higher levels of physical fatigue, mental fatigue, depression, and anxiety than controls and showed cognitive impairment in all the RBANS domains except in Visuospatial/Construction. The subjective mental fatigue correlated with objective impaired cognitive ability in the RBANS test, particularly in the Attention domain. There were no differences between patients and controls regarding macrostructural abnormalities, regional volumes, regional perfusion metrics, gray matter density, or DTI parameters. We observed a significant positive correlation between RBANS Total Scale Index score and gray matter volume in the right superior/middle-temporal gyrus ($p < 0.05$) and a significant negative correlation between the white matter integrity and post-COVID symptoms ($p < 0.05$) in the same area. The connectivity differences were observed between patients and controls in a few regions, including the right

middle frontal gyrus, an important area of convergence of the dorsal and ventral attention networks. We also noted a positive correlation between post-COVID symptoms and increased connectivity in the right temporoparietal junction, which is part of the ventral attention system.

Conclusion: In non-hospitalized subjects with post-COVID, we did not find any structural brain changes or changes in perfusion, compared to controls. However, we noted differences in connectivity within an important area for attention processes, which may be associated with post-COVID brain fog.

KEYWORDS

post-COVID, MRI, attention network, cognitive impairment, resting state fMRI, right middle frontal gyrus, right temporoparietal junction

Introduction

Post-COVID condition occurs in individuals with a history of probable or confirmed SARS CoV-2 infection, usually 3 months from the onset of COVID-19, with symptoms that last for at least 2 months and cannot be explained by an alternative diagnosis, according to Delphi consensus, 2021 (Soriano et al., 2022).

Impaired cognitive ability and physical fatigue are the most frequently reported neuropsychiatric symptoms in post-COVID followed by insomnia, depression, and anxiety (Badenoch et al., 2022).

Other common physical symptoms are dyspnea, postural orthostatic tachycardia syndrome (POTS), widespread muscular pain, dizziness, and headache. Physical and mental fatigue are often accompanied by exertional intolerance and post-exertional malaise. Self-reported word-finding difficulties are among the most frequent neurocognitive complaints, such as impaired memory and attention. Cognitive exhaustion can worsen after even very light physical or mental exertion and leads to social isolation and long-term sick leave. A subset of post-COVID patients also fulfills the diagnostic criteria for myalgic encephalomyelitis (ME) and chronic fatigue syndrome (CFS) (Bonilla et al., 2023).

Depression, sleep disturbance, and anxiety, which have been reported to appear at the same time as the other post-COVID symptoms and are unlikely to be a mere consequence of the impaired cognitive ability, may affect the patient's experience of fatigue and their perception of cognitive impairment (Jaltuszewska et al., 2023).

Many studies show that neuropsychiatric symptoms also occur after a mild COVID infection (Graham et al., 2021) and can persist up to 2 years (Fernández-de-Las-Peñas et al., 2022).

The SARS-CoV-2 virus affects the brain directly from the cribriform plate, which is situated close to the olfactory bulb, or follows a hematogenous route (Singh et al., 2023). At the histopathological level, the three most common brain abnormalities reported during the acute phase of infection are inflammation, hypoxia, and coagulation disorders (Lu et al., 2020). However, the mechanism underlying the pathophysiology of neurologic symptoms in the post-COVID phase, especially after a mild COVID infection, is still debated. Advanced multimodal neuroimaging techniques have been employed to identify structural and functional brain changes in post-COVID patients.

There are a wide range of studies that discuss the alterations in the cerebral structure and cerebral blood flow from the post-acute phase until about 1 year from SARS-CoV-2 infection (Lu et al., 2020; Thapaliya et al., 2023; Hafiz et al., 2022; Tu et al., 2021; Douaud et al., 2022; Bendella et al., 2023; Planchuelo-Gómez et al., 2023; Cecchetti et al., 2022; Paolini et al., 2023; Heine et al., 2023; Du et al., 2022; Latini et al., 2022; Ajčević et al., 2023; Churchill et al., 2023; Qin et al., 2021; Díez-Cirarda et al., 2023), with a primary focus on hospitalized patients. However, there are very few studies investigating non-hospitalized patients with persisting symptoms more than 1 year after infection.

There is a significant heterogeneity in the reported results concerning both the specific regions affected and the types of gray (GM) and white matter (WM) modifications. Studies show evidence of increased (Lu et al., 2020; Thapaliya et al., 2023; Hafiz et al., 2022; Tu et al., 2021), decreased (Douaud et al., 2022; Bendella et al., 2023; Planchuelo-Gómez et al., 2023), and unchanged (Cecchetti et al., 2022) GM volume. Similarly, changes in WM volume in different regions (Lu et al., 2020; Paolini et al., 2023; Heine et al., 2023), WM hyperintensities (Du et al., 2022; Latini et al., 2022), and decreases in perfusion in different regions (Ajčević et al., 2023) have been reported.

There is a general consensus in finding a more pronounced modification in the cortical thickness and the WM microstructure in post-COVID patients with a severe disease than in those with a mild disease (Bendella et al., 2023; Qin et al., 2021).

Many different types of alterations in functional connectivity, such as altered connectivity in the right frontal pole and in the middle-temporal gyrus (Paolini et al., 2023), have been reported in functional magnetic resonance imaging (fMRI) studies (Du et al., 2022; Churchill et al., 2023).

Only a few studies have assessed the association between brain alterations detected using magnetic resonance imaging (MRI) and cognitive impairment measured through a neuropsychological assessment (Douaud et al., 2022; Díez-Cirarda et al., 2023; Andriuta et al., 2022).

In this study, we present a multimodal neuroimaging analysis of GM, WM, brain connectivity, and perfusion-based parameters in 36 post-COVID patients and 36 individually matched controls who had mild SARS-CoV-2 infection from March 2020 to February 2022. The primary aim of this study was to investigate the structural and functional brain alterations

and the secondary aim was to investigate if these alterations are associated with post-COVID symptoms, mental fatigue, and neuropsychological assessment.

Materials and methods

Participants

We recruited 36 post-COVID patients and 36 controls individually matched for age (±5 years) and date of COVID infection (±3 months) from April 2022 to February 2023. The post-COVID patients were enrolled at the Uppsala post-COVID outpatient clinic. The patients included in the study had COVID infection from the beginning of the pandemic through February 2022. The inclusion criteria were age between 18 and 65 years, a previous acute COVID infection that did not require hospitalization, and new onset persisting symptoms for at least 3 months after COVID infection according to the WHO definition (Soriano et al., 2022). The additional inclusion criteria were mental fatigue as one of the three most disabling symptoms, along with physical examination, radiological analysis, and blood tests ruling out other causes of the symptoms. The exclusion criteria were malignancies, autoimmune diseases, chronic diseases, and neurological, psychiatric, lung, and cardiovascular diseases prior to COVID infection.

The patients were not using antidepressants or other drugs that affect the central nervous system (CNS) at the time of recruitment such as anticonvulsants, antiemetics, CNS stimulants, muscle relaxants, narcotics, anxiolytics, or sedatives. In addition, 11 patients had COVID infection during the first wave in Sweden (February 2020–August 2020), 12 patients had COVID infection in the second wave (September 2020–February 2021), six patients in the third wave (March 2021 to July 2021), and seven in the fourth wave (August 2021–April 2022). The fourth wave was primarily driven by the omicron variant.

Every patient was individually matched to a control who had contracted COVID infection during the same period (±3 months) but experienced no post-COVID symptoms. Patients and controls has similar education levels and socioeconomic statuses, with the majority having a high level of education. The matched controls were recruited at the Östhammars primary healthcare center among patients who sought care for simple disabilities not related to COVID infection.

All the participants had a polymerase chain reaction (PCR)-verified COVID infection except for five patients and three controls who had the infection at the beginning of the pandemic when PCR capacity in Sweden was not sufficient to test all the suspected cases.

The time interval between the COVID infection and recording the brain MRI was 20.7 ± 7.6 months for patients and 23.8 ± 7.5 months for controls. The participants who were infected during the fourth wave had a shorter time interval between the infection and brain imaging (8 ± 1.7 months for patients, 11 ± 2.4 months for controls) than those who acquired the infection in the first, second, and third waves (24 ± 4.9 months for patients and 27 ± 4.6 months for controls).

The study was approved by the Swedish Ethical Review Authority (2022-01626-01) and was conducted in accordance with the Declaration of Helsinki. All participants provided their written informed consent.

Clinical and neuropsychological assessment

The study protocol comprised assessments of physical fatigue [Fatigue Severity Scale (FSS)] (Krupp et al., 1989), mental fatigue [Mental Fatigue Scale (MFS)] (Johansson et al., 2010), depression [Montgomery Asberg Depression Rating Scale (MADRS)] (Montgomery and Asberg, 1979), and anxiety [Hospital Anxiety and Depression Scale (HAD)] (Zigmond and Snaith, 1983).

The following cut-offs adjusted for the Swedish populations were used: FSS: score range 0–63, with a cut-off of ≥36. MFS: score range 0–42, with a cut-off of ≥10. MADRS: score range 0–54, categorized as 0–12 for no depression, 13–19 for mild depression, 20–34 for moderate depression, and >35 for severe depression. HAD depression: score 0–21, cut-off ≥7. HAD anxiety: score range 0–21, with a cut-off of ≥7.

Post-COVID symptom severity was assessed using a Symptom Severity Scale (SSS) based on 17 symptoms on a 10-point scale (where 0 indicates no symptom and 10 indicates the maximum severity of the symptom). The score range is from 0 to 170.

The symptoms included in the SSS are shown in Table 1.

Neurocognitive status was assessed using the Repeatable Battery for the Assessment of Neuropsychological Status (RBANS) (Randolph et al., 1998; Birberg Thornberg et al., 2022). RBANS generates index scores for five neurocognitive domains, including immediate memory, visuospatial/constructional, language, attention, and delayed memory, as well as a Total Scale Index score.

All patients except two, who were not possible to reach, were followed up with a new assessment of their post-COVID Symptom Severity Score 1 year after the first test.

Statistical analysis of clinical tests

Continuous data are represented as mean and standard deviation. Categorical data are represented as frequency and percentage.

Clinical symptoms and assessments between patients and controls were compared using the Mann–Whitney *U*-test. The correlation between MFS and RBANS was assessed using the Spearman's correlation coefficient and *p*-values were adjusted using the Bonferroni correction. The symptom scores from the first assessment and 1-year follow-up were compared using the Wilcoxon signed-rank test. Clinical symptoms and assessments between the first three waves and the fourth wave were compared using the Mann–Whitney *U*-test, and *p*-values were adjusted using the Bonferroni correction. p-values < 0.05 were considered statistically significant. Statistical analyses were performed using R (version 4.2.2).

TABLE 1 Clinical characteristics and rating scales.

Variable	Post-COVID	Controls	*P*-value
Age	44.2 ± 10.2	44.6 ± 10.5	
Gender: Women	24 (66.7%)	24 (66.7%)	
Infection period			
Wave 1	11 (30.6%)	13 (36.1%)	
Wave 2	12 (33.3%)	9 (25.0%)	
Wave 3	6 (16.7%)	7 (19.4%)	
Wave 4	7 (19.4%)	7 (19.4%)	
Post-COVID Symptom Severity Score	62.8 ± 24.9	8.6 ± 12.8	<0.001
Cognitive fatigue	7.7 ± 1.9	1.1 ± 1.8	<0.001
Physical fatigue	6.8 ± 2.2	0.9 ± 1.5	<0.001
Dyspnea	5.1 ± 3.2	0.4 ± 1.2	<0.001
Myalgia	4.7 ± 3.4	0.9 ± 1.4	<0.001
Headache	4.6 ± 3.5	1.0 ± 1.5	<0.001
Insomnia	3.9 ± 3.3	0.9 ± 1.3	<0.001
Palpitations	3.6 ± 3.1	0.3 ± 0.8	<0.001
Dizziness	3.2 ± 2.7	0.4 ± 1.3	<0.001
Anxiety	3.4 ± 2.8	0.4 ± 0.9	<0.001
Paresthesia/crawling sensation	2.9 ± 3.1	0.4 ± 1.2	<0.001
Depression	2.9 ± 2.8	0.6 ± 1.4	<0.001
Heaviness in the chest	2.8 ± 2.8	0.4 ± 1.1	<0.001
Diarrhea/abdominal pain	2.4 ± 2.8	0.4 ± 1.4	<0.001
Tinnitus	2.3 ± 3.0	0.2 ± 0.6	<0.001
Hyposmia/hypogeusia	2.2 ± 3.5	0.1 ± 0.5	<0.001
Fainting	2.1 ± 2.4	0.1 ± 0.5	<0.001
Fever	2.0 ± 3.0	0.2 ± 1.0	<0.001
RBANS Total Index score	83.4 ± 25.1	105.2 ± 11.3	<0.001
Immediate memory	85.0 ± 20.1	96.8 ± 15.3	0.027
Visuospatial/ constructional	98.3 ± 13.8	102.4 ± 10.3	0.152
Language	91.0 ± 18.9	106.3 ± 12.7	<0.001
Attention	81.2 ± 24.9	102.9 ± 15.1	<0.001
Delayed memory	87.8 ± 24.9	106.8 ± 14.2	0.002
MADRS	15.7 ± 8.0	4.6 ± 4.7	<0.001
HAD anxiety	6.5 ± 4.1	3.2 ± 2.8	<0.001
HAD depression	7.4 ± 4.5	1.2 ± 1.5	<0.001
FSS	55.4 ± 9.8	18.8 ± 10.6	<0.001
MFS	22.8 ± 6.0	2.1 ± 2.6	<0.001

Data show significant differences between patients and controls in all parameters examined except for the visuospatial/construction domain of the RBANS test. Post-COVID Symptom Severity Score (0–170) includes the 17 following symptoms on a 10-point scale (0 = no symptom, 10 = max severity). RBANS Total Scale Index and five domain-specific index scores. MADRS (depression scale 0–54), HAD anxiety (0–21), HAD depression (0–21), FSS (fatigue severity score 0–63), MFS (mental fatigue score 0–42). Data are presented as mean ± SD and compared using the Mann–Whitney U-test.

Imaging data acquisition

Magnetic resonance imaging

MRI scans was performed at the Uppsala University Hospital. All examinations were performed using a 3T system (Achieva d-Stream, Philips Healthcare, Amsterdam, The Netherlands). All subjects were scanned in a supine position using a 32-channel head coil. The images obtained through three-dimensional (3D) T1-weighted (3D-T1w), axial two-dimensional (2D) T2-weighted (2D-T2w), 3D fluid-attenuated inversion recovery (FLAIR), 2D axial diffusion-weighted imaging (DWI), and susceptibility-weighted imaging (SWI) were acquired for morphological evaluation and volumetric analysis. Perfusion-weighted imaging included a 3D pseudo-continuous arterial spin labeling (pCASL) sequence with gradient spin-echo readout and dynamic susceptibility contrast (DSC) acquisition. Additionally, resting-state fMRI (rs-fMRI) and diffusion tensor imaging (DTI) were acquired as part of the imaging protocol. A full description of the imaging protocol is provided in Supplementary Table 1.

Morphological evaluation

Two certified neuroradiologists (JW and DF) performed independent evaluations regarding WM changes, cortical infarcts, lacunar infarcts, microbleeds, and global atrophy. WM changes were assessed using the FLAIR images and categorized according to the Fazekas scale (0–III) (Fazekas et al., 1987). The number of cortical infarcts, lacunar infarcts, and microbleeds were noted; the infarcts were assessed using mainly FLAIR and 2D-T2-weighted sequences, and microbleeds were assessed in the SWI images. When microbleeds were present, they were assessed using a slightly modified Medication Adherence Rating Scale (MARS) (Gregoire et al., 2009) (using the SWIp sequence instead of GRE T2* and not recording laterality).

The width of the cerebral sulci was assessed using the global cerebral atrophy (GCA) scale (Pasquier et al., 1996).

The differences in routine morphological measures were compared between patients and controls using chi-squared or Fisher tests as appropriate, utilizing SPSS (version 28.0.1.0, IBM SPSS, Armonk, NY). A p-value of <0.05 was regarded as statistically significant.

Volumetry

The 3D-T1w images of all the subjects were processed with FreeSurfer software (http://surfer.nmr.mgh.harvard.edu/, version 7.4.0) using the *recon-all* pipeline. GM volumes and cortical thickness were extracted for the following cortical and subcortical regions: the frontal, parietal, occipital, and temporal lobes (see Supplementary Table 2 for components), cerebellum, hippocampus, putamen, pallidum, and thalamus. In addition, total cerebral gray matter, total cerebral white matter, and total cerebellar white matter were extracted.

TABLE 2 Correlation between the mental fatigue score (MFS) and the neurocognitive test (RBANS).

Scale	Corr. coef.	*P*-value
RBANS Total Index score	−0.46	0.027
Immediate memory	−0.37	0.15
Visuospatial/constructional	−0.36	0.18
Language	−0.16	>0.99
Attention	−0.56	0.002
Delayed memory	−0.36	0.19

Spearman's correlation coefficient. The *p*-values were adjusted using the Bonferroni correction for multiple comparisons across six tests.
MFS score is strongly negatively correlated to the attention domain of the RBANS test.

Perfusion assessment

The pCASL-based cerebral blood flow (CBF) maps (CBF_{pCASL}) were automatically calculated by the scanner according to the model recommended by Alsop et al. (2015). Based on the DSC acquisition, parametric maps of CBF, cerebral blood volume (CBV), mean transit time (MTT), time to peak (TTP), leakage, coefficient of variation (CoV), capillary transit time heterogeneity (CTH), cerebral metabolic rate of oxygen ($CMRO_2$), and oxygen extraction fraction (OEF) were calculated using Cercare Medical Neurosuite (Cercare Medical, Aarhus, Denmark). Parametric maps were registered to the corresponding 3D-T1w image. The perfusion-based measures as listed above were extracted from cortical and subcortical regions derived from FreeSurfer as described above.

Statistical analysis of volumetry and perfusion assessment

Hypothesis testing was focused on the derived regional parameters, that is, perfusion-based metrics, cortical volumes, and thicknesses, comparing the measures between controls and patients. First, the Shapiro–Wilk test was performed to test for normality. To test whether any differences were present between controls and patients, we performed a Kruskal–Wallis test for non-normal distributed data with Dunn's correction for multiple comparisons. The *post-hoc* analysis was performed for all the cortical regions for each parameter.

Voxel-based morphometry analysis

The voxel-based morphometry (VBM) analysis of the gray matter was performed in FSL (the FMRIB Software Library) toolbox (https://fsl.fmrib.ox.ac.uk) version 6.0.6.1 using the standard processing pipeline FSL_VBM as described in detail (Jenkinson et al., 2012).

(i) A group comparison was performed for patients vs. controls using age and gender as non-explanatory co-regressors.
(ii) The analysis of patients vs. controls was conducted using age and gender as non-explanatory co-regressors, adding "time between COVID infection and MRI" as an additional non-explanatory co-regressor.
(iii) A group comparison was performed for patients vs. controls using only the first, second, and third waves again using age and gender as non-explanatory co-regressors.
(iv) A correlation analysis was performed using the three most relevant test scores, notably RBANS total scale index score, MFS, and SSS, again using age and gender as non-explanatory co-regressors.

All variables were transformed into the range of −1 to +1 with a mean of 0. A statistical threshold was defined as $p < 0.05$ corrected using threshold-free cluster enhancement (TFCE) (Smith and Nichols, 2009).

Track-based spatial statistics

The track-based spatial statistics (TBSS) analysis of the white matter was performed in FSL version 6.0.6.1 using the standard processing pipeline FSL_TBSS as described in detail (Jenkinson et al., 2012). The studied parameters related to the white matter integrity included fractional anisotropy (FA), mean diffusivity, and axial and radial diffusivity. Four equivalent analyses were performed similar to the VBM analysis described above. Again, a statistical threshold of TFCE-corrected $p < 0.05$ was applied.

Resting fMRI analysis

Resting fMRI analysis was performed in FSL version 6.0.6.1 using the standard processing pipeline MELODIC as described in detail (Jenkinson et al., 2012). First, a tensorial independent component analysis (TICA) was performed using 20 independent components. Then, a dual regression analysis was performed using the same setup as above: first, a group comparison between patients and controls was carried out and then a correlation analysis was performed with the same three clinical scores, notably RBANS Total Scale Index score, MFS, and SSS, again using age and gender as non-explanatory co-regressors and a statistical threshold of TFCE-corrected $p < 0.05$.

Results

Clinical characteristics

The detailed clinical information regarding the date of COVID infection and responses to rating scales and neurocognitive tests are reported in Supplementary Table 3. The participants were aged between 24 and 64 years. The mean age of COVID patients was 44.2 ± 10.2 years and that of controls was 44.6 ± 10.5 years. The majority (66.6%) of the patients in both groups were women (Table 1).

10.3389/fnins.2024.1435218

TABLE 3 Macrostructural analysis.

Fazekas	Reviewer 1			Reviewer 2		
	Grade 0	Grade 1	Grade 2	Grade 0	Grade 1	Grade 2
Controls	8	25	3	15	19	2
Patients	8	25	3	18	16	2
	$p = 1.00$			$p = 0.77$		
GCA	Grade 0	Grade 1	Grade 2	Grade 0	Grade 1	Grade 2
Controls	2	32	2	29	7	0
Patients	2	32	2	35	1	0
	$p = 1.00$			$p = 0.972$		
Cortical infarcts	0	1 or more		0	1 or more	
Controls	35	1		36	0	
Patients	34	2		36	0	
	$p = 0.5$			NA		
Lacunar infarcts	0	1 or more		0	1 or more	
Controls	36	0		35	1	
Patients	32	4		35	1	
	$p = 0.057$			$p = 0.75$		
Microbleeds	0	1 or more		0	1 or more	
Controls	32	4		35	1	
Patients	32	4		34	2	
	$p = 0.65$			$p = 0.5$		

Comparisons of white matter changes (Fazeka), global cerebral atrophy (GCA), cortical infarcts, lacunar infarcts, and microbleeds between controls and patients for both reviewers. No significant differences were observed.

The post-COVID Symptom Severity Score (values ranging between 0 and 170) was 62.8 ± 24.9 for patients and 8.6 ± 12.8 for controls ($p < 0.001$).

The patient-reported complaints with the highest mean value were cognitive fatigue (7.7 ± 1.9), physical fatigue (6.8 ± 2.2), and dyspnea (5.1 ± 3.2; Table 1).

The patients fulfilled the criteria for mild depression (MADRS 15.7 ± 8.0, HAD depression 7.4 ± 4.5) and were just below the cut-off score for anxiety (HAD anxiety 6.5 ± 4.1). The levels of depressive symptoms and anxiety were anyway higher ($p < 0.001$) compared to healthy controls (Table 1).

They reported higher levels of both physical fatigue (FSS 55.4 ± 9.8) and mental fatigue (MFS 22.8 ± 6.0) compared to healthy controls ($p < 0.001$).

Neurocognitive testing showed a lower RBANS Total Scale Index score in patients ($p < 0.001$). Differences were found between patients and controls in attention and language ($p < 0.001$), immediate memory ($p = 0.027$), and delayed memory domains ($p < 0.002$), whereas no difference was observed in visuospatial/construction domain ($p < 0.152$).

Subjective mental fatigue assessed with the MFS test correlated with objective cognitive impairment measured with the RBANS score ($r = -0.46$, $p < 0.05$, Table 2). Particularly, patients with higher levels of subjective mental fatigue had lower performance in the attention domain ($r = -0.56$, $p = 0.002$; Table 2). The other four RBANS domains did not correlate with the subjective mental fatigue.

When we compared patients who contracted the omicron variant (fourth wave) with patients with earlier COVID variants, there was no significant difference between the groups in symptoms, neurocognitive ability, and responses to rating scales (Supplementary Table 4).

One year after the first assessment, 34 patients were re-evaluated with the post-COVID Symptoms Assessment Scale (SAS). Post-COVID Symptom Severity Score decreased from 62.7 ± 25.6 at the first medical visit to 47.3 ± 26.7 after 1 year ($p < 0.001$). Self-reported cognitive fatigue was also found to be improved (from 7.7 ± 1.9 at the first visit to 6.2 ± 2.5 after 1 year, $p < 0.001$). However, when asked to estimate their health in relation to post-COVID symptoms, only two patients reported feeling completely recovered (Supplementary Table 3).

Routine morphological MRI evaluation

Both reviewers observed that there were no significant differences in the number of cortical infarcts, lacunar infarcts, white

matter hyperintensities, global cerebral atrophy, or microbleeds between patients and controls (Table 3).

MR volumetry

There were no significant differences in volume or cortical thickness in any of the anatomical regions between patients and controls (Figures 1, 2).

MR perfusion

There were no significant differences in CBF_{pCASL}, CBF, CBV, MTT, TTP, leakage, CV, CTH, $CMRO_2$, or OEF in any of the anatomical regions between patients and controls (Supplementary Figures 1–10).

Voxel-based morphometry analysis

(i) There was no significant group difference between patients and controls in gray matter VBM.
(ii) Adding "time between COVID infection and MRI" as an additional co-regressor did not change those results.
(iii) The comparison between patients and controls exclusively in the first, second, and third waves (early variants) resulted still in no significant differences.
(iv) In the whole group, we observed a significant positive correlation with RBANS total index score ($p < 0.05$ TFCE-corrected) for gray matter volume in the right superior/middle-temporal gyrus (Figure 3).

Track-based spatial statistics

(i) There was no significant group difference between patients and controls in the white matter TBSS analysis.
(ii) Adding "time between COVID infection and MRI" as an additional co-regressor did not change the results.
(iii) Again, analysis of patients and controls in only the first, second, and third waves (early variants) resulted in no significant differences.
(iv) In the whole group, we observed a significant negative correlation between FA in the right superior-/middle-temporal gyrus and the SSS (TFCE-corrected $p < 0.05$; Figure 4).

Resting fMRI analysis

Based on dual regression, patients had a significantly stronger connectivity in the right middle frontal gyrus (MFG) compared to controls, while they exhibited a significantly weaker connectivity in the right inferior parietal lobule and the left fronto-parietal junction compared to controls (see Figure 5).

Additionally, we observed a significantly positive correlation in the whole group using the SSS, notably in the right posterior temporoparietal junction (TPJ) and bilateral temporo-occipital junction, and weaker correlations in the left frontobasal and left superior parietal areas were observed. There was a minor negative correlation in the left parietal region (Figure 6).

Discussion

The aim of the present study was to use a multimodal imaging approach to evaluate brain alterations in post-COVID patients after a mild COVID infection and their correlation with post-COVID symptoms (SSS), mental fatigue (MFS), and neuropsychological assessments (RBANS test). We found no significant morphological, microstructural, or perfusion brain changes in non-hospitalized post-COVID patients with brain fog who were treated at an outpatient post-COVID clinic in comparison with age-matched healthy controls who had acquired COVID infection in the same period. However, some differences were observed between the two groups regarding functional brain connectivity, particularly in the right middle frontal gyrus, which may suggest a disturbed regulation mechanism between ventral and dorsal attention networks.

Macro- and microstructure and perfusion

We found no differences in macrostructural abnormalities, such as infarcts and atrophy, microbleeds, number, and localization of WM hyperintensities and general brain volume. The absence of differences in focal lesions is in agreement with a recent review of routine MR imaging studies, which found minimal abnormalities in post-COVID subjects and no conclusive evidence of a correlation between MRI findings and symptoms (Vasilev et al., 2023). As for brain volumes, previous studies have shown divergent results (Lu et al., 2020; Bendella et al., 2023).

Regional perfusion measures were not different in our study between post-COVID subjects and controls. Apart from CBF measurements, we also used novel perfusion-based measures such as CTH, OEF, and $CMRO_2$ (Mouridsen et al., 2014) for an assessment of microvascular derangements. We found no evidence of alterations in post-COVID patients.

Regional GM density and regional WM fractional anisotropy were also similar between the patient groups. The absence of microstructural white matter changes in the whole brain is mostly in line with the findings of Heine et al. (2023) who compared 47 subjects with post-COVID symptoms with subjects without COVID infection although they found aberrant FA of the thalamus. Paolini et al. (2023) also failed to identify any changes in fractional anisotropy but, on the other hand, they showed increases in diffusivity measures in several areas in patients previously hospitalized because of COVID infection, which can be interpreted as an increase in water content. The differences in results may be explained by both differences in infection severity (hospitalized vs. non-hospitalized) and choice of the comparison group (without a medical history of COVID infection vs. with a medical history of COVID infection but without remaining symptoms).

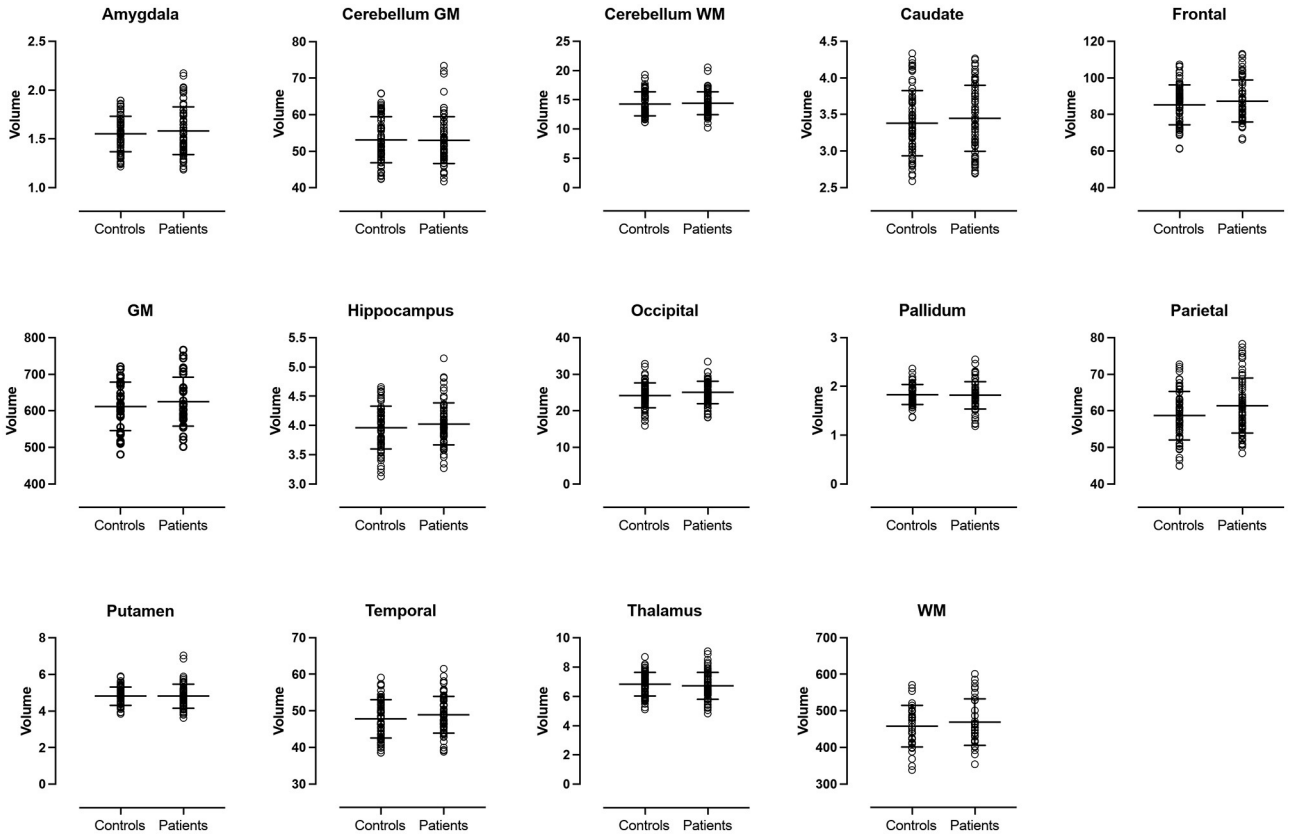

FIGURE 1
Volume analysis. Volumes of the cerebral lobes, cerebral central gray matter structures and cerebellum. No significant differences were observed between patients and controls. GM, total cerebral gray matter. WM, total cerebral white matter.

Connectivity

The only positive findings were differences in resting-state functional connectivity, where post-COVID patients showed higher connectivity in the right middle frontal gyrus. Altered connectivity in a similar frontal region in post-COVID patients was also detected by Paolini et al. (2023). The right middle frontal gyrus has been proposed to be the node that links the ventral and dorsal attention networks by acting as a "circuit-breaker" between exogenous and endogenous attention control (Corbetta et al., 2008). Fox et al. (2006) have shown that the right middle frontal gyrus interrupts ongoing processes in the dorsal network and reorients attention to a novel task-relevant external stimulus. Impaired connectivity in the right MFG and the resulting loss of the flexible modulation between endogenous and exogenous attention may eventually be responsible for certain post-COVID symptoms such as difficulties with focus and concentration in a specific task, as well as oversensitivity to minimal external stimuli, which are perceived as distracting and increasing the mental exhaustion.

This hypothesis is supported by the fact that we additionally found a positive correlation between post-COVID symptoms and increased connectivity in the right TPJ, which is the main part of the ventral attentional system. The increased connectivity in the ventral network in participants with post-COVID symptoms may reflect their inability to filter distracting signals.

Correlation between the neuropsychological test and subjective mental fatigue

Post-COVID patients showed cognitive impairment in all RBANS domains except visuospatial/construction. These results are in accord with another study in which a neurocognitive test was performed using Montreal Cognitive Assessment (MoCA) and where no differences in orientation and visuoconstructive functions were observed (Birberg Thornberg et al., 2022).

The patients who reported a higher value of subjective mental fatigue at the MFS also had a more pronounced objective impaired cognitive ability at the RBANS test, especially in the Attention domain. The fact that impaired attention ability is the neurocognitive domain that correlates with the subjective feeling of mental exhaustion in our patients reinforces the hypothesis that deficit in attention mechanisms can be the basis of the subjective mental fatigue in post-COVID patients and it is in line with our results in connectivity.

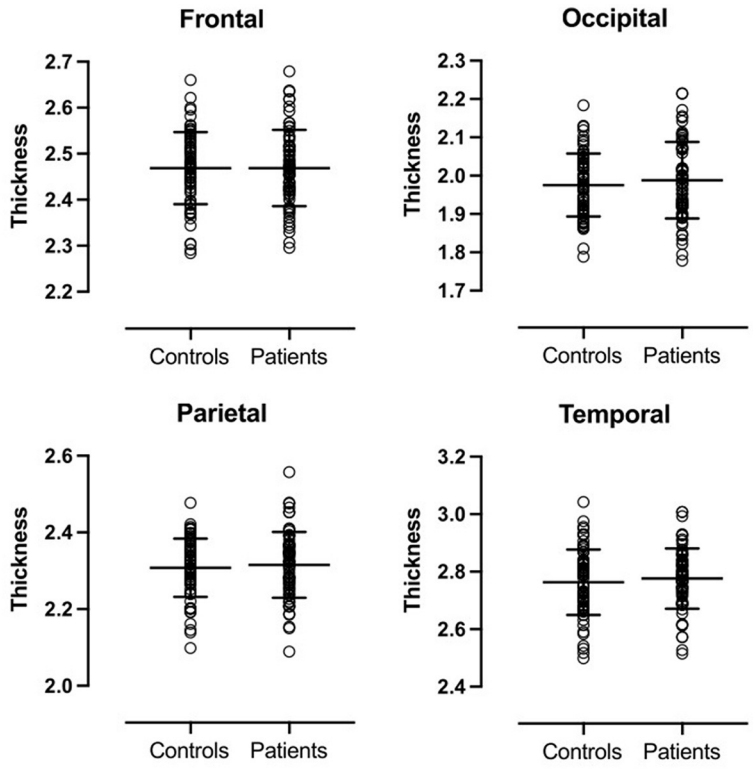

FIGURE 2
Cortical thickness of cerebral lobes. No significant differences were observed between patients and controls.

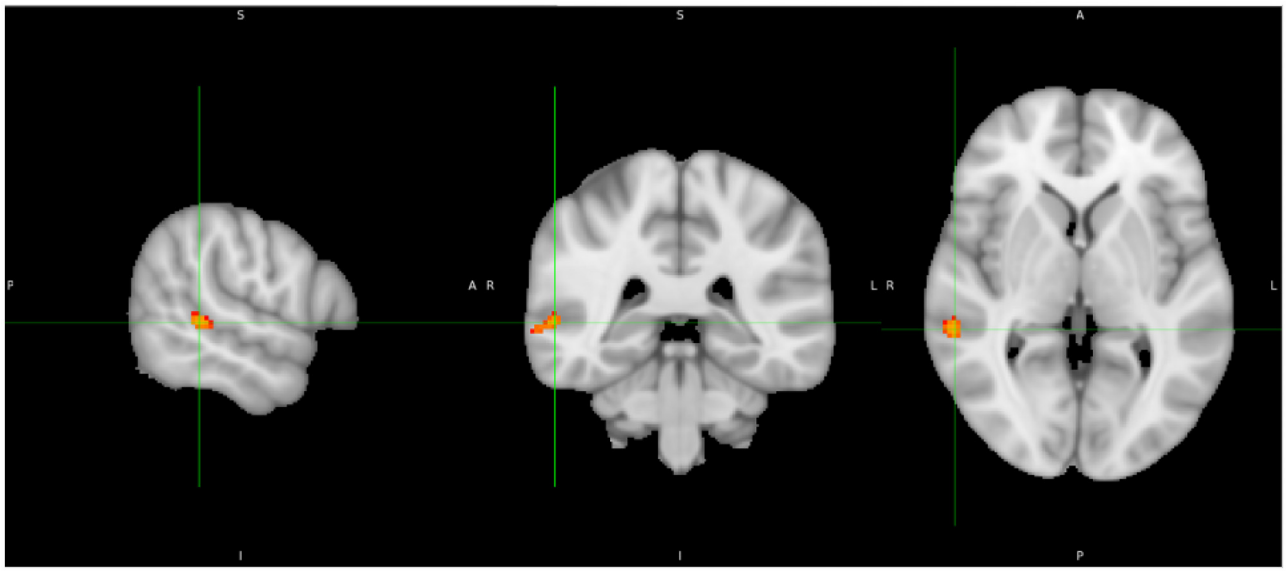

FIGURE 3
Correlation analysis shows a positive correlation between gray matter volume and RBANS Total Index score in the posterior part of the right superior-/middle-temporal gyrus (yellow).

Correlation between the neuropsychological test and MRI

We found a positive correlation between neurocognitive test and GM thickness in the right superior-/middle-temporal gyrus. Interestingly, there was also a correlation between the intensity of post-COVID symptoms (SSS) and WM anisotropy in the same area. These findings are difficult to interpret but imply that this region is involved in both cognitive processes and post-COVID symptoms. Neurocognitive impairment did not correlate with WM

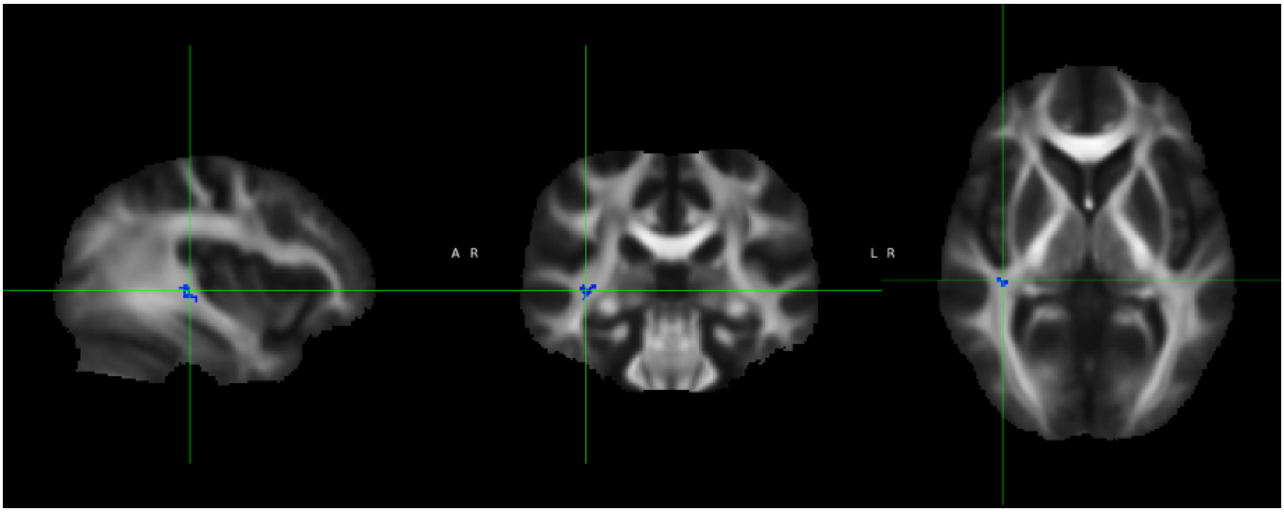

FIGURE 4
Track-based spatial statistics shows a significant negative correlation between Symptom Severity Score (SSS) and FA in the right superior-/middle-temporal gyrus (blue).

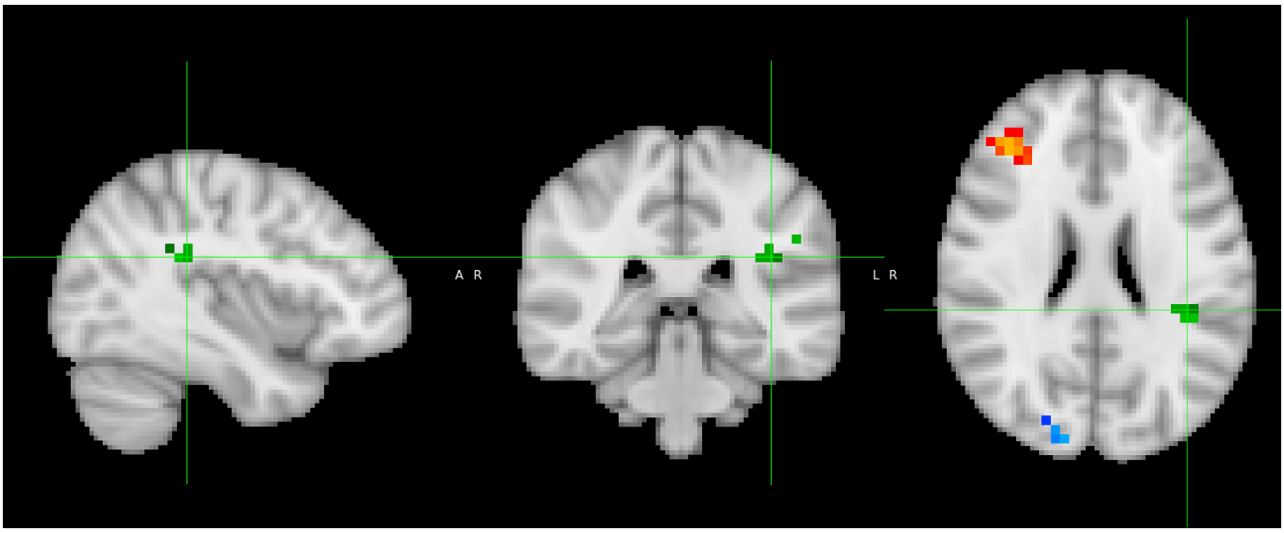

FIGURE 5
Dual regression resting state fMRI analysis shows stronger connectivity in the right middle frontal gyrus (orange) in patients compared to controls and weaker connectivity in the right inferior parietal lobule (blue) and left fronto-parietal junction (green).

anisotropy, similar to a previous study in 86 post-COVID patients (Díez-Cirarda et al., 2023).

Time since infection

Another point of interest to consider is the time of infection. Patients in our study acquired SARS-CoV-2 infection from the beginning of the pandemic in 2020 to February 2022. This period includes four waves of the pandemic in Sweden, where the fourth wave was dominated by the omicron variant. The participants who had the infection in the first three waves were not vaccinated, while those who contracted omicron (the fourth wave) were vaccinated with at least two shots. To assess whether individuals who contracted the virus before receiving the vaccination—during a period when the virus was more aggressive—could have more pronounced structural brain changes, we separately analyzed patients and controls in the first three waves but found no structural differences in brain changes.

There was also no difference in post-COVID symptoms, neurocognitive ability, depression, anxiety, and physical and mental fatigue between the patients who had contracted the infection in the first three waves and those who were infected by the omicron variant. However, the small number of patients in the omicron group may not be sufficient to detect a difference between the two groups (omicron and

10.3389/fnins.2024.1435218

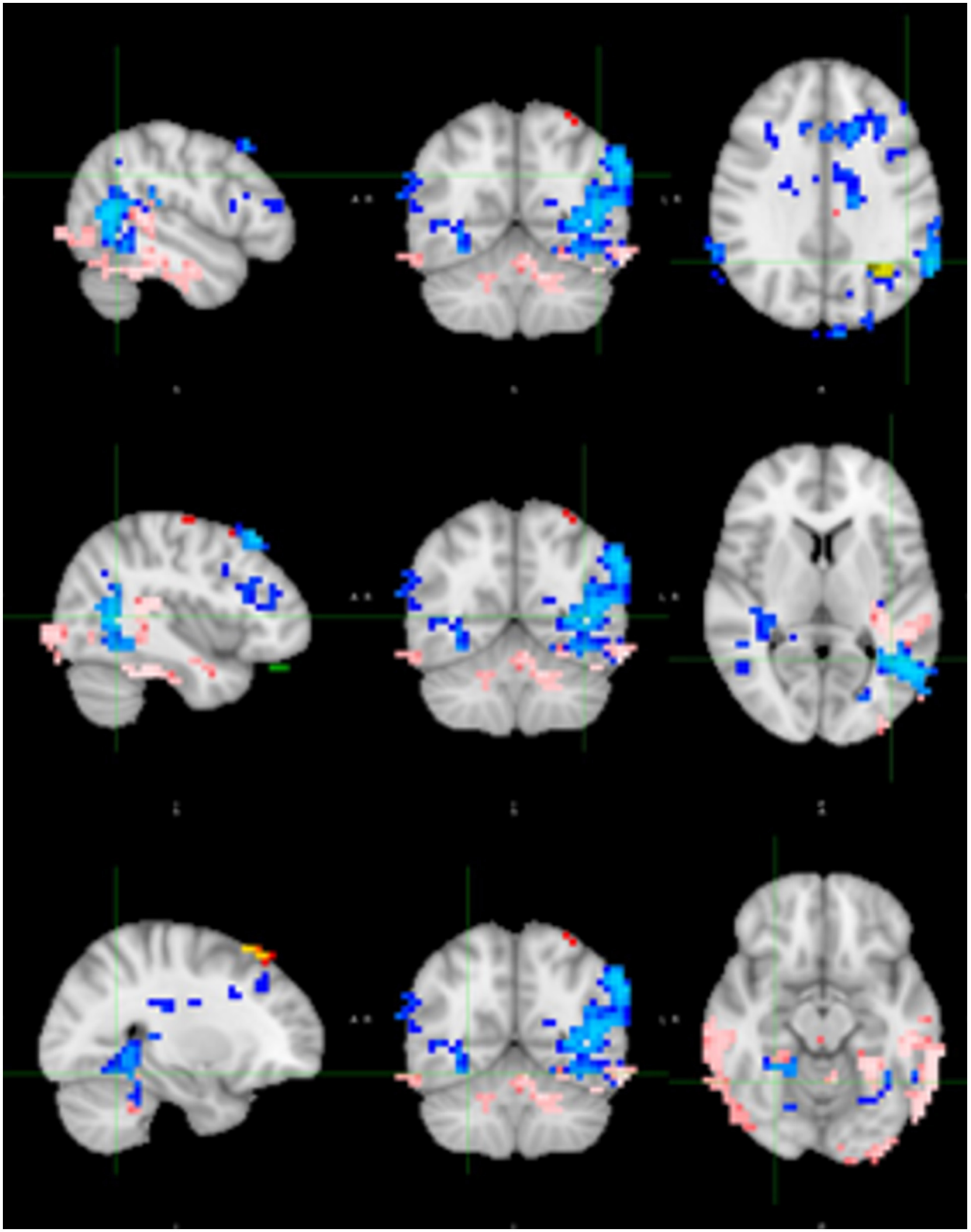

FIGURE 6
Correlation between SSS and connectivity. Positive correlation in the right posterior temporoparietal junction (TPJ; blue) and bilateral temporo-occipital junction (pink), and weaker correlations in the left frontobasal (green) and left superior parietal (red) areas. There was a minor negative correlation in the left parietal region (yellow).

"pre-omicron"). Therefore, these data must be interpreted with caution.

We did not find any correlation between brain changes and the time passed between infection and MRI.

Except for the participants who were infected with the omicron variant (a minority), our patients had experienced post-COVID symptoms for a long time before undergoing MRI (24 ± 5 months), which is longer compared to most other studies.

After 2 years of illness, one patient in our study was diagnosed with myalgic encephalomyelitis/chronic fatigue syndrome (ME/CFS), and others were under investigation since most of the symptoms reported by individuals with ME/CFS and post-COVID are similar. According to evidence from a prospective study, it appears that the subset of post-COVID patients who also fulfill the diagnostic criteria for ME/CFS presents more persistent, high-severity symptoms at a 20-month follow-up, while patients affected by COVID show an overall health improvement in the post-COVID phase (Legler et al., 2023).

In our study, when we reassessed the patients using the post-COVID Symptoms Assessment Scale (SAS) after 1 year, all of them had a lower intensity of symptoms, although only two felt fully recovered; there was thus a trend toward slow improvement.

Interestingly, the localization of the impaired brain connectivity seems different between patients with ME/CFS and post-COVID patients. In ME/CFS, connectivity seems impaired within the brainstem and from the brainstem to key subcortical structures. Moreover, hippocampal connections to the midbrain cuneiform nucleus and the medulla are enhanced, suggesting that the hippocampus has a compensatory role for the impaired connections (Barnden et al., 2019; Inderyas et al., 2024). In our post-COVID study, we could not find any impairment in the brainstem connectivity, suggesting that different brain areas are possibly affected.

Strengths and limitations

A strength of the study is the stringent inclusion criteria for controls. The higher proportion of women (66.6%) in our study reflects the higher prevalence of post-COVID symptoms in women in the general population.

Another strength is the comprehensive MR protocol, including macrostructural, microstructural, perfusion, and cortical activation outcomes. The perfusion protocol included an assessment of capillary transit time heterogeneity, which is a recently introduced metric with the potential to provide significant insights into microvascular function. However, a potential weakness is that the statistical power of the present study may not have been sufficient to detect small structural differences between the study groups. In particular, the results of the subgroup analysis (omicron variant vs. "pre-omicron" variant) can be affected by the low number of patients in the fourth wave.

Potential relevance in clinical practice

Our study presents a hypothesis (post-COVID brain fog is related to attention problem, which in turn is related to impaired connectivity in the right MFG and increased connectivity in the ventral network) that has potential high relevance in clinical practice and future research. This hypothesis needs to be confirmed in larger studies. Additionally, the negative finding concerning the absence of morphological, microstructural, or perfusion brain changes is relevant in clinical practice to avoid unnecessary brain MRI examinations in post-COVID patients, since connectivity studies are not included in the routine MRI examination.

Conclusion

This study found no macrostructural or microstructural brain changes, nor alterations in perfusion, in patients who exhibited persistent subjective and objective impaired cognitive abilities long after a mild COVID infection. However, differences in functional connectivity were observed in a few regions, notably the right medial frontal gyrus, which is an important area for attention processes. These changes could play a role in post-COVID brain fog. However, the results of our exploratory analysis in this region require confirmation through larger studies.

Data availability statement

The raw data supporting the conclusions of this article will be made available by the authors, without undue reservation.

Ethics statement

The studies involving humans were approved by Swedish Ethical Review Authority (2022-01626-01). The studies were conducted in accordance with the local legislation and institutional requirements. The participants provided their written informed consent to participate in this study.

Author contributions

SF: Conceptualization, Writing – original draft, Writing – review & editing, Data curation, Formal analysis, Funding acquisition, Investigation, Methodology, Resources, Supervision. MF: Formal analysis, Investigation, Methodology, Software, Writing – original draft, Writing – review & editing. DF: Data curation, Formal analysis, Investigation, Methodology, Writing – review & editing. SH: Formal analysis, Investigation, Methodology, Software, Writing – review & editing. JW: Conceptualization, Data curation, Formal analysis, Funding acquisition, Investigation, Methodology, Resources, Supervision, Writing – original draft, Writing – review & editing.

Funding

The author(s) declare financial support was received for the research, authorship, and/or publication of this article. The study was funded by grants from the Healthcare Board, Region of Uppsala, Sweden (FoU grant to SF). David Fällmar was supported

by the Swedish Society for Medical Research (SSMF, PD21-0136) and by Hjärnfonden (PS2021-0026).

Acknowledgments

The authors thank the statistician Katja Gabrysch at the Uppsala Clinical Research Center for assisting the statistical analysis of clinical tests.

Conflict of interest

The authors declare that the research was conducted in the absence of any commercial or financial relationships that could be construed as a potential conflict of interest.

Publisher's note

All claims expressed in this article are solely those of the authors and do not necessarily represent those of their affiliated organizations, or those of the publisher, the editors and the reviewers. Any product that may be evaluated in this article, or claim that may be made by its manufacturer, is not guaranteed or endorsed by the publisher.

Supplementary material

The Supplementary Material for this article can be found online at: https://www.frontiersin.org/articles/10.3389/fnins.2024.1435218/full#supplementary-material

References

Ajčević, M., Iscra, K., Furlanis, G., Michelutti, M., Miladinović, A., Buoite Stella, A., et al. (2023). Cerebral hypoperfusion in post-COVID-19 cognitively impaired subjects revealed by arterial spin labeling MRI. *Sci. Rep*. 13:5808. doi: 10.1038/s41598-023-32275-3

Alsop, D. C., Detre, J. A., Golay, X., Günther, M., Hendrikse, J., Hernandez-Garcia, L., et al. (2015). Recommended implementation of arterial spin-labeled perfusion MRI for clinical applications: a consensus of the ISMRM perfusion study group and the European consortium for ASL in dementia. *Magn. Reson. Med*. 73, 102–116. doi: 10.1002/mrm.25197

Andriuta, D., Si-Ahmed, C., Roussel, M., Constans, J. M., Makki, M., Aarabi, A., et al. (2022). Clinical and imaging determinants of neurocognitive disorders in post-acute COVID-19 patients with cognitive complaints. *J. Alzheimers Dis*. 87, 1239–1250. doi: 10.3233/JAD-215506

Badenoch, J. B., Rengasamy, E. R., Watson, C., Jansen, K., Chakraborty, S., Sundaram, R. D., et al. (2022). Persistent neuropsychiatric symptoms after COVID-19: a systematic review and meta-analysis. *Brain Commun*. 4:fcab297. doi: 10.1093/braincomms/fcab297

Barnden, L. R., Shan, Z. Y., Staines, D. R., Marshall-Gradisnik, S., Finegan, K., Ireland, T., et al. (2019). Intra brainstem connectivity is impaired in chronic fatigue syndrome. *Neuroimage Clin*. 24:102045. doi: 10.1016/j.nicl.2019.102045

Bendella, Z., Widmann, C. N., Layer, J. P., Layer, Y. L., Haase, R., Sauer, M., et al. (2023). Brain volume changes after COVID-19 compared to healthy controls by artificial intelligence-based MRI volumetry. *Diagnostics* 13:1716. doi: 10.3390/diagnostics13101716

Birberg Thornberg, U., Andersson, A., Lindh, M., Hellgren, L., Divanoglou, A., Levi, R., et al. (2022). Neurocognitive deficits in COVID-19 patients five months after discharge from hospital. *Neuropsychol. Rehabil*. 14, 1–25. doi: 10.1080/09602011.2022.2125020

Bonilla, H., Quach, T. C., Tiwari, A., Bonilla, A. E., Miglis, M., Yang, P. C., et al. (2023). Myalgic encephalomyelitis/chronic fatigue syndrome is common in post-acute sequelae of SARS-CoV-2 infection (PASC): results from a post-COVID-19 multidisciplinary clinic. *Front. Neurol*. 14:1090747. doi: 10.3389/fneur.2023.1090747

Cecchetti, G., Agosta, F., Canu, E., Basaia, S., Barbieri, A., Cardamone, R., et al. (2022). Cognitive, EEG, and MRI features of COVID-19 survivors: a 10-month study. *J. Neurol*. 269, 3400–3412. doi: 10.1007/s00415-022-11047-5

Churchill, N. W., Roudaia, E., Chen, J. J., Gilboa, A., Sekuler, A., Ji, X., et al. (2023). Effects of post-acute COVID-19 syndrome on the functional brain networks of non-hospitalized individuals. *Front. Neurol*. 14:1136408. doi: 10.3389/fneur.2023.1136408

Corbetta, M., Patel, G., and Shulman, G. L. (2008). The reorienting system of the human brain: from environment to theory of mind. *Neuron* 58, 306–24. doi: 10.1016/j.neuron.2008.04.017

Díez-Cirarda, M., Yus, M., Gómez-Ruiz, N., Polidura, C., Gil-Martínez, L., Delgado-Alonso, C., et al. (2023). Multimodal neuroimaging in post-COVID syndrome and correlation with cognition. *Brain* 146, 2142–2152. doi: 10.1093/brain/awac384

Douaud, G., Lee, S., Alfaro-Almagro, F., Arthofer, C., Wang, C., McCarthy, P., et al. (2022). SARS-CoV-2 is associated with changes in brain structure in UK Biobank. *Nature* 604, 697–707. doi: 10.1038/s41586-022-04569-5

Du, Y. Y., Zhao, W., Zhou, X. L., Zeng, M., Yang, D. H., Xie, X. Z., et al. (2022). Survivors of COVID-19 exhibit altered amplitudes of low frequency fluctuation in the brain: a resting-state functional magnetic resonance imaging study at 1-year follow-up. *Neural Regen Res*. 17, 1576–1581. doi: 10.4103/1673-5374.327361

Fazekas, F., Chawluk, J. B., Alavi, A., Hurtig, H. I., and Zimmerman, RA. (1987). MR signal abnormalities at 1.5 T in Alzheimer's dementia and normal aging. *AJR Am. J. Roentgenol*. 149, 351–356. doi: 10.2214/ajr.149.2.351

Fernández-de-Las-Peñas, C., Rodríguez-Jiménez, J., Cancela-Cilleruelo, I., Guerrero-Peral, A., Martín-Guerrero, J. D., García-Azorín, D., et al. (2022). Post-COVID-19 symptoms 2 years after SARS-CoV-2 Infection among hospitalized vs. nonhospitalized patients. *JAMA Netw. Open* 5:e2242106. doi: 10.1001/jamanetworkopen.2022.42106

Fox, M. D., Corbetta, M., Snyder, A. Z., Vincent, J. L., and Raichle, M. E. (2006). Spontaneous neuronal activity distinguishes human dorsal and ventral attention systems. *Proc. Natl. Acad. Sci. USA*. 103, 10046–10051. doi: 10.1073/pnas.0604187103

Graham, E. L., Clark, J. R., Orban, Z. S., Lim, P. H., Szymanski, A. L., Taylor, C., et al. (2021). Persistent neurologic symptoms and cognitive dysfunction in non-hospitalized Covid-19 "long haulers". *Ann. Clin. Transl. Neurol*. 8, 1073–1085. doi: 10.1002/acn3.51350

Gregoire, S. M., Chaudhary, U. J., Brown, M. M., Yousry, T. A., Kallis, C., Jäger, H. R., et al. (2009). The Microbleed Anatomical Rating Scale (MARS): reliability of a tool to map brain microbleeds. *Neurology* 73, 1759–1766. doi: 10.1212/WNL.0b013e3181c34a7d

Hafiz, R., Gandhi, T. K., Mishra, S., Prasad, A., Mahajan, V., Di, X., et al. (2022). Higher limbic and basal ganglia volumes in surviving COVID-negative patients and the relations to fatigue. *Neuroimage Rep*. 2:100095. doi: 10.1016/j.ynirp.2022.100095

Heine, J., Schwichtenberg, K., Hartung, T. J., Rekers, S., Chien, C., Boesl, F., et al. (2023). Structural brain changes in patients with post-COVID fatigue: a prospective observational study. *EClinicalMedicine* 58:101874. doi: 10.1016/j.eclinm.2023.101874

Inderyas, M., Thapaliya, K., Marshall-Gradisnik, S., Barth, M., and Barnden, L. (2024). Subcortical and default mode network connectivity is impaired in myalgic encephalomyelitis/chronic fatigue syndrome. *Front. Neurosci*. 17:1318094. doi: 10.3389/fnins.2023.1318094

Jaltuszewska, S., Chojnacka-Szawlowska, G., Majkowicz, M., Zdonczyk, S., Homenda, W., Hebel, K., et al. (2023). Illness perception and the severity of depression and anxiety symptoms in patients with multimorbidity: observational cohort studies. *J. Clin. Med*. 13:69. doi: 10.3390/jcm13010069

Jenkinson, M., Beckmann, C. F., Behrens, T. E., Woolrich, M. W., and Smith, S. M. (2012). FSL. *Neuroimage* 62, 782–790. doi: 10.1016/j.neuroimage.2011.09.015

Johansson, B., Starmark, A., Berglund, P., Rödholm, M., and Rönnbäck, L. (2010). A self-assessment questionnaire for mental fatigue and related symptoms after neurological disorders and injuries. *Brain Inj*. 24, 2–12. doi: 10.3109/02699050903452961

Krupp, L. B., LaRocca, N. G., Muir-Nash, J., and Steinberg, A. D. (1989). The fatigue severity scale. Application to patients with multiple sclerosis and systemic lupus erythematosus. *Arch. Neurol*. 46, 1121–1123. doi: 10.1001/archneur.1989.00520460115022

Latini, F., Fahlström, M., Fällmar, D., Marklund, N., Cunningham, J. L., Feresiadou, A., et al. (2022). Can diffusion tensor imaging (DTI) outperform standard magnetic resonance imaging (MRI) investigations in post-COVID-19 autoimmune encephalitis? *Ups J. Med. Sci*. 127. doi: 10.48101/ujms.v127.8562

Legler, F., Meyer-Arndt, L., Mödl, L., Kedor, C., Freitag, H., Stein, E., et al. (2023). Long-term symptom severity and clinical biomarkers in post-COVID-19/chronic fatigue syndrome: results from a prospective observational cohort. *EClinicalMedicine* 63:102146. doi: 10.1016/j.eclinm.2023.102146

Lu, Y., Li, X., Geng, D., Mei, N., Wu, P. Y., Huang, C. C., et al. (2020). Cerebral micro-structural changes in COVID-19 patients - an MRI-based 3-month Follow-up Study. *EClinicalMedicine* 25:100484. doi: 10.1016/j.eclinm.2020.100484

Montgomery, S. A., and Asberg, M. (1979). A new depression scale designed to be sensitive to change. *Br J Psychiatry*. 134, 382–389. doi: 10.1192/bjp.134.4.382

Mouridsen, K., Hansen, M. B., Østergaard, L., and Jespersen, S. N. (2014). Reliable estimation of capillary transit time distributions using DSC-MRI. *J. Cereb. Blood Flow. Metab*. 34, 1511–1521. doi: 10.1038/jcbfm.2014.111

Paolini, M., Palladini, M., Mazza, M. G., Colombo, F., Vai, B., Rovere-Querini, P., et al. (2023). Brain correlates of subjective cognitive complaints in COVID-19 survivors: a multimodal magnetic resonance imaging study. *Eur. Neuropsychopharmacol*. 68, 1–10. doi: 10.1016/j.euroneuro.2022.12.002

Pasquier, F., Leys, D., Weerts, J. G., Mounier-Vehier, F., Barkhof, F., Scheltens, P., et al. (1996). Inter- and intraobserver reproducibility of cerebral atrophy assessment on MRI scans with hemispheric infarcts. *Eur. Neurol*. 36, 268–72. doi: 10.1159/000117270

Planchuelo-Gómez, Á., García-Azorín, D., Guerrero, Á. L., Rodríguez, M., Aja-Fernández, S., and de Luis-García, R. (2023). Structural brain changes in patients with persistent headache after COVID-19 resolution. *J. Neurol*. 270, 13–31. doi: 10.1007/s00415-022-11398-z

Qin, Y., Wu, J., Chen, T., Li, J., Zhang, G., Wu, D., et al. (2021). Long-term microstructure and cerebral blood flow changes in patients recovered from COVID-19 without neurological manifestations. *J. Clin. Invest*. 131:e147329. doi: 10.1172/JCI147329

Randolph, C., Tierney, M. C., Mohr, E., and Chase, T. N. (1998). The Repeatable Battery for the Assessment of Neuropsychological Status (RBANS): preliminary clinical validity. *J. Clin. Exp. Neuropsychol*. 20, 310–3109. doi: 10.1076/jcen.20.3.310.823

Singh, S., Meher, N., Mohammed, A., Razab, M. K. A. A., Bhaskar, L. V. K. S., Nawi, N. M., et al. (2023). Neurological infection and complications of SARS-CoV-2: a review. *Medicine* 102:e30284. doi: 10.1097/MD.0000000000030284

Smith, S. M., and Nichols, T. E. (2009). Threshold-free cluster enhancement: addressing problems of smoothing, threshold dependence and localisation in cluster inference. *Neuroimage* 44, 83–98. doi: 10.1016/j.neuroimage.2008.03.061

Soriano, J. B., Murthy, S., Marshall, J. C., Relan, P., Diaz, J. V., and WHO Clinical Case Definition Working Group on Post-COVID-19 Condition (2022). A clinical case definition of post-COVID-19 condition by a Delphi consensus. *Lancet Infect. Dis*. 22, e102–e107. doi: 10.1016/S1473-3099(21)00703-9

Thapaliya, K., Marshall-Gradisnik, S., Barth, M., Eaton-Fitch, N., and Barnden, L. (2023). Brainstem volume changes in myalgic encephalomyelitis/chronic fatigue syndrome and long COVID patients. *Front Neurosci*. 17:1125208. doi: 10.3389/fnins.2023.1125208

Tu, Y., Zhang, Y., Li, Y., Zhao, Q., Bi, Y., Lu, X., et al. (2021). Post-traumatic stress symptoms in COVID-19 survivors: a self-report and brain imaging follow-up study. *Mol Psychiatry*. 26, 7475–7480. doi: 10.1038/s41380-021-01223-w

Vasilev, Y., Blokhin, I., Khoruzhaya, A., Kodenko, M., Kolyshenkov, V., Nanova, O., et al. (2023). Routine brain MRI findings on the long-term effects of COVID-19: a scoping review. *Diagnostics* 13:2533. doi: 10.3390/diagnostics13152533

Zigmond, A. S., and Snaith, R. P. (1983). The hospital anxiety and depression scale. *Acta Psychiatr. Scand*. 67, 361–370. doi: 10.1111/j.1600-0447.1983.tb09716.x

frontiers | Frontiers in Neuroscience

TYPE Perspective
PUBLISHED 20 September 2024
DOI 10.3389/fnins.2024.1445540

OPEN ACCESS

EDITED BY
Pradeep Kumar,
All India Institute of Medical Sciences, India

REVIEWED BY
George DeMartino,
University of Texas Southwestern Medical Center, United States

*CORRESPONDENCE
Alan Herbert
✉ alan.herbert@insideoutbio.com

RECEIVED 07 June 2024
ACCEPTED 03 September 2024
PUBLISHED 20 September 2024

CITATION
Herbert A (2024) Neurodegenerative diseases reflect the reciprocal roles played by retroelements in regulating memory and immunity.
Front. Neurosci. 18:1445540.
doi: 10.3389/fnins.2024.1445540

Neurodegenerative diseases reflect the reciprocal roles played by retroelements in regulating memory and immunity

Alan Herbert*

InsideOutBio, Charlestown, MA, United States

Tetrapod endogenous retroelements (ERE) encode proteins that have been exapted to perform many roles in development and also in innate immunity, including GAG (group specific antigen) proteins from the ERE long terminal repeat (LTR) family, some of which can assemble into viral-like capsids (VLCs) and transmit mRNA across synapses. The best characterized member of this family is ARC (activity-regulated cytoskeletal gene), that is involved in memory formation. Other types of EREs, such as LINES and SINES (long and short interspersed elements), have instead been exapted for immune defenses against infectious agents. These immune EREs identify host transcripts by forming the unusual left-handed Z-DNA and Z-RNA conformations to enable self/nonself discrimination. Elevated levels of immune EREs in the brain are associated with neurodegenerative disease. Here I address the question of how pathways based on immune EREs are relate to the memory EREs that mediate neural plasticity. I propose that during infection and in other inflammatory states, ERE encoded GAG capsids deliver interferon-induced immune EREs that rapidly inhibit translation of viral RNAs in the dendritic splines by activation of protein kinase R (PKR). The response limits transmission of viruses and autonomously replicating elements, while protecting bystander cells from stress-induced cell death. Further, the PKR-dependent phosphorylation of proteins, like tau, disrupts the endocytic pathways exploited by viruses to spread to other cells. The responses come at a cost. They impair memory formation and can contribute to pathology by increasing the deposition of amyloid beta.

KEYWORDS

flipons, memory, immunity and antiviral strategies, PKR activation, ADAR1 deaminase, retroelements, virus like capsids, ribotransmitter

Background

Retroviruses and Memory: A recent surprise was the discovery that a retrovirally derived GAG (group associated antigen) protein called ARC (activity-regulated cytoskeletal gene, Figure 1A) was associated with memory formation in tetrapods. Even more surprising was the finding that a similar but separate domestication event of an ARC protein impacted a specific set of feeding behavior in *Drosophila melanogaster*. If that was not enough, two groups then revealed that ARC proteins from human, mouse and flies were able to form viral-like capsids (VLCs) (Epstein and Finkbeiner, 2018; Ashley et al., 2018;

Pastuzyn et al., 2018). The Drosophila Arc1 protein also bound *darc1* mRNA in neurons and loaded the transcript into extracellular vesicles that were transferred across the synapse formed between motor neurons and muscles (Ashley et al., 2018). Rat Arc protein assembled *in vitro* in the presence of both *Arc* and enhanced green fluorescent protein (EGFP) RNA into capsids, with little specificity shown. The capsid mediated the transfer of Arc mRNA and EGFP mRNA into new target cells via extracellular vesicles released from neurons (Pastuzyn et al., 2018), and also of luciferase mRNA (de la Pena et al., 2021). The mRNA, referred to here as ribotransmitters, underwent activity-dependent translation in the recipient neuron following uptake by endocytosis (Figure 2) (Pastuzyn et al., 2018), consistent with the proposed role of modulating synaptic connectivity (Wallace et al., 1998).

The tetrapod and *D. melanogaster* ARC proteins are derived from separate branches of the Metaviridae family of long terminal repeat (LTR) endogenous retroelements (ERE) (formerly known as Ty3/Gypsy retrotransposons) (Gifford et al., 2018) (Figure 1). Further, insects are the only protostomes and tetrapods the only deuterostomes that encode ARC, with no other known paralogs that connect to their last common ancestor. The findings support an independent origin of each exaptation (Abrusan et al., 2013). Both tetrapod and insect versions are expressed as neuronal immediate early genes. Whereas the tetrapod version is associated with synaptic plasticity, the insect ARC is not. Rather, the *D. melanogaster* protein increases locomotory activity in response to starvation (Mattaliano et al., 2007). Structural characterization of the drosophila Arc VLC has revealed that the capsid has a number of unique features. While the ancestral Ty3 packages two copies of its 5.2-kb genome into a T = 9 particle, the dArc1 VLC is smaller. At most, it is only able to package two copies of the 2.3-kb dArc1 full length mRNA into its T = 4 structure (Erlendsson et al., 2020). By comparison, the HIV (human immunodeficiency virus) genome is 9.3 kb. The mRNA is also packaged into the capsid as a dimer. The HIV transcript consists of a 1.5 kb GAG, a 2.8 kb POL (polymerase) and a 2.6 kb ENV (envelope) open reading frame (ORF) (**Figure 1A**). LTRs lack the ENV gene found in retroviruses.

The human genome also encodes other proteins able to assemble into VLC. There are 85 human genes known with homology to retroviral or retrotransposon-encoded GAG genes (Campillos et al., 2006; Kokosar and Kordis, 2013). Of these, eight clades are universally retained as at least single intact genes across all placental mammals queried, suggesting they enable important biological functions common to all mammals (Henriques et al., 2024). These include PEG10 that can accommodate large RNAs and is able to bind and secrete its own 6.7 kb mRNA, as well as another 49 mouse RNAs, which have reduced neurological expression in PEG10 knockout mice, suggesting that PEG10 binds and stabilizes these transcripts. Interestingly, flanking a coding sequence with the PEG10 untranslated region (UTR) is sufficient to enable the inclusion of the RNA construct into the PEG10 VLC. The efficiency of VLC uptake and translation of the message in the recipient cells is further increased by incorporating a fusogen to form a virus like particle. Other exapted murine GAGs such as MOAP1, ZCCHC12, RTL1, PNMA3, PNMA5 and PNMA6a are also known to form capsids, but their properties have not yet been fully characterized (Segel et al., 2021). Of these eight GAG variants, hARC is the oldest, dating back an estimated 350 million years. The next oldest is PEG10 (paternally expressed 10) from 160 million years ago. PEG10 marks the first known appearance of genomic imprinting where the sex of the parent determines which copy of an autosomal gene is expressed. The innovation occurred in placental animals and is implemented by the selective methylation of the PEG10 gene in females (Henriques et al., 2024; Suzuki et al., 2007; Shiura et al., 2023).

ARC is important in the formation of tetrapod memories. It is also likely that PEG10 and other GAG proteins can assemble into capsids and contribute to communication between neurons through the synaptic transmission of RNA (Segel et al., 2021). A number of questions remain unanswered beyond those related to which RNAs, other than ARC, function as ribotransmitters and what are the outcomes they regulate? One important question is how did these innovations evolve? These adaptations require time but these autonomously replicating EREs are invasive and pose an existential threat to their host genome. How were these EREs tamed sufficiently for beneficial outcomes to accrue? What accommodations were made to balance the risks associated with EREs and the benefits from their exaptation? How well do the modern-day defenses against autonomous replication by EREs work? What happens to individuals when these defenses fail?

Conflicted genomes

The conflict between an organism and its invasive replicants dates back as far as we can tell. There is no doubt that symbiosis between different entities led to early evolutionary innovations where the parts supplied by each genome benefited all. Two extreme, but successful, examples of this confluence are the mergers that generated chloroplasts and mitochondria (Margulis, 1976). Before those events, many unicellular organisms and viruses exchanged genetic information, supplying parts that the other

Abbreviations: ADAR, Adenosine deaminase, RNA specific; ALU, Family of SINEs first identified using the ALU restriction enzyme; AD, Alzheimer's disease; ARC, Activity-regulated cytoskeletal gene; ATF4, activating transcription factor 4; CFM, contextual fear memory; CAN, Central Nervous System; CREB, cAMP responsive element binding protein; CSF, cerebral spinal fluid; CSR-1, chromosome segregation and RNAi deficient 1; dsRNA, double-stranded RNA; EIF2α, eukaryotic initiation factor 2 alpha; ENV, envelope protein; ERE, endogenous retroelements; GAG, Group Antigen; GABA, Gamma-aminobutyric acid; gRNA, guide RNA; HIV, human immunodeficiency virus; IFN, Interferon, α (alpha), β (beta) and γ (gamma); IPSC, inhibitory postsynaptic currents; IRG1, immune responsive gene1, encoded in humans by ACOD1, aconitate decarboxylase 1); LINES, long interspersed elements; LRP1, low density lipoprotein receptor related protein 1; LTM, long-term memory; LTP, long-term potentiation; LTR, long terminal repeat; MAPT, microtubule associated protein tau; MDA5, melanoma differentiation-associated protein 5, IFIH1, interferon induced with helicase C domain 1; mRNA, messenger RNA; muM, mice lacking the immunoglobulin heavy constant mu gene; HS3ST1, heparan sulfate-glucosamine 3-sulfotransferase 1; ncRNA, noncoding RNA; NFKB1, nuclear factor kappa B subunit 1 encodes NF-κB; ORF, open reading frame; PEG10, paternally expressed 10; phosEIF2α, phosphorylated EIF2α; PKR, Protein Kinase, RNA-activated, encoded in mice by *Eif2ak2*, eukaryotic translation initiation factor 2 alpha kinase 2; POL2, RNA polymerase 2; ptau118, tau with phosphorylated threonine at position 181; RdRp, RNA-dependent RNA polymerases; RTL, retrotransposon GAG like; SCID, severe combined immune deficiency; SINES, short interspersed elements; TLR3, toll-like receptor 3; TFEB, transcription factor EB; UPR, Unfolded protein response; UTR, untranslated region of RNA; tRNA, transfer RNA; VLC, viral-like capsid; ZBP1, Z-DNA binding protein; ZNA, Left-handed Z-RNA or Z-DNA.

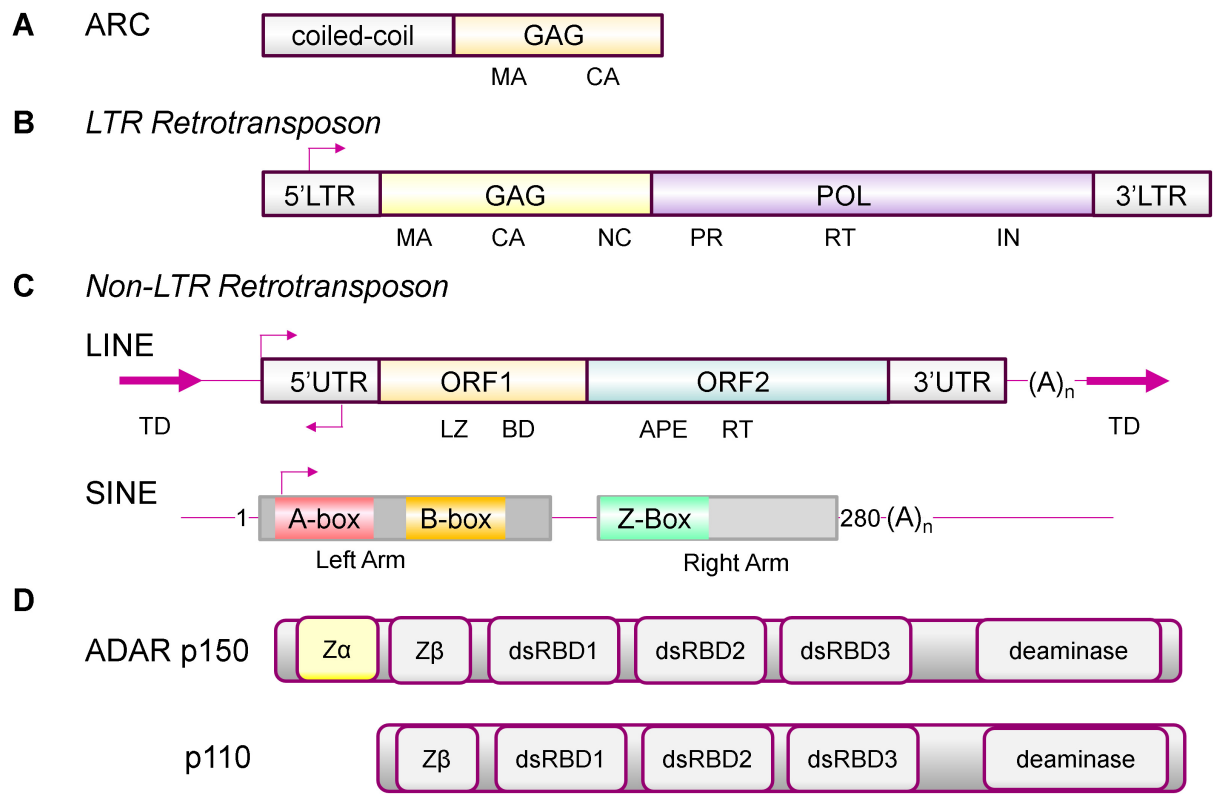

FIGURE 1
ARC, Endogenous Repeat Elements and ADAR1 isoforms. **(A)** ARC has both the coiled-coil and GAG domains that allow formation of higher order structures, including virus-like-capsids (VLC), but lacks a nucleic acid (NA) binding domain (Ashley et al., 2018; Pastuzyn et al., 2018). **(B)** Long Terminal Repeat (LTR) retrotransposons are composed of a group antigen (GAG) with matrix (MA), capsid (CA) and nucleocapsid (NC) domains, a polymerase (POL) with protease (PR), reverse transcriptase (RT) and an integrase (IN) domain, but lack the envelope protein that is found in retroviruses. The terminal duplication (TD) is of the genomic sequence at the site where the insertion occurred. **(C)** Both LINE (long interspersed elements) and SINE (short interspersed elements) are non-LTR retrotransposons. A full-length LINE has two open reading frames (ORF). ORF1 has a leucine zipper (LZ) a C-terminal nucleic acid binding domain (BD). ORF2 has apurinic/apyrimidinic endonuclease (APE) and a central RT domain. SINEs do not encode proteins. They derive from non-coding RNAs such as 7SL RNA and tRNA. Shown is the dimeric 280 base ALU element with a right and left arm. The A- and B-Box are docking sites for RNA polymerase 3. The Z-Box is a region that can flip to a left-handed Z-DNA conformation under physiological conditions. The Z-box can also form Z-RNA in segments of dsRNA formed by foldback of an ALU inverted repeat (Herbert, 2021). **(D)** The interferon induced ADAR p150 has a Zα domain that recognizes Z-RNA present in double-stranded RNAs. The constitutive p110 isoform does not bind Z-RNA (Herbert, 2021). ZBP1 is the only other protein in the human genome to have a canonical Zα domain (Herbert, 2024b). The arrows indirect the direction of transcription.

was missing and providing weapons for attacking and defending against other replicants. The horizontal transfer between species of adaptations and virulence factors often led to quite complex survival strategies. The outcomes are strikingly exemplified by modern day amoeba that have incorporated DNA from all the genomes they have ever encountered, and now harbor in a single individual a cohort of viruses, phages, and bacteria pathogenic to humans (Molmeret et al., 2005; Moliner et al., 2010).

The acceptance of foreign DNAs into a genome often confers a benefit. The strategy also carries risk. The threat is especially serious when the newly acquired DNA is capable of autonomous replication, as is the case with transposable elements that can duplicate themselves exponentially within a host genome. The existing and invasive replicants are often at odds. While an expanded genome increases the coding capacity of an existing organism, the invading replicant often prioritizes smaller genome size and the efficient packaging of as many infectious variants as possible. How organisms cope with such different imperatives shapes their future evolution.

The ARC gene is an example of a beneficial acquisition of a retroviral element by tetrapod genomes. Other examples exist. A retroviral ENV gene required for placenta formation has been independently exapted in seven separate species to produce a syncytin protein, illustrating the selective advantage accruing from this innovation (Dupressoir et al., 2012; Imakawa et al., 2022). ERE regulatory elements have also been exapted in zygotes to control the transition from totipotent to pluripotent stem cells, a key step in embryonic development (Chuong, 2018; Macfarlan et al., 2012).

ERE biology

The GAG proteins like ARC are derived from a LTR retrotransposon (**Figure 1B**). In humans, LTRs can vary in size from 100 to several kilobases, with strong selection against retention of the POL gene that is necessary for their autonomous replication (Lynch and Tristem, 2003). Additionally, capsids like those formed by ARC are likely too small to incorporate both

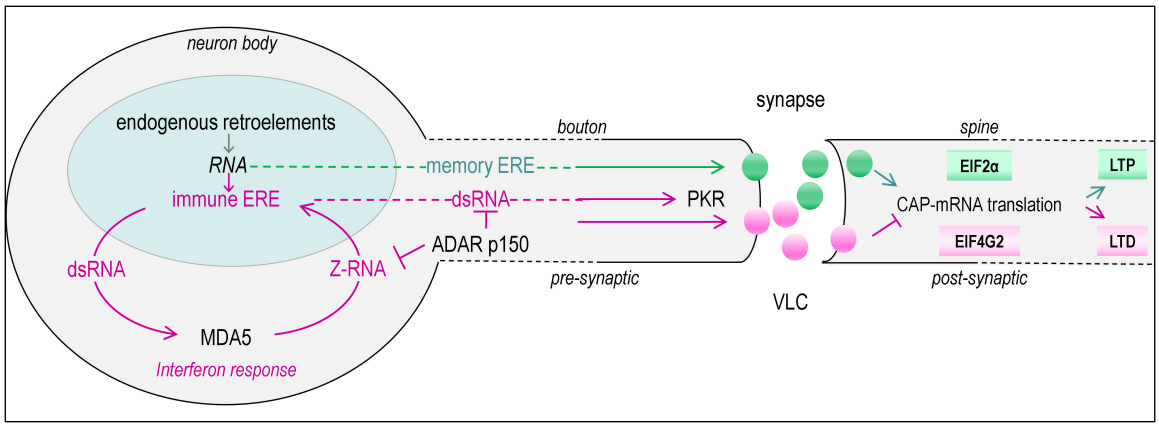

FIGURE 2
Transmission of RNAs (green spheres) from pre- to postsynaptic neuron is regulated by the retroviral derived GAG proteins and modulated by interferon induced expression of endogenous retro-elements (ERE) (pink spheres) that form double-stranded RNAs (dsRNA). The same coloring of lines is used to highlight the pathways involved. Amplification of the interferon response is driven by MDA5 (melanoma differentiation-associated protein 5, IFIH1, interferon induced with helicase C domain 1) that senses dsRNA. The response is suppressed by the interferon induced p150 isoform of ADAR1 that senses Z-RNA in self-transcripts through a Zα domain and performs A to I editing to trigger degradation of dsRNAs substrates by inosine specific nucleases. A set of GAG proteins encoded by the human genome form VLC (virus-like-capsid), that can incorporate RNA and transmit them to other cells where they are translated. For example, transmission of the memory ERE ARC mRNA by an ARC GAG VLC capsid modulates neuroplasticity. It is proposed here that VLC can also transmit dsRNA ERE transcripts (immune ERE) that enable antiviral defenses in the recipient cell by activating PKR (RNA-activated, encoded in mice by Eif2ak2, eukaryotic translation initiation factor 2 alpha kinase 2). Phosphorylation of EIF2α by PKR causes a switch from CAP-dependent translation to CAP-independent protein production that depends on alternative initiation factors such as EIF4G2. The response promotes local dendritic remodeling and disruption of synaptic contacts to prevent transmission of virus across the synapse and also inhibits the translation of viral messages in the postsynaptic neuron. The changes also protect against stress-induced apoptosis and necroptosis, but impair memory formation by altering the balance of LTP (long term potentiation) to LTD (long-term depression). The dotted lines indicate that the axon is much longer than shown as the figure is not drawn to scale.

the GAG and POL transcripts. Other classes of ERE that lack the LTR (called non-LTR transposons) are also present in the human genome (**Figure 1C**). This family includes the autonomous long interspersed elements (LINEs) and the non-autonomous short interspersed elements (SINEs) (Wessler, 2006). LINES are usually flanked by variable length duplication of sequences from the sites where they insert. They have a promoter at the 5′ end of the element and a short 3′UTR that ends in a poly-A tail. Their transcription depends on RNA polymerase 2 (POL2). The full length bicistronic ~6 kb RNA they produce encodes two proteins: ORF1 (an RNA binding protein) and ORF2 (an endonuclease and a reverse transcriptase). LINEs date back to the Precambrian era of 600 million years ago, with 4 of the 15 known clades present in mammals. About 18% of the human genome consists of LINE-1 (L1) EREs. There are roughly 500,000 L1 copies, with some of them still capable of autonomous replication (Goodier and Kazazian, 2008). Their regulatory elements have contributed to many evolutionary innovations (Lowe and Haussler, 2012). Remarkably, these elements now help protect their host. They drive the interferon (IFN) induced expression of genes involved in the innate immune responses (Chuong et al., 2016).

SINEs contribute to about 11% of the human genome, with over 1 million copies, but are absent in D. melanogaster (Sela et al., 2010). They are notable because they do not encode protein but instead are derived from POL3 transcribed small, cellular, noncoding RNAs (ncRNA). The most frequent SINE is derived from the 7SL RNA component of the protein signal recognition particle. In humans, they are named ALU elements for the bacterial restriction enzyme that excises them from genomic DNA. Other SINE families originate from tRNAs and less frequently from snoRNAs and other ncRNAs. ALUs are 90 to 300 bases long, depending on whether they are a single or a duplicated copy of the ancestral RNA (**Figure 1C**). Many ALUs are within genic regions and are now transcribed by POL2 (Deininger, 2011). For their propagation, they capture newly synthesized LINE reverse transcriptases as they emerge from the ribosome. The SINEs then use those enzymes to copy their RNA into DNA. In the process, the new copy is pasted into the genome at a site different from that of the original copy. The freshly inserted SINE can carry with it some regulatory elements from the old ALU neighborhood, altering the readout and processing of RNAs from nearby genes. Unlike mutations, the outcomes are not all or nothing: successful RNA adaptations from the past are not immediately lost, but instead are produced alongside the new transcripts that may differ in their stability, splicing and translation. Malformed pre-mRNAs are purged through processes like nonsense-mediated decay (Herbert, 2020a; Herbert, 2024a). The soft-wiring of RNA processing increases the diversity of protein products produced. Often, SINEs are inserted in the reverse orientation to an existing SINE element. When transcribed, the RNA formed can fold back on itself to produce a double-stranded RNA (dsRNA) (Levanon et al., 2004; Kim et al., 2004; Blow et al., 2004; Athanasiadis et al., 2004). The outcome is common in humans, reflecting the three recent waves of ALU invasion that represented an existential threat to their genome (Herbert, 2020a; Batzer and Deininger, 2002). Those inverted repeats that form dsRNAs are subject to RNA editing by the ADAR (adenosine deaminase, RNA specific) family of enzymes (Schaffer and Levanon, 2021). The enzyme deaminates adenosine in dsRNA to form inosine (A to I editing). Since inosine is translated as guanosine, the readout of adenosine containing

codons is potentially altered, resulting in the incorporation of a different amino acid into a protein. The result is a protein isoform that is not templated by the host genome (Higuchi et al., 2000; Maas et al., 1996; Sommer et al., 1991). As we will see, ADAR1 performs other very important roles in defending the host and in forming memories.

Defending against retroelements

The processes we observe today date from long ago. There was an early need to tame EREs capable of autonomous replication, given the threat they posed to the survival of a species by inserting into and inactivating essential genes. Often, to resolve the conflict, the offensive weapons used by EREs were repurposed to defend against them: a battle of like with like. Often the exapted parts were used to restrict ERE replication. GAG proteins initially used to package EREs into membrane coated vesicles were retooled to disrupt the ERE assembly line. Subsequently, those GAG variants evolved into something else. Some GAGs are now employed as immune sensors in the brain, with RTL5 sensing dsRNA and RTL6 now detecting bacterial lipopolysaccharides (Irie et al., 2022) while RTL9 recognizes fungal zymogens (Ishino et al., 2023). Another strategy was to prevent ERE transcription, so limiting retrotransposon spread. The zinc finger domains encoded by the LTRs to bind their transcripts were repurposed to repress their descendants, leading to clusters of KRAB (Krüppel-associated box) protein families that suppress ERE expression (Ecco et al., 2017). The KRAB genes encode different combinations of the zinc-finger sequences that they have captured and embellished. The clusters potentially produce even more permutations by trans-splicing RNAs from different genes (Umerenkov et al., 2023). The many KRAB variants generated counter any attempted escape by ERE based on the recombination of existing sequences. Such defensive strategies take time to evolve. Before then, organisms required other schemes to ensure their proximate survival.

The destruction of a transposon transcript provides an immediate defense. Mechanisms such as RNA interference enable the instant elimination of autonomously replicating RNAs. Another set of noncoding transcripts, such as microRNAs, prevents the translation of ERE proteins that mediate transposition. Both mechanisms depend on host RNAs complementary to the invasive RNA (Cornec and Poirier, 2023). Indeed, many microRNAs are thought to derive from the dsRNAs formed in the past by retroelement sequences. Later, these microRNAs evolved to play a larger role in host development, targeting the retrotransposons sequences inserted into genes as ERE peppered themselves throughout the genome (Lehnert et al., 2009; Obbard et al., 2009; Borchert et al., 2011).

Avoiding reverse transcriptases

Many organisms have evolved mechanisms to amplify RNAs specifically targeting transposons like ERE. In many species, this pathway uses an RNA-dependent RNA polymerase (RdRp) to generate the dsRNA substrate necessary to produce a guide RNA (gRNA) that paints the target for the defense to destroy. The RdRps involved are generally not very processive, often not in need of priming and usually do not produce long transcripts (Almeida et al., 2019). This strategy is exemplified by the transitive RNAi of the round worm *Caenorhabditis elegans* (Obbard et al., 2009). Of course, this solution requires a companion strategy to avoid an attack on self-RNAs. In C. elegans, there is a dedicated RNAi pathway that prevents the destruction of germline transcripts, one based on the CSR-1 (chromosome segregation and RNAi deficient 1) protein (Wedeles et al., 2013; Seth et al., 2013). *D. melanogaster* instead uses reverse transcription to make a circular DNA copy of the pathogen to generate the required gRNA with the product disseminated via exosomes (Tassetto et al., 2017). The pathway can produce transgenerational immunity. How this strategy discriminates self from nonself is not yet fully understood (Mondotte et al., 2020). *D. melanogaster* also deploys another strategy to defend against EREs, required as the LTRs in fly genomes are still highly active. Here gRNAs are produced by "ping-pong" amplification of short *piwi* RNAs (piRNA). The gRNAs are defined by the piRNA gene clusters that are expressed mostly in the germline. The mechanism does not require a RdRp (Czech et al., 2018).

Interestingly vertebrates have adopted a different system to protect against autonomous replicants. The response does not rely on amplification of the invader's RNA, avoiding the risk of promulgating a pathogen by making further copies of its genome. The strategy also avoids the destruction of essential host transcripts containing embedded EREs. Instead, RNAs that incorporate EREs are used to protect the host. These transcripts are often encoded by parts of the genome that are silent most times. The ERE containing sequences are placed beyond the usual transcription stop site of a gene or removed by splicing. However, when cells are infected by viruses, or become dysregulated, these alarm sequences are transcribed or remain unspliced (Jang and Latchman, 1992; Panning and Smiley, 1993; Karijolich et al., 2017; Tucker and Glaunsinger, 2017). The transcripts produced then form dsRNA that are sensed by their shape rather than by their sequence, triggering an innate immune response that terminates the threat.

The strategy traces back to the earliest known unicellular eukaryotic progenitor, *Capsaspora owczarzaki*. In these organisms, invasive replicants that form dsRNA are targeted for A to I editing by the ADAR1 ancestral protein (Sebe-Pedros et al., 2016; Ros-Rocher et al., 2021). Over time, DNA for these non-self dsRNAs have been copied into host genomes. Their transcription was regulated by the same elements that an invasive replicant used to drive the expression of its own genome (Chuong et al., 2016).

In vertebrates, the acquired dsRNAs were exapted to drive the modern-day IFN-induced, antiviral defense. The dsRNAs produced were repurposed to shutdown translation of the invader's transcripts, preventing their transmission to other cells. Vertebrates evolved PKR (Kinase, RNA-activated, encoded in mice by *Eif2ak2*, eukaryotic translation initiation factor 2 alpha kinase 2) just for this purpose: PKR is both IFN-induced and dsRNA activated (Roberts et al., 1976). As the gene name implies, PKR targeted the EIF2α translation initiation factor. The rapid evolution the PKR gene has undergone in response to viral threats underscores the importance of this innovation (Rothenburg et al., 2009; Bou-Nader et al., 2019; Cesaro and Michiels, 2021). As I will describe, the evolution of PKR

also has impacted the development of adaptive memories within the nervous system.

Self versus Non-self

The dsRNA formed by embedded ERE also enable self/non-self-discrimination without requiring a reverse transcriptase. By flipping from a right-handed A-RNA conformation to left-handed Z-RNA, the ERE dsRNA provides a mechanism for self-recognition, as I will now describe. The Z-DNA is recognized by the IFN the p150 isoform of ADAR. Unlike the constitutively expressed p110 isoform, p150 has a Z-RNA/Z-DNA (collectively called ZNA) binding domain, called Zα, that binds with high affinity the left-handed double helical conformation of both DNA and RNA (**Figure 1B**). While right-handed B-DNA and dsRNA A-RNA are normally the lowest energy nucleic acid helices found in the cell, both left-handed Z-DNA and Z-RNA (collectively called ZNAs) are also present. Like dsRNA, ZNAs convey information by their shape rather than their sequence. They are higher energy forms of DNA and RNA that are most easily adopted by segments with a dinucleotide repeat composed of alternating purine and pyrimidine bases. Z-DNA is formed more easily by $(CG)_n$ than $(TG)_n$ or $(AC)_n$, while $(TA)_n$. is more prone to form hairpins. ZNAs are also formed inside cells by out of alternation sequences like $(CCCG)_n$ (Ho et al., 1986; Nichols et al., 2021). The transition involves flipping the base pairs over and does not require strand cleavage. The dinucleotide sequence motif results in a zig-zag backbone for which the conformation is named.

The genomic elements that convert to ZNA under physiological conditions. are called flipons (Herbert, 2019a). The flip requires energy that can be supplied by hydrolysis of high energy substrates like ATP or other nucleotides. It is driven by polymerases, helicases and opposed by enzymes like topoisomerases that relax the forces such as twisting, stretching, and bending that power the transition both in the nucleus and in stress granules (Chiang et al., 2020; Yi et al., 2022). By changing conformation, flipons flag actively transcribed genes, serving many roles in a cell (Herbert, 2024a; Herbert, 2023). The sequences are enriched in promoters and also in the repeat part of the genome, especially in EREs, that otherwise have little informational value due to their high frequency. Indeed, one repeat looks very much like another (Herbert, 2023).

Like ADAR1, the Zα domain also traces back to *C. owczarzaki* (Herbert, 2024b). Mounting evidence supports the involvement of Zα in recognition of self-RNAs, with noncoding ALU SINE transcripts being the most frequently edited RNAs in the human transcriptome. Importantly, dsRNAs formed from SINE inverted repeats contain a Z-BOX that forms Z-RNA. The flip to Z-RNA provides a tag to label transcripts as self, allowing them to be distinguished from viral RNAs (**Figure 1C**; Nichols et al., 2021; Herbert, 2019b; Herbert, 2021). The Z-RNA tags are recognized by the Zα domain of ADAR p150 and enable the negative regulation of IFN responses against host RNAs (**Figure 1D**). Genetic evidence for this mechanism is provided by Aicardi-Goutières Syndrome type 6 (AGS6). Mutations that lead to a loss of ADAR p150 binding to ZNA are causal for this interferonopathy. In AGS6, responses to self dsRNAs continue unabated (Herbert, 2020b; Guo et al., 2023; Liang et al., 2023).

What then triggers the flip of the ALU Z-BOX to Z-RNA? The IFN responses are activated by dsRNA sensors such as the helicase MDA5 (melanoma differentiation-associated protein 5, encoded by IFIH1, interferon induced with helicase C domain 1) that form filaments on any long A-RNA helix. The stretching of dsRNA by MDA5 as it coats the RNA causes tension that can be relieved by flipping the helix from right-handed A-RNA (pitch = 24.6 Å) to left-handed Z-RNA (pitch = 45.6 Å). The relaxation enables MDA5 to complete ATP hydrolysis, leading to dissociation of the filament and termination of the IFN response (Herbert, 2021). As Z-RNA forms, the IFN-induced ADAR1 p150 isoform that binds Z-RNA docks and can initiate A to I editing to trigger removal of self-RNAs by inosine-specific nucleases (Wu et al., 2019). The Z-BOX of EREs and ADAR p150 work as a tag team to protect the host against immune responses against self.

Eliminating threats

Quite surprisingly, given the age of the Zα domain, there is only one other protein in the human genome, ZBP1 (Z-DNA binding protein 1). This protein can induce inflammatory cell death and serves to amplify anti-pathogen responses. Usually, activation of ZBP1 is squelched by ADAR1 binding through the masking of ZNAs (Zhang T. et al., 2022; Jiao et al., 2022; Hubbard et al., 2022; de Reuver et al., 2022). In normal cells, levels of ADAR1 p150 and ZBP1 are sufficient to maintain homeostasis. However, when IFN responses persist, as happens during viral infection, there is a more than a hundred-fold induction of ZBP1 protein that overcomes any ADAR1 p150 suppression. The IFN induced transcription of the normally silent, Z-RNA forming, EREs then triggers ZBP1 activation. ZBP1 then terminates the threat that triggered the IFN alarm.

Usually the ZBP1-dependent response results in necroptosis, a form of inflammatory programmed cell death (PCD) that activates the acquired immune system. The layered defense amplifies antigen-specific T and B cell memory subsets to protect against future attacks by the pathogen and its relatives. The strategy is quite general. The innate immune response based on host dsRNAs is built in. It does not depend on prior exposure to a pathogen or on whether the threat is old or a newly emergent one. There is no need for a pathogen-specific gRNA. The same process as used to defend against viruses is able to induce adaptive immune responses against dysfunctional and malignant cells. In both cases, the abnormal peptides expressed by host cells target them for elimination by the adaptive immune system, ending the threat. With this strategy, defense is not based on sequence-specific gRNAs. Instead, the response is initiated by ERE-derived dsRNAs with immunity provided by antigen-specific proteins.

Like many other cells, neurons do not normally express ZBP1 (Solon et al., 2024), so they do not usually undergo PCD when ZNAs accumulate in response to elevated IFN levels. However, other brain cells express ZBP1 and are eliminated in this manner. ZBP1 can also activate a different set of pathways to resolve the threat. For example, in response to ZIKA virus, ZBP1 increases expression of IRG1 (immune responsive gene1, encoded in humans by ACOD1, aconitate decarboxylase 1). The enzyme promotes formation of itaconate (Daniels et al., 2019), which leads to the

nuclear translocation of TFEB (transcription factor EB) (Zhang Z. et al., 2022), the master transcriptional regulator of autophagy and lysosomal biogenesis. The endosomes induced in phagocytic cells direct viruses to lysosomes, an attempt to restrict their replication, one that is resisted by many pathogens (Campbell et al., 2015; Contreras et al., 2023; Chen et al., 2023; Zhai et al., 2023).

Not all effects of dsRNA depend on Z-RNA formation. Some are mediated by the dsRNA sensor toll-like receptor 3 (TLR3) that is activated by poly (I-C), an RNA duplex that has inosine on one strand paired to cytosine on the other, but does not form Z-RNA. Administration of the dsRNA polymer to animals of age 4 to 9 months induces TLR3 responses that are protective in the APPswe/PSEN1dE9 transgenic mouse model of Alzheimer's disease (AD) (Wang et al., 2023). Activation of NF-κB (nuclear factor kappa B subunit 1 encoded by NFKB1) that promoted clearance of amyloid was reported but not by induction of IFN or through inflammatory responses. In a separate study, TLR3s activation was prevented by binding of APOE (apolipoprotein E) proteins, variants of which increase the risk of AD. APOE in this case is bound to the heparan sulfate proteoglycans (HSPG) that decorate cell surfaces (Zhu et al., 2010). Interestingly, another study revealed that the APOE4 variant that also confers the greatest risk for AD, binds with much higher affinity to HSPG than other variants. Binding was enhanced by the unusual 3-O-sulfo heparan sulfate (3-OS) modification that is made by the enzyme HS3ST1 (heparan sulfate-glucosamine 3-sulfotransferase 1) (Mah et al., 2023). Two well powered GWAS studies show that variants of HS3T1 gene with highest activity are likely associated with increased risk of AD (Witoelar et al., 2018; Jansen et al., 2019). Whether the binding of APOE4 to 3-OS also inhibits TLR3 activation by immune EREs is currently unknown. Potentially, the interaction provides an additional connection between immune EREs and memory. The non-neuronal cells activated by dsRNA through TLR3 then protect neurons from danger by removing threats, likely via phagocytosis.

Neurological impact of ERE-induced immune responses

In AD and many other human neurological disorders, elevated levels of IFN stimulated transcripts and ERE encoded dsRNAs are present. Many of the outcomes have been attributed previously to oxidative stress from either mitochondrial damage or unfolded protein responses (Larsen et al., 2018; Cheng et al., 2021; Ravel-Godreuil et al., 2021). Besides effects of EREs on innate immune responses in the brain, the induction of chronic IFN also directly impacts neurological memory. This outcome is observed in mouse models of immunodeficiency that impair adaptive immune responses and are characterized by the emergence of endogenous, ecotropic murine leukemia viruses. In a B cell immunodeficiency strain produced by knockout of the immunoglobulin heavy constant mu gene (muM mice), there is cognitive impairment of hippocampus-dependent learning tasks. The deficits are resolved by knockout of MDA5, the cytoplasmic dsRNA sensor that induces IFN responses. Both contextual fear memory (CFM), and spatial learning tasks are improved in animals when both muM and MDA5 coding sequences are absent (Sankowski et al., 2019). Impaired spatial memory is also observed in animals with severe combined immune deficiency (SCID) and in thymic, T cell deficient nude mice. Collectively, the results connect immune and memory EREs (Kipnis et al., 2004).

A separate report provided independent evidence that increased dsRNA plays an essential role in conditioned fear extinction learning (Marshall et al., 2020). In this study, ADAR1 expression in the infralimbic prefrontal cortex was knocked down using short hairpin RNAs. The responses were restored by transduction of ADAR p150 constructs with a wildtype Zα domain, but not by expression of ADAR p110 or ADAR p150 variants that had loss of function mutations in either the Zα or deaminase domain. RNA editing activity was required for fear extinction to occur. The edited RNAs were enriched for postsynaptic membrane, synapse, postsynaptic density, and dendritic spines gene ontology terms. As well as potentially recoding exons, the adenosine to inosine editing likely promoted triage of dsRNAs by inosine-specific nucleases. The editing sites and ADAR binding sites were closely approximated to EREs. Together the results from the studies of ADAR1 p150 transduction and MDA5 knockout immunodeficient mice suggest a different model for long-term impairment of brain function that is observed with chronic viral infection and in neurodegenerative diseases. In these cases, the failure to clear EREs leads to high interferon levels and a reduced ability to form new memories. How then do immune EREs coordinate or interfere with memory EREs?

ERE and neural memory

The increased expression of immune ERE triggers responses to protect the host against viruses and other threats. The evidence suggests that these responses negatively impact the long-term potentiation of memory formation. The findings raise many questions: what is the mechanism involved in cognitive impairment and how does this relate to the enhancement of neuronal plasticity by memory EREs such as ARC? The coevolution of LTR GAGs and non-LTR transcripts raises the possibility that SINEs and other ncRNAs can interfere with the transmission of ribotransmitters between neurons that could also potentially impact neuroplasticity, as in the case of ARC. Further, a class of immune EREs could retain the UTR required for packaging the ERE transcripts into a particular GAG capsid, similar to the way RNA is assembled into PEG10 VLC (Segel et al., 2021). Transmission of immune and memory ERE would then be regulated by expression of those VLC and the RNAs they engage.

Immune ERE potentially could impact cellular function on either side of the synapse through their effects on the translation of ribotransmitters like *ARC*. The effects on the presynaptic side could be via phosphorylation of EIF2α by the IFN induced dsRNA activation of PKR (Kaempfer, 2006; Halliday and Mallucci, 2014). Phosphorylated-EIF2α (phosEIF2α) plays an important regulatory role in neuronal plasticity. It acts by increasing the translation of ATF4 (activating transcription factor 4), a protein that impairs memory by repressing expression of CREB (cAMP responsive element binding protein), an important mediator of L-LTP (long-long-term potentiation) and LTM (long-term memory) (Costa-Mattioli et al., 2007). Notably, PKR loss of function *Eif2ak2*$^{\Delta 12/\Delta 12}$ mice decrease phosEIF2α levels and have

enhanced memory formation. The improved LTM results from a reduction in GABAergic inhibitory postsynaptic currents (IPSC) due to decreased presynaptic levels of phosEIF2α, with no evident effects on excitatory postsynaptic currents (Zhu et al., 2011).

The *Eif2ak2* exon 12 deletion model used in this study removes the PKR catalytic domain (Zhu et al., 2011). The knockout does not affect brain morphology or alter the axonal or synaptic histological markers tested. However, the PKR variant is not, as originally thought, a null allele: the gene still expresses a truncated version of PKR with an intact N-terminal dsRNA binding domain and is able to scaffold both IFN and NF-κB responses (Baltzis et al., 2002). The outcomes are due solely to the loss of the kinase activity. The result is supported by a gain of function mouse model where the PKR kinase is triggered by using AP20187 to dimerize and activate a PKR allele fused to the FK506 binding protein. By increasing phospEIF2α levels, it was possible to promote long term depression (LTD) by reducing the efficacy of synaptic transmission. Unlike LTP, the establishment of LTD required protein synthesis (Di Prisco et al., 2014). Similarly, cognitive function was impaired in wild-type mice treated with IFN. The treatment increased expression of both immune ERE and *Eif2ak2* transcripts, resulting in PKR activation and EIF2α phosphorylation (Zhu et al., 2011). Collectively, the results link the modulation of translation by immune ERE to LTP and LTD.

ARC mRNA translation is also impacted by the phosphorylation status of EIF2α. Normally, EIF2α promotes the 7-methylguanosine CAP-dependent translation of *ARC* mRNA. Following synthesis, the protein is assembled into capsids, which then convey *ARC* mRNA from the presynaptic boutons to postsynaptic structures, such as those present on muscle cells and dendritic spines (Epstein and Finkbeiner, 2018; Ashley et al., 2018; Pastuzyn et al., 2018). The translated *ARC* mRNA modulates the internalization of AMPA receptors through interactions with proteins like endophilin-3 and dynamin-2 that modulate clathrin-mediated endocytosis. The effects likely remain localized to the spine in contact with the bouton. Indeed, live cell imaging reveals that the mixing of the spine contents with those of the cell body is restricted by the constriction at the base of the spine (reviewed in Adrian et al., 2014). Further, effects of activation induced translation are likely more pronounced in splines as the change in ion concentrations following depolarization are magnified due to their small volume (reviewed in Dastidar and Nair, 2022). The design allows the targeted reprogramming of individual synaptic connections between pre- and postsynaptic cells.

During viral infection, the phosphorylation of EIF2α by PKR inhibits the normal path of CAP-dependent translation of transcripts. Instead, the synthesis of ARC proteins depends on the initiation factor EIF4G2 that enables non-CAP dependent translation though an internal ribosome entry site (IRES) (Pinkstaff et al., 2001; Thakor and Holcik, 2012; Hacisuleyman et al., 2024). Besides ARC, EIF4G2 permits translation of other neuronal proteins in neurons that promote local dendritic remodeling and disruption of synaptic contacts (David et al., 2022; Shestakova et al., 2023; Hacisuleyman et al., 2024). Indeed, the disassembly of key structural components in dendritic spines is triggered by herpes simplex virus (HSV) type I infection of neurons (Acuna-Hinrichsen et al., 2021). Further activation of PKR protects against endoplasmic stress that can otherwise induce neural apoptosis and necroptosis (Yuan et al., 2019). So far, there is no published data on HSV infection of *Arc* deficient mice. Such a study would inform on the role of ARC protein in the transmission of immune EREs. Interestingly, in traumatic brain models, knockdown of ARC protein increases neuronal cell death from apoptosis and necrosis (Chen et al., 2020). While the effects described are usually interpreted as due to the effects of ARC on intracellular signaling (Chen et al., 2024), the transmission of ribotransmitters across the synapse by VLC could further protect bystander cells to limit neuronal loss.

VLC and EREs as an antiviral defense

The findings raise the question of whether the ERE encoded immune RNAs and VLC-forming GAG proteins act together to defend against viral infections of the nervous system. The simplest model is that during viral infections, "junk" dsRNAs produced by immune EREs are transported by VLC across the synapse to induce an antiviral state in the recipient cell through the activation of PKR. The process alerts postsynaptic neurons of the threat posed by the virus. The PKR response then restricts the translation of infectious agents transmitted from the presynaptic cells (Taghavi et al., 2013). The defensive strategy is not perfect. This early warning system will also alter the programming of new memories by shutting down the EIF2α dependent translation of the coterie of mRNAs required for strengthening synaptic communication. However, the strategy has major benefits. The effect is localized. Only actively connected synapses are targeted. Further, the response is rapid: there is no need to wait on the recipient cells to mount an IFN-stimulated response to limit the spread of viruses. In extreme cases, these responses eliminate infected cells by inducing necroptosis, countering the protective effects of ADAR p150 and PKR.

If persistent over time, the elevated immune EREs and cell-intrinsic interferon responses may induce more serious neurological sequelae, as occurs in long COVID syndromes (Bungenberg et al., 2022). The chronic elevation of immune EREs within neurons in other types of neurodegenerative diseases may also aggravate the pathology in other ways. The phosphorylation of proteins by PKR other than EIF2α, such as tau protein (encoded by MAPT, microtubule associated protein tau) will also contribute to outcomes. The phosphorylation of tau interferes with its normal role in synaptic vesicle recycling (Hori et al., 2022; Jaye et al., 2024). This effect is likely beneficial during infection. It will inhibit the release and uptake by neurons of viral particles, thus preventing the spread of pathogens by retrograde transport. However, the response will also impair the clearance of protein aggregates from cells, such as those formed by phosphorylated tau. Consistent with this outcome, tau protein modified at sites phosphorylated by PKR accumulates in tauopathies, AD and in other neurodegenerative diseases (Cavallini et al., 2013; Sossin and Costa-Mattioli, 2019; Reimer et al., 2021; Martinez et al., 2021). One of these modifications produced by PKR (and other kinases) results in phosphorylation of tau at threonine 181 (ptau118). Plasma levels of ptau118 predict the presence

of amyloid beta (Aβ) deposits in a number of different brain regions linking PKR activation to disease outcomes (McGrath et al., 2022).

Therapies

How then can we address the potential problems arising from immune ERE suppression of LTP and LCM associated with neurodegenerative disease? Since prevention is preferable to intervention, a focus on decreasing the IFN-induced expression of EREs and decreasing phosEIF2α levels are intriguing approaches. Many studies have established a relationship between PKR activation and disease. In one cohort, PKR levels were elevated in the serum of 17 AD patients compared to 27 unaffected controls and another 19 patients with mild cognitive impairment (Monllor et al., 2021). A similar finding was reported by a different group that found elevated PKR levels in the CSF (cerebral spinal fluid) of 45 AD patients compared to 11 patients with mild cognitive impairment and 35 unaffected controls (Mouton-Liger et al., 2012). Further, CSF levels of phosphorylated PKR positively correlated with those of ptau118 (Mouton-Liger et al., 2012). The potential use of ptau118 as a prospective plasma biomarker for future increased Aβ deposition across multiple brain regions was validated using the Framingham Heart Study cohort (McGrath et al., 2022). Collectively these findings and those described earlier favor selective therapeutic targeting of the PKR catalytic activity, an approach that would leave intact other kinases that promote clearance of amyloid and tau proteins via the UPR. Older PKR inhibitors and current ones like C16 appear to lack sufficient specificity for clinical deployment (Chen et al., 2008; Lo et al., 2019). Newer PKR antagonists are in development (Lopez-Grancha et al., 2021).

Therapeutic strategies aimed at reducing the dsRNA in neurons and thereby reducing PKR activation are less certain. Potentially such approaches could prevent the reactivation of autonomously replicating EREs. Of note is the real-world data analysis that reports a decreased risk of AD in patients prescribed reverse transcriptase inhibitors, a finding validated in the preclinical studies so far performed (Magagnoli et al., 2023). A different strategy focuses on therapeutics that reverse the epigenetic changes associated with an increased expression of ERE (Cao et al., 2022). Unfortunately, the current generation of epigenetic therapeutics have shown greater toxicity than expected (Feehley et al., 2023). Another approach advocates the intranasal administration of IFN (Azarafrouz et al., 2022). However, the manipulation of interferon levels to reduce ERE expression is complicated. IFN-based treatments are reported to promote the autophagy of protein aggregates, yet the same processes also rapidly down-regulate IFN receptors (Tian et al., 2019). Further, *Ifng*$^{-/-}$ knockout mice that do not express type 2 IFN, have enhanced hippocampal spatial learning and novel object recognition, suggesting that stripping this receptor from cell surfaces in the brain may be preferred (Monteiro et al., 2016).

EREs may be of interest as biomarkers. The correlation of cognitive impairment with GAG encoded mRNAs and SINE levels in blood could be useful as a surrogate for ongoing memory impairment and for assessment of treatment responses, especially those transcripts that are associated with ARC and other GAG encoded VLCs. The mRNAs conveyed by these capsids may also provide clues for designing low molecular weight, brain-permeable therapeutics that enhance memory consolidation by either supplying the ribotransmitters or the proteins they encode or that enhance their actions.

Conclusion

Here, I have focused on the potential for reprogramming of postsynaptic dendritic spines by ribotransmitters conveyed by VLCs from pre- to postsynaptic neurons. Transmission by the ARC VLC *ARC* mRNA exemplifies this mechanism. The information delivered from the broadcasting bouton to the recipient cell depends on the current state of both. The exchanges tweak responses to future incoming messages. The optimal pairing requires the upstream neuron to send and receive the correct set of information and exploits the phenotypic plasticity of dentate gyrus granule cells (DGGC). The game of baseball provides an analogy: the presynaptic neuron has the role of a pitcher, with the downstream neuron signaling the type of delivery expected by the catcher. This feed-forward arrangement ensures that both pitcher and catcher are copacetic: it ensures that there is a high degree of synchronicity in their actions. The different pitches correspond to the range of inhibitory and excitatory neurotransmitters expressed by DGGC, but the downstream catcher only expects just one of them at a time. The catcher's response will signal to the pitcher whether the requested ball was thrown. The pitcher will also learn what type of pitches the catcher can handle.

Just as the mix of pitches in baseball determine the outcome of the game, the balancing of LTP and LTD responses enabled by ribotransmitters and receptors of the presynaptic neuron underlies the adaptive memories created (Zhu et al., 2011; Mody, 2002; Gutierrez, 2016). Just as teams over time will choose pitchers that work best with the catchers that they have available, natural selection can optimize the ability of the presynaptic neuron to send and receive the signals that optimize outcomes. Infectious agents exploit the vulnerabilities inherent in the use of memory EREs and ribotransmitters to exchange information across synapses via VLC transported by extracellular vesicles, just as an opposing team might learn the catcher's signals to change the outcome of a game. Such threats are countered by immune EREs that thwart autonomous replicants by immediately inhibiting the translation of their messages in the recipient cell, preventing the hostile takeover of the postsynaptic neuron. The exaptation of ERE proteins and RNAs enhance the ability of a species to reproduce. The coevolution of memory and immune EREs frame the flourishes and functionalities of future generations.

The review highlights the complex role of EREs in mammalian evolution. Memory EREs contribute to synaptic complexity through the capsids they encode and the ribotransmitters they transport. Immune EREs form dsRNAs that activate antiviral defenses to impede the spread of infectious agents from one neuron to the next. Both sets of ERE impact translation through

different initiation factors: EIF2α promotes LTP by cap-dependent translation, while dsRNA activation of PKR produces LTD by the non-CAP mediated translation of a different subset of mRNAs. The balance between LTP and LTD changes according to context and is perturbed during disease. The memory EREs promote neuronal plasticity while the immune EREs are SINEs of forgetfulness.

Data availability statement

The original contributions presented in the study are included in the article/supplementary material, further inquiries can be directed to the corresponding author.

Author contributions

AH: Conceptualization, Investigation, Visualization, Writing – original draft, Writing – review and editing.

Funding

The author(s) declare that no financial support was received for the research, authorship, and/or publication of the article.

Acknowledgments

This review was conceived and created by the author, as were the figures.

Conflict of interest

The author declares that the research was conducted in the absence of any commercial or financial relationships that could be construed as a potential conflict of interest.

Publisher's note

References

Abrusan, G., Szilagyi, A., Zhang, Y., and Papp, B. (2013). Turning gold into 'junk': Transposable elements utilize central proteins of cellular networks. *Nucleic Acids Res.* 41, 3190–3200. doi: 10.1093/nar/gkt011

Acuna-Hinrichsen, F., Covarrubias-Pinto, A., Ishizuka, Y., Stolzenbach, M. F., Martin, C., Salazar, P., et al. (2021). Herpes simplex virus type 1 neuronal infection triggers the disassembly of key structural components of dendritic spines. *Front. Cell. Neurosci.* 15:580717. doi: 10.3389/fncel.2021.580717

Adrian, M., Kusters, R., Wierenga, C. J., Storm, C., Hoogenraad, C. C., and Kapitein, L. C. (2014). Barriers in the brain: Resolving dendritic spine morphology and compartmentalization. *Front. Neuroanat.* 8:142. doi: 10.3389/fnana.2014.00142

Almeida, M. V., Andrade-Navarro, M. A., and Ketting, R. F. (2019). Function and evolution of nematode RNAi pathways. *Noncod. RNA* 5:8.

Ashley, J., Cordy, B., Lucia, D., Fradkin, L. G., Budnik, V., and Thomson, T. (2018). Retrovirus-like Gag protein Arc1 binds RNA and traffics across synaptic boutons. *Cell* 172:262–274.e11. doi: 10.1016/j.cell.2017.12.022

Athanasiadis, A., Rich, A., and Maas, S. (2004). Widespread A-to-I RNA editing of Alu-containing mRNAs in the human transcriptome. *PLoS Biol.* 2:e391. doi: 10.1371/journal.pbio.0020391

Azarafrouz, F., Farhangian, M., Chavoshinezhad, S., Dargahi, S., Nassiri-Asl, M., and Dargahi, L. (2022). Interferon beta attenuates recognition memory impairment and improves brain glucose uptake in a rat model of Alzheimer's disease: Involvement of mitochondrial biogenesis and PI3K pathway. *Neuropeptides* 95:102262. doi: 10.1016/j.npep.2022.102262

Baltzis, D., Li, S., and Koromilas, A. E. (2002). Functional characterization of pkr gene products expressed in cells from mice with a targeted deletion of the N terminus or C terminus domain of PKR. *J. Biol. Chem.* 277, 38364–38372.

Batzer, M. A., and Deininger, P. L. (2002). Alu repeats and human genomic diversity. *Nat. Rev. Genet.* 3, 370–379.

Blow, M., Futreal, P. A., Wooster, R., and Stratton, M. R. (2004). A survey of RNA editing in human brain. *Genome Res.* 14, 2379–2387.

Borchert, G. M., Holton, N. W., Williams, J. D., Hernan, W. L., Bishop, I. P., Dembosky, J. A., et al. (2011). Comprehensive analysis of microRNA genomic loci identifies pervasive repetitive-element origins. *Mob. Genet. Elements* 1, 8–17. doi: 10.4161/mge.1.1.15766

Bou-Nader, C., Gordon, J. M., Henderson, F. E., and Zhang, J. (2019). The search for a PKR code-differential regulation of protein kinase R activity by diverse RNA and protein regulators. *RNA* 25, 539–556. doi: 10.1261/rna.070169.118

Bungenberg, J., Humkamp, K., Hohenfeld, C., Rust, M. I., Ermis, U., Dreher, M., et al. (2022). Long COVID-19: Objectifying most self-reported neurological symptoms. *Ann. Clin. Transl. Neurol.* 9, 141–154. doi: 10.1002/acn3.51496

Campbell, G. R., Rawat, P., Bruckman, R. S., and Spector, S. A. (2015). Human Immunodeficiency virus type 1 nef inhibits autophagy through transcription factor EB sequestration. *PLoS Pathog.* 11:e1005018. doi: 10.1371/journal.ppat.1005018

Campillos, M., Doerks, T., Shah, P. K., and Bork, P. (2006). Computational characterization of multiple Gag-like human proteins. *Trends Genet.* 22, 585–589. doi: 10.1016/j.tig.2006.09.006

Cao, Q., Wang, W., and Yan, Z. (2022). Epigenetics-based treatment strategies for Alzheimer's disease. *Aging (Albany NY)* 14, 4193–4194. doi: 10.18632/aging.204096

Cavallini, A., Brewerton, S., Bell, A., Sargent, S., Glover, S., Hardy, C., et al. (2013). An unbiased approach to identifying tau kinases that phosphorylate tau at sites associated with Alzheimer disease. *J. Biol. Chem.* 288, 23331–23347. doi: 10.1074/jbc.M113.463984

Cesaro, T., and Michiels, T. (2021). Inhibition of PKR by viruses. *Front. Microbiol.* 12:757238. doi: 10.3389/fmicb.2021.757238

Chen, H. M., Wang, L., and D'Mello, S. R. (2008). A chemical compound commonly used to inhibit PKR, 8-(imidazol-4-ylmethylene)-6H-azolidino[5,4-g] benzothiazol-7-one, protects neurons by inhibiting cyclin-dependent kinase. *Eur. J. Neurosci.* 28, 2003–2016. doi: 10.1111/j.1460-9568.2008.06491.x

Chen, T., Li, Y. F., Ren, X., and Wang, Y. H. (2024). The mGluR5-mediated Arc activation protects against experimental traumatic brain injury in rats. *CNS Neurosci. Ther.* 30:e14695. doi: 10.1111/cns.14695

Chen, T., Tu, S., Ding, L., Jin, M., Chen, H., and Zhou, H. (2023). The role of autophagy in viral infections. *J. Biomed. Sci.* 30:5.

Chen, T., Zhu, J., Wang, Y. H., and Hang, C. H. (2020). Arc silence aggravates traumatic neuronal injury via mGluR1-mediated ER stress and necroptosis. *Cell Death Dis.* 11:4. doi: 10.1038/s41419-019-2198-5

Cheng, Y., Saville, L., Gollen, B., Veronesi, A. A., Mohajerani, M., Joseph, J. T., et al. (2021). Increased Alu RNA processing in Alzheimer brains is linked to gene expression changes. *EMBO Rep.* 22:e52255. doi: 10.15252/embr.202052255

Chiang, C., Li, Y., and Ng, S. K. (2020). The role of the Z-DNA binding domain in innate immunity and stress granules. *Front. Immunol.* 11:625504. doi: 10.3389/fimmu.2020.625504

Chuong, E. B. (2018). The placenta goes viral: Retroviruses control gene expression in pregnancy. *PLoS Biol.* 16:e3000028. doi: 10.1371/journal.pbio.3000028

Chuong, E. B., Elde, N. C., and Feschotte, C. (2016). Regulatory evolution of innate immunity through co-option of endogenous retroviruses. *Science* 351, 1083–1087. doi: 10.1126/science.aad5497

Contreras, P. S., Tapia, P. J., Jeong, E., Ghosh, S., Altan-Bonnet, N., and Puertollano, R. (2023). Beta-coronaviruses exploit cellular stress responses by modulating TFEB and TFE3 activity. *iScience* 26:106169. doi: 10.1016/j.isci.2023.106169

Cornec, A., and Poirier, E. Z. (2023). Interplay between RNA interference and transposable elements in mammals. *Front. Immunol.* 14:1212086. doi: 10.3389/fimmu.2023.1212086

Costa-Mattioli, M., Gobert, D., Stern, E., Gamache, K., Colina, R., Cuello, C., et al. (2007). eIF2alpha phosphorylation bidirectionally regulates the switch from short- to long-term synaptic plasticity and memory. *Cell* 129, 195–206. doi: 10.1016/j.cell.2007.01.050

Czech, B., Munafo, M., Ciabrelli, F., Eastwood, E. L., Fabry, M. H., Kneuss, E., et al. (2018). piRNA-guided genome defense: From biogenesis to silencing. *Annu. Rev. Genet.* 52, 131–157.

Daniels, B. P., Kofman, S. B., Smith, J. R., Norris, G. T., Snyder, A. G., Kolb, J. P., et al. (2019). The nucleotide sensor ZBP1 and kinase RIPK3 induce the enzyme IRG1 to promote an antiviral metabolic state in neurons. *Immunity* 50:64–76.e4. doi: 10.1016/j.immuni.2018.11.017

Dastidar, S. G., and Nair, D. (2022). A ribosomal perspective on neuronal local protein synthesis. *Front. Mol. Neurosci.* 15:823135. doi: 10.3389/fnmol.2022.823135

David, M., Olender, T., Mizrahi, O., Weingarten-Gabbay, S., Friedlander, G., Meril, S., et al. (2022). DAP5 drives translation of specific mRNA targets with upstream ORFs in human embryonic stem cells. *RNA* 28, 1325–1336. doi: 10.1261/rna.079194.122

de la Pena, J. B., Barragan-Iglesias, P., Lou, T. F., Kunder, N., Loerch, S., Shukla, T., et al. (2021). Intercellular Arc signaling regulates vasodilation. *J. Neurosci.* 41, 7712–7726.

de Reuver, R., Verdonck, S., Dierick, E., Nemegeer, J., Hessmann, E., Ahmad, S., et al. (2022). ADAR1 prevents autoinflammation by suppressing spontaneous ZBP1 activation. *Nature* 607, 784–789. doi: 10.1038/s41586-022-04974-w

Deininger, P. (2011). Alu elements: Know the SINEs. *Genome Biol.* 12:236.

Di Prisco, G. V., Huang, W., Buffington, S. A., Hsu, C. C., Bonnen, P. E., Placzek, A. N., et al. (2014). Translational control of mGluR-dependent long-term depression and object-place learning by eIF2alpha. *Nat. Neurosci.* 17, 1073–1082. doi: 10.1038/nn.3754

Dupressoir, A., Lavialle, C., and Heidmann, T. (2012). From ancestral infectious retroviruses to bona fide cellular genes: Role of the captured syncytins in placentation. *Placenta* 33, 663–671. doi: 10.1016/j.placenta.2012.05.005

Ecco, G., Imbeault, M., and Trono, D. (2017). KRAB zinc finger proteins. *Development* 144, 2719–2729.

Epstein, I., and Finkbeiner, S. (2018). The Arc of cognition: Signaling cascades regulating Arc and implications for cognitive function and disease. *Semin. Cell Dev. Biol.* 77, 63–72. doi: 10.1016/j.semcdb.2017.09.023

Erlendsson, S., Morado, D. R., Cullen, H. B., Feschotte, C., Shepherd, J. D., and Briggs, J. A. G. (2020). Structures of virus-like capsids formed by the Drosophila neuronal Arc proteins. *Nat. Neurosci.* 23, 172–175.

Feehley, T., O'Donnell, C. W., Mendlein, J., Karande, M., and McCauley, T. (2023). Drugging the epigenome in the age of precision medicine. *Clin. Epigenet.* 15:6. doi: 10.1186/s13148-022-01419-z

Gifford, R. J., Blomberg, J., Coffin, J. M., Fan, H., Heidmann, T., Mayer, J., et al. (2018). Nomenclature for endogenous retrovirus (ERV) loci. *Retrovirology* 15:59.

Goodier, J. L., and Kazazian, H. H. Jr. (2008). Retrotransposons revisited: The restraint and rehabilitation of parasites. *Cell* 135, 23–35. doi: 10.1016/j.cell.2008.09.022

Guo, X., Liu, S., Sheng, Y., Zenati, M., Billiar, T., Herbert, A., et al. (2023). ADAR1 Zalpha domain P195A mutation activates the MDA5-dependent RNA-sensing signaling pathway in brain without decreasing overall RNA editing. *Cell Rep.* 42:112733. doi: 10.1016/j.celrep.2023.112733

Gutierrez, R. (2016). The plastic neurotransmitter phenotype of the hippocampal granule cells and of the moss in their messy fibers. *J. Chem. Neuroanat.* 73, 9–20. doi: 10.1016/j.jchemneu.2015.11.007

Hacisuleyman, E., Hale, C. R., Noble, N., Luo, J. D., Fak, J. J., Saito, M., et al. (2024). Neuronal activity rapidly reprograms dendritic translation via eIF4G2:uORF binding. *Nat. Neurosci.* 27, 822–835. doi: 10.1038/s41593-024-01615-5

Halliday, M., and Mallucci, G. R. (2014). Targeting the unfolded protein response in neurodegeneration: A new approach to therapy. *Neuropharmacology* 76, 169–174.

Henriques, W. S., Young, J. M., Nemudryi, A., Nemudraia, A., Wiedenheft, B., and Malik, H. S. (2024). The diverse evolutionary histories of domesticated metaviral capsid genes in mammals. *Mol. Biol. Evol.* 41:8119.

Herbert, A. (2019a). A genetic instruction code based on DNA conformation. *Trends Genet.* 35, 887–890.

Herbert, A. (2019b). Z-DNA and Z-RNA in human disease. *Commun. Biol.* 2:7.

Herbert, A. (2020a). ALU non-B-DNA conformations, flipons, binary codes and evolution. *R. Soc. Open Sci.* 7:200222. doi: 10.1098/rsos.200222

Herbert, A. (2020b). Mendelian disease caused by variants affecting recognition of Z-DNA and Z-RNA by the Za domain of the double-stranded RNA editing enzyme ADAR. *Eur. J. Hum. Genet.* 28, 114–117. doi: 10.1038/s41431-019-0458-6

Herbert, A. (2021). To "Z" or not to "Z": Z-RNA, self-recognition, and the MDA5 helicase. *PLoS Genet.* 17:e1009513. doi: 10.1371/journal.pgen.1009513

Herbert, A. (2023). Flipons and small RNAs accentuate the asymmetries of pervasive transcription by the reset and sequence-specific microcoding of promoter conformation. *J. Biol. Chem.* 299:105140. doi: 10.1016/j.jbc.2023.105140

Herbert, A. (2024a). *Flipons and the logic of soft-wired genomes*. Boca Raton, FL: CRC Press.

Herbert, A. (2024b). The ancient Z-DNA and Z-RNA specific Zα fold has evolved modern roles in immunity and transcription through the natural selection of flipons. *R. Soc. Open Sci.* 11:80.

Higuchi, M., Maas, S., Single, F. N., Hartner, J., Rozov, A., Burnashev, N., et al. (2000). Point mutation in an AMPA receptor gene rescues lethality in mice deficient in the RNA-editing enzyme ADAR2. *Nature* 406, 78–81. doi: 10.1038/35017558

Ho, P. S., Ellison, M. J., Quigley, G. J., and Rich, A. (1986). A computer aided thermodynamic approach for predicting the formation of Z-DNA in naturally occurring sequences. *EMBO J.* 5, 2737–2744. doi: 10.1002/j.1460-2075.1986.tb04558.x

Hori, T., Eguchi, K., Wang, H. Y., Miyasaka, T., Guillaud, L., Taoufiq, Z., et al. (2022). Microtubule assembly by tau impairs endocytosis and neurotransmission via dynamin sequestration in Alzheimer's disease synapse model. *Elife* 11:e73542. doi: 10.7554/eLife.73542

Hubbard, N. W., Ames, J. M., Maurano, M., Chu, L. H., Somfleth, K. Y., Gokhale, N. S., et al. (2022). ADAR1 mutation causes ZBP1-dependent immunopathology. *Nature* 607, 769–775. doi: 10.1038/s41586-022-04896-7

Imakawa, K., Kusama, K., Kaneko-Ishino, T., Nakagawa, S., Kitao, K., Miyazawa, T., et al. (2022). Endogenous retroviruses and placental evolution, development, and diversity. *Cells* 11:2458.

Irie, M., Itoh, J., Matsuzawa, A., Ikawa, M., Kiyonari, H., Kihara, M., et al. (2022). Retrovirus-derived RTL5 and RTL6 genes are novel constituents of the innate immune system in the eutherian brain. *Development* 149:dev200976. doi: 10.1242/dev.200976

Ishino, F., Itoh, J., Irie, M., Matsuzawa, A., Naruse, M., Suzuki, T., et al. (2023). Retrovirus-derived RTL9 plays an important role in innate antifungal immunity in the eutherian brain. *Int. J. Mol. Sci.* 24:14884. doi: 10.3390/ijms241914884

Jang, K. L., and Latchman, D. S. (1992). The herpes simplex virus immediate-early protein ICP27 stimulates the transcription of cellular Alu repeated sequences by increasing the activity of transcription factor TFIIIC. *Biochem. J.* 284, 667–673. doi: 10.1042/bj2840667

Jansen, I. E., Savage, J. E., Watanabe, K., Bryois, J., Williams, D. M., Steinberg, S., et al. (2019). Genome-wide meta-analysis identifies new loci and functional pathways influencing Alzheimer's disease risk. *Nat. Genet.* 51, 404–413.

Jaye, S., Sandau, U. S., and Saugstad, J. A. (2024). Clathrin mediated endocytosis in Alzheimer's disease: Cell type specific involvement in amyloid beta pathology. *Front. Aging Neurosci.* 16:1378576. doi: 10.3389/fnagi.2024.1378576

Jiao, H., Wachsmuth, L., Wolf, S., Lohmann, J., Nagata, M., Kaya, G. G., et al. (2022). ADAR1 averts fatal type I interferon induction by ZBP1. *Nature* 607, 776–783. doi: 10.1038/s41586-022-04878-9

Kaempfer, R. (2006). Interferon-gamma mRNA attenuates its own translation by activating PKR: A molecular basis for the therapeutic effect of interferon-beta in multiple sclerosis. *Cell Res.* 16, 148–153. doi: 10.1038/sj.cr.7310020

Karijolich, J., Zhao, Y., Alla, R., and Glaunsinger, B. (2017). Genome-wide mapping of infection-induced SINE RNAs reveals a role in selective mRNA export. *Nucleic Acids Res.* 45, 6194–6208. doi: 10.1093/nar/gkx180

Kim, D. D., Kim, T. T., Walsh, T., Kobayashi, Y., Matise, T. C., Buyske, S., et al. (2004). Widespread RNA editing of embedded alu elements in the human transcriptome. *Genome Res.* 14, 1719–1725. doi: 10.1101/gr.2855504

Kipnis, J., Cohen, H., Cardon, M., Ziv, Y., and Schwartz, M. (2004). T cell deficiency leads to cognitive dysfunction: Implications for therapeutic vaccination for schizophrenia and other psychiatric conditions. *Proc. Natl. Acad. Sci. U.S.A.* 101, 8180–8185. doi: 10.1073/pnas.0402268101

Kokosar, J., and Kordis, D. (2013). Genesis and regulatory wiring of retroelement-derived domesticated genes: A phylogenomic perspective. *Mol. Biol. Evol.* 30, 1015–1031. doi: 10.1093/molbev/mst014

Larsen, P. A., Hunnicutt, K. E., Larsen, R. J., Yoder, A. D., and Saunders, A. M. (2018). Warning SINEs: Alu elements, evolution of the human brain, and the spectrum of neurological disease. *Chromosome Res.* 26, 93–111. doi: 10.1007/s10577-018-9573-4

Lehnert, S., Van Loo, P., Thilakarathne, P. J., Marynen, P., Verbeke, G., and Schuit, F. C. (2009). Evidence for co-evolution between human microRNAs and Alu-repeats. *PLoS One* 4:e4456. doi: 10.1371/journal.pone.0004456

Levanon, E. Y., Eisenberg, E., Yelin, R., Nemzer, S., Hallegger, M., Shemesh, R., et al. (2004). Systematic identification of abundant A-to-I editing sites in the human transcriptome. *Nat. Biotechnol.* 22, 1001–1005. doi: 10.1038/nbt996

Liang, Z., Chalk, A. M., Taylor, S., Goradia, A., Heraud-Farlow, J. E., and Walkley, C. R. (2023). The phenotype of the most common human ADAR1p150 Zalpha mutation P193A in mice is partially penetrant. *EMBO Rep.* 24:e55835. doi: 10.15252/embr.202255835

Lo, Y. C., Liu, T., Morrissey, K. M., Kakiuchi-Kiyota, S., Johnson, A. R., Broccatelli, F., et al. (2019). Computational analysis of kinase inhibitor selectivity using structural knowledge. *Bioinformatics* 35, 235–242.

Lopez-Grancha, M., Bernardelli, P., Moindrot, N., Genet, E., Vincent, C., Roudieres, V., et al. (2021). A novel selective PKR inhibitor restores cognitive deficits and neurodegeneration in Alzheimer disease experimental models. *J. Pharmacol. Exp. Ther.* 378, 262–275. doi: 10.1124/jpet.121.000590

Lowe, C. B., and Haussler, D. (2012). 29 mammalian genomes reveal novel exaptations of mobile elements for likely regulatory functions in the human genome. *PLoS One* 7:e43128. doi: 10.1371/journal.pone.0043128

Lynch, C., and Tristem, M. (2003). A co-opted gypsy-type LTR-retrotransposon is conserved in the genomes of humans, sheep, mice, and rats. *Curr. Biol.* 13, 1518–1523. doi: 10.1016/s0960-9822(03)00618-3

Maas, S., Melcher, T., Herb, A., Seeburg, P. H., Keller, W., Krause, S., et al. (1996). Structural requirements for RNA editing in glutamate receptor pre-mRNAs by recombinant double-stranded RNA adenosine deaminase. *J. Biol. Chem.* 271, 12221–12226. doi: 10.1074/jbc.271.21.12221

Macfarlan, T. S., Gifford, W. D., Driscoll, S., Lettieri, K., Rowe, H. M., Bonanomi, D., et al. (2012). Embryonic stem cell potency fluctuates with endogenous retrovirus activity. *Nature* 487, 57–63. doi: 10.1038/nature11244

Magagnoli, J., Yerramothu, P., Ambati, K., Cummings, T., Nguyen, J., Thomas, C. C., et al. (2023). Reduction of human Alzheimer's disease risk and reversal of mouse model cognitive deficit with nucleoside analog use. *medRxiv* [Preprint]. doi: 10.1101/2023.03.17.23287375

Mah, D., Zhu, Y., Su, G., Zhao, J., Canning, A., Gibson, J., et al. (2023). Apolipoprotein E recognizes Alzheimer's disease associated 3-O sulfation of heparan sulfate. *Angew. Chem. Int. Ed. Engl.* 62:e202212636. doi: 10.1002/anie.202212636

Margulis, L. (1976). Genetic and evolutionary consequences of symbiosis. *Exp. Parasitol.* 39, 277–349.

Marshall, P. R., Zhao, Q., Li, X., Wei, W., Periyakaruppiah, A., Zajaczkowski, E. L., et al. (2020). Dynamic regulation of Z-DNA in the mouse prefrontal cortex by the RNA-editing enzyme Adar1 is required for fear extinction. *Nat. Neurosci.* 23, 718–729. doi: 10.1038/s41593-020-0627-5

Martinez, N. W., Gomez, F. E., and Matus, S. (2021). The potential role of protein kinase r as a regulator of age-related neurodegeneration. *Front. Aging Neurosci.* 13:638208. doi: 10.3389/fnagi.2021.638208

Mattaliano, M. D., Montana, E. S., Parisky, K. M., Littleton, J. T., and Griffith, L. C. (2007). The *Drosophila* ARC homolog regulates behavioral responses to starvation. *Mol. Cell. Neurosci.* 36, 211–221. doi: 10.1016/j.mcn.2007.06.008

McGrath, E. R., Beiser, A. S., O'Donnell, A., Yang, Q., Ghosh, S., Gonzales, M. M., et al. (2022). Blood phosphorylated tau 181 as a biomarker for amyloid burden on brain PET in cognitively healthy adults. *J. Alzheimers Dis.* 87, 1517–1526.

Mody, I. (2002). The GAD-given right of dentate gyrus granule cells to become GABAergic. *Epilepsy Curr.* 2, 143–145. doi: 10.1111/j.1535-7597.2002.00053.x

Moliner, C., Fournier, P. E., and Raoult, D. (2010). Genome analysis of microorganisms living in amoebae reveals a melting pot of evolution. *FEMS Microbiol. Rev.* 34, 281–294. doi: 10.1111/j.1574-6976.2010.00209.x

Molmeret, M., Horn, M., Wagner, M., Santic, M., and Abu Kwaik, Y. (2005). Amoebae as training grounds for intracellular bacterial pathogens. *Appl. Environ. Microbiol.* 71, 20–28.

Mondotte, J. A., Gausson, V., Frangeul, L., Suzuki, Y., Vazeille, M., Mongelli, V., et al. (2020). Evidence for long-lasting transgenerational antiviral immunity in insects. *Cell Rep.* 33:108506. doi: 10.1016/j.celrep.2020.108506

Monllor, P., Giraldo, E., Badia, M. C., de la Asuncion, J. G., Alonso, M. D., Lloret, A., et al. (2021). Serum levels of clusterin, PKR, and RAGE correlate with amyloid burden in Alzheimer's disease. *J. Alzheimers Dis.* 80, 1067–1077.

Monteiro, S., Ferreira, F. M., Pinto, V., Roque, S., Morais, M., de Sa-Calcada, D., et al. (2016). Absence of IFNgamma promotes hippocampal plasticity and enhances cognitive performance. *Transl. Psychiatry* 6:e707. doi: 10.1038/tp.2015.194

Mouton-Liger, F., Paquet, C., Dumurgier, J., Lapalus, P., Gray, F., Laplanche, J. L., et al. (2012). Increased cerebrospinal fluid levels of double-stranded RNA-dependant protein kinase in Alzheimer's disease. *Biol. Psychiatry* 71, 829–835. doi: 10.1016/j.biopsych.2011.11.031

Nichols, P. J., Bevers, S., Henen, M., Kieft, J. S., Vicens, Q., and Vögeli, B. (2021). Recognition of non-CpG repeats in Alu and ribosomal RNAs by the Z-RNA binding domain of ADAR1 induces A-Z junctions. *Nat. Commun.* 12:93. doi: 10.1038/s41467-021-21039-0

Obbard, D. J., Gordon, K. H., Buck, A. H., and Jiggins, F. M. (2009). The evolution of RNAi as a defence against viruses and transposable elements. *Philos. Trans. R. Soc. Lond. B Biol. Sci.* 364, 99–115.

Panning, B., and Smiley, J. R. (1993). Activation of RNA polymerase III transcription of human Alu repetitive elements by adenovirus type 5: Requirement for the E1b 58-kilodalton protein and the products of E4 open reading frames 3 and 6. *Mol. Cell Biol.* 13, 3231–3244. doi: 10.1128/mcb.13.6.3231-3244.1993

Pastuzyn, E. D., Day, C. E., Kearns, R. B., Kyrke-Smith, M., Taibi, A. V., McCormick, J., et al. (2018). The neuronal gene arc encodes a repurposed retrotransposon gag protein that mediates intercellular RNA transfer. *Cell* 172:275–288.e18.

Pinkstaff, J. K., Chappell, S. A., Mauro, V. P., Edelman, G. M., and Krushel, L. A. (2001). Internal initiation of translation of five dendritically localized neuronal mRNAs. *Proc. Natl. Acad. Sci. U.S.A.* 98, 2770–2775. doi: 10.1073/pnas.051623398

Ravel-Godreuil, C., Znaidi, R., Bonnifet, T., Joshi, R. L., and Fuchs, J. (2021). Transposable elements as new players in neurodegenerative diseases. *FEBS Lett.* 595, 2733–2755.

Reimer, L., Betzer, C., Kofoed, R. H., Volbracht, C., Fog, K., Kurhade, C., et al. (2021). PKR kinase directly regulates tau expression and Alzheimer's disease-related tau phosphorylation. *Brain Pathol.* 31, 103–119. doi: 10.1111/bpa.12883

Roberts, W. K., Hovanessian, A., Brown, R. E., Clemens, M. J., and Kerr, I. M. (1976). Interferon-mediated protein kinase and low-molecular-weight inhibitor of protein synthesis. *Nature* 264, 477–480. doi: 10.1038/264477a0

Ros-Rocher, N., Perez-Posada, A., Leger, M. M., and Ruiz-Trillo, I. (2021). The origin of animals: An ancestral reconstruction of the unicellular-to-multicellular transition. *Open Biol.* 11:200359. doi: 10.1098/rsob.200359

Rothenburg, S., Seo, E. J., Gibbs, J. S., Dever, T. E., and Dittmar, K. (2009). Rapid evolution of protein kinase PKR alters sensitivity to viral inhibitors. *Nat. Struct. Mol. Biol.* 16, 63–70. doi: 10.1038/nsmb.1529

Sankowski, R., Strohl, J. J., Huerta, T. S., Nasiri, E., Mazzarello, A. N., D'Abramo, C., et al. (2019). Endogenous retroviruses are associated with hippocampus-based memory impairment. *Proc. Natl. Acad. Sci. U.S.A.* 116, 25982–25990. doi: 10.1073/pnas.1822164116

Schaffer, A. A., and Levanon, E. Y. (2021). ALU A-to-I RNA editing: Millions of sites and many open questions. *Methods Mol. Biol.* 2181, 149–162. doi: 10.1007/978-1-0716-0787-9_9

Sebe-Pedros, A., Ballare, C., Parra-Acero, H., Chiva, C., Tena, J. J., Sabido, E., et al. (2016). The dynamic regulatory genome of capsaspora and the origin of animal multicellularity. *Cell* 165, 1224–1237.

Segel, M., Lash, B., Song, J., Ladha, A., Liu, C. C., Jin, X., et al. (2021). Mammalian retrovirus-like protein PEG10 packages its own mRNA and can be pseudotyped for mRNA delivery. *Science* 373, 882–889. doi: 10.1126/science.abg6155

Sela, N., Kim, E., and Ast, G. (2010). The role of transposable elements in the evolution of non-mammalian vertebrates and invertebrates. *Genome Biol.* 11:R59.

Seth, M., Shirayama, M., Gu, W., Ishidate, T., Conte, D. Jr., and Mello, C. C. (2013). The *C. elegans* CSR-1 argonaute pathway counteracts epigenetic silencing to promote germline gene expression. *Dev. Cell* 27, 656–663. doi: 10.1016/j.devcel.2013.11.014

Shestakova, E. D., Smirnova, V. V., Shatsky, I. N., and Terenin, I. M. (2023). Specific mechanisms of translation initiation in higher eukaryotes: The eIF4G2 story. *RNA* 29, 282–299. doi: 10.1261/rna.079462.122

Shiura, H., Kitazawa, M., Ishino, F., and Kaneko-Ishino, T. (2023). Roles of retrovirus-derived PEG10 and PEG11/RTL1 in mammalian development and evolution and their involvement in human disease. *Front. Cell. Dev. Biol.* 11:1273638. doi: 10.3389/fcell.2023.1273638

Solon, M., Ge, N., Hambro, S., Haller, S., Jiang, J., Baca, M., et al. (2024). ZBP1 and TRIF trigger lethal necroptosis in mice lacking caspase-8 and TNFR1. *Cell Death Differ.* 31, 672–682. doi: 10.1038/s41418-024-01286-6

Sommer, B., Köhler, M., Sprengel, R., and Seeburg, P. H. (1991). NA editing in brain controls a determinant of ion flow in glutamate-gated channels. *Cell* 67, 11–19. doi: 10.1016/0092-8674(91)90568-j

Sossin, W. S., and Costa-Mattioli, M. (2019). Translational control in the brain in health and disease. *Cold Spring Harb. Perspect. Biol.* 11:a032912.

Suzuki, S., Ono, R., Narita, T., Pask, A. J., Shaw, G., Wang, C., et al. (2007). Retrotransposon silencing by DNA methylation can drive mammalian genomic imprinting. *PLoS Genet.* 3:e55. doi: 10.1371/journal.pgen.0030055

Taghavi, N., Samuel, C. E., and dependent, R. (2013). Protein kinase PKR and the Z-DNA binding orthologue PKZ differ in their capacity to mediate initiation factor eIF2alpha-dependent inhibition of protein synthesis and virus-induced stress granule formation. *Virology* 443, 48–58. doi: 10.1016/j.virol.2013.04.020

Tassetto, M., Kunitomi, M., and Andino, R. (2017). Circulating immune cells mediate a systemic RNAi-based adaptive antiviral response in *Drosophila*. *Cell* 169:314–325.e13. doi: 10.1016/j.cell.2017.03.033

Thakor, N., and Holcik, M. (2012). IRES translation of cellular messenger RNA operates in eIF2alpha- independent manner during stress. *Nucleic Acids Res.* 40, 541–552. doi: 10.1093/nar/gkr701

Tian, Y., Wang, M. L., and Zhao, J. (2019). Crosstalk between autophagy and type i interferon responses in innate antiviral immunity. *Viruses* 11:132.

Tucker, J. M., and Glaunsinger, B. A. (2017). Host noncoding retrotransposons induced by DNA viruses: A SINE of infection? *J. Virol.* 91:e00982–17.

Umerenkov, D., Herbert, A., Konovalov, D., Danilova, A., Beknazarov, N., Kokh, V., et al. (2023). Z-flipon variants reveal the many roles of Z-DNA and Z-RNA in health and disease. *Life Sci. Alliance* 6:e202301962. doi: 10.26508/lsa.202301962

Wallace, C. S., Lyford, G. L., Worley, P. F., and Steward, O. (1998). Differential intracellular sorting of immediate early gene mRNAs depends on signals in the mRNA sequence. *J. Neurosci.* 18, 26–35. doi: 10.1523/JNEUROSCI.18-01-00026.1998

Wang, S., Zhu, T., Ni, W., Zhou, C., Zhou, H., Lin, L., et al. (2023). Early activation of toll-like receptor-3 reduces the pathological progression of Alzheimer's disease in APP/PS1 mouse. *Alzheimers Res. Ther.* 15:33. doi: 10.1186/s13195-023-01186-w

Wedeles, C. J., Wu, M. Z., and Claycomb, J. M. (2013). Protection of germline gene expression by the C. elegans Argonaute CSR-1. *Dev. Cell* 27, 664–671. doi: 10.1016/j.devcel.2013.11.016

Wessler, S. R. (2006). Transposable elements and the evolution of eukaryotic genomes. *Proc. Natl. Acad. Sci. U.S.A.* 103, 17600–17601.

Witoelar, A., Rongve, A., Almdahl, I. S., Ulstein, I. D., Engvig, A., White, L. R., et al. (2018). Meta-analysis of Alzheimer's disease on 9,751 samples from Norway and IGAP study identifies four risk loci. *Sci. Rep.* 8:18088. doi: 10.1038/s41598-018-36429-6

Wu, J., Samara, N. L., Kuraoka, I., and Yang, W. (2019). Evolution of inosine-specific endonuclease V from bacterial DNase to eukaryotic RNase. *Mol. Cell* 76:44–56.e3. doi: 10.1016/j.molcel.2019.06.046

Yi, J., Yeou, S., and Lee, N. K. (2022). DNA bending force facilitates Z-DNA formation under physiological salt conditions. *J. Am. Chem. Soc.* 144, 13137–13145. doi: 10.1021/jacs.2c02466

Yuan, J., Amin, P., and Ofengeim, D. (2019). Necroptosis and RIPK1-mediated neuroinflammation in CNS diseases. *Nat. Rev. Neurosci.* 20, 19–33.

Zhai, H., Wang, T., Liu, D., Pan, L., Sun, Y., and Qiu, H. J. (2023). Autophagy as a dual-faced host response to viral infections. *Front. Cell. Infect. Microbiol.* 13:1289170. doi: 10.3389/fcimb.2023.1289170

Zhang, T., Yin, C., Fedorov, A., Qiao, L., Bao, H., Beknazarov, N., et al. (2022). ADAR1 masks the cancer immunotherapeutic promise of ZBP1-driven necroptosis. *Nature* 606, 594–602. doi: 10.1038/s41586-022-04753-7

Zhang, Z., Chen, C., Yang, F., Zeng, Y. X., Sun, P., Liu, P., et al. (2022). Itaconate is a lysosomal inducer that promotes antibacterial innate immunity. *Mol. Cell* 82. 2844–2857.e10. doi: 10.1016/j.molcel.2022.05.009

Zhu, P. J., Huang, W., Kalikulov, D., Yoo, J. W., Placzek, A. N., Stoica, L., et al. (2011). Suppression of PKR promotes network excitability and enhanced cognition by interferon-gamma-mediated disinhibition. *Cell* 147, 1384–1396. doi: 10.1016/j.cell.2011.11.029

Zhu, Y., Kodvawala, A., and Hui, D. Y. (2010). Apolipoprotein E inhibits toll-like receptor (TLR)-3- and TLR-4-mediated macrophage activation through distinct mechanisms. *Biochem. J.* 428, 47–54. doi: 10.1042/BJ20100016

frontiers | Frontiers in Neuroscience

TYPE Original Research
PUBLISHED 01 November 2024
DOI 10.3389/fnins.2024.1484777

OPEN ACCESS

EDITED BY
Pradeep Kumar,
All India Institute of Medical Sciences, India

REVIEWED BY
Silvia Pozzi,
Laval University, Canada
Hongjian Pu,
University of Pittsburgh, United States

*CORRESPONDENCE
Shiming Huang
✉ 18848488563@163.com

†These authors share first authorship

RECEIVED 22 August 2024
ACCEPTED 14 October 2024
PUBLISHED 01 November 2024

CITATION
Fu Z, Miao X, Luo X, Yuan L, Xie Y and Huang S (2024) Analysis of the correlation and influencing factors between delirium, sleep, self-efficacy, anxiety, and depression in patients with traumatic brain injury: a cohort study. *Front. Neurosci.* 18:1484777. doi: 10.3389/fnins.2024.1484777

Analysis of the correlation and influencing factors between delirium, sleep, self-efficacy, anxiety, and depression in patients with traumatic brain injury: a cohort study

Zhongmin Fu[1,2†], Xiaoju Miao[1,2†], Xian Luo[1,2], Lili Yuan[1,2], Yan Xie[3] and Shiming Huang[1*]

[1]Department of Nursing, Affiliated Hospital of Zunyi Medical University, Zunyi, China, [2]The First Ward of the Neurosurgery Department, Affiliated Hospital of Zunyi Medical University, Zunyi, China, [3]Department of Nursing, West China Hospital of Sichuan University, Chengdu, China

Background: Patients with traumatic brain injury (TBI) often experience post-injury anxiety and depression, which can persist over time. However, the relationships between anxiety and depression in TBI patients and delirium, sleep quality, self-efficacy, and serum inflammatory markers require further investigation.

Objective: This study aims to explore the associations of delirium, sleep quality, self-efficacy, and serum inflammatory markers with anxiety and depression in TBI patients, and to examine potential influencing factors.

Methods: We conducted a cohort study involving 127 patients with TBI. Delirium was assessed using the Confusion Assessment Method (CAM) and CAM-ICU, while anxiety, depression, sleep quality, self-efficacy, and pain were evaluated using the appropriate tools, respectively. Serum inflammatory markers (CRP, TNF-α, IL-6) were collected within 1 day post-injury. Generalized estimating equations (GEE) were used to analyze the relationships between delirium, sleep, self-efficacy, and anxiety/depression.

Results: The study identified 56 patients with delirium. Patients with delirium differed significantly from those without delirium in age, TBI classification, sleep duration, CRP levels, TNF-α levels, pain, self-efficacy, and insomnia ($P < 0.05$). The GEE analysis revealed that delirium, CRP levels, self-efficacy, underlying diseases, insomnia, TBI classification, age, and sleep duration were associated with anxiety symptoms in TBI patients at 6 months post-discharge ($P < 0.05$). Depression in TBI patients at 6 months post-discharge was not associated with delirium or insomnia but correlated with CRP levels, TBI classification, and self-efficacy ($P < 0.05$).

Conclusion: TBI patients who experience delirium, insomnia, and low self-efficacy during the acute phase are likely to exhibit more anxiety at the 6-month follow-up. Depression in TBI patients is not associated with delirium or insomnia but is negatively correlated with self-efficacy. CRP levels post-TBI may serve as a biomarker to identify patients at risk of emotional symptoms and potentially accelerate patient recovery.

KEYWORDS

traumatic brain injury, anxiety, depression, delirium, sleep, self-efficacy

1 Introduction

Traumatic brain injury (TBI) is a significant cause of disability and mortality worldwide. It is estimated that ~10 million people globally experience TBI annually, with 52,000 deaths attributed to TBI and nearly 100,000 new cases of disability resulting from it (Ahmed et al., 2017; Capizzi et al., 2020l Hyder et al., 2007). TBI can lead to a spectrum of cognitive, social, emotional, physical, and behavioral impairments, including sleep disturbances, depression/anxiety, and cognitive deficits (Draper and Ponsford, 2008; Langlois et al., 2006; Morganti-Kossmann et al., 2019; Dikmen et al., 2009). Studies have reported prevalence rates of anxiety disorders among TBI patients ranging from 21 to 70% (Moore et al., 2006; Scholten et al., 2016), and depression rates ranging from 17 to 50% (Scholten et al., 2016; Riggio, 2011; Osborn et al., 2014). These mental health issues not only significantly reduce patients' quality of life but also potentially impact their recovery process and social functioning (Duan et al., 2021; Rapoport et al., 2006; Zahniser et al., 2019). Given the complex etiology of psychological manifestations in TBI patients, which involve a combination of brain dysfunction and psychological trauma, as well as interrelationships between cognitive, emotional, and physical symptoms, epidemiology and underlying mechanisms of psychological health in TBI patients remain areas worthy of exploration (Piantino et al., 2022; Brett et al., 2022; Dikmen et al., 2009).

Delirium is characterized by an acute alteration in mental status marked by confusion, impaired attention, and fluctuating levels of arousal. Trauma-induced agitation and delirium generally manifest within the initial 24 h of TBI admission but can occur at any point during hospitalization and are frequent during the recovery phase (Roberson et al., 2021). Prior research indicates that patients experiencing trauma-induced delirium are susceptible to severe acute and long-term psychiatric outcomes (Teasdale and Jennett, 1976; Draper et al., 2007; Rocca et al., 2019). However, there is currently no direct investigation into the correlation between trauma-induced delirium in TBI patients and anxiety or depression during the recovery period.

Insomnia is highly prevalent among individuals with TBI, affecting 29% of patients (Mathias and Alvaro, 2012). Within 10 days post-TBI, about 13.3% of patients report sleep disturbances, increasing to 33.5% within 6 weeks (Chaput et al., 2009). Chaput et al. (2009) investigated sleep complaints in 493 mild TBI patients at 10 days and 6 weeks post-injury, revealing that those with sleep issues faced heightened risks of headaches, depressive symptoms, and irritability. Moreover, TBI patients experiencing sleep problems were more likely to concurrently suffer from depressive symptoms (Chaput et al., 2009), and prolonged insomnia has been linked with worsening depression over time (Lequerica et al., 2020; Huang et al., 2013). Nonetheless, there remains limited longitudinal and temporal research on the interplay between sleep quality, depression, and anxiety (Saravanan et al., 2024; Rao et al., 2014), highlighting the need for additional prospective studies to clarify the causal relationship between acute insomnia during TBI and the heightened occurrence of post-injury depression and anxiety symptoms.

Self-efficacy refers to one's confidence in managing symptoms, indicating greater persistence in related tasks (Bandura, 1977). In acquired brain injury, higher self-efficacy is associated with reduced anxiety and depression symptoms (Lewin et al., 2013; Longworth et al., 2018; Volz et al., 2016; Brands et al., 2015). Studies indicate that patients with higher self-efficacy, goal resilience, and adaptive goal adjustment tend to experience fewer emotional disturbances post-injury (Brands et al., 2015). Improving self-efficacy levels may be crucial for addressing psychological distress in mild TBI patients (Belanger et al., 2020). However, research on the relationship between self-efficacy and anxiety/depression has predominantly focused on stroke patients with acquired brain injury, with limited exploration in TBI patients.

Inflammation is a significant secondary mechanism following TBI (Das et al., 2012), potentially linked to various neurological symptoms such as anxiety, depression, cognitive impairment, and sleep disturbances (Malik et al., 2022; Rathbone et al., 2015; McAfoose and Baune, 2009). Research suggests interleukin-6 (IL-6), tumor necrosis factor α (TNFα), and C-reactive protein (CRP) are the predominant cytokines associated with adverse psychological outcomes in mild TBI patients (Malik et al., 2022; Rathbone et al., 2015). Additionally, systemic inflammation appears to correlate with psychological conditions like depression and anxiety in non-TBI populations (Osimo et al., 2020; Silva-Fernandes et al., 2024). However, it remains unclear whether these inflammatory mediators exhibit heightened activity in individuals experiencing post-TBI depression and anxiety. Discrepancies in the timing of cytokine assessments post-injury were noted in a systematic review, with most studies evaluating participants during the chronic phase of TBI (ranging from 1 month to several years) (Malik et al., 2022). Currently, the relationship between elevated acute-phase serum inflammatory markers in TBI and increased emotional symptoms requires further investigation.

This study aims to explore relationships between anxiety and depression symptoms, delirium, sleep, self-efficacy, and acute-phase serum inflammatory markers in TBI patients through a prospective cohort study. Findings are expected to deepen understanding of anxiety and depression mechanisms post-TBI, support future clinical interventions, and enhance long-term recovery and quality of life for patients.

2 Methods

2.1 Study design

This is a 6-month prospective cohort study approved by the Medical Ethics Committee of Affiliated Hospital of Zunyi Medical University. The study adheres to the Helsinki Declaration (Goodyear et al., 2007) and follows the Strengthening the Reporting of Observational Studies in Epidemiology (STROBE) guidelines (von Elm et al., 2007).

2.2 Study setting

This study was conducted at the Neurosurgery Ward of the Affiliated Hospital of Zunyi Medical University, a tertiary hospital

in Guizhou Province, China. The study commenced in June 2022 and concluded in December 2023. Patient recruitment began upon admission from June 2022 to April 2023. A research assistant (LX) explained the study objectives to patients and their families, ensuring informed consent was obtained and documented. Follow-up was conducted by designated nurses (FZM), starting from the discharge of the first patient until 6 months post-discharge, with follow-up intervals at 1-, 3-, and 6-months post-discharge.

2.3 Study population

This study is a prospective, population-based cohort study focusing on patients with TBI. Convenience sampling was employed to select patients from the Neurosurgery Ward of the Affiliated Hospital of Zunyi Medical University from June 2022 to April 2023. Inclusion criteria: ① confirmed history of TBI using CT or MRI; ② patients discharged from the hospital; ③ stable vital signs at discharge. Exclusion criteria: ① severe endocrine and metabolic diseases, hematologic disorders, malignant tumors, chronic pulmonary insufficiency, liver or kidney failure; ② patients who died within 3 days post-injury; ③ inability to participate in follow-up due to speech impediment or refusal.; ④ history of previous TBI, stroke, brain tumors, epilepsy, cognitive impairments or other brain disorders. Chronic inflammation associated with these comorbidities could distort the study results. Excluding these patients helps reduce confounding factors, enabling a more accurate analysis of the relationship between post-traumatic brain injury inflammation and clinical outcomes.

2.4 Data collection

2.4.1 Basic information

Basic information was registered via the hospital information system from patient admission to discharge. This included baseline socio-demographic characteristics and medical history, encompassing age, gender (male and female), residential types, marital status, education, underlying diseases, body mass index (BMI), monthly family income, and TBI classification. Underlying diseases refer to pre-existing conditions upon admission, such as hypertension, diabetes, and chronic obstructive pulmonary disease. TBI was classified based on the Glasgow Coma Scale (GCS) score at admission, with scores of 13–15 indicating mild TBI, 9–12 indicating moderate TBI, and 3–8 indicating severe TBI (Rimel et al., 1982).

2.4.2 Measurement of serum CRP, TNF-α, and IL-6

Fasting venous blood samples (3 mL) were collected from patients on the morning of the first post-injury day in citrate anticoagulant tubes. After centrifugation at 3,000 rpm for 15 min, the supernatant was stored at −20°C until analysis. Serum CRP, TNF-α, and IL-6 levels were determined using the ELISA sandwich method. Experimental procedures adhered strictly to the manufacturer's instructions.

2.4.3 Pain

Pain assessment was conducted within 1-day post-injury using the critical-care pain observation tool (Gélinas et al., 2006). This tool evaluates four dimensions: facial expression, body movements, muscle tension, and compliance with ventilator synchrony or vocalization. The dimension "ventilator synchrony" applies to intubated patients, while "vocalization" applies to non-intubated patients. Each dimension is scored from 0 to 2, yielding a total score of 8 points. A score of 0 indicates no pain, while 8 indicates maximum pain. Evaluation was performed by physicians.

2.4.4 Sleep duration

On the day of discharge, nurses investigated patients' self-reported sleep duration by asking, "How many hours did you sleep each night in the past week ?"

2.4.5 Sleep quality

The Athens Insomnia Scale (AIS) was employed to assess patient sleep quality scores. This assessment was conducted upon discharge. The AIS comprises eight dimensions: sleep onset latency (time from lights out to falling asleep), nocturnal awakenings, early morning awakenings before desired time, total sleep time, overall sleep quality (irrespective of duration), daytime mood disturbance, daytime physical functioning (physical or mental, e.g., memory, cognition, attention), and daytime sleepiness (Soldatos et al., 2000). Each dimension is rated from 0 (no impact) to 3 (severe impact), with a total score of 24. Higher scores indicate poorer sleep quality. Scores below 4 indicate no insomnia, 4–6 suggest suspected insomnia, and scores above 6 indicate insomnia.

2.4.6 Self efficacy

Schwarzer et al. (2009) developed the general self-efficacy scale (GSES) to evaluate how individuals cope in different situations and their confidence facing new challenges. The scale comprises 10 items rated on a 4-point Likert scale, ranging from 1 (completely incorrect) to 4 (completely correct). The final score is obtained by summing the scores of all items and dividing by 10. A higher score indicates greater self-efficacy in patients. Scores between 1.0 and 2.0 suggest low self-efficacy, scores between 2.1 and 3.0 indicate moderate self-efficacy, and scores between 3.1 and 4.0 indicate high levels of self-efficacy. Assessment using the GSES was conducted at the patients' discharge.

2.4.7 Delirium

Delirium assessment was conducted using the confusion assessment method (CAM) (Marcantonio et al., 2014) or the CAM-ICU (Ely et al., 2001) by responsible nurses and physicians at 8:00 a.m. and 8:00 p.m. daily for target patients post-injury. If any assessment during hospitalization met the delirium criteria, the patient was considered to have developed delirium. All nurses and physicians were trained in using delirium assessment tools to ensure accuracy. CAM evaluates delirium based on four features corresponding to four specific question items: (1) acute onset or fluctuating course of mental status; (2) inattention; (3) disorganized

thinking; (4) altered level of consciousness. The CAM diagnostic algorithm requires the simultaneous presence of criteria (1) and (2), and either criterion (3) or (4). For patients in the ICU or those unable to communicate verbally due to endotracheal intubation, the CAM-ICU was used to assess delirium. When using this scale, initial assessment of sedation depth was performed using the Richmond agitation-sedation scale (RASS) (Ely et al., 2003). Delirium assessment was conducted if the RASS score was −3 or higher. A RASS score below −3 indicated the patient was unconscious, in which case delirium assessment was temporarily suspended.

2.4.8 Anxiety and depression assessment

Psychological status among patients was evaluated using the hospital anxiety and depression scale (HADS) at discharge and during follow-ups at 1-, 3-, and 6-months post-discharge. We selected discharge time as the baseline since it marks a stable recovery phase and the end of primary treatment, enhancing comparability. Developed by Zigmond and Snaith (1983) in 1983, the HADS comprises two subscales: anxiety (HADS-A) and depression (HADS-D). Each subscale comprises seven items, each scored from 0 to 3 points, resulting in a maximum subscale score of 21 points, with higher scores indicating more severe psychological distress. The scores of 0–7 indicate normal psychological status, 8–10 suggest mild anxiety or depression, 11–14 indicate moderate levels, and scores between 15 and 21 signify severe anxiety or depression. These assessments provide valuable insights into the patients' mental health over time, aiding in appropriate intervention and support strategies.

2.5 Sample size

The sample size was calculated using PASS 15 software based on the longitudinal data sample size formula provided by Diggle (2002). The primary outcome was the HADS-A score at four time points. A pilot study of 30 patients (15 in the delirium group and 15 in the non-delirium group) showed an expected mean difference in anxiety scores of 6.2, with a pooled standard deviation of 3.87 and a repeated measures correlation of 0.812. Considering a two-sided significance level of 0.05, a power of 0.9, and a 20% dropout rate, the sample size was calculated to be 20. Ultimately, 130 patients were enrolled, with 127 completing follow-up.

2.6 Statistical analysis

Data were exported using Excel 2016 and reviewed by two individuals for accuracy. Statistical analyses were conducted using STATA 17 software. Continuous variables following a normal distribution were described using mean and standard deviation (SD). Between-group comparisons were assessed using *t*-tests. Non-normally distributed continuous variables were described using median (M) and interquartile range (IQR), with between-group comparisons evaluated using the Wilcoxon rank-sum test. Categorical variables were described as frequencies and percentages, with between-group comparisons analyzed using the chi-square test. Given the repeated measures of anxiety and depression scores among TBI patients and potential missing data, the generalized estimating equation (GEE) model was used with the maximum likelihood estimation method. As the missing data was <5%, no sensitivity analysis was conducted (Schafer, 1997). A preliminary normality test of the HADS scores was performed before the GEE analysis. Since the scores followed a normal distribution, a Gaussian distribution with an identity link function was chosen. Dummy variables were used in the GEE model to identify factors influencing anxiety and depression. Further analyses using the GEE model compared HADS-A scores between delirium and non-delirium groups, non-insomnia, suspected insomnia and insomnia groups, and low, medium, and high self-efficacy groups at different time points relative to discharge day. Graphs were created using GraphPad Prism 9.0. A significance level of $\alpha = 0.05$ (two-sided) was used, with $P < 0.05$ indicating statistical significance.

3 Results

3.1 Comparison of baseline characteristics between delirium and non-delirium groups in TBI patients

A total of 130 TBI patients were recruited for this study, with three patients lost to follow-up: one patient died, one patient developed speech impairment making communication impossible upon discharge, and one patient withdrew. Ultimately, data from 127 patients were included in the final analysis. Details of patient recruitment and follow-up are illustrated in Figure 1. Among these 127 TBI patients, 56 (44.1%) experienced delirium. General characteristics of all TBI patients and differences between the delirium and non-delirium groups are summarized in Table 1. Significant differences between the delirium and non-delirium groups were observed in terms of age, TBI classification, sleep duration, CRP levels, TNFα levels, pain scores, self-efficacy, and insomnias ($P < 0.05$, Table 1).

3.2 Factors influencing anxiety in patients with TBI

Using HADS-A scores as the dependent variable, the GEE analysis revealed that delirium, CRP levels, self-efficacy, underlaying disease, insomnias, TBI classification, age, and sleep duration were significant factors influencing anxiety in traumatic brain injury patients post-discharge ($P < 0.05$, Table 2).

3.3 Factors influencing depression in patients with TBI

Using HADS-D scores as the dependent variable, the GEE analysis revealed that post-discharge depression in traumatic brain injury patients was not associated with delirium, insomnias but

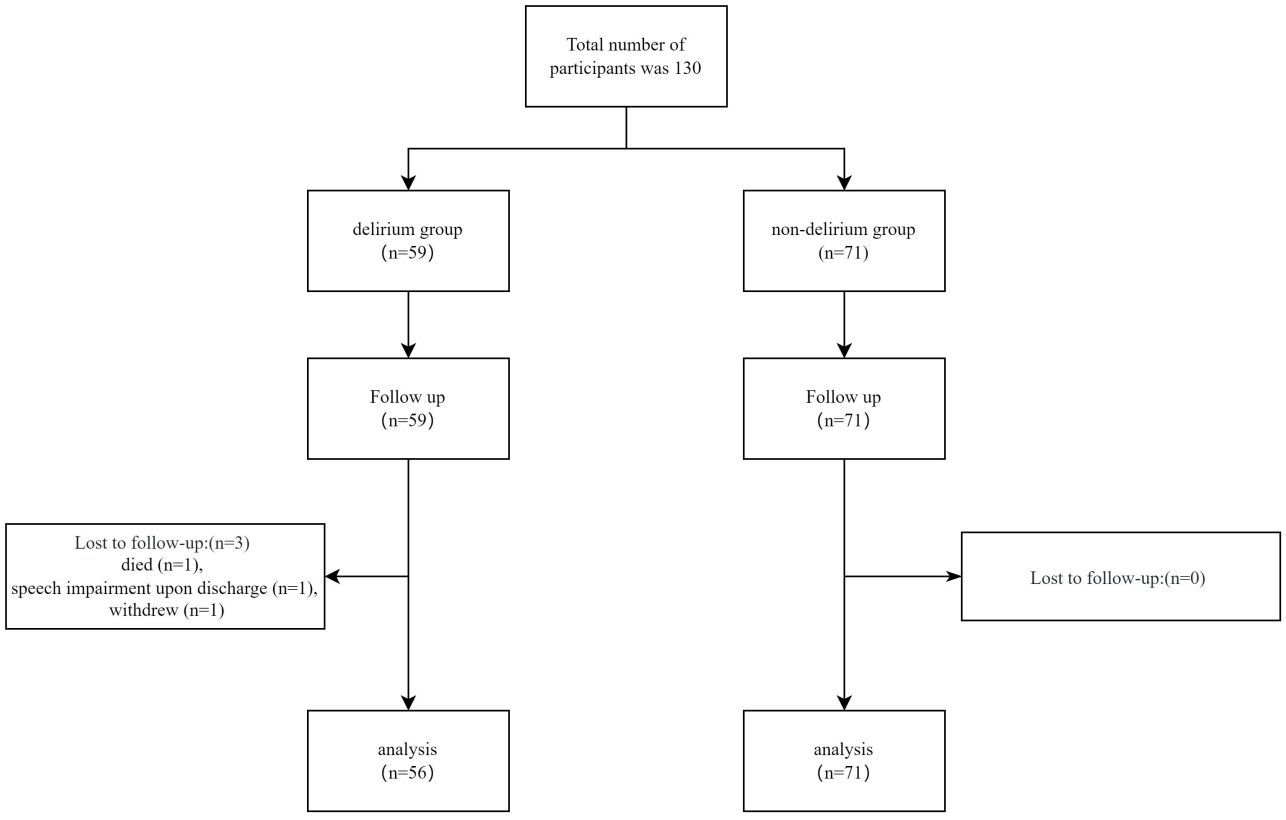

FIGURE 1
Flowchart of participant enrollment.

showed significant correlations with CRP levels, TBI classification, and self-efficacy ($P < 0.05$, Table 3).

3.4 Comparison of HADS-A scores between delirium and non-delirium patients with TBI

According to the separate effects analysis of the GEE model, significant differences in HADS-A scores were observed between delirium and non-delirium groups on discharge day, at one, three, and 6 months post-discharge ($P < 0.001$, Supplementary Table S1; Figure 2). Compared to discharge day, non-delirium patients showed significant differences in HADS-A scores at 3 and 6 months post-discharge ($P < 0.05$), while delirium patients exhibited significant differences at 1, 3, and 6 months post-discharge ($P < 0.05$).

3.5 Comparison of HADS-A scores among TBI patients with different sleep quality levels

The separate effects analysis of the GEE model revealed significant differences in HADS-A scores among patients categorized into normal sleep, suspected insomnia, and insomnia groups on discharge day, as well as at 1, 3, and 6 months post-discharge ($P < 0.001$, see Supplementary Table S2; Figure 3). Compared to discharge day, patients with normal sleep exhibited significant differences in HADS-A scores at 3 and 6 months post-discharge ($P < 0.05$). Similarly, the suspected insomnia group showed significant differences at 3 and 6 months post-discharge ($P < 0.05$), while the insomnia group displayed significant differences at 1, 3, and 6 months post-discharge ($P < 0.05$).

3.6 Comparison of HADS-A scores among TBI patients with different levels of self-efficacy

According to the separate effects analysis of the GEE model, significant differences in HADS-A scores were observed between patients with low self-efficacy and those with moderate self-efficacy, low self-efficacy and high self-efficacy, as well as moderate self-efficacy and high self-efficacy groups on discharge day, at 1, 3, and 6 months post-discharge ($P < 0.05$, see Supplementary Table S3; Figure 4). Compared to discharge day, the low self-efficacy group showed significant

TABLE 1 General characteristics of delirium and non-delirium groups in patients with traumatic brain injury.

Variable		Non-delirium group ($n = 71$)	Delirium group ($n = 56$)	$\chi^2/t/Z$	*P*-value
Gender, *n* (%)	Man	49 (69.0)	36 (64.3)	0.316	0.574
	Woman	22 (31.0%)	20 (35.7%)		
Age, *n* (%)	18–30	4 (7.2)	14 (19.7)	14.374	0.001
	31–59	27 (48.2)	11 (15.5)		
	≥60	25 (44.6)	46 (64.8)		
Residential types, *n* (%)	Rural	23 (32.4)	18 (32.1)	0.001	0.976
	Urban	48 (67.6)	38 (67.9)		
Marital status, *n* (%)	Married	43 (60.6)	34 (60.7)	0.001	0.986
	Single	28 (39.4)	22 (39.3)		
Work status, *n* (%)	Employed	43 (60.6)	30 (46.4)	0.626	0.429
	Unemployed	28 (39.4)	26 (53.6)		
Education, *n* (%)	Primary school and below	10 (14.1)	8 (14.3)	0.703	0.951
	Middle school	18 (25.3)	11 (19.6)		
	High school	22 (31.0)	20 (35.7)		
	Junior college	13 (18.3)	10 (17.9)		
	Bachelor and above education degree	8 (11.3)	7 (12.5)		
Underlaying disease, *n* (%)	No	33 (46.5)	18 (32.1)	2.677	0.102
	Yes	38 (53.5)	38 (67.9)		
BMI (kg/m^2), *n* (%)	<18.5	3 (4.3)	2 (3.6)	0.645	0.886
	18.5–23.9	26 (36.6)	17 (30.4)		
	24–27.9	28 (39.4)	25 (44.6)		
	≥28	14 (19.7)	12 (21.4)		
Monthly family income (yuan), *n* (%)	<5,000	8 (11.3)	4 (7.1)	0.937	0.626
	5,000–10,000	27 (38.0)	25 (44.7)		
	>10,000	36 (50.7)	27 (48.2)		
TBI classification, *n* (%)	Mild TBI	47 (66.2)	2 (3.6)	51.816	<0.001
	Moderate TBI	24 (33.8)	54 (96.4)		
Sleep duration (min)		308.82 ± 50.56	282.47 ± 51.31	2.897	0.004
CRP (mg/L)		25.18 (14.91)	44.80 (12.07)	−5.189	<0.001
TNFα (pg/ml)		173.91 (38.55)	268.74 (51.99)	−6.517	<0.001
IL6 (pg/ml)		285.34 (214.81)	288.67 (222.44)	−1.513	0.13
CPOT score		3.15 ± 1.54	4.53 ± 1.29	−5.386	<0.001
AIS		11.31 ± 5.87	13.41 ± 4.41	−2.225	0.028
GSES		2.81 ± 1.26	1.74 ± 0.49	5.961	<0.001

TBI, traumatic brain injury; GSES, general self-efficacy scale; CPOT, critical-care pain observation tool; AIS, Athens insomnia scale; CRP, C-reactive protein; TNF α, tumor necrosis factor α; IL-6, interleukin-6.

differences in HADS-A scores at 1, 3, and 6 months post-discharge ($P < 0.05$), the moderate self-efficacy group exhibited significant differences at 3 and 6 months post-discharge ($P < 0.05$), and the high self-efficacy group displayed significant differences at 3 and 6 months post-discharge ($P < 0.05$).

10.3389/fnins.2024.1484777

TABLE 2 Parameter estimation of anxiety factors based on generalized estimation equation.

Parameter	β	SE	95%CI		Waldχ^2	*P*-value
			Lower limit	Upper limit		
Intercept	5.804	2.0171	1.851	9.758	8.281	0.004
Time						
6 months	−3.071	0.1206	−3.307	−2.835	648.647	0.000
3 months	−2.159	0.1008	−2.357	−1.962	458.898	0.000
1 months	−0.429	0.1021	−0.630	−0.229	17.670	0.000
Baseline	0[a]	–	–	–	–	–
Gender						
Female	0.208	0.2673	−0.316	0.732	0.605	0.437
Male	0[a]	–	–	–	–	–
Age						
18–39 y	1.211	0.3686	0.488	1.933	10.790	0.001
40–59 y	0.532	0.3674	−0.188	1.253	2.099	0.147
≥60 y	0[a]	–	–	–	–	–
Residential types						
Rural	0.029	0.3519	−0.661	0.718	0.007	0.935
Urban	0[a]	–	–	–	–	–
Marital status						
Single	0.340	0.3097	−0.267	0.947	1.203	0.273
Married	0[a]	–	–	–	–	–
Work status						
Unemployed	−0.138	0.2559	−0.640	0.363	0.292	0.589
Employed	0[a]	–	–	–	–	–
Education						
Bachelor and above education degree	0.232	0.5140	−0.775	1.240	0.204	0.652
Junior college	0.188	0.5416	−0.873	1.250	0.121	0.728
High school	−0.225	0.4382	−1.083	0.634	0.263	0.608
Middle school	−0.218	0.4727	−1.144	0.709	0.212	0.645
Primary school and below	0[a]	–	–	–	–	–
Underlaying disease						
Existence	0.779	0.2583	0.272	1.285	9.089	0.003
Non-existence	0[a]	–	–	–	–	–
BMI (kg/m^2)						
≥28	0.022	0.9239	−1.789	1.833	0.001	0.981
24–27.9	0.414	0.9566	−1.461	2.289	0.187	0.665
18.5–23.9	0.252	0.9136	−1.538	2.043	0.076	0.782
<18.5	0[a]	–	–	–	–	–
Monthly family income (yuan)						
>10,000	−0.943	0.5740	−2.068	0.182	2.697	0.101
5,000–10,000	−0.715	0.6187	−1.928	0.497	1.337	0.248

(Continued)

TABLE 2 (Continued)

Parameter	β	SE	95%CI		Waldχ^2	*P*-value
			Lower limit	Upper limit		
<5,000	0[a]	–	–	–	–	–
TBI classification						
Mild TBI	1.508	0.3535	0.815	2.201	18.208	0.000
Moderate TBI	0[a]	–	–	–	–	–
Delirium						
Yes	1.148	0.3866	0.390	1.906	8.819	0.003
No	0[a]	–	–	–	–	–
AIS score						
>6	0.953	0.4874	−0.002	1.909	3.826	0.050
4–6	0.366	0.4345	−0.486	1.218	0.709	0.400
0–4	0[a]	–	–	–	–	–
GSES score						
5–6	−1.076	0.4006	−1.861	−0.291	7.219	0.007
3–4	−0.093	0.2941	−0.669	0.484	0.099	0.753
1–2	0[a]	–	–	–	–	–
CPOT score	−0.063	0.1084	−0.276	0.149	0.340	0.560
CRP (mg/L)	0.057	0.0156	0.026	0.087	13.258	0.000
TNFα (pg/ml)	0.001	0.0033	−0.007	0.006	0.019	0.889
IL−6 (pg/ml)	0.002	0.0011	0.000	0.004	2.536	0.111
Sleep duration (min)	−0.020	0.0097	−0.039	−0.001	4.110	0.043

TBI, traumatic brain injury; GSES, general self-efficacy scale; CPOT, critical-care pain observation tool; AIS, Athens insomnia scale; CRP, C-reactive protein; TNF α, tumor necrosis factor α; IL-6, Interleukin-6.
0[a] refers to the redundant parameter; β refers to the regression coefficient or model parameter; "–" indicates that the group is the reference group.

3.7 Comparison of HADS-D scores among TBI patients with different levels of self-efficacy

According to the separate effects analysis of the GEE model, significant differences in HADS-D scores were observed between patients with low self-efficacy and those with moderate self-efficacy, low self-efficacy and high self-efficacy, as well as moderate self-efficacy and high self-efficacy groups on discharge day, at 1, 3, and 6 months post-discharge ($P < 0.05$, see Supplementary Table S4; Figure 5). Compared to discharge day, the low self-efficacy group showed significant differences in HADS-D scores at 1, 3, and 6 months post-discharge ($P < 0.05$), the moderate self-efficacy group exhibited significant differences at 3 and 6 months post-discharge ($P < 0.05$), and the high self-efficacy group displayed significant differences at 3 and 6 months post-discharge ($P < 0.05$).

4 Discussion

Our study identified several key factors associated with heightened anxiety symptoms in TBI patients: younger age, underlaying disease, TBI classification, delirium, elevated CRP levels, diminished self-efficacy, and insomnia. These findings underscore the intricate interplay of biological, psychosocial, and clinical elements contributing to anxiety development post-TBI. Interestingly, depression symptoms did not correlate significantly with delirium or insomnia but exhibited significant associations with serum CRP levels, TBI classification, and self-efficacy.

4.1 The relationship between CRP, delirium, anxiety, and depression in patients with TBI

In this study, both HADS-A and HADS-D scores were higher in patients with delirium compared to non-delirious patients. However, only the intergroup difference in HADS-A was statistically significant. Consistent with Barker et al., anxiety symptoms were more prevalent than depression symptoms when using HADS (Barker-Collo et al., 2018). There was no statistically significant difference in HADS-D scores between the delirium and non-delirium groups, potentially explained by the majority (96.4%) of the delirium group being moderate TBI patients, who may have more severe cognitive deficits, potentially masking emotional symptoms and/or poorer insight, resulting in fewer self-reported emotional symptoms (Uiterwijk et al., 2022). The GEE analysis in this study revealed that mild TBI patients reported more severe

TABLE 3 Parameter estimation of depression factors based on generalized estimation equation.

Parameter	β	SE	95%CI		Waldχ^2	*P*-value
			Lower limit	Upper limit		
Intercept	6.775	2.7695	1.347	12.203	5.984	0.014
Time						
6 months	−3.537	0.1596	−3.850	−3.224	490.878	0.000
3 months	−3.007	0.2125	−3.423	−2.591	200.324	0.000
1 months	−0.587	0.1265	−0.835	−0.339	21.542	0.000
Baseline	0[a]	–	–	–	–	–
Gender						
Female	0.105	0.3644	−0.609	0.819	0.083	0.773
Male	0[a]					
Age						
18–39 y	0.540	0.4601	−0.362	1.441	1.376	0.241
40–59 y	0.035	0.4394	−0.826	0.896	0.006	0.937
≥60 y	0[a]	–	–	–	–	–
Residential types						
Rural	−0.562	0.3352	−1.219	0.095	2.808	0.094
Urban	0[a]	–	–	–	–	–
Marital status						
Single	0.327	0.3428	−0.345	0.999	0.910	0.340
Married	0[a]	–	–	–	–	–
Work status						
Unemployed	−0.244	0.2878	−0.808	0.320	0.718	0.397
Employed	0[a]	–	–	–	–	–
Education						
Bachelor and above education degree	−0.331	0.5938	−1.495	0.832	0.311	0.577
Junior college	−0.038	0.6204	−1.254	1.178	0.004	0.951
High school	−0.151	0.5158	−1.161	0.860	0.085	0.770
Middle school	−0.015	0.4563	−0.909	0.880	0.001	0.975
Primary school and below	0[a]	–	–	–	–	–
Underlaying disease, *n* (%)						
Existence	0.393	0.2716	−0.139	0.925	2.093	0.148
Non-existence	0[a]	–	–	–	–	–
BMI (kg/m^2)						
≥28	−1.600	1.2553	−4.060	0.860	1.625	0.202
24–27.9	−1.792	1.2621	−4.266	0.681	2.017	0.156
18.5–23.9	−1.412	1.2554	−3.873	1.048	1.266	0.261
<18.5	0[a]	–	–	–	–	–
Monthly family income (yuan)						
>10,000	−0.575	0.5038	−1.563	0.412	1.304	0.253
5,000–10,000	−0.752	0.5534	−1.836	0.333	1.844	0.174

(Continued)

TABLE 3 (Continued)

Parameter	β	SE	95%CI		Waldχ^2	*P*-value
			Lower limit	Upper limit		
<5,000	0[a]	–	–	–	–	–
TBI classification						
Mild TBI	0.922	0.3862	0.165	1.679	5.695	0.017
Moderate TBI	0[a]	–	–	–	–	–
Delirium						
Yes	0.222	0.4522	−0.665	1.108	0.240	0.624
No	0a	–	–	–	–	–
AIS score						
>6	0.658	0.5830	−0.485	1.800	1.272	0.259
4–6	0.499	0.4871	−0.456	1.453	1.048	0.306
0–4	0[a]	–	–	–	–	–
GSES score						
5–6	−0.971	0.3788	−1.714	−0.229	6.573	0.010
3–4	−0.981	0.5046	−1.970	0.008	3.780	0.052
1–2	0[a]	–	–	–	–	–
CPOT	0.040	0.1046	−0.165	0.245	0.147	0.702
CRP (mg/L)	0.037	0.0166	0.005	0.070	5.003	0.025
TNFα (pg/ml)	0.007	0.0046	−0.002	0.016	2.316	0.128
IL−6 (pg/ml)	0.000	0.0016	−0.003	0.003	0.003	0.955
Sleep duration (min)	−0.012	0.0094	−0.030	0.006	1.629	0.202

TBI, traumatic brain injury; GSES, general self-efficacy scale; CPOT, critical-care pain observation tool; AIS, Athens insomnia scale; CRP, C-reactive protein; TNF α, tumor necrosis factor α; IL-6, Interleukin-6.
0[a] refers to the redundant parameter; β refers to the regression coefficient or model parameter; "–" indicates that the group is the reference group.

anxiety and depression than moderate TBI patients, indirectly confirming this speculation. TBI-related delirium is a complex and poorly understood complication occurring in a heterogeneous patient population (Sherer et al., 2020). It is speculated that the pathophysiology of TBI-related delirium differs from other delirium processes (Povlishock and Katz, 2005). Even mild or moderate TBI patients may experience post-traumatic delirium without significant structural damage detected by neuroimaging (Ganau et al., 2018). The underlying pathophysiology remains incompletely understood, but severe and persistent inflammation is associated with a series of molecular, biochemical, and cellular changes in the brain that lead to neuronal injury and apoptosis (Ganau et al., 2018; Sun et al., 2019). The mechanisms underlying anxiety and depression following TBI are currently unclear, but inflammation post-TBI is speculated to be a contributing factor, associated with elevated levels of TNF-α, IL-6, IFN-α, and CRP (Malik et al., 2022; Rathbone et al., 2015).

In our study, delirious patients exhibited higher post-injury CRP levels compared to non-delirious patients, and elevated CRP levels were associated with higher anxiety and depression scores in patients. Studies have shown elevated CRP levels have also been associated with delirium (Lozano-Vicario et al., 2023; Vasunilashorn et al., 2017) and psychological disorders (Wium-Andersen et al., 2013; Bekkevold et al., 2023) even in the absence of a TBI event. Increased CRP concentrations may relate to emotional disturbances and cognitive impairments, but the mechanisms remain unclear (Su et al., 2014). Systemic inflammatory responses likely play a significant role. First, systemic inflammation activates the hypothalamic-pituitary-adrenal (HPA) axis (Murray et al., 2013) and triggers stress responses, releasing stress hormones like cortisol. These hormones help manage short-term stress, but prolonged HPA activation may lead to anxiety symptoms (Tsigos and Chrousos, 2002; Juruena et al., 2020; Haroon et al., 2012). Second, systemic inflammation may increase the conversion of tryptophan to kynurenine and quinolinic acid through the indoleamine 2,3-dioxygenase pathway, reducing serotonin production. Lower serotonin levels correlate closely with anxiety, while kynurenine and quinolinic acid may harm the central nervous system and raise anxiety risk (Christmas et al., 2011; Dantzer et al., 2008). Third, systemic inflammation activates microglia in the brain, resulting in neuroinflammation (Qin et al., 2007). Neuroinflammation contributes to the pathophysiology of anxiety and depression (Briones and Woods, 2014). Finally, systemic inflammation can increase oxidative stress, damaging neurons, disrupting neurotransmitter balance, and worsening anxiety symptoms

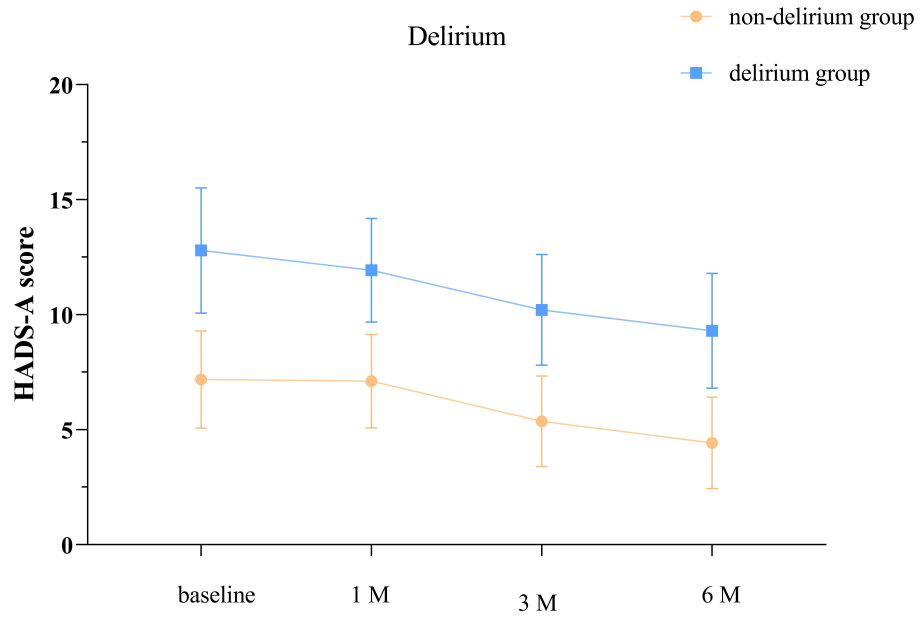

FIGURE 2
Anxiety scores at different time points in the delirium and non-delirium groups. The baseline refers to the day of discharge. HADS-A: hospital anxiety and depression scale- anxiety score. The error bars indicate the standard deviation, the larger the error bars, the greater the variability or uncertainty in the data.

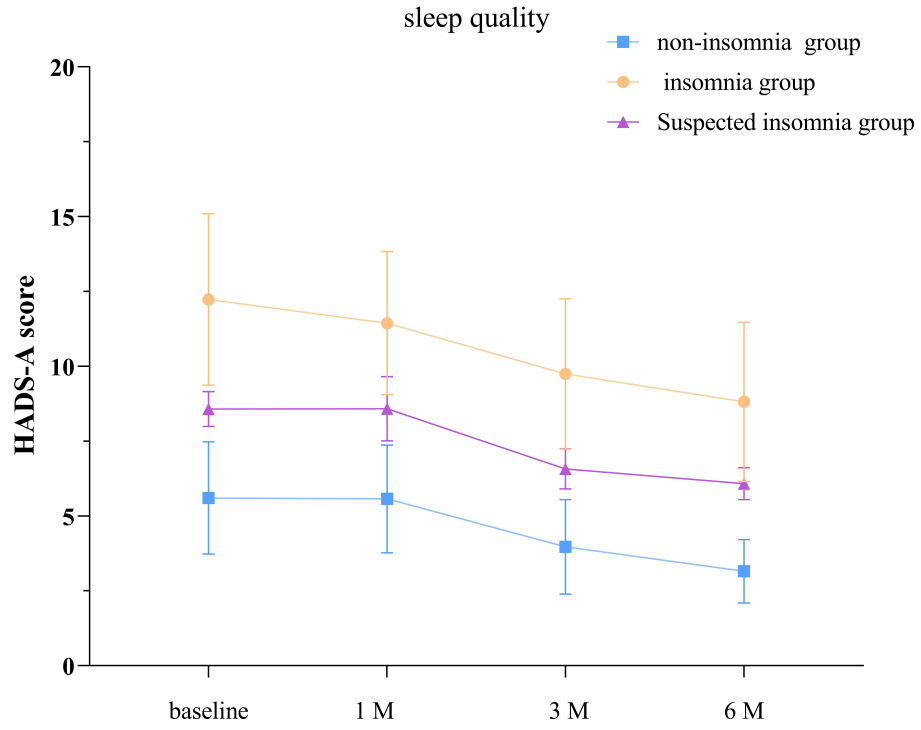

FIGURE 3
Anxiety scores in groups with different sleep quality. The baseline refers to the day of discharge. HADS-A: hospital anxiety and depression scale-anxiety score. The error bars indicate the standard deviation, the larger the error bars, the greater the variability or uncertainty in the data.

(Dantzer et al., 2008; Fedoce et al., 2018). We measured CRP at a single time point, but its link to anxiety may reflect an early inflammatory surge that increases the risk of subsequent psychological issues. This emphasizes the necessity of identifying TBI patients at high risk for delirium and psychological problems based on early CRP concentrations.

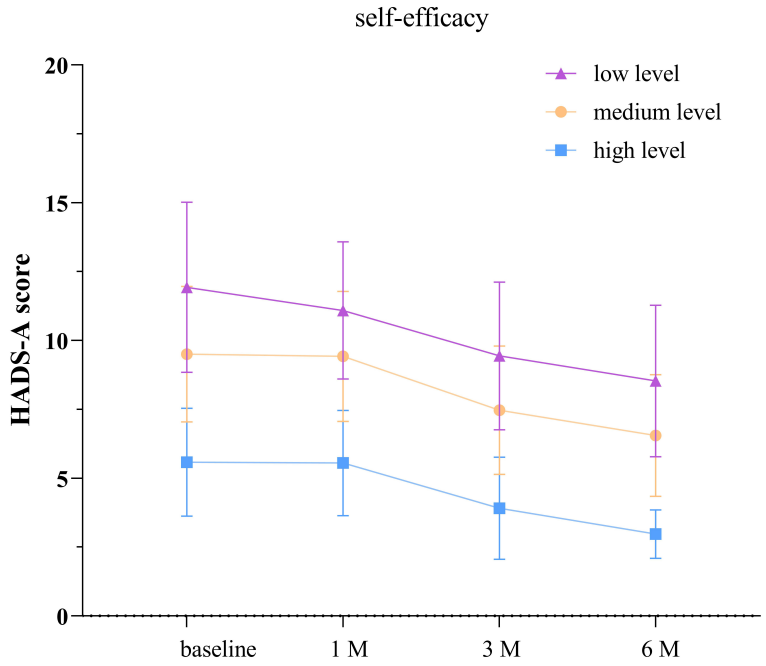

FIGURE 4
Anxiety scores in groups with different levels of self-efficacy. The baseline refers to the day of discharge. HADS-A: hospital anxiety and depression scale- anxiety score. The error bars indicate the standard deviation, the larger the error bars, the greater the variability or uncertainty in the data.

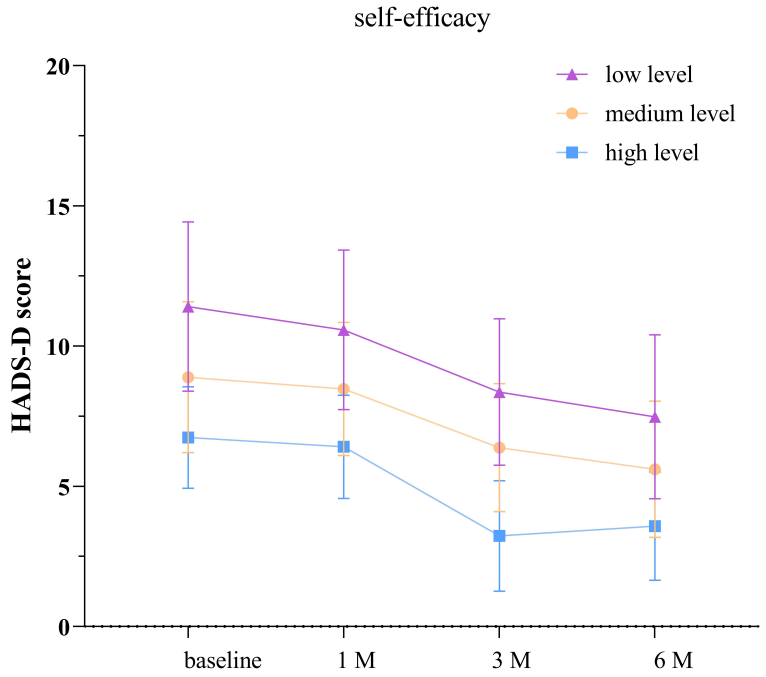

FIGURE 5
Depression scores in groups with different levels of self-efficacy. The baseline refers to the day of discharge. HADS-D: hospital anxiety and depression scale- depression score. The error bars indicate the standard deviation, the larger the error bars, the greater the variability or uncertainty in the data.

Additionally, research has reported gender-specific associations between CRP levels and symptoms of depression and anxiety, with significant positive correlations observed only in females (Yang et al., 2020). Therefore, further research in specific populations is necessary to explore the correlation between CRP levels in TBI patients and delirium, anxiety, and depression.

4.2 The relationship between insomnia, anxiety, and depression in patients with TBI

Our study indicates a close association between insomnia and anxiety symptoms following TBI, while its connection with depression remains unclear. In the general population, sleep issues and mental health problems often co-occur bidirectionally, a well-established phenomenon (Scott et al., 2021). However, in the context of TBI, poor sleep may be influenced by various mechanisms including severity of injury (Fichtenberg et al., 2000; Mahmood et al., 2004), location of injury (Leduc et al., 2007), post-injury physiological factors (e.g., biochemical changes due to injury) (Mathias and Alvaro, 2012), alterations in melatonin levels (Grima et al., 2016), and psychological factors (Fogelberg et al., 2012). These factors could potentially impact our study outcomes. Previous studies have shown that subjective poor sleep quality and insomnia in TBI patients are significantly associated with increased levels of depression and/or anxiety (Huang et al., 2013; Johnson et al., 2019). However, these associations were not consistently reported when objectively measuring sleep quality (El-Khatib et al., 2019; Botchway et al., 2019). These findings suggest inconsistency in objectively reporting sleep quality in relation to depression and anxiety. Future research in this population should include longitudinal tracking of sleep in TBI patients to understand changes in subjective and objective sleep quality and their relationship with psychopathology. Prompt identification of insomnia patients is essential to improve sleep quality and reduce anxiety. Timely identification of insomnia patients is essential to improve sleep quality and reduce anxiety.

4.3 The relationship between self-efficacy and anxiety/depression in patients with TBI

Higher levels of self-efficacy are negatively correlated with anxiety and depression. Enhancing self-efficacy in TBI patients may effectively improve their mental health in clinical practice. Consistent with previous research findings, patients with higher self-efficacy experience fewer emotional disturbances and enjoy a higher quality of life (Brands et al., 2015). The common-sense model of self-regulation suggests that when facing health threats, individuals navigate emotional responses to the threat, develop perceptions about the threat and potential therapeutic actions, formulate action plans to cope with the threat, and integrate continuous feedback on the effectiveness of their action plans and the progression of the threat (Leventhal et al., 2016). Other models of adaptation following acquired brain injury also emphasize the ongoing interaction between behavior and emotions, as well as the critical role of self-efficacy and coping in disease management (Brands et al., 2012). Brands et al. (2014) demonstrated that high self-efficacy in managing symptoms related to brain injury can prevent negative impacts of emotion-focused coping. This suggests that enhancing self-efficacy in patients may be a potential strategy for managing mental health issues following TBI. Research has already indicated that self-efficacy and quality of life improve following neuropsychological rehabilitation (Brands et al., 2017; Belanger et al., 2020). Hawley et al. (2022) employed a self-advocacy independent living (SAIL) program to enhance self-efficacy in TBI patients.

Future therapeutic approaches for anxiety and depression in TBI patients should explicitly focus on reinforcing patient self-belief to enhance self-efficacy.

4.4 Limitations

Despite revealing complex relationships between various factors and symptoms like anxiety, depression, delirium, sleep, and self-efficacy among TBI patients, our study has several limitations that must be considered. Firstly, the small sample size and short follow-up period may not capture all potential influencing factors, and selection bias among patients could affect the generalizability of the results. Secondly, identifying the independent impact of delirium still poses challenges, as this condition typically results from the interaction of multiple pathological factors (Maldonado, 2018). Thirdly, a significant proportion of the included population is male. Future research should aim to include more female participants to better represent the TBI population. Additionally, in this study, we only measured CRP, TNF-α, and IL-6 levels on day 1 post-injury. Future research should dynamically monitor serum inflammatory factors at multiple time points to clarify their effects on anxiety and depression. Given that only three mild TBI patients showed delirium, we could not perform subgroup analyses based on TBI classification. Therefore, it is unclear if the observed links between delirium and pain, sleep quality, and self-efficacy are due to differences in TBI classification. Lastly, approximately half of the patients in our study had comorbidities such as hypertension and diabetes, which could be a factor influencing cytokine levels in the studied patient group (Feng et al., 2022; Wang et al., 2024). Future studies could further expand our findings by validating them through larger-scale randomized controlled trials and delving deeper into the exact mechanisms of inflammation response in mental health issues post-TBI. Additionally, long-term follow-up studies could assess the prolonged impacts of these factors on the long-term mental health outcomes of TBI patients.

5 Conclusion

Our study identified significant correlations between younger age, underlying diseases, TBI classification, delirium, elevated CRP levels, lower self-efficacy, insomnia, and more severe anxiety symptoms. Conversely, there was no significant association between depression symptoms and delirium or insomnia, but significant relationships were found with serum CRP levels, TBI classification, and self-efficacy. In the future, serum CRP levels post-TBI hold promise as a biomarker to identify patients at risk for emotional symptoms. Additionally, comprehensive interventions targeting prevention and treatment of delirium, timely management of insomnia, and enhancement of patient self-efficacy could be promising strategies to improve mental health outcomes.

Data availability statement

The original contributions presented in the study are included in the article/Supplementary material, further inquiries can be directed to the corresponding author.

Ethics statement

The studies involving humans were approved by Biomedical Ethics Committee, Affiliated Hospital of Zunyi Medical University. The studies were conducted in accordance with the local legislation and institutional requirements. Written informed consent for participation in this study was provided by the participants' legal guardians/next of kin.

Author contributions

ZF: Conceptualization, Investigation, Software, Writing – original draft. XM: Writing – original draft, Writing – review & editing. XL: Data curation, Methodology, Software, Writing – review & editing. LY: Data curation, Formal analysis, Supervision, Writing – review & editing. YX: Investigation, Writing – review & editing. SH: Conceptualization, Supervision, Writing – review & editing.

Funding

The author(s) declare financial support was received for the research, authorship, and/or publication of this article. This work was supported by Zunyi City Science and Technology Plan Project: Zuncity Kehe HZ character (2023) No. 293.

Acknowledgments

The authors would like to express their gratitude to the staff who participated in this research.

Conflict of interest

The authors declare that the research was conducted in the absence of any commercial or financial relationships that could be construed as a potential conflict of interest.

Publisher's note

Supplementary material

The Supplementary Material for this article can be found online at: https://www.frontiersin.org/articles/10.3389/fnins.2024.1484777/full#supplementary-material

References

Ahmed, S., Venigalla, H., Mekala, H. M., Dar, S., Hassan, M., and Ayub, S. (2017). Traumatic brain injury and neuropsychiatric complications. *Indian J. Psychol. Med.* 39, 114–121. doi: 10.4103/0253-7176.203129

Bandura, A. (1977). Self-efficacy: toward a unifying theory of behavioral change. *Psychol. Rev.* 84, 191–215. doi: 10.1037/0033-295X.84.2.191

Barker-Collo, S., Theadom, A., Jones, K., Starkey, N., Kahan, M., and Feigin, V. (2018). Depression and anxiety across the first 4 years after mild traumatic brain injury: findings from a community-based study. *Brain Inj.* 32, 1651–1658. doi: 10.1080/02699052.2018.1540797

Bekkevold, O. J., Damås, J. K., Brumpton, B. M., and Åsvold, B. O. (2023). The causal role of C-reactive protein and interleukin-6 on anxiety and depression symptoms and life satisfaction: Mendelian randomisation analyses in the HUNT study. *Psychol. Med.* 53, 7561–7568. doi: 10.1017/S0033291723001290

Belanger, H. G., Vanderploeg, R. D., Curtiss, G., Armistead-Jehle, P., Kennedy, J. E., Tate, D. F., et al. (2020). Self-efficacy predicts response to cognitive rehabilitation in military service members with post-concussive symptoms. *Neuropsychol. Rehabil.* 30, 1190–1203. doi: 10.1080/09602011.2019.1575245

Botchway, E. N., Godfrey, C., Anderson, V., Nicholas, C. L., and Catroppa, C. (2019). Outcomes of subjective sleep-wake disturbances twenty years after traumatic brain injury in childhood. *J. Neurotrauma* 36, 669–678. doi: 10.1089/neu.2018.5743

Brands, I., Custers, M., and Van Heugten, C. (2017). Self-efficacy and quality of life after low-intensity neuropsychological rehabilitation: a pre-post intervention study. *NeuroRehabilitation* 40, 587–594. doi: 10.3233/NRE-171446

Brands, I., Köhler, S., Stapert, S., Wade, D., and Van Heugten, C. (2014). Influence of self-efficacy and coping on quality of life and social participation after acquired brain injury: a 1-year follow-up study. *Arch. Phys. Med. Rehabil.* 95, 2327–2334. doi: 10.1016/j.apmr.2014.06.006

Brands, I., Stapert, S., Köhler, S., Wade, D., and Van Heugten, C. (2015). Life goal attainment in the adaptation process after acquired brain injury: the influence of self-efficacy and of flexibility and tenacity in goal pursuit. *Clin. Rehabil.* 29, 611–622. doi: 10.1177/0269215514549484

Brands, I. M., Wade, D. T., Stapert, S. Z., and Van Heugten, C. M. (2012). The adaptation process following acute onset disability: an interactive two-dimensional approach applied to acquired brain injury. *Clin. Rehabil.* 26, 840–852. doi: 10.1177/0269215511432018

Brett, B. L., Gardner, R. C., Godbout, J., Dams-O'connor, K., and Keene, C. D. (2022). Traumatic brain injury and risk of neurodegenerative disorder. *Biol. Psychiatry* 91, 498–507. doi: 10.1016/j.biopsych.2021.05.025

Briones, T. L., and Woods, J. (2014). Dysregulation in myelination mediated by persistent neuroinflammation: possible mechanisms in chemotherapy-related cognitive impairment. *Brain Behav. Immun.* 35, 23–32. doi: 10.1016/j.bbi.2013.07.175

Capizzi, A., Woo, J., and Verduzco-Gutierrez, M. (2020). Traumatic brain injury: an overview of epidemiology, pathophysiology, and medical management. *Med. Clin. North Am.* 104, 213–238. doi: 10.1016/j.mcna.2019.11.001

Chaput, G., Giguère, J. F., Chauny, J. M., Denis, R., and Lavigne, G. (2009). Relationship among subjective sleep complaints, headaches, and mood alterations following a mild traumatic brain injury. *Sleep Med.* 10, 713–716. doi: 10.1016/j.sleep.2008.07.015

Christmas, D. M., Potokar, J., and Davies, S. J. (2011). A biological pathway linking inflammation and depression: activation of indoleamine 2, 3-dioxygenase. *Neuropsychiatr. Dis. Treat.* 431–439. doi: 10.2147/NDT.S17573

Dantzer, R., O'connor, J. C., Freund, G. G., Johnson, R. W., and Kelley, K. W. (2008). From inflammation to sickness and depression: when the immune system subjugates the brain. *Nat. Rev. Neurosci.* 9, 46–56. doi: 10.1038/nrn2297

Das, M., Mohapatra, S., and Mohapatra, S. S. (2012). New perspectives on central and peripheral immune responses to acute traumatic brain injury. *J. Neuroinflamm.* 9:236. doi: 10.1186/1742-2094-9-236

Diggle, P. (2002). *Analysis of Longitudinal Data*. Oxford: Oxford University Press.

Dikmen, S. S., Corrigan, J. D., Levin, H. S., Machamer, J., Stiers, W., and Weisskopf, M. G. (2009). Cognitive outcome following traumatic brain injury. *J. Head Trauma Rehabil.* 24, 430–438. doi: 10.1097/HTR.0b013e3181c133e9

Draper, K., and Ponsford, J. (2008). Cognitive functioning ten years following traumatic brain injury and rehabilitation. *Neuropsychology* 22, 618–625. doi: 10.1037/0894-4105.22.5.618

Draper, K., Ponsford, J., and Schönberger, M. (2007). Psychosocial and emotional outcomes 10 years following traumatic brain injury. *J. Head Trauma Rehabil.* 22, 278–287. doi: 10.1097/01.HTR.0000290972.63753.a7

Duan, K., Mayer, A. R., Shaff, N. A., Chen, J., Lin, D., Calhoun, V. D., et al. (2021). DNA methylation under the major depression pathway predicts pediatric quality of life four-month post-pediatric mild traumatic brain injury. *Clin. Epigenet.* 13:140. doi: 10.1186/s13148-021-01128-z

El-Khatib, H., Arbour, C., Sanchez, E., Dumont, M., Duclos, C., Blais, H., et al. (2019). Towards a better understanding of increased sleep duration in the chronic phase of moderate to severe traumatic brain injury: an actigraphy study. *Sleep Med.* 59, 67–75. doi: 10.1016/j.sleep.2018.11.012

Ely, E. W., Inouye, S. K., Bernard, G. R., Gordon, S., Francis, J., May, L., et al. (2001). Delirium in mechanically ventilated patients: validity and reliability of the confusion assessment method for the intensive care unit (CAM-ICU). *JAMA* 286, 2703–2710. doi: 10.1001/jama.286.21.2703

Ely, E. W., Truman, B., Shintani, A., Thomason, J. W., Wheeler, A. P., Gordon, S., et al. (2003). Monitoring sedation status over time in ICU patients: reliability and validity of the Richmond Agitation-Sedation Scale (RASS). *JAMA* 289, 2983–2991. doi: 10.1001/jama.289.22.2983

Fedoce, A. D. G., Ferreira, F., Bota, R. G., Bonet-Costa, V., Sun, P. Y., and Davies, K. J. (2018). The role of oxidative stress in anxiety disorder: cause or consequence? *Free Radic. Res.* 52, 737–750. doi: 10.1080/10715762.2018.1475733

Feng, L., Gao, Q., Hu, K., Wu, M., Wang, Z., Chen, F., et al. (2022). prevalence and risk factors of sarcopenia in patients with diabetes: a meta-analysis. *J. Clin. Endocrinol. Metab.* 107, 1470–1483. doi: 10.1210/clinem/dgab884

Fichtenberg, N. L., Millis, S. R., Mann, N. R., Zafonte, R. D., and Millard, A. E. (2000). Factors associated with insomnia among post-acute traumatic brain injury survivors. *Brain Inj.* 14, 659–667. doi: 10.1080/02699050050044015

Fogelberg, D. J., Hoffman, J. M., Dikmen, S., Temkin, N. R., and Bell, K. R. (2012). Association of sleep and co-occurring psychological conditions at 1 year after traumatic brain injury. *Arch. Phys. Med. Rehabil.* 93, 1313–1318. doi: 10.1016/j.apmr.2012.04.031

Ganau, M., Lavinio, A., and Prisco, L. (2018). Delirium and agitation in traumatic brain injury patients: an update on pathological hypotheses and treatment options. *Minerva Anestesiol.* 84, 632–640. doi: 10.23736/S0375-9393.18.12294-2

Gélinas, C., Fillion, L., Puntillo, K. A., Viens, C., and Fortier, M. (2006). Validation of the critical-care pain observation tool in adult patients. *Am. J. Crit. Care* 15, 420–427. doi: 10.4037/ajcc2006.15.4.420

Goodyear, M. D., Krleza-Jeric, K., and Lemmens, T. (2007). The declaration of Helsinki. *BMJ* 335, 624–625. doi: 10.1136/bmj.39339.610000.BE

Grima, N. A., Ponsford, J. L., St Hilaire, M. A., Mansfield, D., and Rajaratnam, S. M. (2016). Circadian melatonin rhythm following traumatic brain injury. *Neurorehabil. Neural Repair* 30, 972–977. doi: 10.1177/1545968316650279

Haroon, E., Raison, C. L., and Miller, A. H. (2012). Psychoneuroimmunology meets neuropsychopharmacology: translational implications of the impact of inflammation on behavior. *Neuropsychopharmacology* 37, 137–162. doi: 10.1038/npp.2011.205

Hawley, L., Morey, C., Sevigny, M., Ketchum, J., Simpson, G., Harrison-Felix, C., et al. (2022). Enhancing self-advocacy after traumatic brain injury: a randomized controlled trial. *J. Head Trauma Rehabil.* 37, 114–124. doi: 10.1097/HTR.0000000000000689

Huang, W., Bliwise, D. L., Johnson, T. M., Long, Q., Kutner, N., and Stringer, A. Y. (2013). Correlates of persistent sleep complaints after traumatic brain injury. *Neuropsychol. Rehabil.* 23, 698–714. doi: 10.1080/09602011.2013.803488

Hyder, A. A., Wunderlich, C. A., Puvanachandra, P., Gururaj, G., and Kobusingye, O. C. (2007). The impact of traumatic brain injuries: a global perspective. *NeuroRehabilitation* 22, 341–353. doi: 10.3233/NRE-2007-22502

Johnson, K. A., Gordon, C. J., and Grunstein, R. R. (2019). Somatic symptoms are associated with insomnia disorder but not obstructive sleep apnoea or hypersomnolence in traumatic brain injury. *NeuroRehabilitation* 45, 409–418. doi: 10.3233/NRE-192868

Juruena, M. F., Eror, F., Cleare, A. J., and Young, A. H. (2020). The role of early life stress in HPA axis and anxiety. *Adv. Exp. Med. Biol.* 1191, 141–153. doi: 10.1007/978-981-32-9705-0_9

Langlois, J. A., Rutland-Brown, W., and Wald, M. M. (2006). The epidemiology and impact of traumatic brain injury: a brief overview. *J. Head Trauma Rehabil.* 21, 375–378. doi: 10.1097/00001199-200609000-00001

Leduc, B. E., Dagher, J. H., Mayer, P., Bellemare, F., and Lepage, Y. (2007). Estimated prevalence of obstructive sleep apnea-hypopnea syndrome after cervical cord injury. *Arch. Phys. Med. Rehabil.* 88, 333–337. doi: 10.1016/j.apmr.2006.12.025

Lequerica, A. H., Weber, E., Dijkers, M. P., Dams-O'connor, K., Kolakowsky-Hayner, S. A., Bell, K. R., et al. (2020). Factors associated with the remission of insomnia after traumatic brain injury: a traumatic brain injury model systems study. *Brain Inj.* 34, 187–194. doi: 10.1080/02699052.2019.1682193

Leventhal, H., Phillips, L. A., and Burns, E. (2016). The Common-Sense Model of Self-Regulation (CSM): a dynamic framework for understanding illness self-management. *J. Behav. Med.* 39, 935–946. doi: 10.1007/s10865-016-9782-2

Lewin, A., Jöbges, M., and Werheid, K. (2013). The influence of self-efficacy, pre-stroke depression and perceived social support on self-reported depressive symptoms during stroke rehabilitation. *Neuropsychol. Rehabil.* 23, 546–562. doi: 10.1080/09602011.2013.794742

Longworth, C., Deakins, J., Rose, D., and Gracey, F. (2018). The nature of self-esteem and its relationship to anxiety and depression in adult acquired brain injury. *Neuropsychol. Rehabil.* 28, 1078–1094. doi: 10.1080/09602011.2016.1226185

Lozano-Vicario, L., García-Hermoso, A., Cedeno-Veloz, B. A., Fernández-Irigoyen, J., Santamaría, E., Romero-Ortuno, R., et al. (2023). Biomarkers of delirium risk in older adults: a systematic review and meta-analysis. *Front. Aging Neurosci.* 15:1174644. doi: 10.3389/fnagi.2023.1174644

Mahmood, O., Rapport, L. J., Hanks, R. A., and Fichtenberg, N. L. (2004). Neuropsychological performance and sleep disturbance following traumatic brain injury. *J. Head Trauma Rehabil.* 19, 378–390. doi: 10.1097/00001199-200409000-00003

Maldonado, J. R. (2018). Delirium pathophysiology: AN updated hypothesis of the etiology of acute brain failure. *Int. J. Geriatr. Psychiatry* 33, 1428–1457. doi: 10.1002/gps.4823

Malik, S., Alnaji, O., Malik, M., Gambale, T., and Rathbone, M. P. (2022). Correlation between mild traumatic brain injury-induced inflammatory cytokines and emotional symptom traits: a systematic review. *Brain Sci.* 12:102. doi: 10.3390/brainsci12010102

Marcantonio, E. R., Ngo, L. H., O'connor, M., Jones, R. N., Crane, P. K., Metzger, E. D., et al. (2014). 3D-CAM: derivation and validation of a 3-minute diagnostic interview for CAM-defined delirium: a cross-sectional diagnostic test study. *Ann. Intern. Med.* 161, 554–561. doi: 10.7326/M14-0865

Mathias, J. L., and Alvaro, P. K. (2012). Prevalence of sleep disturbances, disorders, and problems following traumatic brain injury: a meta-analysis. *Sleep Med.* 13, 898–905. doi: 10.1016/j.sleep.2012.04.006

McAfoose, J., and Baune, B. T. (2009). Evidence for a cytokine model of cognitive function. *Neurosci. Biobehav. Rev.* 33, 355–366. doi: 10.1016/j.neubiorev.2008.10.005

Moore, E. L., Terryberry-Spohr, L., and Hope, D. A. (2006). Mild traumatic brain injury and anxiety sequelae: a review of the literature. *Brain Inj.* 20, 117–132. doi: 10.1080/02699050500443558

Morganti-Kossmann, M. C., Semple, B. D., Hellewell, S. C., Bye, N., and Ziebell, J. M. (2019). The complexity of neuroinflammation consequent to traumatic brain injury: from research evidence to potential treatments. *Acta Neuropathol.* 137, 731–755. doi: 10.1007/s00401-018-1944-6

Murray, K. N., Buggey, H. F., Denes, A., and Allan, S. M. (2013). Systemic immune activation shapes stroke outcome. *Mol. Cell. Neurosci.* 53, 14–25. doi: 10.1016/j.mcn.2012.09.004

Osborn, A. J., Mathias, J. L., and Fairweather-Schmidt, A. K. (2014). Depression following adult, non-penetrating traumatic brain injury: a meta-analysis examining methodological variables and sample characteristics. *Neurosci. Biobehav. Rev.* 47, 1–15. doi: 10.1016/j.neubiorev.2014.07.007

Osimo, E. F., Pillinger, T., Rodriguez, I. M., Khandaker, G. M., Pariante, C. M., and Howes, O. D. (2020). Inflammatory markers in depression: a meta-analysis of mean differences and variability in 5,166 patients and 5,083 controls. *Brain Behav. Immun.* 87, 901–909. doi: 10.1016/j.bbi.2020.02.010

Piantino, J. A., Iliff, J. J., and Lim, M. M. (2022). The bidirectional link between sleep disturbances and traumatic brain injury symptoms: a role for glymphatic dysfunction? *Biol. Psychiatry* 91, 478–487. doi: 10.1016/j.biopsych.2021.06.025

Povlishock, J. T., and Katz, D. I. (2005). Update of neuropathology and neurological recovery after traumatic brain injury. *J. Head Trauma Rehabil.* 20, 76–94. doi: 10.1097/00001199-200501000-00008

Qin, L., Wu, X., Block, M. L., Liu, Y., Breese, G. R., Hong, J. S., et al. (2007). Systemic LPS causes chronic neuroinflammation and progressive neurodegeneration. *Glia* 55, 453–462. doi: 10.1002/glia.20467

Rao, V., Mccann, U., Han, D., Bergey, A., and Smith, M. T. (2014). Does acute TBI-related sleep disturbance predict subsequent neuropsychiatric disturbances? *Brain Inj.* 28, 20–26. doi: 10.3109/02699052.2013.847210

Rapoport, M. J., Kiss, A., and Feinstein, A. (2006). The impact of major depression on outcome following mild-to-moderate traumatic brain injury in older adults. *J. Affect. Disord.* 92, 273–276. doi: 10.1016/j.jad.2005.05.022

Rathbone, A. T., Tharmaradinam, S., Jiang, S., Rathbone, M. P., and Kumbhare, D. A. (2015). A review of the neuro- and systemic inflammatory responses in post

concussion symptoms: Introduction of the "post-inflammatory brain syndrome" PIBS. *Brain Behav. Immun.* 46, 1–16. doi: 10.1016/j.bbi.2015.02.009

Riggio, S. (2011). Traumatic brain injury and its neurobehavioral sequelae. *Neurol. Clin.* 29, 35–47, vii. doi: 10.1016/j.ncl.2010.10.008

Rimel, R. W., Giordani, B., Barth, J. T., and Jane, J. A. (1982). Moderate head injury: completing the clinical spectrum of brain trauma. *Neurosurgery* 11, 344–351. doi: 10.1227/00006123-198209000-00002

Roberson, S. W., Patel, M. B., Dabrowski, W., Ely, E. W., Pakulski, C., and Kotfis, K. (2021). Challenges of delirium management in patients with traumatic brain injury: from pathophysiology to clinical practice. *Curr. Neuropharmacol.* 19, 1519–1544. doi: 10.2174/1570159X19666210119153839

Rocca, G., Caputo, F., Frigiolini, F. M. E., Verde, A., and Ventura, F. (2019). Delirium resulting from traumatic brain injury as an acute risk factor for suicide: a case report and review of the literature. *J. Neuropsychiatry Clin. Neurosci.* 31, 86–88. doi: 10.1176/appi.neuropsych.18080172

Saravanan, K., Downey, L., Sawyer, A., Jackson, M. L., Berlowitz, D. J., and Graco, M. (2024). Understanding the relationships between sleep quality and depression and anxiety in neurotrauma: a scoping review. *J. Neurotrauma* 41, 13–31. doi: 10.1089/neu.2023.0033

Schafer, J. L. (1997). *Analysis of Incomplete Multivariate Data* (1st ed.). New York, NY: Chapman and Hall/CRC. doi: 10.1201/9780367803025

Scholten, A. C., Haagsma, J. A., Cnossen, M. C., Olff, M., Van Beeck, E. F., and Polinder, S. (2016). Prevalence of and risk factors for anxiety and depressive disorders after traumatic brain injury: a systematic review. *J. Neurotrauma* 33, 1969–1994. doi: 10.1089/neu.2015.4252

Schwarzer, R., Jerusalem, M., and Juczyński, Z. (2009). The general self-efficacy scale (GSE). *Anxiety, Stress, Coping* 12, 329–345.

Scott, A. J., Webb, T. L., Martyn-St James, M., Rowse, G., and Weich, S. (2021). Improving sleep quality leads to better mental health: a meta-analysis of randomised controlled trials. *Sleep Med. Rev.* 60:101556. doi: 10.1016/j.smrv.2021.101556

Sherer, M., Katz, D. I., Bodien, Y. G., Arciniegas, D. B., Block, C., Blum, S., et al. (2020). Post-traumatic confusional state: a case definition and diagnostic criteria. *Arch. Phys. Med. Rehabil.* 101, 2041–2050. doi: 10.1016/j.apmr.2020.06.021

Silva-Fernandes, A., Conde, A., Marques, M., Caparros-Gonzalez, R. A., Fransson, E., Mesquita, A. R., et al. (2024). Inflammatory biomarkers and perinatal depression: a systematic review. *PLoS ONE* 19:e0280612. doi: 10.1371/journal.pone.0280612

Soldatos, C. R., Dikeos, D. G., and Paparrigopoulos, T. J. (2000). Athens Insomnia Scale: validation of an instrument based on ICD-10 criteria. *J. Psychosom. Res.* 48, 555–560. doi: 10.1016/S0022-3999(00)00095-7

Su, S. H., Xu, W., Li, M., Zhang, L., Wu, Y. F., Yu, F., et al. (2014). Elevated C-reactive protein levels may be a predictor of persistent unfavourable symptoms in patients with mild traumatic brain injury: a preliminary study. *Brain Behav. Immun.* 38, 111–117. doi: 10.1016/j.bbi.2014.01.009

Sun, Y., Bai, L., Niu, X., Wang, Z., Yin, B., Bai, G., et al. (2019). elevated serum levels of inflammation-related cytokines in mild traumatic brain injury are associated with cognitive performance. *Front. Neurol.* 10:1120. doi: 10.3389/fneur.2019.01120

Teasdale, G., and Jennett, B. (1976). Assessment and prognosis of coma after head injury. *Acta Neurochir.* 34, 45–55. doi: 10.1007/BF01405862

Tsigos, C., and Chrousos, G. P. (2002). Hypothalamic-pituitary-adrenal axis, neuroendocrine factors and stress. *J. Psychosom. Res.* 53, 865–871. doi: 10.1016/S0022-3999(02)00429-4

Uiterwijk, D., Stargatt, R., Humphrey, S., and Crowe, S. F. (2022). The relationship between cognitive functioning and symptoms of depression, anxiety, and post-traumatic stress disorder in adults with a traumatic brain injury: a meta-analysis. *Neuropsychol. Rev.* 32, 758–806. doi: 10.1007/s11065-021-09524-1

Vasunilashorn, S. M., Dillon, S. T., Inouye, S. K., Ngo, L. H., Fong, T. G., Jones, R. N., et al. (2017). High C-reactive protein predicts delirium incidence, duration, and feature severity after major noncardiac surgery. *J. Am. Geriatr. Soc.* 65, e109–e116. doi: 10.1111/jgs.14913

Volz, M., Möbus, J., Letsch, C., and Werheid, K. (2016). The influence of early depressive symptoms, social support and decreasing self-efficacy on depression 6 months post-stroke. *J. Affect. Disord.* 206, 252–255. doi: 10.1016/j.jad.2016.07.041

von Elm, E., Altman, D. G., Egger, M., Pocock, S. J., Gøtzsche, P. C., and Vandenbroucke, J. P. (2007). The Strengthening the Reporting of Observational Studies in Epidemiology (STROBE) statement: guidelines for reporting observational studies. *Lancet* 370, 1453–1457. doi: 10.1016/S0140-6736(07)61602-X

Wang, C., Li, S., Song, Y., Yuan, X., Zhu, H., and Yu, B. (2024). Prospective association of comorbid hypertension and depressive symptoms with C-reactive protein in older adults. *J. Affect. Disord.* 354, 286–292. doi: 10.1016/j.jad.2024.03.066

Wium-Andersen, M. K., Ørsted, D. D., Nielsen, S. F., and Nordestgaard, B. G. (2013). Elevated C-reactive protein levels, psychological distress, and depression in 73, 131 individuals. *JAMA Psychiatry* 70, 176–184. doi: 10.1001/2013.jamapsychiatry.102

Yang, Q. Q., Shao, D., Li, J., Yang, C. L., Fan, M. H., and Cao, F. L. (2020). Positive association between serum levels of high-sensitivity C-reactive protein and depression/anxiety in female, but not male, patients with type 2 diabetes mellitus. *Biol. Res. Nurs.* 22, 178–187. doi: 10.1177/1099800419894641

Zahniser, E., Nelson, L. D., Dikmen, S. S., Machamer, J. E., Stein, M. B., Yuh, E., et al. (2019). The temporal relationship of mental health problems and functional limitations following mTBI: A TRACK-TBI and TED study. *J. Neurotrauma* 36, 1786–1793. doi: 10.1089/neu.2018.6172

Zigmond, A. S., and Snaith, R. P. (1983). The hospital anxiety and depression scale. *Acta Psychiatr. Scand.* 67, 361–370. doi: 10.1111/j.1600-0447.1983.tb09716.x

frontiers | Frontiers in Neuroscience

TYPE Hypothesis and Theory
PUBLISHED 06 November 2024
DOI 10.3389/fnins.2024.1479830

OPEN ACCESS

EDITED BY
Pradeep Kumar,
All India Institute of Medical Sciences, India

REVIEWED BY
Eun-Jin Bae,
Seoul National University, Republic of Korea
Xing-Jun Liu,
Nantong University, China

*CORRESPONDENCE
Athanasia Alexoudi
✉ a.alexoudi@nioa.gr

RECEIVED 12 August 2024
ACCEPTED 21 October 2024
PUBLISHED 06 November 2024

CITATION
Alexoudi A, Donadio V and Karageorgiou E (2024) The potential role of CGRP in synuclein-associated neurodegenerative disorders. *Front. Neurosci.* 18:1479830. doi: 10.3389/fnins.2024.1479830

The potential role of CGRP in synuclein-associated neurodegenerative disorders

Athanasia Alexoudi[1]*, Vincenzo Donadio[2] and Elissaios Karageorgiou[1]

[1]Neurological Institute of Athens, Athens, Greece, [2]IRCCS Institute of Neurological Sciences of Bologna, Bologna, Italy

In this hypothesis article, the potential clinicopathological associations of Calcitonin Gene Related Peptide (CGRP) with the development of synuclein-associated neurodegenerative disorders (SAND) are discussed. The presence of α-syn and CGRP in the CNS and the ENS and the intricate role of CGRP and its related pathways in inflammation, apoptosis, metabolism, neuromodulation, and brain-gut communication are analyzed. Since this hypothesis is confirmed, modulating CGRP-potential related pathways may lead to novel disease-modifying therapies.

KEYWORDS

CGRP, synuclein-associated neurodegenerative disorders, neuroinflammation, GLP-1, apoptosis, neuromodulation

1 Introduction

1.1 Overview of SAND

SAND are defined by aggregates of abnormally misfolded α-synuclein (α-syn) in the peripheral and central nervous systems, which cumulatively refer to Parkinson's disease (PD), Lewy body degeneration (LBD), and multiple system atrophy (MSA) pathologies (Lim et al., 2016). A special case of SAND is Pure Autonomic Failure (PAF) where α-syn aggregates are almost exclusively observed in the autonomic nerves of the peripheral nervous system. Differences in the macroscopic distribution and microscopic features of α-syn are associated with different clinical SAND phenotypes. Typical microscopic features in SAND are intracellular α-syn inclusions [Lewy bodies (LBs)] deposited in neurons [Lewy neurites (LNs)], present in LBD and PD, and also in brain glial cells and skin Remak non-myelinating Schwann cells in MSA (Lim et al., 2016; Donadio et al., 2023). Even more, dopaminergic neuronal loss in the substantia nigra pars compacta (SNpc) is observed across SAND, explaining common symptoms of parkinsonism. The aggregation and spread of α-syn are associated with disease severity and prognosis (Stewart et al., 2015; Lim et al., 2016), explaining the high morbidity and mortality (1.75–3.86 higher mortality risk in PD, 3.94 in LBD, and 10.51 in MSA) (Savica et al., 2017).

1.2 Role of neuroinflammation

For the past 30 years there is accumulating evidence that neuroinflammation is associated with the PD pathological processes, from which the following main narratives have emerged. First, early studies indicated the activation of microglial cells and infiltration of T lymphocytes in brain regions with pathological α-syn accumulation in patients with PD. Second, modified cellular immunity changes in monocytes and T lymphocytes have been described in peripheral

blood, including increased phagocytic capacity, decreased effector CD8+ T cells and lower cytotoxicity natural killer (NK) cells. These inflammatory mechanisms have been supported by the increased expression of proinflammatory cytokines in blood, cerebrospinal fluid, and brain tissue. Third, examining the inflammasome's integral role in inflammatory mechanisms, α-syn has been shown to contribute to inflammasome activation (Codolo et al., 2013). Fourth, genes mediating immune responses have been associated with presence of PD (including LRRK2, DJ-1, PINK1, GBA, SNCA, PARK2, MAPT, ER β, PDLIM2, STK39, DYRK1A), strengthening the neuroinflammation theory. The above, however, have not verified a specific pathophysiological sequence of events through which inflammation triggers PD (Kung et al., 2022). Considering that CGRP modulates lymphocyte activity, and that CGRP and its related pathways are known to contribute to inflammation in other conditions, we postulate that CGRP pathways are also critical in inflammatory-driven SAND pathology, although dedicated studies in SAND are lacking. As we expand on below, CGRP belongs to the calcitonin family of peptides and is widely expressed in neuronal tissue (Wimalawansa et al., 1990). CGRP receptor binding leads to activation of multiple signaling pathways with downstream effects, where their modulation could prove causal to neurodegeneration (Umoh et al., 2014). In the case of Alzheimer's disease, it has been suggested that exogenous administration of CGRP inhibits tissue infiltration of macrophages and expression of various inflammatory mediators, which in turn attenuate inflammatory responses (Singh et al., 2017). Therefore, from a bird's eye view, the potentially protective role of CGRP and its related pathways in SAND deserve further examination.

In this hypothesis article we will discuss the clinicopathological associations of Calcitonin Gene Related Peptide (CGRP) and synuclein-associated neurodegenerative disorders (SAND). CGRP is a key molecule in inflammatory processes, with the development of SAND, suggesting novel disease-modifying therapeutic pathways worth examining. This follows on recent research supporting neuroinflammatory processes as key players in the pathogenesis of SAND (Lim et al., 2016).

2 CGRP structure and physiologic pathways

2.1 CGRP structure

CGRP expression is abundant across tissues, including neuronal tissue (Russell et al., 2014). There are two major CGRP isoforms, α and βCGRP or CGRPI and II. They differ by only three amino acids in rats and by one in humans, and although they have similar structure and biological activities, they are synthesized from different genes at different sites on chromosome 11 (Wimalawansa et al., 1990). Functional comparisons indicate that αCGRP is severalfold more immunoreactive compared to its β isoform (Schulz et al., 1999; Schütz et al., 2004). αCGRP is formed via alternative splicing of the calcitonin/CGRP gene. It is widely expressed in neuronal tissue and is primarily localized on C and Aδ sensory fibers. βCGRP is produced from its own second human calcitonin gene (hCGRP-II, or CALC II). CGRP is a multifunctional peptide with high vasodilation potential (Russell et al., 2014). Historically, αCGRP has been presumed to exist in both the central and peripheral nervous systems (CNS and PNS), whereas βCGRP to exist predominantly in the enteric nervous system (ENS). It has become clear, however, that both isoforms are expressed in the CNS and ENS (Russell et al., 2014). This common theme of CGRP and pathologic α-syn being expressed in the CNS and the ENS was one of the triggers in examining their potential relationship.

The two isoforms bind to the CGRP receptor, which is composed of two subunits. The "calcitonin receptor-like receptor" (CLR), discovered in early 1990s, which is unresponsive to CGRP binding on its own (Chang et al., 1993; Russell et al., 2014). As such, another protein co-expressed with CLR is required to effect CGRP binding and is known as the "receptor activity modifying protein" (RAMP). Three RAMPs have been recognized (RAMP1, RAMP2, RAMP3). The resulting heterodimeric complex of CLR and RAMP in the cell membrane is stable. The receptor composed of CLR and RAMP1 has high affinity for CGRP. Instead, the CLR/RAMP2 (AM1 receptor) and CLR/RAMP3 (AM2 receptor) combinations respond to the adrenomedullin peptide, of which the AM2 receptor shows affinity for CGRP as well (Choksi et al., 2002). Even when CLR/RAMP are combined, the CGRP receptor is not functional without the mediation of a third protein; the receptor component protein (RCP). Although the absence of RCP has no effect on CGRP binding affinity, downstream signal transduction is attenuated (Evans et al., 2000).

2.2 Production and release of CGRP

Despite extensive research to date, the process of CGRP synthesis and release is not fully clarified. It is suggested that CGRP is produced in both the CNS and PNS, and its synthesis is promoted after nerve damage and inflammatory responses (Saito et al., 2022). In the CNS, it is suggested that CGRP is synthesized in the anterior horn of the spinal cord and the cell bodies of motor neurons (Evangelista, 2013). It is postulated that nerve growth factor (NGF) released from cells such as macrophages and keratinocytes, as well as other factors, such as brain-derived neurotrophic factor (BDNF), participate in the process (Salio et al., 2007). In the PNS, there is evidence that CGRP release is mediated through transient receptor potential vanilloid 1 (TRPV1, also known as the capsaicin receptor and the vanilloid receptor 1) and TRP ankyrin 1 (TRPA1) activity, which in turn are dependent on Protease Activated Receptor 2 (PAR2) activation during inflammatory processes (Saito et al., 2022). Once CGRP is produced, it is stored in vesicles located at the sensory nerve terminal (Matteoli et al., 1988). Besides peripheral neurons, different types of immune cells (activated B-lymphocytes, mononuclear cells, and macrophages) can produce CGRP, suggesting an additional possible mechanism of immune response down-regulation (Linscheid et al., 2004).

2.3 Receptor activation

Binding of CGRP to the CLR/RAMP1 receptor leads to receptor activation and coupling to Gαs, Gαi/o or Gαq/11 proteins resulting in downstream effects as depicted in Figure 1.

Gαs and Gαi families regulate adenylyl cyclase (AC) activity. The Gαs family stimulates, while Gαi/o exerts an inhibitory effect. Vasodilation, inflammation, and gene transcription are regulated through a direct Gαs protein pathway (Saito et al., 2022; Rysiewicz et al., 2023). The CGRP receptor-induced crosstalk between PI3K/Akt

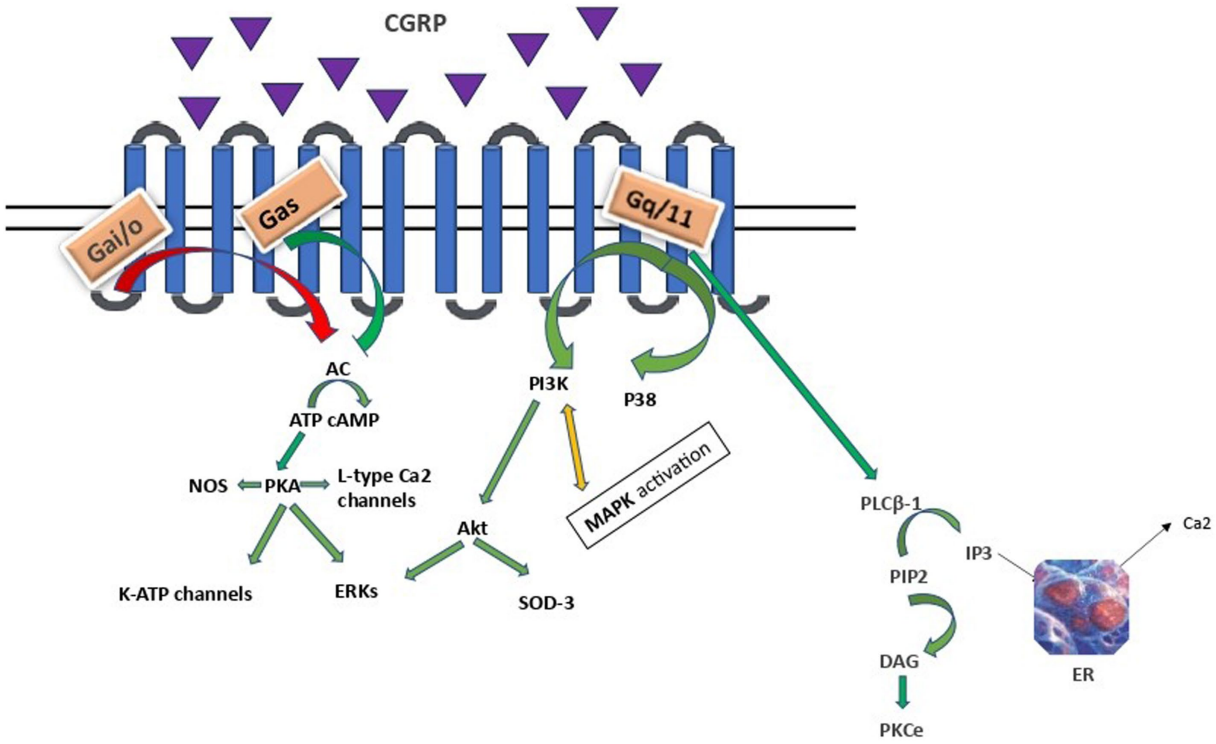

FIGURE 1
CGRP intracellular signalling. AC, adenylyl cyclase; cAMP, cyclic adenosine monophosphate; PKA, protein kinase A; ERKs, extracellular signal-related kinases; PLCB-1, phosphoinositide-phospholipase CB 1; PIP2, phosphatidylinositol 4,5-bisphosphate, IP3, inositol trisphosphate; DAG, diacylglycerol; PKCe, protein kinase C epsilon type, PI3K/Akt, Phosphoinositide 3- kinase/Protein kinase B; MAPK, mitogen - activated protein kinase; SOD3, superoxide dismutase 3; ER, endoplasmic reticulum. Arrows: green: facilitation, red: inhibition, orange: conflicting association.

and ERK, leading to decreased Akt, NFkB, and SOD-3, as well as increased ERK1/2 and p38 MAPK expressions, suggests that CGRP weakens anti-apoptotic and strengthens proliferative signaling pathways in an Akt/ERK-dependent manner (Umoh et al., 2014). Specifically, Akt regulates neuronal toxicity and mediates neuronal survival through the PI3K signaling pathway. ERK is a kinase and once phosphorylated can promote different processes in different cellular targets under particular conditions, such as neural differentiation, migration, apoptosis and neurogenesis. Apparently, PI3K/Akt and ERK pathways play opposite roles in the prevention of neuronal apoptosis. Besides, α-syn promotes inflammation via activating p38 and ERK in human microglial cells. Therefore, these proteins and their related pathways play a vital role in the pathogenesis of neurodegenerative diseases, including PD (Rai et al., 2019; Albert-Gascó et al., 2020). Finally, CGRP activation of the Gαq/11-dependent pathway generates inositol trisphosphate (IP3) and diacylglycerol (DAG). DAG activates and anchors PKC to the plasma membrane, whereas IP3 diffuses to the endoplasmic reticulum (ER), toward the release of calcium in the cytoplasm (Cottrell, 2019).

2.4 Internalization and desensitization

The aforementioned CGRP receptor signaling is modulated by CGRP internalization and CGRP receptor/b-arrestin complex desensitization and trafficking. Specifically, early studies on desensitization revealed that signaling was attenuated after a second exposure to CGRP, where the CLR component of the receptor is phosphorylated and internalized through the participation of arrestin, clathrin, and G protein–coupled receptor kinases (Walker et al., 2010).

Interestingly, there seem to be different acute and chronic effects of CGRP on inflammation. In acute peripheral inflammation, increased synthesis of CGRP is present, attenuating in chronic phase (Liu et al., 2012). We hypothesize that this difference is partially explained by the duration of CGRP receptor stimulation. Acute stimulation induces CLR/RAMP1 receptor recycling, correlated with resensitization, whereas chronic stimulation leads the CGRP receptors to degradation by lysosomes (Cottrell et al., 2007).

CGRP role as a biomarker in the field of pain is substantial. Cytokine activin C mainly expressed in small diameter dorsal root ganglion (DRG) neuron, significantly influences the release of calcitonin gene-related peptide (CGRP) in the nervous system, particularly following peripheral nerve injury. It appears to enhance CGRP release through its interaction with TRPV1, as evidenced by the loss of analgesic effects in TRPV1 knockout mice. The normalized data on CGRP support the idea that activin C plays a complex role in modulating chronic neuropathic pain, and its action is linked to inhibiting pro-inflammatory mediator-induced ERK phosphorylation. Moreover, activin C levels are reduced during early persistent inflammation, but its intrathecal application can effectively inhibit inflammation-induced hyperalgesia (Zhang et al., 1994; Liu et al., 2012; Huang et al., 2020; Chen et al., 2024).

3 Supposed CGRP mechanisms involved in sand

There are five main CGRP pathophysiological mechanisms that can have an effect on SAND pathology (Figure 2): (a) neuroinflammatory, (b) anti-apoptotic and proliferative, (c) metabolic, (d) neuromodulatory, and (e) anti-microbial. Of these mechanisms, most data explain CGRP-related neuroinflammatory processes in SAND, which also overlap with the other mechanisms. Although there is evidence of potentially beneficial treatments across specific CGRP pathways, targeting CGRP pathways upstream may allow for more impactful multi-pathway effects as we discuss below.

3.1 CGRP, Neuroinflammation, and SAND

A key mechanism through which CGRP mediates its effect is by modulating neuroinflammatory pathways. Neuroinflammation has been implicated in the triggering and evolution of pathological changes in many neurodegenerative diseases, including PD (Lim et al., 2016). Key inflammatory processes involve the excessive activation of microglia, especially through NOD-, LRR-, and pyrin domain-containing protein 3 (NLRP3) inflammasome pathways, which have been observed in tissues collected from patients with SAND (Haque et al., 2020). It follows that downstream anti-inflammatory interventions have been considered in delaying PD progression, albeit without any definite benefits from clinical trials to-date (Hung and Schwarzschild, 2020). Within this framework, studies support CGRP having anti-inflammatory properties through CD8 proliferation, and NK killing activity inhibition, production of mononuclear phagocyte promotion, macrophage regulation, especially microglia, and NLRP3 inflammasome inhibition (Zhu et al., 2023).

3.1.1 Microglia in SAND

Microglia, the resident immune cells of the brain, fulfil a variety of different tasks within the central nervous system (CNS) and display several different characteristics across resting (non-phagocytic) and activated (phagocytic) states (Wake et al., 2009). Resting microglia contact neuronal synapses, undergo transformation similar to that of macrophages, and respond to stimuli such as neuronal death (Wake et al., 2009). The activation of microglia through distinct signaling pathways is responsible for both their beneficial effect on clearance and blocking of detrimental inflammation, as well as for cascades contributing to neurodegeneration. This differential modulation of microglia explains existing controversies on their role in neurodegeneration (Lim et al., 2016). Research over the last decade revealed their contribution as both an active and re-active player in neurodegeneration, highlighting the significance of developing selective microglia-mediated treatment interventions that either inhibit or enhance neurodegenerative pathways, rather than pursuing non-specific inhibition of microglia. Microglia are activated as a response to extracellular stimuli, including endotoxins, cytokines, chemokines, mis-folded proteins, and ATP. With regards to SAND, it is possible that microglia activation follows systemic infection (e.g., Western equine encephalitis virus, Japanese-encephalitis, bacterial infections) or exposure to factors which promote oxidative stress (Wake et al., 2009). Beyond the aforementioned stimuli, microglia are triggered from α-syn into activating inflammatory pathways. Specifically, α-syn exists either as monomeric or fibrillar form in the brain. Under certain conditions, α-syn secretion leads to the increase of misfolded and/or aggregated proteins, which have been typically associated with direct neurotoxicity via impaired vesicle recycling, endoplasmic reticulum transport, mitochondrial energy production, and protein degradation (Haque et al., 2020). In addition to direct α-syn neurotoxicity, an indirect α-syn-induced neurodegeneration pathway involves microglial activation towards inflammation. In this pathway, neuron-secreted α-syn binds on microglial Toll-like receptor 2 (TLR2), facilitating their activation with secretion of cytokines and chemokines, leading to inflammation and neurotoxicity (Figure 3). Additionally, TLR4 is also involved in these pathways, where it has been suggested it mediates both microglial and astrocytic α-syn-dependent activation toward α-syn clearance (Fellner et al., 2013). Subsequent to α-synuclein uptake, multiple inflammatory signaling pathways are activated in microglia, with more prominent the critical dopamine receptor- mediated NLRP3 inflammasome pathway, which leads to neuroinflammation and subsequent neurodegeneration. Across cells, microglia and peripheral macrophages are the main cell types responsible for inflammasome activation, further explaining their critical role in inflammation-mediated disorders (Martinon et al., 2002). Considering the above microglial effects on SAND, study results suggest that exogenous administration of CGRP inhibits infiltration of macrophages and expression of various inflammatory mediators, raising the possibility of CGRP receptor stimulation becoming a potential target for SAND therapy (Singh et al., 2017).

3.1.2 The role of the inflammasome in SAND

Inflammasomes are a group of cytosolic multiprotein complexes of the innate immune system that activate inflammatory caspases, allowing for the release of cytokines and alarmins into circulation and inducing pyroptosis, a type of inflammatory programmed cell death. Each inflammasome consists of three components (Figure 3): (1) a nucleotide-binding domain and leucine-rich repeat receptor (NLR) [or an absent in melanoma 2-like receptor (ALR) in the special case of melanoma], (2) an adaptor component named Apoptosis-Associated Speck-like Protein Containing a Caspase Activation and Recruitment Domain (ASC), and (3) an effector component named pro-caspase 1. The inflammasome complex achieves cytosolic sensing of pathogen (or danger)-associated molecular patterns via the NLR (or ALR). At least five different types of NLRs have been recognized as inflammasome components, and naming of an inflammasome has conventionally been defined by their NLR component. NLR protein complexes (NLRP) have different subtypes depending on the differential combination of their components. Of all NLRPs, NLRP3 is the best studied inflammasome involved in human diseases. The ASC is usually recruited by activated NLR (and ALR) toward engaging caspase-1 activation. Finally, pro-caspase 1 activation to caspase 1 leads to the secretion of proinflammatory cytokines (Martinon et al., 2002). Activation of the inflammasome is responsible for inflammatory responses by promoting proteolytic cleavage, maturation, and secretion of pro-inflammatory cytokines interleukin 1β (IL-1β) and IL-18, and eventually pyroptosis (Figure 3) (Martinon et al., 2002).

When examining the inflammasome role in SAND, monomeric and fibrillar α-syn released by degenerating neurons into the extracellular space are first recognized by microglial TLR, and thus activate the NF-κB pathway and the production of IL-1β precursor protein. However, only fibrillar α-syn induces the NLRP3 response,

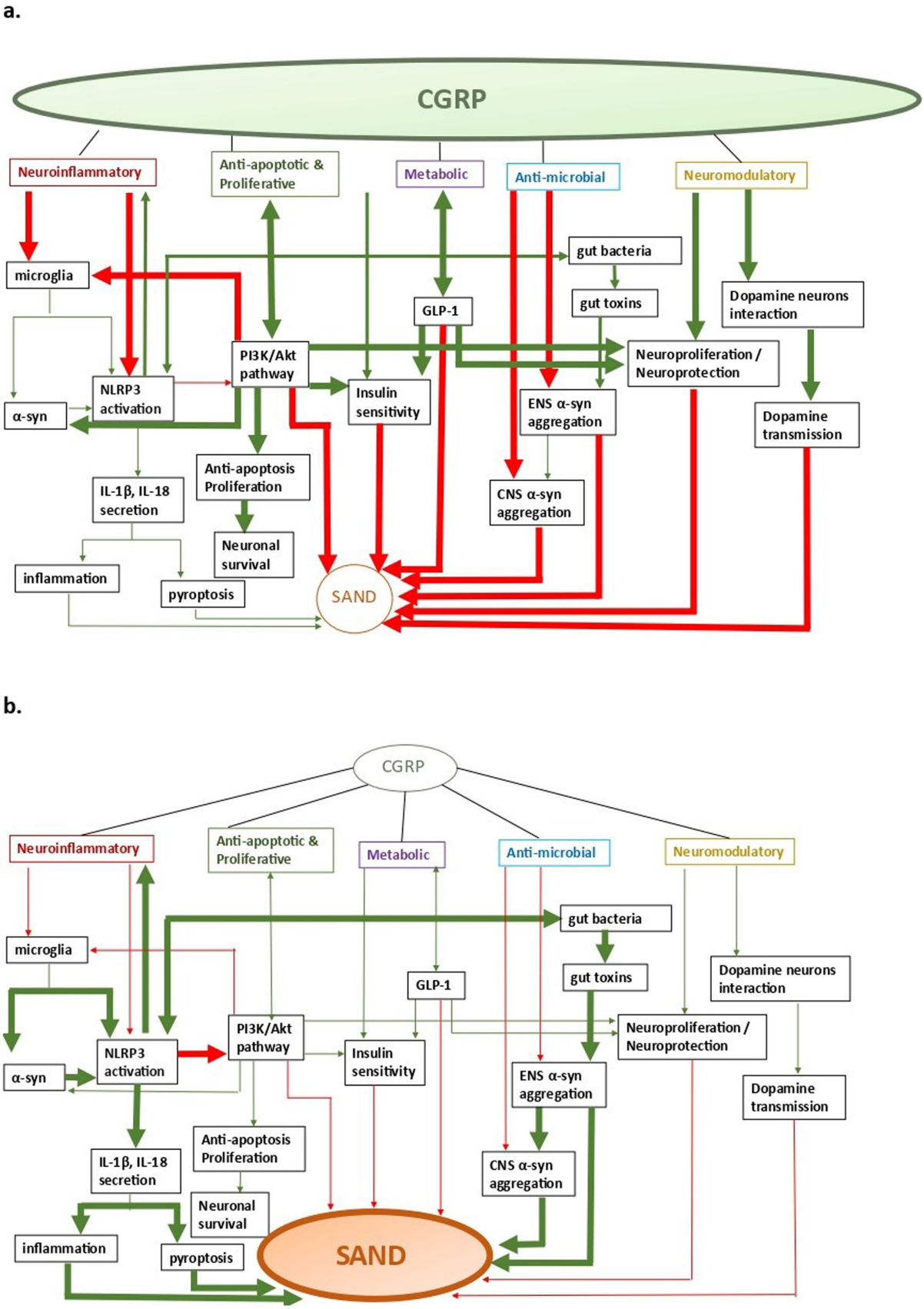

FIGURE 2
CGRP-related pathways in SAND; a. CGRP-pathway activation, b. SAND evolution (a) neuroinflammatory, (b) anti-apoptotic and proliferative, (c) metabolic, (d) anti- microbial, and (e) neuromodulatory. Arrows: green: facilitation, red: inhibition.

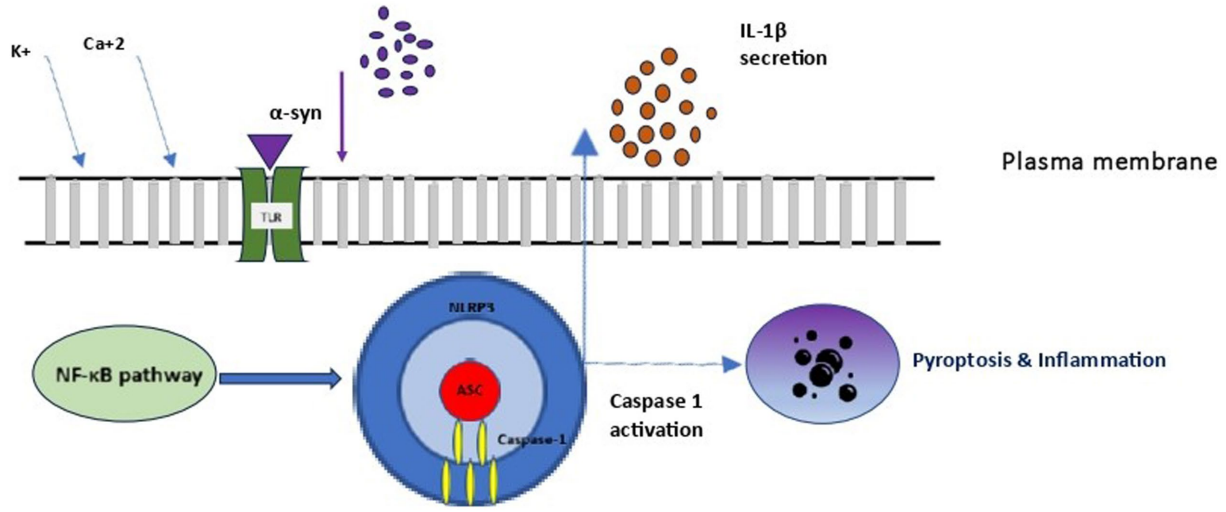

FIGURE 3
Microglial NLRP3 inflammasome activation. NLRP3, NOD-LRR- and PYD-containing protein 3; PC1: procaspase 1; ASC, apoptosis associated speck-like protein containing a CARD.

which acts as an endogenous trigger that activates microglial cells and induces a strong inflammatory response and pyroptosis in SAND (Codolo et al., 2013). In a vicious cycle, the extracellular secretion of mature IL-1β leads to inflammatory damage and death to dopamine neurons in the substantia nigra, as demonstrated in a murine model (Ferrari et al., 2006). Although the exact pathophysiology of this process is unclear, the secretion of mature IL-1β by the activated inflammasome leads to pyroptosis, during which, IL-1β is also secreted, further accentuating inflammation. To the above microglial-mediated process, both astrocytes and peripheral immune cells that enter the central nervous system participate in and amplify the core microglial-mediated inflammatory response. MCC950 is a well-known NLRP3 inhibition factor, which suppressing NLRP3 activity allows inflammation reduction and neurons' protection in the substantial nigra in experimental models (Cheng et al., 2020).

Studies from the field of Diabetes Mellitus (DM) directly link NLRP3 and CGRP-related pathways, where NLRP3 activation (e.g., via reactive oxygen species) and consequent IL-1β production have been shown to affect receptor resistance and apoptosis in DM models (Guo et al., 2015). It has been demonstrated that IL-1β activation leads to disrupted PI3K-Akt signaling, as well as increased TNF-α, in insulin-targeted cells by decreasing insulin sensitivity and inducing JNK-dependent serine phosphorylation of insulin receptor substrate-1 (IRS-1) (Wen et al., 2011). IL-1β also leads to pancreatic β-cell loss in DM. The inverse effects have been observed in animal models exposed to a high-fat diet where deficiency of NLRP3, ASC, and/or caspase-1 lead to reduced inflammatory cytokine levels, increased insulin-PI3K-Akt signaling, and improved glucose tolerance and insulin sensitivity (Vandanmagsar et al., 2011; Wen et al., 2011). CGRP is a B-cell growth factor and probably an inhibitory factor for insulin secretion (Manaka et al., 1998). Additionally, as we discussed above, CGRP is known to lead to similar downstream effects in PI3K-Akt signaling, but there are no known studies in SAND on dopaminergic neurons or α-syn pathology. By extension, the fact that patients with DM are 40% more likely to develop PD is further suggestive of their common pathophysiological pathways, including inflammasome activation.

Overall, a crosstalk between CGRP and NLRP3 seems to be at play. The NLRP3 inflammasome triggers the CGRP increase and therefore blockade of NLRP3 or IL-1β reduces the upregulation of CGRP and attenuates expression of the neuronal activation marker p-ERK in the CNS (He et al., 2019). Conversely, CGRP directly inhibits NLRP3 activation, as typically seen in bacterial infections. Cytosolic CGRP binds directly to NLRP3 and inhibits any downstream inflammatory response (Zhu et al., 2023).

A more recently identified mechanism through which NLRP3 participates in inflammation is through the gut-brain axis, where NLRP3 is modulated by gut bacteria. It has been proposed that altered composition of enteric microbiota may lead to dysbiosis and promote inflammation via gut-brain communication. The involvement of the enteric plexus in PD justifies further studies to assess if an altered microbiome truly contributes to the degenerative process.

In a more traditional approach, the close relationship between inflammasome activation and SAND is corroborated by a series of studies that examined biosamples from patients with PD. Specifically, NLRP3 has comparatively higher activation in serum samples of patients with PD compared to controls. This activation is modulated by genetic variations of NLRP3 single-nucleotide polymorphisms (SNPs), impacting the progression of PD (von Herrmann et al., 2018). In keeping with the above, patients with PD also have higher levels of IL-1β and IL-18 in serum and cerebrospinal fluid compared to controls (Zhang et al., 2016). Even more, and of clinical significance, higher levels of IL-1β and total plasma α-syn have been associated with worse motor function in PD (Fan et al., 2020). Beyond PD, the density of microglia expressing NLRP3 inflammasome-related proteins have been significantly upregulated in the putamen of patients with MSA, and correlate with severity of neurodegeneration (Li et al., 2018).

Considering the above, the NLRP3 inflammasome and its related pathways are attractive therapeutic targets in SAND by mitigating neuroinflammatory effects and delaying progression of

synuclein-associated pathology. Indeed, there are already a couple of key observations of inflammasome regulation with potential therapeutic implications. First, NLRP3 activity is attenuated by activation of the dopamine D1 receptor cyclic adenosine monophosphate (cAMP) signaling pathway in primary microglia and astrocytes (Yan et al., 2015). The second mechanism is via caspase-1 deficiency, an important component of the NLRP3 inflammasome, which inhibits α-syn-induced microglial activation, resulting in neuroprotection of mesencephalic dopaminergic neurons, as observed in a murine model (Zhu et al., 2023).

Taking all these together, one may hypothesize that a neurotropic pathogen infection enhances neuronal expressions of CGRP. CGRP is overexpressed in order to impede the aggregation of α-synuclein. Once PD manifests clinically, the loss of CGRP immunoreactive neurons might be an additional pathological finding further to a reaction to the accumulation of pathological synuclein (Figure 2). This hypothesis might offer a possible causal link between PD and CGRP, which however needs to be further investigated. Studies have revealed elevated neocortical pro- and anti-inflammatory cytokines in AD, but not in late-stage LBD. Furthermore, significant CGRP neuronal loss has been observed in the parabrachial nucleus (PBN) and Kolliker-Fuse (KF) nucleus in progressed MSA. These findings are in keeping with our model, where the inflammatory process is more pronounced at the beginning stages of the disease and then is attenuated over time.

3.2 CGRP anti-apoptotic and proliferative effects

Beyond anti-inflammatory mechanisms that are better studied in CGRP-related pathways, CGRP-mediated activation of the Akt/ERK signaling kinase cascade leads to both neurotoxic and neuroprotective downstream effects. The neuroprotective role of CGRP in multiple neuronal populations against neurotoxicity is mediated through pathways whose disruption affects neuronal cell proliferation, differentiation, and survival, thus causing neurodegeneration (Abushik et al., 2017). A key mechanism in this process is apoptosis, which is also a main mechanism of neuronal death in PD. Thus, treatments against apoptosis have been considered in SAND (Schulz et al., 1999). One such therapeutic target involves stimulation of a proliferation signaling cascade to promotes neuronal survival and increase neurite outgrowth and regeneration. There is evidence that CGRP weakens anti-apoptotic and strengthens proliferative pathways in an Akt/ERK- dependent manner (Umoh et al., 2014).

The PI3K-AKT pathway promotes survival and development of dopamine neurons by suppressing apoptosis via inhibition of B cell lymphoma 2 survival protein (Bcl-2)-antagonist of cell death. During the pathogenesis of PD, activation of the multifunctional serine/threonine protein kinase GSK-3 leads to apoptosis of dopaminergic neurons. Noteworthy, the same pathway inhibits GSK-3. Moreover, AKT and phosphorylated AKT are significantly decreased in the SNpc of patients with PD.

Finally, within the premise of its anti-apoptotic neuroprotective effects, CGRP reduced mitochondrial toxicity of the apoptosis-inducing toxin N-methyl-4-phenylpyridinium (MPP+) and protected a midbrain subpopulation of α-synuclein overexpressing PC12 dopamine cells *in vitro* (Chung et al., 2005). PC12 is a cell line that synthesizes, releases and stores catecholamines (Greene and Rein, 1977; Greene and Tischler, 1976). They are sensitive to mitochondrial toxins, such as 1-methyl-4-phenylpyridinium (MPP+), and rotenone (Nakamura et al., 2000; Hirata and Nagatsu, 2005). Therefore, it could be suggested even a potential neuroprotective effect of CGRP in adult dopamine neurons *in vivo*.

3.3 CGRP metabolic mechanisms in SAND

Another avenue through which CGRP-related pathways may mediate protective effects in SAND is metabolism. Beyond the inflammatory common pathways between DM and SAND, the two also share common metabolic pathways that engage additional processes.

One such mechanism involves Glucagon-like peptide effects, where it has been demonstrated in animal models that long-acting CGRP analogues have potential therapeutic benefits via positive metabolic effects of Glucagon-like peptide-1 (GLP-1) secretion (Nilsson et al., 2016). At the same time, GLP-1 receptor activation has been shown to increase gene expression of energy balance regulating peptides, IL-6, and CGRP within the parabrachial nucleus (Richard et al., 2014). Thus, there is a positive feedback pathway between GLP-1 and CGRP, that is regulated by a yet unknown mechanism. Metabolic benefits are further supported through a study in humans indicating that use of Dipeptidyl peptidase 4 (DPP4) inhibitors and/or GLP-1 mimetics are associated with a lower rate of PD compared to other oral antidiabetic drugs (Brauer et al., 2020). Whether this benefit hinges on people having DM rather than people without DM, and, even more, people who have already developed PD or other SAND, remains to be seen.

Another metabolic pathway involves fatty acids, which are involved in both inflammatory and energy metabolism processes. Specifically, saturated fatty acids induce NLRP3 inflammasome activation (Vandanmagsar et al., 2011). Additionally, α-synuclein highly co-localizes with fatty acid-binding protein (FABP) and dopamine long-type Dopamine-2 receptors, leading to impaired dopamine production via mitochondrial dysfunction. Instead, inhibition of FABP prevents FABP-induced neurotoxicity (Kawahata and Fukunaga, 2022).

The above raise the possibility that CGRP effects on downstream metabolic pathways may exert benefits in SAND. Nevertheless, the above conjecture is incomplete and should be interpreted with caution, since in a high-fat diet mouse model of DM, anti-αCGRP drugs reduced adiposity, albeit without changes on glucose homeostasis (Halloran et al., 2020).

3.4 CGRP-mediated neuromodulation

One of the most intriguing, and less understood, mechanisms CGRP-related pathways may be involved in SAND is neuromodulation. The neuromodulating role of CGRP is supported by its interaction with the dopaminergic system within the CNS. The high CGRP receptor densities that have been found in many brain regions, including basal ganglia, cortex, hippocampus, thalamus, hypothalamus, pituitary, and amygdala, facilitate the pervasive effects on dopamine transmission in these areas and modulate the activity of

specific dopaminergic neurons that innervate selective dopamine terminal field regions (Deutch and Roth, 1987).

The overall concentration of CGRP in brain is fluctuating. It has been noted that CGRP expression is markedly increased by stress (e.g., injury, ischemia, hyperthermia, seizures, toxins) (Bulloch et al., 1996, 1998; Harada et al., 2009; Hashikawa-Hobara et al., 2015; Liu et al., 2010; Sharma et al., 2000; Zhang et al., 2010). Additionally, CGRP promotes neuroprotective/ neurotrophic processes via insulin-like growth factor-1 (IGF-1), basic fibroblast growth factor (bFGF), nerve growth factor (NGF), and strengthens antiapoptotic signaling via the Akt/ERK- pathway, cyclic AMP response element-binding transcription factor (CREB), and B cell lymphoma 2 survival protein (Bcl-2) (Umoh et al., 2014).

It seems these processes are activated by CGRP, toward ensuring cell survival and preventing apoptosis and neuronal death.

3.5 CGRP-microbiome interactions across the brain-gut axis

An association between CGRP and SAND is also suggested by the observed co-expression of α-syn and CGRP in the CNS and the ENS, especially given the hypothesis over the past two decades that ENS involvement may also be critical in the initiation and spread of SAND. This brain-gut axis hypothesis has opened interesting perspectives in the pathogenesis of neurodegenerative diseases, especially SAND. It has been suggested that gut microbial toxins may induce the production of α-syn aggregates in the ENS, which can be subsequently propagated to and proliferated in the CNS in a prion-like manner through the vagus nerve (Santos et al., 2019). Considering that germ-free mice have higher levels of CGRP, it is reasonable to postulate that, if α-syn aggregation in the ENS is secondary to microbial toxins, this effect is mediated by inhibiting CGRP and its pathways (Pujo et al., 2023). The inverse is also reasonable given the above, i.e., that CGRP-pathway activation protects from α-syn aggregation, since CGRP also has antimicrobial effects, but this and, more importantly, protection of dopamine network function, remain to be seen.

Additional support to a gut-brain axis mechanism is provided by studies where intestinal infection with potential pathogens (e.g., *H. pylori*, small intestinal bacterial overgrowth) is not only associated with worse motor fluctuations but may also contribute to the pathogenesis of the disease (Fasano et al., 2015). *H. pylori* infection contributes to neurodegeneration with different mechanisms. *H. pylori* disrupts the equilibrium of gastrointestinal microbiota with an excessive growth of small intestinal bacterial overgrowth. Besides the dysbiosis, the autotoxin produced by *H. pylori* induces pro-inflammatory cytokines release, thereby facilitating the occurrence of CNS inflammation through microbiome-gut-brain axis, leading to neuronal damage (Wei et al., 2024). Adding one more piece to the puzzle, CGRP expression is increased in the gastric mucosa and in the dorsal horn of the spinal cord of mice inoculated with *H. pylori*, further supporting our hypothesis that a pathogenetic factor (e.g., *H. pylori* infection), upregulates CGRP pathways both in the intestine and in the CNS, and thus makes CGRP a neuroprotective candidate in the neurodegenerative process (Li et al., 2009).

Neuroimmune interactions are vital for intestinal tissue homeostasis and host defense, yet the specifics remain unclear. Using a chemogenetic approach, eight distinct neuronal subsets were activated, revealing differential immune responses. Notably, nociceptor neurons expressing TRPV1 induced extensive immunomodulation by altering innate lymphocytes, macrophages, and RORγ+ regulatory T (Treg) cells. Specifically, TRPV1+ neurons in the dorsal root ganglia decreased Treg cell numbers through the neuropeptide CGRP. This finding suggests a significant link between pain signaling and the regulation of gut Treg cell function, highlighting CGRP's critical role in neuroimmune crosstalk (Zhu et al., 2024).

Finally, another possible bidirectional brain-gut route of pathological α-syn spread between the CNS and the ENS is via the general circulation. Following on the selective vulnerability hypothesis, where certain areas of the nervous system are key hubs from where neurodegenerative diseases start and spread from (e.g., via prion-like mechanisms), the above can explain the differential pathology burden between PD, LBD, and MSA. In this model, the differential distribution of CGRP in both the brain and gut raises the possibility that it may play a role in this brain-gut relationship in SAND. Although interesting, especially for certain SAND phenotypes, adequate data to verify the above hypotheses are lacking.

4 CGRP-associated pathways as novel therapeutic targets in SAND pathogenesis

4.1 Potential therapeutic strategies

The above mechanisms justify targeting CGRP-related pathways in treating SAND. Overall, their disruption promote a number of pathophysiological conditions that are linked to SAND (Figure 2) (Russell et al., 2014). CGRP has a neuromodulating role facilitating the pervasive effects on dopamine transmission in many brain areas and modulating the activity of specific dopaminergic neurons which innervate selective DA terminal field regions (Deutch and Roth, 1987). It has been shown that CGRP and its receptor modulate the PI3K/Akt signaling pathway (Umoh et al., 2014). Additionally, CGRP is related to the regulation of macrophage polarization and the reduction of the NLRP3 and IL-1β in animal models, indicating that the molecule may alleviate inflammatory reactions (Zhu et al., 2023). The use of GLP-1 mimetics is associated with a lower rate of PD compared to the use of other oral antidiabetic drugs (Brauer et al., 2020). Long-acting CGRP analogues cause a specific concentration dependent CGRP-induced increased GLP-1 secretion, reduction in fasting insulin levels, a tendency to reduce fasting blood glucose and glycosylated hemoglobin, a decrease in food intake, and a significant decline in body weight in diet-induced obese rats. Thus, CGRP may have a therapeutic potential for the treatment of type 2 diabetes through positive metabolic effects and effect on GLP-1 secretion (Nilsson et al., 2016).

4.2 Existing and emerging therapies

The multiple potential neuroprotective effects activating CGRP-related pathways are likely to benefit neurological disorders beyond SAND. Nonetheless, GLP-1 analogs (i.e., exenatide and liraglutide) have shown potent neuroprotective activity in clinical and preclinical

studies of PD. The therapeutic potential of the GLP1 analogues is mainly mediated through the involvement of PI3K/ERK/MAPK and PI3K/AKT-dependent pathways in terms of evading apoptosis toward cell survival (Athauda and Foltynie, 2016).

At the same time, these therapeutics may also increase the risk for other disorders by attenuated modulation of CGRP pathways. After all, it may be that optimized dynamic fluctuations of such complex pathways allow for homeostasis and cell survival, and, in the end, we may require to consider such chronotherapy dimensions when implementing novel treatments. Additionally, treatments for other conditions may be contributors to SAND evolution. A prime example is migraine and its novel therapies that suppress CGRP and improve migraine symptoms. Currently, a direct connection between PD and migraine has not yet been established and it is also unknown if anti-CGRP therapies increase the risk for developing SAND.

In the "AGES-Reykjavik Study" midlife migraine has been correlated to late-life parkinsonism. The results imply that there is a link between migraine with multiple indicators of parkinsonism (Scher et al., 2014).

In summary, CGRP-related pathways could prove to be novel targets in PD and other SAND therapeutics, as they contribute not only with their anti-inflammatory and anti-apoptotic properties, but also their positive metabolic effects on GLP-1 secretion, neuromodulation, and brain-gut communication. Clinical trials will have to be considered across both (a) upstream targets that mediate effects across multiple pathways, but also risk more widespread side effects, as well as (b) downstream specific CGRP-related pathway targets that engage fewer mechanisms and, thus, lead to fewer adverse events, but are more likely to have smaller effects.

5 Conclusion and future directions

5.1 Summary of findings

The presence of α-syn and CGRP in the CNS and the ENS and the intricate role of CGRP in inflammation, apoptosis, metabolism, neuromodulation, and brain-gut communication triggered our investigation of the possible association of CGRP-related pathways to alpha-synuclein aggregation and SAND. Prominent among its effects is CGRP regulation of multiple- complex signaling pathways, including PI3K/ERK/MAPK and PI3K/AKT, which in turn decrease inflammation and increase anti-apoptotic effects. There are already drugs, including anti-migraine targeting the CGRP pathway (i.e., anti-CGRP Monoclonal Antibodies and Gepants) in the market that could be candidates that effect upstream or downstream CGRP-related pathway effects on the evolution of SAND (Khan et al., 2019; Dodick et al., 2023; Haanes and Edvinsson, 2023; Reuter, 2023). However, despite the above suggesting that dynamic modulation of CGRP pathways can contribute to SAND, concrete causal associations are still and their circadian lacking to support our model as necessary or sufficient, nor does one specific target stand out compared to others as a better candidate for treatments.

5.2 Ongoing investigations and implications for future research

Given that many of the above hypotheses are extrapolations from other neurodegenerative disorders and pathological processes, we are currently pursuing a study supported by the Alzheimer's Association, and planned to be completed in late 2025, on CGRP-related pathways in the development and progression of Clinicopathologically-established Parkinson's Disease (CGRP in CPPD), in order to better establish whether CGRP and its downstream effects are indeed associated with PD pathology across dynamic (sleep–wake) cycles and across disease stages. Through this study we examine through a novel clinicopathological protocol in people with PD and non-impaired controls the unexplored cross-sectional and dynamic associations of blood and skin biopsy CGRP-related pathway biomarkers to multidimensional real-world data. Specifically, in the CGRP in CPPD study we will: (a) explore whether CGRP and inflammatory biomarkers (i.e., NLPR3 inflammasome, IL-1ß and IL-18) are associated to quantified phosphorylated a-synuclein in plasma and skin biopsy samples and their prognostic accuracy in CPPD clinical and pathological progression, (b) examine CGRP-related pathway associations dynamic fluctuations with regards to motor, cognitive, sleep features, cross-sectionally and longitudinally, and (c) investigate the association between medications known to modulate CGRP-related pathways and clinical and pathological CPPD progression. The results of the study will inform the extent of CGRP-related pathway contribution to PD across disease stages, and guide on possible specific therapeutic targets.

Data availability statement

The original contributions presented in the study are included in the article/supplementary material, further inquiries can be directed to the corresponding author.

Author contributions

AA: Conceptualization, Formal analysis, Funding acquisition, Investigation, Writing – original draft, Writing – review & editing. VD: Supervision, Writing – review & editing. EK: Supervision, Writing – review & editing, Conceptualization.

Funding

The author(s) declare that financial support was received for the research, authorship, and/or publication of this article. This study was supported by an ACSF-22-971298 fellowship grant to Athanasia Alexoudi and the Horizon 2020 program (No 965422) on Multidisciplinary Expert System for the Assessment and Management of Complex Brain Disorders.

Conflict of interest

The authors declare that the research was conducted in the absence of any commercial or financial relationships that could be construed as a potential conflict of interest.

The author(s) declared that they were an editorial board member of Frontiers, at the time of submission. This had no impact on the peer review process and the final decision.

Publisher's note

References

Abushik, P. A., Bart, G., Korhonen, P., Leinonen, H., Giniatullina, R., Sibarov, D. A., et al. (2017). Pro-nociceptive migraine mediator CGRP provides neuroprotection of sensory, cortical and cerebellar neurons via multi-kinase signaling. *Cephalalgia* 37, 1373–1383. doi: 10.1177/0333102416681588

Albert-Gascó, H., Ros-Bernal, F., Castillo-Gómez, E., and Olucha-Bordonau, F. E. (2020). Map/erk signaling in developing cognitive and emotional function and its effect on pathological and neurodegenerative processes. *Int. J. Mol. Sci.* 21:4471. doi: 10.3390/ijms21124471

Athauda, D., and Foltynie, T. (2016). The glucagon-like peptide 1 (GLP) receptor as a therapeutic target in Parkinson's disease: mechanisms of action. *Drug Discov. Today* 21, 802–818. doi: 10.1016/j.drudis.2016.01.013

Brauer, R., Wei, L., Ma, T., Athauda, D., Girges, C., Vijiaratnam, N., et al. (2020). Diabetes medications and risk of Parkinson's disease: a cohort study of patients with diabetes. *Brain* 143, 3067–3076. doi: 10.1093/brain/awaa262

Bulloch, K., Milner, T. A., Prasad, A., Hsu, M., Buzsaki, G., and McEwen, B. S. (1998). Induction of calcitonin gene-related peptide-like immunoreactivity in hippocampal neurons following ischemia: a putative regional modulator of the CNS injury/immune response. *Exp. Neurol.* 150, 195–205. doi: 10.1006/exnr.1997.6765

Bulloch, K., Prasad, A., Conrad, C. D., McEwen, B. S., and Milner, T. A. (1996). Calcitonin gene-related peptide level in the rat dentate gyrus increases after damage. *Neuroreport* 7, 1036–1040. doi: 10.1097/00001756-199604100-00016

Chang, C. P., Pearse, R. V., O'Connell, S., and Rosenfeld, M. G. (1993). Identification of a seven transmembrane helix receptor for corticotropin-releasing factor and sauvagine in mammalian brain. *Neuron* 11, 1187–1195. doi: 10.1016/0896-6273(93)90230-O

Chen, H. H., Mohsin, M., Ge, J. Y., Feng, Y. T., Wang, J. G., Ou, Y. S., et al. (2024). Optogenetic activation of peripheral somatosensory neurons in transgenic mice as a neuropathic pain model for assessing the therapeutic efficacy of analgesics. *ACS Pharmacol. Transl. Sci.* 7, 236–248. doi: 10.1021/acsptsci.3c00254

Cheng, J., Liao, Y., Dong, Y., Hu, H., Yang, N., Kong, X., et al. (2020). Microglial autophagy defect causes parkinson disease-like symptoms by accelerating inflammasome activation in mice. *Autophagy* 16, 2193–2205. doi: 10.1080/15548627.2020.1719723

Choksi, T., Hay, D. L., Legon, S., Poyner, D. R., Hagner, S., Bloom, S. R., et al. (2002). Comparison of the expression of calcitonin receptor-like receptor (CRLR) and receptor activity modifying proteins (RAMPs) with CGRP and adrenomedullin binding in cell lines. *Br. J. Pharmacol.* 136, 784–792. doi: 10.1038/sj.bjp.0704761

Chung, C. Y., Seo, H., Sonntag, K. C., Brooks, A., Lin, L., and Isacson, O. (2005). Cell type-specific gene expression of midbrain dopaminergic neurons reveals molecules involved in their vulnerability and protection. *Hum. Mol. Genet.* 14, 1709–1725. doi: 10.1093/hmg/ddi178

Codolo, G., Plotegher, N., Pozzobon, T., Brucale, M., Tessari, I., Bubacco, L., et al. (2013). Triggering of Inflammasome by aggregated α-Synuclein, an inflammatory response in Synucleinopathies. *PLoS One* 8:e55375. doi: 10.1371/journal.pone.0055375

Cottrell, G. S. (2019). CGRP receptor signalling pathways. *Handb Exp Pharmacol.* 255. doi: 10.1007/164_2018_130

Cottrell, G. S., Padilla, B., Pikios, S., Roosterman, D., Steinhoff, M., Grady, E. F., et al. (2007). Post-endocytic sorting of calcitonin receptor-like receptor and receptor activity-modifying protein 1. *J. Biol. Chem.* 282, 12260–12271. doi: 10.1074/jbc.M606338200

Deutch, A. Y., and Roth, R. H. (1987). Calcitonin gene-related peptide in the ventral tegmental area: selective modulation of prefrontal cortical dopamine metabolism. *Neurosci. Lett.* 74, 169–174. doi: 10.1016/0304-3940(87)90144-3

Dodick, D. W., Goadsby, P. J., Schwedt, T. J., Lipton, R. B., Liu, C., Lu, K., et al. (2023). Ubrogepant for the treatment of migraine attacks during the prodrome: a phase 3, multicentre, randomised, double-blind, placebo-controlled, crossover trial in the USA. *Lancet* 402, 2307–2316. doi: 10.1016/S0140-6736(23)01683-5

Donadio, V., Incensi, A., Rizzo, G., Westermark, G. T., Devigili, G., De Micco, R., et al. (2023). Phosphorylated α-synuclein in skin Schwann cells: a new biomarker for multiple system atrophy. *Brain* 146, 1065–1074. doi: 10.1093/brain/awac124

Evangelista, S. (2013). Handbook of biologically active peptides. *2nd* Edn. Oxford: Elsevier Inc.

Evans, B. N., Rosenblatt, M. I., Mnayer, L. O., Oliver, K. R., and Dickerson, I. M. (2000). CGRP-RCP, a novel protein required for signal transduction at calcitonin gene-related peptide and adrenomedullin receptors. *J. Biol. Chem.* 275, 31438–31443. doi: 10.1074/jbc.M005604200

Fan, Z., Pan, Y. T., Zhang, Z. Y., Yang, H., Yu, S. Y., Zheng, Y., et al. (2020). Systemic activation of NLRP3 inflammasome and plasma α-synuclein levels are correlated with motor severity and progression in Parkinson's disease. *J. Neuroinflammation* 17:11. doi: 10.1186/s12974-019-1670-6

Fasano, A., Visanji, N. P., Liu, L. W. C., Lang, A. E., and Pfeiffer, R. F. (2015). Gastrointestinal dysfunction in Parkinson's disease. *Lancet Neurol.* 14, 625–639. doi: 10.1016/S1474-4422(15)00007-1

Fellner, L., Irschick, R., Schanda, K., Reindl, M., Klimaschewski, L., Poewe, W., et al. (2013). Toll-like receptor 4 is required for α-synuclein dependent activation of microglia and astroglia. *Glia* 61, 349–360. doi: 10.1002/glia.22437

Ferrari, C. C., Pott Godoy, M. C., Tarelli, R., Chertoff, M., Depino, A. M., and Pitossi, F. J. (2006). Progressive neurodegeneration and motor disabilities induced by chronic expression of IL-1β in the substantia nigra. *Neurobiol. Dis.* 24, 183–193. doi: 10.1016/j.nbd.2006.06.013

Greene, L. A., and Rein, G. (1977). Release of [3H]norepinephrine from a clonal line of pheochromocytoma cells (PC12) by nicotinic cholinergic stimulation. *Brain Res.* 138, 521–528. doi: 10.1016/0006-8993(77)90687-4

Greene, L. A., and Tischler, A. S. (1976). Establishment of a noradrenergic clonal line of rat adrenal pheochromocytoma cells which respond to nerve growth factor. *Proc. Natl. Acad. Sci. USA* 73, 2424–2428. doi: 10.1073/pnas.73.7.2424

Guo, H., Callaway, J. B., and Ting, J. P. Y. (2015). Inflammasomes: mechanism of action, role in disease, and therapeutics. *Nat. Med.* 21, 677–687. doi: 10.1038/nm.3893

Haanes, K. A., and Edvinsson, L. (2023). Atogepant, the first oral preventive treatment for chronic migraine. *Lancet* 402, 748–749. doi: 10.1016/S0140-6736(23)01462-9

Halloran, J., Lalande, A., Zang, M., Chodavarapu, H., and Riera, C. E. (2020). Monoclonal therapy against calcitonin gene-related peptide lowers hyperglycemia and adiposity in type 2 diabetes mouse models. *Metabol. Open* 8. doi: 10.1016/j.metop.2020.100060

Haque, M. E., Akther, M., Jakaria, M., Kim, I. S., Azam, S., and Choi, D. K. (2020). Targeting the microglial NLRP3 inflammasome and its role in Parkinson's disease. *Mov. Disord.* 35, 20–33. doi: 10.1002/mds.27874

Harada, N., Narimatsu, N., Kurihara, H., Nakagata, N., and Okajima, K. (2009). Stimulation of sensory neurons improves cognitive function by promoting the hippocampal production of insulin-like growth factor-I in mice. *Transl. Res.* 154, 90–102. doi: 10.1016/j.trsl.2009.05.001

Hashikawa-Hobara, N., Ogawa, T., Sakamoto, Y., Matsuo, Y., Ogawa, M., Zamami, Y., et al. (2015). Calcitonin gene-related peptide pre-administration acts as a novel antidepressant in stressed mice. *Sci. Rep.* 5:12559. doi: 10.1038/srep12559

He, W., Long, T., Pan, Q., Zhang, S., Zhang, Y., Zhang, D., et al. (2019). Microglial NLRP3 inflammasome activation mediates IL-1β release and contributes to central sensitization in a recurrent nitroglycerin-induced migraine model. *J. Neuroinflammation* 16:78. doi: 10.1186/s12974-019-1459-7

Hirata, Y., and Nagatsu, T. (2005). Rotenone and CCCP inhibit tyrosine hydroxylation in rat striatal tissue slices. *Toxicology* 216, 9–14. doi: 10.1016/j.tox.2005.07.010

Huang, Y. K., Lu, Y. G., Zhao, X., Zhang, J. B., Zhang, F. M., Chen, Y., et al. (2020). Cytokine activin C ameliorates chronic neuropathic pain in peripheral nerve injury rodents by modulating the TRPV1 channel. *Br. J. Pharmacol.* 177, 5642–5657. doi: 10.1111/bph.15284

Hung, A. Y., and Schwarzschild, M. A. (2020). Approaches to disease modification for Parkinson's disease: clinical trials and lessons learned. *Neurotherapeutics* 17, 1393–1405. doi: 10.1007/s13311-020-00964-w

Kawahata, I., and Fukunaga, K. (2022). Impact of fatty acid-binding proteins and dopamine receptors on α-synucleinopathy. *J. Pharmacol. Sci.* 148, 248–254. doi: 10.1016/j.jphs.2021.12.003

Khan, S., Olesen, A., and Ashina, M. (2019). CGRP, a target for preventive therapy in migraine and cluster headache: systematic review of clinical data. *Cephalalgia* 39, 374–389. doi: 10.1177/0333102417741297

Kung, P. J., Elsayed, I., Reyes-Pérez, P., and Bandres-Ciga, S. (2022). Immunogenetic determinants of Parkinson's disease etiology. *J. Parkinsons Dis.* 12, S13–S27. doi: 10.3233/JPD-223176

Li, F., Ayaki, T., Maki, T., Sawamoto, N., and Takahashi, R. (2018). NLRP3 inflammasome-related proteins are upregulated in the putamen of patients with multiple system atrophy. *J. Neuropathol. Exp. Neurol.* 77, 1055–1065. doi: 10.1093/jnen/nly090

Li, X. B., Chen, H. M., Lu, H., Zheng, Q., Chen, X. Y., Peng, Y. S., et al. (2009). Role of *Helicobacter pylori* infection on neuronal expression in the stomach and spinal cord of a murine model. *J. Dig. Dis.* 10, 286–292. doi: 10.1111/j.1751-2980.2009.00397.x

Lim, S., Chun, Y., Lee, J. S., and Lee, S. J. (2016). Neuroinflammation in Synucleinopathies. *Brain Pathol.* 26, 404–409. doi: 10.1111/bpa.12371

Linscheid, P., Seboek, D., Schaer, D. J., Zulewski, H., Keller, U., and Müller, B. (2004). Expression and secretion of procalcitonin and calcitonin gene-related peptide by adherent monocytes and by macrophage-activated adipocytes. *Crit. Care Med.* 32, 1715–1721. doi: 10.1097/01.CCM.0000134404.63292.71

Liu, G., Cai, H., Xu, X., Liu, Z., Wang, Q., Feng, G., et al. (2010). The effects of calcitonin gene-related peptide on bFGF and AQP4 expression after focal cerebral ischemia reperfusion in rats. *Pharmazie* 65, 274–78. doi: 10.1691/ph.2010.9755

Liu, X. J., Zhang, F. X., Liu, H., Li, K. C., Lu, Y. J., Wu, Q. F., et al. (2012). Activin C expressed in nociceptive afferent neurons is required for suppressing inflammatory pain. *Brain* 135, 391–403. doi: 10.1093/brain/awr350

Manaka, Y., Watanabe, M., Yamaguchi, K., Manaka, H., Kato, T., Yamatani, K., et al. (1998). Sequential changes in CGRP-like immunoreactivity in NIDDM model Otsuka long-Evans Tokushima fatty (OLETF) rat pancreatic islets. *Pancreas* 17, 72–79. doi: 10.1097/00006676-199807000-00009

Martinon, F., Burns, K., and Tschopp, J. (2002). The Inflammasome: a molecular platform triggering activation of inflammatory caspases and processing of proIL-β. *Mol. Cell* 10, 417–426. doi: 10.1016/S1097-2765(02)00599-3

Matteoli, M., Haimann, C., Torri-Tarelli, F., Polak, J. M., Ceccarelli, B., and De Camilli, P. (1988). Differential effect of α-latrotoxin on exocytosis from small synaptic vesicles and from large dense-core vesicles containing calcitonin gene-related peptide at the frog neuromuscular junction. *Proc. Natl. Acad. Sci. USA* 85, 7366–7370. doi: 10.1073/pnas.85.19.7366

Nakamura, K., Bindokas, V. P., Marks, J. D., Wright, D. A., Frim, D. M., Miller, R. J., et al. (2000). The selective toxicity of 1-methyl-4-phenylpyridinium to dopaminergic neurons: the role of mitochondrial complex I and reactive oxygen species revisited. *Mol. Pharmacol.* 58, 271–278. doi: 10.1124/mol.58.2.271

Nilsson, C., Hansen, T. K., Rosenquist, C., Hartmann, B., Kodra, J. T., Lau, J. F., et al. (2016). Long acting analogue of the calcitonin gene-related peptide induces positive metabolic effects and secretion of the glucagon-like peptide-1. *Eur. J. Pharmacol.* 773, 24–31. doi: 10.1016/j.ejphar.2016.01.003

Pujo, J., De Palma, G., Lu, J., Galipeau, H. J., Surette, M. G., Collins, S. M., et al. (2023). Gut microbiota modulates visceral sensitivity through calcitonin gene-related peptide (CGRP) production. *Gut Microbes* 15:2188874. doi: 10.1080/19490976.2023.2188874

Rai, S. N., Dilnashin, H., Birla, H., Singh, S. S., Zahra, W., Rathore, A. S., et al. (2019). The role of PI3K/Akt and ERK in neurodegenerative disorders. *Neurotox. Res.* 35, 775–795. doi: 10.1007/s12640-019-0003-y

Reuter, U. (2023). A nasal CGRP receptor antagonist for acute migraine therapy. *Lancet Neurol.* 22, 190–191. doi: 10.1016/S1474-4422(23)00037-6

Richard, J. E., Farkas, I., Anesten, F., Anderberg, R. H., Dickson, S. L., Gribble, F. M., et al. (2014). GLP-1 receptor stimulation of the lateral parabrachial nucleus reduces food intake: neuroanatomical, electrophysiological, and behavioral evidence. *Endocrinology* 155, 4356–4367. doi: 10.1210/en.2014-1248

Russell, F. A., King, R., Smillie, S. J., Kodji, X., and Brain, S. D. (2014). Calcitonin gene-related peptide: physiology and pathophysiology. *Physiol. Rev.* 94, 1099–1142. doi: 10.1152/physrev.00034.2013

Rysiewicz, B., Błasiak, E., Mystek, P., Dziedzicka-Wasylewska, M., and Polit, A. (2023). Beyond the G protein α subunit: investigating the functional impact of other components of the Gαi3 heterotrimers. *Cell Commun. Signal.* 21:279. doi: 10.1186/s12964-023-01307-w

Saito, N., Kimura, M., Ouchi, T., Ichinohe, T., and Shibukawa, Y. (2022). Gαs-coupled CGRP receptor signaling Axis from the trigeminal ganglion neuron to odontoblast negatively regulates dentin mineralization. *Biomol. Ther.* 12:1747. doi: 10.3390/biom12121747

Salio, C., Averill, S., Priestley, J. V., and Merighi, A. (2007). Costorage of BDNF and neuropeptides within individual dense-core vesicles in central and peripheral neurons. *Dev. Neurobiol.* 67, 326–338. doi: 10.1002/dneu.20358

Santos, S. F., De Oliveira, H. L., Yamada, E. S., Neves, B. C., and Pereira, A. (2019). The gut and Parkinson's disease - a bidirectional pathway. *Front. Neurol.* 10:574. doi: 10.3389/fneur.2019.00574

Savica, R., Grossardt, B. R., Bower, J. H., Ahlskog, J. E., Boeve, B. F., Graff-Radford, J., et al. (2017). Survival and causes of death among people with clinically diagnosed Synucleinopathies with parkinsonism: a population-based study. *JAMA Neurol.* 74, 839–846. doi: 10.1001/jamaneurol.2017.0603

Scher, A. I., Ross, G. W., Sigurdsson, S., Garcia, M., Gudmundsson, L. S., Sveinbjörnsdóttir, S., et al. (2014). Midlife migraine and late-life parkinsonism: AGES-reykjavik study. *Neurology* 83, 1246–1252. doi: 10.1212/WNL.0000000000000840

Schulz, J. B., Weller, M., and Moskowitz, M. A. (1999). Caspases as treatment targets in stroke and neurodegenerative diseases. *Ann. Neurol.* 45, 421–429. doi: 10.1002/1531-8249(199904)45:4<421::AID-ANA2>3.0.CO;2-Q

Schütz, B., Mauer, D., Salmon, A. M., Changeux, J. P., and Zimmer, A. (2004). Analysis of the cellular expression pattern of β-CGRP in α-CGRP-deficient mice. *J. Comp. Neurol.* 476, 32–43. doi: 10.1002/cne.20211

Sharma, H. S., Westman, J., and Nyberg, F. (2000). Selective alteration of calcitonin gene related peptide in hyperthermic brain injury. An experimental study in the rat brain using immunohistochemistry. *Acta Neurochir. Suppl.* 76, 541–545. doi: 10.1007/978-3-7091-6346-7_113

Singh, Y., Gupta, G., Shrivastava, B., Dahiya, R., Tiwari, J., Ashwathanarayana, M., et al. (2017). Calcitonin gene-related peptide (CGRP): a novel target for Alzheimer's disease. *CNS Neurosci. Ther.* 23, 457–461. doi: 10.1111/cns.12696

Stewart, T., Sossi, V., Aasly, J. O., Wszolek, Z. K., Uitti, R. J., Hasegawa, K., et al. (2015). Phosphorylated α-synuclein in Parkinson's disease: correlation depends on disease severity. *Acta Neuropathol. Commun.* 3:7. doi: 10.1186/s40478-015-0185-3

Umoh, N. A., Walker, R. K., Millis, R. M., Al-Rubaiee, M., Gangula, P. R., and Haddad, G. E. (2014). Calcitonin gene-related peptide regulates cardiomyocyte survival through regulation of oxidative stress by PI3K/Akt and MAPK signaling pathways. Ann. *Clin. Exp. Hypertens.* 2:1007

Vandanmagsar, B., Youm, Y. H., Ravussin, A., Galgani, J. E., Stadler, K., Mynatt, R. L., et al. (2011). The NLRP3 inflammasome instigates obesity-induced inflammation and insulin resistance. *Nat. Med.* 17, 179–188. doi: 10.1038/nm.2279

von Herrmann, K. M., Salas, L. A., Martinez, E. M., Young, A. L., Howard, J. M., Feldman, M. S., et al. (2018). NLRP3 expression in mesencephalic neurons and characterization of a rare NLRP3 polymorphism associated with decreased risk of Parkinson's disease. *NPJ Parkinsons Dis.* 4:24. doi: 10.1038/s41531-018-0061-5

Wake, H., Moorhouse, A. J., Jinno, S., Kohsaka, S., and Nabekura, J. (2009). Resting microglia directly monitor the functional state of synapses in vivo and determine the fate of ischemic terminals. *J. Neurosci.* 29, 3974–3980. doi: 10.1523/JNEUROSCI.4363-08.2009

Walker, C. S., Conner, A. C., Poyner, D. R., and Hay, D. L. (2010). Regulation of signal transduction by calcitonin gene-related peptide receptors. *Trends Pharmacol. Sci.* 31, 476–483. doi: 10.1016/j.tips.2010.06.006

Wei, B., Zhao, Y. J., Cheng, Y. F., Huang, C., and Zhang, F. (2024). *Helicobacter pylori* infection and Parkinson's disease: etiology, pathogenesis and levodopa bioavailability. *Immun. Ageing* 21:1. doi: 10.1186/s12979-023-00404-1

Wen, H., Gris, D., Lei, Y., Jha, S., Zhang, L., Huang, M. T. H., et al. (2011). Fatty acid-induced NLRP3-ASC inflammasome activation interferes with insulin signaling. *Nat. Immunol.* 12, 408–415. doi: 10.1038/ni.2022

Wimalawansa, S. J., Morris, H. R., Etienne, A., Blench, I., Panico, M., and MacIntyre, I. (1990). Isolation, purification and characterization of β-hCGRP from human spinal cord. *Biochem. Biophys. Res. Commun.* 167, 993–1000. doi: 10.1016/0006-291X(90)90621-S

Yan, Y., Jiang, W., Liu, L., Wang, X., Ding, C., Tian, Z., et al. (2015). Dopamine controls systemic inflammation through inhibition of NLRP3 inflammasome. *Cell* 160, 62–73. doi: 10.1016/j.cell.2014.11.047

Zhang, X., Bao, L., Xu, Z. Q., Kopp, J., Arvidsson, U., Elde, R., et al. (1994). Localization of neuropeptide Y Y1 receptors in the rat nervous system with special reference to somatic receptors on small dorsal root ganglion neurons. *Proc. Natl. Acad. Sci. USA* 91, 11738–11742. doi: 10.1073/pnas.91.24.11738

Zhang, Z. H., Fang, X. B., Xi, G. M., Li, W. C., Ling, H. Y., and Qu, P. (2010). Calcitonin gene-related peptide enhances CREB phosphorylation and attenuates tau protein phosphorylation in rat brain during focal cerebral ischemia/reperfusion. *Biomed. Pharmacother.* 64, 430–436. doi: 10.1016/j.biopha.2009.06.009

Zhang, P., Shao, X. Y., Qi, G. J., Chen, Q., Bu, L. L., Chen, L. J., et al. (2016). Cdk5-dependent activation of neuronal Inflammasomes in Parkinson's disease. *Mov. Disord.* 31, 366–376. doi: 10.1002/mds.26488

Zhu, Y., Meerschaert, K. A., Galvan-Pena, S., Bin, N. R., Yang, D., Basu, H., et al. (2024). A chemogenetic screen reveals that Trpv1-expressing neurons control regulatory T cells in the gut. *Science* 385:eadk1679. doi: 10.1126/science.adk1679

Zhu, F., Yu, D., Qin, X., Qian, Y., Ma, J., Li, W., et al. (2023). The neuropeptide CGRP enters the macrophage cytosol to suppress the NLRP3 inflammasome during pulmonary infection. *Cell. Mol. Immunol.* 20, 264–276. doi: 10.1038/s41423-022-00968-w

frontiers | Frontiers in Neuroscience

TYPE Original Research
PUBLISHED 11 November 2024
DOI 10.3389/fnins.2024.1480000

OPEN ACCESS

EDITED BY
Pradeep Kumar,
All India Institute of Medical Sciences, India

REVIEWED BY
Janakiraman Udaiyappan,
Southern Methodist University, United States
Samir Ranjan Panda,
National Institute of Pharmaceutical Education and Research, India

*CORRESPONDENCE
Linlin Fu
✉ 363504347@qq.com
Qisi Lin
✉ qslin074@126.com
Fenfen Sun
✉ fen_1208@163.com

†These authors have contributed equally to this work and share first authorship

RECEIVED 13 August 2024
ACCEPTED 28 October 2024
PUBLISHED 11 November 2024

CITATION
Yuan L, Song G, Xu W, Liu S, Zhang Y, Pan W, Ding X, Fu L, Lin Q and Sun F (2024) Diethyl butylmalonate attenuates cognitive deficits and depression in 5×FAD mice. *Front. Neurosci.* 18:1480000. doi: 10.3389/fnins.2024.1480000

Diethyl butylmalonate attenuates cognitive deficits and depression in 5×FAD mice

Lai Yuan[1,2†], Ge Song[1,2†], Wangwei Xu[3,4†], Shuni Liu[1,2†], Yongsheng Zhang[1,2], Wei Pan[1], Xiaohui Ding[1], Linlin Fu[1*], Qisi Lin[3*] and Fenfen Sun[1*]

[1]Jiangsu Key Laboratory of Immunity and Metabolism, Department of Pathogen Biology and Immunology, Xuzhou Medical University, Xuzhou, China, [2]The First Clinical Medical College, Xuzhou Medical University, Xuzhou, China, [3]Jiangsu Key Laboratory of New Drug Research and Clinical Pharmacy, Xuzhou Medical University, Xuzhou, China, [4]Suqian Affiliated Hospital of Xuzhou Medical University, Suqian, China

Background: Alzheimer's disease (AD), characterized by cognitive impairment and depression, is currently one of the intractable problems due to the insufficiency of intervention strategies. Diethyl butylmalonate (DBM) has recently attracted extensive interest due to its anti-inflammatory role in macrophages. However, it is still unknown whether DBM has a beneficial effect on cognitive deficits and depression.

Methods: DBM was administrated to 5×FAD and C57BL/6J mice by intraperitoneal injection. Novel object recognition, Y-maze spatial memory, Morris water maze and nest building tests were used to evaluate cognitive function. Moreover, the tail suspension test, forced swimming test, open field test and the elevated plus maze test were used to assess depression. Transmission electron microscopy, Golgi-Cox staining, immunofluorescence, RT-qPCR and western blot were utilized to determine the neuropathological changes in the hippocampus and amygdala of mice.

Results: Multiple behavioral tests showed that DBM effectively mitigated cognitive deficit and depression in 5×FAD mice. Moreover, DBM significantly attenuated synaptic ultrastructure and neurite impairment in the hippocampus of 5×FAD mice, paralleled by the improvement of the deficits of PSD95 and BDNF proteins. In addition, DBM decreased the accumulation of microglia and downregulated neuroinflammation in the hippocampus and amygdala of 5×FAD mice.

Conclusion: This study provides evidence that DBM ameliorates cognitive deficits and depression via improvement of the impairment of synaptic ultrastructure and neuroinflammation, suggesting that DBM is a potential drug candidate for treating AD-related neurodegeneration.

KEYWORDS

Alzheimer's disease, cognitive, depression, neuroinflammation, synaptic plasticity, diethyl butylmalonate

1 Introduction

Alzheimer's disease (AD) is a multifactorial neurodegenerative disorder and the leading cause of dementia (Paul, 2022). AD patients are characterized by cognitive impairment, including memory deficits and depression (Lyketsos et al., 2011; Kogan et al., 2000; Koenig et al., 2016). Neuroinflammation is critical in AD progression via impairing synaptic plasticity and neurite outgrowth (Hou et al., 2021; Hartmann et al., 2024; Bohlson and Tenner, 2023; Li et al., 2023). Neuroinflammation plays a vital role in the AD progression (Leng and Edison, 2021). In AD, activated microglia release a range of proinflammatory cytokines, including IL-1β, IL-6, and TNF-α (Cai et al., 2019), directly inducing neuronal apoptosis and synaptic dysfunction (Zhao et al., 2019). These activated microglia can also engulf synapses, compromising synaptic structure (Hong et al., 2016). Consequently, reducing neuroinflammation may help alleviate cognitive impairment by enhancing synaptic plasticity and preserving synaptic ultrastructure in AD.

Succinate dehydrogenase (SDH), an enzyme in Kreb's cycle, is a arbiter of pro-inflammatory response in macrophages (Mills et al., 2016). It is reported that SDH governs the increased inflammatory gene expression and reciprocally decreased anti-inflammatory gene expression via succinate oxidation (Mills et al., 2016). Diethyl butylmalonate (DBM) is known to be a competitive inhibitor of SDH. It rapidly hydrolyzes to form malonate, preventing succinate accumulation and oxidation, thereby exerting an anti-inflammatory effect by inhibiting ROS production (Zhang et al., 2021; Fan et al., 2022; Prag et al., 2022). It is reported that DBM administration can alleviate brain damage in a mouse model of cardiac arrest (Leng and Edison, 2021). Additionally, recent research has demonstrated that DBM suppresses microglial activation and reduces neuroinflammation in LPS-stimulated microglia (Sangineto et al., 2023). However, it remains largely enigmatic whether DBM could improve cognitive impairment and depression in AD.

Transgenic mice have become essential tools for exploring the neuropathology of AD and evaluating potential therapeutic agents (Wong et al., 2002). Here, utilizing the 5×FAD mice model, which showed cognitive impairment and depression (Jawhar et al., 2012; Xu et al., 2018), we comprehensively evaluated the protective effects of DBM on the condition of AD. Our results indicate that DBM treatment improves cognitive function and alleviates depression in these transgenic mice, alongside enhancements in synaptic ultrastructure, neurite growth, and reductions in neuroinflammation. This suggests that DBM holds promise as a therapeutic molecule for preventing neurodegenerative diseases, including AD.

Abbreviations: DBM, Diethyl butylmalonate; AD, Alzheimer's disease; Con, Control; Veh, Vehicle; TEM, Transmission electron microscope; IF, Immunofluorescence; SYN, Synaptophysin; BDNF, Brain-derived neurotrophic factor; PSD95, Postsynaptic density 95; AZ, Active zone; SC, Synaptic cleft; SV, Synaptic vesicle; Iba1, Ionized calcium-binding adaptor molecule1; IL-1β, Interleukin-1 beta; IL-6, Interleukin-6; TNF-α, Tumor necrosis factor-α; SEM, Standard error of the mean; ANOVA, Analysis of variance; MWM, Morris water maze; NOR, Novel object recognition; NB, Nest building; OFT, Open field test; FST, Forced swimming test; TST, Tail suspension test; CA1, Cornu ammonis 1; CA3, Cornu ammonis 3; DG, Dentate gyrus; PBS, Phosphate buffered solution; RT-qPCR, Quantitative reverse transcription polymerase chain reaction; SDH, Succinate dehydrogenase; LPS, Lipopolysaccharide; CNS, Central nervous system; APP, Amyloid precursor protein; Aβ, β-amyloid.

2 Materials and methods

2.1 Animals

C57BL/6J mice were obtained from Jiangsu Jicui Pharmaceutical Technology Corporation (Jiangsu Province, China) and the transgenic mouse line 5×FAD (MMRRC catalog #034840-JAX, RRID: MMRRC_034840-JAX) were purchased from the Jackson Laboratory. 5×FAD mice overexpress the 695-amino acid isoform of the human amyloid precursor protein (APP695) carrying the Swedish, London, and Florida mutations under the control of the murine Thy-1 promoter. They were housed in environmentally controlled conditions (temperature 24°C, 12 h light/dark cycle) and given free access to standard food and water in specific pathogen free (SPF) experimental animal Center of Xuzhou Medical University. The mice were acclimatized for 1 week before the experiment. All animal care and experiments were carried out in strict accordance with the recommendation of the Guide for the Care and Use of Laboratory Animals of the Ministry of Health (China) and approved by the Ethics Committee of Xuzhou Medical University (Xuzhou, China, SCXK (Su) 2020-0048).

2.2 Experimental design

5×FAD mice (4 month old) and C57BL/6J mice (4 month old) were randomly divided into the following four groups (12 mice for each group, including 6 males and 6 females): (I) C57BL/6J mice received phosphate buffer solution (PBS) as vehicle control (Con + Veh) group; (II) C57BL/6J mice received intraperitoneal injections (two times weekly) of 40 mg/kg DBM (Cat. 112038-100ML, Sigma-Aldrich, St. Louis, United States) as Con + DBM group; (III) 5×FAD group as AD model for mice received PBS as 5×FAD + Veh group; (IV) 5×FAD + DBM group received DBM (two times weekly) with intraperitoneal injections in 5×FAD mice. Following 4 weeks of intervention, a series of behavioral tests were performed. Mice were then anesthetized with pentobarbitone sodium (100 mg/kg body weight) and sacrificed 3 days after behavioral tests. The fresh hippocampus and amygdala tissues were collected and preserved at −80°C for western blotting and RT-qPCR. The whole brains were taken and placed in Golgi fixative for Golgi-Cox staining. For transmission electron microscope, the left hippocampus was sectioned and cut into 1 cm^3 pieces and stored in electron microscope fixative. For immunofluorescence analysis, the whole brains were placed in a 4% paraformaldehyde-fixed solution and then transferred into a 30% sucrose solution for dehydration and cryoprotection.

2.3 Behavioral tests

To investigate the impact of DBM administration on spontaneous rodent behaviors and recognition memory and depression in 5×FAD mice, behavioral tests were conducted, including Morris water maze, Y-maze spatial memory, the novel object recognition, Y-maze test, nest building test, elevated plus maze test, open field test, tail suspension test and forced swimming test. The procedures followed were comparable to those described in earlier studies.

2.3.1 Morris water maze test

The test was conducted in accordance with previously established protocols (Liu et al., 2020). The Morris water maze (MWM) test was performed in a circular tank measuring 150 cm in diameter and 35 cm in height (XR-XM101, Shanghai Xinruan Information Technology Co., Ltd.) in a dimly lit room. The water temperature was maintained between 22–25°C to prevent the mice from floating. The mice were placed in predefined pseudo-random locations. On day 0, the mice underwent four habituation training sessions. The platform was positioned 2 cm above the water's surface, with the water left undyed. Mice were trained for five consecutive days, with each mouse undergoing four trials per day. A trial ended when the mouse located the platform or after 60 s had passed. A mouse was guided to the platform if it failed to locate the submerged platform within the time limit. All data were automatically recorded using a video tracking system (SuperMaze software, Shanghai Xinruan Information Technology Co., Ltd.).

2.3.2 Y-maze spatial memory test

The test was conducted in accordance with previously established protocols (Dellu et al., 2000). The Y-maze consists of three identical arms (30 cm × 10 cm × 16 cm). During the training phase, one arm, referred to as the novel arm, was closed, while the remaining two arms were designated as the start arm and the familiar arm. Mice were introduced into the start arm and allowed to explore the start and familiar arms for 5 min. After 1 h, the mice were given 5 min to explore all three arms. The percentage of time spent in the novel arm was calculated using the formula: (time in the novel arm/total exploration time) × 100. The arena was cleaned with 70% ethanol to minimize olfactory cues before the commencement of trial for every mouse.

2.3.3 Novel object recognition test

The novel object recognition (NOR) test comprises three stages. In the habituation stage, mice were allowed to explore an open field for 5 min. After 24 h, the training stage began, where mice explored the arena for 5 min with two identical objects placed in parallel. One hour later, during the testing stage, mice explored the arena again for 5 min, with one familiar object and one novel object placed side by side. To minimize olfactory cues, the open field was cleaned with 70% ethanol before each trial. Testing took place in a soundproof chamber maintained at 22–25°C. The arena was cleaned with 70% ethanol to minimize olfactory cues before the commencement of trial for every mouse. The novel object discrimination index (NODI) was calculated using the formula: (time spent with the novel object/total object exploration time) × 100 (Liu et al., 2022).

2.3.4 Y-maze test

The Y-maze test, used to measure spatial working memory, was performed according to previously described methods (Kraeuter et al., 2019). After acclimatizing the mice, each arm of the Y-maze was marked with distinct visual cues. Mice were placed in the center of the maze and allowed to explore freely for 8 min. The total number of arm entries and spontaneous alternations were recorded. A spontaneous alternation was defined as consecutive entries into each of the three arms without repetition (e.g., arms one, two, three, or three, two, one, but not three, one, three). The arena was cleaned with 70% ethanol to minimize olfactory cues before the commencement of trial for every mouse. The alternation percentage was calculated using the formula: [number of spontaneous alternations/(total arm entries)] × 100.

2.3.5 Nest building test

One hour before the onset of the dark phase, mice were individually housed in separate cages, each provided with a 3-gram pressed-cotton square. The next morning, the quality of the nest and the weight of the untorn nestlet were assessed. Nest scores were evaluated using a definitive 5-point rating scale based on a previously described system (Deacon, 2006).

2.3.6 Elevated plus maze test

In the elevated plus maze test, mice were placed at the intersection of the four arms of the maze, and their behavior was recorded for 5 min. The arena was cleaned with 70% ethanol to minimize olfactory cues before the commencement of trial for every mouse. The primary behaviors observed include the time spent in and entries made into the open and closed arms. Activity in the open arms reflects a balance between the rodent's preference for secure areas (e.g., closed arms) and their natural curiosity to explore new environments (Walf and Frye, 2007).

2.3.7 Open field test

The open field test (OFT) was used to assess locomotor activity. The test was performed as described in previous studies. The apparatus consisted of a black metallic box measuring 60 × 80 × 50 cm, equipped with a video analysis system. Mice were placed in the center of the open field and allowed to explore freely for 6 min. After a 2-min adaptation period, the number of crossings was automatically recorded over the following 4 min (Lin et al., 2023). The arena was cleaned with 70% ethanol to minimize olfactory cues before the commencement of trial for every mouse.

2.3.8 Forced swimming test

The forced swimming test (FST) was conducted in a cylindrical glass tank with a height of 25 cm, a diameter of 10 cm, and water maintained at 25°C. Each mouse was placed in the tank to adapt for 2 min, and then the cumulative immobility time was recorded for the following 4 min using ANY-maze software. Detailed procedures were based on previously published methods (Lin et al., 2023; Harro, 2018; Zhao et al., 2022).

2.3.9 Tail suspension test

The tail suspension test (TST) was performed as previously described (Cryan et al., 2005). Mice were individually suspended upside down by the tail, using a clamp placed 1 cm from the tip. Each mouse was suspended for 6 min, and immobility time was recorded during the final 4 min when the mice remained completely motionless. The immobility time for each mouse during the last 4 min was analyzed using ANY-maze software.

2.4 Transmission electron microscope

After cardiac perfusion with saline and 4% paraformaldehyde-fixed solution, the CA1 region in the left side of hippocampus was sectioned and cut into 1 cm^3 pieces and fixed in 2.5% glutaraldehyde at 4°C for 24 h. The sections were then washed three times in PBS, post-fixed with 1% osmium tetroxide, stained with 2% uranyl acetate, dehydrated in a graded series of ethanol and acetone, and embedded in epoxy resin. The sections were subsequently sliced into 70 nm thick sections using an

ultramicrotome and stained with 4% uranyl acetate and 0.5% lead citrate after being mounted on copper grids. The ultrastructure of synapses in the hippocampus was observed using transmission electron microscopy (TEM) (FEI Company, Hillsboro, OR, United States), and synaptic morphometrics were analyzed. Synaptic parameters, including postsynaptic density (PSD), synaptic cleft width, synaptic interface curvature, and active zone length, were quantified using ImageJ software (version 1.53n; https://imagej.nih.gov/ij/).

2.5 Golgi-Cox staining

Golgi-Cox staining analyzed neuronal morphology Variations using the FD Rapid Golgi Stain Kit (Nanjing Well-Offex Biotechnology Co., Ltd., Nanjing, China; catalog number: PK401) as previously described (Du, 2019; Restivo et al., 2005). Briefly, the whole mouse brains were dissected, immersed in a mixture of solution A and solution B, and stored at room temperature in the dark for 14 days, with the solution replaced every 48 h. The brain tissues were then placed in solution C for 5 days, sectioned into 100-μm-thick slices using a vibratome, mounted on gelatin-coated slides, and stained with a mixture of solution D and solution E. The sections were dehydrated through a graded alcohol series, cleared with xylene, and covered with Permount. Images were captured using a digital camera attached to a microscope (Olympus Corp., Tokyo, Japan). Researchers blinded to the experimental conditions randomly selected dendritic shafts and spines of pyramidal neurons from CA1 region of the hippocampus for analysis. Morphological data, including total neurite length, individual neurite length, and neurite count per neuron, were analyzed using the NeuronJ plugin of ImageJ software. Spine density was estimated by counting the number of spines along a 10-μm section of a 30–50 μm-long distal dendritic branch using the Cell Counter plugin in ImageJ. Additionally, Sholl analysis was conducted to evaluate dendritic complexity with the Sholl plugin in ImageJ (Srinivasan et al., 2020). Images of Golgi-stained neurons were superimposed with concentric circles of increasing diameters (in 10-μm increments) around the soma (10–300 μm). The number of neurite intersections with each circle was counted manually, and the following indicators were calculated: (i) total intersections and (ii) maximum intersection distance.

2.6 Immunofluorescence

For image analysis of hippocampal immunofluorescence, sections were processed as previously described (Shi et al., 2021). Fresh brain tissues were soaked in a 4% paraformaldehyde-fixed solution and then transferred into a 30% sucrose solution for dehydration and cryoprotection. The mouse brain was embedded with an embedding agent and snap-frozen at −20°Cin a frozen sectioning machine, sectioned into 20-μm-thick slices, and washed three times for 10 min each. The sections were then treated with 1% H_2O_2 in PBS for 30 min. All sections were blocked with BSA (G5001, Servicebio) for 30 min and incubated overnight at 4°C with the indicated primary anti-Iba1$^+$ antibody (Abcam, Cambridge, United Kingdom; catalog number Ab178847) and anti-beta-Amyloid-1-42 (HA721789, HUABIO, Hangzhou, China). Subsequently, the sections were incubated with a goat anti-rabbit IgG secondary antibody (GB23303, Servicebio Technology Co., Ltd., China) for 2 h at room temperature. Nuclei were stained using DAPI solution (G1012, Servicebio Technology Co., Ltd., China). Representative images were captured using a fluorescence microscope (OLYMPUS IX51), and the quantification of positively stained cells was performed using ImageJ.

2.7 RNA extraction and quantitative reverse transcription polymerase chain reaction

RNA extraction and quantitative reverse transcription polymerase chain reaction (RT-qPCR) were performed based on methods previously described (Yang et al., 2022). The fresh hippocampus and amygdala were collected and preserved at −80°C for RT-qPCR. The amygdala was removed from the brain where located in the most ventrocaudal part of the brain, near the hippocampus, in the frontal portion of the temporal lobe, below the subcortical nuclei, expanding to its basal structures (Nikolenko et al., 2020). Total RNA was extracted from hippocampal or amygdala tissues using TRIzol (Thermo Fisher Scientific, United States). The quantity of RNA was measured at 260 nm, and purity was assessed by the ratio of absorbance at 260 nm to 280 nm. Subsequently, 1 μg of purified RNA was reverse-transcribed into cDNA using the HiScript II Q RT SuperMix for qPCR (+gDNA wiper) (Vazyme Biotech Co., Ltd., Nanjing, China). qPCR was performed using the ChamQ SYBR qPCR Master Mix (Vazyme Biotech Co., Ltd., Nanjing, China) on a real-time PCR detection system (Roche, Switzerland). The relative mRNA expression levels were determined using the comparative CT method ($2^{-\Delta\Delta Ct}$) and normalized to the expression of the housekeeping gene β-actin. Primer sequences were shown in Table 1.

2.8 Western blotting

Western blot assays were performed as described previously (Wu et al., 2021). The hippocampus was collected and preserved at −80°C for western blotting. Total protein concentration from hippocampal samples was determined using a BCA protein assay kit. Equal amounts

TABLE 1 The RT-qPCR primer sequences used in this study.

No.	Gene symbol	Forward primer (5′–3′)	Reverse primer (5′–3′)
1	TNF-α	CTTGTTGCCTCCTCTTTTGCTTA	CTTTATTTCTCTCAATGACCCGTAG
2	IL-6	CTGCTCATTCACGAAAAGGGA	TCACAGAAGGAGTGGCTAAGGACC
3	IL-1β	TGGGAAACAACAGTGGTCAGG	CTGCTCATTCACGAAAAGGGA
4	β-actin	CGTGGGCCGCCCTAGGCACCA	TTGGCCTTAGGGTTCAGGGGGG

10.3389/fnins.2024.1480000

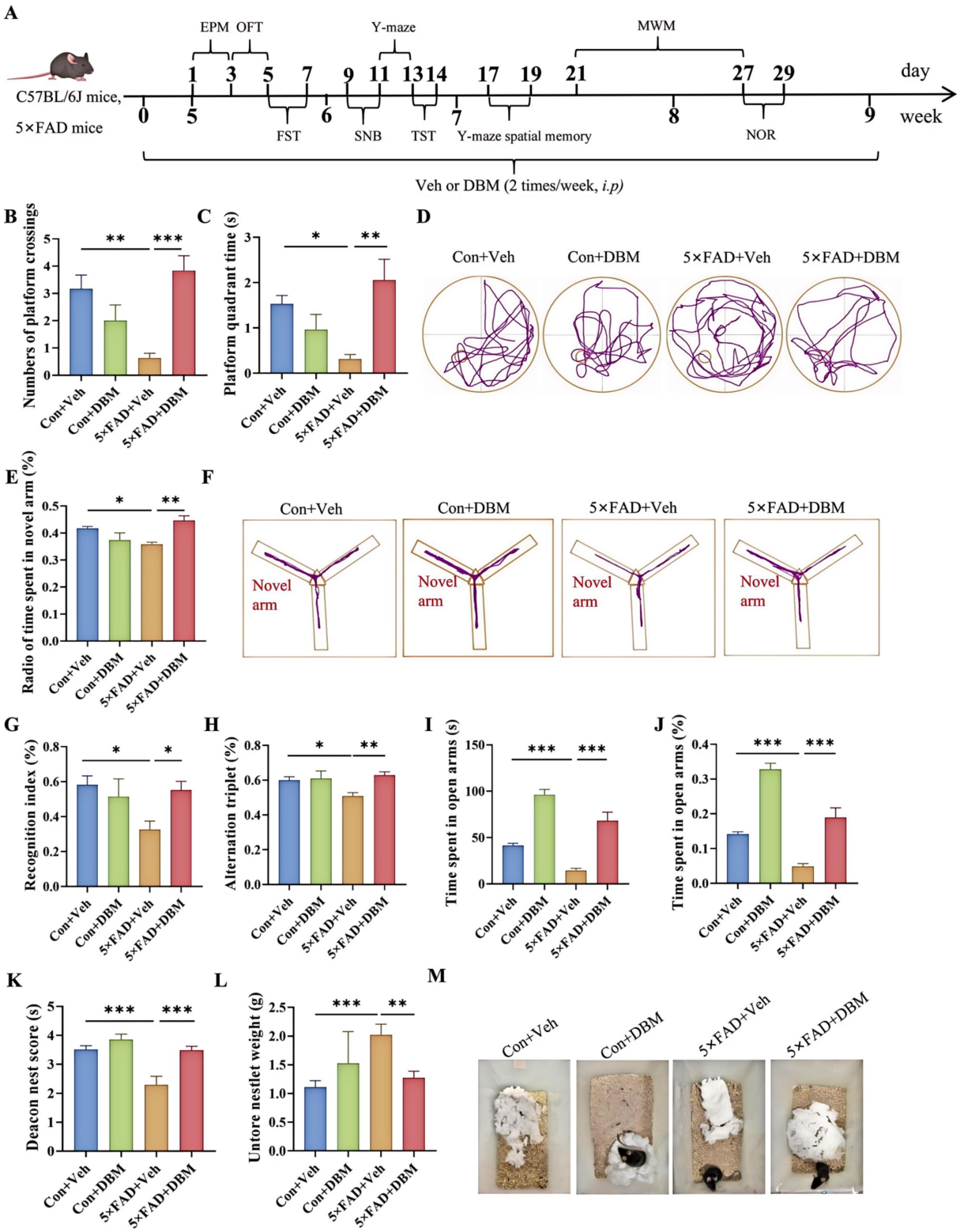

FIGURE 1
Diethyl butylmalonate ameliorates cognitive deficits in 5×FAD mice. **(A)** Schematic timeline for DBM treatment on cognitive deficits and depression in 5×FAD mice. **(B)** Number of platform crossings and **(C)** the platform quadrant time in the Morris water maze were recorded. **(D)** Representative track plots of Con + Veh, Con + DBM, 5×FAD + Veh and 5×FAD + DBM groups recorded by SMART video tracking system in the testing place. **(E)** Radio of time spent in novel arm was recorded in Y-maze spatial memory test. **(F)** Representative track plots of Con + Veh, Con + DBM, 5×FAD + Veh and 5×FAD + DBM groups recorded by SMART video tracking system in the testing place. **(G)** Recogniton index and **(H)** total time were recorded in novel object recognition test. **(I)** Time spent in open arms and **(J)** the index of time spent in open arms were recorded in Y-maze test. **(K)** Deacon nest score and **(L)** untorn nestlet weight (amount of untorn nesting material). **(M)** Representative images of nesting result in Con + Veh, Con + DBM, 5×FAD + Veh and 5×FAD + DBM groups. $n = 12$ mice for each group. Values are mean ± SEM. $^{*}p < 0.05$, $^{**}p < 0.01$, and $^{***}p < 0.001$.

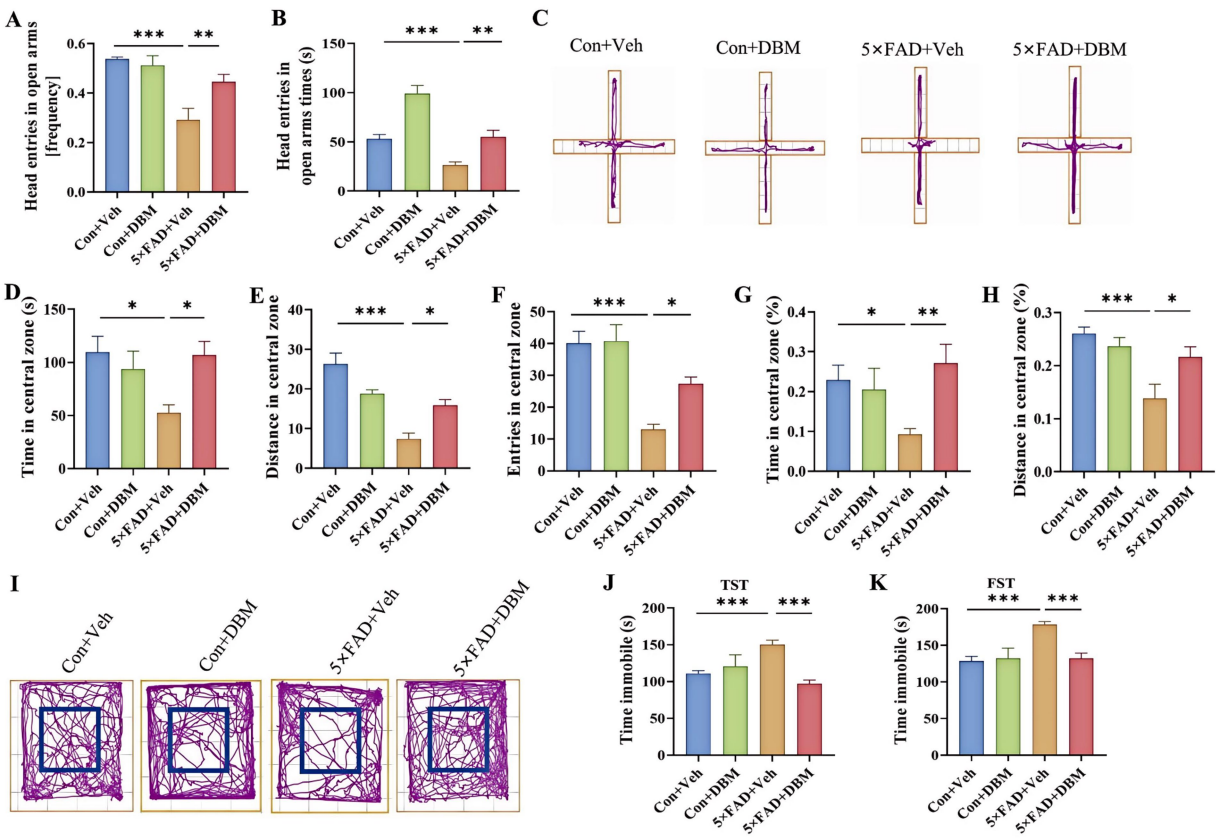

FIGURE 2
Diethyl butylmalonate improves depression in 5×FAD mice. **(A)** The frequency entries in open arms, **(B)** head entries in open arms times, **(C)** representative track plots of Con + Veh, Con + DBM, 5×FAD + Veh and 5×FAD + DBM groups recorded by SMART video tracking system in the elevated plus maze test. **(D)** Time in the central zone, **(E)** distance in the central zone, **(F)** entries in the central zone, **(G)** index of time in the central zone and **(H)** index of distance in the central zone were recorded in the open field test. **(I)** Representative track plots of Con + Veh, Con + DBM, 5×FAD + Veh and 5×FAD + DBM groups recorded by SMART video tracking system in the open field test. **(J)** Time immobile was recorded in tail suspension test. **(K)** Time immobile in forced swimming test. $n = 12$ mice for each group. Values are mean ± SEM. $^{*}p < 0.05$, $^{**}p < 0.01$, and $^{***}p < 0.001$.

of protein were separated via sodium dodecyl sulfate-polyacrylamide gel electrophoresis (SDS-PAGE) and transferred to polyvinylidene difluoride (PVDF) membranes. The membranes were blocked with 5% non-fat milk for 1 h at room temperature, followed by overnight incubation at 4°C with primary antibodies. Primary antibodies included anti-BDNF (Alomone Labs, Jerusalem, Israel; catalog number ANT-010), anti-PSD95 (Cell Signaling Technology; catalog number 3450) and β-actin (ABclonal, AS003). After washing the membranes three times in TBST, they were incubated with an HRP-linked anti-rabbit IgG secondary antibody (ABclonal, AS014) for 1 h at room temperature. After three additional washes, protein bands were detected using Clarity™ ECL Western Blot Substrate (Bio-Rad, 1705060) and visualized with the ChemiDoc Touch imaging system (Bio-Rad). Protein expression levels were normalized to β-actin expression. The procedure for image quantification of western blot band involves scanning the blot to obtain a digital image, followed by ImageJ software analysis. First, background correction is applied to remove non-specific signals. Then, the intensity of each protein band is measured by defining areas of interest. The intensity values are normalized to β-actin, to account for variations in protein loading. Finally, results are analyzed and quantified relative to control samples or other experimental conditions.

2.9 Statistical analysis

Data were presented as mean ± standard error of the mean (SEM) and analyzed using GraphPad Prism software 8.0. One-way analysis of variance (ANOVA) was used to compare four groups, followed by the *post hoc* Tukey–Kramer test for multiple comparisons. p-value <0.05 was considered to indicate statistical significance.

3 Results

3.1 Diethyl butylmalonate ameliorates cognitive deficits in 5×FAD mice

The cognitive function (including recognition memory, spatial memory and ability to perform activities of daily living) can be evaluated by Morris water maze, Y-maze spatial memory, NOR, Y-maze test and nest building test (Hattiangady et al., 2014; Broadbent et al., 2004; Dellu et al., 2000; Deacon, 2006; Yoshizaki et al., 2020). The strategy was shown in Figure 1A. In brief, DBM administration (twice per week), started from the beginning until the ending of behavioral

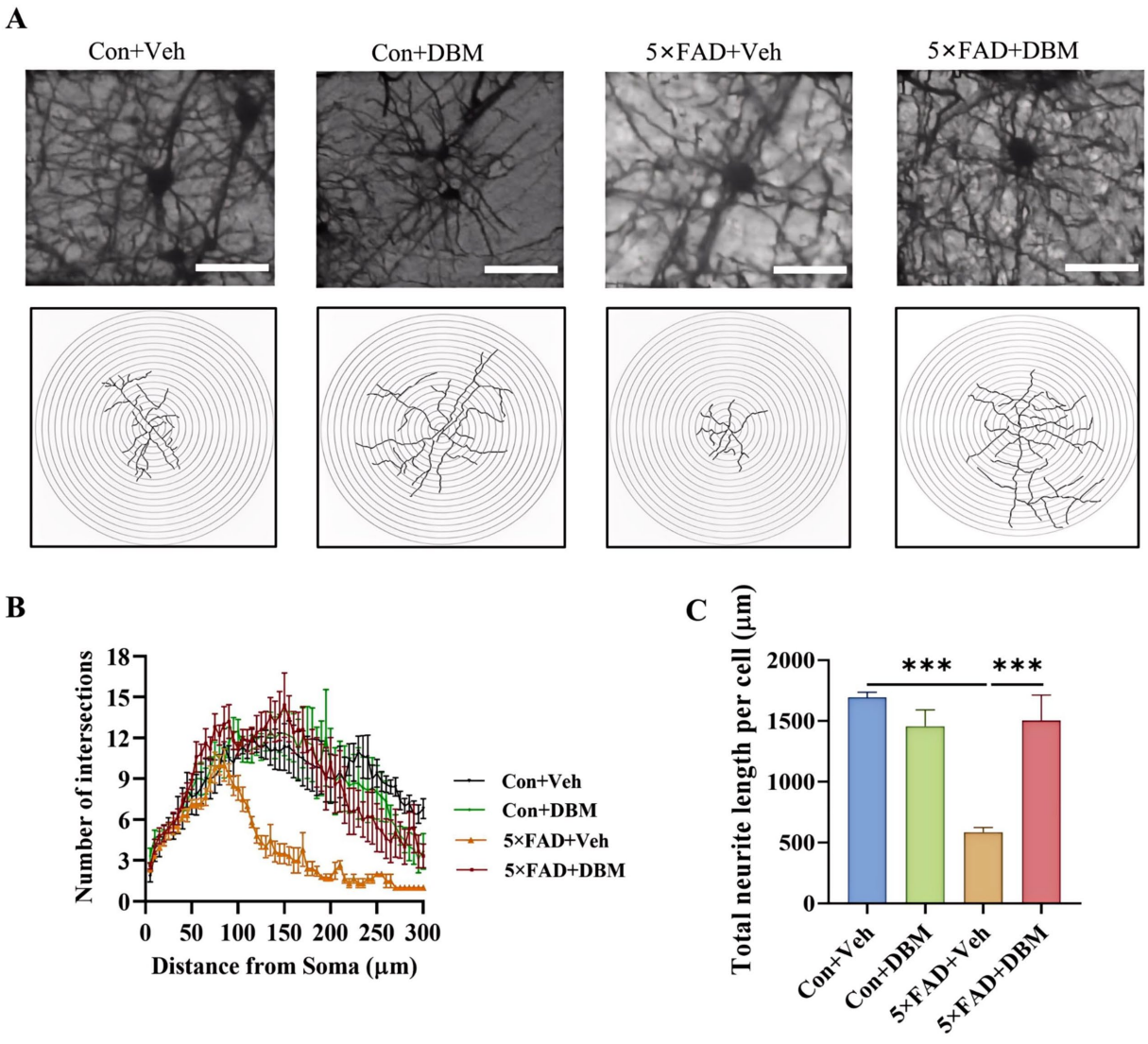

FIGURE 3
Diethyl butylmalonate relieves neuron degeneration in the hippocampus of female 5×FAD mice. Golgi-Cox staining was used to analyze the neuronal morphological variations in the cornu ammonis 1 (CA1) region of the hippocampus of female mice. **(A)** Representative images of pyramidal neurons. **(B)** Sholl analysis of dendritic branching complexity of pyramidal neurons. **(C)** Total neurite length per cell. $n = 3$, scale bars: 100 μm. Values are mean ± SEM. $^{*}p < 0.05$, $^{**}p < 0.01$, and $^{***}p < 0.001$.

tests. In Morris water maze test, the numbers of platform crossings and the platform quadrant time were decreasing in 5×FAD mice compared with the Con + Veh mice ($p < 0.01$, Figure 1B; $p < 0.05$, Figures 1C,D); however, DBM supplementation significantly improved exploration ability, increasing the numbers of platform crossings and the platform quadrant time in 5×FAD mice ($p < 0.001$, Figure 1B; $p < 0.01$, 1B; $p < 0.05$, Figures 1C,D). In Y-maze spatial memory test, DBM supplementation improved spatial recognition memory impairment in 5×FAD mice, as demonstrated by an increase in the ratio of time spent in the novel arm (percentage of time spent in novel arm) (both $p < 0.01$, Figures 1E,F). In NOR, DBM supplementation could prevent recognition memory impairment in 5×FAD mice, with an increase in the novel object recognition index (percentage of time spent with the novel object) ($p < 0.05$, Figure 1G), and there is no significant difference in the total exploration time ($p > 0.05$, Figure 1H). In the Y-maze test, the time spent in open arms and the index of it in the 5×FAD mice was clearly lower than that in the Con + Veh mice, while DBM significantly improved the exploration ability in 5×FAD mice ($p < 0.001$, Figures 1I,J). In NB, the nesting ability of 5×FAD mice was reduced compared to the control + Veh mice and DBM supplementation could recover the nesting building ability ($p < 0.001$, Figure 1K). In contrast, the untore nestlet weight (nest-building deficit) of 5×FAD + DBM mice was significantly decreased compared with that of the 5×FAD group ($p < 0.01$, Figures 1L,M). Overall, these findings indicate that DBM ameliorates cognitive impairment.

3.2 Diethyl butylmalonate attenuates depression in 5×FAD mice

We next evaluated the effects of DBM on depression-like behaviors in 5×FAD mice using elevated plus maze test, open field

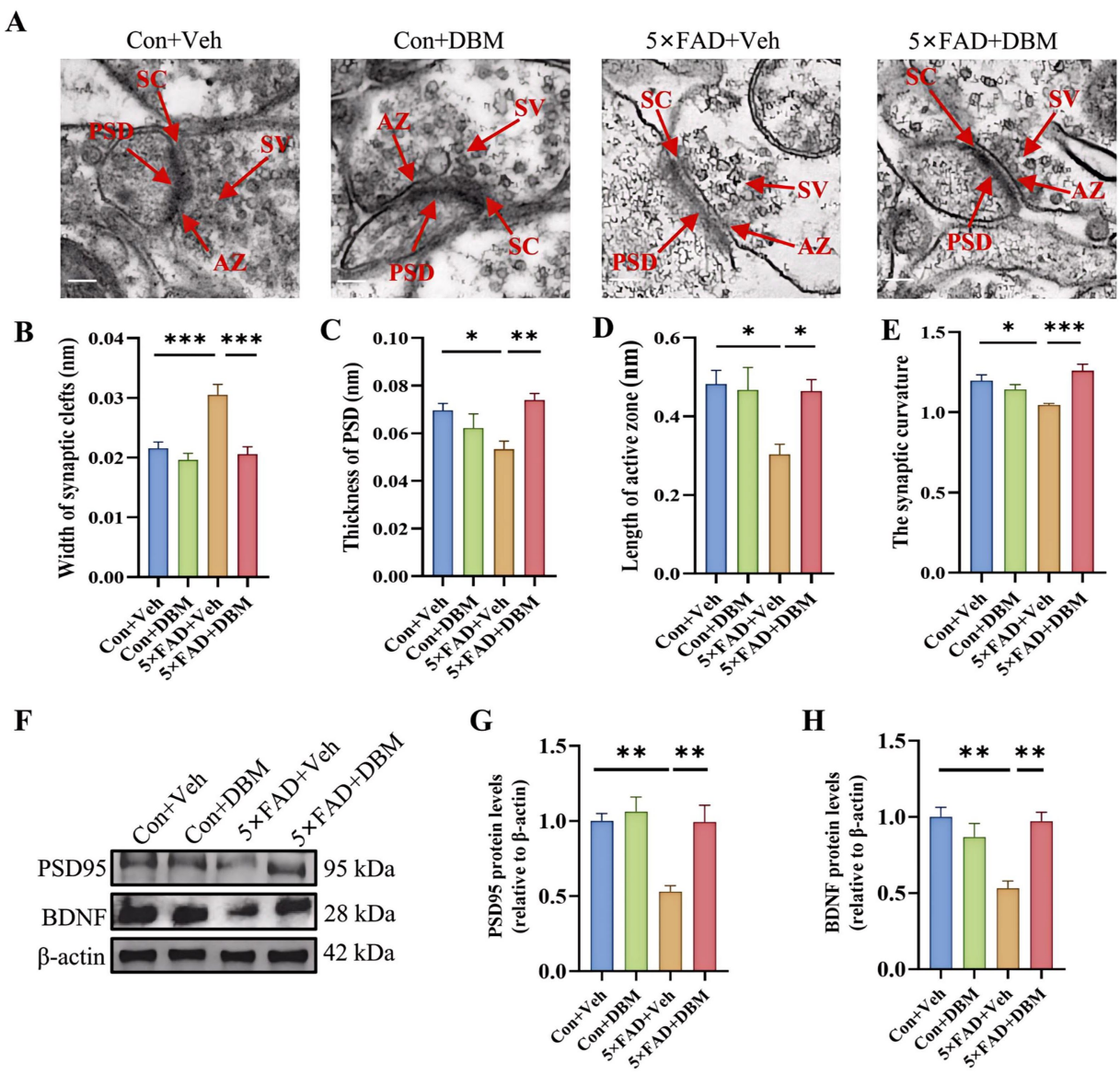

FIGURE 4
Diethyl butylmalonate ameliorates synaptic ultrastructural impairment in the hippocampus of 5×FAD female mice. **(A–E)** Synaptic ultrastructure in the cornu ammonis 1 (CA1) region of the hippocampus of mice was analyzed by transmission electron microscope ($n = 3$, scale bars: 100 nm): **(A)** representative images of synaptic ultrastructure, **(B–E)** the statistical analysis of the synaptic ultrastructure associated indexes ($n = 3$, 5 figures for each group): **(B)** width of synaptic cleft, **(C)** thickness of PSD, **(D)** length of active zone, **(E)** synaptic curvature. **(F–H)** The protein expression of PSD95 **(F, G)**, BDNF **(F, H)** in the hippocampus of mice ($n = 4$). Values are mean ± SEM. *$p < 0.05$, **$p < 0.01$, and ***$p < 0.001$.

test (OFT), tail suspension test (TST) and forced swimming test (FST) (Yoshizaki et al., 2020; Dang et al., 2022; Sithisarn et al., 2013). In the elevated plus maze test, 5×FAD mice showed a significantly reduced frequency of head entries in open arms and the time of head entries in open arms as compared to the Con + Veh mice ($p < 0.001$, Figures 2A–C); while DBM supplementation significantly increased the novel object discrimination index ($p < 0.01$, Figures 2A–C). In OFT, DBM supplementation induced a protective effect on 5×FAD mice represented by an increase in the time in the central zone, the entries in the central zone, the entries in the central zone, the index of the time in the central zone and the index of the distance in the central zone (all $p < 0.05$, Figures 2D–I). Subsequently, in TST, we found that 5×FAD mice displayed a higher level of immobility in comparison to the Con + Veh mice, while DBM supplementation could attenuate the depression-like behavior in 5×FAD mice ($p < 0.001$, Figure 2J). In FST, the result of the time immobile was the same as TST ($p < 0.001$, Figure 2K). Overall, these results suggest that DBM improves depression in 5×FAD mice.

3.3 Diethyl butylmalonate mitigated neurite impairment in the hippocampus of 5×FAD mice

The hippocampus, lying just beneath the neocortex, is implicated in cognitive processing, social recognition and memory (Alexander et al., 2016; Zhou et al., 2015). Neurite impairment in the hippocampus is the key event in AD (Wong et al., 2002). Using

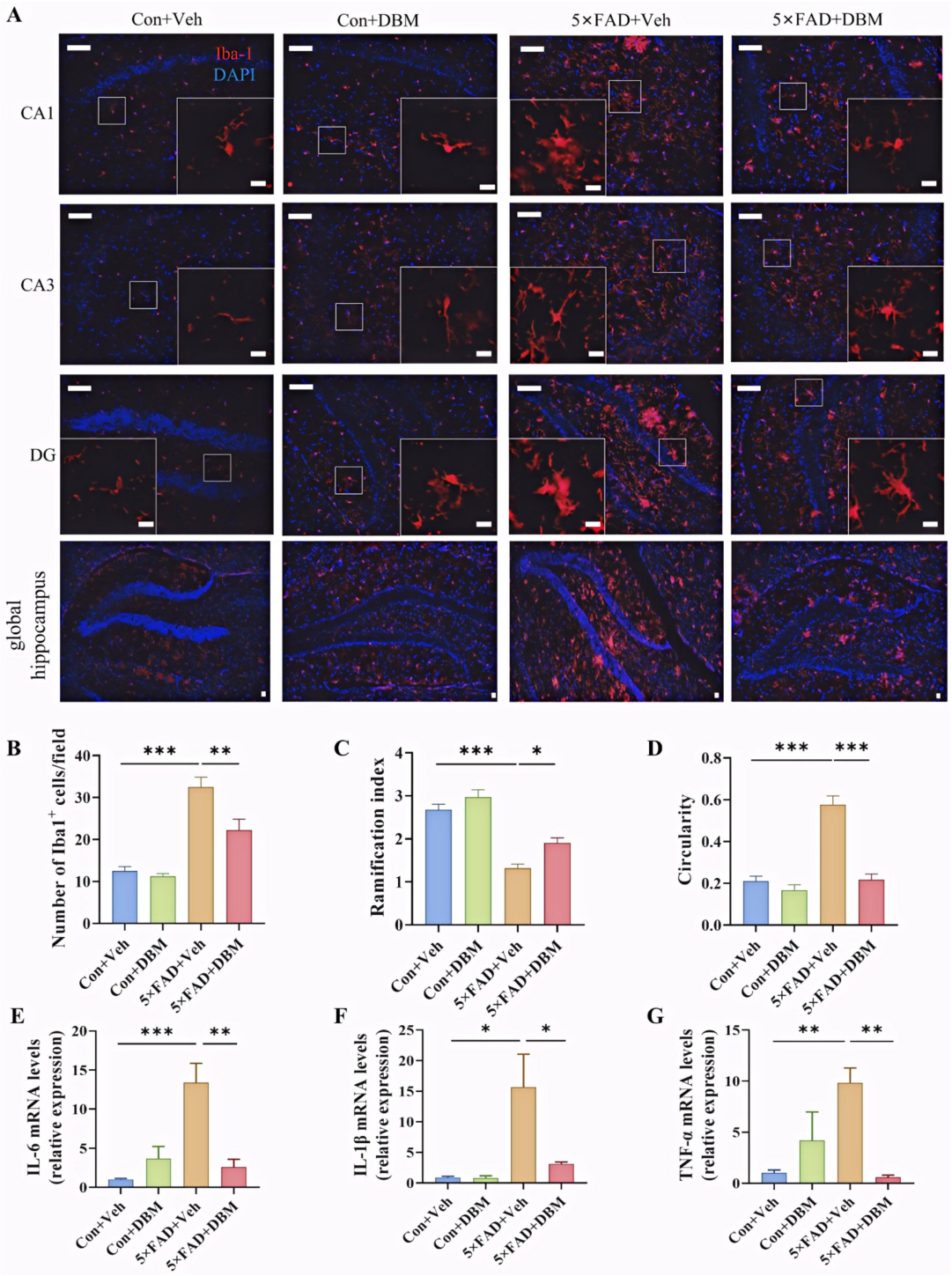

FIGURE 5
Diethyl butylmalonate ameliorates the neuroinflammation in the hippocampus of 5×FAD female mice. **(A)** Representative immunofluorescent staining of the Iba-1$^+$ cells in the CA1, CA3 and DG regions of hippocampus and the global hippocampus ($n = 3$). **(B)** The quantification of Iba-1 cells number in the hippocampus ($n = 3$, 10 images per mouse per region, scale bar: 50 μm). **(C)** The ramification of microglia in the hippocampus ($n = 3$, 10 images per mouse per region, scale bar: 50 μm). **(D)** The circularity of microglia in the hippocampus ($n = 3$, 10 images per mouse per region, scale bar: 50 μm). **(E–G)** The mRNA expression of IL-1β, IL-6 and TNF-α in the hippocampus ($n = 4$). Con + Veh, control mice with vehicle control treatment; Con + DBM, control mice with DBM treatment; 5×FAD + Veh, 5×FAD mice with vehicle control treatment; 5×FAD + DBM: 5×FAD mice with DBM treatment. Values are mean ± SEM. *$p < 0.05$, **$p < 0.01$, and ***$p < 0.001$.

Golgi-Cox staining, we investigated the effects of DBM supplementation on neurite impairment in the hippocampus, a critical brain region responsible for cognition or memory. Sholl analysis showed that 5×FAD + DBM mice had increased dendritic complexity by increasing the sum number of dendritic intersections and the distance of the maximum intersections from the soma (Figures 3A,B). A significant decrease in the total neurite length per cell was observed in 5×FAD mice, while DBM supplementation

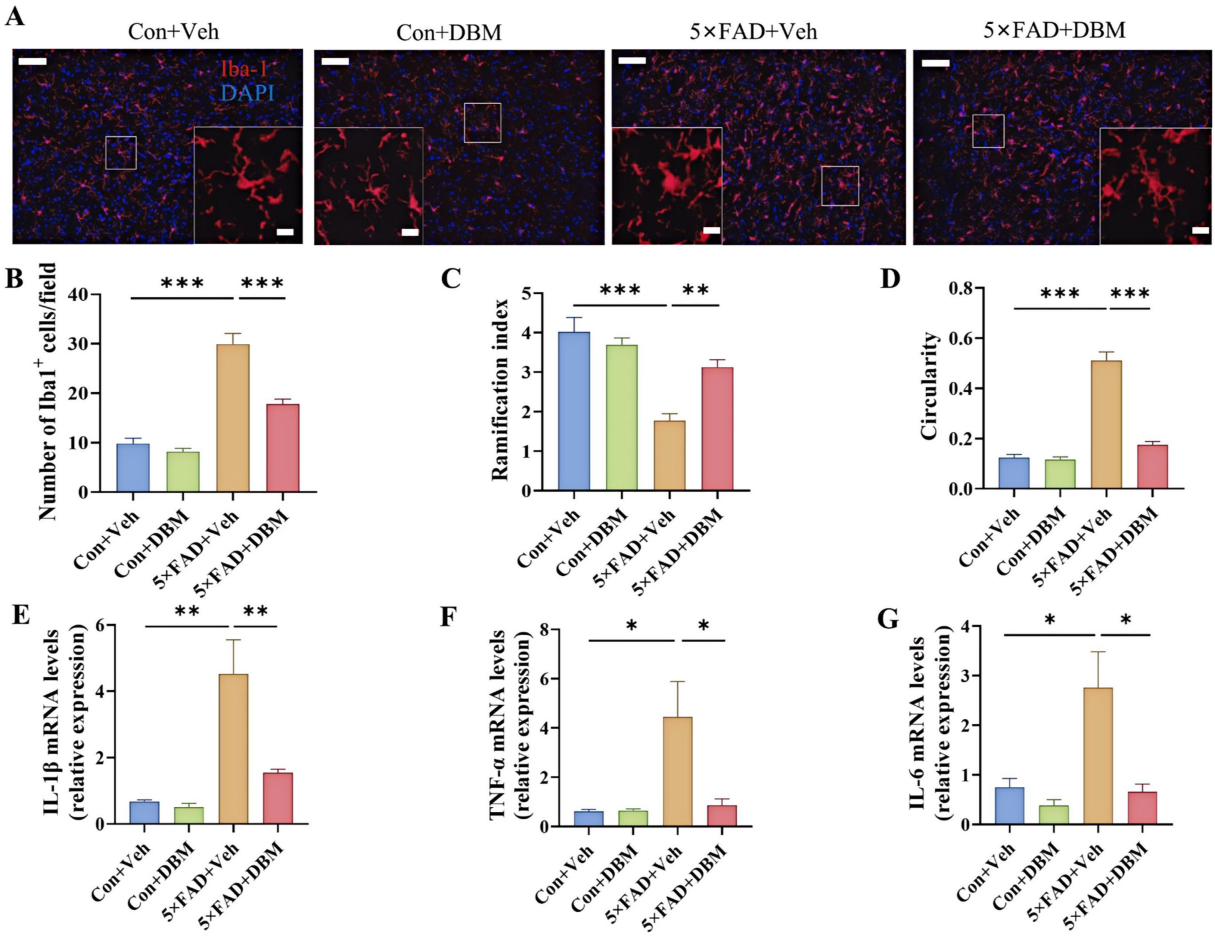

FIGURE 6
Diethyl butylmalonate ameliorates the neuroinflammation in the amygdala of 5×FAD female mice. **(A)** Representative immunofluorescent staining of the Iba-1 cells in the amygdala ($n = 3$). **(B)** The quantification of Iba-1 cells number in the amygdala ($n = 3$, 10 images per mouse per region, scale bar: 50 μm). **(C)** The ramification of microglia in the amygdala ($n = 3$, 10 images per mouse per region, scale bar: 50 μm). **(D)** The circularity of microglia in the amygdala ($n = 3$, 10 images per mouse per region, scale bar: 50 μm). **(E–G)** The mRNA expression of IL-1β, IL-6 and TNF-α the amygdala ($n = 4$). Con + Veh, control mice with vehicle control treatment; Con + DBM, control mice with DBM treatment; 5×FAD + Veh, 5×FAD mice with vehicle control treatment; 5×FAD + DBM: 5×FAD mice with DBM treatment. Values are mean ± SEM. $^{*}p < 0.05$, $^{**}p < 0.01$, and $^{***}p < 0.001$.

increased the length of total neurite per cell ($p < 0.001$, Figures 3A,C). These results indicate that DBM can prevent neurite degeneration and increase neuronal complexity in the hippocampus of 5×FAD mice.

3.4 Diethyl butylmalonate prevents synaptic ultrastructural impairment in the hippocampus of 5×FAD mice

Impairment of synaptic ultrastructure has been implicated in cognitive impairment and AD (Head et al., 2009; Whitfield et al., 2014). Using transmission electron microscopy, we observed an increased width of the synaptic cleft ($p < 0.001$, Figures 4A,B) and a reduction in PSD thickness ($p < 0.05$, Figures 4A,C) in hippocampal CA1 region of 5×FAD mice. However, DBM supplementation shortened the width of synaptic cleft and prevented the decrease in the thickness of PSD ($p < 0.001$, Figure 4B; $p < 0.01$, Figure 4C). It also increase the length of active zone and the synaptic curvature ($p < 0.001$, Figure 4E; $p < 0.05$, Figure 4D) in 5×FAD mice. Furthermore, we found that DBM supplementation prevented the reduction of postsynaptic density protein 95 (PSD95) and brain-derived neurotrophic factor (BDNF) in the hippocampus of the 5×FAD mice ($p < 0.01$, Figures 4F–H). However, DBM did not obviously reduce Aβ deposition in the hippocampus of 5×FAD mice (Supplementary Figure S1). Therefore, DBM plays the protective effect on cognitive memory via improvement of synaptic ultrastructure damage in 5×FAD mice.

3.5 Diethyl butylmalonate ameliorates neuroinflammation in the hippocampus of 5×FAD mice

Activation of microglia is implicated in neuroinflammation and is considered critical in the pathogenesis of AD (Leng and

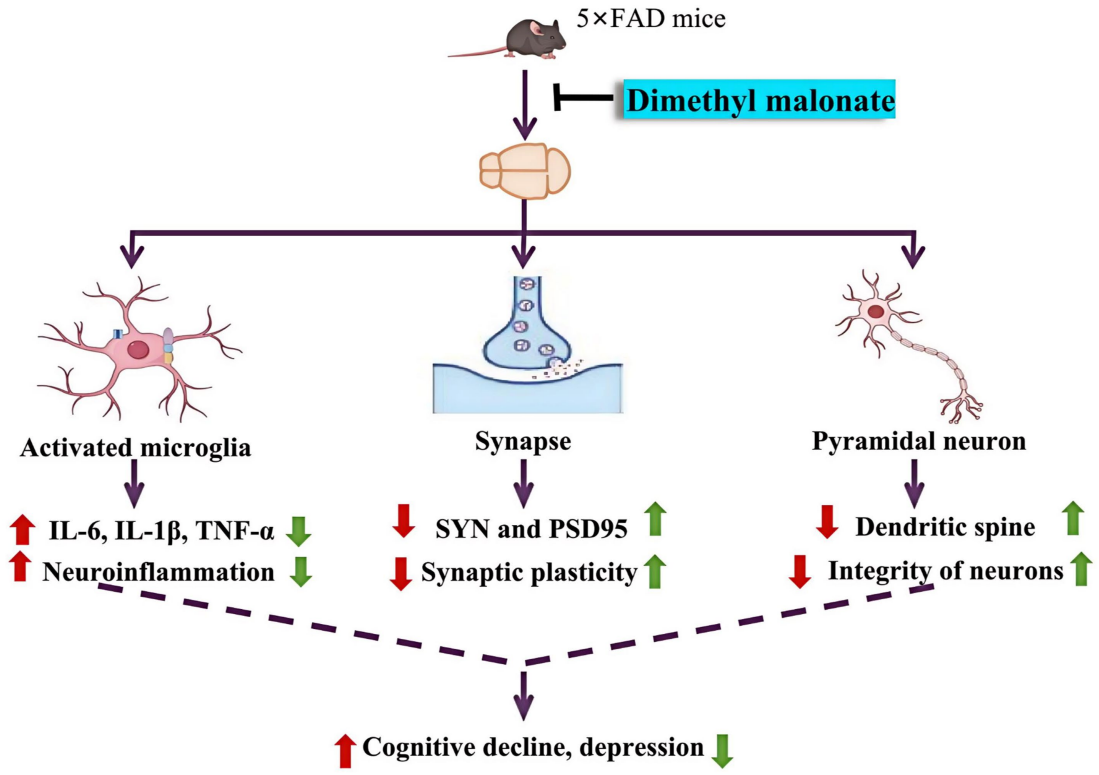

FIGURE 7
Graphical summary of DBM's protective effects on cognitive impairment and depression in 5×FAD mice. In 5×FAD mice, activation of microglia induces the production of pro-inflammatory cytokines in the brains, including the hippocampus and amygdala, reduces the integrity of pyramidal neurons, and impairs synaptic ultrastructure along with the deficits of synapse-related proteins, and consequently causing cognitive decline and depression. However, DBM supplementation alleviates these pathological alterations by inhibiting microglia activation and neuroinflammation. Red arrows represent key events in 5×FAD mice; green arrows represent the amelioration by DBM administration.

Edison, 2021; Subhramanyam et al., 2019; Thakur et al., 2023; Cunningham, 2013). Here, the morphological alteration of microglia was investigated by immunofluorescent staining with Iba1$^+$ (microglia marker) antibody (Figure 5A). We observed the increased microglia number in the hippocampus of the 5×FAD group ($p < 0.001$, Figure 5B). In the 5×FAD group, the majority of Iba1$^+$ microglia showed the morphology of activated microglia with elongated soma and fewer branches in the hippocampus of the hippocampus ($p < 0.001$, Figures 5C,D). In the control and DBM supplementation groups, the Iba1$^+$ microglia showed the characteristic of resting microglia consisting of a rod-shaped cell body with thin processes ($p < 0.05$, Figure 5A; $p < 0.001$, Figure 5D). These results suggest that DBM inhibits the activation of microglia.

Furthermore, we investigated whether DBM could improve the neuroinflammation in the hippocampus. DBM supplementation significantly prevented an increase in the microglia number in these areas ($p < 0.01$, Figure 5B) and the circularity in 5×FAD mice ($p < 0.001$, Figure 5D). DBM supplementation also prevented a decrease in the ramification index in 5×FAD mice ($p < 0.05$, Figure 5C), with a decrease in the mRNA levels of pro-inflammatory cytokines (IL-1β, IL-6, TNF-α) in 5×FAD mice ($p < 0.05$, Figures 5E–G). These results showed that DBM attenuates the neuroinflammation in the hippocampus of 5×FAD mice.

3.6 Diethyl butylmalonate reduces neuroinflammation in the amygdala of 5×FAD mice

Neuroinflammation in the amygdala is closely associated with depression (Zheng et al., 2021). We further characterized the effects of DBM on neuroinflammatory profiles in the amygdala. We observed the increased microglia number in the amygdala of the 5×FAD group and DBM supplementation significantly reduced the microglia number in this region ($p < 0.001$, Figures 6A,B). Correspondingly, in compared with Con + Veh and 5×FAD + DBM groups, the decreased ramification index and increased circularity of microglia were observed in 5×FAD group ($p < 0.01$, Figure 6C; $p < 0.001$, Figure 6D). Furthermore, DBM supplementation significantly prevented the upregulation of IL-1β, IL-6 and TNF-α mRNA expression in the amygdala of 5×FAD ($p < 0.01$, Figure 6E; $p < 0.05$, Figures 6F,G). These results show that DBM attenuates the neuroinflammation in the amygdala of 5×FAD mice.

4 Discussion

The discovery of new effective drugs for AD is imperative yet challenging (Cummings et al., 2023; Price and Duman, 2019). Here,

we investigated the effects of DBM on abnormal behaviors in 5×FAD mice. We showed that DBM supplementation alleviates cognitive impairment and depression along with the improvement of neurite outgrowth, synaptic ultrastructure damage and neuroinflammation (Figure 7). Our findings support that DBM may be a drug candidate for treating neurodegeneration.

AD is a progressive form of dementia marked by cognitive and memory deficits (Leng and Edison, 2021; Fang et al., 2021). Also, depression is one of the most common neuropsychiatric disorders that accompanies AD, appearing in up to 50% of patients (Chi et al., 2014). Neuroinflammation is one of the hallmarks of neuropsychiatric disorders (Leng and Edison, 2021). It is reported that activated microglia release TNF-α, IL-1β and IL-6, and other pro-inflammatory factors that mediate secondary brain damage (Heneka et al., 2015). These pro-inflammatory factors cause harm and neuron loss, ultimately leading to learning and memory dysfunction (Zhao et al., 2021). In addition, neuroinflammation can also adversely affect cognitive function by interfering with normal signaling between neurons (Cunningham, 2013). Thus, neuroinflammation mediated by microglia activation is key for AD progression. Here, using classic behavioral tests, we showed that DBM, a competitive inhibitor of SDH, can attenuate cognitive deficits and depression in 5×FAD mice, which is associated with reduced neuroinflammation.

It has been reported that SDH increases mitochondrial succinate oxidation and mitochondrial membrane potential, thereby promoting ROS production. Inhibiting SDH in macrophages prevents the induction of a range of pro-inflammatory factors typified by IL-1β (Mills et al., 2016). Here, we showed that *in vivo* DBM administration reduces the accumulation of microglia and inhibits the upregulation of pro-inflammatory cytokines in the hippocampus and amygdala, two brain regions associated with cognitive deficits and depression. It is also reported that DBM can downregulate pro-inflammatory response in LPS-stimulated microglia cells (Zhao et al., 2019). Therefore, DBM's anti-inflammatory effect may be attributed to pro-cognition and anti-depression function in AD mice. Furthermore, microglia are able to bind to soluble β-amyloid (Aβ) oligomers and Aβ fibrils via cell-surface receptors and Toll-like receptors in AD (Thakur et al., 2023; Heneka et al., 2015). The deposition in β-amyloid (Aβ) protein are characteristic of the AD brain (Ghosh et al., 2015; Holtzman et al., 2011). However, we only observed a slight decrease of Aβ deposition in the hippocampal region of 5×FAD mice after DBM treatment.

Neurite outgrowth and synaptic plasticity are manipulated by neuroinflammation, and consequently, cognitive deficits and depression (Cai et al., 2019; Heneka et al., 2015). We observed that DBM administration increases the structural integrity and the complexity of neurons in the hippocampus. Furthermore, the dysregulation of synaptic ultrastructure has been implicated in AD patients (Head et al., 2009; Whitfield et al., 2014). Here, we found that the impairment of synaptic ultrastructure in the hippocampus of AD mice is attenuated by DBM treatment. Previous studies have shown the deficits of postsynaptic proteins PSD95 and synaptic plasticity-related protein BDNF in synaptic plasticity, cognitive function and depression (Choo et al., 2017; Wang et al., 2024; Liu et al., 2010). This study showed that DBM supplementation alleviates the protein deficits of PSD95 and BDNF. These data further explain why DBM improves cognitive deficits and depression.

Overall, our study shows that DBM has a beneficial effect on cognitive deficits and depression in AD mice via manipulating neuroinflammation, which provides a novel drug candidate for treating neurodegenerative diseases, including AD. However, this study also has several shortcomings. We only evaluated the protective effect of DBM in female AD mice, since that female mice display accelerated disease progression (Poon et al., 2023). It should be pointed out that DBM's effect on male AD mice should also be investigated in the future. Moreover, we did a series of behavioral tests to confirm the effect of DBM on cognitive impairment and depression. However, in Morris Water Maze test, we did not record the learning curve (the latency time to get on the platform), which might affect the behavioral performance.

Data availability statement

The original contributions presented in the study are included in the article/Supplementary material, further inquiries can be directed to the corresponding authors.

Ethics statement

The animal study was approved by the Guide for the Care and Use of Laboratory Animals of the Ministry of Health (China) and approved by the Ethics Committee of Xuzhou Medical University (Xuzhou, China, SCXK (Su) 2020-0048). The study was conducted in accordance with the local legislation and institutional requirements.

Author contributions

LY: Writing – original draft, Data curation, Formal analysis, Funding acquisition. GS: Writing – original draft, Formal analysis, Methodology. WX: Writing – original draft, Methodology. SL: Writing – original draft, Methodology. YZ: Writing – original draft, Methodology, Visualization. WP: Writing – review & editing, Funding acquisition, Conceptualization. XD: Writing – original draft, Methodology. LF: Writing – review & editing, Conceptualization. QL: Writing – review & editing, Methodology. FS: Writing – original draft, Writing – review & editing, Conceptualization.

Funding

The author(s) declare that financial support was received for the research, authorship, and/or publication of this article. Project support was provided in part by the Natural Science Foundation of Jiangsu Province (No. BK20201459), the Jiangsu Qing Lan Project, the Training Programs of Innovation and Entrepreneurship for College Students in Jiangsu Province (Nos. 202310313092Y and 202410313047Y).

Conflict of interest

The authors declare that the research was conducted in the absence of any commercial or financial relationships that could be construed as a potential conflict of interest.

Publisher's note

All claims expressed in this article are solely those of the authors and do not necessarily represent those of their affiliated organizations, or those of the publisher, the editors and the reviewers. Any product that may be evaluated in this article, or claim that may be made by its manufacturer, is not guaranteed or endorsed by the publisher.

Supplementary material

The Supplementary material for this article can be found online at: https://www.frontiersin.org/articles/10.3389/fnins.2024.1480000/full#supplementary-material

References

Alexander, G. M., Farris, S., Pirone, J. R., Zheng, C., Colgin, L. L., and Dudek, S. M. (2016). Social and novel contexts modify hippocampal CA2 representations of space. *Nat. Commun.* 7:10300. doi: 10.1038/ncomms10300

Bohlson, S. S., and Tenner, A. J. (2023). Complement in the brain: contributions to neuroprotection, neuronal plasticity, and neuroinflammation. *Annu. Rev. Immunol.* 41, 431–452. doi: 10.1146/annurev-immunol-101921-035639

Broadbent, N. J., Squire, L. R., and Clark, R. E. (2004). Spatial memory, recognition memory, and the hippocampus. *Proc. Natl. Acad. Sci. U.S.A.* 101, 14515–14520. doi: 10.1073/pnas.0406344101

Cai, M., Lee, J.-H., and Yang, E. J. (2019). Electroacupuncture attenuates cognition impairment via anti-neuroinflammation in an Alzheimer's disease animal model. *J. Neuroinflammation* 16:264. doi: 10.1186/s12974-019-1665-3

Chi, S., Yu, J. T., Tan, M. S., and Tan, L. (2014). Depression in Alzheimer's disease: epidemiology, mechanisms, and management. *J. Alzheimers Dis.* 42, 739–755. doi: 10.3233/JAD-140324

Choo, M., Miyazaki, T., Yamazaki, M., Kawamura, M., Nakazawa, T., Zhang, J., et al. (2017). Retrograde BDNF to TrkB signaling promotes synapse elimination in the developing cerebellum. *Nat. Commun.* 8:195. doi: 10.1038/s41467-017-00260-w

Cryan, J. F., Mombereau, C., and Vassout, A. (2005). The tail suspension test as a model for assessing antidepressant activity: review of pharmacological and genetic studies in mice. *Neurosci. Biobehav. Rev.* 29, 571–625. doi: 10.1016/j.neubiorev.2005.03.009

Cummings, J. L., Osse, A. M. L., and Kinney, J. W. (2023). Alzheimer's disease: novel targets and investigational drugs for disease modification. *Drugs* 83, 1387–1408. doi: 10.1007/s40265-023-01938-w

Cunningham, C. (2013). Microglia and neurodegeneration: the role of systemic inflammation. *Glia* 61, 71–90. doi: 10.1002/glia.22350

Dang, R. Z., Wang, M., Li, X., Wang, H., Liu, L., Wu, Q., et al. (2022). Edaravone ameliorates depressive and anxiety-like behaviors via Sirt1/Nrf2/HO-1/Gpx4 pathway. *J. Neuroinflammation* 19:41. doi: 10.1186/s12974-022-02400-6

Deacon, R. M. (2006). Assessing nest building in mice. *Nat. Protoc.* 1, 1117–1119. doi: 10.1038/nprot.2006.170

Dellu, F., Contarino, A., Simon, H., Koob, G. F., and Gold, L. H. (2000). Genetic differences in response to novelty and spatial memory using a two-trial recognition task in mice. *Neurobiol. Learn. Mem.* 73, 31–48. doi: 10.1006/nlme.1999.3919

Du, F. (2019). Golgi-Cox staining of neuronal dendrites and dendritic spines with FD rapid GolgiStain™ kit. *Curr. Protoc. Neurosci.* 88:e69. doi: 10.1002/cpns.69

Fan, M., Liu, Y., Shang, Y., Xue, Y., Liang, J., and Huang, Z. (2022). JADE2 is essential for hippocampal synaptic plasticity and cognitive functions in mice. *Biol. Psychiatry* 92, 800–814. doi: 10.1016/j.biopsych.2022.05.021

Fang, F., Gao, Y., Schulz, P. E., Selvaraj, S., and Zhang, Y. (2021). Brain controllability distinctiveness between depression and cognitive impairment. *J. Affect. Disord.* 294, 847–856. doi: 10.1016/j.jad.2021.07.106

Ghosh, C., Seal, M., Mukherjee, S., and Ghosh Dey, S. (2015). Alzheimer's disease: a heme–Aβ perspective. *Acc. Chem. Res.* 48, 2556–2564. doi: 10.1021/acs.accounts.5b00102

Harro, J. (2018). Animal models of depression: pros and cons. *Cell Tissue Res.* 377, 5–20. doi: 10.1007/s00441-018-2973-0

Hartmann, J., Bajaj, T., Otten, J., Klengel, C., Ebert, T., Gellner, A. K., et al. (2024). SKA2 regulated hyperactive secretory autophagy drives neuroinflammation-induced neurodegeneration. *Nat. Commun.* 15:2635. doi: 10.1038/s41467-024-46953-x

Hattiangady, B., Mishra, V., Kodali, M., Shuai, B., Rao, X., and Shetty, A. K. (2014). Object location and object recognition memory impairments, motivation deficits and depression in a model of gulf war illness. *Front. Behav. Neurosci.* 8:78. doi: 10.3389/fnbeh.2014.00078

Head, E., Corrada, M. M., Kahle-Wrobleski, K., Kim, R. C., Sarsoza, F., Goodus, M., et al. (2009). Synaptic proteins, neuropathology and cognitive status in the oldest-old. *Neurobiol. Aging* 30, 1125–1134. doi: 10.1016/j.neurobiolaging.2007.10.001

Heneka, M. T., Carson, M. J., el Khoury, J., Landreth, G. E., Brosseron, F., Feinstein, D. L., et al. (2015). Neuroinflammation in Alzheimer's disease. *Lancet Neurol.* 14, 388–405. doi: 10.1016/S1474-4422(15)70016-5

Holtzman, D. M., Morris, J. C., and Goate, A. M. (2011). Alzheimer's disease: the challenge of the second century. *Sci. Transl. Med.* 3:77sr1. doi: 10.1126/scitranslmed.3002369

Hong, S., Beja-Glasser, V. F., Nfonoyim, B. M., Frouin, A., Li, S., Ramakrishnan, S., et al. (2016). Complement and microglia mediate early synapse loss in Alzheimer mouse models. *Science* 352, 712–716. doi: 10.1126/science.aad8373

Hou, Y., Wei, Y., Lautrup, S., Yang, B., Wang, Y., Cordonnier, S., et al. (2021). NAD^+ supplementation reduces neuroinflammation and cell senescence in a transgenic mouse model of Alzheimer's disease via cGAS-STING. *Proc. Natl. Acad. Sci. U.S.A.* 118:e2011226118. doi: 10.1073/pnas.2011226118

Jawhar, S., Trawicka, A., Jenneckens, C., Bayer, T. A., and Wirths, O. (2012). Motor deficits, neuron loss, and reduced anxiety coinciding with axonal degeneration and intraneuronal Abeta aggregation in the 5XFAD mouse model of Alzheimer's disease. *Neurobiol. Aging* 33:196.e29. doi: 10.1016/j.neurobiolaging.2010.05.027

Koenig, A. M., Arnold, S. E., and Streim, J. E. (2016). Agitation and irritability in Alzheimer's disease: evidenced-based treatments and the black-box warning. *Curr. Psychiatry Rep.* 18:3. doi: 10.1007/s11920-015-0640-7

Kogan, J. H., Frankland, P. W., and Silva, A. J. (2000). Long-term memory underlying hippocampus-dependent social recognition in mice. *Hippocampus* 10, 47–56. doi: 10.1002/(SICI)1098-1063(2000)10:1<47::AID-HIPO5>3.0.CO;2-6

Kraeuter, A. K., Guest, P. C., and Sarnyai, Z. (2019). The Y-maze for assessment of spatial working and reference memory in mice. *Methods Mol. Biol.* 1916, 105–111. doi: 10.1007/978-1-4939-8994-2_10

Leng, F., and Edison, P. (2021). Neuroinflammation and microglial activation in Alzheimer disease: where do we go from here? *Nat. Rev. Neurol.* 17, 157–172. doi: 10.1038/s41582-020-00435-y

Li, Q., Zhao, Y., Guo, H., Li, Q., Yan, C., Li, Y., et al. (2023). Impaired lipophagy induced-microglial lipid droplets accumulation contributes to the buildup of TREM1 in diabetes-associated cognitive impairment. *Autophagy* 19, 2639–2656. doi: 10.1080/15548627.2023.2213984

Lin, S.-S., Zhou, B., Chen, B. J., Jiang, R. T., Li, B., Illes, P., et al. (2023). Electroacupuncture prevents astrocyte atrophy to alleviate depression. *Cell Death Dis.* 14:343. doi: 10.1038/s41419-023-05839-4

Liu, J., Chang, L., Roselli, F., Almeida, O. F., Gao, X., Wang, X., et al. (2010). Amyloid-beta induces caspase-dependent loss of PSD-95 and synaptophysin through NMDA receptors. *J. Alzheimers Dis.* 22, 541–556. doi: 10.3233/JAD-2010-100948

Liu, S., Fan, M., Xu, J. X., Yang, L. J., Qi, C. C., Xia, Q. R., et al. (2022). Exosomes derived from bone-marrow mesenchymal stem cells alleviate cognitive decline in AD-like mice by improving BDNF-related neuropathology. *J. Neuroinflammation* 19:35. doi: 10.1186/s12974-022-02393-2

Liu, B., Kou, J., Li, F., Huo, D., Xu, J., Zhou, X., et al. (2020). Lemon essential oil ameliorates age-associated cognitive dysfunction via modulating hippocampal synaptic density and inhibiting acetylcholinesterase. *Aging* 12, 8622–8639. doi: 10.18632/aging.103179

Lyketsos, C. G., Carrillo, M. C., Ryan, J. M., Khachaturian, A. S., Trzepacz, P., Amatniek, J., et al. (2011). Neuropsychiatric symptoms in Alzheimer's disease. *Alzheimers Dement.* 7, 532–539. doi: 10.1016/j.jalz.2011.05.2410

Mills, E. L., Kelly, B., Logan, A., Costa, A. S. H., Varma, M., Bryant, C. E., et al. (2016). Succinate dehydrogenase supports metabolic repurposing of mitochondria to drive inflammatory macrophages. *Cell* 167, 457–470.e13. doi: 10.1016/j.cell.2016.08.064

Nikolenko, V. N., Oganesyan, M. V., Rizaeva, N. A., Kudryashova, V. A., Nikitina, A. T., Pavliv, M. P., et al. (2020). Amygdala: neuroanatomical and morphophysiological

features in terms of neurological and neurodegenerative diseases. *Brain Sci.* 10:502. doi: 10.3390/brainsci10080502

Paul, B. D. (2022). DUB'ling down uncovers an X-linked vulnerability in Alzheimer's disease. *Cell* 185, 3854–3856. doi: 10.1016/j.cell.2022.09.029

Poon, C. H., Wong, S. T. N., Roy, J., Wang, Y., Chan, H. W. H., Steinbusch, H., et al. (2023). Sex differences between neuronal loss and the early onset of amyloid deposits and behavioral consequences in 5xFAD transgenic mouse as a model for Alzheimer's disease. *Cells* 12:780. doi: 10.3390/cells12050780

Prag, H. A., Pala, L., Kula-Alwar, D., Mulvey, J. F., Luping, D., Beach, T. E., et al. (2022). Ester prodrugs of malonate with enhanced intracellular delivery protect against cardiac ischemia-reperfusion injury *in vivo*. *Cardiovasc. Drugs Ther.* 36, 1–13. doi: 10.1007/s10557-020-07033-6

Price, R. B., and Duman, R. (2019). Neuroplasticity in cognitive and psychological mechanisms of depression: an integrative model. *Mol. Psychiatry* 25, 530–543. doi: 10.1038/s41380-019-0615-x

Restivo, L., Ferrari, F., Passino, E., Sgobio, C., Bock, J., Oostra, B. A., et al. (2005). Enriched environment promotes behavioral and morphological recovery in a mouse model for the fragile X syndrome. *Proc. Natl. Acad. Sci. U.S.A.* 102, 11557–11562. doi: 10.1073/pnas.0504984102

Sangineto, M., Ciarnelli, M., Cassano, T., Radesco, A., Moola, A., Bukke, V. N., et al. (2023). Metabolic reprogramming in inflammatory microglia indicates a potential way of targeting inflammation in Alzheimer's disease. *Redox Biol.* 66:102846. doi: 10.1016/j.redox.2023.102846

Shi, H., Ge, X., Ma, X., Zheng, M., Cui, X., Pan, W., et al. (2021). A fiber-deprived diet causes cognitive impairment and hippocampal microglia-mediated synaptic loss through the gut microbiota and metabolites. *Microbiome* 9:223. doi: 10.1186/s40168-021-01172-0

Sithisarn, P., Rojsanga, P., Jarikasem, S., Tanaka, K., and Matsumoto, K. (2013). Ameliorative effects of acanthopanax trifoliatus on cognitive and emotional deficits in olfactory bulbectomized mice: an animal model of depression and cognitive deficits. *Evid. Based Complement. Alternat. Med.* 2013:701956. doi: 10.1155/2013/701956

Srinivasan, A., Srinivasan, A., and Ferland, R. J. (2020). AutoSholl allows for automation of Sholl analysis independent of user tracing. *J. Neurosci. Methods* 331:108529. doi: 10.1016/j.jneumeth.2019.108529

Subhramanyam, C. S., Wang, C., Hu, Q., and Dheen, S. T. (2019). Microglia-mediated neuroinflammation in neurodegenerative diseases. *Semin. Cell Dev. Biol.* 94, 112–120. doi: 10.1016/j.semcdb.2019.05.004

Thakur, S., Dhapola, R., Sarma, P., Medhi, B., and Reddy, D. H. K. (2023). Neuroinflammation in Alzheimer's disease: current Progress in molecular signaling and therapeutics. *Inflammation* 46, 1–17. doi: 10.1007/s10753-022-01721-1

Walf, A. A., and Frye, C. A. (2007). The use of the elevated plus maze as an assay of anxiety-related behavior in rodents. *Nat. Protoc.* 2, 322–328. doi: 10.1038/nprot.2007.44

Wang, C. S., McCarthy, C. I., Guzikowski, N. J., Kavalali, E. T., and Monteggia, L. M. (2024). Brain-derived neurotrophic factor scales presynaptic calcium transients to modulate excitatory neurotransmission. *Proc. Natl. Acad. Sci. U.S.A.* 121:e2303664121. doi: 10.1073/pnas.2303664121

Whitfield, D. R., Vallortigara, J., Alghamdi, A., Howlett, D., Hortobágyi, T., Johnson, M., et al. (2014). Assessment of ZnT3 and PSD95 protein levels in Lewy body dementias and Alzheimer's disease: association with cognitive impairment. *Neurobiol. Aging* 35, 2836–2844. doi: 10.1016/j.neurobiolaging.2014.06.015

Wong, P. C., Cai, H., Borchelt, D. R., and Price, D. L. (2002). Genetically engineered mouse models of neurodegenerative diseases. *Nat. Neurosci.* 5, 633–639. doi: 10.1038/nn0702-633

Wu, J., Zhu, Y., Zhou, L., Lu, Y., Feng, T., Dai, M., et al. (2021). Parasite-derived excretory-secretory products alleviate gut microbiota dysbiosis and improve cognitive impairment induced by a high-fat diet. *Front. Immunol.* 12:710513. doi: 10.3389/fimmu.2021.710513

Xu, J., Pan, H., Xie, X., Zhang, J., Wang, Y., and Yang, G. (2018). Inhibiting succinate dehydrogenase by dimethyl malonate alleviates brain damage in a rat model of cardiac arrest. *Neuroscience* 393, 24–32. doi: 10.1016/j.neuroscience.2018.09.041

Yang, X., Zheng, M., Zhou, M., Zhou, L., Ge, X., Pang, N., et al. (2022). Lentinan supplementation protects the gut-liver axis and prevents steatohepatitis: the role of gut microbiota involved. *Front. Nutr.* 8:803691. doi: 10.3389/fnut.2021.803691

Yoshizaki, K., Asai, M., and Hara, T. (2020). High-fat diet enhances working memory in the Y-maze test in male C57BL/6J mice with less anxiety in the elevated plus maze test. *Nutrients* 12:2036. doi: 10.3390/nu12072036

Zhang, Z., Lu, Z., Liu, C., Man, J., Li, X., Cui, K., et al. (2021). Protective effects of dimethyl malonate on neuroinflammation and blood-brain barrier after ischemic stroke. *Neuroreport* 32, 1161–1169. doi: 10.1097/WNR.0000000000001704

Zhao, Y. F., Ren, W. J., Zhang, Y., He, J. R., Yin, H. Y., Liao, Y., et al. (2022). High, in contrast to low levels of acute stress induce depressive-like behavior by involving astrocytic, in addition to microglial P2X7 receptors in the rodent hippocampus. *Int. J. Mol. Sci.* 23:1904. doi: 10.3390/ijms23031904

Zhao, W., Xu, Z., Cao, J., Fu, Q., Wu, Y., Zhang, X., et al. (2019). Elamipretide (SS-31) improves mitochondrial dysfunction, synaptic and memory impairment induced by lipopolysaccharide in mice. *J. Neuroinflammation* 16:230. doi: 10.1186/s12974-019-1627-9

Zhao, Y., Zhang, J., Zheng, Y., Zhang, Y., Zhang, X. J., Wang, H., et al. (2021). NAD^+ improves cognitive function and reduces neuroinflammation by ameliorating mitochondrial damage and decreasing ROS production in chronic cerebral hypoperfusion models through Sirt1/PGC-1alpha pathway. *J. Neuroinflammation* 18:207. doi: 10.1186/s12974-021-02250-8

Zheng, Z.-H., Tu, J. L., Li, X. H., Hua, Q., Liu, W. Z., Liu, Y., et al. (2021). Neuroinflammation induces anxiety- and depressive-like behavior by modulating neuronal plasticity in the basolateral amygdala. *Brain Behav. Immun.* 91, 505–518. doi: 10.1016/j.bbi.2020.11.007

Zhou, X., Zhang, F., Hu, X., Chen, J., Wen, X., Sun, Y., et al. (2015). Inhibition of inflammation by astaxanthin alleviates cognition deficits in diabetic mice. *Physiol. Behav.* 151, 412–420. doi: 10.1016/j.physbeh.2015.08.015

frontiers | Frontiers in Neuroscience

TYPE Original Research
PUBLISHED 02 December 2024
DOI 10.3389/fnins.2024.1488820

OPEN ACCESS

EDITED BY
Pradeep Kumar,
All India Institute of Medical Sciences, India

REVIEWED BY
Igor Straka,
Comenius University, Slovakia
Małgorzata Wojtkowska,
Adam Mickiewicz University, Poland

*CORRESPONDENCE
Lifang Zhao
✉ zhaolifang@xwhosp.org

†These authors have contributed equally to this work and share first authorship

RECEIVED 30 August 2024
ACCEPTED 18 November 2024
PUBLISHED 02 December 2024

CITATION
Ying C, Li Y, Zhang H, Pang S, Hao S, Hu S and Zhao L (2024) Probing the diagnostic values of plasma cf-nDNA and cf-mtDNA for Parkinson's disease and multiple system atrophy.
Front. Neurosci. 18:1488820.
doi: 10.3389/fnins.2024.1488820

Probing the diagnostic values of plasma cf-nDNA and cf-mtDNA for Parkinson's disease and multiple system atrophy

Chao Ying[1,2,3,4†], Yuan Li[5†], Hui Zhang[5], Shimin Pang[5], Shuwen Hao[6], Songnian Hu[1,2,3,4] and Lifang Zhao[7*]

[1]Department of Neurobiology, Xuanwu Hospital, Capital Medical University, Beijing, China, [2]Beijing Municipal Geriatric Medical Research Center, Beijing, China, [3]Key Laboratory for Neurodegenerative Diseases of the Ministry of Education, Beijing Key Laboratory on Parkinson's Disease, Parkinson's Disease Center for Beijing Institute on Brain Disorders, Clinical and Research Center for Parkinson's Disease, Capital Medical University, Beijing, China, [4]National Clinical Research Center for Geriatric Disorders, Xuanwu Hospital, Capital Medical University, Beijing, China, [5]Department of Neurology, Xuanwu Hospital, Capital Medical University, Beijing, China, [6]Department of Neurology, The First Hospital of Hebei Medical University, Shijiazhuang, China, [7]Department of Clinical Biobank and Central Laboratory, Xuanwu Hospital, Capital Medical University, Beijing, China

Background: Cell loss and mitochondrial dysfunction are key pathological features of idiopathic Parkinson's disease (PD) and multiple system atrophy (MSA). It remains unclear whether disease-specific changes in plasma circulating cell-free nuclear DNA (cf-nDNA) and mitochondrial DNA (cf-mtDNA) occur in patients with PD and MSA. In this study, we investigated whether plasma cf-nDNA, cf-mtDNA levels, as well as cf-mtDNA integrity, are altered in patients with PD and MSA.

Methods: TaqMan probe-based quantitative PCR was employed to measure plasma cf-nDNA levels, cf-mtDNA copy numbers, and cf-mtDNA deletion levels in 171 participants, including 76 normal controls (NC), 62 PD patients, and 33 MSA patients. A generalized linear model was constructed to analyze differences in circulating cell-free DNA (cfDNA) biomarkers across clinical groups, while a logistic regression model was applied to assess the predictive values of these biomarkers for developing PD or MSA. Spearman correlations were used to explore associations between the three cfDNA biomarkers, demographic data, and clinical scales.

Results: No significant differences in plasma cf-nDNA levels, cf-mtDNA copy numbers, or cf-mtDNA deletion levels were observed among the PD, MSA, and NC groups (all $P > 0.05$). Additionally, these measures were not associated with the risk of developing PD or MSA. In PD patients, cf-nDNA levels were positively correlated with Hamilton Anxiety Rating Scale scores (Rho = 0.382, FDR adjusted $P = 0.027$). In MSA patients, cf-nDNA levels were positively correlated with International Cooperative Ataxia Rating Scale scores (Rho = 0.588, FDR adjusted $P = 0.011$) and negatively correlated with Montreal Cognitive Assessment scores (Rho = −0.484, FDR adjusted $P = 0.044$). Subgroup analysis showed that PD patients with constipation had significantly lower plasma cf-mtDNA copy numbers than those without constipation ($P = 0.049$). MSA patients with cognitive impairment had significantly higher cf-nDNA levels compared to those without ($P = 0.008$).

Conclusion: Plasma cf-nDNA level, cf-mtDNA copy number, and cf-mtDNA deletion level have limited roles as diagnostic biomarkers for PD and MSA. However, their correlations with clinical symptoms support the hypothesis that cell loss and mitochondrial dysfunction are involved in PD and MSA development.

KEYWORDS

circulating cell-free DNA, Parkinson's disease, multiple system atrophy, biomarker, diagnosis, cell-free nuclear DNA, cell-free mitochondrial DNA

Introduction

Parkinson's disease (PD) is a gradually progressive and highly disabling disorder of the central nervous system, primarily affecting the elderly (Opara et al., 2017). The primary clinical manifestations of PD include bradykinesia, rigidity, resting tremor, and postural instability. Non-motor symptoms encompass a reduced sense of smell, depression, and dementia (Calne, 2005; Kummer et al., 2009). Lewy bodies and dopaminergic neuron degeneration are hallmark pathological features of PD. Motor symptoms emerge when 60–80% of dopaminergic neurons in the striatum within the substantia nigra pars compacta are lost (Fearnley and Lees, 1991; Eriksen et al., 2005). Multiple system atrophy (MSA) is a rare and rapidly progressive neurodegenerative disorder classified as an alpha-synucleinopathy. It is characterized by various combinations of clinical manifestations, including autonomic dysfunction, Parkinson's syndrome, cerebellar ataxia, and pyramidal signs. The neuropathological hallmark of MSA is the accumulation of abnormal fibrillar alpha-synuclein in glial cells, forming glial inclusions (Jellinger and Wenning, 2016). Limited accessibility to the central nervous system, combined with the complexity and heterogeneity of symptoms, makes early and accurate diagnosis of these diseases is challenging (Tolosa et al., 2006; Schrag et al., 2015; Dutta et al., 2023). A minimally invasive and reliable assay for early and precise diagnosis of PD and MSA is urgently needed (Postuma and Berg, 2016).

Mitochondrial dysfunction is closely linked to the pathogenesis of PD and MSA. Mitochondria, the cell's energy reservoirs, contain their own DNA. Mitochondrial DNA (mtDNA) is a multicopy extrachromosomal genome that is transcribed and replicated independently of the cell cycle and directs mitochondrial protein synthesis. The mitochondrial genome consists of a double-stranded loop with an outer heavy chain and an inner light chain. The coding region contains 13 genes for the electron transport chain complex, 22 transfer RNAs, 2 ribosomal RNAs, and a non-coding control region with the promoter and the initiation site for heavy chain replication (Phillips et al., 2014). Mitochondrial DNA, typically located near the inner mitochondrial membrane, is exposed to high levels of reactive oxygen species and free radicals generated by the electron transport chain, rendering it susceptible to damage (Raha and Robinson, 2000; Masayesva et al., 2006). Mitochondrial dysfunction is a recognized mechanism potentially involved in the pathogenesis of synucleinopathies, such as PD and MSA. Mitochondrial genome integrity defects have been observed in idiopathic preclinical models and postmortem PD brain tissue (Sanders et al., 2014; Gonzalez-Hunt and Sanders, 2021). Dysfunction in mitochondrial respiratory chain activity, particularly in complex I, has been observed in PD (Schapira et al., 1989). Mitochondrial inhibitors like MPTP and fisetin one contribute to the clinical and neuropathological features of PD (Hatcher et al., 2008). Mitochondrial DNA alterations, including copy number reductions, deletions, point mutations, and impaired maintenance, have been associated with PD development (Autere et al., 2004; Pyle et al., 2016). While most studies focus on PD, mitochondrial defects have also been identified in MSA (Compagnoni et al., 2018). Two studies evaluated respiratory chain activity in MSA patients and healthy controls found reduced complex I activity in patients' skeletal muscle (Blin et al., 1994), but not in platelets or substantia nigra (Gu et al., 1997). Furthermore, studies have reported selective reductions in coenzyme Q10 levels in the cerebellar regions of MSA patients and decreased plasma levels of coenzyme Q10 in these patients as well (Barca et al., 2016; Mitsui et al., 2016; Schottlaender et al., 2016).

Circulating cell-free DNA (cfDNA) carries markers indicative of mitochondrial dysfunction. cfDNA typically comprises nuclear and mitochondrial DNA fragments in the bloodstream, mainly 160–180 bp in length, derived from apoptosis and necrosis (Bruno et al., 2020). The short half-life of cfDNA, approximately 2 h, enables it to accurately reflect dynamic changes in disease-related pathological conditions (Rostami et al., 2020; Loft et al., 2023). cfDNA can be detected months before radiological changes and is used for multiple non-invasive longitudinal assessments. cfDNA can cross the blood-brain barrier, significantly enhancing its clinical utility compared to conventional biomarkers (Loft et al., 2023). Several studies have explored the role of cfDNA in diagnosing and understanding neurodegenerative diseases like PD, with a primary focus on concentration quantification and methylation analysis (Gaitsch et al., 2023; Malhotra et al., 2023). Wojtkowska et al. (2024) analyzed serum circulating cell-free nuclear DNA (cf-nDNA) levels in 30 PD patients and 15 controls by measuring the expression of the nuclear gene *KRAS*, revealing a slight but significant increase in PD patients. However, the increase of cf-nDNA level in PD patients disappeared after adjusting for age (Wojtkowska et al., 2024). In contrast, Scalzo et al. (2009) reported significantly lower cf-nDNA levels in PD patients compared to controls, based on the expression of the nuclear gene β-*globin* in 42 PD patients and 20 controls. Additionally, some studies analyzed circulating cell-free mitochondrial DNA (cf-mtDNA) levels in

cerebrospinal fluid (CSF) and serum of PD patients, though the results were inconsistent (Müller-Nedebock et al., 2019; Kunze et al., 2023). Another critical issue is that current cf-mtDNA studies primarily rely on cerebrospinal fluid (CSF) and serum. Due to the invasive nature of CSF collection and the risk of leukocyte DNA contamination in serum, plasma-derived cfDNA may be more suitable for biomarker studies (Kerachian et al., 2021; Malhotra et al., 2023).

This study aimed to evaluate whether plasma cf-nDNA level, cf-mtDNA copy number, and cf-mtDNA deletion level are altered in patients with PD and MSA, and whether these changes correlate with the risk of developing PD and MSA. Furthermore, we explored the relationships between these cfDNA markers and motor as well as non-motor symptoms in patients with PD and MSA.

Materials and methods

Study subjects

This cross-sectional study recruited 171 participants from May to November 2022 at Xuanwu Hospital, Capital Medical University. Sixty-two participants with PD were diagnosed using the 2015 MDS clinical diagnostic criteria (Postuma et al., 2015). Individuals with a first- or second-degree relative with a family history of PD or onset before age 50 were excluded. Probable MSA was diagnosed according to the second consensus statement on MSA diagnosis (Gilman et al., 2008). Patients were then classified into two subtypes based on predominant motor symptoms: MSA-P (predominant parkinsonism) and MSA-C (predominant cerebellar ataxia). Diagnoses were confirmed by at least two experienced specialists in movement disorders. Patients were excluded if they had: (i) Severe dementia or communication difficulties; (ii) Complications like aphasia and severe dysarthria affecting clinical evaluation; (iii) Parkinsonian syndromes due to cerebrovascular, hypoxic, traumatic, infectious, metabolic, or systemic diseases affecting the central nervous system (Li et al., 2020). The study included 76 NCs with no known medical conditions. Exclusion criteria for NCs included a family history of synucleinopathy, neuropathy, psychiatric illness, a history of head injury, or signs of Rapid Eye Movement sleep behavior disorder (RBD). Additionally, individuals with cancer, end-stage renal disease, active infections, significant trauma, autoimmune disease, or chronic inflammatory disorders were excluded from both groups. All procedures were approved by the Xuanwu Hospital Medical Research Ethics Committee and Institutional Review Board (approval number: [2022]047), following the Declaration of Helsinki. All participants and/or their legal proxies provided written informed consent.

Clinical assessment

Site investigators thoroughly assessed participants' demographics and clinical characteristics. Blood samples were collected within one week of the clinical assessments. Demographic data included age, sex, body mass index (BMI), education level, disease duration, and smoking and drinking history. BMI was calculated as weight (kg) divided by height squared (m^2). Smoking and drinking history were categorized as "ever" or "never." Disease duration was defined as the time from the onset of first motor symptoms to the blood sampling date. Medical histories of diabetes, hypertension, coronary heart disease, cerebrovascular disease, and hyperlipidemia were self-reported. Clinical characteristics were assessed using multiple scales for motor and non-motor symptoms. Motor symptoms were assessed using part III of the Movement Disorder Society-Unified Parkinson's Disease Rating Scale (MDS-UPDRS) for PD and MSA patients, and the Unified Multiple System Atrophy Rating Scale (UMSARS) for MSA patients. PD patients with Hoehn and Yahr (H&Y) stage ≤ 2 were considered to have early-stage PD, while those with H&Y stage 2.5–5 were classified as intermediate- to late-stage PD. Cognitive function was assessed using the Mini-Mental State Examination (MMSE) and Montreal Cognitive Assessment (MoCA). Depression and anxiety were evaluated using the Hamilton Depression Rating Scale (HAM-D) and Hamilton Anxiety Rating Scale (HAM-A). RBD symptom history and severity were evaluated using the RBD Questionnaire-Hong Kong (RBDQ-HK). The overall non-motor symptoms burden was assessed using the Non-Motor Symptom Scale (NMSS), and constipation was screened by the part 21 of NMSS. Olfactory function was assessed using the Argentine Hyposmia Rating Scale (AHRS). The International Cooperative Ataxia Rating Scale (ICARS) was used to evaluate ataxia severity in MSA patients. PD Motor subtypes were classified as tremor dominant (TD), postural instability and gait difficulty (PIGD), or mixed (MIX) phenotype based on the ratio of mean tremor score to mean PIGD score in MDS-UPDRS (Stebbins et al., 2013). Considering the effect of education level on cognition, 1 point was added to MoCA scores (< 30) for subjects with ≤ 12 years of education. H&Y stage and MDS-UPDRS were assessed in the OFF state for PD patients.

Sample collection and cfDNA isolation

Blood samples were collected in EDTA tubes and centrifuged at 1,600 *g* for 10 min at 4°C, within 2 h of collection. The supernatant, free of cellular components, was carefully transferred to a new tube, minimizing disruption of the cell pellet. A second centrifugation at 16,000 *g* for 10 min at 4°C was performed to remove residual cellular debris. The clarified supernatant was gently mixed by inversion to achieve uniformity aliquoted, and stored at −80°C for cfDNA extraction. Plasma stored at −80°C was purified for cfDNA within six months. cfDNA was isolated from 500 μL of plasma aliquots using the VAHTS§ Serum/Plasma Circulating DNA Kit (Vazyme Biotech, Nanjing, China) according to the manufacturer's protocol. The eluted cfDNA was divided into three aliquots to minimize degradation from repeated freeze-thaw cycles and stored at −80°C.

Quantification of cf-nDNA levels, cf-mtDNA copy numbers and cf-mtDNA deletion levels

TaqMan-based quantification of cf-nDNA and cf-mtDNA levels was performed using established methods (Lowes et al.,

2019; Davis et al., 2020). The nuclear housekeeping gene (*RPP30*) and two mitochondrial regions (*MT-ND1* and *MT-ND4*) were measured in three independent PCR runs and were expressed as ng/mL of plasma. *RPP30* levels represent total plasma cf-nDNA concentration. cf-mtDNA copy number was determined by comparing mitochondrial *MT-ND1* to the single-copy nuclear gene *RPP30*. cf-mtDNA deletion level was expressed as the ratio of *MT-ND1* to *MT-ND4*. *RPP30* was amplified and quantified using the following primers and probe: 5′-AGATTTGGACCTGCGAGCG-3′ (forward), 5′-GAGCGGCTGTCTCCACAAGT-3′ (reverse), 5′-FAM-TTCTGACCTGAAGGCTCTGCGCG-BHQ1-3′ (probe). The *ND1* region was amplified and quantified using the following primers and probe: 5′-CCCTAAAACCCGCCACATCT-3′ (forward), 5′-GAGCGATGGTGAGAGCTAAGGT-3′ (reverse), 5′-HEX-CCATCACCCTCTACATCACCGCCC-BHQ1-3′ (probe). The *ND4* region was amplified and quantified using the following primers and probe: 5′-CCATTCTCCTCCTATCCCTCAAC-3′ (forward), 5′-CACAATCTGATGTTTTGGTTAAACTATATTT-3′ (reverse), 5′-FAM-CCGACATCATTACCGGGTTTTCCTCTTG-BHQ1-3′ (probe). Each reaction was run on a LightCycler 480 (Roche, Mannheim, Germany) in a 20 μL volume, containing 2 μL of isolated cfDNA template, 2 μL of 10 × Ex Taq Buffer (Mg^{2+} plus) (20 mM), 1 μL of dNTP Mixture (2.5 mM each), 0.2 μL of TaKaRa Ex Taq HS (5 U/μL), 0.4 μL of each primer and probe (10 μM), and 13.6 μL of double-distilled water. Thermal cycling profiles for *RPP30*, *ND1*, and *ND4* included initial denaturation at 94°C for 1 min, followed by 40 cycles of denaturation at 95°C for 15 s, and annealing/extension at 64°C for 1 min, with fluorescence data collected at 64°C.

Quality control of qPCR

To ensure accuracy and reliability, blinded quantitative polymerase chain reaction (qPCR) assays were performed following a standardized and rigorous approach. Melting curve analysis was conducted after each reaction to confirm PCR product specificity and identity. Triplicate reactions were performed, and mean values were calculated with a standard deviation (SD) of less than 0.5 for Cq values. All cfDNA samples were required to fall within the linear range of a standard curve established through serial dilutions of pooled human leukocyte genomic DNA. Amplified target concentrations were computed by correlating Cq values with the standard curve, accounting for dilution factors from the initial plasma sample to the final PCR reaction. The standard curve concentration range was 4.0 ng/μL to 0.0165 ng/μL for *RPP30*, and 38.0 ng/μL to 0.125 ng/μL for *ND1* and *ND4*. Standard curve accuracy was confirmed by ensuring an R^2 value greater than 0.999 and amplification efficiency between 90 – 110%. Calibrator DNA from healthy donors was included on each plate to normalize Cq values and compensate for inter-plate variations in PCR efficiency. The inter-assay coefficient of variation was calculated for each target, with measurements repeated if it exceeded two SD. A negative control was always included to ensure no product detection until at least five cycles beyond the lowest concentration on the standard curve, avoiding false-positive results.

Statistical analysis

Sample size was not determined using statistical methods but was similar to that in previous studies (Park et al., 2022; Wojtkowska et al., 2024). Participants were classified into NC, PD, and MSA groups by diagnoses. Baseline characteristics were summarized and compared between groups. Continuous variables were evaluated for normality with the Shapiro–Wilk test and homogeneity with Levene's chi-square test. Normally distributed data were reported as mean ± SD and compared with one-way ANOVA. Non-normally distributed data were presented as median with interquartile range and compared using the Mann–Whitney U or Kruskal–Wallis H test. Categorical variables were presented as counts (percentage) and compared with chi-square tests or Fisher's exact test. Additional *post hoc* comparisons were conducted between groups using Bonferroni correction. A general linear regression model was used to compare plasma cf-nDNA levels, cf-mtDNA copy numbers, and cf-mtDNA deletion levels across disease groups and subgroups, adjusting for age, sex, BMI, and education level. Spearman's rank correlation analyses with false discovery rate (FDR) adjustment were performed, controlling for age, sex, BMI, and education level, to assess correlations between cfDNA biomarkers and various clinical factors, including age, disease duration, H&Y stage, MMSE, MoCA, HAM-D, HAM-A, RBDQ-HK, UPDRS-III, NMSS, UMSARS, and ICARS scores. Univariate and multivariate logistic regression models were constructed to compute odds ratio (OR) and 95% confidence interval (CI) to evaluate the association between three significant biomarkers and the risk of PD and MSA. The multivariate model was adjusted for age, sex, BMI, education level, and other potential confounders. Additionally, cfDNA biomarkers were included in models as continuous variables (per SD) and categorical variables (in tertiles) to verify the robustness of the association. Linear trend was examined by using the median of each tertile subgroup as a continuous variable. All statistical analyses were conducted using SPSS V.22.0 (IBM Corp., New York, NY, USA) and R3.2.3 (AT&T, now Lucent Technologies, Vienna, Austria). A two-tailed $P < 0.05$ was considered statistically significant.

Results

Subject characteristics

The study included 171 participants: 62 with PD, 33 with MSA, and 76 NC. Table 1 presents the baseline demographic and clinical characteristics of participants. Significant differences in age and education levels were observed among the NC, MSA, and PD groups. Additionally, distinct differences in lifestyle factors (e.g., smoking) and comorbid conditions (e.g., hypertension, coronary heart disease, cerebrovascular disease) were observed among the three groups. Participants with PD and MSA scored significantly lower on cognitive assessments, as indicated by lower MMSE and MoCA scores. Furthermore, the PD and MSA groups had significantly higher scores on the HAM-D, the HAM-A, and the RBDQ-HK compared to the NC group. No significant differences in the prevalence of hyperlipidemia were observed among the three groups.

TABLE 1 Baseline characteristics of the participants in the study.

Characteristics	NC (*n* = 76)	PD (*n* = 62)	MSA (*n* = 33)
Age, years	70.05 ± 5.12	65.77 ± 5.63***‡‡	62.39 ± 4.23†††
Female (%)	50 (65.8%)	40 (64.5%)	15 (45.5%)
BMI	23.95 [22.00; 25.83]	24.35 [22.75; 25.98]	25.10 [23.80; 26.40]
Education, years	12.58 [11.00; 15.00]	11.43 [9.00; 15.00]	10.94 [9.00; 12.00]†
Disease duration, years	NA	3.03 [1.80; 4.64]	2.37 [1.89; 3.27]
Smoke (%)	6 (7.9%)	12 (19.4%)	12 (36.4%)†††
Drink (%)	30 (39.5%)	14 (22.6%)	9 (27.3%)
Hypertension (%)	31 (40.8%)	30 (48.4%)‡	7 (21.2%)
Diabetes (%)	11 (14.5%)	15 (24.2%)	10 (30.3%)
Coronary heart disease (%)	2 (2.6%)	13 (21.0%)**	1 (3.0%)
Cerebrovascular disease (%)	0 (0.0%)	15 (24.2%)***	6 (18.2%)††
Hyperlipidemia (%)	29 (38.2%)	15 (24.2%)	12 (36.4%)
H&Y stage	NA	2.00 [2.00; 2.00]‡‡‡	2.50 [2.00; 3.00]
MDS-UPDRS-III	NA	32.00 [22.00; 42.00]	29.00 [21.00; 39.00]
UMSARS-II	NA	NA	15.38 ± 7.02
ICARS scores	NA	NA	21.39 ± 9.93
NMSS scores	NA	29.00 [8.00; 55.00]	37.00 [26.00; 61.00]
AHRS scores	NA	20.00 [12.00; 24.00]‡‡‡	24.00 [24.00; 24.00]
MMSE scores	29.00 [28.00; 30.00]	27.00 [25.25; 28.00]***	27.00 [26.00; 28.00]†††
MOCA scores	26.00 [25.00; 27.25]	22.50 [20.00; 26.00]***	22.00 [20.00; 25.00]†††
HAM-D scores	2.00 [1.00; 4.00]	7.00 [2.00; 13.00]***	6.00 [3.00; 13.00]†††
HAM-A scores	4.50 [2.00; 7.25]	9.50 [3.25; 17.75]***	10.00 [4.00; 17.00]††
RBDQ-HK scores	1.00 [0.00; 3.00]	15.00 [2.00; 32.75]***	32.00 [22.00; 49.00]†††
cf-nDNA level (ng/ml)	8.66 [6.20; 12.38]	8.51 [6.43; 9.95]	7.48 [5.84; 9.30]
ND1 (ng/ml)	95.69 [48.55; 137.23]	73.88 [33.22; 133.23]	73.01[49.94; 127.62]
ND4 (ng/ml)	86.46 [44.37; 129.09]	69.46 [30.62; 123.68]	67.46 [44.08; 119.32]
cf-mtDNA copy number	10.26 [4.91; 17.18]	9.39 [3.91; 16.78]	9.19 [6.65; 16.68]
cf-mtDNA deletion level	1.07 ± 0.07	1.07 ± 0.06	1.08 ± 0.07

Continuous variables are reported as mean ± standard deviation or median (interquartile range), and categorical variables are displayed as numbers (%). BMI, body mass index; NC, normal control; H&Y, Hoehn and Yahr; MDS-UPDRS-III: movement disorder society-unified Parkinson's disease rating scale part III; UMSARS, unified multiple system atrophy rating scale part II; NMSS, non-motor symptom scale; MMSE, mini-mental state examination; AHRS, Argentine Hyposmia Rating Scale; ICARS, international cooperative ataxia rating scale; MoCA, montreal cognitive assessment; HAM-D, Hamilton depression scale; HAM-A, Hamilton anxiety scale; RBDQ-HK, rapid eye movement sleep behavior disorder questionnaire-Hong Kong; PD, Parkinson's disease; MSA, multiple system atrophy; cf-mtDNA, circulating cell-free mitochondrial DNA; cf-nDNA, circulating cell-free nuclear DNA; NA, not applicable. PD vs. NC, $^{**}P < 0.01$, $^{***}P < 0.001$; MSA vs. NC, $^{\dagger}P < 0.05$, $^{\dagger\dagger}P < 0.01$, $^{\dagger\dagger\dagger}P < 0.001$; PD vs. MSA, $^{\ddagger}P < 0.05$, $^{\ddagger\ddagger}P < 0.01$, $^{\ddagger\ddagger\ddagger}P < 0.001$.

Intergroup and subgroup comparisons of plasma cfDNA biomarkers

A generalized linear model, adjusted for age, sex, BMI, and education level, was used to compare cf-nDNA levels, cf-mtDNA copy numbers and cf-mtDNA deletion levels across the different groups. The analysis showed no significant differences in plasma cf-nDNA levels between the PD, MSA, and NC groups (all $P > 0.05$; Figure 1A). Similarly, cf-mtDNA copy numbers and deletion levels did not differ significantly among the PD, MSA, and NC groups (all $P > 0.05$; Figures 1B, C). Additionally, when grouping PD patients according to disease stage and motor typing, or grouping MSA patients according to disease subtype, no significant differences were observed in the three plasma cfDNA biomarkers among these groupings (all $P > 0.05$; Figures 2A–I).

Associations between cfDNA biomarkers and risk of developing PD and MSA

We investigated the associations between cfDNA biomarkers and the risks of developing PD and MSA. After adjusting for age, sex, BMI, education level, hypertension, coronary heart disease, and cerebrovascular disease, no significant associations were found between cf-nDNA level (OR: 0.74; 95% CI: 0.42–1.20; $P = 0.247$), cf-mtDNA copy number (OR: 1.21; 95% CI: 0.75–1.92; $P = 0.427$), or cf-mtDNA deletion level (OR: 1.02; 95% CI: 0.64–1.61; $P = 0.943$)

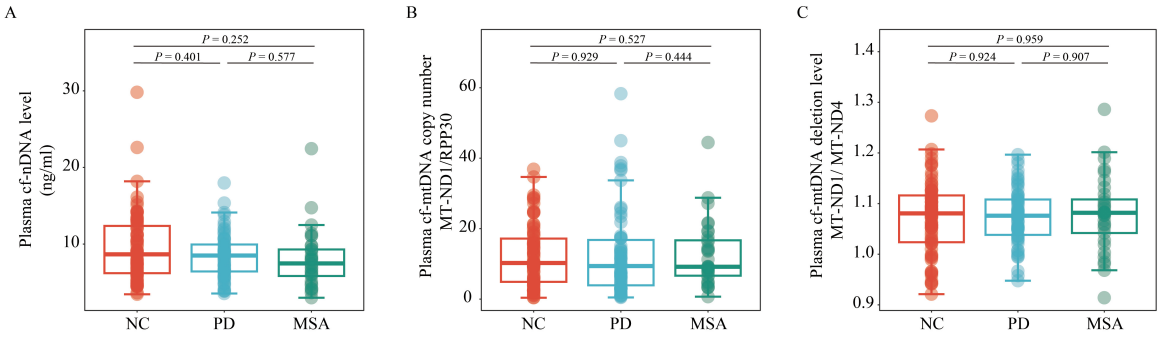

FIGURE 1
Comparison of plasma cf-nDNA levels, cf-mtDNA copy numbers and deletion levels among NC (n = 76), PD (n = 62), and MSA (n = 33). The figure illustrates plasma: **(A)** cf-nDNA level, represented by *RPP30*; **(B)** cf-mtDNA copy number, represented by the ratio of *MT-ND1* to *RPP30*; **(C)** cf-mtDNA deletion level, represented by the ratio of *MT-ND1* to *MT-ND4*, across the three groups. Statistical analysis was performed using a generalized linear model, adjusting for age, gender, BMI, and educational level. Boxplots indicate the median and IQR. The upper whisker extends to the highest value within 1.5 times the IQR, and the lower whisker to the lowest value within 1.5 times the IQR. Data points outside the whiskers are classified as "outliers." PD, Parkinson's disease; MSA, multiple system atrophy; NC, normal control; cf-mtDNA, circulating cell-free mitochondrial DNA; cf-nDNA, circulating cell-free nuclear DNA; IQR, interquartile range.

and the risk of developing PD (Table 2). Similar findings were observed when the levels of the three cfDNA markers were stratified into tertiles. Additionally, trend tests did not show significant linear correlations between cf-nDNA level (P for trend = 0.422), cf-mtDNA copy number (P for trend = 0.462), or cf-mtDNA deletion levels (P for trend = 0.689) and the risk of developing PD (Table 2).

In MSA patients, those in the highest tertile of cf-nDNA level had a 64% lower risk of developing MSA compared to those in the lowest tertile (OR: 0.34; 95% CI: 0.11–1.00; P = 0.058), indicating a significant dose-response relationship (P for trend = 0.046). However, these associations were no longer significant after adjusting for age, sex, BMI, education level, smoking status, and cerebrovascular disease (OR: 3.06; 95% CI: 0.50–2.34; P = 0.243; P for trend = 0.252). Similarly, no significant associations were observed between cf-nDNA level (OR: 1.39; 95% CI: 0.68–2.74; P = 0.340), cf-mtDNA copy number (OR: 0.97; 95% CI: 0.50–1.91; P = 0.937), or cf-mtDNA deletion level (OR: 1.31; 95% CI: 0.66–2.69; P = 0.447) per SD and the risk of developing MSA, after adjusting for confounding factors (Table 2).

Associations between plasma cfDNA biomarkers and clinical features

We performed correlation analyses between plasma cfDNA biomarkers and clinical characteristics in different subgroups, correcting for confounders such as age, sex, years of education, and BMI, with FDR correction. The results showed a significantly positive correlation between plasma cf-nDNA levels and HAM-A scores in PD patients (Rho = 0.382, FDR adjusted P = 0.027). Similarly, in MSA patients, cf-nDNA levels showed a significantly positive correlation with ICARS scores (Rho = 0.588, FDR adjusted P = 0.011) and a significantly negative correlation with MoCA scores (Rho = −0.484, FDR adjusted P = 0.044). No correlations were found for cf-nDNA level, cf-mtDNA copy number and cf-mtDNA deletion level with other clinical characteristics (Table 3).

We also performed subgroup comparisons of plasma cfDNA biomarkers in PD and MSA patients with different clinical presentations, correcting for confounders such as age, sex, years of education, and BMI (Table 4). We found that plasma cf-mtDNA copy numbers were significantly lower in PD patients with constipation compared to those without constipation (P = 0.049). Similarly, MSA patients with constipation showed a trend toward lower plasma cf-mtDNA copy numbers than those without this symptom (P = 0.076). MSA patients with cognitive impairment had significantly higher cf-nDNA levels than those without cognitive impairment (P = 0.008). Notably, there was a trend toward higher plasma cf-nDNA levels in PD patients with anxiety or depression compared to PD patients without anxiety or depression (P = 0.065, P = 0.061).

Discussion

This study offers the first comprehensive assessment of plasma cf-nDNA levels, cf-mtDNA copy numbers, and cf-mtDNA deletion levels in patients with PD and MSA. Our cross-sectional study found no significant differences in plasma cf-nDNA levels, cf-mtDNA copy numbers, and cf-mtDNA deletion levels among the PD, MSA, and NC groups. Additionally, there was no correlations between these cfDNA biomarkers and the risk of developing PD or MSA. Notably, in PD patients, there was a significantly positive correlation between plasma cf-nDNA levels and HAM-A scores. In MSA patients, cf-nDNA levels were positively correlated with ICARS scores and negatively correlated with MoCA scores. Additionally, we found that cf-mtDNA copy numbers were significantly lower in PD patients with constipation compared to those without. MSA patients with cognitive impairment had significantly higher cf-nDNA levels compared to those without.

Plasma cfDNA is derived from DNA released from dying cells, with a half-life of about 5–150 min. This "global snapshot" capability makes it an ideal molecular marker for many diseases, especially neurodegenerative diseases where tissue biopsy is not possible (Song et al., 2022). Many neurological disorders are not characterized by alterations in DNA sequences, and therefore, except for epigenetics, the application of cfDNA from nuclear

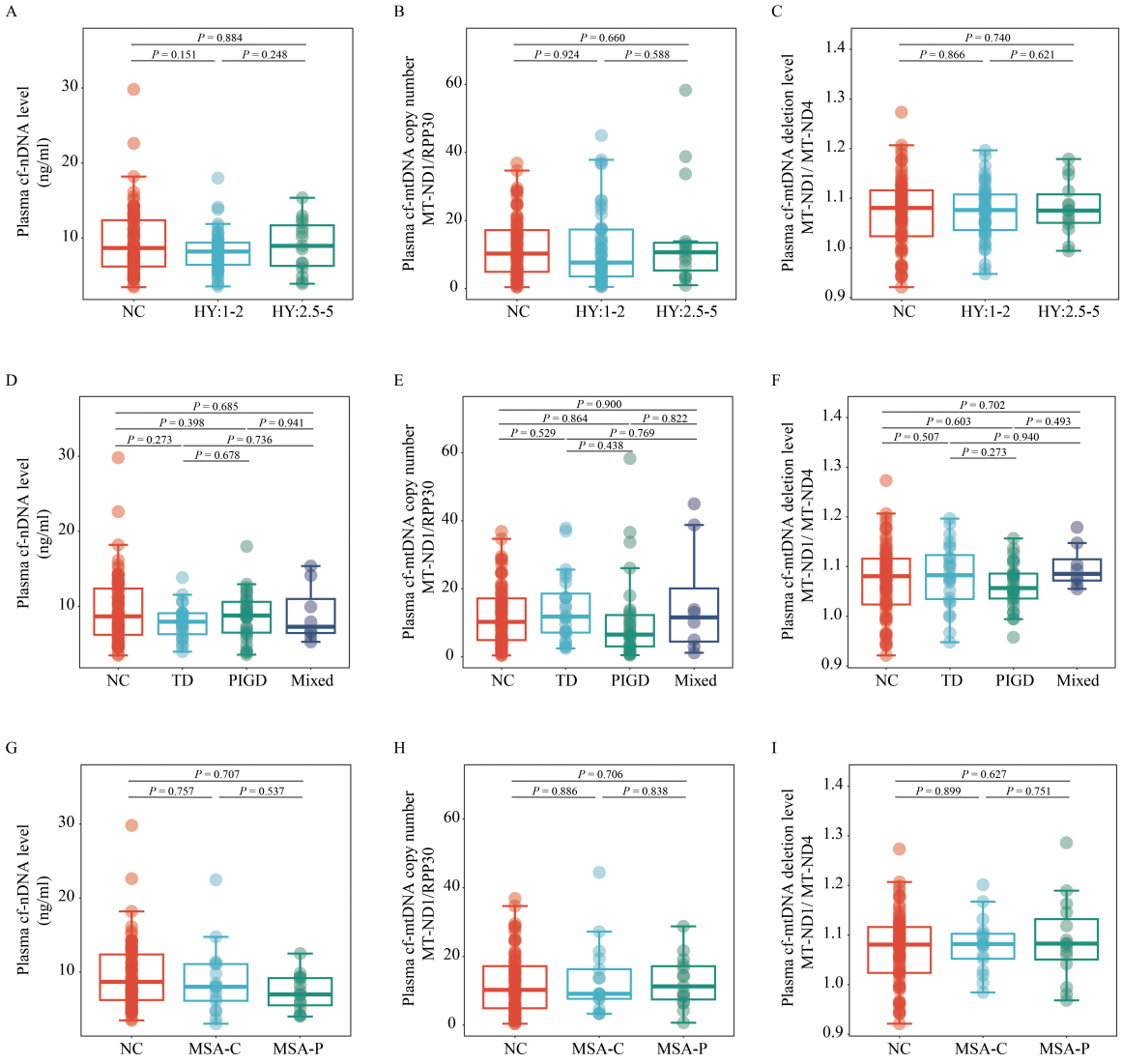

FIGURE 2
Comparison of plasma cf-nDNA levels, cf-mtDNA copy numbers and cf-mtDNA deletion levels between NC (n = 76) and patients with various PD and MSA subtypes. The figure displays variations in plasma cf-nDNA levels [*RPP30*; panels **(A,D,G)**], cf-mtDNA copy numbers [*MT-ND1* to *RPP30* ratio; panels **(B,E,H)**], and cf-mtDNA deletion levels [*MT-ND1* to *MT-ND4* ratio; panels **(C,F,I)**]. Panels **(A,B,C)** classify PD into early stages (H&Y stage 1–2; n = 47) and mid-late stages (H&Y stage 2.5–5; n = 15). Panels **(D,E,F)** classify PD into TD (n = 24), PIGD (n = 30), and Mix (n = 8) groups. Panels **(G,H,I)** classify MSA into MSA-C (n = 18) and MSA-P (n = 15) subtypes. Statistical analysis was conducted using multivariable linear regression, adjusted for age, sex, BMI, and education level, to assess P-values. Boxplots depict the median and IQR, with whiskers extending to values within 1.5 times the IQR. Data points outside the whiskers are labeled as "outliers." PD, Parkinson's disease; MSA, multiple system atrophy; NC, normal control; TD, tremor dominant; PIGD, postural instability and gait disorder; Mix, mixed symptomatology; H&Y, Hoehn and Yahr; MSA-C, Multiple System Atrophy-Cerebellar type; MSA-P, Multiple System Atrophy-Parkinsonian type; cf-mtDNA, circulating cell-free mitochondrial DNA; cf-nDNA, circulating cell-free nuclear DNA; IQR, interquartile range.

genes in neurodegenerative disorders has been mostly based on the quantification of cfDNA (Supplementary Table 1). Our study found no significant differences in cf-nDNA levels among the PD, MSA, and NC groups. This suggests that plasma cf-nDNA levels may not serve as a reliable biomarker for diagnosing PD and MSA. Further analysis showed no significant association between plasma cf-nDNA levels and the risk of developing PD or MSA. These findings are consistent with previous reports on cf-nDNA concentrations in PD patients. Wojtkowska et al. (2024) investigated serum cf-nDNA levels in 30 PD patients and 15 NC by detecting the nuclear gene *KRAS*, revealing a non-significant elevation in cf-nDNA levels among PD patients after adjusting for age. In contrast, Scalzo et al. (2009) observed a significant reduction in cf-nDNA levels in PD patients compared to controls, based on detecting the nuclear gene β-*globin* in 42 PD patients and 20 controls. However, two cross-sectional studies from Chen M. et al. (2017) and Chen Y. S. et al. (2017) reported a significant increase in cf-nDNA levels in PD patients. Our study improves on these previous studies. First, they did not consider confounding factors like age, sex, BMI, and years of education when analyzing differences in cf-nDNA levels. Second, low statistical power due to small sample sizes was a significant limitation in most of these studies, potentially leading to inconsistent results. In addition, for quantification of cf-nDNA concentrations, some studies have used simple fluorescence

TABLE 2 Associations between cfDNA biomarkers and risk of developing MSA and PD in logistic regression models.

Plasma measures	PD						MSA					
	Crude model			Multivariate model			Crude model			Multivariate model		
	OR	95% CI	*P*-value	OR	95% CI	*P*-value	OR	95% CI	*P*-value	OR	95% CI	*P*-value
cf-nDNA level												
Per SD	0.73	0.50–1.05	0.102	0.74	0.42–1.20	0.247	0.65	0.38–1.03	0.094	1.39	0.68–2.74	0.340
Q1	ref			ref			ref			ref		
Q2	1.55	0.68–3.55	0.298	1.56	0.51–4.93	0.437	1.13	0.43–2.95	0.808	2.03	0.40–1.16	0.401
Q3	0.58	0.24–1.34	0.202	0.65	0.20–2.04	0.463	0.34	0.11–1.00	0.058	3.06	0.50–2.34	0.243
P-value for trend			0.162			0.422			**0.046**			0.252
cf-mtDNA copy number												
Per SD	1.06	0.75–1.49	0.742	1.21	0.75–1.92	0.427	1.04	0.68– 1.56	0.851	0.97	0.50–1.91	0.937
Q1	ref			ref			ref			ref		
Q2	1.19	0.52–2.71	0.676	1.69	0.54–5.48	0.372	1.47	0.54–4.06	0.449	1.15	0.16–7.67	0.885
Q3	0.77	0.33–1.75	0.527	0.76	0.23–2.48	0.651	0.96	0.34–2.72	0.943	1.06	0.18–6.22	0.945
P-value for trend			0.458			0.462			0.831			0.987
cf-mtDNA deletion level												
Per SD	1.04	0.74–1.47	0.823	1.02	0.64–1.61	0.943	1.11	0.73–1.69	0.619	1.31	0.66–2.69	0.447
Q1	ref			ref			ref			ref		
Q2	1.31	0.57–3.01	0.527	0.98	0.33–2.93	0.975	1.73	0.65–4.79	0.278	1.56	0.30–8.36	0.594
Q3	0.83	0.36–1.93	0.670	0.78	0.24–2.45	0.672	0.87	0.30–2.49	0.789	1.26	0.25–6.51	0.781
P-value for trend			0.714			0.689			0.945			0.748

Bold values: *P*-value < 0.05. Crude model: unadjusted model; Multivariate model: adjusted for age, sex, BMI, education level, hypertension, coronary heart disease, and cerebrovascular disease in PD patients; adjusted for age, sex, BMI, education level, smoking status, and cerebrovascular disease in MSA patients; Trend analysis utilized the median value of each tertile. cf-mtDNA, circulating cell-free mitochondrial DNA; cf-nDNA, circulating cell-free nuclear DNA; PD, Parkinson's disease; MSA, multiple system atrophy; OR, odds ratio; CI, confidence interval; SD, standard deviation; -, not available.

quantification as well as qPCR assays based on the SYBR Green method. Considering our wider subject population, more accurate TaqMan probe qPCR method, and rigorous statistical correction, we believe the presented data in this study will inspire future follow-up studies.

Mitochondrial dysfunction is widely believed to play a crucial role in PD and MSA (Nakamoto et al., 2018; Monzio et al., 2020; Asghar et al., 2022). In 1979, studies showed that the toxin MPTP, which inhibits mitochondrial respiratory complex I, can induce substantia nigra cell loss and Parkinson's disease (Davis et al., 1979). Additionally, patients with mutations in mitochondrial polymerase γ and other mitochondrial disorders exhibit nigrostriatal neurodegeneration, Lewy body pathology, and clinical features of Parkinson's disease (Gonzalez-Hunt and Sanders, 2021). Pathological changes in mtDNA gradually accumulate in the brains of patients. Various studies have implicated mtDNA related processes as possible alternative avenues of mitochondrial dysfunction in PD risk (Bender et al., 2006; Lin et al., 2012; Dölle et al., 2016). Therefore, The pathophysiological role of cfDNA, particularly cf-mtDNA, in neurodegeneration is increasingly evident. Released from stressed or damaged cells, cfDNA serves as a potent danger-associated molecular pattern (DAMP) that activates pattern recognition receptors (e.g., TLRs, cGAS/STING) in brain-resident cells such as microglia, astrocytes, and neurons. This activation initiates inflammatory signaling cascades—especially via the NF-κB pathway—that lead to the release of pro-inflammatory cytokines (e.g., IL-1β, IL-6), which intensify neuroinflammation and neuronal injury. Additionally, cf-mtDNA contributes to oxidative stress, compounding cellular damage and further promoting inflammation. In the aging brain, where mitochondrial dysfunction and oxidative stress are already elevated, cfDNA levels tend to rise, perpetuating chronic inflammation that drives neurodegenerative progression (Kunze et al., 2023; Legati and Ghezzi, 2023). Several studies have linked CSF-derived cf-mtDNA to PD. Pyle et al. (2015) examined CSF from PD patients and found significantly reduced levels of cf-mtDNA compared to healthy controls. Lowes et al. (2020) found that the reduction in CSF cf-mtDNA copy number may be related to the initiation, type, and duration of treatment. Similar studies have been conducted in other neurodegenerative diseases, including Alzheimer's disease (Podlesniy et al., 2020) and multiple sclerosis (Varhaug et al., 2017; Fissolo et al., 2019). This suggests that assessing mitochondrial molecules involved in neurodegenerative processes may provide a sensitive indicator of mitochondrial dysfunction in neurodegenerative diseases.

cfDNA can cross the blood-brain barrier and enter the peripheral circulation, thus measuring disease-related changes in cf-mtDNA copy numbers and deletion levels in blood samples is

TABLE 3 Spearman correlations between plasma cfDNA biomarkers and clinical parameters across the diagnostic groups.

Group	Plasma measures		Duration	H&Y stage	MMSE	MOCA	HAM-D	HAM-A	RBDQ-HK	MDS-UPDRS-III	NMSS	UMSARS-II	ICARS
NC	cf-nDNA level	Rho			0.227	0.082	0.228	0.208	−0.185				
		P			0.055	0.494	0.054	0.080	0.121				
		FDR adjusted *P*			0.133	0.494	0.133	0.133	0.151				
	cf-mtDNA copy number	Rho			0.070	−0.139	0.098	−0.034	0.167				
		P			0.559	0.243	0.414	0.775	0.160				
		FDR adjusted *P*			0.699	0.608	0.690	0.775	0.608				
	cf-mtDNA deletion level	Rho			0.033	−0.040	0.214	0.059	0.016				
		P			0.786	0.743	0.076	0.625	0.897				
		FDR adjusted *P*			0.897	0.897	0.380	0.897	0.897				
PD	cf-nDNA level	Rho	0.182	0.060	−0.108	−0.123	0.196	0.382	0.107	−0.073	0.184		
		P	0.171	0.656	0.422	0.357	0.141	0.003	0.426	0.591	0.172		
		FDR adjusted *P*	0.387	0.656	0.548	0.548	0.387	**0.027**	0.548	0.656	0.387		
	cf-mtDNA copy number	Rho	−0.136	0.013	0.089	0.097	−0.135	−0.191	−0.186	−0.025	−0.057		
		P	0.309	0.923	0.504	0.469	0.311	0.150	0.162	0.852	0.675		
		FDR adjusted *P*	0.700	0.923	0.756	0.756	0.700	0.700	0.700	0.923	0.868		
	cf-mtDNA deletion level	Rho	0.114	−0.072	0.052	0.003	−0.025	−0.038	−0.019	−0.149	−0.184		
		P	0.397	0.595	0.703	0.981	0.885	0.779	0.886	0.273	0.174		
		FDR adjusted *P*	0.981	0.981	0.981	0.981	0.981	0.981	0.981	0.981	0.981		
MSA	cf-nDNA level	Rho	0.271	0.251	−0.382	−0.484	0.267	0.186	0.048	0.178	0.444	0.412	0.588
		P	0.154	0.189	0.041	0.008	0.162	0.334	0.805	0.354	0.016	0.029	0.001
		FDR adjusted *P*	0.255	0.260	0.090	**0.044**	0.255	0.389	0.805	0.389	0.059	0.080	**0.011**

(Continued)

10.3389/fnins.2024.1488820

10.3389/fnins.2024.1488820

TABLE 3 (Continued)

Group	Plasma measures		Duration	H&Y stage	MMSE	MOCA	HAM-D	HAM-A	RBDQ-HK	MDS-UPDRS-III	NMSS	UMSARS-II	ICARS
	cf-mtDNA copy number	Rho	−0.051	−0.230	0.080	0.184	0.250	0.145	−0.021	−0.088	−0.108	−0.189	−0.153
		P	0.792	0.230	0.681	0.339	0.190	0.452	0.914	0.650	0.578	0.336	0.447
		FDR adjusted *P*	0.871	0.829	0.832	0.829	0.829	0.829	0.914	0.832	0.832	0.829	0.829
	cf-mtDNA deletion level	Rho	0.034	−0.090	−0.289	0.015	0.007	0.035	0.060	0.230	0.026	0.123	0.014
		P	0.859	0.641	0.129	0.937	0.970	0.857	0.757	0.231	0.894	0.532	0.946
		FDR adjusted *P*	0.970	0.970	0.970	0.970	0.970	0.970	0.970	0.970	0.970	0.970	0.970

Bold values: FDR adjusted *P*-value < 0.05. Adjusted for age, sex, BMI and education years. NC, normal control; H&Y, Hoehn and Yahr; MDS-UPDRS-III, movement disorder society-unified Parkinson's disease rating scale part III; UMSARS, unified multiple system atrophy rating scale part II; NMSS, non-motor symptom scale; MMSE, mini-mental state examination; MoCA, montreal cognitive assessment; HAM-D, Hamilton depression scale; HAM-A, Hamilton anxiety scale; RBDQ-HK, rapid eye movement sleep behavior disorder questionnaire-Hong Kong; ICARS, international cooperative ataxia rating scale; cf-mtDNA, circulating cell-free mitochondrial DNA; cf-nDNA, circulating cell-free nuclear DNA; FDR, false discovery rate; PD, Parkinson's disease; MSA, multiple system atrophy.

appealing. As shown in Supplementary Table 1, there has been a significant increase in research on cf-mtDNA in serum or plasma as potential biomarkers for neurodegenerative diseases, indicating the great potential of blood cf-mtDNA as a non-invasive biomarker for these diseases. This study is the first to find no statistically significant differences in plasma cf-mtDNA copy numbers and cf-mtDNA deletion levels between PD and MSA patients and healthy controls. Similarly, Borsche et al. (2020) reported no differences in serum cf-mtDNA levels between idiopathic PD patients and healthy controls. However, affected heterozygous and double allele *PRKN/PINK1* mutation carriers have higher serum cf-mtDNA levels than idiopathic PD patients and healthy controls (Borsche et al., 2020). Similar results were obtained in two studies focusing on CSF from the same team. They found that high cf-mtDNA levels in CSF occurred only in *LRRK2* mutation carriers with PD, not in idiopathic PD patients (Podlesniy et al., 2016; Puigròs et al., 2022). These findings were in agreement with the work published by Wojtkowska et al. (2024), who demonstrated that after correcting for the confounding factor of age, there were no significant differences in serum or CSF cf-mtDNA levels in PD patients compared to NC. While various forms of cell death occur in neurons or glial cells within the brain of patients, leukocytes are the primary contributors to almost 50–80% of cfDNA derived from plasma. Neutrophil-derived cfDNA makes up the majority, while neuron-derived cfDNA represents only 1–2% of the plasma DNA pool (Sun et al., 2015; Moss et al., 2018; Loyfer et al., 2023). This fraction of cfDNA in PD and MSA patients is likely released from peripheral blood neutrophils, similar to what is observed in cancer patients and healthy individuals undergoing acute exercise (Fridlich et al., 2023; Mattox et al., 2023). Therefore, the results of this experiment may reflect the mitochondrial function of the patient's general immune cells rather than brain-specific mitochondrial dysfunction. Although many studies on neurodegenerative diseases have reported changes in cf-mtDNA copy numbers and deletion levels, differences in assay processes across laboratories often result in non-comparable data. These differences include variations in target genes, biological sample types, blood collection timing, centrifugation conditions, DNA extraction methods, and qPCR protocols (Trumpff et al., 2021; Park et al., 2022). Inconsistent results have been observed between different neurodegenerative diseases and even in the same disease, such as Parkinson's disease. This suggests that the relationship between cf-mtDNA and neurodegenerative diseases may be more complex, reflecting the diversity and multifaceted etiology of each disease. Additionally, sample heterogeneity and inaccuracies in cf-mtDNA assay methods may partly explain the conflicting results frequently reported in the literature. Therefore, establishing standardized blood processing methods and analytical workflows is essential, along with the systematic characterization of both cf-mtDNA and cf-nDNA, potentially utilizing samples from large clinical cohorts (Bronkhorst et al., 2022). In this study, a two-step centrifugation method was used, with no significant impact on nuclear DNA. However, at a force of 16,000 *g*, larger structures like platelets precipitate, leading to a decline in mtDNA concentration in the plasma supernatant and the loss of around 75% of mtDNA. Consequently, it needs to be clarified that the analyzed cf-mtDNA was related to small extracellular vesicles, exosomes, and protein complexes under such centrifugal conditions (Pisareva et al., 2023).

TABLE 4 Comparisons of cfDNA biomarkers between PD and MSA subgroups.

Plasma measures	PD		*P*-value	MSA		*P*-value
	Without cognitive impairment (*n* = 37)	With cognitive impairment (*n* = 25)		Without cognitive impairment (*n* = 18)	With cognitive impairment (*n* = 15)	
cf-nDNA level	7.985 ± 2.743	9.095 ± 3.221	0.123	6.852 ± 2.933	9.403 ± 4.272	**0.008**
cf-mtDNA copy number	13.072 ± 10.826	12.462 ± 14.426	0.472	13.530 ± 10.380	11.448 ± 7.303	0.925
cf-mtDNA deletion level	1.077 ± 0.064	1.071 ± 0.041	0.576	1.062 ± 0.077	1.101 ± 0.067	0.226
	Without depression (*n* = 32)	With depression (*n* = 30)		Without depression (*n* = 19)	With depression (*n* = 14)	
cf-nDNA level	7.901 ± 3.053	9.000 ± 2.820	0.061	7.972 ± 4.448	8.064 ± 2.757	0.392
cf-mtDNA copy number	12.756 ± 11.066	12.900 ± 13.675	0.606	11.431 ± 9.927	14.147 ± 7.748	0.294
cf-mtDNA deletion level	1.079 ± 0.048	1.069 ± 0.063	0.638	1.078 ± 0.072	1.081 ± 0.080	0.975
	Without anxiety (*n* = 27)	With anxiety (*n* = 35)		Without anxiety (*n* = 11)	With anxiety (*n* = 22)	
cf-nDNA level	7.557 ± 2.286	9.108 ± 3.280	0.065	8.564 ± 5.662	7.735 ± 2.483	0.291
cf-mtDNA copy number	14.280 ± 11.832	11.704 ± 12.694	0.375	13.570 ± 12.863	12.090 ± 6.702	0.810
cf-mtDNA deletion level	1.076 ± 0.058	1.073 ± 0.054	0.986	1.062 ± 0.069	1.088 ± 0.077	0.549
	Without RBD (*n* = 34)	With RBD (*n* = 28)		Without RBD (*n* = 5)	With RBD (*n* = 28)	
cf-nDNA level	8.506 ± 3.054	8.344 ± 2.920	0.779	7.335 ± 2.609	8.132 ± 3.968	0.874
cf-mtDNA copy number	13.861 ± 11.342	11.569 ± 13.463	0.351	11.243 ± 8.107	12.823 ± 9.310	0.940
cf-mtDNA deletion level	1.069 ± 0.060	1.081 ± 0.049	0.631	1.067 ± 0.061	1.082 ± 0.077	0.513
	Without constipation (*n* = 21)	With constipation (*n* = 40)		Without constipation (*n* = 5)	With constipation (*n* = 28)	
cf-nDNA level	7.803 ± 2.943	8.749 ± 3.006	0.362	7.727 ± 2.905	8.062 ± 3.948	0.746
cf-mtDNA copy number	17.097 ± 11.896	10.717 ± 12.195	**0.049**	18.947 ± 6.522	11.447 ± 9.037	0.076
cf-mtDNA deletion level	1.086 ± 0.065	1.069 ± 0.050	0.292	1.070 ± 0.033	1.081 ± 0.080	0.948
	Without olfaction loss (*n* = 29)	With olfaction loss (*n* = 33)		Without olfaction loss (*n* = 28)	With olfaction loss (*n* = 5)	
cf-nDNA level	8.367 ± 3.242	8.491 ± 2.760	0.821	7.797 ± 3.877	9.214 ± 3.192	0.408
cf-mtDNA copy number	12.879 ± 12.558	12.779 ± 12.252	0.726	12.926 ± 9.511	10.667 ± 6.119	0.804
cf-mtDNA deletion level	1.073 ± 0.053	1.076 ± 0.058	0.508	1.084 ± 0.077	1.058 ± 0.055	0.642

Bold values: *P*-value < 0.05 after adjusted for age, sex, BMI and education years. Data are expressed as the mean ± SD. Definition of abnormal: for cognitive impairment, a cut-off of 26 on the MMSE score; for depression, a cut-off of 8 on the HAMD score; for anxiety, a cut-off of 7 on the HAMA score; for RBD, a cut-off of 19 on the RBDQ-HK score; for olfactory loss, a cut-off of 22 on the AHRS score; constipation was screened by the part 21 of NMSS. RBD, rapid eye movement sleep behavior disorder; cf-mtDNA, circulating cell-free mitochondrial DNA; cf-nDNA, circulating cell-free nuclear DNA; PD, Parkinson's disease; MSA, multiple system atrophy.

Future studies need to consider the limitations of previous research and the challenges of analyzing mtDNA to improve study designs.

In synucleinopathies, α-synuclein released from neurons or oligodendrocytes activates microglia, initiating an inflammatory response in the central nervous system (Yuan et al., 2024). This inflammatory and immune response is observed not only in the central nervous system, but also in the peripheral blood (Passaro et al., 2021; Jun and Kim, 2023). Neutrophils release neutrophil extracellular traps (NETs) when activated by various endogenous and exogenous inflammatory factors, further contributing to inflammation. NETs can directly release DNA fragments into the microenvironment, creating a positive feedback loop that perpetuates chronic inflammation (Pisetsky, 2012). Furthermore, two studies have reported an association between α-synuclein and NETs formation (Azevedo et al., 2012; Peelaerts et al., 2023). Notably, we observed PD patients with anxiety or depression tended to have higher plasma cf-nDNA levels compared to those without these conditions. Previous studies (Eraly et al., 2014; Milaneschi et al., 2021; Zeng et al., 2024) have found that associations of C-reactive protein, lymphocyte to monocyte ratio and neutrophil to lymphocyte ratio with the risks of any psychiatric disorder, depression, anxiety, and stress-related

disorders. Possible explanations include blood-brain barrier disruption, microglial activation, neurotransmission disorders, and interactions between inflammation and neuropathology (Zeng et al., 2024). This aligns with our findings that cf-nDNA levels in PD patients are positively correlated with HAM-A scores. In addition, our results indicate that cf-nDNA levels were significantly elevated in MSA patients exhibiting cognitive impairment than those with normal cognition, and a significantly negative correlation was identified between MoCA scores and cf-nDNA levels in MSA patients. This is consistent with previous findings. Nidadavolu et al. (2022) analyzed serum cf-nDNA from 631 community-dwelling individuals, finding that high baseline cf-nDNA levels were associated with lower overall cognitive functioning, increased risk of dementia, and faster cognitive decline over 8 years. We also found a significantly positive correlation between plasma cf-nDNA levels and ICARS scores in MSA patients. Although the mechanisms linking cfDNA levels with cognitive loss and ataxia symptoms remain unclear, this is not surprising given MSA's inflammatory nature and cfDNA's role as a biomarker of systemic inflammation (Leńska-Mieciek et al., 2023). Chronic neuroinflammation in MSA patients' brains leads to neuronal damage and blood-brain barrier disruption, releasing DNA into peripheral circulation. These cfDNAs themselves can also act as DAMPs to induce immune responses, triggering further inflammation and peripheral cell death (Chen et al., 2015; Kunze et al., 2023). Although we could not determine a causal relationship between the clinical symptoms and plasma cf-nDNA levels, this result paves the way for further studies on the correlation between plasma cf-nDNA levels and MSA severity. Another notable finding is that, although both PD and MSA are α-synucleinopathies, the correlations mentioned above do not show a consistent trend between these diseases. This may suggest that, despite sharing common pathological mechanisms, PD and MSA exhibit different peripheral inflammation and immune characteristics (Folke et al., 2019; Yuan et al., 2024), which could lead to variations in the interactions between cf-nDNAs and the inflammatory responses. It should also be noted that, beyond concentration, cfDNA fragment size and the specific sequences of cfDNA are related to the inflammatory responses (Storci et al., 2018; Deng et al., 2022). This highlights the need for further research to better understand the specificities and commonalities of these diseases.

Constipation is one of the most common functional gastrointestinal disorders in patients with PD and MSA. Evidence suggests that both PD and MSA patients exhibit disruption of intestinal barrier integrity, endotoxin-mediated intestinal inflammation, and pro-inflammatory microbiota. This intestinal-sourced inflammatory cascade may lead to local and systemic inflammation, elevated pro-inflammatory cytokines, and oxidative stress (Engen et al., 2017; Tan et al., 2021). At the same time, changes in microbial metabolites caused by intestinal microbiota imbalance in PD patients can also affect mitochondrial dysfunction (Liang et al., 2021). This is consistent with our results. Our study showed that PD and MSA patients with constipation had lower cf-mtDNA copy numbers compared to those without. Considering the high energy demands of neural, muscular, and inflammatory cells involved in gastrointestinal tract function (Camilleri et al., 2009), and the fact that low mtDNA copy number is associated with high inflammatory markers (Wu et al., 2017; Kang et al., 2021), it is plausible that patients with constipation present with reduced cf-mtDNA copy numbers. Another piece of evidence for this phenomenon is that previous research has linked constipation to reduced mtDNA copy numbers in individuals with autism spectrum disorder and intellectual disability compared to NC (Valiente-Pallejà et al., 2018). Future studies should further explore the complex interactions between intestinal inflammation and mitochondrial dysfunction to reveal new therapeutic targets.

Limitations of this study need to be noted. Firstly, the sample size was relatively small and the study is single-centered. Findings in this study need to be validated in larger, more diverse sample groups and multiple centers. Secondly, demographic data show a significant difference in the history of hypertension, coronary heart disease and cerebrovascular disease among the three groups. Whether this difference leads to changes in plasma cf-nDNA or cf-mtDNA is unknown. To address this, we conducted additional statistical analyses and the results are shown in Supplementary Table 2. Overall, there were no significant differences in plasma cf-nDNA or cf-mtDNA levels between subjects with hypertension, coronary heart disease, cerebrovascular disease, and those without these comorbidities. This suggests that these comorbidities may not significantly impact plasma cf-nDNA or cf-mtDNA levels. Considering that both PD and MSA are age-related, it is likely that all subjects will have some degree of comorbidities. Future research should focus on the impact of various comorbidities on cfDNA levels in the elderly and rigorously control for these factors statistically to minimize their impact. Thirdly, since simultaneous release of nuclear and mitochondrial genomes may indicate cell death or injury, we opted to assess changes in mtDNA copy numbers using real-time quantitative PCR, quantifying the ratio of mitochondrial to nuclear genomes. This method produces relative measurements compared to nuclear DNA copy numbers in the sample rather than absolute mtDNA copy number values, it complicates cross-study comparisons and objective clinical utility assessments. Future studies might consider using digital droplet PCR for absolute mtDNA copy number assessment and standardized pre-analytical cf-mtDNA procedures. Finally, plasma cf-nDNA concentrations are exceedingly low due to limited plasma inputs and the fragmented double-stranded structure of cfDNA. Therefore, the elevated Cq values observed in quantitative PCR analyses may have compromised the study's reliability. Future investigations could mitigate this issue by developing reference primers targeting either short or long interspersed nuclear elements.

In future neurodegenerative disease research, plasma cfDNA markers alone may have limited utility but could be combined with other biomarkers to enhance specificity. For instance, cfDNA could be combined with DNA methylation indicators. DNA methylation profiles can help trace the tissue origin of cfDNA from damaged cells, as cfDNA fragments retain tissue-specific methylation patterns. Additionally, certain differentially methylated sites are strongly linked to neurodegenerative diseases and exhibit high specificity. Beyond cfDNA methylation, cfDNA markers could be integrated with symptomatic markers, imaging markers, biochemical markers, and genetic markers to significantly enhance diagnostic sensitivity and specificity. A promising future approach involves using AI models to integrate multimodal data—demographics, medical history, lab results, medication profiles, neuropsychological tests, functional assessments, and multimodal neuroimaging—to diagnose and identify α-synucleinopathies.

In conclusion, our study suggests that plasma cf-nDNA level, cf-mtDNA copy number, and cf-mtDNA deletion level may not be

distinct indicators for identifying PD and MSA patients. Moreover, significant associations between these three cfDNA biomarkers and the risk of developing PD and MSA are lacking. Nevertheless, their notable correlations with clinical features suggest that these biomarkers can still offer valuable insights into disease burden and progression. These findings underscore the necessity for further exploration of these relationships and the clinical applications of these biomarkers in PD and MSA diagnosis and management.

Data availability statement

The raw data supporting the conclusions of this article will be made available by the authors, without undue reservation.

Ethics statement

The studies involving humans were approved by the Ethics Committee of Xuanwu Hospital. The studies were conducted in accordance with the local legislation and institutional requirements. The participants provided their written informed consent to participate in this study.

Author contributions

CY: Formal analysis, Methodology, Validation, Writing – original draft, Writing – review and editing. YL: Formal analysis, Resources, Writing – original draft, Writing – review and editing. HZ: Investigation, Writing – original draft. SP: Investigation, Writing – original draft. ShH: Methodology, Writing – original draft. SoH: Writing – original draft. LZ: Formal analysis, Resources, Supervision, Visualization, Writing – original draft, Writing – review and editing.

Funding

The authors declare that financial support was received for the research, authorship, and/or publication of this article. This work was supported by the National Natural Science Foundation of China (No. 82201409).

Conflict of interest

The authors declare that the research was conducted in the absence of any commercial or financial relationships that could be construed as a potential conflict of interest.

Publisher's note

All claims expressed in this article are solely those of the authors and do not necessarily represent those of their affiliated organizations, or those of the publisher, the editors and the reviewers. Any product that may be evaluated in this article, or claim that may be made by its manufacturer, is not guaranteed or endorsed by the publisher.

Supplementary material

The Supplementary Material for this article can be found online at: https://www.frontiersin.org/articles/10.3389/fnins.2024.1488820/full#supplementary-material

References

Asghar, M., Odeh, A., Fattahi, A. J., Henriksson, A. E., Miglar, A., Khosousi, S., et al. (2022). Mitochondrial biogenesis, telomere length and cellular senescence in Parkinson's disease and lewy body dementia. *Sci. Rep.* 12:17578. doi: 10.1038/s41598-022-22400-z

Autere, J., Moilanen, J. S., Finnilä, S., Soininen, H., Mannermaa, A., Hartikainen, P., et al. (2004). Mitochondrial DNA polymorphisms as risk factors for Parkinson's disease and Parkinson's disease dementia. *Hum. Genet.* 115, 29–35. doi: 10.1007/s00439-004-1123-9

Azevedo, E. P., Guimaraes-Costa, A. B., Torezani, G. S., Braga, C. A., Palhano, F. L., Kelly, J. W., et al. (2012). Amyloid fibrils trigger the release of neutrophil extracellular traps (nets), causing fibril fragmentation by net-associated elastase. *J. Biol. Chem.* 287, 37206–37218. doi: 10.1074/jbc.M112.369942

Barca, E., Kleiner, G., Tang, G., Ziosi, M., Tadesse, S., Masliah, E., et al. (2016). Decreased coenzyme q10 levels in multiple system atrophy cerebellum. *J. Neuropathol. Exp. Neurol.* 75, 663–672. doi: 10.1093/jnen/nlw037

Bender, A., Krishnan, K. J., Morris, C. M., Taylor, G. A., Reeve, A. K., Perry, R. H., et al. (2006). High levels of mitochondrial DNA deletions in substantia nigra neurons in aging and Parkinson disease. *Nat. Genet.* 38, 515–517. doi: 10.1038/ng1769

Blin, O., Desnuelle, C., Rascol, O., Borg, M., Paul, H. P. S., Azulay, J. P., et al. (1994). Mitochondrial respiratory failure in skeletal muscle from patients with Parkinson's disease and multiple system atrophy. *J. Neurol. Sci.* 125, 95–101. doi: 10.1016/0022-510x(94)90248-8

Borsche, M., Konig, I. R., Delcambre, S., Petrucci, S., Balck, A., Bruggemann, N., et al. (2020). Mitochondrial damage-associated inflammation highlights biomarkers in prkn/pink1 Parkinsonism. *Brain* 143, 3041–3051. doi: 10.1093/brain/awaa246

Bronkhorst, A. J., Ungerer, V., Oberhofer, A., Gabriel, S., Polatoglou, E., Randeu, H., et al. (2022). New perspectives on the importance of cell-free DNA biology. *Diagnostics (Basel, Switzerland)* 12:2147. doi: 10.3390/diagnostics12092147

Bruno, D., Donatti, A., Martin, M., Almeida, V. S., Geraldis, J. C., Oliveira, F. S., et al. (2020). Circulating nucleic acids in the plasma and serum as potential biomarkers in neurological disorders. *Braz. J. Med. Biol. Res.* 53:e9881. doi: 10.1590/1414-431x20209881

Calne, D. (2005). A definition of Parkinson's disease. *Parkinsonism Relat. Disord.* 11, S39–S40. doi: 10.1016/j.parkreldis.2005.01.008

Camilleri, M., Carlson, P., Zinsmeister, A. R., Mckinzie, S., Busciglio, I., Burton, D., et al. (2009). Mitochondrial DNA and gastrointestinal motor and sensory functions in health and functional gastrointestinal disorders. *Am. J. Physiol. Gastroint. Liver Physiol.* 296, G510–G516. doi: 10.1152/ajpgi.90650.2008

Chen, H. L., Lu, C. H., Lin, H. C., Chen, P. C., Chou, K. H., Lin, W. M., et al. (2015). White matter damage and systemic inflammation in obstructive sleep apnea. *Sleep* 38, 361–370. doi: 10.5665/sleep.4490

Chen, M., Chen, P., Lu, C., Chen, H., Chao, Y., Li, S., et al. (2017). Plasma DNA mediate autonomic dysfunctions and white matter injuries in patients with Parkinson's disease. *Oxidative Med. Cell. Longev.* 2017, 7371403. doi: 10.1155/2017/7371403

Chen, Y. S., Chen, M. H., Lu, C. H., Chen, P. C., Chen, H. L., Yang, I. H., et al. (2017). Associations among cognitive functions, plasma DNA, and white matter integrity in patients with early-onset parkinson's disease. *Front. Neurosci.* 11:9. doi: 10.3389/fnins.2017.00009

Compagnoni, G. M., Kleiner, G., Bordoni, A., Fortunato, F., Ronchi, D., Salani, S., et al. (2018). Mitochondrial dysfunction in fibroblasts of multiple system atrophy. *Biochim. Biophys. Acta Mol. Basis Dis.* 1864, 3588–3597. doi: 10.1016/j.bbadis.2018.09.018

Davis, G. C., Williams, A. C., Markey, S. P., Ebert, M. H., Caine, E. D., Reichert, C. M., et al. (1979). Chronic Parkinsonism secondary to intravenous injection of meperidine analogues. *Psychiatry Res.* 1, 249–254. doi: 10.1016/0165-1781(79)90006-4

Davis, R. L., Wong, S. L., Carling, P. J., Payne, T., Sue, C. M., and Bandmann, O. (2020). Serum fgf-21, gdf-15, and blood mtDNA copy number are not biomarkers of Parkinson disease. *Neurol. Clin. Pract.* 10, 40–46. doi: 10.1212/CPJ.0000000000000702

Deng, J., Pan, W., Ji, N., Liu, N., Chen, Q., Chen, J., et al. (2022). Cell-free DNA promotes inflammation in patients with oral lichen planus via the sting pathway. *Front. Immunol.* 13:838109. doi: 10.3389/fimmu.2022.838109

Dölle, C., Fløtnes, I., Nido, G. S., Miletic, H., Osuagwu, N., Kristoffersen, S., et al. (2016). Defective mitochondrial DNA homeostasis in the substantia nigra in Parkinson disease. *Nat. Commun.* 7:13548. doi: 10.1038/ncomms13548

Dutta, S., Hornung, S., Taha, H. B., and Bitan, G. (2023). Biomarkers for parkinsonian disorders in cns-originating evs: Promise and challenges. *Acta Neuropathol.* 145, 515–540. doi: 10.1007/s00401-023-02557-1

Engen, P. A., Dodiya, H. B., Naqib, A., Forsyth, C. B., Green, S. J., Voigt, R. M., et al. (2017). The potential role of gut-derived inflammation in multiple system atrophy. *J. Parkinsons Dis.* 7, 331–346. doi: 10.3233/JPD-160991

Eraly, S. A., Nievergelt, C. M., Maihofer, A. X., Barkauskas, D. A., Biswas, N., Agorastos, A., et al. (2014). Assessment of plasma C-reactive protein as a biomarker of posttraumatic stress disorder risk. *JAMA Psychiatry* 71, 423–431. doi: 10.1001/jamapsychiatry.2013.4374

Eriksen, J. L., Wszolek, Z., and Petrucelli, L. (2005). Molecular pathogenesis of Parkinson disease. *Arch. Neurol.* 62:353. doi: 10.1001/archneur.62.3.353

Fearnley, J. M., and Lees, A. J. (1991). Ageing and Parkinson's disease: Substantia nigra regional selectivity. *Brain* 114, 2283–2301. doi: 10.1093/brain/114.5.2283

Fissolo, N., Cervera-Carles, L., Guimerans, L. M. V., Lleó, A., Clarimón, J., Drulovic, J., et al. (2019). Cerebrospinal fluid mitochondrial DNA levels in patients with multiple sclerosis. *Multiple Sclerosis (Houndmills, Basingstoke, England)* 25, 1535–1538. doi: 10.1177/1352458518786055

Folke, J., Rydbirk, R., Løkkegaard, A., Salvesen, L., Hejl, A., Starhof, C., et al. (2019). Distinct autoimmune anti-α-synuclein antibody patterns in multiple system atrophy and Parkinson's disease. *Front. Immunol.* 10:2253. doi: 10.3389/fimmu.2019.02253

Fridlich, O., Peretz, A., Fox-Fisher, I., Pyanzin, S., Dadon, Z., Shcolnik, E., et al. (2023). Elevated cfDNA after exercise is derived primarily from mature polymorphonuclear neutrophils, with a minor contribution of cardiomyocytes. *Cell Rep. Med.* 4:101074. doi: 10.1016/j.xcrm.2023.101074

Gaitsch, H., Franklin, R., and Reich, D. S. (2023). Cell-free DNA-based liquid biopsies in neurology. *Brain* 146, 1758–1774. doi: 10.1093/brain/awac438

Gilman, S., Wenning, G. K., Low, P. A., Brooks, D. J., Mathias, C. J., Trojanowski, J. Q., et al. (2008). Second consensus statement on the diagnosis of multiple system atrophy. *Neurology* 71, 670–676. doi: 10.1212/01.wnl.0000324625.00404.15

Gonzalez-Hunt, C. P., and Sanders, L. H. (2021). DNA damage and repair in Parkinson's disease: Recent advances and new opportunities. *J. Neurosci. Res.* 99, 180–189. doi: 10.1002/jnr.24592

Gu, M., Gash, M. T., Cooper, J. M., Wenning, G. K., Daniel, S. E., Quinn, N. P., et al. (1997). Mitochondrial respiratory chain function in multiple system atrophy. *Mov. Disord.* 12, 418–422. doi: 10.1002/mds.870120323

Hatcher, J. M., Pennell, K. D., and Miller, G. W. (2008). Parkinson's disease and pesticides: A toxicological perspective. *Trends Pharmacol. Sci.* 29, 322–329. doi: 10.1016/j.tips.2008.03.007

Jellinger, K. A., and Wenning, G. K. (2016). Multiple system atrophy: Pathogenic mechanisms and biomarkers. *J. Neural. Transm.* 123, 555–572. doi: 10.1007/s00702-016-1545-2

Jun, J. S., and Kim, R. (2023). Peripheral blood inflammatory cytokines in prodromal and overt alpha-synucleinopathies: A review of current evidence. *Encephalitis* 3, 81–86. doi: 10.47936/encephalitis.2023.00031

Kang, J. I., Park, C. I., Lin, J., Kim, S. T., Kim, H. W., and Kim, S. J. (2021). Alterations of cellular aging markers in obsessive- compulsive disorder: Mitochondrial DNA copy number and telomere length. *J. Psychiatry. Neurosci.* 46, E451–E458. doi: 10.1503/jpn.200238

Kerachian, M. A., Azghandi, M., Mozaffari-Jovin, S., and Thierry, A. R. (2021). Guidelines for pre-analytical conditions for assessing the methylation of circulating cell-free DNA. *Clin. Epigenetics* 13:193. doi: 10.1186/s13148-021-01182-7

Kummer, A., Cardoso, F., and Teixeira, A. L. (2009). Frequency of psychiatric disorders in young-onset parkinson's disease does not differ from typical-onset Parkinson's disease. *Parkinsonism Relat. Disord.* 15, 153–155. doi: 10.1016/j.parkreldis.2008.04.001

Kunze, R., Fischer, S., Marti, H. H., and Preissner, K. T. (2023). Brain alarm by self-extracellular nucleic acids: From neuroinflammation to neurodegeneration. *J. Biomed. Sci.* 30:64. doi: 10.1186/s12929-023-00954-y

Legati, A., and Ghezzi, D. (2023). Parkinson's disease, parkinsonisms, and mitochondria: The role of nuclear and mitochondrial DNA. *Curr. Neurol. Neurosci. Rep.* 23, 131–147. doi: 10.1007/s11910-023-01260-8

Leńska-Mieciek, M., Madetko-Alster, N., Alster, P., Królicki, L., Fiszer, U., and Koziorowski, D. (2023). Inflammation in multiple system atrophy. *Front. Immunol.* 14:1214677. doi: 10.3389/fimmu.2023.1214677

Li, X. Y., Yang, W., Li, X., Li, X. R., Li, W., Song, Q., et al. (2020). Phosphorylated alpha-synuclein in red blood cells as a potential diagnostic biomarker for multiple system atrophy: A pilot study. *Parkinsons Dis.* 2020:8740419. doi: 10.1155/2020/8740419

Liang, Y., Cui, L., Gao, J., Zhu, M., Zhang, Y., and Zhang, H. L. (2021). Gut microbial metabolites in Parkinson's disease: Implications of mitochondrial dysfunction in the pathogenesis and treatment. *Mol. Neurobiol.* 58, 3745–3758. doi: 10.1007/s12035-021-02375-0

Lin, M. T., Cantuti-Castelvetri, I., Zheng, K., Jackson, K. E., Tan, Y. B., Arzberger, T., et al. (2012). Somatic mitochondrial DNA mutations in early Parkinson and incidental lewy body disease. *Ann. Neurol.* 71, 850–854. doi: 10.1002/ana.23568

Loft, M., To, Y. H., Gibbs, P., and Tie, J. (2023). Clinical application of circulating tumour DNA in colorectal cancer. *Lancet Gastroenterol. Hepatol.* 8:837. doi: 10.1016/S2468-1253(23)00146-2

Lowes, H., Pyle, A., Duddy, M., and Hudson, G. (2019). Cell-free mitochondrial DNA in progressive multiple sclerosis. *Mitochondrion* 46, 307–312. doi: 10.1016/j.mito.2018.07.008

Lowes, H., Pyle, A., Santibanez-Koref, M., and Hudson, G. (2020). Circulating cell-free mitochondrial DNA levels in Parkinson's disease are influenced by treatment. *Mol. Neurodegener.* 15:10. doi: 10.1186/s13024-020-00362-y

Loyfer, N., Magenheim, J., Peretz, A., Cann, G., Bredno, J., Klochendler, A., et al. (2023). A DNA methylation atlas of normal human cell types. *Nature* 613, 355–364. doi: 10.1038/s41586-022-05580-6

Malhotra, S., Miras, M. C. M., Pappolla, A., Montalban, X., and Comabella, M. (2023). Liquid biopsy in neurological diseases. *Cells (Basel, Switzerland)* 12:1911. doi: 10.3390/cells12141911

Masayesva, B. G., Mambo, E., Taylor, R. J., Goloubeva, O. G., Zhou, S., Cohen, Y., et al. (2006). Mitochondrial DNA content increase in response to cigarette smoking. *Cancer Epidemiol. Biomark. Prevent.* 15, 19–24. doi: 10.1158/1055-9965.EPI-05-0210

Mattox, A. K., Douville, C., Wang, Y., Popoli, M., Ptak, J., Silliman, N., et al. (2023). The origin of highly elevated cell-free DNA in healthy individuals and patients with pancreatic, colorectal, lung, or ovarian cancer. *Cancer Discov.* 13, 2166–2179. doi: 10.1158/2159-8290.CD-21-1252

Milaneschi, Y., Kappelmann, N., Ye, Z., Lamers, F., Moser, S., Jones, P. B., et al. (2021). Association of inflammation with depression and anxiety: Evidence for symptom-specificity and potential causality from UK biobank and nesda cohorts. *Mol. Psychiatry* 26, 7393–7402. doi: 10.1038/s41380-021-01188-w

Mitsui, J., Matsukawa, T., Yasuda, T., Ishiura, H., and Tsuji, S. (2016). Plasma coenzyme q10 levels in patients with multiple system atrophy. *JAMA Neurol.* 73, 977–980. doi: 10.1001/jamaneurol.2016.1325

Monzio, C. G., Di Fonzo, A., Corti, S., Comi, G. P., Bresolin, N., and Masliah, E. (2020). The role of mitochondria in neurodegenerative diseases: The lesson from Alzheimer's disease and Parkinson's disease. *Mol. Neurobiol.* 57, 2959–2980. doi: 10.1007/s12035-020-01926-1

Moss, J., Magenheim, J., Neiman, D., Zemmour, H., Loyfer, N., Korach, A., et al. (2018). Comprehensive human cell-type methylation atlas reveals origins of circulating cell-free DNA in health and disease. *Nat. Commun.* 9:5068. doi: 10.1038/s41467-018-07466-6

Müller-Nedebock, A. C., Brennan, R. R., Venter, M., Pienaar, I. S., van der Westhuizen, F. H., Elson, J. L., et al. (2019). The unresolved role of mitochondrial DNA in Parkinson's disease: An overview of published studies, their limitations, and future prospects. *Neurochem. Int.* 129:104495. doi: 10.1016/j.neuint.2019.104495

Nakamoto, F. K., Okamoto, S., Mitsui, J., Sone, T., Ishikawa, M., Yamamoto, Y., et al. (2018). The pathogenesis linked to coenzyme q10 insufficiency in IPSC-derived neurons from patients with multiple-system atrophy. *Sci. Rep.* 8:14215. doi: 10.1038/s41598-018-32573-1

Nidadavolu, L. S., Feger, D., Wu, Y., Grodstein, F., Gross, A. L., Bennett, D. A., et al. (2022). Circulating cell-free genomic DNA is associated with an increased risk of dementia and with change in cognitive and physical function. *J. Alzheimers Dis.* 89, 1233–1240. doi: 10.3233/JAD-220301

Opara, J., Małecki, A., Małecka, E., and Socha, T. (2017). Motor assessment in Parkinson's disease. *Ann. Agr. Env. Med.* 24, 411–415. doi: 10.5604/12321966.1232774

Park, S. S., Jeong, H., and Andreazza, A. C. (2022). Circulating cell-free mitochondrial DNA in brain health and disease: A systematic review and meta-analysis. *World J. Biol. Psychiatry* 23, 87–102. doi: 10.1080/15622975.2021.1938214

Passaro, A. P., Lebos, A. L., Yao, Y., and Stice, S. L. (2021). Immune response in neurological pathology: Emerging role of central and peripheral immune crosstalk. *Front. Immunol.* 12:676621. doi: 10.3389/fimmu.2021.676621

Peelaerts, W., Mercado, G., George, S., Villumsen, M., Kasen, A., Aguileta, M., et al. (2023). Urinary tract infections trigger synucleinopathy via the innate immune response. *Acta Neuropathol.* 145, 541–559. doi: 10.1007/s00401-023-02562-4

Phillips, N. R., Simpkins, J. W., and Roby, R. K. (2014). Mitochondrial DNA deletions in Alzheimer's brains: A review. *Alzheimer's Dement.* 10, 393–400. doi: 10.1016/j.jalz.2013.04.508

Pisareva, E., Roch, B., Sanchez, C., Pastor, B., Mirandola, A., Diab-Assaf, M., et al. (2023). Comparison of the structures and topologies of plasma extracted circulating nuclear and mitochondrial cell-free DNA. *Front. Genet.* 14:1104732. doi: 10.3389/fgene.2023.1104732

Pisetsky, D. S. (2012). The origin and properties of extracellular DNA: From pamp to damp. *Clinical immunology (Orlando, Fla.)* 144, 32–40. doi: 10.1016/j.clim.2012.04.006

Podlesniy, P., Llorens, F., Puigròs, M., Serra, N., Sepúlveda-Falla, D., Schmidt, C., et al. (2020). Cerebrospinal fluid mitochondrial DNA in rapid and slow progressive forms of Alzheimer's disease. *Int. J. Mol. Sci.* 21:10.3390/ijms21176298.

Podlesniy, P., Vilas, D., Taylor, P., Shaw, L. M., Tolosa, E., and Trullas, R. (2016). Mitochondrial DNA in csf distinguishes lrrk2 from idiopathic Parkinson's disease. *Neurobiol. Dis.* 94, 10–17. doi: 10.1016/j.nbd.2016.05.019

Postuma, R. B., and Berg, D. (2016). Advances in markers of prodromal Parkinson disease. *Nat. Rev. Neurol.* 12, 622–634. doi: 10.1038/nrneurol.2016.152

Postuma, R. B., Berg, D., Stern, M., Poewe, W., Olanow, C. W., Oertel, W., et al. (2015). Mds clinical diagnostic criteria for Parkinson's disease. *Mov. Disord.* 30, 1591–1601. doi: 10.1002/mds.26424

Puigròs, M., Calderon, A., Pérez-Soriano, A., de Dios, C., Fernández, M., Colell, A., et al. (2022). Cell-free mitochondrial DNA deletions in idiopathic, but not lrrk2, Parkinson's disease. *Neurobiol. Dis.* 174, 105885. doi: 10.1016/j.nbd.2022.105885

Pyle, A., Anugrha, H., Kurzawa-Akanbi, M., Yarnall, A., Burn, D., and Hudson, G. (2016). Reduced mitochondrial DNA copy number is a biomarker of Parkinson's disease. *Neurobiol. Aging* 38, 216–217. doi: 10.1016/j.neurobiolaging.2015.10.033

Pyle, A., Brennan, R., Kurzawa-Akanbi, M., Yarnall, A., Thouin, A., Mollenhauer, B., et al. (2015). Reduced cerebrospinal fluid mitochondrial DNA is a biomarker for early-stage Parkinson's disease. *Ann. Neurol.* 78, 1000–1004. doi: 10.1002/ana.24515

Raha, S., and Robinson, B. H. (2000). Mitochondria, oxygen free radicals, disease and ageing. *Trends Biochem. Sci.* 25, 502–508. doi: 10.1016/s0968-0004(00)01674-1

Rostami, A., Lambie, M., Yu, C. W., Stambolic, V., Waldron, J. N., and Bratman, S. V. (2020). Senescence, necrosis, and apoptosis govern circulating cell-free DNA release kinetics. *Cell Rep.* 31, 107830. doi: 10.1016/j.celrep.2020.107830

Sanders, L. H., Mccoy, J., Hu, X., Mastroberardino, P. G., Dickinson, B. C., Chang, C. J., et al. (2014). Mitochondrial DNA damage: Molecular marker of vulnerable nigral neurons in parkinson's disease. *Neurobiol. Dis.* 70, 214–223. doi: 10.1016/j.nbd.2014.06.014

Scalzo, P. L., Ikuta, N., Cardoso, F., Regner, A., and Teixeira, A. L. (2009). Quantitative plasma DNA analysis in Parkinson's disease. *Neurosci. Lett.* 452, 5–7. doi: 10.1016/j.neulet.2009.01.031

Schapira, A. H., Cooper, J. M., Dexter, D., Jenner, P., Clark, J. B., and Marsden, C. D. (1989). Mitochondrial complex i deficiency in Parkinson's disease. *Lancet (London, England)* 1:1269. doi: 10.1016/s0140-6736(89)92366-0

Schottlaender, L. V., Bettencourt, C., Kiely, A. P., Chalasani, A., Neergheen, V., Holton, J. L., et al. (2016). Coenzyme q10 levels are decreased in the cerebellum of multiple-system atrophy patients. *PLoS One* 11:e149557. doi: 10.1371/journal.pone.0149557

Schrag, A., Horsfall, L., Walters, K., Noyce, A., and Petersen, I. (2015). Prediagnostic presentations of Parkinson's disease in primary care: A case-control study. *Lancet Neurol.* 14, 57–64. doi: 10.1016/S1474-4422(14)70287-X

Song, P., Wu, L. R., Yan, Y. H., Zhang, J. X., Chu, T., Kwong, L. N., et al. (2022). Limitations and opportunities of technologies for the analysis of cell-free DNA in cancer diagnostics. *Nat. Biomed. Eng.* 6, 232–245. doi: 10.1038/s41551-021-00837-3

Stebbins, G. T., Goetz, C. G., Burn, D. J., Jankovic, J., Khoo, T. K., and Tilley, B. C. (2013). How to identify tremor dominant and postural instability/gait difficulty groups with the movement disorder society unified Parkinson's disease rating scale: Comparison with the unified Parkinson's disease rating scale. *Mov. Disord.* 28, 668–670. doi: 10.1002/mds.25383

Storci, G., De Carolis, S., Olivieri, F., and Bonafè, M. (2018). Changes in the biochemical taste of cytoplasmic and cell-free DNA are major fuels for inflamm-aging. *Semin. Immunol.* 40, 6–16. doi: 10.1016/j.smim.2018.08.003

Sun, K., Jiang, P., Chan, K. C. A., Wong, J., Cheng, Y. K. Y., Liang, R. H. S., et al. (2015). Plasma DNA tissue mapping by genome-wide methylation sequencing for noninvasive prenatal, cancer, and transplantation assessments. *Proc. Natl. Acad. Sci. U.S.A.* 112, E5503–E5512. doi: 10.1073/pnas.1508736112

Tan, A. H., Chong, C. W., Lim, S. Y., Yap, I., Teh, C., Loke, M. F., et al. (2021). Gut microbial ecosystem in Parkinson disease: New clinicobiological insights from multi-omics. *Ann. Neurol.* 89, 546–559. doi: 10.1002/ana.25982

Tolosa, E., Wenning, G., and Poewe, W. (2006). The diagnosis of Parkinson's disease. *Lancet Neurol.* 5, 75–86. doi: 10.1016/S1474-4422(05)70285-4

Trumpff, C., Michelson, J., Lagranha, C. J., Taleon, V., Karan, K. R., Sturm, G., et al. (2021). Stress and circulating cell-free mitochondrial DNA: A systematic review of human studies, physiological considerations, and technical recommendations. *Mitochondrion* 59, 225–245. doi: 10.1016/j.mito.2021.04.002

Valiente-Pallejà, A., Torrell, H., Muntané, G., Cortés, M. J., Martínez-Leal, R., Abasolo, N., et al. (2018). Genetic and clinical evidence of mitochondrial dysfunction in autism spectrum disorder and intellectual disability. *Hum. Mol. Genet.* 27, 891–900. doi: 10.1093/hmg/ddy009

Varhaug, K. N., Vedeler, C. A., Myhr, K., Aarseth, J. H., Tzoulis, C., and Bindoff, L. A. (2017). Increased levels of cell-free mitochondrial DNA in the cerebrospinal fluid of patients with multiple sclerosis. *Mitochondrion* 34, 32–35. doi: 10.1016/j.mito.2016.12.003

Wojtkowska, M., Karczewska, N., Pacewicz, K., Pacak, A., Kopeæ, P., Florczak-Wyspiańska, J., et al. (2024). Quantification of circulating cell-free DNA in idiopathic Parkinson's disease patients. *Int. J. Mol. Sci.* 25:2818. doi: 10.3390/ijms25052818

Wu, I. C., Lin, C. C., Liu, C. S., Hsu, C. C., Chen, C. Y., and Hsiung, C. A. (2017). Interrelations between mitochondrial DNA copy number and inflammation in older adults. *J. Gerontol. Ser. A-Biol. Sci. Med. Sci.* 72, 937–944. doi: 10.1093/gerona/glx033

Yuan, X., Wan, L., Chen, Z., Long, Z., Chen, D., Liu, P., et al. (2024). Peripheral inflammatory and immune landscape in multiple system atrophy: A cross-sectional study. *Mov. Disord.* 39, 391–399. doi: 10.1002/mds.29674

Zeng, Y., Chourpiliadis, C., Hammar, N., Seitz, C., Valdimarsdottir, U. A., Fang, F., et al. (2024). Inflammatory biomarkers and risk of psychiatric disorders. *JAMA Psychiatry* 81, 1118–1129. doi: 10.1001/jamapsychiatry.2024.2185

frontiers | Frontiers in Neuroscience

TYPE Original Research
PUBLISHED 28 January 2025
DOI 10.3389/fnins.2025.1472010

OPEN ACCESS

EDITED BY
Pradeep Kumar,
All India Institute of Medical Sciences, India

REVIEWED BY
Hongwei Wen,
Southwest University, China
Hai-Feng Shi,
Changzhou No.2 People's Hospital, China

*CORRESPONDENCE
Hailing Zhou
✉ ZHL13590049931@163.com

RECEIVED 28 July 2024
ACCEPTED 06 January 2025
PUBLISHED 28 January 2025

CITATION
Ni W, Liu WV, Li M, Wei S, Xu X, Huang S, Zhu L, Wang J, Wen F and Zhou H (2025) Altered brain functional network connectivity and topology in type 2 diabetes mellitus. *Front. Neurosci.* 19:1472010. doi: 10.3389/fnins.2025.1472010

Altered brain functional network connectivity and topology in type 2 diabetes mellitus

Weiwei Ni[1], Weiyin Vivian Liu[2], Mingrui Li[3], Shouchao Wei[4], Xuanzi Xu[5], Shutong Huang[6], Lanhui Zhu[1], Jieru Wang[7], Fengling Wen[7] and Hailing Zhou[7]*

[1]Physical Examination Centre, Central People's Hospital of Zhanjiang, Zhanjiang, China, [2]MR Research, GE Healthcare, Beijing, China, [3]Department of Magnetic Resonance Imaging, Zhanjiang First Hospital of Traditional Chinese Medicine, Zhanjiang, China, [4]Central People's Hospital of Zhanjiang, Zhanjiang Institute of Clinical Medicine, Zhanjiang, China, [5]Department of Teaching and Training, Central People's Hospital of Zhanjiang, Zhanjiang, China, [6]Department of Clinical Laboratory, Central People's Hospital of Zhanjiang, Zhanjiang, China, [7]Department of Radiology, Central People's Hospital of Zhanjiang, Zhanjiang, China

Introduction: Type 2 diabetes mellitus (T2DM) accelerates brain aging and disrupts brain functional network connectivity, though the specific mechanisms remain unclear. This study aimed to investigate T2DM-driven alterations in brain functional network connectivity and topology.

Methods: Eighty-five T2DM patients and 67 healthy controls (HCs) were included. All participants underwent clinical, neuropsychological, and laboratory tests, followed by MRI examinations, including resting-state functional magnetic resonance imaging (rs-fMRI) and three-dimensional high-resolution T1-weighted imaging (3D-T1WI) on a 3.0 T MRI scanner. Post-image preprocessing, brain functional networks were constructed using the Dosenbach atlas and analyzed with the DPABI-NET toolkit through graph theory.

Results: In T2DM patients, functional connectivity within and between the default mode network (DMN), frontal parietal network (FPN), subcortical network (SCN), ventral attention network (VAN), somatosensory network (SMN), and visual network (VN) was significantly reduced compared to HCs. Conversely, two functional connections within the VN and between the DMN and SMN were significantly increased. Global network topology analysis showed an increased shortest path length and decreased clustering coefficient, global efficiency, and local efficiency in the T2DM group. MoCA scores were negatively correlated with the shortest path length and positively correlated with global and local efficiency in the T2DM group. Node network topology analysis indicated reduced clustering coefficient, degree centrality, eigenvector centrality, and nodal efficiency in multiple nodes in the T2DM group. MoCA scores positively correlated with clustering coefficient and nodal efficiency in the bilateral precentral gyrus in the T2DM group.

Discussion: This study demonstrated significant abnormalities in connectivity and topology of large-scale brain functional networks in T2DM patients. These findings suggest that brain functional network connectivity and topology could serve as imaging biomarkers, providing insights into the underlying neuropathological processes associated with T2DM-related cognitive impairment.

KEYWORDS

type 2 diabetes mellitus, functional magnetic resonance imaging, blood oxygenation level-dependent imaging, brain functional network connectivity, graph theory

1 Introduction

Type 2 diabetes mellitus (T2DM) affects approximately 450 million adults worldwide (American Diabetes Association Professional Practice, 2024), leading to systemic complications. This chronic metabolic disease accelerates brain aging (Biessels et al., 2020) and nerve damage, resulting in cognitive impairment. T2DM facilitates the progression from mild cognitive impairment (MCI) to dementia, significantly diminishing quality of life. Understanding the mechanisms underlying cognitive impairment in T2DM is crucial for early detection and treatment (Srikanth et al., 2020).

Neurodegenerative and neuropsychological disorders, including T2DM, often have a prolonged preclinical phase lasting a decade or more. Subtle changes in brain function frequently precede overt structural neuropathology and behavioral symptoms. T2DM is characterized by hyperinsulinemia as reduced insulin receptor expression and receptor-activating enzymes, leading to the deposition of amyloid beta (Aβ) and Tau proteins (Arnold et al., 2018). Chronic hyperglycemia and insulin resistance disrupt neuronal function, synaptic plasticity and neurovascular integrity, contributing to neuroinflammation and oxidative stress exacerbate damage (van Sloten et al., 2020). The brain volume reduction and cognitive decline in associated brain regions (Zhang et al., 2014; Cao et al., 2024). Advancements in neuroimaging, particularly resting-state functional magnetic resonance imaging (rs-fMRI), have enabled the identification of numerous neuroimaging biomarkers. This non-invasive, repeatable, and straightforward technique has revealed alterations in blood oxygenation level-dependent (BOLD) signals in T2DM patients (Marquez and Yassa, 2019; Van Bussel et al., 2017; Zackova et al., 2021; Franke and Gaser, 2019). Post-processing of BOLD images facilitates the classification and mapping of brain functional networks, offering new insights into the pathophysiological mechanisms of T2DM-related cognitive disorders (Wang et al., 2016; Lv et al., 2018; Cole et al., 2010).

Significant progress has been made in understanding T2DM-driven brain functional networks. Both reduced and increased functional connectivity between various brain regions in T2DM patients have been observed (Cui et al., 2016; Liu et al., 2018; Li et al., 2020; Liu et al., 2017; Tan et al., 2019). Earlier studies primarily focused on local brain region connections, but it is now recognized that most cognitive functions involve multiple brain regions working together. Consequently, initial changes in brain regions were often overlooked (Fuster, 2006). The focus has shifted toward systematically identifying and understanding the functional organization of large-scale brain networks and their roles in cognitive and emotional processing (Bressler and Menon, 2010). Few studies, however, have examined changes in T2DM-related large-scale networks, with the default mode network (DMN) receiving more attention (Chen et al., 2015; Liu et al., 2019; Chen et al., 2016; Deng et al., 2021; Cui et al., 2015) while other large-scale networks are not fully understood. At present, the mechanism between changes in large-scale network functional connectivity and cognitive dysfunction is still not clearly understood. Graph theory analysis can elucidate important topological features of the whole brain, including small-world attributes, modulators, and hub nodes (Farahani et al., 2019). Several studies have reported differences in graph theory-derived parameters of brain functional networks between T2DM patients and healthy individuals. However, these studies often included small sample sizes and did not simultaneously analyze large-scale brain network connectivity and topological changes in T2DM patients (van Bussel et al., 2016; Xin et al., 2024; Zhou et al., 2022; Zhang et al., 2021). Differences in graph theory-derived parameters of brain functional networks between T2DM patients and healthy individuals are reported based on small cohorts without analyzing large-scale brain network connectivity and topological changes.

This study aimed to construct large-scale network connections in T2DM patients using BOLD-based rs-fMRI data and to display whole-brain and nodal topological features through graph theory analysis. This approach seeks to enhance the understanding of the mechanisms underlying cognitive dysfunction in T2DM and provide further ideas for the delay or prevention of brain disease in T2DM patients.

2 Materials and methods

2.1 Participants

This study was approved by the ethics committee of our hospital. Participants, all right-handed Han Chinese native speakers, attended the endocrinology department and health examination center between November 2022 and January 2024. Written informed consent was secured from all participants prior to enrollment. Inclusion criteria for T2DM group: 1. diagnoses of type 2 diabetes were established by an endocrinologist following the American Diabetes Association guidelines, and inclusion criteria for T2DM group were: 1. hyperglycemia was diagnosed with typical diabetic symptoms plus glycated hemoglobin A1C (HbA1c) ≥6.5% or fasting blood glucose (FBG) ≥7.0 mmol/L or fasting two-hour blood glucose (OGTT2h) ≥11.1 mmol/L or random FBG ≥ 11.1 mmol/L. Fasting was defined as no energy intake for at least 8 h prior to the examination; OGTT uses 75 g of anhydrous glucose dissolved in 300 mL of warm water (American Diabetes Association Professional Practice, 2024); 2. aged 18–65, Han nationality, right-handed; 3. blood pressure is normal; 4. complete cognitive function assessment and MRI examination. The inclusion criteria for the healthy controls (HCs) group were as follows: 1. those with matched gender, age and years of education to the T2DM group; 2. no history of diabetes and normal blood pressure; 3. complete cognitive function assessment and MRI examination. Exclusion criteria included individuals younger than 18 or older than 65 years, those with organic central nervous system diseases, a history of mental illness or familial mental illness, severe head trauma, severe hypoglycemia, significant vascular complications, alcohol dependence or substance abuse, noticeable hearing or visual impairments, women who were pregnant, breastfeeding, or using contraceptives, and those with contraindications for MRI. In total, 85 T2DM patients and 67

HCs were enrolled. Demographic data, including gender, age, and education, were self-reported by all participants.

2.2 Laboratory analysis and cognition testing

Blood samples were obtained from all subjects to measure glycated hemoglobin A_{1c} (HbA_{1c}), fasting blood glucose (FBG), triglyceride (TG), total cholesterol (TC), and low-density lipoprotein (LDL) levels. All participants underwent neuropsychological assessments, including the Montreal cognitive assessment (MoCA) (Li et al., 2018), the digital span test (DST, comprising forward and backward tasks) (Diamond, 2013), and the clock drawing test (CDT) (Zhou et al., 2010), with each test lasting 5–10 min.

2.3 MRI acquisition

All participants were subjected to MRI examinations on a 3.0 T MRI scanner (SIGNA Pioneer, GE Healthcare) with a 16-channel phased-array head coil. Routine imaging included T1-weighted, T2-weighted, and T2-fluid attenuated inversion recovery (T2-FLAIR) sequences to rule out organic brain lesions. Blood oxygenation level-dependent (BOLD) imaging was then conducted with the following parameters: flip angle = 90.0°, bandwidth = 250.0 kHz, TR = 2000 ms, TE = 30.0 ms, slices = 48, thickness = 3.0 mm, pixel size = 3.0 × 3.0 × 3.0 mm^3, FOV = 256 × 256 mm^2, and NEX = 1. Additionally, three-dimensional high-resolution T1-weighted brain volume imaging (3D-T1WI BRAVO) was performed with these parameters: flip angle = 12.0°, bandwidth = 31.25 kHz, TR = 7.8 ms, TE = 3.1 ms, slices = 1,024, thickness = 1.0 mm, pixel size = 1.0 × 1.0 × 1.0 mm^3, FOV = 25.6 × 25.6 cm^2, and NEX = 1.

2.4 Assessment of small-vessel disease

White matter degeneration and lacunar infarction in five brain regions (bilateral frontal lobes, parietal and occipital lobes, temporal lobes, cerebellum and brainstem, and basal ganglia) were quantitatively assessed on T2-FLAIR images using the age-related white matter changes (ARWMC) Wahlund score (Wahlund et al., 2001). These assessments were conducted by two experienced radiologists who were blinded to the group assignments. Discrepancies were resolved through joint discussion to reach consensus. Participants with ratings above 2 were excluded from the study.

2.5 Image processing

All rs-fMRI data were processed using SPM12 and DPABI (version 8.1) toolkits in MATLAB (Yan et al., 2016). The preprocessing steps were as follows: 1. DICOM-NIFTI data format conversion. 2. Removal of the first 10 time points. 3. Temporal correction. 4. Head movement correction: ensure that the head motion displacement of all enrolled subjects is <2 mm and the head motion rotation is <2 °, and the mean FD_Jenkinson is obtained as the covariate for the subsequent comparison between the groups. 5. Nuisnace covariate regression: to remove the nuisance signals, the Friston 24-parameter model was utilized to regress out head motion effects from the realigned data. The signals from WM and CSF were regressed out to reduce respiratory and cardiac effects. 6. Spatial normalization: We first registered the 3D-T1WI images to the fMRI images. We selected the "New Segment + Dartel" option. The "New Segment + Dartel" option performs the New Segment operation on the 3D-T1WI structural images to obtain tissue maps for gray matter, white matter, and cerebrospinal fluid. Additionally, DARTEL transforms the structural and tissue images into MNI space and generates transformation matrices. Finally, we chose the "Normalize by DARTEL" option, which uses the transformation matrices to convert the functional images into MNI space. 7. Filtering: select signals in the frequency band of 0.01 Hz to 0.08 Hz. These procedures were applied to enhance image data quality, reduce confounding factors, and prepare the data for further analysis.

2.6 Construction of brain function networks

A total of 142 ROIs from the Dosenbach atlas were used as nodes and classified into seven large-scale networks (Dosenbach et al., 2010; Yeo et al., 2011). Seven large-scale networks include: default mode network (DMN), frontal parietal network (FPN), subcortical network (SCN), ventral attention network (VAN), somatosensory network (SMN), visual network (VN), and dorsal attention network (DAN). The BOLD signals for each node were averaged, and Pearson correlation coefficients were calculated to determine the correlation between BOLD signals across nodes. Functional connectivity (FC) between nodes was then computed using Z transformation, with these connections represented as edges within the brain functional network. Since the current negative functional connection is still controversial, we set the negative functional connection to 0 and keep only the positive functional connection, so as to obtain the undirected weighted positive resting state functional connection matrix (Pang et al., 2022). The details, including node names, networks, and MNI coordinates, are listed in Supplementary Table S1.

2.7 Graph theory analysis of brain functional networks

The topological attributes of the brain functional network were computed across sparsity levels ranging from 0.1 to 0.34, with a step size of 0.01 (Yang et al., 2021), using the DPABI-NET toolkit in MATLAB. Global topological attributes assessed included sigma, gamma, lambda, shortest path length, clustering coefficient, global efficiency, and local efficiency. Node-specific attributes evaluated comprised clustering coefficient, degree centrality, eigenvector centrality, and nodal efficiency.

2.8 Statistics

Statistical analyses were performed using SPSS (IBM, SPSS, version 25). Differences in demographic data and neurocognitive test scores between groups were assessed using either independent

TABLE 1 Demographic data, clinical biochemical indicators and neuropsychological result of all subjects.

	T2DM (n = 85)	HC (n = 67)	Statistics	p-value
Age (years)	50.29 ± 9.62	47.88 ± 8.05	t = 1.648	0.101
Sex (female/male)	30/55	31/36	$\chi2$ = 1.878	0.171
Education (years)	12.00 (9.00;15.00)	12 (9.00;16.00)	z = −0.087	0.930
HbA1c (%)	8.91 ± 2.06	N/A	N/A	N/A
FBG (mmol/L)	7.88 (6.77;10.63)	N/A	N/A	N/A
TG (mmol/L)	1.89 (1.11;2.52)	N/A	N/A	N/A
TC (mmol/L)	5.16 ± 1.27	N/A	N/A	N/A
LDL (mmol/L)	3.13 (2.58;3.84)	N/A	N/A	N/A
CDT	3.00 (3.00;4.00)	3.00 (3.00;4.00)	z = −0.355	0.722
MoCA	26.00 (24.00;27.00)	27.00 (27.00;29.00)	z = −5.831	<0.001*
DST(forward)	8.00 (7.00;9.00)	8.00 (8.00;9.00)	z = −1.105	0.269
DST(inverse)	4.00 (3.00;5.00)	4.00 (3.00;4.00)	z = −0.276	0.783

FBG, fasting blood glucose; TG, triglyceride; TC, total cholesterol; LDL, low-density lipoprotein; DST, the digital span test; CDT, the clock drawing test; MoCA, Montreal cognitive assessment. *P < 0.05.

two-sample t-tests or Mann–Whitney U tests, based on the distribution normality and variance equality of the data. Chi-square tests were used to evaluate gender differences between groups. Connectivity between functional network nodes was compared with two-sample t-tests, adjusting for gender, age, education level, and average head motion. Results were corrected for false discovery rate (FDR) using the Benjamini-Hochberg (B-H) procedure, with statistical significance set at $p < 0.05$.

Network topology attributes were analyzed using analysis of covariance (ANCOVA), incorporating gender, age, education level, and average head motion as covariates. The significance threshold for global network topology attributes was set at $p < 0.05$. For node-specific attributes, FDR correction was applied, with significance defined as $Q < 0.05$ after adjustment. Gender, age, education level and average head movement were used as covariables to conduct partial correlation analysis of MoCA scores, clinical measurements, and brain network topological parameters in the T2DM group, with statistical significance determined as $p < 0.05$.

3 Results

3.1 Demographic data, clinical measurements, and cognitive testing

Gender, age, and education were not comparable between the T2DM and HC groups. However, the T2DM group exhibited significantly lower MoCA scores than the HC group (Table 1).

3.2 Changes in connectivity of large-scale functional networks

The T2DM group showed significantly reduced functional connections within and between the DMN, FPN, SCN, VAN, DAN, SMN, and VN compared to the HC group. However, two functional connections were significantly increased within the VN and between the DMN and SMN (Figure 1).

3.3 Group differences in global network metrics

In the global network topology analysis, the T2DM group showed a lower clustering coefficient, global efficiency, and local efficiency, along with a higher shortest path length compared to the HC group. No significant differences were observed in sigma, gamma, and lambda between the groups (Table 2; Figure 2).

3.4 Group differences in node-level network metrics

In the node network topology analysis, the clustering coefficient was lower in the left basal ganglia and bilateral precentral gyrus in the T2DM group compared to the HC group. Degree and eigenvector centrality were reduced in the bilateral thalamus, and degree centrality alone was decreased in the right basal ganglia. Nodal efficiency was also lower in several brain regions (Table 3; Figure 3).

3.5 Correlation between network theory parameters and MoCA scores

In the global network topology analysis, MoCA scores negatively correlated with shortest path length and positively correlated with both global and local efficiency in the T2DM group. Node network topology analysis revealed that MoCA scores positively correlated with the clustering coefficient of the right precentral gyrus and with nodal efficiency in the right frontal cortex, left ventromedial frontal cortex, and both the right and left precentral gyri (Figure 4).

3.6 Correlation between network parameters and laboratory indicators

Global network graph analysis revealed no significant correlations between network parameters and laboratory indicators in T2DM

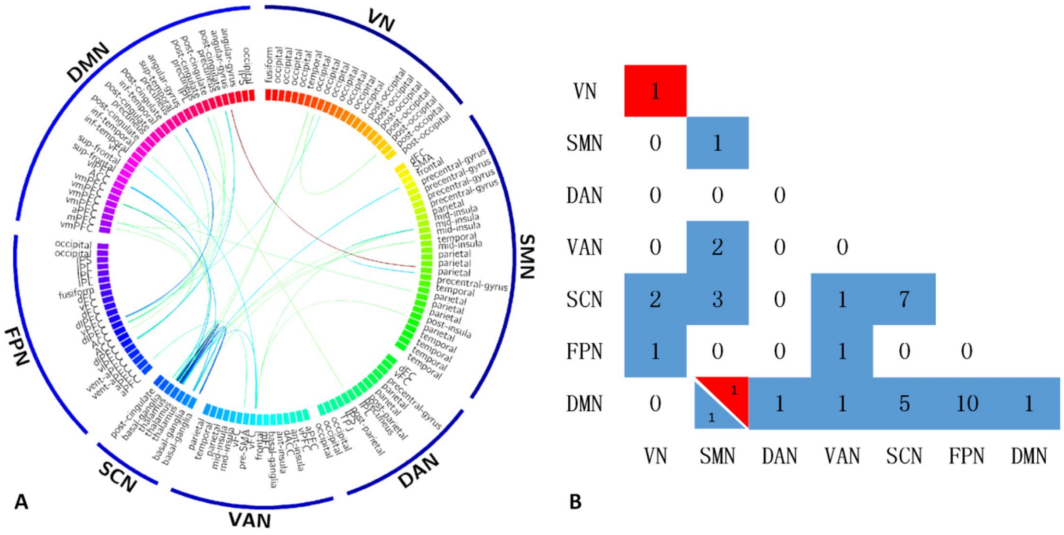

FIGURE 1
The T2DM group showed significantly reduced functional connections within and between the DMN, FPN, SCN, VAN, DAN, SMN, and VN compared to the HC group. However, two functional connections were significantly increased within the VN and between the DMN and SMN **(A)**. Maps show the number of significant edges for each pair of networks for each of the two contrasts **(B)**. DMN, default mode network; FPN, frontal parietal network; SCN, subcortical network; VAN, ventral attention network; SMN, somatosensory network; VN, visual network; DAN, dorsal attention network.

TABLE 2 **Global network metrics of all subjects.**

	T2DM (n = 85)	HC (n = 67)	Statistics(F)	P-value
Lp	1.059 ± 0.185	0.992 ± 0.158	5.991	0.016*
Cp	0.039 ± 0.009	0.042 ± 0.008	4.651	0.033*
Eg	0.056 ± 0.009	0.060 ± 0.009	6.131	0.014*
Eloc	0.082 ± 0.017	0.088 ± 0.016	5.858	0.017*
Sigma	1.195 ± 0.229	1.202 ± 0.229	0.021	0.884
Gamma	0.409 ± 0.066	0.417 ± 0.069	0.113	0.737
Lambda	0.089 ± 0.004	0.090 ± 0.004	1.428	0.234

Lp, shortest path length; Cp, clustering coefficient; Eg, global efficiency; Eloc, local efficiency. *$P < 0.05$.

patients compared to the HC group. However, node network topology analysis showed that FBG negatively correlated with nodal efficiency in the left ventromedial frontal cortex and left thalamus, as well as with eigenvector centrality in the left thalamus. Additionally, TG negatively correlated with both eigenvector and degree centrality in the left thalamus (Figure 5).

4 Discussion

This study identifies significant alterations in brain functional connectivity in T2DM patients compared to healthy controls, suggesting that cognitive impairment in T2DM is influenced by interactions among different brain regions and networks.

The DMN plays a critical role in cognition-related functions such as memory, future planning, and social planning (Yeshurun et al., 2021). Consistent with previous findings, connectivity within the DMN network as well as connectivity between the DMN and other networks, particularly involving the posterior cingulate gyrus, prefrontal cortex, precuneus, and angular gyrus reduced in T2DM patients (Deng et al., 2021; Chen et al., 2016). Meng et al. demonstrated large-scale network damage centered on DMN in T2DM patients through a meta-analysis, which provides key insights into the neural mechanisms of diabetes-related cognitive decline (Meng et al., 2022). Significantly decreased connectivity between the DMN and the FPN was also observed (Meng et al., 2022), suggesting deficits in execution, attention and emotional regulation in T2DM patients (Nielsen et al., 2017). Previous report about increased connectivity in the pre-DMN and decreased connectivity in the post-DMN (Cui et al., 2015), both increased and decreased connections between DMN and SMN networks were also found in our study, dissociative patterns in the DMN likely triggered the T2DM-related cognition decline.

Additionally, our results reveal reduced functional connectivity between the SCN and several other networks, including the VN, DMN, and SMN. This suggests that diminished connectivity in T2DM affects both cognitive regions and integration centers. Significant connectivity reductions were also found in the three sensory

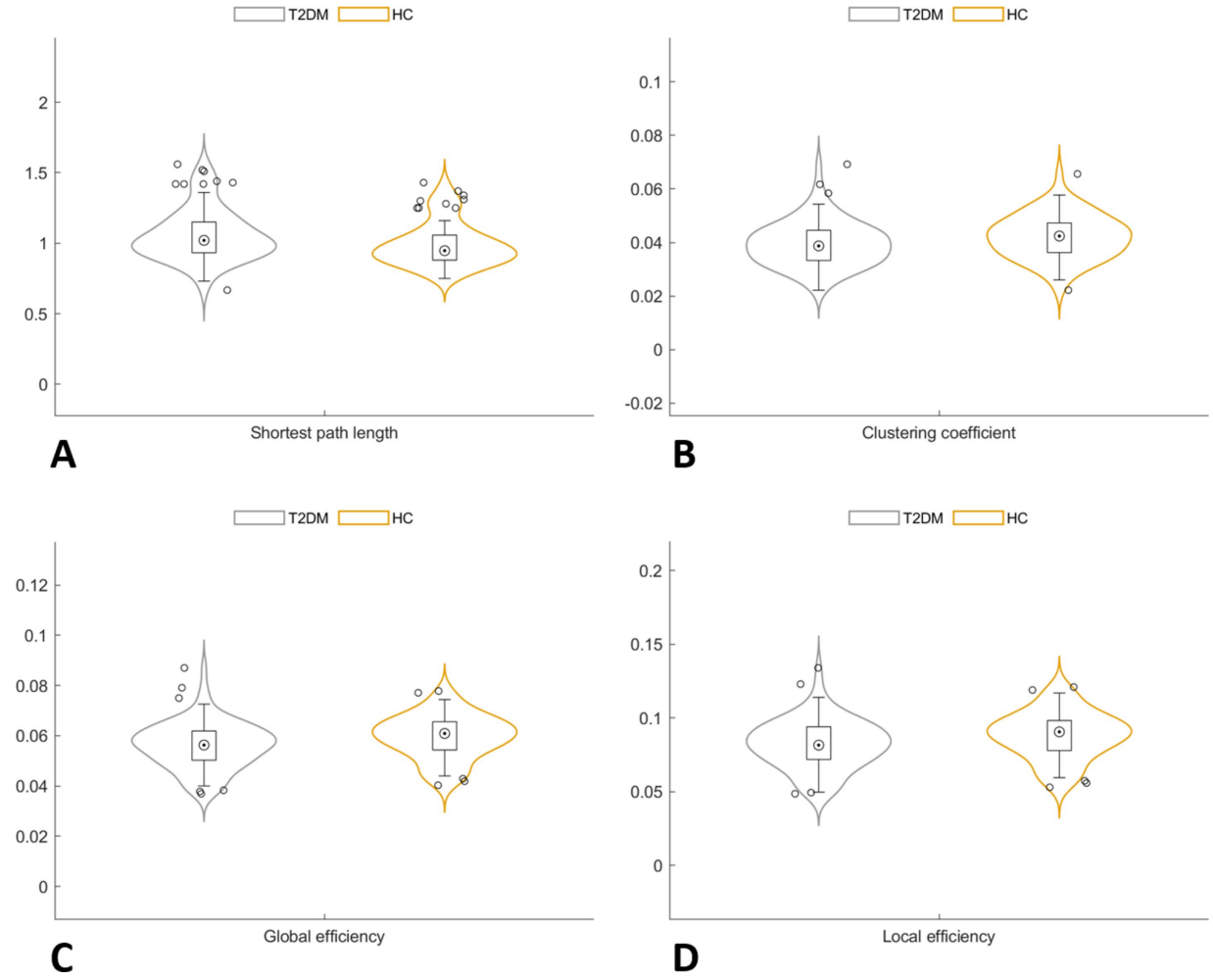

FIGURE 2
In the global network topology analysis, the T2DM group showed a higher shortest path length **(A)**, along with a lower clustering coefficient **(B)**, global efficiency **(C)** and local efficiency **(D)** compared to the HC group.

networks—the VAN, SMN, and VN—correlating with abnormalities in attention, sensation, and vision reported in T2DM patients (Zhang et al., 2015; Xia et al., 2015; Faskowitz et al., 2022). The VN, in particular, is highly susceptible and often shows disruptions in T2DM (Ni et al., 2024; Kaewput et al., 2019). While T2DM is commonly associated with disconnections in the DAN (Meng et al., 2022), our study found only a slight abnormality in the connection between DAN and DMN. Possibly due to the relatively short duration of diabetes in our study cohort.

T2DM impairs brain functional network connectivity through several mechanisms. It leads to neuron loss, disrupts cell proliferation in the dentate gyrus, and damages synaptic plasticity, as evidenced by both human and animal studies (Jackson-Guilford et al., 2000; Li et al., 2002; Stranahan et al., 2008). Neuroplasticity, which involves structural and functional adjustments in response to stimuli or damage (Cramer et al., 2011; Fu and Zuo, 2011), is crucial here. Enhanced functional connectivity often reflects compensatory mechanisms that the nervous system employs to preserve normal function and optimize between-network interactions (Jing et al., 2023; Fang et al., 2019). Additionally, treatments such as blood glucose reduction and improved perfusion of small blood vessels can enhance network connectivity. For example, intranasal insulin has been found to improve resting-state functional connectivity in the hippocampus (Zhang et al., 2015), potentially explaining our observations of increased connectivity within the VN and between the DMN and the SMN. This is consistent with previous findings of increased connectivity between the thalamus and VN in pre-T2DM patients (Jing et al., 2023).

We compared 7 global indicators between the two groups. We believed that these 7 indicators were independent of each other, so we did not conduct multiple contrast correction for these 7 indicators, which is similar to most relevant studies (Shang et al., 2023; Xin et al., 2024). Whole-brain network analysis revealed that T2DM is associated with decreased global network connectivity, characterized by lower clustering coefficient, global efficiency, and local efficiency, as well as increased shortest path length (Farahani et al., 2019; van Bussel et al., 2016; Yang et al., 2020). The clustering coefficient, which measures the interconnection among adjacent nodes, decreased in T2DM, indicating reduced information processing within clustered brain regions. Our results also show diminished global and local efficiency, suggesting less effective network processing, and an increased shortest path length, reflecting slower information transmission between brain

TABLE 3 Node-level network metrics of all subjects.

Node name	MNI coordinates			Statistics(*F*)	*P*-value	*Q*-value
	X	Y	Z			
Clustering coefficient						
Basal ganglia (L) (ROI 30)	−6	17	34	12.729	0.000	0.035*
Precentral gyrus (R) (ROI 51)	46	−8	24	13.748	0.000	0.042*
Precentral gyrus (L) (ROI 52)	−54	−9	23	11.730	0.001	0.038*
Degree centrality						
Thalamus (L) (ROI 57)	−12	−12	6	21.270	0.000	0.001*
Thalamus (R) (ROI 58)	11	−12	6	15.468	0.000	0.009*
Basal ganglia (R) (ROI 71)	11	−24	2	11.579	0.001	0.041*
Eigenvector centrality						
Thalamus (L) (ROI 57)	−12	−12	6	14.025	0.000	0.037*
Thalamus (R) (ROI 58)	11	−12	6	13.172	0.000	0.028*
Nodal efficiency						
vPFC (L) (ROI 23)	−52	28	17	9.454	0.003	0.045*
Basal ganglia (L) (ROI 30)	−6	17	34	11.681	0.001	0.039*
Frontal (R) (ROI 32)	58	11	14	8.176	0.005	0.049*
Basal ganglia (L) (ROI 38)	−20	6	7	9.923	0.002	0.047*
Basal ganglia (R) (ROI 39)	14	6	7	8.120	0.005	0.047*
vFC (L) (ROI 40)	−48	6	1	12.170	0.001	0.046*
Precentral gyrus (R) (ROI 51)	46	−8	24	9.755	0.002	0.044*
Precentral gyrus (L) (ROI 52)	−54	−9	23	9.308	0.003	0.043*
Parietal (L) (ROI 54)	−47	−12	36	8.739	0.004	0.043*
Thalamus (L) (ROI 57)	−12	−12	6	11.574	0.001	0.031*
basal ganglia (R) (ROI 71)	11	−24	2	8.832	0.003	0.045*
Angular gyrus (L) (ROI 101)	−41	−47	29	10.189	0.002	0.049*
Temporal (L) (ROI 102)	−59	−47	11	9.122	0.003	0.042*
Occipital (R) (ROI 120)	19	−66	−1	8.658	0.004	0.041*
Post occipital (L) (ROI 135)	−5	−80	9	8.097	0.005	0.045*

vPFC, ventromedial prefrontal cortex; vFC, ventral frontal cortex; *$Q < 0.05$.

10.3389/fnins.2025.1472010

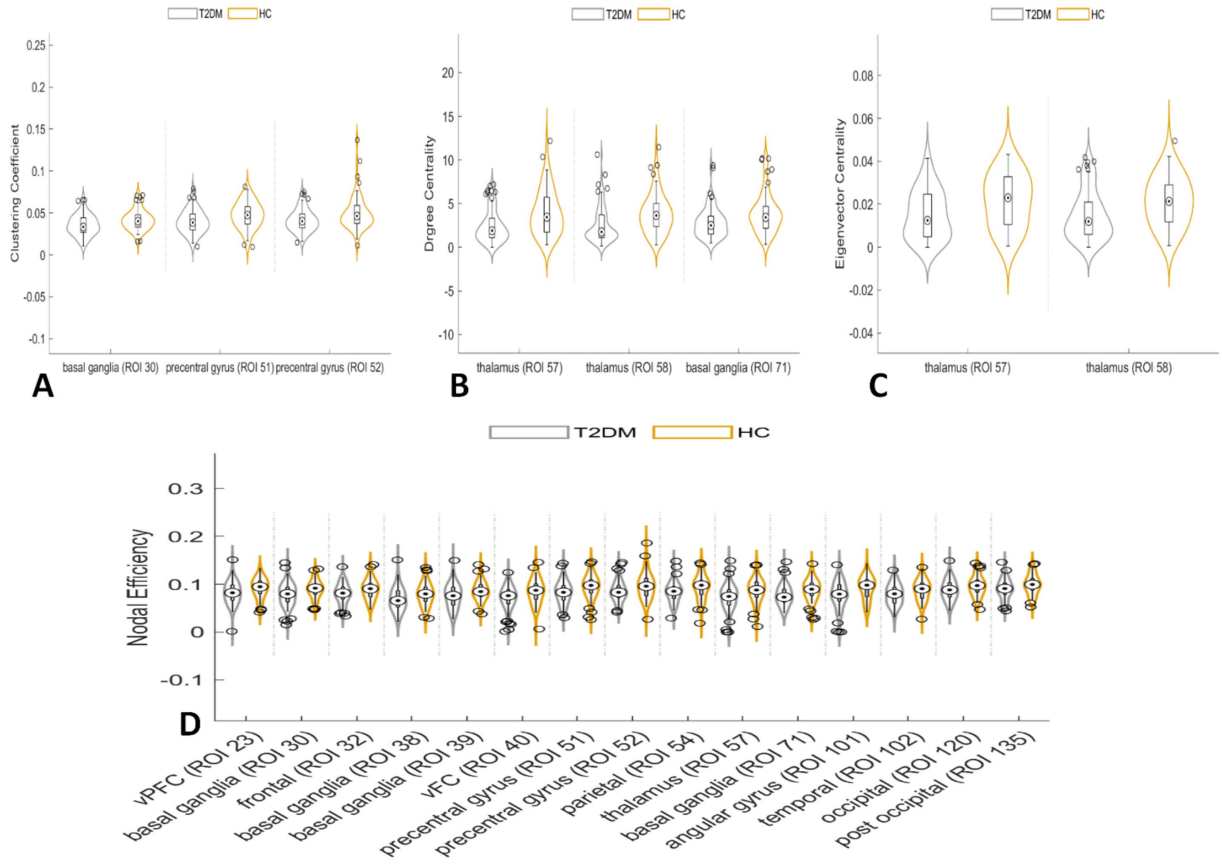

FIGURE 3
In the node network topology analysis, the clustering coefficient was lower in the left basal ganglia and bilateral precentral gyrus in the T2DM group compared to the HC group **(A)**. Degree centrality and eigenvector centrality were reduced in the bilateral thalamus, and degree centrality alone was decreased in the right basal ganglia **(B,C)**. Nodal efficiency was also lower in several brain regions **(D)**.

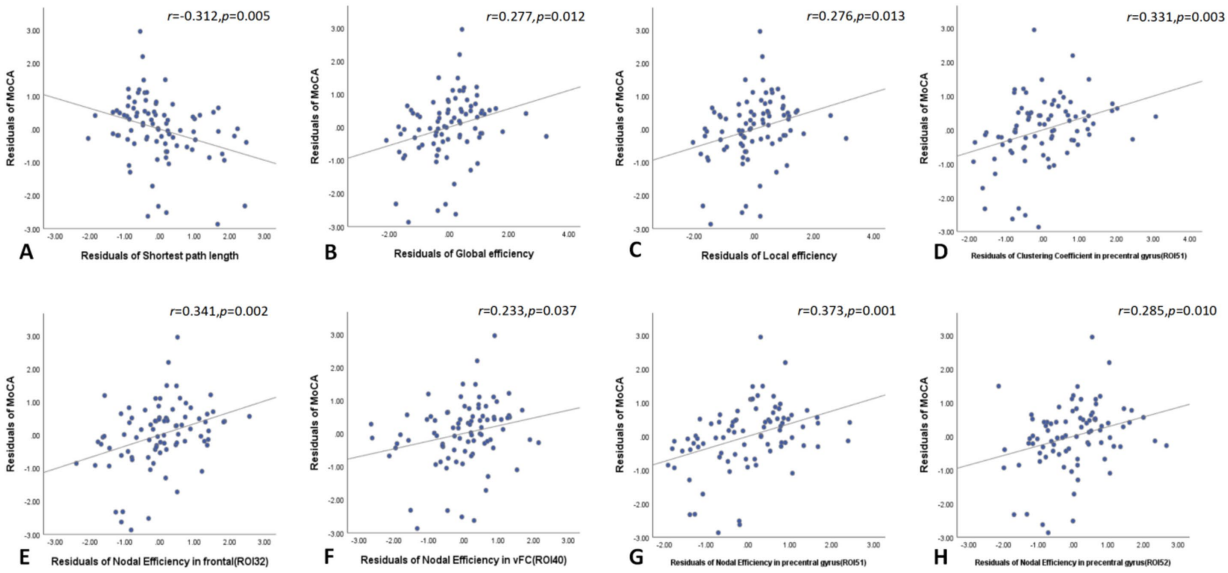

FIGURE 4
In the global network topology analysis, MoCA scores negatively correlated with shortest path length and positively correlated with both global and local efficiency in the T2DM group **(A–C)**. Node network topology analysis revealed that MoCA scores positively correlated with the clustering coefficient of the right precentral gyrus and with nodal efficiency in the right frontal cortex, left ventromedial frontal cortex, and both the right and left precentral gyri **(D–H)**. MoCA, Montreal cognitive assessment.

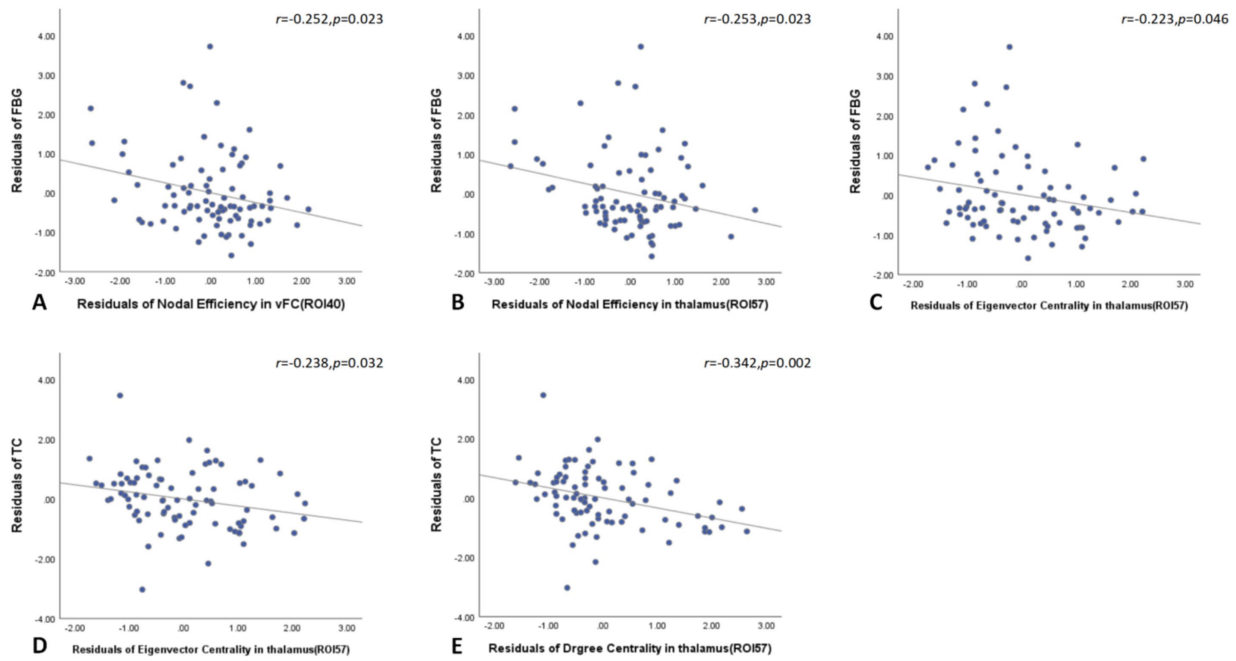

FIGURE 5
Node network topology analysis showed that FBG negatively correlated with nodal efficiency in the left ventromedial frontal cortex and left thalamus, as well as with eigenvector centrality in the left thalamus in T2DM patients **(A–C)**. Additionally, TG negatively correlated with both eigenvector and degree centrality in the left thalamus **(D,E)**. FBG, fasting blood glucose; TG, triglyceride.

regions. Although some studies have reported increased clustering coefficient, global efficiency, and local efficiency with a decreased shortest path length in T2DM (van Bussel et al., 2016; Xin et al., 2024; Zhou et al., 2022; Zhang et al., 2021), our findings are consistent with observations in dementia, where functional connectivity is notably reduced and information processing efficiency is compromised (delEtoile and Adeli, 2017). The increased connectivity seen in early T2DM may be a compensatory response, yet it results in reduced between-network efficacy. These similar topological changes in T2DM and dementia suggest that T2DM may be a risk factor for developing dementia.

In nodal brain network analysis, T2DM is associated with a decreased clustering coefficients of the left basal ganglia and bilateral anterior central gyrus, indicating reduced connectivity between any one of three brain regions and adjacent brain regions, which would reduce the speed of information processing between adjacent node brain regions. The study of degree centrality helps to identify important nodes, and the reduced degree centrality in the bilateral thalamus and right basal ganglia suggests these areas are less synchronized in the network, resulting in a lower degree of integration of the entire brain network. Eigenvector centrality is a hierarchical measure as the sum of the centrality for any one node adjacent one and represents the "hub" in the functional brain network (Lorenzini et al., 2023). Decreased eigenvector centrality in the bilateral thalamus represents a weakened role as a "transit station" connecting to other essential brain regions. Overall, reduced nodal efficiency across multiple brain regions in T2DM signifies diminished information processing capability (Yang et al., 2020; delEtoile and Adeli, 2017; Jacob et al., 2022), supporting our study of a damaged state in T2DM patients. Some previous studies have concluded that the topology of T2DM networks with different states is mainly characterized by reduced efficiency (van Bussel et al., 2016; Xin et al., 2024). Our study results also support this view, indicating that the node network of T2DM patients included in our study is in a damaged state. The observed reduction in eigenvector centrality, an aspect infrequently highlighted in previous studies, indicates a notable alterations in network connectivity as a "hub" region in brain networks. Comprehensive brain and nodal graph theory analyses reveal a reduction in information processing efficiency in both nodes and connections across extensive brain networks.

Insulin, a growth factor with neurotrophic properties, is essential for regulating learning and memory (Rachdaoui, 2020). In T2DM, characterized by hyperinsulinemia, insulin resistance in the brain can arise from reduced insulin receptor expression and receptor-activating enzymes. This resistance can lead to the accumulation of amyloid β-protein (Aβ) and Tau proteins, contributing to cognitive decline (Arnold et al., 2018). The MoCA effectively detects mild cognitive impairment (Li et al., 2018), and lower MoCA scores in T2DM patients are linked to decreased efficiency in large-scale brain network connections. Poor glycemic control is associated with reduced global and local network efficiency and increased shortest path length, exacerbating cognitive decline. Node analysis reveals that elevated FBG further diminishes node performance. Specifically, decreased performance in the precentral gyrus (PreCG), which is crucial for verbal motor memory tasks (Sakurai et al., 2018), correlates with declining MoCA scores. This decline may impair speech motor functions, affecting MoCA outcomes. Previous

studies have also connected MoCA scores in T2DM with PreCG volume and noted that increased centrality in PreCG is linked to abnormalities in brain tissue connections (Roy et al., 2020). Additionally, elevated TG levels are associated with reduced efficacy in the left thalamus. Elevated lipids not only affect the brain functional network in T2DM patients, but also further aggravate the decreased brain functional network caused by elevated blood glucose (Kassab et al., 2023; Yang et al., 2023). These findings highlight the necessity of controlling both blood glucose and lipid levels to reduce brain damage in T2DM patients.

This study has several limitations. First, being cross-sectional, it does not capture the effects of T2DM duration on brain connectivity. Future research should address this by incorporating longitudinal follow-up. Second, incomplete data on medication use limits our ability to control for their potential effects on brain functional networks.

In summary, our study identified abnormalities in large-scale brain networks in T2DM patients, suggesting that cognition decline is caused by large-scale DMN-centered networks instead of one single region. Graph theory analysis revealed reduced efficacy in T2DM brain topology, with cognitive decline linked to diminished efficiency in both global and node-specific networks. These findings suggest that brain functional connectivity and topology could serve as valuable imaging biomarkers for understanding the biological mechanisms underlying cognitive impairment in T2DM.

Data availability statement

The raw data supporting the conclusions of this article will be made available by the authors, without undue reservation.

Ethics statement

The studies involving humans were approved by Ethics Committee of Zhanjiang Central People's Hospital. The studies were conducted in accordance with the local legislation and institutional requirements. The participants provided their written informed consent to participate in this study. Written informed consent was obtained from the individual(s) for the publication of any potentially identifiable images or data included in this article.

Author contributions

HZ: Writing – review & editing. WN: Writing – original draft. WL: Writing – original draft. ML: Writing – original draft. SW: Writing – original draft. XX: Writing – original draft. SH: Writing – original draft. LZ: Writing – original draft. JW: Writing – original draft. FW: Writing – original draft.

Funding

The author(s) declare that financial support was received for the research, authorship, and/or publication of this article. This study was funded by the Medical Scientific Research Foundation of Guangdong Province (No. A2024369), the Project of Traditional Chinese Medicine Bureau of Guangdong Province (No. 20221444), the Basic and Applied Basic Research Foundation of GuangDong (No. 2021A151515010827), the Zhanjiang Science and Technology Project (No. 2021A05115), and the Doctoral Cooperation Project of Central People's Hospital of Zhanjiang (No. 2021H03).

Conflict of interest

WL was employed by the GE Healthcare.

The remaining authors declare that the research was conducted in the absence of any commercial or financial relationships that could be construed as a potential conflict of interest.

Publisher's note

Supplementary material

The Supplementary material for this article can be found online at: https://www.frontiersin.org/articles/10.3389/fnins.2025.1472010/full#supplementary-material

References

American Diabetes Association Professional Practice (2024). 2. Diagnosis and classification of diabetes:standards of care in diabetes—2024. *Diabetes Care* 47, S20–S42. doi: 10.2337/dc24-S002

Arnold, S. E., Arvanitakis, Z., Macauley-Rambach, S. L., Koenig, A. M., Wang, H. Y., Ahima, R. S., et al. (2018). Brain insulin resistance in type 2 diabetes and Alzheimer disease: concepts and conundrums. *Nat. Rev. Neurol.* 14, 168–181. doi: 10.1038/nrneurol.2017.185

Biessels, G. J., Nobili, F., Teunissen, C. E., Simó, R., and Scheltens, P. (2020). Understanding multifactorial brain changes in type 2 diabetes: a biomarker perspective. *Lancet Neurol.* 19, 699–710. doi: 10.1016/s1474-4422(20)30139-3

Bressler, S. L., and Menon, V. (2010). Large-scale brain networks in cognition: emerging methods and principles. *Trends Cogn. Sci.* 14, 277–290. doi: 10.1016/j.tics.2010.04.004

Cao, Z., Ge, L., Lu, W., Zhao, K., Chen, Y., Sun, Z., et al. (2024). Altered subcortical brain volume and cortical thickness related to insulin resistance in type 2 diabetes mellitus. *Brain Behav.* 14:e70055. doi: 10.1002/brb3.70055

Chen, Y., Liu, Z., Wang, A., Zhang, J., Zhang, S., Qi, D., et al. (2016). Dysfunctional organization of default mode network before memory impairments in type 2 diabetes. *Psychoneuroendocrinology* 74, 141–148. doi: 10.1016/j.psyneuen.2016.08.012

Chen, Y., Liu, Z., Zhang, J., Tian, G., Li, L., Zhang, S., et al. (2015). Selectively disrupted functional connectivity networks in type 2 diabetes mellitus. *Front. Aging Neurosci.* 7:233. doi: 10.3389/fnagi.2015.00233

Cole, D. M., Smith, S. M., and Beckmann, C. F. (2010). Advances and pitfalls in the analysis and interpretation of resting-state FMRI data. *Front. Syst. Neurosci.* 4:8. doi: 10.3389/fnsys.2010.00008

Cramer, S. C., Sur, M., Dobkin, B. H., O'Brien, C., Sanger, T. D., Trojanowski, J. Q., et al. (2011). Harnessing neuroplasticity for clinical applications. *Brain* 134, 1591–1609. doi: 10.1093/brain/awr039

Cui, Y., Jiao, Y., Chen, H. J., Ding, J., Luo, B., Peng, C. Y., et al. (2015). Aberrant functional connectivity of default-mode network in type 2 diabetes patients. *Eur. Radiol.* 25, 3238–3246. doi: 10.1007/s00330-015-3746-8

Cui, Y., Li, S. F., Gu, H., Hu, Y. Z., Liang, X., Lu, C. Q., et al. (2016). Disrupted brain connectivity patterns in patients with type 2 diabetes. *AJNR Am. J. Neuroradiol.* 37, 2115–2122. doi: 10.3174/ajnr.A4858

Deletoile, J., and Adeli, H. (2017). Graph theory and brain connectivity in Alzheimer's disease. *Neuroscientist* 23, 616–626. doi: 10.1177/1073858417702621

Deng, L., Liu, H., Liu, H., Liu, J., Liu, W., Liu, Y., et al. (2021). Concomitant functional impairment and reorganization in the linkage between the cerebellum and default mode network in patients with type 2 diabetes mellitus. *Quant. Imaging Med. Surg.* 11, 4310–4320. doi: 10.21037/qims-21-41

Diamond, A. (2013). Executive functions. *Annu. Rev. Psychol.* 64, 135–168. doi: 10.1146/annurev-psych-113011-143750

Dosenbach, N. U., Nardos, B., Cohen, A. L., Fair, D. A., Power, J. D., Church, J. A., et al. (2010). Prediction of individual brain maturity using fMRI. *Science* 329, 1358–1361. doi: 10.1126/science.1194144

Fang, F., Lai, M. Y., Huang, J. J., Kang, M., Ma, M. M., Li, K. A., et al. (2019). Compensatory hippocampal connectivity in young adults with early-stage type 2 diabetes. *J. Clin. Endocrinol. Metab.* 104, 3025–3038. doi: 10.1210/jc.2018-02319

Farahani, F. V., Karwowski, W., and Lighthall, N. R. (2019). Application of graph theory for identifying connectivity patterns in human brain networks: a systematic review. *Front. Neurosci.* 13:585. doi: 10.3389/fnins.2019.00585

Faskowitz, J., Betzel, R. F., and Sporns, O. (2022). Edges in brain networks: contributions to models of structure and function. *Netw. Neurosci.* 6, 1–28. doi: 10.1162/netn_a_00204

Franke, K., and Gaser, C. (2019). Ten years of BrainAGE as a neuroimaging biomarker of brain aging: what insights have we gained? *Front. Neurol.* 10:789. doi: 10.3389/fneur.2019.00789

Fu, M., and Zuo, Y. (2011). Experience-dependent structural plasticity in the cortex. *Trends Neurosci.* 34, 177–187. doi: 10.1016/j.tins.2011.02.001

Fuster, J. M. (2006). The cognit: a network model of cortical representation. *Int. J. Psychophysiol.* 60, 125–132. doi: 10.1016/j.ijpsycho.2005.12.015

Jackson-Guilford, J., Leander, J. D., and Nisenbaum, L. K. (2000). The effect of streptozotocin-induced diabetes on cell proliferation in the rat dentate gyrus. *Neurosci. Lett.* 293, 91–94. doi: 10.1016/s0304-3940(00)01502-0

Jacob, Y., Morris, L. S., Verma, G., Rutter, S. B., Balchandani, P., and Murrough, J. W. (2022). Altered hippocampus and amygdala subregion connectome hierarchy in major depressive disorder. *Transl. Psychiatry* 12:209. doi: 10.1038/s41398-022-01976-0

Jing, J., Liu, C., Zhu, W., Pan, Y., Jiang, J., Cai, X., et al. (2023). Increased resting-state functional connectivity as a compensatory mechanism for reduced brain volume in prediabetes and type 2 diabetes. *Diabetes Care* 46, 819–827. doi: 10.2337/dc22-1998

Kaewput, W., Thongprayoon, C., Rangsin, R., Ruangkanchanasetr, P., Mao, M. A., and Cheungpasitporn, W. (2019). Associations of renal function with diabetic retinopathy and visual impairment in type 2 diabetes: a multicenter nationwide cross-sectional study. *World J. Nephrol.* 8, 33–43. doi: 10.5527/wjn.v8.i2.33

Kassab, H. S., Osman, N. A., and Elrahmany, S. M. (2023). Assessment of triglyceride-glucose index and ratio in patients with type 2 diabetes and their relation to microvascular complications. *Endocr. Res.* 48, 94–100. doi: 10.1080/07435800.2023.2245909

Li, X., Jia, S., Zhou, Z., Jin, Y., Zhang, X., Hou, C., et al. (2018). The role of the Montreal cognitive assessment (MoCA) and its memory tasks for detecting mild cognitive impairment. *Neurol. Sci.* 39, 1029–1034. doi: 10.1007/s10072-018-3319-0

Li, Y., Liang, Y., Tan, X., Chen, Y., Yang, J., Zeng, H., et al. (2020). Altered functional hubs and connectivity in type 2 diabetes mellitus without mild cognitive impairment. *Front. Neurol.* 11:1016. doi: 10.3389/fneur.2020.01016

Li, Z. G., Zhang, W., Grunberger, G., and Sima, A. A. (2002). Hippocampal neuronal apoptosis in type 1 diabetes. *Brain Res.* 946, 221–231. doi: 10.1016/s0006-8993(02)02887-1

Liu, D., Duan, S., Zhou, C., Wei, P., Chen, L., Yin, X., et al. (2018). Altered brain functional hubs and connectivity in type 2 diabetes mellitus patients: a resting-state fMRI study. *Front. Aging Neurosci.* 10:55. doi: 10.3389/fnagi.2018.00055

Liu, L., Li, W., Zhang, Y., Qin, W., Lu, S., and Zhang, Q. (2017). Weaker functional connectivity strength in patients with type 2 diabetes mellitus. *Front. Neurosci.* 11:390. doi: 10.3389/fnins.2017.00390

Liu, H., Liu, J., Liu, H., Peng, L., Feng, Z., Rong, P., et al. (2019). Pathological between-network positive connectivity in early type 2 diabetes patients without cerebral small vessel diseases. *Front. Neurosci.* 13:731. doi: 10.3389/fnins.2019.00731

Lorenzini, L., Ingala, S., Collij, L. E., Wottschel, V., Haller, S., Blennow, K., et al. (2023). Eigenvector centrality dynamics are related to Alzheimer's disease pathological changes in non-demented individuals. *Brain Commun.* 5:fcad088. doi: 10.1093/braincomms/fcad088

Lv, H., Wang, Z., Tong, E., Williams, L. M., Zaharchuk, G., Zeineh, M., et al. (2018). Resting-state functional MRI: everything that nonexperts have always wanted to know. *AJNR Am. J. Neuroradiol.* 39, 1390–1399. doi: 10.3174/ajnr.A5527

Marquez, F., and Yassa, M. A. (2019). Neuroimaging biomarkers for Alzheimer's disease. *Mol. Neurodegener.* 14:21. doi: 10.1186/s13024-019-0325-5

Meng, J., Liu, J., Li, H., Gao, Y., Cao, L., He, Y., et al. (2022). Impairments in intrinsic functional networks in type 2 diabetes: a meta-analysis of resting-state functional connectivity. *Front. Neuroendocrinol.* 66:100992. doi: 10.1016/j.yfrne.2022.100992

Ni, M. H., Yu, Y., Yang, Y., Li, Z. Y., Ma, T., Xie, H., et al. (2024). Functional-structural decoupling in visual network is associated with cognitive decline in patients with type 2 diabetes mellitus: evidence from a multimodal MRI analysis. *Brain Imaging Behav.* 18, 73–82. doi: 10.1007/s11682-023-00801-6

Nielsen, J. D., Madsen, K. H., Wang, Z., Liu, Z., Friston, K. J., and Zhou, Y. (2017). Working memory modulation of Frontoparietal network connectivity in first-episode schizophrenia. *Cereb. Cortex* 27, 3832–3841. doi: 10.1093/cercor/bhx050

Pang, L., Fan, B., Chen, Z., Chen, Z., Lv, C., and Zheng, J. (2022). Disruption of cerebellar-cerebral functional connectivity in temporal lobe epilepsy and the connection to language and cognitive functions. *Front. Neurosci.* 16:871128. doi: 10.3389/fnins.2022.871128

Rachdaoui, N. (2020). Insulin: the friend and the foe in the development of type 2 diabetes mellitus. *Int. J. Mol. Sci.* 21. doi: 10.3390/ijms21051770

Roy, B., Ehlert, L., Mullur, R., Freeby, M. J., Woo, M. A., Kumar, R., et al. (2020). Regional brain gray matter changes in patients with type 2 diabetes mellitus. *Sci. Rep.* 10:9925. doi: 10.1038/s41598-020-67022-5

Sakurai, Y., Furukawa, E., Kurihara, M., and Sugimoto, I. (2018). Frontal phonological agraphia and Acalculia with impaired verbal short-term memory due to left inferior precentral gyrus lesion. *Case Rep. Neurol.* 10, 72–82. doi: 10.1159/000487849

Shang, S., Zhu, S., Wu, J., Xu, Y., Chen, L., Dou, W., et al. (2023). Topological disruption of high-order functional networks in cognitively preserved Parkinson's disease. *CNS Neurosci. Ther.* 29, 566–576. doi: 10.1111/cns.14037

Srikanth, V., Sinclair, A. J., Hill-Briggs, F., Moran, C., and Biessels, G. J. (2020). Type 2 diabetes and cognitive dysfunction-towards effective management of both comorbidities. *Lancet Diabetes Endocrinol.* 8, 535–545. doi: 10.1016/s2213-8587(20)30118-2

Stranahan, A. M., Arumugam, T. V., Cutler, R. G., Lee, K., Egan, J. M., and Mattson, M. P. (2008). Diabetes impairs hippocampal function through glucocorticoid-mediated effects on new and mature neurons. *Nat. Neurosci.* 11, 309–317. doi: 10.1038/nn2055

Tan, X., Liang, Y., Zeng, H., Qin, C., Li, Y., Yang, J., et al. (2019). Altered functional connectivity of the posterior cingulate cortex in type 2 diabetes with cognitive impairment. *Brain Imaging Behav.* 13, 1699–1707. doi: 10.1007/s11682-018-0017-8

Van Bussel, F., Backes, W. H., Hofman, P. A. M., van Oostenbrugge, R., van Boxtel, M., Verhey, F. R. J., et al. (2017). Cerebral pathology and cognition in diabetes: the merits of multiparametric neuroimaging. *Front. Neurosci.* 11:188. doi: 10.3389/fnins.2017.00188

Van Bussel, F. C., Backes, W. H., Van Veenendaal, T. M., Hofman, P. A., Van Boxtel, M. P., Schram, M. T., et al. (2016). Functional brain networks are altered in type 2 diabetes and prediabetes: signs for compensation of cognitive decrements? The Maastricht study. *Diabetes* 65, 2404–2413. doi: 10.2337/db16-0128

Van Sloten, T. T., Sedaghat, S., Carnethon, M. R., Launer, L. J., and Stehouwer, C. D. A. (2020). Cerebral microvascular complications of type 2 diabetes: stroke, cognitive dysfunction, and depression. *Lancet Diabetes Endocrinol.* 8, 325–336. doi: 10.1016/s2213-8587(19)30405-x

Wahlund, L. O., Barkhof, F., Fazekas, F., Bronge, L., Augustin, M., Sjogren, M., et al. (2001). A new rating scale for age-related white matter changes applicable to MRI and CT. *Stroke* 32, 1318–1322. doi: 10.1161/01.str.32.6.1318

Wang, Y. F., Ji, X. M., Lu, G. M., and Zhang, L. J. (2016). Resting-state functional MR imaging shed insights into the brain of diabetes. *Metab. Brain Dis.* 31, 993–1002. doi: 10.1007/s11011-016-9872-4

Xia, W., Wang, S., Rao, H., Spaeth, A. M., Wang, P., Yang, Y., et al. (2015). Disrupted resting-state attentional networks in T2DM patients. *Sci. Rep.* 5:11148. doi: 10.1038/srep11148

Xin, H., Fu, Y., Wen, H., Feng, M., Sui, C., Gao, Y., et al. (2024). Cognition and motion dysfunction-associated brain functional network disruption in diabetic peripheral neuropathy. *Hum. Brain Mapp.* 45:e26563. doi: 10.1002/hbm.26563

Yan, C. G., Wang, X. D., Zuo, X. N., and Zang, Y. F. (2016). DPABI: Data Processing & Analysis for (resting-state) brain imaging. *Neuroinformatics* 14, 339–351. doi: 10.1007/s12021-016-9299-4

Yang, H., Chen, X., Chen, Z. B., Li, L., Li, X. Y., Castellanos, F. X., et al. (2021). Disrupted intrinsic functional brain topology in patients with major depressive disorder. *Mol. Psychiatry* 26, 7363–7371. doi: 10.1038/s41380-021-01247-2

Yang, J., Gohel, S., and Vachha, B. (2020). Current methods and new directions in resting state fMRI. *Clin. Imaging* 65, 47–53. doi: 10.1016/j.clinimag.2020.04.004

Yang, Q., Xu, H., Zhang, H., Li, Y., Chen, S., He, D., et al. (2023). Serum triglyceride glucose index is a valuable predictor for visceral obesity in patients with type 2 diabetes: a cross-sectional study. *Cardiovasc. Diabetol.* 22:98. doi: 10.1186/s12933-023-01834-3

Yeo, B. T., Krienen, F. M., Sepulcre, J., Sabuncu, M. R., Lashkari, D., Hollinshead, M., et al. (2011). The organization of the human cerebral cortex estimated by intrinsic functional connectivity. *J. Neurophysiol.* 106, 1125–1165. doi: 10.1152/jn.00338.2011

Yeshurun, Y., Nguyen, M., and Hasson, U. (2021). The default mode network: where the idiosyncratic self meets the shared social world. *Nat. Rev. Neurosci.* 22, 181–192. doi: 10.1038/s41583-020-00420-w

Zackova, L., Jani, M., Brazdil, M., Nikolova, Y. S., and Mareckova, K. (2021). Cognitive impairment and depression: Meta-analysis of structural magnetic resonance imaging studies. *Neuroimage Clin.* 32:102830. doi: 10.1016/j.nicl.2021.102830

Zhang, H., Hao, Y., Manor, B., Novak, P., Milberg, W., Zhang, J., et al. (2015). Intranasal insulin enhanced resting-state functional connectivity of hippocampal regions in type 2 diabetes. *Diabetes* 64, 1025–1034. doi: 10.2337/db14-1000

Zhang, D., Huang, Y., Gao, J., Lei, Y., Ai, K., Tang, M., et al. (2021). Altered functional topological organization in type-2 diabetes mellitus with and without microvascular complications. *Front. Neurosci.* 15:726350. doi: 10.3389/fnins.2021.726350

Zhang, Y., Zhang, X., Zhang, J., Liu, C., Yuan, Q., Yin, X., et al. (2014). Gray matter volume abnormalities in type 2 diabetes mellitus with and without mild cognitive impairment. *Neurosci. Lett.* 562, 1–6. doi: 10.1016/j.neulet.2014.01.006

Zhou, H., Lu, W., Shi, Y., Bai, F., Chang, J., Yuan, Y., et al. (2010). Impairments in cognition and resting-state connectivity of the hippocampus in elderly subjects with type 2 diabetes. *Neurosci. Lett.* 473, 5–10. doi: 10.1016/j.neulet.2009.12.057

Zhou, B., Wang, X., Yang, Q., Wu, F., Tang, L., Wang, J., et al. (2022). Topological alterations of the brain functional network in type 2 diabetes mellitus patients with and without mild cognitive impairment. *Front. Aging Neurosci.* 14:834319. doi: 10.3389/fnagi.2022.834319

Frontiers in Neuroscience

Provides a holistic understanding of brain function from genes to behavior

Part of the most cited neuroscience journal series which explores the brain - from the new eras of causation and anatomical neurosciences to neuroeconomics and neuroenergetics.

Discover the latest Research Topics

See more →

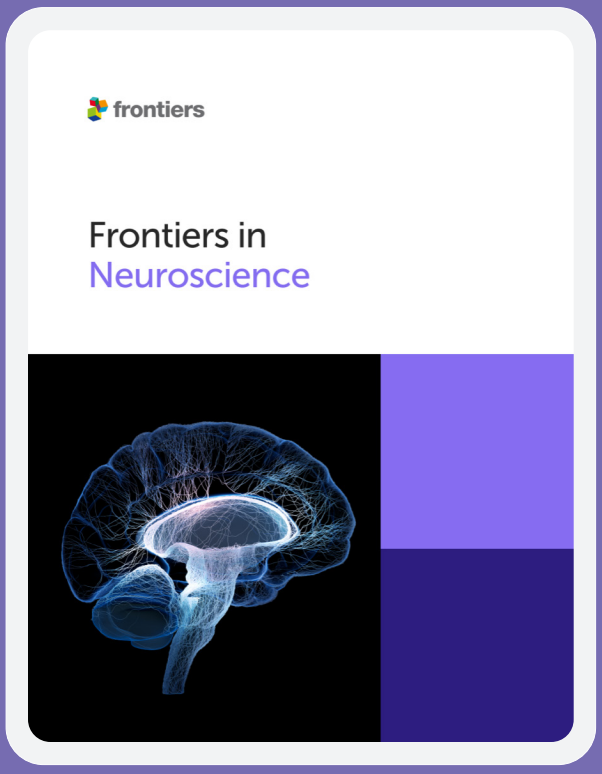

Frontiers

Avenue du Tribunal-Fédéral 34
1005 Lausanne, Switzerland
frontiersin.org

Contact us

+41 (0)21 510 17 00
frontiersin.org/about/contact